CHEMICAL
REVIEWS

pubs.acs.org/CR Review

# Molecular Probes, Chemosensors, and Nanosensors for Optical Detection of Biorelevant Molecules and Ions in Aqueous Media and Biofluids

Joana Krämer,[‖] Rui Kang,[‖] Laura M. Grimm,[‖] Luisa De Cola, Pierre Picchetti,* and Frank Biedermann*

Cite This: *Chem. Rev.* 2022, 122, 3459−3636

Read Online

ACCESS | Metrics & More | Article Recommendations | Supporting Information

**ABSTRACT:** Synthetic molecular probes, chemosensors, and nanosensors used in combination with innovative assay protocols hold great potential for the development of robust, low-cost, and fast-responding sensors that are applicable in biofluids (urine, blood, and saliva). Particularly, the development of sensors for metabolites, neurotransmitters, drugs, and inorganic ions is highly desirable due to a lack of suitable biosensors. In addition, the monitoring and analysis of metabolic and signaling networks in cells and organisms by optical probes and chemosensors is becoming increasingly important in molecular biology and medicine. Thus, new perspectives for personalized diagnostics, theranostics, and biochemical/medical research will be unlocked when standing limitations of artificial binders and receptors are overcome. In this review, we survey synthetic sensing systems that have promising (future) application potential for the detection of small molecules, cations, and anions in aqueous media and biofluids. Special attention was given to sensing systems that provide a readily measurable optical signal through dynamic covalent chemistry, supramolecular host−guest interactions, or nanoparticles featuring plasmonic effects. This review shall also enable the reader to evaluate the current performance of molecular probes, chemosensors, and nanosensors in terms of sensitivity and selectivity with respect to practical requirement, and thereby inspiring new ideas for the development of further advanced systems.

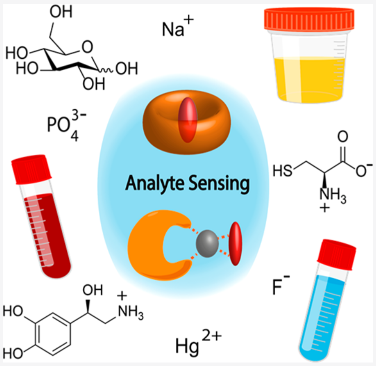

## CONTENTS

**Received:** August 25, 2021
**Published:** January 7, 2022

## 1. INTRODUCTORY REMARKS

Since its beginning, supramolecular chemistry has received increasing attention due to the wide range of possibilities for new practical applications.[1−7] Among those, novel molecular probes, supramolecular binders, and chemosensors may in combination with innovative assays lead to a revolution of sensing and medical diagnostics. To date, instrumental-based analytics, *e.g.*, well-known, highly sensitive, and powerful methods, such as HPLC-MS, GC-MS, or NMR, are commonly used for biofluid analysis in clinics. However, these methods require the use of large and complex machines that are difficult to operate and therefore cannot be used in private households or in point-of-care applications for routine diagnostics. In the last decades of research, molecular recognition-based diagnostics have produced varied and promising results in terms of sensing technology. So far, these are mainly based on biological building blocks and processes, namely immune-based diagnostics (antibody−antigen interactions),[8,9] genetically modified receptor proteins,[10] DNA and RNA technologies (including polymerase chain reaction (PCR) test),[11−13] and enzymatic reaction-based diagnostics.[14,15] Sensing methods adapted from electrochemistry are already highly advanced but are mainly restricted to the small subset of redox active analytes. Synthetic, non-biobased chemistry and particularly supramolecular chemistry has by now contributed relatively little to diagnostic applications. This somewhat disappointing status quo was summarized in 2013 by Otto S. Wolfbeis in his editorial article as "*Probes, Sensors, and Labels: Why is Real Progress Slow?*",[16] which still serves as a blueprint for describing the situation in 2021.

There are some inspiring exceptions demonstrating the future potential of synthetic artificial chemosensing systems for medical diagnostics. For instance, the molecular recognition-based glucose sensors developed separately by Senseonics (Figure 1a) and GlySure Ltd. (Figure 1b) are based on fluorescent boronic acid probes. These devices can be used for monitoring the intravenous glucose levels in real time over the period of several months.[17,18] Moreover, cation-selective chemosensors have been utilized in developing a supramolecular sensor cassette distributed by OPTI Medical Systems, Inc., which can be used for the detection of $Na^+$, $K^+$, $Ca^{2+}$, $CO_2$ (indirectly), and pH in untreated whole blood (Figure 1c).[19,20]

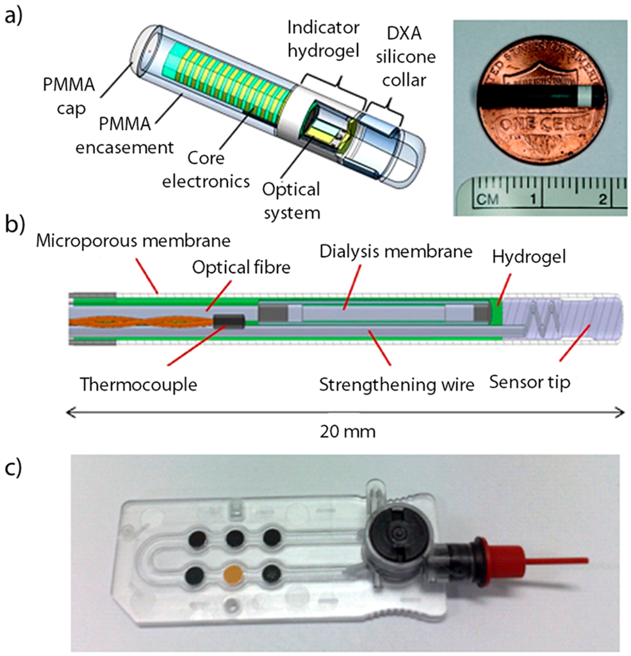

**Figure 1.** (a) Schematic representation of the "Eversense system" by Senseonics used for the detection of glucose. The hydrogel of the sensor contains glucose-selective and fluorescent phenylboronic acid probes. (b) Schematic representation of the GlySure Ltd. system used for intravenous glucose sensing through immobilized glucose-selective and fluorescent phenylboronic acid probes. Reproduced with permission from ref 18. Copyright 2015 SAGE Publishing. (c) Image of the sensor cassette sold by OPTI Medical Systems, Inc. (www.optimedical.com). The black spots carry the organic polymer fiber mats with the fluorescent sensor molecules that measure the concentration of $Na^+$, $K^+$, $Ca^{2+}$, and $CO_2$ (indirectly) in whole blood. Reproduced with permission from ref 19. Copyright 2008 The Royal Society of Chemistry.

In this review article, we focus on molecular probe, chemosensor, and nanosensor developments that are either already operational in aqueous environments or that have the potential to be developed into functional chemosensors in aqueous media. We were particularly interested in highlighting literature reports on molecular recognition-based sensing coupled to an optical readout. Moreover, we provide a general overview of the most important small molecule analyte classes found in biofluids and compare different molecular probes, chemosensors, and nanosensors for each analyte. In this respect, our review article is meant to be complementary to other review articles that are organized according to design principles or classifications of probes or chemosensors. For further reading, we can recommend the excellent review articles by Anslyn and coworkers (2015),[21] Levine and coworkers (2020),[22] and the comprehensive textbooks on chemosensors (2011)[23] and artificial receptors (2010),[24] as representative literature materials. We cover the important developments of molecular sensors, probes, and assays made in the last two decades but also present challenging tasks to the reader that chemists have yet to face. While there is some ambiguity in the literature about the terms, we follow the widely accepted convention and classify the chemical sensing systems into three categories, i.e., molecular probes, chemosensors, and nanosensors, see Figure 2.

**(Molecular) probes** are systems that form strong, essentially irreversible bonds with their target analytes (Figure 2a). This is coupled to the emergence of a pronounced optical response, *e.g.*, changes in fluorescence emission or absorbance bands. Typically, molecular probes undergo covalent-like bonding through organic reaction mechanisms. However, metal complexes are also considered as molecular probes if the binding of the target analyte results in strongly bonded, kinetically nearly inert metal−analyte complexes.

**Chemosensors** are defined in this review as systems that (under the experimental assay conditions) reversibly bind their target analytes (Figure 2b). Most chemosensors engage in noncovalent bonding through, *e.g.*, hydrogen-bonding and electrostatic interactions with the analytes. However, also metal complexes that form labile, readily exchanging complexes with their ligands (= analytes) can function as chemosensors. According to the definition used here, chemosensors generate an optical signal in the presence of the analyte. Importantly, chemosensors can be used for monitoring of (bio)chemical and (bio)physical processes such as enzymatic reactions and analyte diffusion through membranes in real time because they readily adjust (= equilibrate) to the changes in the composition of the sample, whereas molecular probes typically report a static picture.

**Nanosensors** can be obtained by combining molecular probes or chemosensors with nanoparticles (NPs) (Figure 2c). According to the IUPAC and the EU definitions of nanomaterials, NPs have at least one external dimension in the range of 1−100 nm[25,26] and feature unique physicochemical characteristics, *e.g.*, modulated optical properties (plasmon resonances).[27,28] Besides, many authors extend the term "nanoparticle" to include particles larger than 100 nm (up to several hundred nanometers) as long as physicochemical properties other than in the bulk phase are observed.[29,30] Nanoparticles can be functionalized with one or multiple copies of the same as well as with different probes or chemosensors. In addition, they can be co-functionalized, *e.g.*, with additional dyes, performance enhancers, or cellular targeting molecules, and can serve as colloidal carriers for water-insoluble molecular probes and chemosensors.[31,32]

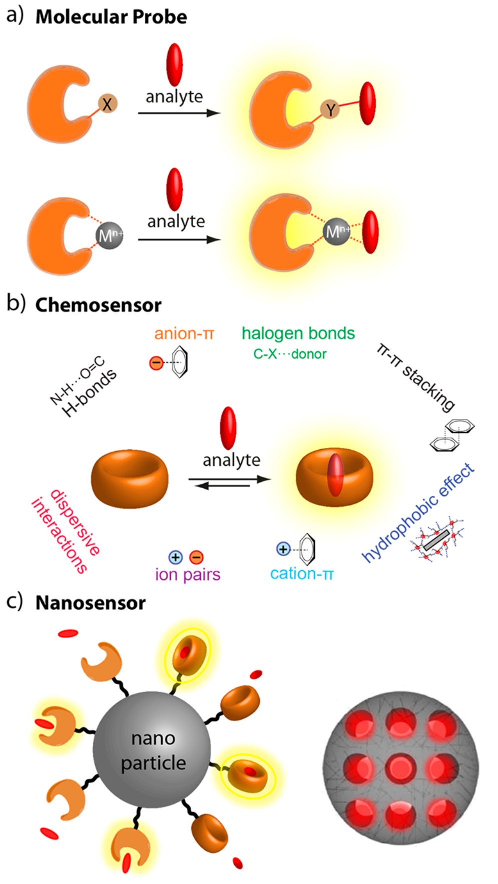

**Figure 2.** Schematic representation of a molecular probe, a chemosensor, and a nanosensor. An emission turn-on response is shown as an exemplary signal response to the presence of an analyte. (a) Molecular probes typically undergo a strong and irreversible covalent-like bond formation with analytes that carry reactive functional groups. (b) Chemosensors bind their target analytes reversibly through a combination of noncovalent binding interactions. The binding and unbinding kinetics are typically fast on the time scale of the experiment/assay. (c) Nanosensors are (nano)particle-based systems that are either surface functionalized with multiple copies of chemosensors or probes or that possess pores as binding stations for the analyte.

When molecular probes or chemosensors are coupled to NPs, different photophysical features can emerge, *e.g.*, as a result of energy transfer between the probes/chemosensors and NPs. For instance, plasmonic gold nanoparticles (AuNPs) have been extensively researched for the preparation of nanosensors, as they can be readily functionalized with molecular probes or chemosensors and show tunable plasmonic properties.[33−36] In addition to surface-functionalized NPs, there are also some examples of nanosensors based on porous organic or inorganic materials, such as metal−organic frameworks (MOFs) or mesoporous silica particles, where confinement effects, *e.g.*, aggregation-induced emission, or quenching, can be exploited for signal transduction.

Both affinity and selectivity of chemosensors and probes are often the main practical limitation for their use in realistic diagnostic applications, *e.g.*, in biofluids such as urine, saliva, and blood. Therefore, we emphasize herein the typical concentration ranges in which the analyte of interest occurs in the biofluid compared to the reported assay conditions. Moreover, we consistently specified and tabulated the

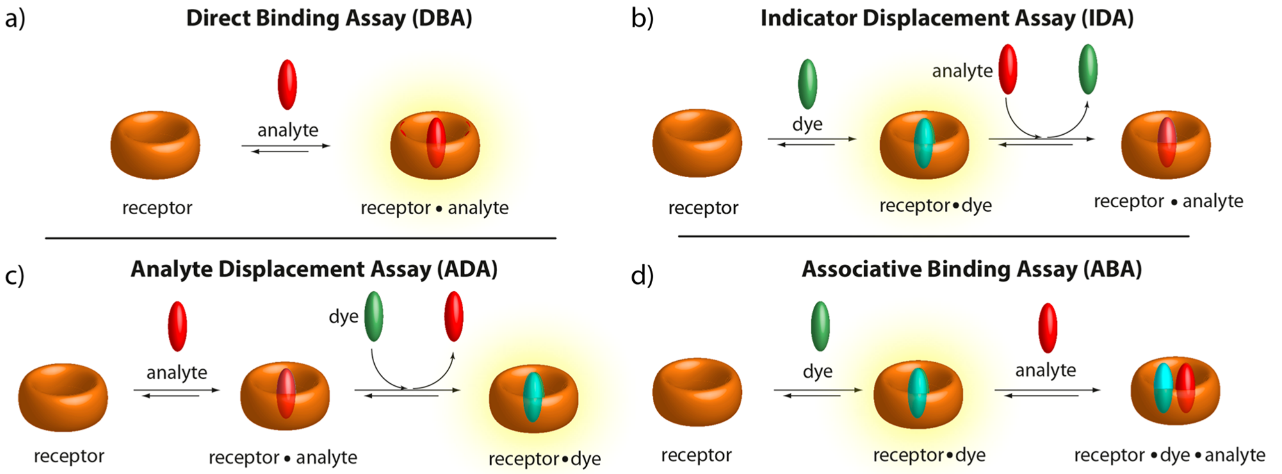

**Figure 3.** Schematic representation of the different assay types. For details, see text.

experimental conditions, *i.e.*, co-solvents used (if any), presence of salts, and the pH, under which the assays were carried out because the binding parameters of molecular recognition-based chemosensors and probes can strongly depend on these factors. For example, chemosensors based on the cucurbit[*n*]uril (CB*n*) macrocycles display unprecedently high binding affinities in water for many hydrophobic and/or positively charged guests.[37,38] However, CB*n* also interact competitively with metal cations such as $Na^+$ and $K^+$,[39,40] which are ubiquitously occurring in millimolar concentrations in biofluids, leading in most cases to greatly reduced actual binding affinities of CB*n* and biorelevant target analytes in saline biofluids (see, for instance, the binding parameters for CB*n* complexes that are made accessible at SupraBank.org).[41] Current obstacles that are encountered when attempting to extrapolate the binding properties of chemosensors reported in pure water or low concentrated salt buffers to their performance in complex biofluids are pointed out in this review. Additionally, possible strategies to overcome these barriers are presented.

We assume that the reader has already come across different assay types used for optical signal generation such that we keep the following introduction to this topic brief. The interested reader can find more information in several literature reviews.[42−44]

Most probes and some chemosensors operate in a direct binding assay (DBA), meaning that analyte binding directly results in an easily quantifiable signal change, such as the emergence or disappearance of a spectroscopic feature (Figure 3a). If applicable, this assay type is often the easiest and most practical choice. Particularly attractive DBAs are those in which the target analyte provides a unique spectroscopic response upon binding that can be distinguished from the signal caused by cross-reactive analytes.

For those probes and chemosensors that are not chromophoric/emissive or that do not produce a significant spectroscopic response upon analyte binding, the so-called indicator displacement assay (IDA)[45,46] is a viable option (Figure 3b). In an IDA, an indicator dye is first pre-complexed with the receptor molecule and displaced again when a stronger binding or higher concentrated analyte is present. Counterbalancing their simplicity, IDA-based sensing may fail to distinguish the target analyte from cross-reactive analytes (of unknown concentrations) because the displacement of the indicator from the chemosensor leads to an analyte independent spectroscopic response.

On some occasions, it can be advantageous to first complex the analyte (= guest) by the receptor and then displace it through subsequent addition of the indicator dye, which we recently introduced as a guest displacement assay (GDA). However, in an analytical context, it may be better referred to as an analyte displacement assay (ADA, Figure 3c).[47,48]

Finally, sometimes it has been feasible to establish associative binding assays (ABA) (Figure 3d).[44,49] Suitable receptors for ABA are capable of simultaneously binding dye and analyte, thereby bringing them in close spatial contact and enabling their electronic coupling. This unique binding mode offers interesting opportunities for distinguishing analytes from each other through the resulting analyte-specific spectroscopic fingerprints (see also section 2.3).

As already pointed out, we directed our efforts towards identifying sensors and their corresponding assay types that are potentially applicable for diagnostics and thus functional in biofluids. One interesting biofluid is urine, as it is becoming increasingly more evident that urinalysis can provide diagnostic data which is difficult to obtain otherwise.[50−54] Figure 4 shows representative small molecules (metabolites) that are commonly found in the human urine metabolome, whereas Figure 5 lists representative small molecules (metabolites) commonly found in human saliva. For human urine, we selected those compounds that are typically present at concentrations of >10 $\mu$M/mM creatinine.[50]

This small subset of compounds already demonstrates that urine is a rather complex mixture of many substances and substance classes that share structural similarities. In fact, there are several thousands of different metabolites, most occurring at trace levels but some also reaching micromolar concentrations that are regularly found in this protein-free biofluid.[50] A rich metabolome is of great diagnostic value because it can be used to identify and distinguish many different diseases and body dysfunctions.[55−57] Furthermore, urine is a sterile biofluid that can be conveniently obtained even by the layman on a daily basis. Urinalysis has therefore the potential to revolutionize diagnostics in home-use and in point-of-care units if sensing systems become available that are easy to use and cost efficient. However, the molecular composition complexity of urine is also a challenge to be embraced when designing selectively responding chemosensors and probes.

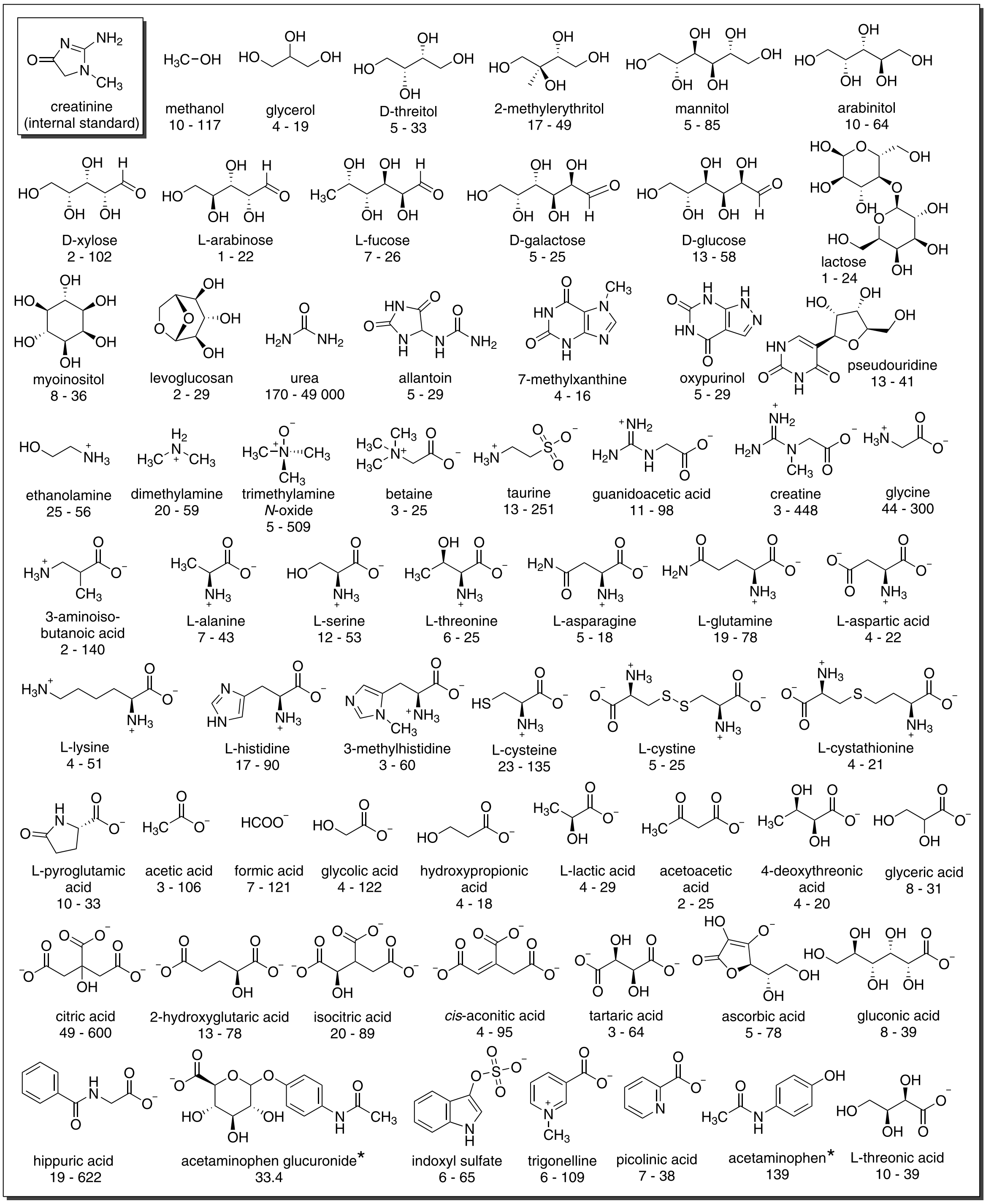

**Figure 4.** Overview of representative organic substances found in urine. The numbers indicate the concentration range (shown as $\mu$M/mM creatinine) at which the compounds were reported in a comprehensive metabolomic study based on NMR spectroscopy.[50] Typical creatinine levels found in human adult urine are 97−230 $\mu$mol kg$^{-1}$ d$^{-1}$.[61] Many more organic compounds, including additional amino acids, sugars, lipids, *etc.*, are found in the full metabolome at micromolar to trace levels. *Compounds found in urine samples from individuals that had been administered paracetamol (acetaminophen).

Note also that it is not only required to detect the target analyte in urine, but that the real information lies in its concentration profile, such that both quantitative and qualitative sensing methods are needed. In addition, inorganic cations and anions are present in urine at varying concentrations (depending on the volume that is excreted), and the pH of urine typically varies from 4.5 to 7.8 even for healthy patients.[58] These fluctuations in the matrix background further challenge the development of functional chemical sensor systems for urinalysis.

It is generally desirable to measure the urine composition regularly over a long period of time due to the highly varying urine composition from patient to patient, as well as the temporal metabolite fluctuations during a day.[59,60] In this way, normal concentration variations can be distinguished from systematically occurring changes that may indicate the

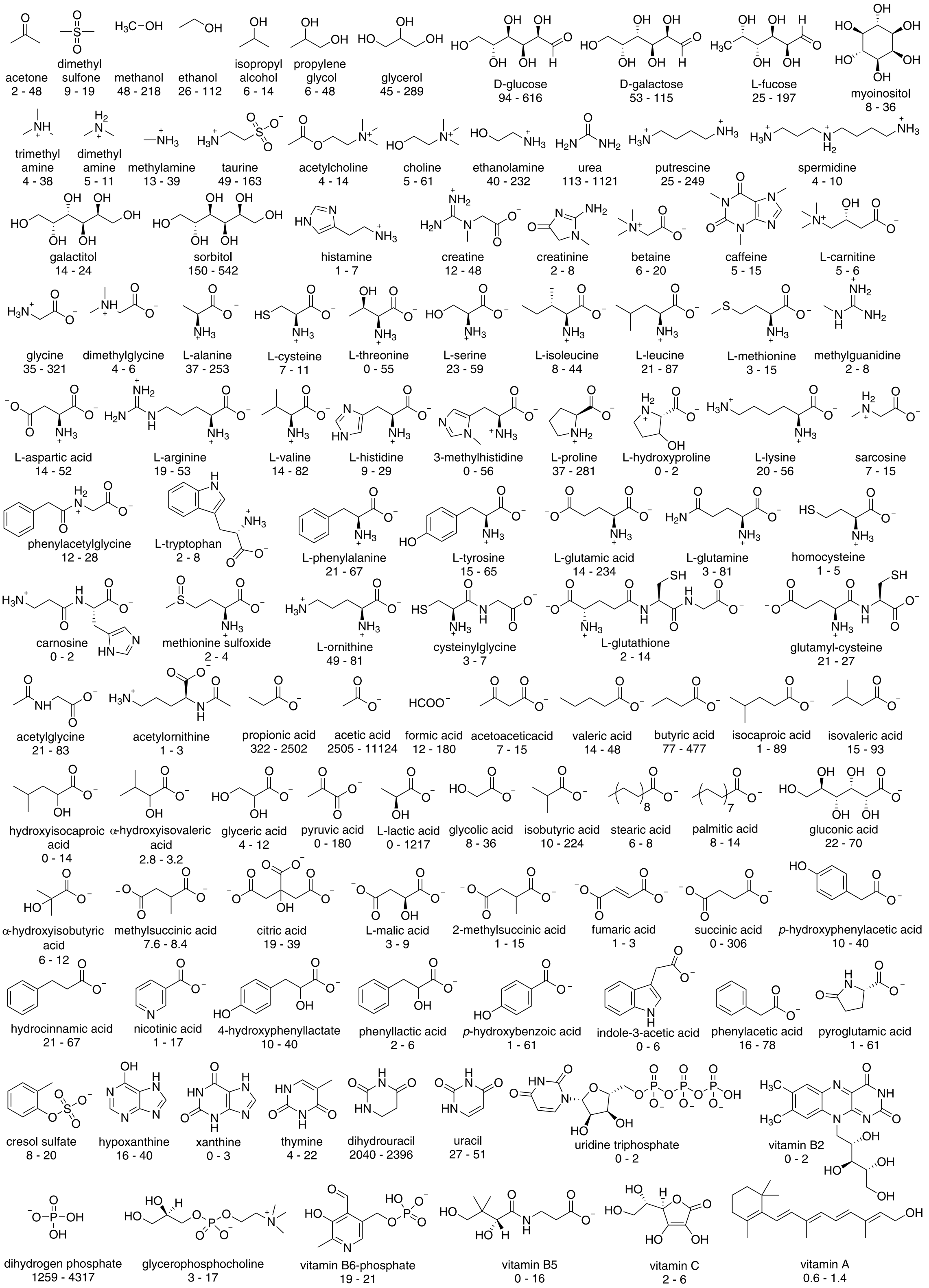

**Figure 5.** Overview of representative organic substances found in saliva. The numbers indicate the concentration range (values given in $\mu$M) at which the compounds were reported in a comprehensive metabolomic study based on NMR, GC-MS, and HPLC methods.[62]

emergence of a disease or body malfunction. The development of chemosensors and molecular probes for the facile and low-cost detection and quantification of target analytes in urine is one promising approach to fulfil these practical requirements. Similar approaches can be put forward for developing chemosensing methods for the use in saliva or blood. We have aimed to provide the reader a comprehensive overview on the status of molecular probes, chemosensors, and nanosensors for application in aqueous media, including fresh and wastewater sources and particularly biofluids.

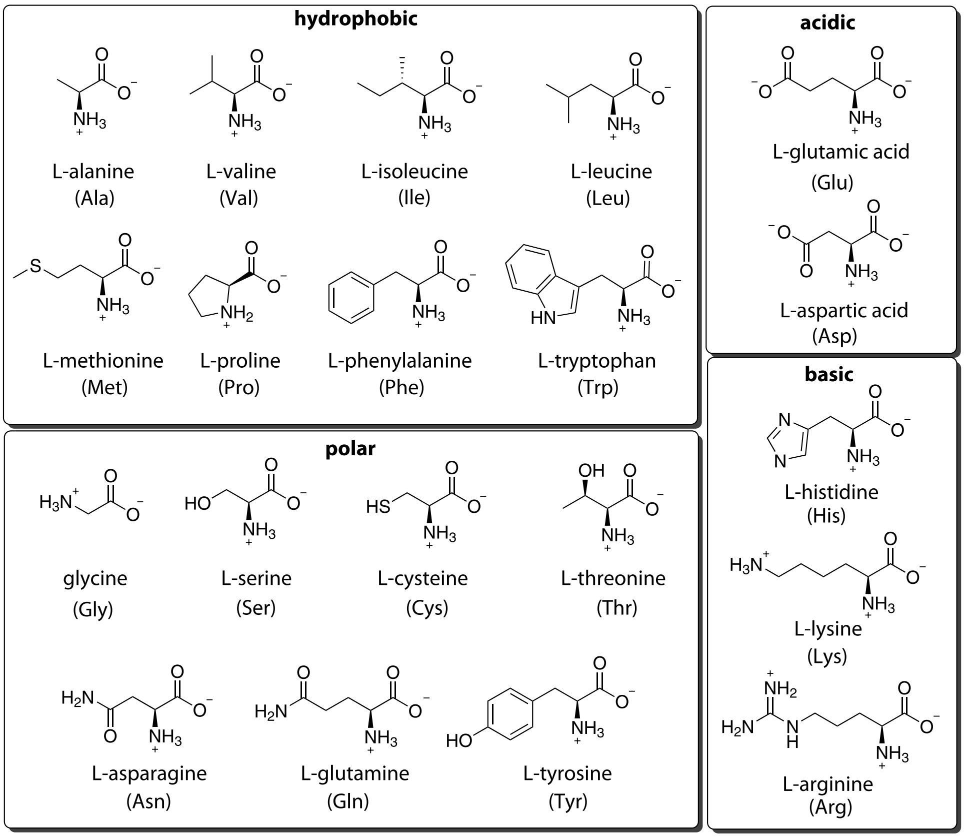

**Figure 6.** Chemical structures of the 20 proteinogenic L-amino acids.

## 2. AMINO ACIDS

Amino acids are a class of organic molecules that are composed of a basic amino group and an acidic carboxyl group bonded directly to a central carbon atom called the $\alpha$-carbon, which carries an organic residue. Except for glycine, all amino acids are chiral, while most naturally occurring amino acids are S-configured. Figure 9 shows the chemical structure of the 20 genetically encoded proteinogenic amino acids, which are the building blocks of proteins. Both amino acids and their derivatives are commonly found in biofluids, typically in the micromolar to millimolar concentration range (e.g., Figures 4 and 5 and Table 7) and are important targets for molecular diagnostics.[61] Many diseases are linked and/or indicated by the alteration of the relative concentration of amino acids,[63−66] thus only an exemplary number of them are presented herein. For a detailed discussion of the amino acid catabolism and its associated diseases, which is beyond the scope of this review, we would refer the interested reader to other excellent literature sources.[67−75] Phenylketonuria (PKU) is the most common congenital disorder of the amino acid metabolism and is characterized by abnormal concentrations of phenylalanine (Phe) in the body.[76] On the basis of plasma concentrations of Phe, different types of PKU can be classified, namely classical PKU (c(Phe) > 1200 $\mu$M), moderate PKU (600 $\mu$M < c(Phe) < 1200 $\mu$M), and hyperphenylalaninemia (Phe = 120−600 $\mu$M).[67,68] When untreated, PKU can lead to intellectual disability, seizures, behavioral problems, and psychological disorders.[77,78] Tyrosinemia type 1 is an example of impaired tyrosine catabolism that is characterized by elevated levels of tyrosine in the blood and can lead to liver, kidney, and peripheral nerve damage if left untreated.[68,78,79]

Tryptophan (Trp) is another essential amino acid that both itself as well as its metabolites are directly or indirectly involved in many physiological processes, including neuronal functions, immunity, and gut homeostasis.[80−82] Because of the strong link between altered tryptophan metabolism and physiology, abnormal Trp concentrations in biofluids such as plasma, serum, and urine are considered as potential biomarkers that can be associated with disorders of the central nervous system such as psychiatric and neurological diseases.[72,83,84] Abnormal levels of histidine and its metabolites are associated with diseases such as aging-related disorders, metabolic syndrome, atopic dermatitis, ulcers, inflammatory bowel diseases, ocular diseases, and neurological disorders.[73] For example, it was reported by the Zhai group that the ratio of branched-chain amino acids to histidine can potentially be used as a biomarker for osteoarthritis.[85] Sulfur-containing amino acids, *i.e.*, methionine, cysteine, and homocysteine, play an important role in the maintenance and integrity of cellular systems by participating in cellular redox reactions and affecting the ability of cells to detoxify from free radicals and reactive oxygen species.[70] Therefore, genetic defects that affect the regulation of the sulfur containing amino acids can be the cause for a variety of diseases, including homo- and cystinuria, homo- and cysteinemia, and neural tube defects as well as vascular disease, Alzheimer's disease, HIV, and special types of cancer.[70] For example, high levels of homocysteine (in serum or plasma) were shown to be a risk factor for cardiovascular diseases, especially for people with significant carotid stenosis.[69,71,86,87] Overall, amino acids play an essential role in the human body, and their detection in aqueous media and biofluids holds a great potential for molecular diagnostics applications.

## 2.1. General Approaches for Amino Acid Detection

Amino acids are popular targets for chemosensors and probes as they offer several reactive moieties, for instance their $-NH_2$ and $-COOH$ groups that can be used as chemical anchors (Figure 6). They possess additional functional groups that can be targeted by molecular recognition or chemically reactive sites, *e.g.*, thiol or amino groups. Other unique features are intrinsic azaheterocyclic moieties, *e.g.*, for His, that can serve as ligands for metal ions and metal−organic complexes. Additionally, positively charged side chains (*e.g.*, lysine) or negatively charged side chains (*e.g.*, glutamic acid) are of utility when designing chemosensors and probes. Furthermore, the hydrogen bonding capabilities of the $-CONH_2$ amide moieties found in asparagine and glutamine and that of the −OH hydroxyl moieties found in serine and threonine might be considered, even though intermolecular H-bonding is generally screened by water as a solvent. Finally, the hydrophobic aromatic residues (*e.g.*, tryptophan) and the hydrophobic aliphatic residues (*e.g.*, leucine) can be exploited as target sites for chemosensor binding.

In the following, first, molecular probes and chemosensors are described that have a broad scope, *i.e.*, that detect all or a wide range of amino acids. Then, chemosensors and probes that were designed to target specifically the side chains of certain amino acids are discussed. In addition, we refer the reader to a specialized critical review by Zhou and Yoon on the matter of amino acid sensing by probes and chemosensors.[88] Lastly, it is worth pointing out that enzyme-based assay kits for the detection and quantification of several amino acids in biofluids have become commercially available. Therefore, any probe or chemosensor that is hoped to reach practical utility must outperform the existing technology, for instance, in terms of sensitivity, ease of handling, assay times, and costs.

## 2.2. Molecular Probes for Amino Acids (and Proteins)

Most known molecular probes for amino acids operate through a chemical reaction with the amino functionality. Several (pro)dyes have been developed that feature a readily visible color change or become emissive after the reaction with amino acids. The molecular probes discussed within this section are summarized in Tables 1 and 2.

For instance, ninhydrin (**P2.1**) is a popular amino acid reactive probe that gives a deep-blue or purple color, known as Ruhemann's purple, when reacting with primary amines through a sequence of condensation and decarboxylation steps (Figure 7).[89−96] Ninhydrin is widely used to detect fingerprints[97−99] because it yields a clearly visible stain in the presence of amino acids, peptides, and proteins (mostly the $-NH_2$ groups of lysine) that are deposited on a surface upon touching it. It has been proposed that even the gender of a "person of interest" can be determined from fingerprints through a ninhydrin-based, LC/HPLC-coupled colorimetric assay because the amino acid content in male and female fingerprints is different.[100]

The spiro compound fluorescamine (**P2.2**) that forms highly fluorescent products upon reaction with primary amino groups in basic aqueous media is a representative emission-based probe for amino acids and amines (Figure 8).[101] While fluorescamine is generally selective toward primary amines, also amino acids and their derivatives containing secondary amines, such as proline, can be detected by using a modified protocol.[102]

**Table 1. Summary of Molecular Probes for Amino Acids (and Proteins) (LOD, Limit of Detection)**

| probe | media | concentration range | ref |
|---|---|---|---|
| Amino Acids Analyte | | | |
| **P2.1** | water | μM range | 89−96 |
| **P2.2** | water (pH >9.0) | μM range | 101,102 |
| **P2.3**[a] | 400 mM boric acid buffer, pH 9.7 | pM range | 106 |
| **P2.4**[a] | borate buffer, pH 9.5 | μM range | 107 |
| **P2.5** | 1% MeCN in 10 mM PBS, pH 7.4 | μM range | 112 |
| **P2.7**[b] | 85 mM MES, phosphate or CHES buffer, pH 5.7−9.0 | μM range | 113 |
| **P2.8** | 50% MeOH in 50 mM HEPES buffer, pH 7.5 | mM range | 114 |
| **P2.9**[c] | 100 mM NaCl in 50 mM HEPES buffer, pH 7.4 | mM range | 115 |
| Bovine Serum Albumin (BSA) Analyte | | | |
| **P2.6** | HeLa cells | 0−25 μM;<br>LOD, 62 nM | 112 |
| Lysine (Lys) Analyte | | | |
| **P2.6**[3] | 1% MeCN in 10 mM PBS, pH 7.4 | 0−25 μM;<br>LOD, 62 nM | 112 |

[a] Other nucleophiles such as thiols, carboxylic acids, and cyanides need to be present for the reaction with amines to occur. [b] Sensor array with different indicator dyes was used to differentiate between 20 amino acids. [c] Cross-reactivity with arginine and other amino acids.

Ninhydrin and fluorescamine indiscriminately react with all accessible (primary) amino moieties. Furthermore, these probes are not selective for metabolites and also label and detect proteins. On the one hand, this is an advantage as, for instance, fluorescamine is useful for determining protein concentrations.[103−105] On the other hand, these probes can therefore only be used for detecting and quantifying amino acids and their derivatives if proteins are not present in the biofluid (*e.g.*, in urine of healthy patients) or if the biofluid is first purified from proteins, which is, for example, required for blood serum samples.

Dialdehydes such as *o*-phthaldialdehyde (**P2.3**) and naphthalene-2,3-dicarboxaldehyde (**P2.4**) are useful and highly sensitive fluorescent probes for the detection of amines and amino acids in alkaline aqueous media.[106,107] For **P2.3** and **P2.4**, the co-addition of a nucleophile such as a thiol or a cyanide salt is required for the formation of fluorescent isoindoles (Figure 9). Thus, **P2.3** and **P2.4** can also be applied for the detection of other nucleophiles such as thiols,[108,109] carboxylic acids,[110] and cyanides[111] in biofluids in an alternative assay protocol.

Very recently, an exciting new class of amine-reactive probes and labels that can be used for the detection of amines, amino acids, and proteins, as well as for biolabeling, was disclosed by Bouffard, Kim, and coworkers.[112] Unlike other known pentafluorophenyl esters or NHS-ester reactive dyes, these amine-reactive *meso*-ester BODIPYs motifs (**P2.5** and **P2.6** in Figure 10) did not only form stable amide bonds with primary $NH_2$-groups but also provided both changes in their absorbance and emission spectra ($\Delta\lambda$ = 70−100 nm) as well as an emission intensity increase (up to 3000-fold) in a practically convenient time scale (5 min). The authors demonstrated that the large emission turn-on response is an outstanding reflection of the extreme sensitivity of *meso*-ester BODIPYs to modest electronic differences between esters and

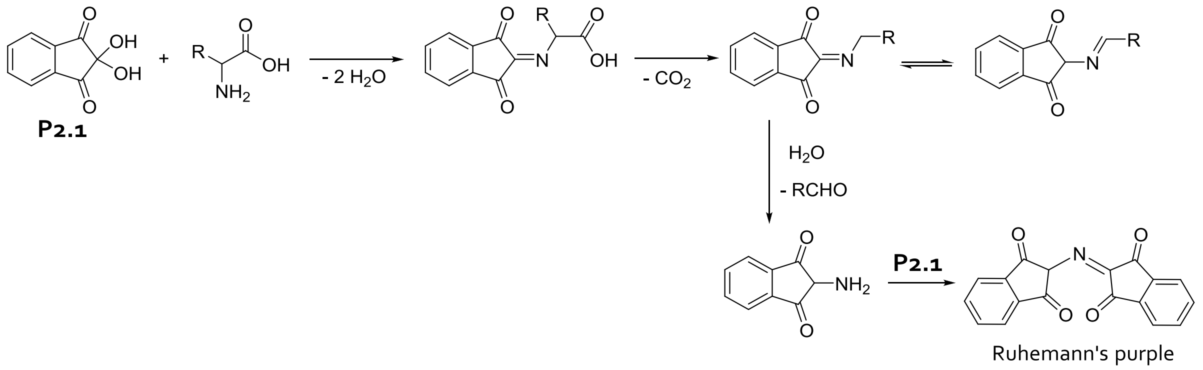

**Figure 7.** Schematic representation of the reaction sequence of ninhydrin (**P2.1**) with an $\alpha$-amino acid.

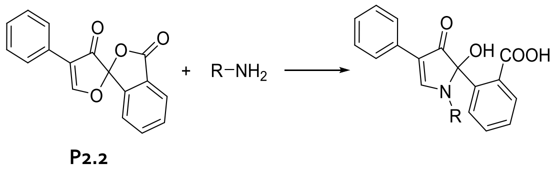

**Figure 8.** Schematic representation of the reaction of a primary amine with fluorescamine (**P2.2**).

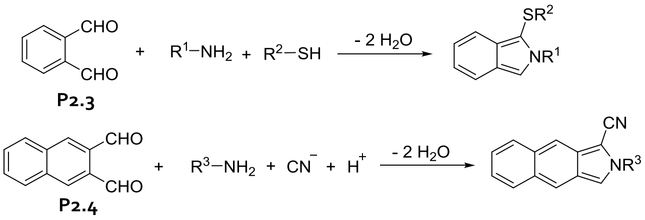

**Figure 9.** Schematic representation of the reaction of **P2.3** and **P2.4** with amines, thiols, and cyanides.

amides. Furthermore, probe **P2.6** was used for protein labeling in living cells. This new class of amine-reactive probes will certainly find a wide range of applications in the life sciences given the already successful examples for monitoring food spoilage and for staining of proteins on electrophoretic gels or in living cells.

Aforementioned (commercial) probes for amino acids cannot directly distinguish different amino acids from each other, and hence they are often used in combination with separation methods such as (high-performance) liquid chromatography. This causes certain restrictions in terms of assay times and parallelization opportunities. Thus, general amino acid binding probes with which many or all amino acids can be directly distinguished from each other, *e.g.*, through reactivity differences or on account of analyte-indicative spectroscopic fingerprints, are also of interest.

Severin and coworkers developed a colorimetric indicator displacement assay (IDA)-based on the combination of a reactive rhodium complex (**P2.7** in Figure 11) and three colorimetric indicator dyes (gallocyanin, xylenol orange, and calcein blue). With this assay, which was conducted in aqueous buffers (MES, CHES, or phosphate buffer, pH 5.7−9.0) with an analyte concentration of 750 $\mu$M, it was possible to distinguish the 20 proteinogenic amino acids from each other in a stepwise process ("decision tree") and through coupled multivariate analysis (Figure 11b).[113]

Anslyn and coworkers introduced an enantioselective IDA that was used to determine the enantiomeric excess (*ee*) of $\alpha$-amino acids in methanolic buffer mixtures in the low millimolar concentration range.[114] The assay exploited the ability of the $Cu^{II}$-complex (**P2.8** in Figure 12) to coordinate with amino acids, providing an analyte-indicative spectroscopic information. The maximum absorbance value difference between the L- and the D-form of the amino acids were used for enantioselective sensing. The authors demonstrated the capability of their assay for high-throughput screening

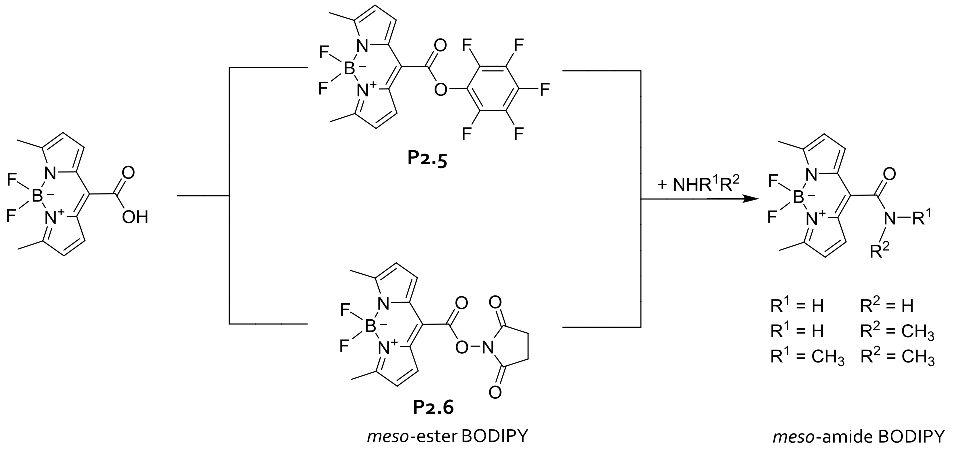

**Figure 10.** Amine-reactive BODIPY-based probes **P2.5** and **P2.6** respond with changes in their absorbance and emission properties upon amide bond formation.

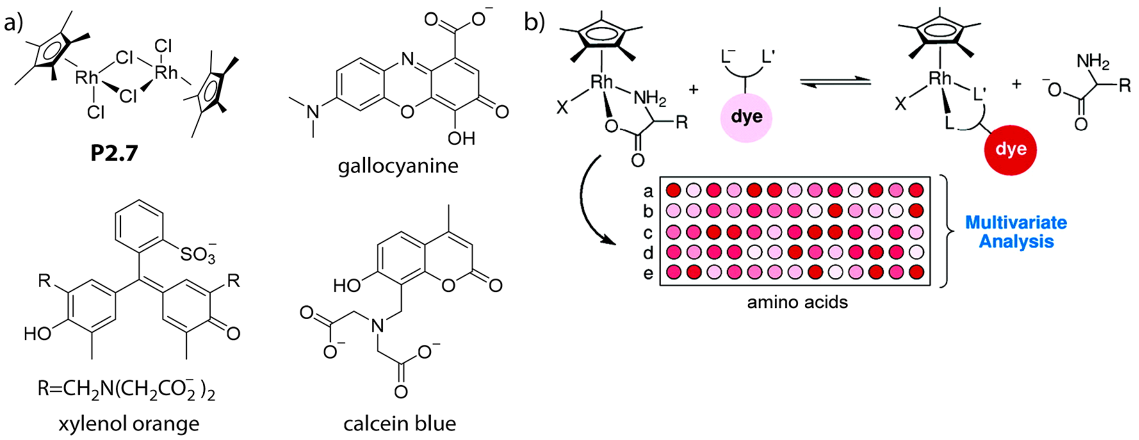

**Figure 11.** (a) Chemical structures of probe **P2.7** and its corresponding indicator dyes. (b) Principle of the colorimetric identification of 20 natural amino acids using indicator-displacement arrays composed of **P2.7** and the indicator dyes at different pH. Adapted with permission from ref 113. Copyright 2004 American Chemical Society.

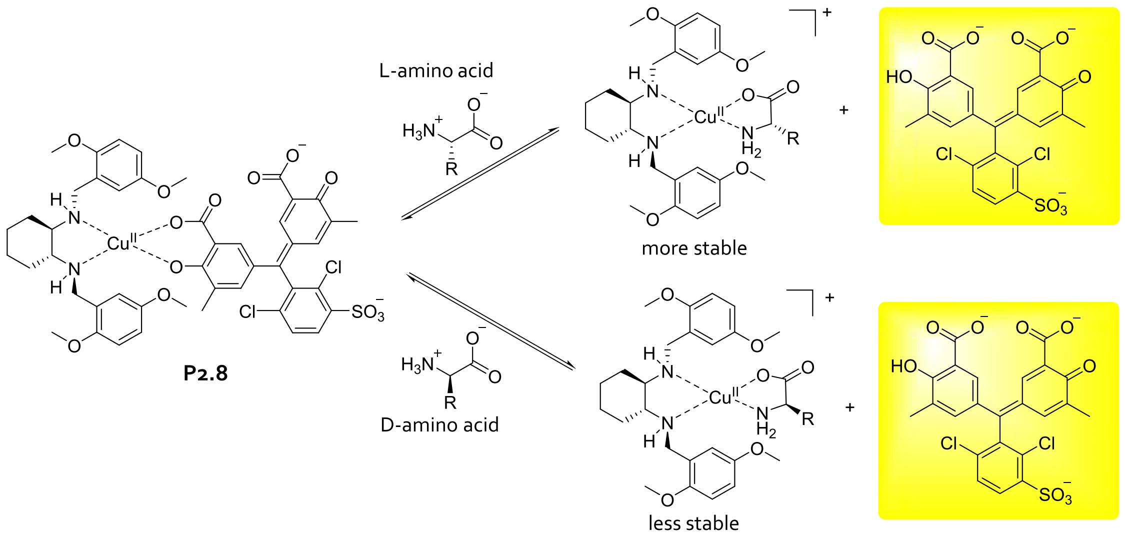

**Figure 12.** Schematic representation of an enantioselective IDA for amino acids based on $Cu^{II}$-complex **P2.8**. Adapted with permission from ref 114. Copyright 2008 American Chemical Society.

applications, *e.g.*, the *ee* values of 96 amino acid samples were determined with acceptable accuracy.[114]

In some cases, it was possible to distinguish amino acids from each other using just one simple probe. For instance, Glass and coworkers presented an aldehyde-functional amino coumarin probe (**P2.9**) that was found to react with amino acids (and amines) through the formation of hydrogen bonding stabilized iminium bonds in 50 mM HEPES buffer containing 100 mM NaCl, pH 7.4 (Figure 13).[115] While the binding affinities are rather low, restricting its applicability to high millimolar analyte concentrations and above, this emission turn-on probe nevertheless showcases that different amino acids can be distinguished from each other by taking the complementary information on their $K_a$ values and their signal response factors into account.

In a real-life scenario, metabolites have to be detected, quantified, and distinguished from several other possible interferents commonly found in biofluids. Nonselective probes such as ninhydrin or fluorescamine are suitable for the task of quantifying the total amino (acid) amount of a sample. However, IDAs can in principle distinguish different amino acids from each other will likely provide a convolute response when applied to real biofluidic samples of unknown mixture compositions. The development of more selectively reacting or responding probes for amino acids and their derivates remains an important task for the future.

### 2.2.1. Molecular Probes for Thiol Containing Amino Acids (and Glutathione).

A wide range of different thiol-reactive probes has been developed already, which can roughly be divided into two classes: (i) probes that form stable covalent conjugates with the thiol-containing analytes, and (ii) systems in which the thiol triggers the chemical cleavage of the probe, resulting in an uncaging event or the release of a chromophoric/emissive indicator. We restrict our focus here to systems that are applicable to sensing in aqueous media and refer the reader to the excellent reviews on thiol probes available in the literature.[88,116−120] The chemical structures of thiol-containing amino acids and derivatives are depicted in Figure 14.

With respect to probes that react with thiols forming covalent conjugates, the ability of thiols to undergo Michael addition, $S_N$-type reactions, and addition-condensation reactions are most commonly exploited.

a)

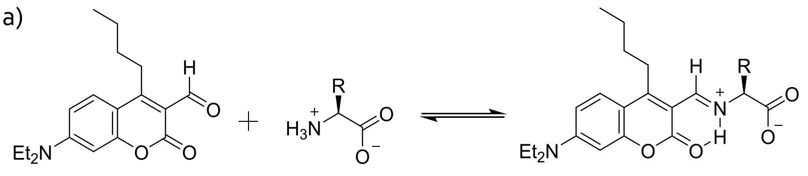

**P2.9**

b)

| Analyte | $K_{eq}$ ($M^{-1}$) | $I_{max}/I_0$ |
|---|---|---|
| Glycine | 4.0 | 26 |
| Aspartate | 2.3 | 40 |
| Glutamate | 2.4 | 45 |
| Lysine | 6.5 | 29 |
| Serine | 5.2 | 23 |
| β-Alanine | 2.5 | 23 |
| Alanine | 1.4 | 29 |
| Ethanolamine | 6.7 | 15 |
| 1,3-Diaminopropane | 12.5 | 22 |
| Lactic acid | - | - |
| Diethylamine | - | - |

**Figure 13.** (a) Schematic representation of amine-reactive probe (**P2.9**). (b) Table of binding constant and signal transduction selectivity of **P2.9** for certain amino acids.[115]

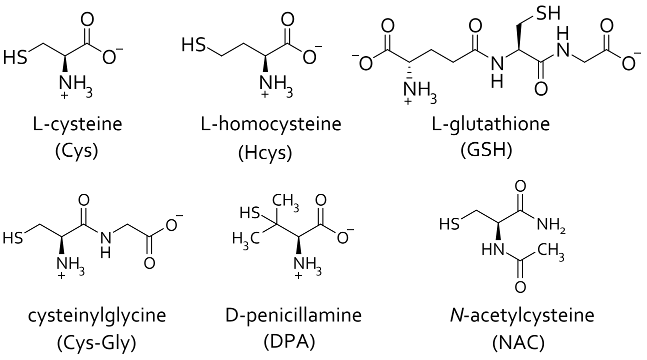

**Figure 14.** Chemical structures of thiol-functional amino acids.

Typical Michael-type reactive probes contain maleimides or other *α*,*β*-unsaturated acyl species. For instance, promising results were reported by the Nagano group that designed the maleimide-pendant BODIPY fluorophore (**P2.10** in Figure 15), which showed an up to 350-fold emission enhancement upon reacting with thiols, *e.g.*, *N*-acetylcysteine (NAC), in 100 mM sodium phosphate buffer, pH 7.4.[121] Through a systematic variation of the substituent pattern, the authors had arrived at an optimum where the probe−thiol conjugate possessed a large emission quantum yield, while the emission of the probe itself was nearly fully quenched due to a donor-excited photoinduced electron transfer (PET). A maleimide-linked chromenoquinoline (**P2.11** in Figure 15) was synthesized by Talukdar and coworkers, which showed nanomolar detection limits for cysteine (Cys), homocysteine (Hcys), and glutathione (GSH) in 10 mM HEPES buffer, pH 7.4.[122] Furthermore, the fast reactivity of maleimides with thiols was utilized by Gunnlaugsson and coworkers, who designed a $Tb^{III}$-cyclen maleimide-based lanthanide luminescence turn-on probe (**P2.12** in Figure 15) that responded with an emission enhancement in the presence of GSH, Cys, and Hcys but not to other (non-thiol functional) amino acids in 20 mM HEPES buffer containing 135 mM KCl, pH 7.4.[123]

Lin and coworkers installed an *α*,*β*-unsaturated keto moiety on a (diethylamino)coumarin through a facile synthetic sequence.[124] Probe **P2.13** (Figure 16) responded with an emission enhancement (factor >200) to the presence of thiols and showed a submicromolar detection limit in 25 mM sodium phosphate buffer, pH 7.4. Reactivity differences were found between different thiols (reaction rate: Cys > Hcys > GSH) that were rationalized by steric effects. Furthermore, the authors succeeded in determining the total thiol concentration

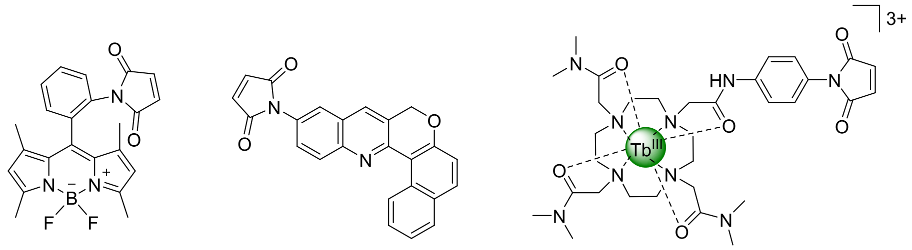

**P2.10** **P2.11** **P2.12**

**Figure 15.** Chemical structures of the probes **P2.10**, **P2.11**, and **P2.12**.

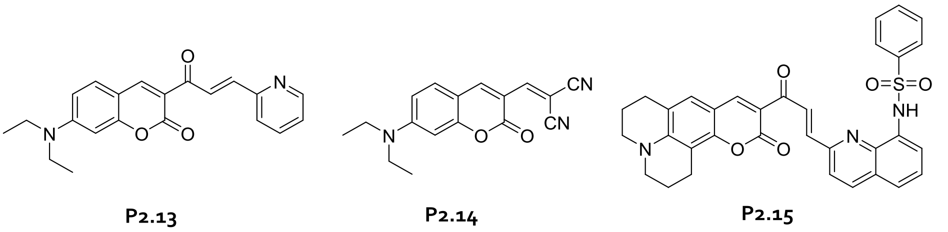

**P2.13** **P2.14** **P2.15**

**Figure 16.** Chemical structure of the probes **P2.13**, **P2.14**, and **P2.15**.

in urine of healthy individuals. Kim and coworkers found that the addition reaction of the weakly fluorescent coumarin malononitrile conjugate **P2.14** (Figure 16) with thiols led to an approximately 10× emission intensity increase in 100 mM HEPES containing 33% DMSO, pH 7.4.[125] A modest kinetic selectivity for cysteine was obtained with another coumarin-based probe (**P2.15** in Figure 16) featuring an $\alpha,\beta$-unsaturated keto moiety as the reactive site. The faster reaction rate for cysteine compared to other thiols was ascribed to steric differences and a lower p$K_a$ value, corresponding to a higher nucleophilicity of cysteine in the used reaction mixture of 10% DMSO in 10 mM PBS at pH 7.4.[126]

Akkaya and coworkers covalently attached a nitroalkene unit to a water-soluble BODIPY dye, obtaining the thiol-responsive probe **P2.16** (Figure 17) that showed a higher emission enhancement upon reacting with Cys than with Hcys and GSH in an aqueous-organic medium of 20% MeCN in 50 mM HEPES, pH 7.2.[127]

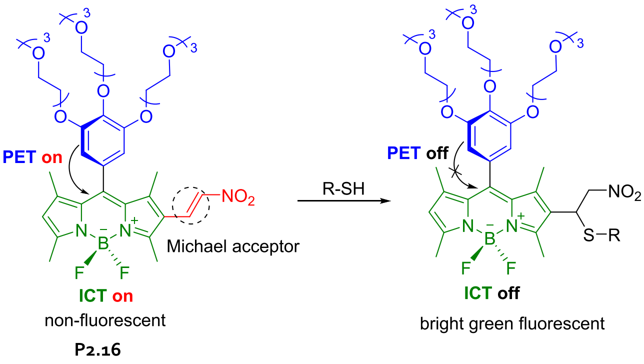

**Figure 17.** Schematic representation of the reaction of probe **P2.16** with a thiol-containing analyte. Adapted with permission from ref 127. Copyright 2012 American Chemical Society.

A squaraine-based chromophore (**P2.17** in Figure 18) reported by Ajayaghosh and coworkers was highly reactive towards Cys and GSH, enabling its use as a ratiometric fluorescent probe for the detection of aminothiols in blood plasma.[128] The detection of Cys was investigated in 50% MeOH in 10 mM CHES, pH 9.6. In fact, the probe correctly indicated the known increase of thiols in the blood of smokers. While the authors stressed the detection of Cys and GSH in their original report, other thiols may cause a similar emission response.

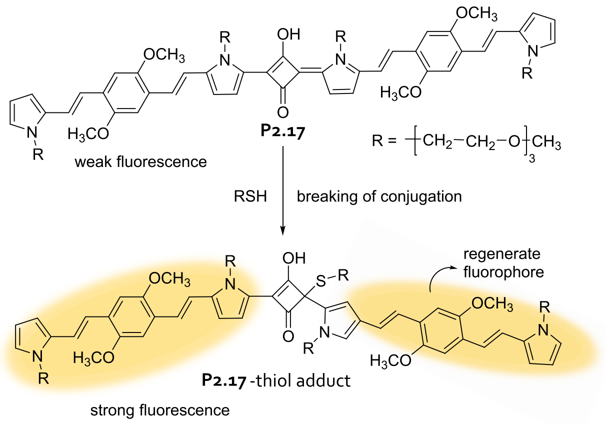

**Figure 18.** Schematic representation of probe **P2.17** and its reaction with a thiol. Adapted with permission from ref 128. Copyright 2008 Wiley-VCH.

Probes that form stable conjugates with thiols in a one-step-reaction typically suffer from the same issue already pointed out for general amino-acid-reactive probes, *i.e.*, it is difficult or impossible to distinguish different thiols from each other. Thus, their use may be restricted to examine the total thiol content of a sample for which established protocols with commercially available probes such as Ellman's reagent[129] or Aldrithiol[130,131] are competitive options.

To distinguish thiols from each other, which is of diagnostic relevance,[133−135] a probe design that capitalizes on the presence of a second recognition point, *e.g.*, the amino group in thiol-containing amino acids, appears to be promising. Strongin, Yang, and coworkers designed a benzothiazole fluorophore with an adjacent phenyl acrylate moiety (**P2.18** in Figure 19) that undergoes a Michael addition with thiols, causing an emission turn-on of the probe in the blue wavelength range ($\lambda_{ex}$ = 304 nm, $\lambda_{em}$ = 377 nm).[132] Importantly, probe **P2.18** can undergo a rapid (<10 min) addition−elimination reaction with Hcys. The uncaging of the probe causes an emission signal increase with a maximum at 487 nm. The homologous thiol amino acid Cys also follows this addition−elimination cycle, however, at a reduced kinetic rate. The authors also demonstrated that their probe remains functional in deproteinized human plasma. In contrast, many alternative acrylate-based probe designs feature a kinetic selectivity for the addition−elimination reaction with cysteine over homocysteine and glutathione, for instance, a 1,8-naphthalimide-based probe (**P2.19** in Figure 20) developed by Liu and coworkers.[136] This emission turn-on probe reached a detection limit of 1.8 $\mu$M for cysteine in 10 mM PBS, pH 7.4.

A thiol- and amine-reactive probe (**P2.20** in Figure 20), which leads to the uncaging of a two-photon active merocyanine dye, was introduced by Wong, Li, Dong, and coworkers. **P2.20** was utilized for cellular imaging application. Their probe-based cysteine quantification assay displayed linearity in the concentration range from 0.5 to 40 $\mu$M. The subsequent amine-moiety triggered addition−elimination mechanism was found to occur faster for cysteine than for

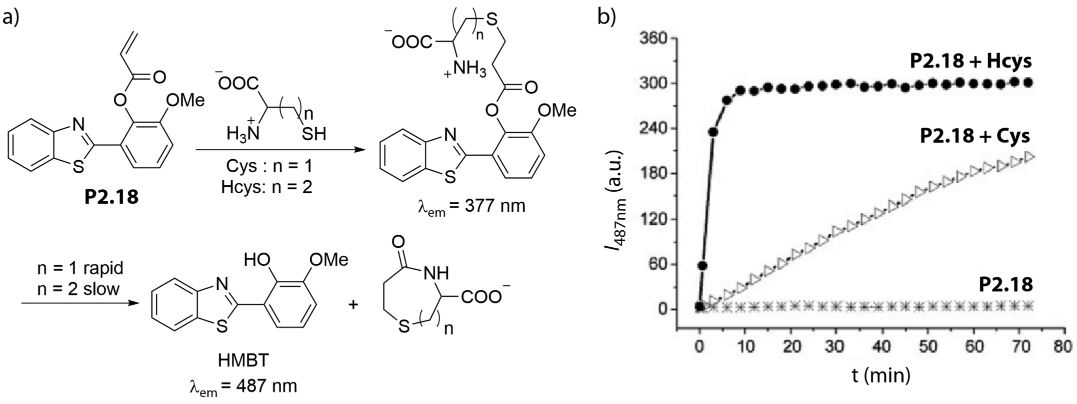

**Figure 19.** (a) Schematic representation of the reaction of **P2.18** with Cys and Hcys. (b) Kinetic traces of probe **P2.18** (10 $\mu$M) with 20 $\mu$M Hcys and Cys in 1 mM CTAB in 20 mM phosphate buffer, pH 7.4, as obtained by emission intensity monitoring. Adapted with permission from ref 132. Copyright 2011 Wiley-VCH.

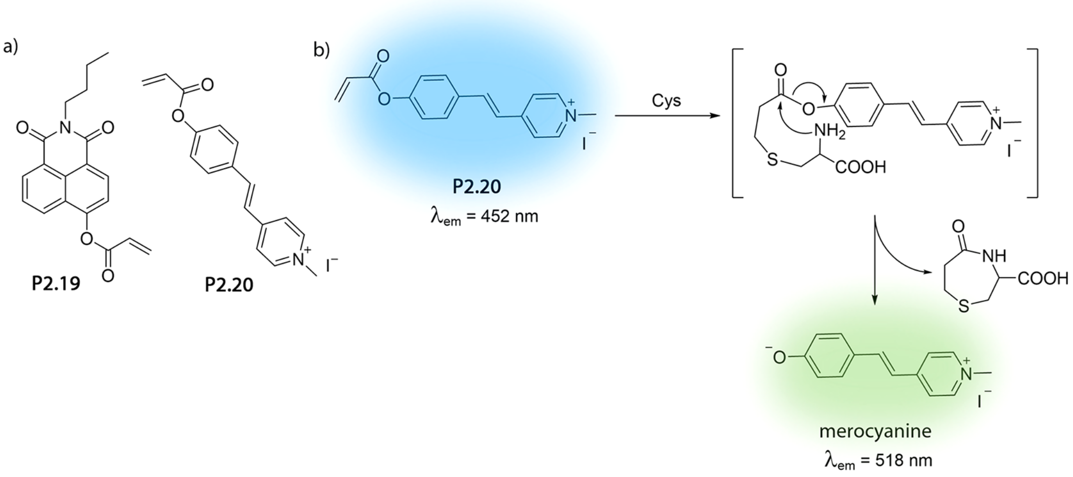

**Figure 20.** (a) Chemical structures of the thiol-reactive probe **P2.19**. (b) Schematic representation of the reaction of **P2.20** with Cys. Adapted with permission from ref 137. Copyright 2015 American Chemical Society.

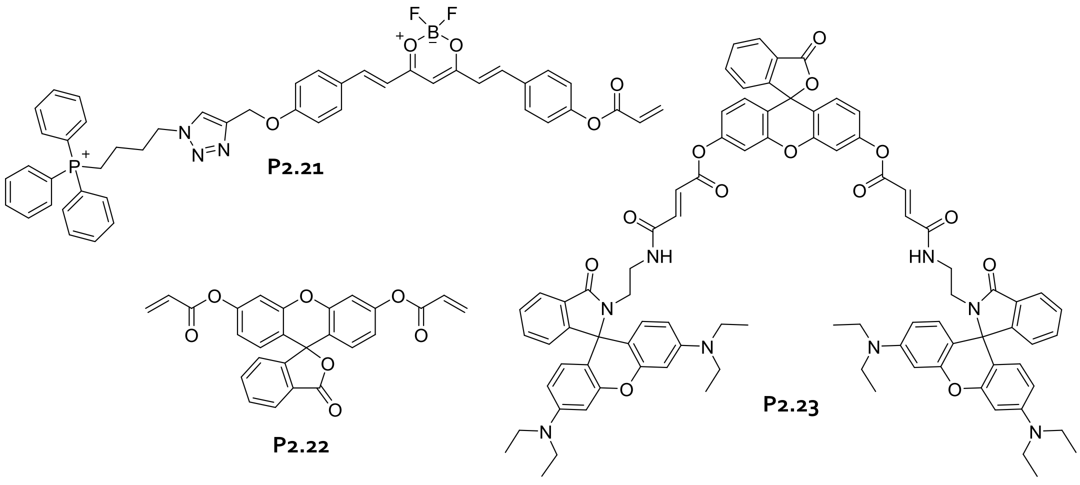

**Figure 21.** Chemical structures of probes **P2.21**−**P2.23**.

homocysteine or glutathione in 50% DMSO in 10 mM PBS, pH 7.4.[137]

Following a similar design idea, Guo and coworkers more recently introduced an acrylate-type Michael acceptor probe for thiols, particularly for cysteine in 50% DMSO in 10 mM PBS, pH 7.4.[138] Their probe (**P2.21** in Figure 21) responds with an emission turn-on response in the near-infrared (NIR) region of the electromagnetic spectrum and features a $Ph_3P^+$-R group as a mitochondria-targeting group. The authors demonstrated the functionality of the probe for imaging applications of cysteine inside living cells. Fluorescein acrylates (**P2.22** in Figure 21), which can be easily prepared in a one-

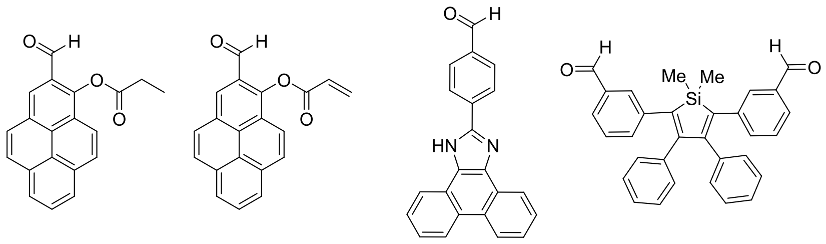

**P2.24** **P2.25** **P2.26** **P2.27**

**Figure 22.** Chemical structures of probes **P2.24**−**P2.27**.

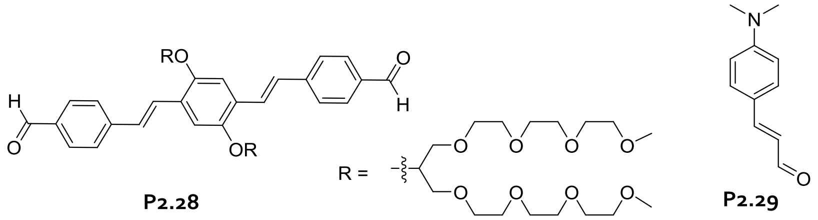

**P2.28** **P2.29**

**Figure 23.** Chemical structures of probes **P2.28** and **P2.29**.

step reaction from commercial fluorescein, have been presented by Chen and coworkers as cysteine-selective molecular probes and provided an excellent detection limit of around 100 nM in mixed aqueous-organic media such as 20% EtOH in 20 mM phosphate buffer, pH 7.4.[139] Bao, Zhu, and coworkers also utilized the discussed addition−elimination mechanism, arriving at a thiol reactive probe **P2.23** that was (kinetically) selective for cysteine over homocysteine, glutathione, and non-thiol-functional amino acids and that can be applied for imaging in cells (Figure 21).[140] The authors reported a detection limit of 88 nM for cysteine in 10 mM HEPES, pH 7.4, containing 20% MeCN with their rhodamine−fluorescein based probe.

Molecular probes that are selective for homocysteine have been devised by exploiting the formation of a six-membered thiazine ring. This motif emerges upon addition of the −SH and $-NH_2$ moieties of the target analyte to the probes' aldehyde group that is adjacent to a chromophoric aromatic system. In favorable cases, this conjugation reaction can cause an emission turn-on of the probe in the presence of homocysteine but not with cysteine, glutathione, or other amino acids. This was indeed observed for a pyrene−aldehyde based probe reported by Lee, Shin, Yoon, and coworkers.[141] In their design, an additionally present acrylate or acetate moiety (**P2.24** and **P2.25** in Figure 22) engaged in a hydrogen bonding contact with the −NH group of the formed thiazine ring. A low detection limit in the submicromolar range, fast reaction times (∼5 min), and strong signal response factors (∼50× emission enhancement) were found in 10% DMSO in 10 mM HEPES, pH 7.4. The probe is applicable for homocysteine detection in living cells. In contrast, **P2.26** (Figure 22) was shown to react with both homocysteine and cysteine alike, leading to nearly identical ratiometric emission responses in the presence of these amino acids in 75% DMF in 10 mM HEPES buffer, pH 7.4.[142] Likewise, an aldehyde-functionalized silacyclopentadienes (silole) derivative **P2.27** (Figure 22) was used by the Tang group to distinguish homocysteine from cysteine based on their kinetic rates of thioaminal formation, which was found to be faster for cysteine in 60% DMSO in 10 mM HEPES, pH 7.4.[143] Thus, it appears that the aforementioned hydrogen bonding capability of an adjacent acrylate or acetate moiety installed in **P2.24** and **P2.25** was of key significance for tuning the selectivity towards homocysteine.

Bunz, Dreuw, and coworkers have synthesized a water-soluble aromatic aldehyde (**P2.28** in Figure 23) that was shown to respond with emission turn-on to cysteine through thioaminal formation in phosphate buffer (pH 11).[144] This probe was generally not reactive to other amino acids. However, lysine and potentially all primary amines are interfering species due to their cross-reactivity in imine-formation. Also, $\alpha,\beta$-unsaturated aldehydes are reactive towards amino thiols, resulting in the formation of a cyclic addition−condensation product with the −CHO moiety. For instance, the commercially available **P2.29** (Figure 23) was introduced in a seminal report by Strongin, Rusin, and coworkers as a cysteine selective probe, which responds to the presence of Cys with a decrease in its absorbance at 400 nm.[145] In this way, low micromolar concentrations of cysteine were detected in aqueous buffers (100 mM carbonate buffer, pH 9.5).

Conversely, a naphthalimide-based glyoxal hydrazone (**P2.30** in Figure 24), introduced by Guo and coworkers, showed a ratiometric emission response for both Cys and Hcys in 50% DMSO in 100 mM HEPES, pH 7.4.[146] Apparently both amino thiols form a cyclic reaction product that engages in intramolecular hydrogen-bonding interactions. Interestingly, glutathione can also be selectively detected though aldehyde-based thiol-(amine)-recognition. Wang, Zhao, and coworkers

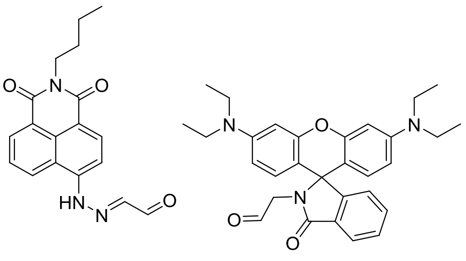

**P2.30** **P2.31**

**Figure 24.** Chemical structures of probes **P2.30** and **P2.31**.

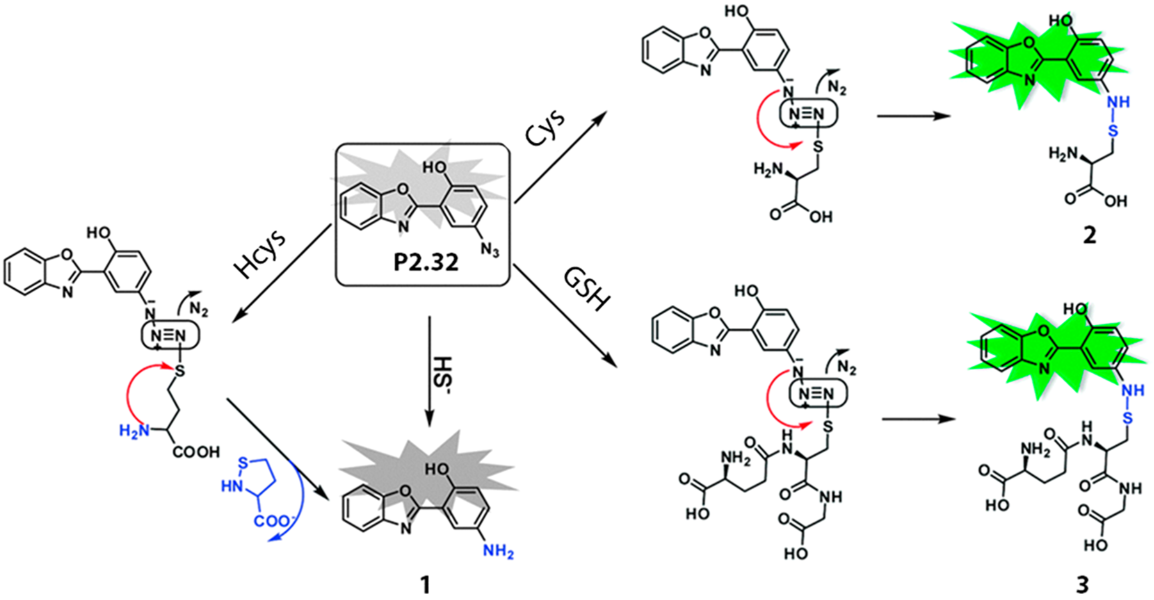

**Figure 25.** Schematic representation of the reactions of probe **P2.32** with Cys, Hcys, and GSH, leading to the formation of weakly emissive product 1 (Hcys) or strongly emissive product 2 (Cys) and product 3 (GSH). Adapted with permission from ref 148. Copyright 2016 The Royal Society of Chemistry.

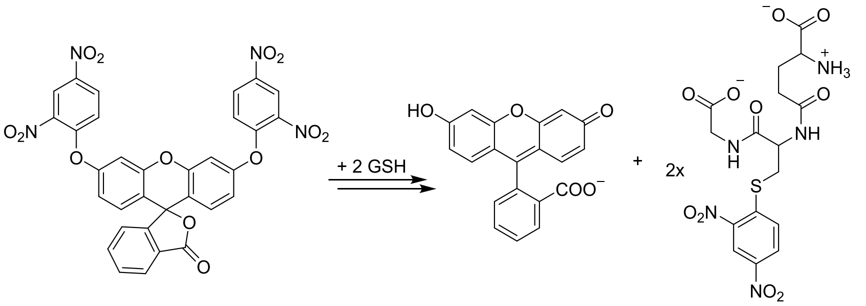

**P2.33** fluorescein 2,4-dinitrobenzene-GSH

**Figure 26.** Schematic representation of the reaction of probe **P2.33**, with GSH leading to the uncaging of fluorescein in buffered aqueous media. Reproduced with permission from ref 149. Copyright 2013 Elsevier BV.

installed a $-CH_2CHO$ moiety on the spirolactam-N of a rhodamine derivative, which was only weakly emissive.[147] Through reaction of the probe **P2.31** (Figure 24) with GSH but not with other thiols, the ring-opening of the spirolactam occurred, resulting in an emission turn-on response in 20 mM PBS at pH 5.8.

For the authors of this review, it remains so far not fully predictable under which circumstances aldehyde-based probes for amino thiols will be selective for homocysteine, cysteine, toward both, and toward other thiol species. It is also worth noting that biogenic amines, *e.g.*, putrescine, cadaverine, or the amino acid lysine, can potentially react with aldehyde-based probes to form imines. This possibility should be considered when developing quantitative assays for cysteine and homocysteine sensing in living cells and biofluids.

An innovative method for selective thiol sensing was exploited by the Xu group, who designed probe **P2.32** (Figure 25) that features an aryl azide. With **P2.32**, it was possible to distinguish Cys as well as GSH from Hcys and hydrogen sulfide in mixed aqueous-organic media, such as 50% MeCN in HEPES buffer, pH 7.4, with a detection limit of 90 nM.[148] Here, the additional amine reactivity of homocysteine causes a further decomposition of the thiol-azide intermediate, leading to a weakly emissive compound, whereas the addition products of cysteine and glutathione and other non-amino reactive thiols, such as *N*-acetylcysteine, convert *via* a rearrangement reaction into stable and emissive conjugates (Figure 25).

A conceptually different approach, exploiting the nucleophilicity of thiols in $S_N$-type reactions, has been often successful for detecting glutathione. Typically, the probes are designed in such a way that either an emission-quenching moiety is displaced through a substitution reaction, or an aforequenched fluorophore is uncaged upon the reaction with the target analyte.

A conceptually simple yet powerful probe was introduced by the Chen group, who functionalized fluorescein with two dinitrophenol moieties, causing a complete emission quenching (Figure 26).[149] The authors then demonstrated that upon GSH addition an emission turn-on response occurred after 15−30 min through uncaging of the fluorescein fluorophore. None of the other amino acids tested caused a significant emission turn-on response. Probe **P2.33** showed an excellent detection limit of 22 nM for glutathione, in mixed aqueous-organic medium such as 30% EtOH in 20 mM PBS, pH 7.4, and can be used for cellular imaging. The authors reasoned that the two carboxylate moieties present in glutathione

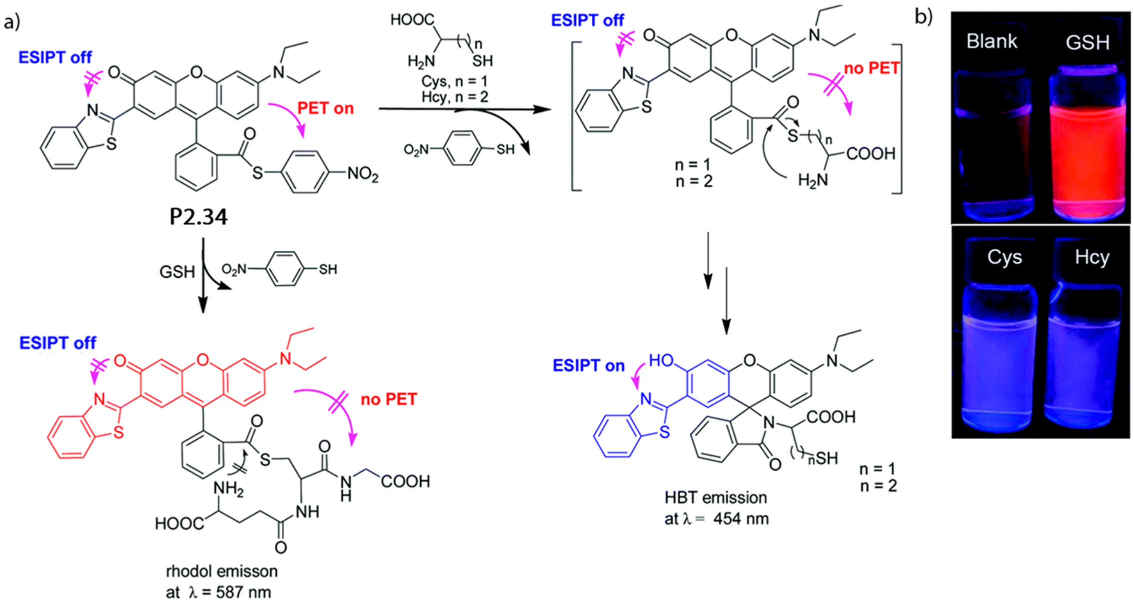

**Figure 27.** (a) Schematic representation of the mechanism for the discriminative detection of GSH and Cys/Hcys by using **P2.34**. (b) Image of aqueous solutions of **P2.34** in the presence of GSH, Cys, and Hcys under UV-light ($\lambda_{ex}$ = 365 nm). Reproduced with permission from ref 150. Copyright 2014 The Royal Society of Chemistry.

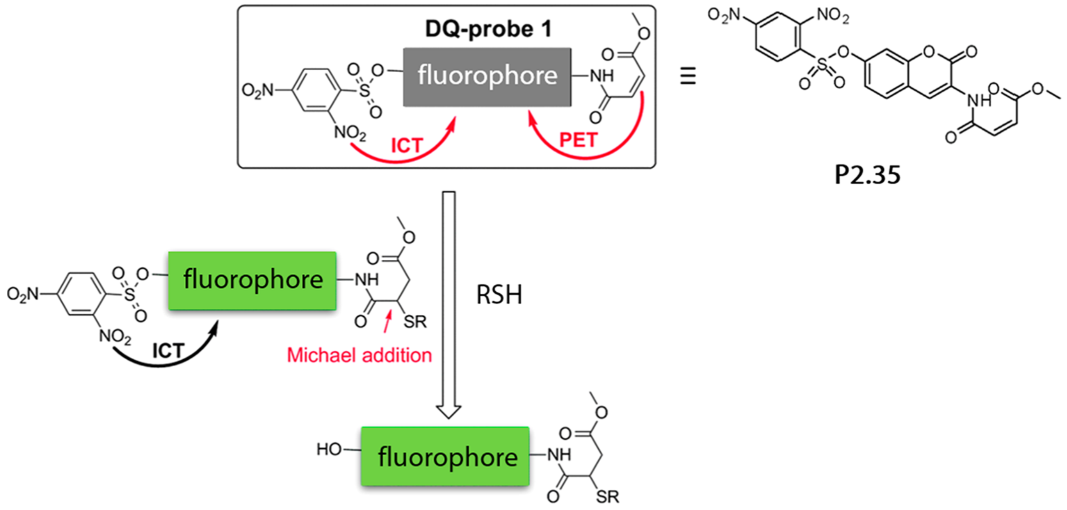

**Figure 28.** Sensing of thiols with probe **P2.35**. Reproduced with permission from ref 151. Copyright 2015 The Royal Society of Chemistry.

enhance the rate of the nucleophilic substitution reaction. Indeed, the peptide Glu-Cys-Glu, possessing three carboxylate functionalities, showed even higher reaction rates than glutathione.

In the same year, Yang, Li, and Strongin communicated a rhodol thioester **P2.34**, which is a rhodamine derivative that can distinguish GSH from Cys and Hcys through emerging unique emission colors, *i.e.*, red in the presence of GSH and blue for Cys and Hcys in 30% DMF in 20 mM phosphate buffer, pH 7.4 (Figure 27).[150] In the first step, all thiols displace the quencher 4-nitrothiophenol to form a fluorescent thiol ester featuring the typical rhodol emission at 587 nm. However, thiol-conjugated Cys and Hcys rapidly undergo a subsequent addition−elimination mechanism through involvement of their accessible amino groups (*S*,*N*-acyl shift reaction), leading to the formation of a thermodynamically stable spirolactam. The probe was designed in such a way that the intramolecular spirocyclization led to a "quinone-phenol"-type signal transduction of rhodol dyes due to an excited state intramolecular proton transfer (ESIPT) process that caused the emergence of the 2-(2-hydroxyphenyl)benzothiazole (HBT) emission at 454 nm. For GSH, the *S*,*N*-acyl shift reaction is kinetically impaired. Noteworthy, the rhodol thioester has been successfully applied to the differential sensing of GSH and cysteine in breast cancer cells and in reduced human blood serum.

The dual use of a Michael-type acceptor and quencher moiety, and of an additional displaceable quencher moiety, has been put forward by the Sun and Yi group in 2015.[151] Their tailor-made probe **P2.35** has an extremely low residual emission in the absence of thiols and thereby reaches a detection limit of 20 nM for Cys, Hcys, and GSH in 10 mM PBS, pH 7.4 (Figure 28).

In the same year, the Zhu group introduced a dual-response *S*,*N*-fluorescent probe **P2.36** for Cys, Hcys, und GSH containing two thiol-reactive moieties installed on a BODIPY

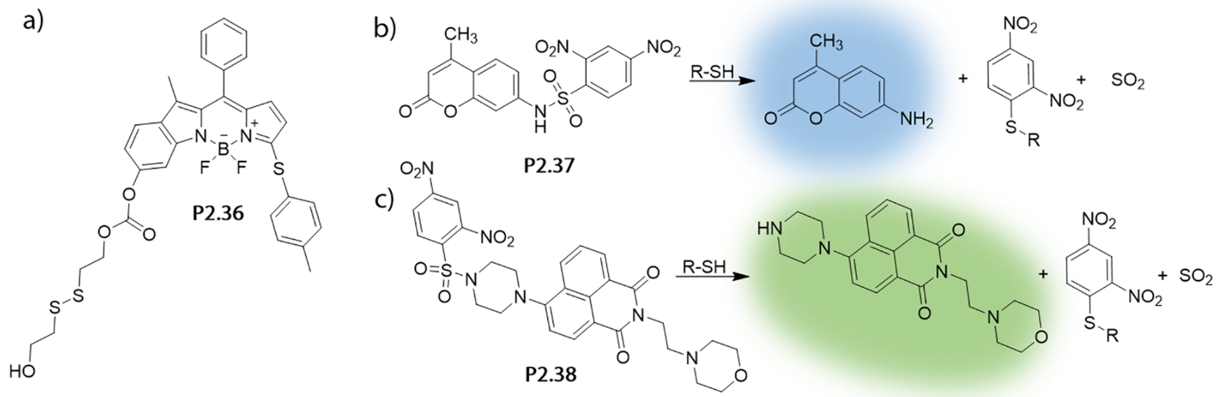

**Figure 29.** (a) Chemical structure of molecular probe **P2.36**. (b,c) Schematic representation of the reaction of probe **P2.37** and probe **P2.38** with thiols. (b) Adapted with permission from ref 152. Copyright 2015 The Royal Society of Chemistry. (c) Adapted with permission from ref 153. Copyright 2016 Springer Nature.

chromophore (Figure 29a).[154] Through their design, it is possible to distinguish GSH from Cys/Hcys through the emerging different emission colors in 20 mM HEPES, pH 7.4, containing 50% MeCN. Like the aforementioned rhodol-based system, distinction between the biorelevant thiols is again based on their reactivity differences, *e.g.*, thiol and amine reactivity of Cys and Hcys and exclusive thiol reactivity of glutathione.

The use of cleavable sulfonyl and sulfonamide moieties is another popular strategy for the development of thiol-reactive probes, as for instance demonstrated by the groups of Yao, Peng, Ma, Li, Deng, and Wang.[152,153,155−158] An amino-coumarin that was conjugated through a sulfonamide group to a dinitrophenyl quencher uncaged in the presence of thiols, resulting in a strong emission enhancement (**P2.37** in Figure 29b).[152] This probe reacted equally well with cysteine and glutathione in 10 mM phosphate buffer, pH 9.0. Note that the basic pH chosen increases the nucleophilicity of the thiol analytes and thus the reaction rate of the probe. Similar observations were made for a sulfonamide linked naphthalimide−dinitrophenyl conjugate **P2.38** (Figure 29c) that possesses a lysosomal thiol-targeting moiety. Also, this probe reacted indiscriminately with Cys, Hcys, and GSH within 10 min at 37°C, displaying a low micromolar detection limit in aqueous-organic media, *i.e.*, 30% DMSO in 10 mM HEPES buffer, pH 7.4, and the potential for two-photon imaging applications.[153]

The dinitrobenzylsulfonyl moiety can analogously be employed to conjugate a thiol-cleavable quencher to hydroxyl-functional dyes, as was shown for Nile red as the fluorophore (**P2.39** in Figure 30). This probe reacts with Cys, Hcys, and GSH in a similar fashion but has been shown to provide an extrapolated thiol-detection limit in the nanomolar regime in 50 mM HEPES, pH 7.4, containing 50% DMSO.[155] The same design concept can also be applied to BODIPY fluorophores (**P2.40** in Figure 30), leading to a similar performance in terms of detection limit and signal response, albeit with a somewhat unexpected overall selectivity for cysteine over homocysteine and glutathione in 50% DMSO in 50 mM HEPES, pH 7.8.[156]

A conceptually related probe design has been shown to furbish kinetic selectivity for aromatic thiols over aliphatic thiols and showed very high sensitivity with a detection limit of 20 nM in 10 mM phosphate buffer, pH 8.0 (**P2.41** in Figure 31a).[157] Similar reactivity differences were also observed for a nitrobenzofurazan (NBD)-based probe **P2.42** (Figure 31b) that reacted much faster with aromatic than with aliphatic thiols because of the lower $pK_a$ value of aromatic thiols and thus their higher nucleophilicity at pH 7.3 in 10 mM phosphate buffer.[158]

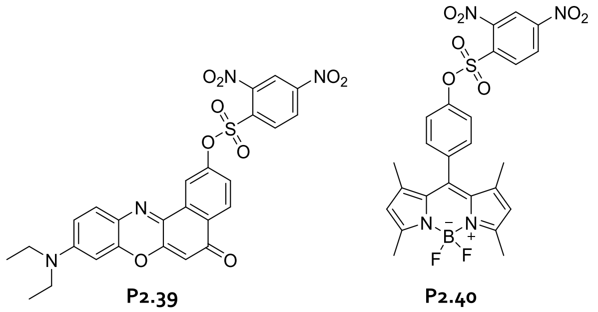

**Figure 30.** Chemical structures of probes **P2.39** and **P2.40**.

Besides sulfonamide and sulfonyl esters, thioesters can also be utilized as thiol amine reactive moieties that undergo native chemical ligation combined with spirocyclization. This was demonstrated by Guo, Yang, and coworkers through probe **P2.43** (Figure 32), achieving ratiometric distinction of homocysteine and cysteine in aqueous organic mixtures, *i.e.*, 40% EtOH in 20 mM phosphate buffer, pH 7.4.[159] Furthermore, probe **P2.43** displayed excellent selectivity for Cys and Hcys over other thiols that lack an adjacent amino functionality (Figure 32).

The inherent reactivity of NBD derivatives towards nucleophilic species can be directly exploited to design thiolamine reactive probes, as demonstrated for instance by Yang and coworkers with their probe **P2.44** (Figure 33).[160] Typically, the more nucleophilic SH-group first attacks the NBD chromophore and causes the departure of the leaving group, *e.g.*, a halogen or thiophenol residue. Subsequently, the probe−thiol conjugate rearranges then *via* an intramolecular displacement reaction to form an amine-linked NBD fluorophore that has a much higher emission quantum yield than its thiol-linked analogue in 20 mM phosphate buffer, pH

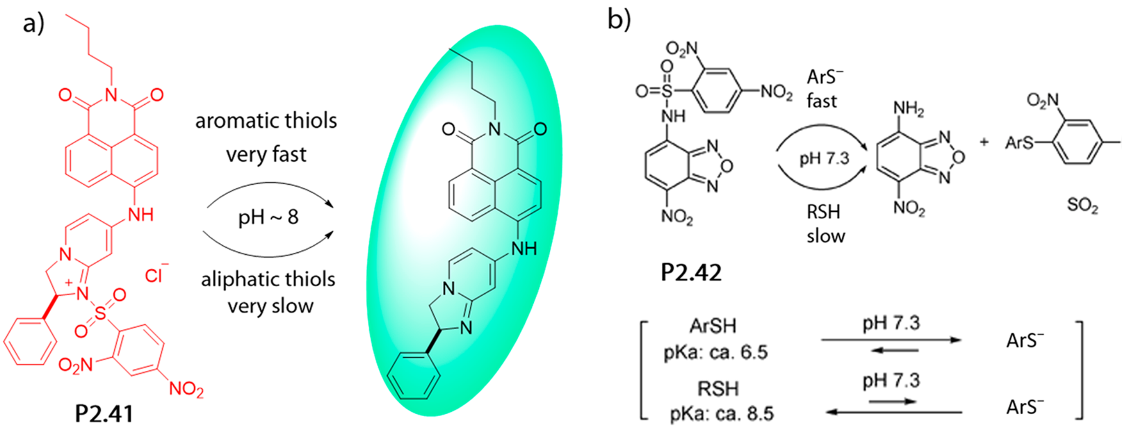

**Figure 31.** Reaction of (a) probe **P2.41** and (b) probe **P2.42** for aromatic and aliphatic thiols. (a) Reproduced with permission from ref 157. Copyright 2012 American Chemical Society. (b) Reproduced with permission from ref 158. Copyright 2010 The Royal Society of Chemistry.

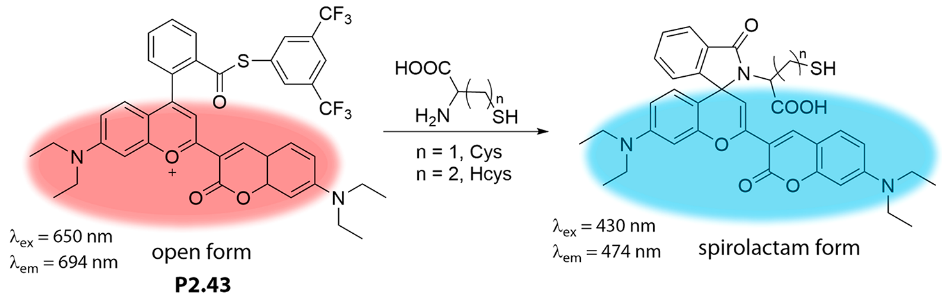

**Figure 32.** Schematic representation of probe **P2.43** upon reaction with Cys and Hcys. Reproduced with permission from ref 159. Copyright 2014 American Chemical Society.

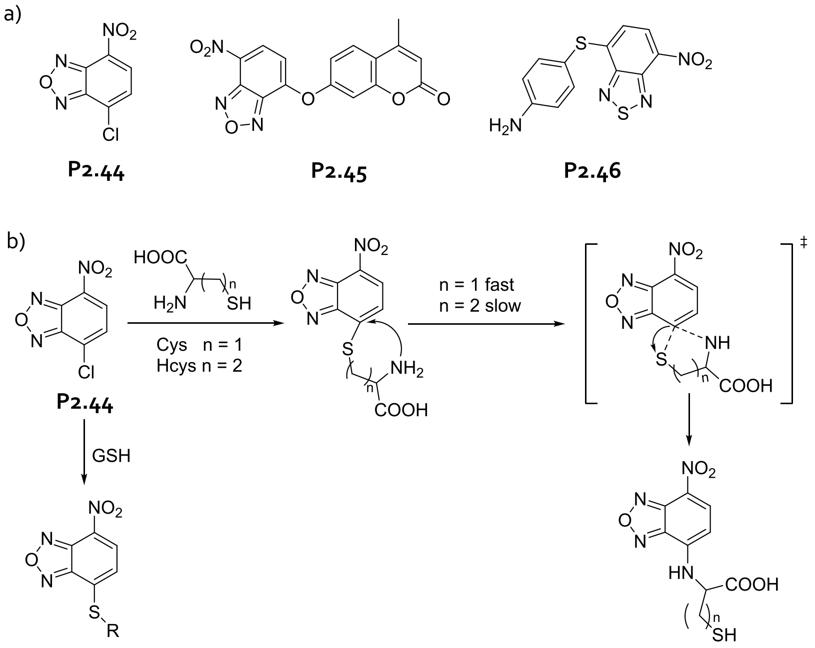

**Figure 33.** (a) Chemical structures of probe **P2.44**−**P2.46**. (b) Schematic representation of the reaction mechanism with GSH or Cys and Hcys. Reproduced with permission from ref 160. Copyright 2014 The Royal Society of Chemistry.

7.4, containing 25% MeCN. The amine reactivity of homocysteine and cysteine allows for distinguishing them from glutathione that does not undergo the rearrangement reaction. The Song group has exploited this feature by designing a NBD-coumarin-conjugated probe (**P2.45** in Figure 33a) that responds with a coumarin-based emission increase in the presence of glutathione, whereas the combined emission of NBD-amine and coumarin is observed upon addition of cysteine or homocysteine. This system showed a micromolar detection limit in aqueous-organic mixtures (30% MeCN in 10 mM PBS, pH 7.4).[161] Moreover, by using a nitrobenzothiadiazole chromophore for the probe design, Yoon, Yin, and coworkers demonstrated that only cysteine but not homocysteine reacts with **P2.46** (Figure 33a) when the pH is adjusted to 6 (due to the lower p$K_a$ value of Cys compared to Hcys), while at pH 7.4 both amino thiols undergo the same reaction sequence in 10 mM HEPES (containing 1% DMSO).[162] Note that amines are also directly reactive towards NBD derivatives, nevertheless, in the neutral pH range, the reaction rate is so low that amines do not effectively interfere with thiol amine sensing.

Thiols are also known to engage in disulfide exchange reactions. Figure 34 shows the operational principle of the commercial Ellman (**P2.47**) and Aldrithiol (**P2.48**) probes.[131] These reactions are obviously not analyte selective but rather serve as a general thiol detection method. In some cases, the diselenide exchange reaction can be advantageous for thiol sensing, as the Han group has demonstrated by an emission turn-on assay (**P2.49** in Figure 35) that responds within milliseconds to the presence of glutathione under physiological conditions (20 mM PBS, pH 7.4).[163] The diselenide-based probe can be applied for live cell imaging. Moreover, probes containing N−Se bonds also rapidly undergo an exchange reaction in the presence of thiols. This was utilized by Chen and coworkers for a cyanine-based probe **P2.50**, that upon uncaging emits in the NIR region and that was operational in physiological buffers (15 mM PBS, pH 7.4) in cells and in tissues.[164]

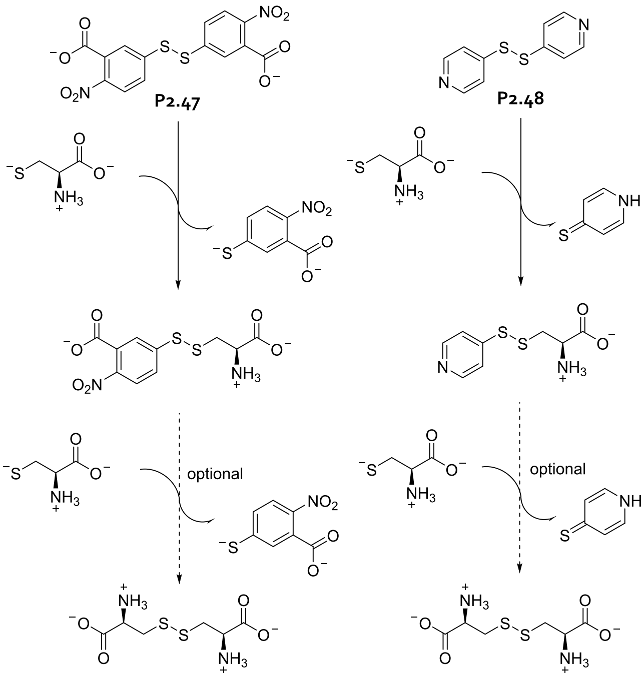

**Figure 34.** Reaction mechanism of Ellman's reagent (**P2.47**) and Aldrithiol (**P2.48**) with Cys. Reproduced with permission from ref 131. Copyright 2016 American Chemical Society.

Tang and coworkers designed a rhodamine-based probe **P2.51** (Figure 35), where a nitrophenol quencher was attached through a thiol-cleavable N−Se bond.[165] This probe can detect thiols with a nanomolar detection limit in 1% DMSO in PBS, pH 7.4, requiring less than 10 min of incubation time. Kim, Kang, and coworkers developed a disulfide reaction-based probe **P2.52** (Figure 35) that was successfully applied to the detection of thioredoxin, a class of small redox proteins found in the mitochondria of living cells.[166] Interestingly, this probe showed a much lower reactivity with cysteine, homocysteine, and glutathione.

Advanced probes can both form thiol- and amine-conjugate products that show strong but wavelength-shifted fluorescence emission signals, allowing for the ratiometric sensing of GSH (thiol-conjugate) as well as Cys and Hcys (amine-conjugate). Yang and coworkers have developed such a probe **P2.53** in Figure 36, based on a chlorinated BODIPY-chromophore that responds with a bathochromic emission shift upon reacting with glutathione, while a hypsochromic shift is observed upon reacting with Hcys and Cys in 5% MeCN in 20 mM HEPES, pH 7.4.[167] The authors also demonstrated the utility of their probe for ratiometric imaging of glutathione in living cells.

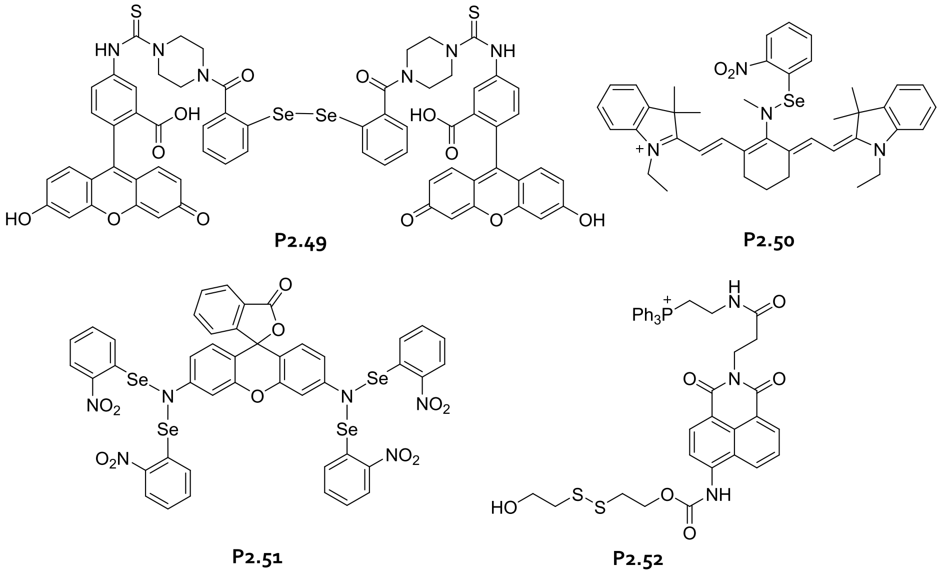

**Figure 35.** Chemical structures of probe **P2.49**−**P2.52**.

A powerful new strategy for thiol amine detection and differentiation was introduced by the Guo group that designed a chlorinated coumarin-hemicyanine probe (**P2.54** in Figure

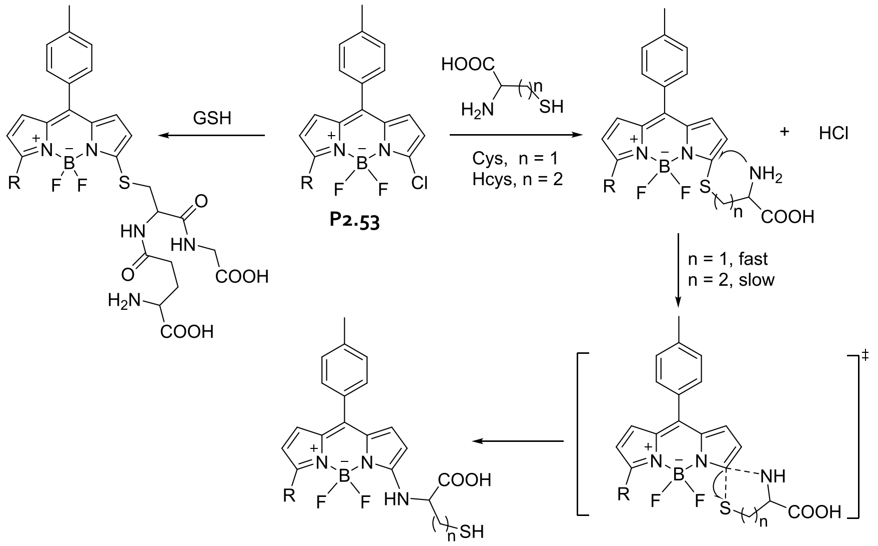

**Figure 36.** Reaction mechanism of probe **P2.53** with Cys, Hcys, and GSH. Reproduced with permission from ref 167. Copyright 2012 American Chemical Society.

37) with three potential binding sites.[168] The authors rationalized that the activated *para*-position of the coumarin dye should be the favored reaction side for thiol conjugation through a $S_NAr$ mechanism. If the thiol does not contain a free amino functionality, such as *N*-acetylcysteine, the reaction stops here and yields only a weakly fluorescent product (Figure 37a). For the glutathione−probe conjugate, its dangling amine was expected to proceed with a nucleophilic attack on the benzothiazolium cation for steric reasons (Figure 37b). In contrast, for Cys and Hcys, the amino group can participate in a rearrangement reaction to form amino coumarin with an altered emission profile. The displaced −SH moiety can subsequently undergo a Michael addition with the *α*,*β*-unsaturated keto moiety (Figure 37c). This reaction sequence was expected to be fast for cysteine and slow for homocysteine due to kinetic differences for the formation of a seven- and an eight-membered ring, respectively. Overall, the chlorinated coumarin−hemicyanine probe was uniquely capable of distinguishing cysteine from homocysteine and glutathione, *e.g.*, in 10 mM phosphate buffer, pH 7.4, to which 1 mM of CTAB was added. Moreover, probe **P2.54** was successfully applied for the simultaneous monitoring of Cys and GSH in COS-7 cells through multicolor imaging (Figure 37d).

While most thiol-reactive probes exploit the nucleophilic or redox properties of thiols in organic reactions, it is also possible to develop thiol probes that capitalize on the strong, near-covalent bonding interactions of thiols with soft transition metal ions functional in aqueous media. For instance, our group has recently communicated the smallest green emissive fluorophore HINA (3-hydroxyisonicotinealdehyde) known so far (**P2.55** in Figure 38) and found that its binding to a $Pt^{II}$-complex results in its emission quenching in 900 $\mu$M CTAB in 25 mM carbonate buffer, pH 9.4.[169] Through subsequent addition of a thiol, *e.g.*, cysteine, to the in situ formed probe **P2.55**, the HINA indicator is released within seconds, providing an emission turn-on response. The assay can be used for general thiol detection in buffered aqueous media with micromolar sensitivity.

The emission-quenching metal−organic compound **P2.56** (Figure 39) was considered by the Chan group as a probe for thiol-based amino acids.[170] While the −SH moiety expectedly exchanges chloride on the platinum center, the charge promoted hydrogen-bonding between the ammonium group of the amino acid and the carboxyl functional group of the probe assists in providing a modest binding selectivity for cysteine ($K_a$ = 7.9 × $10^4$ $M^{-1}$) over homocysteine ($K_a$ = 4.5 × $10^3$ $M^{-1}$) and 1-octanethiol ($K_a$ = 8.5 × $10^2$ $M^{-1}$) in 80% DMSO in Tris buffer, pH 7.2. Other proteinogenic amino acids did not cause a noticeable emission quenching of the probe. However, a slight emission increase was observed upon addition of the metal-coordinating amino acid histidine, which may indicate its binding to the probe. Detection of thiols by this probe is possible in the (high) micromolar concentration regime, but its applicability is so far limited by the need for organic solvents.

Thiols also strongly bind to $Au^+$ metal centers, which inspired Yang, Tae, and coworkers to design the $Au^I$-complex **P2.57** as a thiol probe.[171] They first prepared a substituted rhodamine dye that featured a binding station for $Au^+$ and then exposed the resulting metal−organic probe to different amino acids, including Cys, Hcys, and GSH (Figure 40). Only Cys and Hcys gave rise to a readily visible colorimetric and emission turn-on response, which was much stronger in magnitude for Cys than for Hcys. While a binding constant of only ∼$10^3$ $M^{-1}$ has been reported for the interaction of the probe with Cys, it has been experimentally demonstrated that 100 nM cysteine can be detected in water (1% MeOH) by using 1 $\mu$M of the probe.

Copper- and mercury-based metal complexes (**P2.58** and **P2.59** in Figure 41) have been utilized for the detection of thiol amino acids (and of histidine, see next section), but in these instances, often an indicator displacement assay strategy has been pursued. In the first step, $Cu^{II}$ or $Hg^{II}$ salts were introduced to a fluorescent dye, typically causing quenching of its emission, which was then restored in the presence of thiols such as cysteine due to competitive binding to the metal ion species.[172−174] The aforementioned systems are suitable for the detection of thiols in the micromolar range in aqueous media.

The development of chromophoric and emissive probes for thiol-containing amino acids and their derivatives is certainly one of the greatest achievements in the area of optical

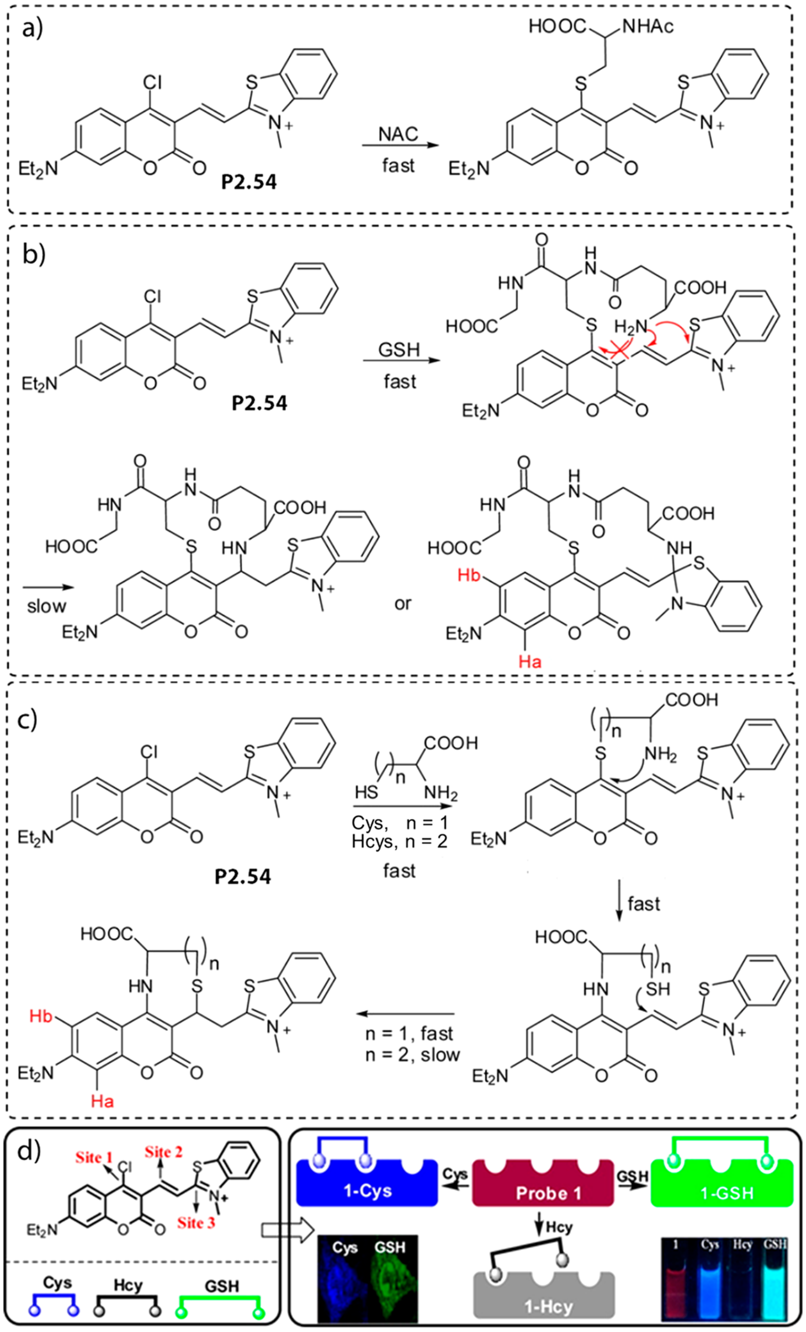

**Figure 37.** Reaction mechanism of probe **P2.54** upon reaction with (a) NAC, (b) GSH, and (c) Cys/Hcys. (d) Schematic representation of simultaneous sensing of Cys and GSH. Adapted with permission from ref 168. Copyright 2014 American Chemical Society.

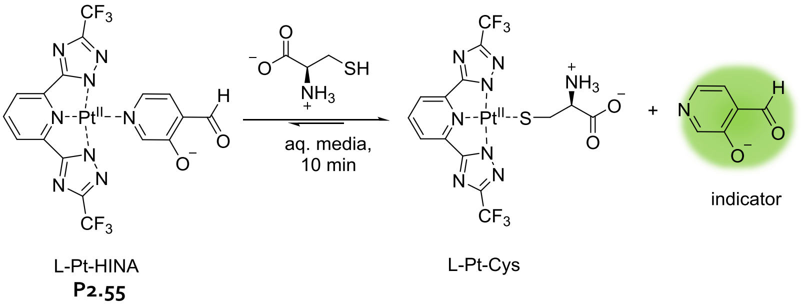

**Figure 38.** Schematic representation of the reaction of HINA with a $Pt^{II}$-precursor to form a non-emissive L-$Pt^{II}$–HINA (**P2.55**). Upon addition of Cys, the HINA ligand is displaced and becomes emissive. Reproduced with permission from ref 169. Copyright 2021 The Royal Society of Chemistry.

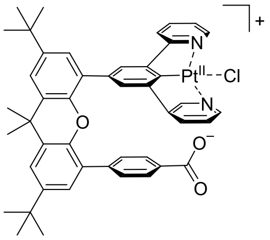

**P2.56**

**Figure 39.** Chemical structure of probe **P2.56**.

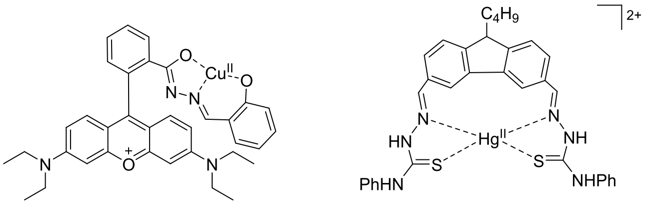

**P2.58** **P2.59**

**Figure 41.** Chemical structures of probes **P2.58** and **P2.59**.

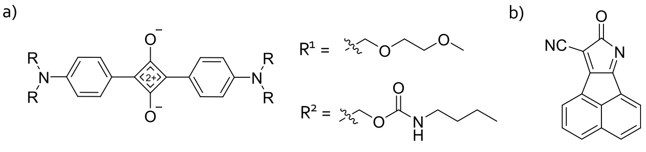

**P2.60** **P2.61**

**Figure 42.** Some of the earliest examples for (a) a thiol-probe (**P2.60**) that is operational in blood serum, and (b) a thiol probe (**P2.61**) that can be used for distinction of cysteine and homocysteine from GSH and other amino acids.

chemosensing. It was not until 2004 that one of the first emission turn-off probes that is applicable for thiol determination in human plasma was showcased by the Martínez-Máñez group (**P2.60** in Figure 42).[175] Only in 2007, one of the first visible light excitable probes for homocysteine and cysteine in 70% MeOH in HEPES buffer, pH 7.0, was introduced by Huang and coworkers (**P2.61** in Figure 42).[176] Not even two decades later, there is now a library of probes available that can be used for selective sensing of cysteine, homocysteine, as well as glutathione, alongside the many broad-range thiol detection probes that are known. The probes have also much improved in terms of sensitivity and applicability to cellular imaging applications. Additionally, many fully water-soluble systems are now available.

When searching and comparing literature reports, we made some curious observations. Many reports on new thiol probes start with the potential diagnostic advantages that could be unleashed when homocysteine, cysteine, or glutathione levels are accurately and rapidly determined in a routine biofluid diagnostics. Indeed, the sensitivity of current thiol probes appears sufficient for detecting thiols at the diagnostically relevant micromolar concentration range in biofluids; see Tables 2 and 3 for comparison. However, we have hardly found any medical reports where such probes are considered. In fact, most research reports from the medical and clinical area discuss data for thiol-containing metabolites that were obtained by simple unselective probes, resulting in the total thiol concentration of the biofluid. Besides, the concentration profile of individual thiols is commonly obtained through chromatographic methods such as HPLC-MS. There is surely more work to do for bringing selectively binding thiol-reactive probes into molecular diagnostics.

We have also noticed a certain imbalance between the most popular thiols tested for the design of new probes, *i.e.*, homocysteine, cysteine, glutathione, and the thiol-containing species present in biofluids. For instance, thiol amino acid derivatives, *e.g.*, *N*-acetylcysteine, thioglycolic acid, and the dipeptide Cys-Gly, all occurring at a similar concentration level in human urine as homocysteine,[177] are rarely considered as potential targets or cross-reactive interferents in the developers of new thiol-reactive probes. For instance, it would be very interesting to observe if the Cys-Gly dipeptide can be distinguished from cysteine because both contain reactive −SH and $-NH_2$ moieties that are arranged in a similar distance/angle. Moreover, several thiol-functional drugs, *e.g.*, tiopronin, D-penicillamine, methimazole, propylthiouracil, and thioguanine, that are routinely prescribed to patients, are excreted in urine.[177] It would be likewise informative to see experimental data if their presence interferes with the current probe-based assays for thiol detection in biofluids.

The vast number of publications found for the development of thiol-reactive probes also presents some contrast to the comparably low attention thiols have received so far in molecular diagnostics, *e.g.*, compared to carbohydrates, keto compounds, or neurotransmitters that are much more frequently discussed in the medical journals. In our view, this imbalance clearly pinpoints those current abilities and standing limitations that govern the design of molecular probes and not yet the practical medical needs.

### 2.2.2. Molecular Probes for Non-thiol Containing Amino Acids.

There appear to be only a few systems that form covalent-like bonding motifs with amino acids side chains

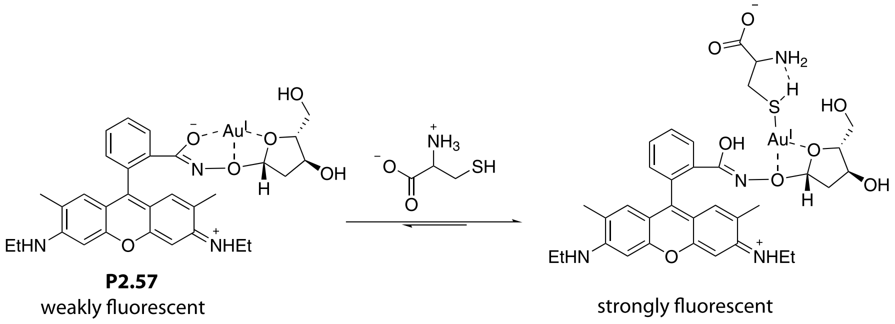

**Figure 40.** Schematic representation of the selective detection of cysteine and homocysteine in water with probe **P2.57** consisting of $Au^+$ and 2-deoxyribose-functionalized rhodamine.

## Table 2. Summary of Molecular Probes for Amino Acids with Thiol Functional Group (LOD, Limit of Detection)

| probe | media | concentration range | ref |
|---|---|---|---|
| | Aminothiols Analyte | | |
| **P2.17** | 10 mM MES buffer, pH 9.6, containing 50% MeCN; | μM range | 128 |
| | human blood plasma (blood of smokers) | | |
| | Cysteine (Cys)[f] Analyte | | |
| **P2.11** | 1% DMSO in 10 mM HEPES buffer, pH 7.4 | 0−100 μM;<br>LOD, nM | 122 |
| **P2.12** | 135 mM KCl in 20 mM HEPES buffer, pH 7.4 | 0−100 μM | 123 |
| **P2.13**[a] | 25 mM phosphate buffer, pH 7.4 | 0−20.0 μM;<br>LOD, sub-μM | 124 |
| **P2.15**[b] | 10% DMSO in 10 mM PBS, pH 7.4 | 0−900 μM<br>LOD, 1 μM | 126 |
| **P2.16** | 20% MeCN in 50 mM HEPES, pH 7.2 | 900 μM | 127 |
| **P2.18**[c] | 10% human plasma (deproteinized) diluted with 20% EtOH in 20 mM phosphate buffer, pH 7.4 | 0−40.0 μM | 132 |
| | 20% EtOH in 20 mM phosphate buffer, pH 7.4 | 0−40.0 μM | 132 |
| | 1 mM CTAB in 20 mM phosphate buffer, pH 7.4, containing 20% EtOH | 0−20.0 μM | 132 |
| **P2.19**[b] | 0.2% DMSO in 10 mM PBS, pH 7.4 | 0−16.0 μM;<br>LOD, 1.8 μM | 136 |
| **P2.20** | 50% DMSO in 10 mM PBS, pH 7.4 | 0.5−40.0 μM (linear range) | 137 |
| **P2.21**[d] | 50% DMSO in 10 mM PBS, pH 7.4 | 0−200 μM | 138 |
| **P2.22** | 20% EtOH in 20 mM phosphate buffer, pH 7.4 | 0−500 nM (linear range);<br>LOD, 100 nM | 139 |
| **P2.23**[b] | 20% MeCN in 10 mM HEPES buffer, pH 7.4 | 0−270 μM;<br>LOD, 88 nM | 140 |
| **P2.26** | 75% DMF in 10 mM HEPES buffer, pH 7.4 | 0−2.0 mM | 142 |
| **P2.27** | 60% DMSO in 10 mM HEPES buffer, pH 7.4 | 0−2.5 mM | 143 |
| **P2.28** | borate buffer, pH 11.0; borate buffer, pH 9.0; phosphate buffer, pH 7.0 | mM range | 144 |
| **P2.29** | 100 mM carbonate buffer, pH 9.5 | 0−1.5 mM | 145 |
| **P2.30** | 50% DMSO in 100 mM HEPES, pH 7.4 | 0−500 μM | 146 |
| **P2.32** | 50% MeCN in HEPES buffer, pH 7.4 | 0−7.0 μM;<br>LOD, 90 nM | 148 |
| **P2.34** | 30% DMF in 20 mM phosphate buffer, pH 7.4 | 0−40.0 μM | 150 |
| **P2.35** | 10 mM PBS, pH 7.4 | 0.1−1.0 μM;<br>LOD, 20 nM | 151 |
| **P2.36** | 50% MeCN in 20 mM HEPES buffer, pH 7.4 | 0−200 μM;<br>LOD, 0.8 μM | 154 |
| **P2.37** | 10 mM phosphate buffer, pH 9.0 | 0−60.0 μM | 152 |
| **P2.38** | 30% DMSO in 10 mM HEPES buffer, pH 7.4 | 0−160 μM;<br>LOD, low mM | 153 |
| **P2.39** | 50% DMSO in 50 mM HEPES buffer, pH 7.4 | 0−6.0 μM;<br>LOD, 43 nM | 155 |
| **P2.40** | 50% DMSO in 50 mM HEPES buffer, pH 7.8 | 0−12.0 μM | 156 |
| **P2.43** | 40% EtOH in 20 mM phosphate buffer, pH 7.4 | 0−250 μM | 159 |
| **P2.44** | 25% MeCN in 20 mM HEPES buffer, pH 7.4 | 0−50.0 μM;<br>LOD, 50 nM | 160 |
| **P2.45** | 30% MeCN in 10 mM PBS, pH 7.4 | 0−500 mM | 161 |
| **P2.46** | 1% DMSO in 10 mM HEPES buffer, pH 7.4 | 0−500 μM | 162 |
| | 1% DMSO in 10 mM citric acid−$Na_2HPO_4$, pH 6.0 | 0−500 μM | |
| **P2.53** | 5% MeCN in 20 mM HEPES buffer, pH 7.4 | 0−60.0 μM;<br>LOD, 86 nM | 167 |
| | Cysteine (Cys)[f] Analyte | | |
| **P2.54** | 1 mM CTAB in 10 mM phosphate buffer, pH 7.4 | 0−20 μM;<br>LOD, 0.4 μM | 168 |
| **P2.56**[6] | 80% DMF in Tris buffer, pH 7.2 | high mM range | 170 |
| **P2.57** | 1% MeOH in water | 0−250 μM;<br>LOD, 100 nM | 171 |
| **P2.59** | 1% DMSO in 25 mM HEPES buffer, pH 7.4 | 0−45.0 μM | 173 |
| | Glutathione (GSH) Analyte | | |
| **P2.11** | 1% DMSO in 10 mM HEPES buffer, pH 7.4 | 0−100 μM;<br>LOD, nM | 122 |
| **P2.12** | 135 mM KCl in 20 mM HEPES buffer, pH 7.4 | 0−100 μM | 123 |
| **P2.13**[a] | 25 mM phosphate buffer, pH 7.4 | 0−20.0 μM;<br>LOD, sub-μM | 124 |
| **P2.31** | 20 mM PBS, pH 5.8 | 0−90.0 μM | 147 |
| **P2.32** | 50% MeCN in HEPES buffer, pH 7.4 | 0−7.0 μM;<br>LOD, 90 nM | 148 |
| **P2.33**[e] | 30% EtOH in 20 mM PBS, pH 7.4 | 0−10.0 μM;<br>LOD, 22 nM | 149 |
| **P2.34** | 30% DMF in 20 mM phosphate buffer, pH 7.4 | 0−40.0 μM | 150 |
| **P2.35** | 10 mM PBS, pH 7.4 | 0.1−1.0 μM | 151 |
| **P2.36** | 50% MeCN in 20 mM HEPES buffer, pH 7.4 | 0−200 μM;<br>LOD, 0.8 μM | 154 |
| **P2.37** | 10 mM phosphate buffer, pH 9.0 | 0−60.0 μM | 152 |
| **P2.38** | 30% DMSO in 10 mM HEPES buffer, pH 7.4 | 0−130 μM;<br>LOD, low μM | 153 |
| **P2.39** | 50% DMSO in 50 mM HEPES buffer, pH 7.4 | 0−6.0 μM;<br>LOD, 43 nM | 155 |
| **P2.45** | 30% MeCN in 10 mM PBS, pH 7.4 | 0−500 mM | 161 |
| **P2.49** | 20 mM PBS, pH 7.4 | 0−2.0 μM | 163 |
| **P2.53** | 5% MeCN in 20 mM HEPES buffer, pH 7.4 | 0−60.0 μM;;<br>LOD, 86 nM | 167 |
| **P2.54** | 1 mM CTAB in 10 mM phosphate buffer, pH 7.4 | 0−40 μM | 168 |
| **P2.61** | 70% MeOH in HEPES, pH 7.0 | 0−300 μM | 176 |
| | Homocysteine (Hcys) Analyte | | |
| **P2.11** | 1% DMSO in 10 mM HEPES buffer, pH 7.4 | 0−100 μM;<br>LOD, nM | 122 |
| **P2.12** | 135 mM KCl in 20 mM HEPES buffer, pH 7.4 | 0−100 μM | 123 |
| **P2.13**[a] | 25 mM phosphate buffer, pH 7.4 | 0−20.0 μM;<br>LOD, sub-mM | 124 |
| **P2.18**[c] | 10% human plasma (deproteinized) diluted with 20% EtOH in 20 mM phosphate buffer, pH 7.4 | 0−12.0 μM | 132 |
| | 20% EtOH in 20 mM phosphate buffer, pH 7.4 | 0−40.0 μM | |
| | 1 mM CTAB in 20 mM phosphate buffer containing 20% EtOH, pH 7.4 | 0−20 μM | |
| **P2.24** | 10% DMSO in 10 mM HEPES buffer, pH 7.4 | 0−100 μM;<br>LOD, sub-μM | 141 |
| **P2.25** | 10% DMSO in 10 mM HEPES buffer, pH 7.4 | 0−100 μM;<br>LOD, sub-μM | 141 |
| **P2.26** | 75% DMF in 10 mM HEPES buffer, pH 7.4 | 0−2.0 mM | 142 |
| **P2.27** | 60% DMSO in 10 mM HEPES buffer, pH 7.4 | 0−2.5 mM | 143 |
| **P2.30** | 50% DMSO in 100 mM HEPES buffer, pH 7.4 | 0−2.0 mM | 146 |
| **P2.32** | 50% MeCN in HEPES buffer, pH 7.4 | mM range | 148 |
| **P2.34** | 30% DMF in 20 mM phosphate buffer, pH 7.4 | 0−40.0 μM | 150 |
| **P2.35** | 10 mM PBS, pH 7.4 | 0.1−1.0 μM | 151 |
| **P2.36** | 50% MeCN in 20 mM HEPES buffer, pH 7.4 | 0−200 μM;<br>LOD, 0.8 μM | 154 |

### Table 2. continued

| probe | media | concentration range | ref |
|---|---|---|---|
| | Homocysteine (Hcys) Analyte | | |
| **P2.38** | 30% DMSO in 10 mM HEPES buffer, pH 7.4 | mM range;<br>LOD, sub-mM | 153 |
| **P2.39** | 50% DMSO in 50 mM HEPES buffer, pH 7.4 | 0–6.0 $\mu$M;<br>LOD, 43 nM | 155 |
| **P2.43** | 40% EtOH in 20 mM phosphate buffer, pH 7.4 | 0–250 mM | 159 |
| **P2.44** | 25% MeCN in 20 mM HEPES buffer, pH 7.4 | 0–50.0 $\mu$M;<br>LOD, 50 nM | 160 |
| **P2.45** | 30% MeCN in 10 mM PBS, pH 7.4 | 0–500 $\mu$M | 161 |
| **P2.46** | 1% DMSO in 10 mM HEPES buffer, pH 7.4 | 0–500 $\mu$M | 162 |
| **P2.53** | 5% MeCN in 20 mM HEPES buffer, pH 7.4 | 0–60.0 $\mu$M;<br>LOD, 86 nM | 167 |
| **P2.54** | 1 mM CTAB in 10 mM phosphate buffer, pH 7.4 | 0–40 $\mu$M;<br>LOD, 0.4 nM | 168 |
| **P2.61** | 70% MeOH in HEPES, pH 7.0 | 0–200 $\mu$M | 176 |
| | *N*-Acetylcysteine (NAC) Analyte | | |
| **P2.34** | 30% DMF in 20 mM phosphate buffer, pH 7.4 | $\mu$M range | 150 |
| **P2.54** | 1 mM CTAB in 10 mM phosphate buffer, pH 7.4 | 0–40 $\mu$M;<br>LOD, 0.4 nM | 168 |
| | Thiol Analytes | | |
| **P2.10** | 100 mM phosphate buffer, pH 7.4 | $\mu$M range | 121 |
| **P2.14** | 33% DMSO in 100 mM HEPES buffer, pH 7.4 | mM range | 125 |
| **P2.47** | 100 mM phosphate buffer, pH 8.0 | $\mu$M range;<br>LOD, 1.2 $\mu$M | 131 |
| **P2.48** | 10–100 mM phosphate buffer, pH 7.0–7.5<br>10 mM MES buffer, pH 9.6, containing 50% MeCN | $\mu$M range | 131 |
| **P2.50** | 15 mM PBS, pH 7.4 | $\mu$M range | 164 |
| **P2.51** | 1% DMSO in 15 mM PBS, pH 7.4 | 0–1.0 $\mu$M | 165 |
| **P2.55** | 900 $\mu$M CTAB in 25 mM carbonate buffer, pH 9.4 | $\mu$M range | 169 |
| **P2.58** | 40% EtOH in Tris buffer, pH 7.1 | 0–10.0 $\mu$M | 172 |
| **P2.60** | 20% MeCN in 10 mM MES buffer, pH 6.0; human plasma | $\mu$M range | 175 |
| **P2.13**[a] | 25 mM phosphate buffer, pH 7.4 | 0–20.0 $\mu$M;<br>LOD, sub-$\mu$M | 124 |
| **P2.41** | 10 mM phosphate buffer, pH 8.0 | 0–9.9 $\mu$M;<br>LOD, 20 nM | 157 |
| **P2.42** | 10 mM phosphate buffer, pH 7.3 | 0–5.0 $\mu$M;<br>LOD, 200 nM | 158 |
| **P2.52** | PBS, pH 7.4 | 0–5.0 $\mu$M | 166 |

[a] Can react with Hcys and GSH, the reactivity is Cys>Hcys>GSH. [b] Kinetic rates for Cys are faster compared to other thiols. [c] The reaction rate with Hcys is faster than Cys. [d] Detects also other thiols, imaging in living cells. [e] The peptide Glu-Cys-Glu shows higher reaction rates than GSH. [f] Cys binds with $K_a$ = $10^4$ $M^{-1}$, Hcys binds with $K_a$ = $10^3$ $M^{-1}$, octanethiol binds with $K_a$ = $10^2$ $M^{-1}$.

### Table 3. Summary of the Normal Concentration Range of Thiols in Blood, Urine, and Saliva[a]

| concentration range | media | ref |
|---|---|---|
| Cysteine (Cys) Analyte | | |
| 189–235 $\mu$M | blood | 178 |
| 36.7–148 $\mu$mol/mmol creatinine = 0.367–148 mM | urine | 50 |
| 1.04–1.56 $\mu$M | saliva | 179 |
| Glutathione (GSH) Analyte | | |
| 8.23–17.4 $\mu$M | blood | 178 |
| 5.0–85.0 nmol/mmol creatinine = 50–850 nM | urine | 50 |
| 9.29–24.7 $\mu$M | saliva | 180 |
| Homocysteine (Hcys) Analyte | | |
| 7.30–11.3 $\mu$M | blood | 178 |
| 0.60–1.70 $\mu$mol/mmol creatinine = 6.00–17.0 $\mu$M | urine | 50 |
| 2.27–4.95 $\mu$M | saliva | 180 |
| *N*-Acetylcysteine (NAC) Analyte | | |
| 1.00–2.14 $\mu$mol/mmol creatinine = 10.0–21.4 $\mu$M | urine | 181 |

[a] Urinary analyte concentrations were converted assuming a representative creatinine level of 10 mmol/L.

other than thiols (see Table 4). In fact, we are only aware of probes capable of selectively detecting the amino acid histidine.

### Table 4. Summary of Molecular Probes for Non-thiol-functional Amino Acids (LOD, Limit of Detection)

| probe | media | concentration range | ref |
|---|---|---|---|
| | Histidine (His) Analyte | | |
| **P2.62** | 1× PBS, pH 7.0 | $\mu$M range | 182 |
| **P2.63** | HEPES buffer, pH 7.4 | 0–400 $\mu$M | 183 |

Soft transition metals are known to coordinate strongly to azaheterocycles, and thus nonsurprisingly can also bind the amino acid histidine. This feature has been exploited by the Wong group that reported a water-soluble metal organic probe **P2.62** (Figure 43a), which is selective for histidine and histidine-rich proteins such as bovine serum albumin (BSA).[182] The available data suggested that the bidentate complexation of one equivalent of histidine is accompanied by the displacement of two weakly coordinated solvent molecules. Thus, it is somewhat surprising that four equivalents of His were needed to reach a signal saturation with an emission enhancement by a factor of 180 in 1× PBS (pH 7.0). The probe was found to be highly selective for histidine over other natural amino acids. In terms of application potential, it was found that the Ir$^{III}$-based probe can be used for staining of proteins in a Western blot and enables the detection of as little as 1.5 ng of a poly(amino acid) per band after 10 min of reaction time.

Very recently, the Hu group synthesized a structurally related, luminescence-quenched iridium complex (**P2.63** in Figure 43b) that became emissive upon exchange of its two acetonitrile ligands for one equivalent of His.[183] It was verified that histidine functions as a chelating ligand by simultaneous involvement of its azaheterocycle ring and amino group. Probe **P2.63** shows a low LOD of 0.6 $\mu$M for histidine in HEPES buffer, pH 7.4, and was verified to be highly selective for its target analyte over all other proteogenic amino acids, including also Cys and GSH. Again, the histidine-rich protein BSA also caused a strong emission enhancement of the probe. It appears that free His and BSA can be distinguished through their characteristic spectral shift by the probe. The reaction times needed, *e.g.*, >40 min for completion of the reaction of 10 $\mu$M probe with 200 $\mu$M histidine in aqueous media, are unfortunately somewhat limiting the practical prospects.

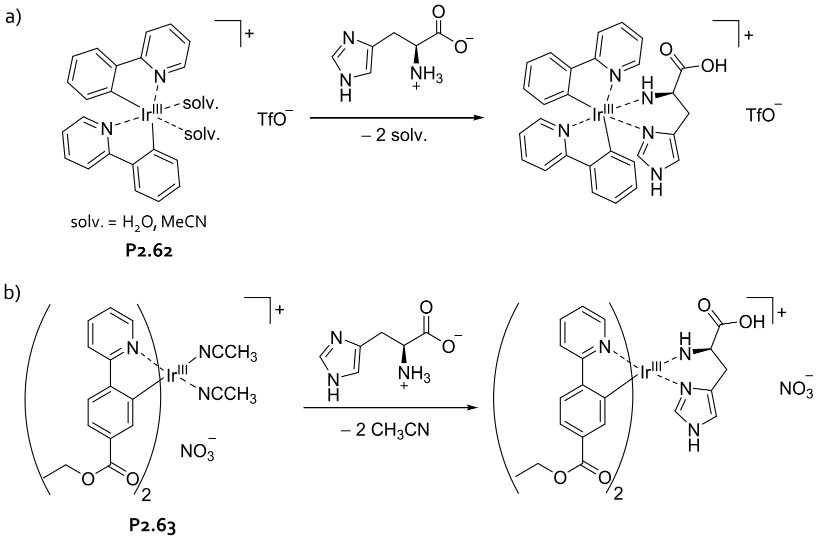

**Figure 43.** Iridium$^{III}$-based metal complexes (a) **P2.62** and (b) **P2.63** function as selective luminescence turn-on probes for histidine as well as the His-rich protein BSA.

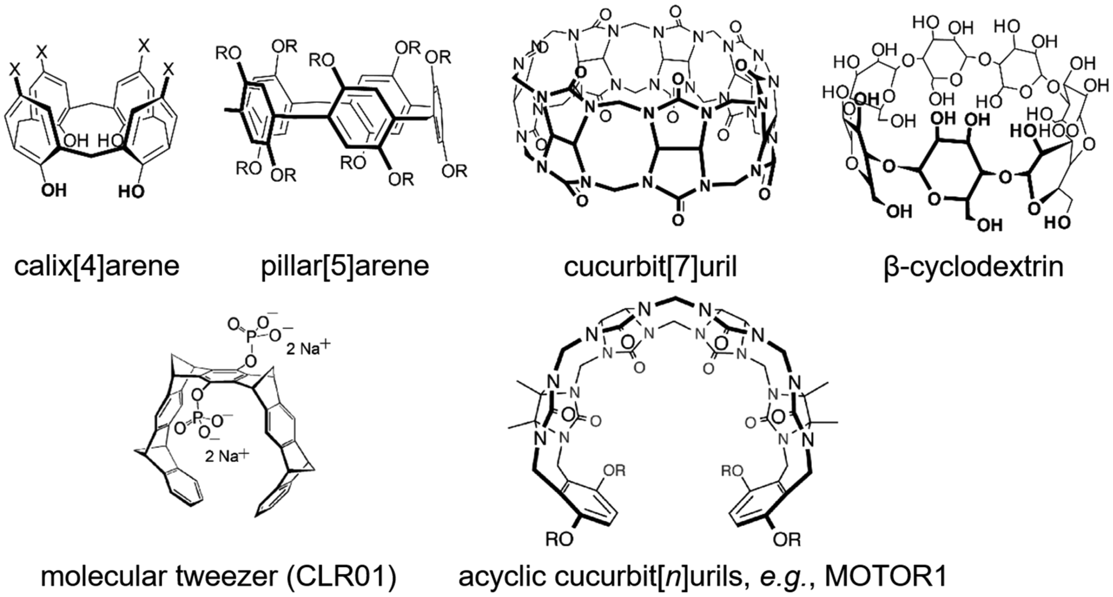

**Figure 44.** Chemical structures of representative macrocyclic hosts that were used as a scaffold for the construction of chemosensors for amino acids.

A self-assembling luminescent metal–organic probe was introduced by our group that responds to a range of azaheterocyclic compounds, such as the metabolites histamine, histidine, and the drugs nicotine, clotrimazole, fluconazole, and miconazole.[184] This probe is covered in more detail the commencing section on "Chemosensors and Probes for Drug Sensing" (section 9.1).

There are many other literature examples for histidine detecting systems that were introduced as probes but which should be preferably termed chemosensors because they form reversible bonding motifs with modest binding energies. Those systems are covered in section 2.3.1.

## 2.3. Chemosensors for Amino Acids (and Proteins)

Amino acids are popular choices as potential guests for newly discovered synthetic binders, *e.g.*, macrocyclic hosts, and thus, a vast number of binding parameters have become available for systems that noncovalently bind amino acids; see, for instance SupraBank.org.[41] In the spirit of this review, we will only discuss those systems that provide a useful optical response, be it directly or as part of an indirect detection method such as IDA. Moreover, we give preference to those systems that are operational in aqueous media and that can possibly, either already or with some future improvements, be adopted for realistic sensing applications in biofluids. Readers interested in the fundamentals of the molecular recognition of amino acids by synthetic binders and hosts, *e.g.*, calix[*n*]arenes (C*xn*), cucurbit[*n*]urils (CB*n*), pillar[*n*]arenes, and cyclodextrins (Figure 44), are referred to one of the many literature sources that are available.[185−201] Within this section, discussed chemosensors are summarized in Table 5.

To date, two classes of hosts are most widely utilized for amino acid sensing applications, *i.e.*, the C*xn* and CB*n* due to their comparably high binding affinity values for these target analytes.[44,185,202] Both (unmodified) hosts have an inherent

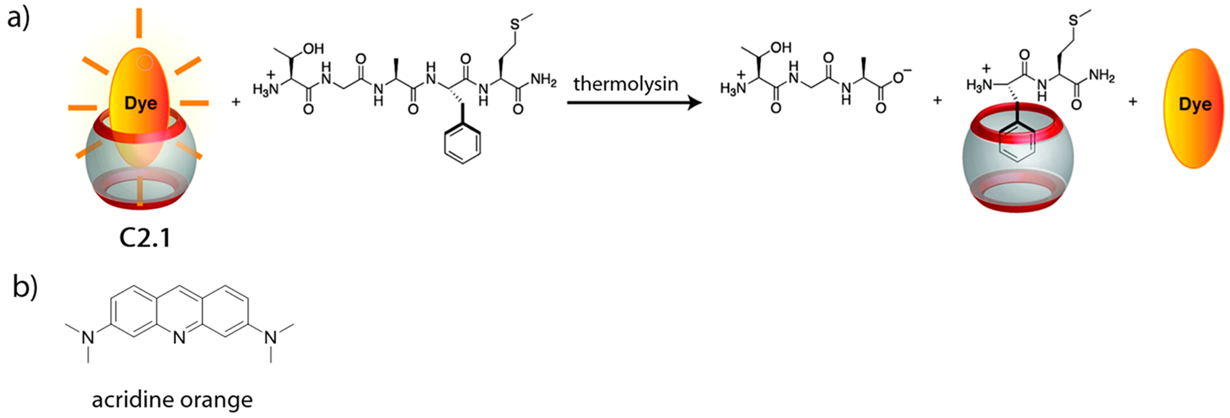

**Figure 45.** (a) Schematic representation of a product-selective tandem assay with chemosensor **C2.1** for monitoring of the hydrolysis of the Thr-Gly-Ala-Phe-Met-$NH_2$ peptide by the endopeptidase thermolysin. (b) Chemical structure of the dye acridine orange. Reproduced with permission from ref 221. Copyright 2011 American Chemical Society.

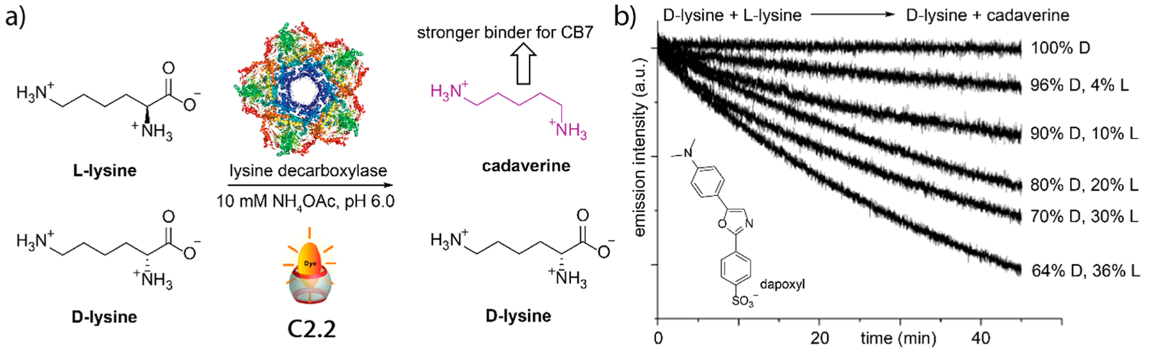

**Figure 46.** (a) Addition of decarboxylases to mixtures of L- and D-amino acids results in the enantioselective decarboxylation of L-amino acids to their corresponding biogenic amines. In the presence of a CB7•dye reporter pair, *e.g.*, CB7•dapoxyl, (**C2.2**), this enzymatic process can be followed in real time by emission spectroscopy. (b) Representative emission traces for the decarboxylation of D-/L-mixtures of lysine (50 $\mu$M total concentration) with lysine decarboxylase in the presence of CB7 (10 $\mu$M) and dapoxyl (2.5 $\mu$M) as the reporter pair in 10 mM ammonium acetate buffer, pH 6.0. Figure and data traces adapted from ref 226. Copyright 2008 Wiley-VCH.

binding preference for positively charged amino acids, *e.g.*, Lys and Arg, due to attractive cation···$\pi$ interactions and cation···O=C interactions. However, these macrocyclic hosts differ in many other characteristics. Calixarenes can be readily modified at their rim with charged residues, and thereby their binding preference can be tuned and directed towards negatively charged analytes, including negatively charged amino acids. Cucurbit[*n*]urils are comparably difficult to functionalize,[202,203] and when successful, equatorial-substituted derivatives are often obtained that do not appear to show significant binding selectivity differences compared to the parent hosts. However, cucurbit[*n*]urils generally provide one of the strongest binding affinities of any known host because of high-energy cavity water release.[187,204−207] CB*n* particularly favor the binding of hydrophobic species such as the amino acid phenylalanine, as well as peptides and proteins (*e.g.*, insulin) with an accessible N-terminal Phe residue.[196,208−211] Cucurbit[*n*]urils generally discriminate against negatively charged species, *e.g.*, the amino acids aspartate and glutamate are not bound at all. In the following, we discuss several representative examples where calix[*n*]arene and cucurbit[*n*]uril-based systems have been used for sensing of amino acids.

Both parent calix[*n*]arenes and cucurbit[*n*]urils are optically silent, *i.e.*, they are not emissive and absorb light in the UV region, which is practically not suitable for optical sensing applications. Thus, binding of the analyte does not result in a detectable optical response and both unmodified Cx*n* and CB*n* are not inherently chemosensors. However, both systems are ideally suited for setting up an IDA or GDA; see also section 1.[44,47,212,213]

Chemosensors bind their target analytes reversibly and usually with faster binding kinetics than probes, which is a distinct advantage when striving to monitor biophysical processes and enzymatic reactions. This concept, which was pioneered by the Nau group, has been successfully applied in a broad number of applications, ranging from surveying enzymatic reactions to the monitoring of membrane permeation of label-free analytes in real time.[49,213−224] In the following, only a few of the highlights related to amino acid and peptide target molecules are presented.

The low but differential selectivity of CB*n* complexes for amino acids and proteins can be an advantage for designing general assays capable of monitoring chemical transformations.[215] For instance, if the product of an enzymatic reaction is a stronger binder than the reactant, the equilibrium of host, dye, and reactant/product (= guest) shifts towards the formation of a CB*n*•guest complex. This was termed a product-selective tandem assay. Likewise, if the enzymatic substrate to product conversion yields a weaker host-binding species, the host-dye equilibrium shifts towards higher concentrations of the host•dye complex during the enzymatic reaction. This is called a substrate-selective tandem assay.

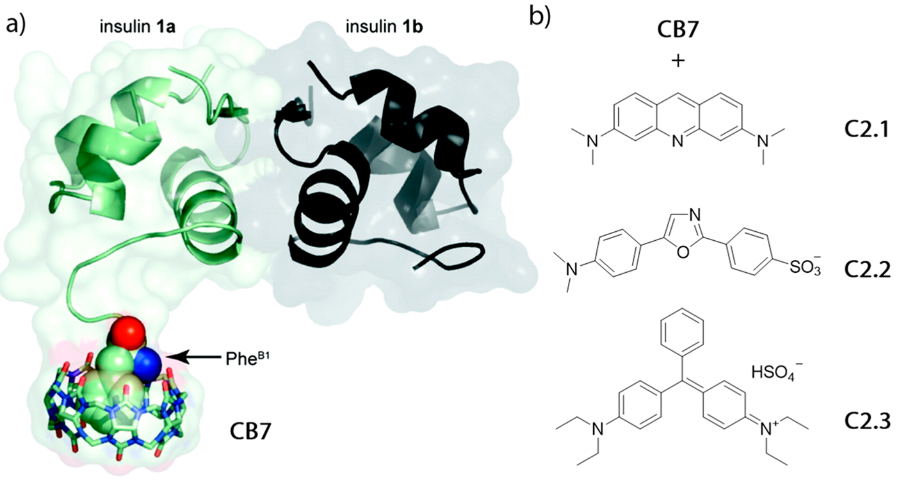

**Figure 47.** (a) Crystal structure of the complex between the N-terminal Phe-residue of insulin and the host CB7. Acridine orange was used as an indicator dye. Reproduced with permission from ref 211. Copyright 2011 American Chemical Society. (b) Chemical structures of the chemosensors **C2.1**, **C2.2**, and **C2.3**.

The cleavage of the Thr-Gly-Ala-Phe-Met-$NH_2$ peptide by the endopeptidase thermolysin monitored by the CB7•acridine orange (AO) chemosensor (**C2.1**) serves as one representative example for a product-selective tandem assay (Figure 45).[221] The affinity of the indicator dye for CB7 ($K_a$ = $2.0 \times 10^5$ $M^{-1}$ in water, pH 7.0)[225] lies between that of the peptidic substrate ($K_a$ = $1.3 \times 10^4$ $M^{-1}$) and that of the produced dipeptide Phe-Met-$NH_2$ ($K_a$ = $1.5 \times 10^7$ $M^{-1}$), both in 10 mM ammonium phosphate buffer, pH 7.2, 37 °C. Thus, during the enzymatic reaction, the indicator dye is subsequently set free by the competitive binding of the produced Phe-Met-$NH_2$ dipeptide to the host CB7. This process can be monitored conveniently by fluorescence spectroscopy in real time. Such assays can be utilized to determine the enzymatic key parameters, such as catalytic rate constant ($k_{cat}$) and Michaelis constant ($K_m$) in a label-free fashion and can be employed for screening enzyme inhibiting drugs (unless they display a strong competitive binding for the host). With respect to possible use in diagnostics, the elegant combination of an enzymatic reaction that provides a high substrate specificity and a chemosensor-based signal transduction step, may solve the binding selectivity problem of conventional assays. For instance, several amino acids (*e.g.*, His, Arg, Lys, Tyr, Trp) can be selectively detected by a CB7-based tandem assay through the use of a substrate-specific decarboxylase enzyme, *e.g.*, lysine decarboxylase.[226] The decarboxylase was shown to selectively act only on its intended substrate even when other amino acids were present in the mixture, resulting in the exclusive formation of the corresponding, more strongly CB7-binding, biogenic amine, *e.g.*, cadaverine. During the enzymatic reaction, the indicator dye, *e.g.*, dapoxyl, is therefore displaced from the CB7•dye chemosensor (*e.g.*, CB7•dapoxyl, **C2.2**) by the competitive action of the formed biogenic amine (Figure 46a). The corresponding characteristic kinetic profile can be monitored by fluorescence spectroscopy and correlated to the amount of biogenic amine produced. Thus, the initial amount of the amino acid substrate present in the sample can be calculated. Importantly, any background binding of matrix components to the host that causes partial displacement of the host•indicator complex is a static effect and thus can be distinguished from the dynamic information available from the enzymatic time-course data (Figure 46b). Indeed, Nau and coworkers succeeded in detecting representative amino acids in the low micromolar regime, even in mixtures of amino acids in 10 mM ammonium acetate buffer, pH 6.0. The assay can be applied to the cost-efficient microplate reader format.

Spectacularly, this assay format was adopted for determining the enantiomeric purity of amino acid samples within an enantiomeric excess wide range of 64 to 99.98 *ee*% because D-amino acids cannot be converted by decarboxylases (Figure 46).[226] Additionally, the Nau group demonstrated that their sensing format is also capable of monitoring the course of two sequentially operating enzymes ("enzymatic cascades"), *e.g.*, lysine decarboxylase and diamine oxidase, by combining a product-selective and a substrate-selective tandem assay.[213]

Notably, the IDA format is also applicable to other signal transduction methods besides absorbance and fluorescence spectroscopy. For instance, $^{129}$Xe can be used as an NMR indicator to follow *in vitro* and *in vivo* binding of spectroscopically silent analytes to CB6 and CB7, as has been demonstrated by the Dmochowski group, the Albert group, and by Schröder, Hennig, and coworkers.[227−230]

In some cases, the interaction of native proteins with CB*n*-based chemosensors can also be exploited. Urbach and coworkers demonstrated the selective targeting of the natural proteins insulin and the human growth hormone (hGH) by CB7•AO (**C2.1**) in an IDA format, thereby providing a path towards their detection and quantification in biological fluids.[211,231] In these cases, protein binding to CB7 leads to a displacement of the indicator dye because the host binds sterically accessible amino acid residues, such as the N-terminal Phe of insulin (Figure 47). In contrast, BSA is recognized by a CB7•brilliant green (**C2.3**) chemosensing ensemble, resulting in the formation of a ternary complex that shows a strongly enhanced emission compared to the CB7•dye and the BSA•dye pairs in aqueous media.[232] This effect, which was discovered by Bhasikuttan, Nau, and coworkers, can be used for BSA detection and quantification in the low micromolar concentration regime.

Fluorescent cucurbit[*n*]uril analogues have been introduced by the Isaacs group who installed chromophoric and emissive aromatic moieties into the host's cavity wall. These hosts bind, like the parent cucurbit[*n*]urils, a wide range of analytes, including amino acids. For instance, a cyclic fluorescent CB6-

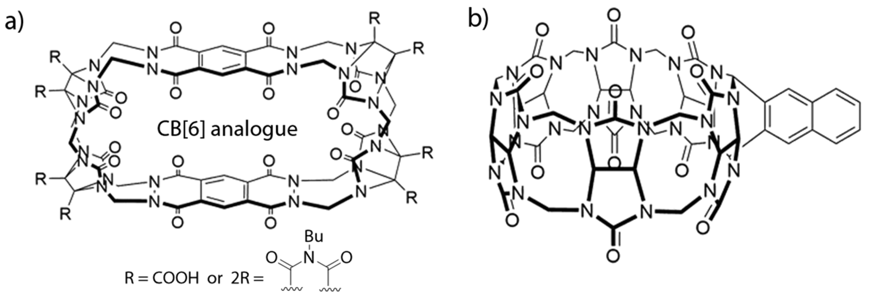

**C2.4** **C2.5**

**Figure 48.** Chemical structures of chromophoric and emissive cucurbit[6]uril analogues: (a) **C2.4** and (b) **C2.5**.

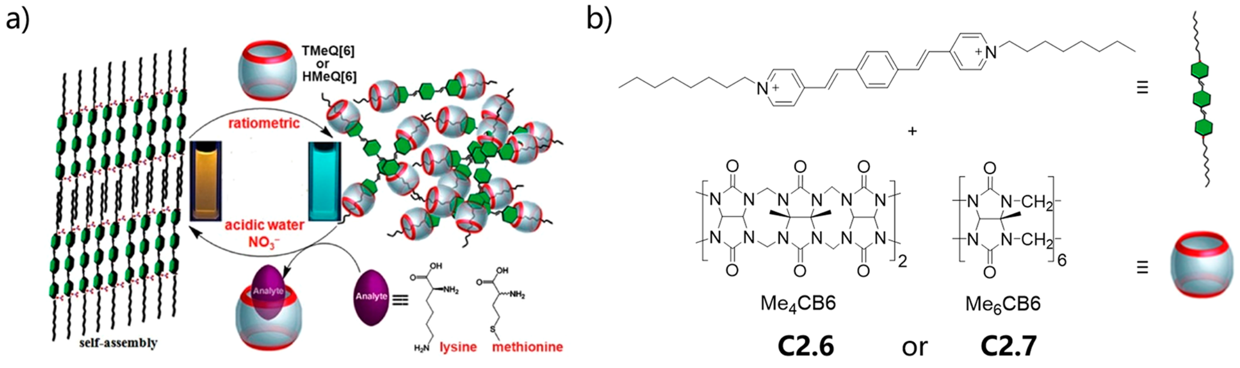

**Figure 49.** (a) Schematic representation of an IDA with **C2.6**/**C2.7** and lysine or methionine as analytes. (b) Chemical structures of the partially methyl substituted CB6 derivatives $Me_4CB6$ and $Me_6CB6$ and a bipyridinium phenylene-vinylene dye. Adapted with permission from ref 236. Copyright 2017 Wiley-VCH.

analogue (**C2.4** in Figure 48a) was shown to bind Phe, Tyr, and Trp with affinities of $K_a = 4.2 \times 10^4$ $M^{-1}$, $5.7 \times 10^4$ $M^{-1}$, and $3.2 \times 10^6$ $M^{-1}$, respectively, in 50 mM sodium acetate buffer, pH 4.7.[233] Surprisingly, the more hydrophilic amino acid tyrosine is even slightly stronger bound than phenylalanine by this CB6 analogue, while the parent CB*n* hosts strongly favor the binding of the more hydrophobic Phe.[44,202] Moreover, unlike for CB6, the biogenic diamines cadaverine and putrescine are only weakly bound by **C2.4**. Nevertheless, like cucurbit[*n*]urils, also this cyclic analogue shows a rather broad analyte spectrum and thus may be of limited utility for sensing applications in complex biofluids. For instance, besides the aforementioned amino acids, also the neurotransmitter dopamine (see also section 4.2), and the nucleobases adenine, thymine, uracil, and cytosine are bound with $10^3$–$10^4$ $M^{-1}$ affinities by **C2.4** in the same medium.[233]

Isaacs, Anzenbacher Jr., and coworkers developed a CB6 analogue (**C2.5** in Figure 48b), where the chromophore naphthalene is attached on the outside of the cavity.[234] The maintained cavity shape of the CB6 binds basic amino acids, *e.g.*, Lys ($K_a = 1.6 \times 10^3$ $M^{-1}$), Arg ($K_a = 1.8 \times 10^3$ $M^{-1}$), ornithine ($K_a = 9.9 \times 10^2$ $M^{-1}$), and His ($K_a = 1.7 \times 10^3$ $M^{-1}$), but also the derived biogenic amines cadaverine, agmatine, putrescine (each $K_a > 10^6$ $M^{-1}$), and histamine ($K_a = 1.7 \times 10^4$ $M^{-1}$) in water, pH 7.0. In fact, the use of a $Eu^{III}$ salt was required as an additive to furbish a quantifiable emission change upon guest binding. The $Eu^{III}$ cation binds to the carbonyl-fringed rim of the host and partially quenches the emission of the naphthalene fluorophore through energy transfer. Upon guest binding, $Eu^{III}$ is displaced and the emission intensity is restored. This chemosensing ensemble can distinguish large analytes from smaller analytes. Large analytes completely fill the host cavity and displace $Eu^{III}$ from both portals, whereas smaller analytes only cause partial $Eu^{III}$ displacement. The authors demonstrated that the analytes can be correctly classified through multivariate analysis methods. To judge the potential of the host for amino acid sensing in diagnostic applications, it remains to be seen how the system performs in mixtures of analytes as found in biofluids. One step toward this direction has been achieved by Isaacs, Anzenbacher Jr., and coworkers for the sensing of addictive over-the-counter (OTC) drugs in human urine by the same system;[235] see the following section (section 9) on drug detection in this review.

A ratiometric indicator displacement assay was established by Ni, Tao, and coworkers using the self-aggregating bipyridinium phenylene-vinylene dye, which self-assembles in the presence of nitrate salts. Upon addition of the partially methyl-substituted CB6 derivatives, $Me_4CB6$ (**C2.6**) and $Me_6CB6$ (**C2.7**), the dye is disaggregated through its binding inside the host cavity and the emission color is hypsochromically shifted by 120 nm (Figure 49).[236] These chemosensing ensembles selectively responded to the presence of lysine (Lys) and methionine (Met), whereas other proteinogenic amino acids did not cause a significant fluorescence change. It is noteworthy that $Me_4CB6$ and $Me_6CB6$ display different analyte binding preferences compared to the parent CB6 host, which can be rationalized by the elliptical distortion of substituted CB6 derivatives.[236,237] Thus, it should be possible to set up differential sensing arrays for amino acids and other metabolites using CB6 and its partially methylated analogues.

Isaacs and coworkers introduced a set of acyclic cucurbit[*n*]urils, *e.g.*, **C2.8** (Figure 50c), that adopt a tweezer-like conformation and contain chromophoric and emissive aromatic moieties as part of the cavity walls.[238,239] These

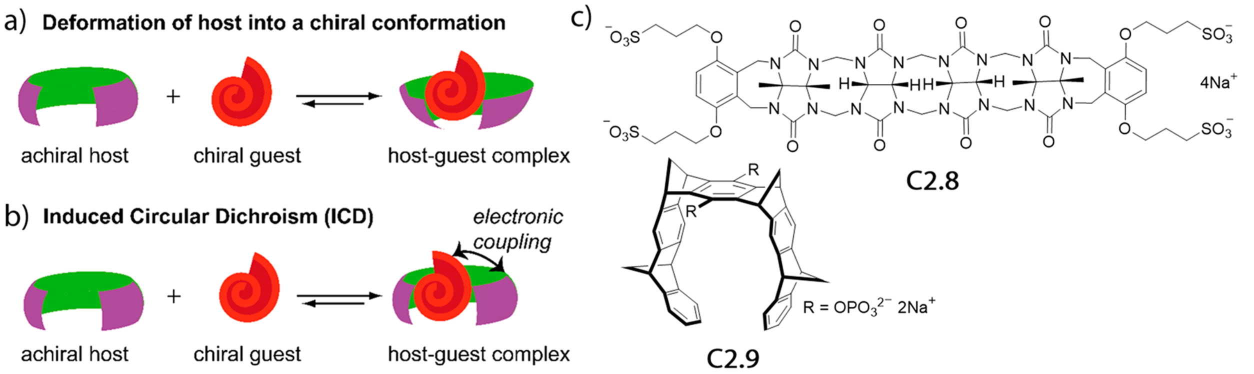

**Figure 50.** Schematic representation of chiral guest complexation by achiral hosts, leading to CD signal generation (a) through deformation of the host into a chiral conformation and (b) *via* induced circular dichroism (ICD) through electronic coupling between chromophoric hosts and guests. (c) Chemical structures of chemosensor **C2.8** and **C2.9**. Reproduced with permission from ref 246. Copyright 2020 The Royal Society of Chemistry.

hosts are promiscuous binders, forming complexes with structurally diverse guests, *e.g.,* blockbuster drugs, neuromuscular blocking agents, hydrocarbons, and carbon nanotubes.[234,240−245] On the one hand, using these compounds for analytical sensing tasks in complex biofluids likely faces selectivity challenges. On the other hand, the wide analyte-binding scope of synthetic binders can be a very useful feature for setting up general analytical assays.

We have recently utilized acyclic cucurbit[*n*]urils (**C2.8** in Figure 50) in combination with CD spectroscopy for chirality sensing. It was found that the complex formation of nonchromophoric amino acids and other chiral guests, such as terpenes, steroids, and drugs, in combination with chromophoric achiral hosts, lead to the formation of chiral, chromophoric complexes that display characteristic spectroscopic fingerprints. Capitalizing on this concept, it was also feasible to monitor base-catalyzed racemization of amino acids and peptides in various solvents.[246] This chirality-sensing approach was extended to other host classes, *e.g.,* molecular tweezers (*e.g.,* CLR01, **C2.9** in Figure 50c), that were introduced by Schrader and Klärner and that have a strong binding preference for Lys and Arg.[247−251] Molecular tweezers that have so far mainly be utilized to target protein misfolds and viruses with sterically accessible Lys and Arg residues[248,251−254] may therefore become useful chemosensors for Lys and Arg in biofluids, particularly if their signal transduction capabilities are further improved.

A larger member of the cucurbit[*n*]uril family, namely CB8, offers additional exciting possibilities for modifying the binding affinities and installing a signal transduction moiety. CB8 uniquely can form 1:1:1 heteroternary complexes with aromatic guests, allowing the setting up of associative binding assays (ABA; Figure 3).[44] It has been early noticed by Kim and coworkers, and was later further investigated by the Urbach group, that CB8 can simultaneously complex an electron-poor aromatic compound such as methyl viologen (MV, Figure 51) and an electron-rich aromatic molecule such as naphthol or the amino acids Trp and Phe in a face-to-face $\pi-\pi$ stacking orientation.[196,208,210,255−260] ABAs with self-assembled CB8•dye complexes overcome certain shortcomings of indicator IDAs, *e.g.,* with CB7•dye reporter pairs. First, the ABA sensing method does not "waste" the binding energy of the analyte for displacing a dye, and thus, the analyte detection sensitivity is higher with ABA than in the IDA format.[44,49,222,223] For instance, with liposome encapsulated chemosensors, even the submicromolar to nanomolar analyte detection range can be accessed while comparable IDA-based sensors require orders of magnitude higher analyte concentrations.[223] Furthermore, the ABA sensing format possesses superior analyte-differentiation potential. Firstly, CB8•dye complexes show mostly a binding preference towards analytes with at least one aromatic recognition motif, whereas CB7•dye reporter pairs that operate through an IDA mechanism bind both aromatic and aliphatic guests, *e.g.,* Phe and Lys. Secondly, different analytes can be identified by clearly distinguishable spectroscopic fingerprints that arise from the "communication" between the dye and the analyte inside the cavity of CB8. The ternary complexes are typically uniquely colored due to charge transfer (CT) interactions between both aromatic guests.[255,261] Upon binding by CB8•MV (**C2.10**), different analytes, *e.g.,* Phe and Trp, can be spectroscopically distinguished from each other based on the emerging CT bands. The CT bands in the absorbance spectra correlate to the HOMO−LUMO gap between the electron-rich aromatic analyte and the accepting electron-poor dye.[261] Unfortunately, such CT bands are rather weak in magnitude, requiring typically an operational concentration of ≫100 $\mu$M for both the analytes and the CB8•MV chemosensor for reliable signal transduction by absorbance spectroscopy. More pronounced CT bands were found for aryl-substituted viologens as the dye component.[261]

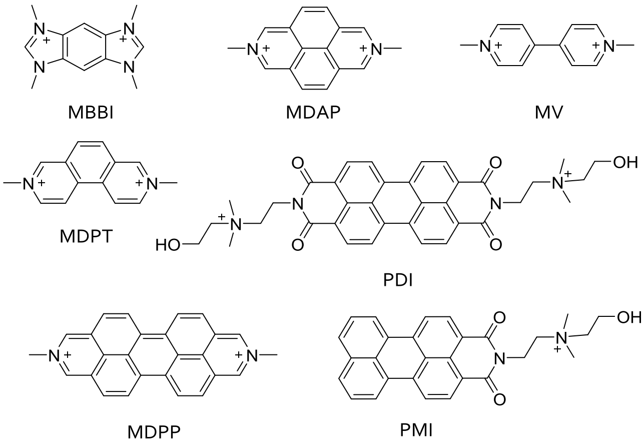

**Figure 51.** Chemical structures of selected dyes (typically halide salts), which are commonly used together in combination with CB8 to form CB8•dye chemosensors.

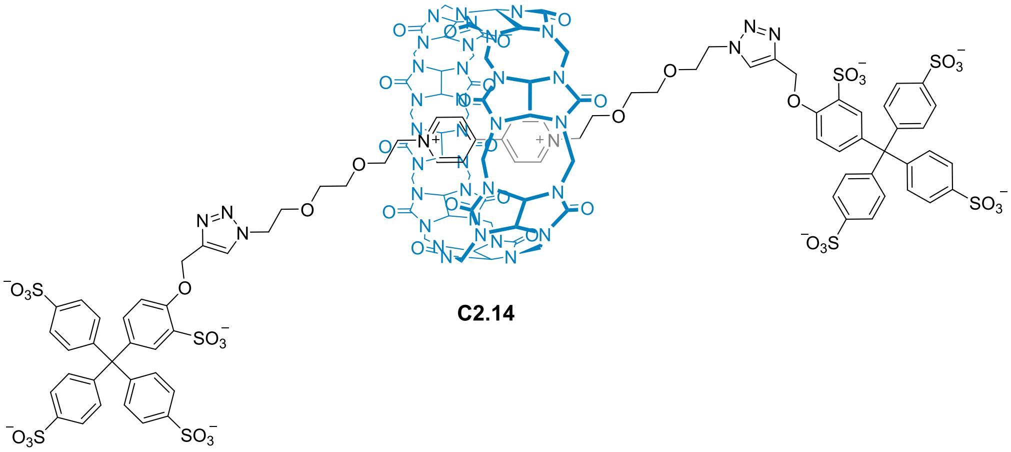

**Figure 52.** Chemical structure of the CB8•dye rotaxane-type chemosensor **C2.14**.

Moreover, the complexation of inherently fluorescent analytes, *e.g.*, Trp and its derivatives as well as peptides, by **C2.10** causes a strong quenching of their emission, which can be monitored also at low $\mu$M concentrations.[260,262]

Fluorescence-based associative binding assays with CB8•dye-based chemosensors can be established by utilizing the combination of CB8 and size-matching fluorescent dyes (Figure 51).[49] For instance, Kaifer and coworkers have self-assembled 1:1 complexes of CB8 with 2,7-dimethyldiazapyrenium (MDAP) or with 2,7-dimethyldiazaphenanthrenium (MDPT), furbishing promising chemosensors for catechol and indole derivatives.[263,264] Biedermann, Nau, and coworkers have later utilized such systems for the monitoring of enzymatic reactions and of membrane permeation processes of aromatic compounds, including Trp, its derivatives, and peptides in the micromolar concentration range in water or low salt buffers, *e.g.*, 10 mM HEPES or 10 mM phosphate buffer, pH ~7.0.[44,49,220,223] Phenylalanine is bound by CB8•MDAP (**C2.11**) but only provides partial quenching of the fluorescence of the chemosensor. The more electron-poor fluorescent dye tetramethyl benzobis(imidazolium) (MBBI) introduced by Urbach, Bielawski, Scherman, and coworkers can be used as an alternative when aiming to detect Phe and its derivatives and peptides because the CB8•MBBI complex responds with nearly complete emission quenching upon binding of most aromatic compounds.[223,265] Other suitable fluorescent dyes used as components for self-assembled CB8-based chemosensors are perylene bisdiimides (PDI; Scherman and coworkers) and perylene monoimides (PMI; Huang, Hunter, and coworkers).[261,266−268] Noteworthy, the corresponding self-assembled CB8•PDI chemosensor preferentially binds and responds with emission quenching to either rather electron-poor, *e.g.*, MV and azobenzene or significantly electron-rich aromatic compounds such as Trp species.[266] In contrast, the CB8•PMI complex (**C2.12**) dissociates upon addition of micromolar quantities of Phe-containing peptides, providing an indicator displacement assay with emission quenching in aqueous media.[267] High binding affinities for Trp- and Phe-type compounds and useful spectroscopic responses (emission, absorbance, CD) can be achieved with CB8-based chemosensors that utilize the methylated diazaperoperylenium (MDPP) as dye.[49,222] Di, Xu, and Hu utilized the CB8•MDPP chemosensor (**C2.13**) to visualize the enzymatic activity of cytosolic enzyme indoleamine 2,3-dioxygenase 1 (IDO1) in living cells.[269] This enzyme catalyzes the oxidation of tryptophan into *N*′-formylkynurenine, which is a much weaker binder and poorer fluorescence quencher for the chemosensor. Thus, the enzymatic activity of IDO1 in malignant HeLa and HepG2 cells overexpressing IDO1 was readily monitored by following the emission turn-on response of the chemosensor upon consumption of Trp.

Even better analyte differentiation capabilities are achieved when induced circular dichroism (ICD) is recorded for the complexes formed by CB8•dye with chiral guests (see also Figure 50). The cofacial arrangement of the dye and the aromatic moiety of a chiral analyte induces chiroptical properties in the CB8•dye chemosensor complex, *e.g.*, a distinct CD signal.[222] These CD signals contain much more analyte-related information than conventional absorbance and emission spectra. Indeed, by using CD spectral fingerprints generated by chiral analyte binding to CB8•MDAP (**C2.10**) and CB8•MDPP (**C2.13**) chemosensors, it was possible to differentiate Phe-containing from Trp-containing analytes. Besides, it was possible to distinguish N-terminal from C-terminal positioned peptidic aromatic amino acids. Even Trp-containing peptides differing in their adjacent nonaromatic amino acids were distinguishable by their ICD signals.[222] Also penicillin-type antibiotics and the protein insulin can be detected in low salinity buffers in this way.

Alternatively, array-based sensing formats are attractive strategies for enhancing amino acids distinction capabilities. Bunz and coworkers self-assembled an eight-element sensor array based on the combination of poly[*para*-phenyleneethynylene] dyes (PPE) and a supercharged green fluorescent protein (GFP) variant. The assay was combined with different additives such as metal salts and CB7•AO (**C2.1**) to increase the responsivity of the assay in order to distinguish all 20 natural amino acids from each other (each at 25 mM concentration in water).[270] The extension of the sensor array to different mixtures of analytes and biofluids will be exciting. Recently, it was reported by Wei and coworkers that combining CB*n* and CD recognition elements through immobilization on $MoS_2$ nanosheets dramatically improves the distinguishability of amino acids in an IDA-type format.[271] Astonishingly, 39 amino acids (19 L-amino acid, 19 D-amino acids, glycine) were classifiable and distinguishable from each other at a 0.5 mM concentration level. The authors also reported the application of their surface-immobilized chemosensor to the differentiation and identification of bacterial peptidoglycans and bacterial species.

Besides the selectivity problems that one faces when choosing cucurbit[*n*]urils as a host for binding and detecting analytes, their millimolar binding affinities[40] with alkaline and earth alkaline metals cations also cause competitive weakening of their complexes with amino acids and other analytes in buffered aqueous media or any biofluid. Thus, many reports for CB*n*-based sensing applications were conducted in deionized water or minimal buffers, *e.g.*, 10 mM phosphate buffer. It will be an important step forward in the field when more binding data in physiological buffers or biofluids become available.

The rotaxanated CB8•dye-based chemosensor **C2.14** in Figure 52 was reported by the Urbach group utilizing mechanical bonding as a strategy to prevent chemosensor disintegration caused by competitive binding of matrix components.[272] This system can be used for the detection of the fluorescent amino acid tryptophan ($K_a = 1.8 \times 10^4$ M$^{-1}$ in 5 mM sodium phosphate buffer, pH 7.4) and of its derived biogenic amine tryptamine ($K_a = 1.1 \times 10^5$ M$^{-1}$), whose emission is quenched upon binding to the rotaxanated chemosensor. While the authors were primarily interested in the binding difference of their rotaxanated system in aqueous and organic solvents, we believe that a similar strategy will be useful to arrive at fluorescent CB8-based chemosensors for applications in biofluids.

The same group developed a dilution-stable chemosensor by linking CB7 covalently to tetramethyl rhodamine (**C2.15** in Figure 53). It was found that this system retains a high binding affinity for representative guests, *e.g.*, $K_a = 6.3 \times 10^6$ M$^{-1}$ and $6.7 \times 10^6$ M$^{-1}$ for Phe-Gly-Gly binding to the chemosensor and to CB7 in 10 mM sodium phosphate buffer, pH 7.4, respectively.[273] These findings indicated that the dye is only weakly interacting with the CB7 host. Nevertheless, analyte binding to this covalent CB7−dye conjugate caused partial emission quenching, which was exploited to detect the permeation of some analytes into cells that were beforehand incubated with the chemosensor. This system is likely to respond similarly to all analytes that are known CB7 binders, and thus can be used for the detection of the amino acids Phe and Lys, as well as derivatives and peptides thereof, in the micromolar concentration regime in aqueous media. We have shown recently that dilution-stable, unimolecular CB*n*-based chemosensors can be obtained by covalently linking an indicator dye to CB*n* through a flexible tether.[274] Here, the tethered dye forms an inclusion complex with the host and thus tunes the selectivity of the chemosensor towards strongly binding guests. This design strategy improved the tolerance of the chemosensors towards salts, allowing for sensing applications in human urine, saliva, and concentrated buffers. It also provides a promising pathway to establish a practically exploitable kinetic binding selectivity between different analytes.

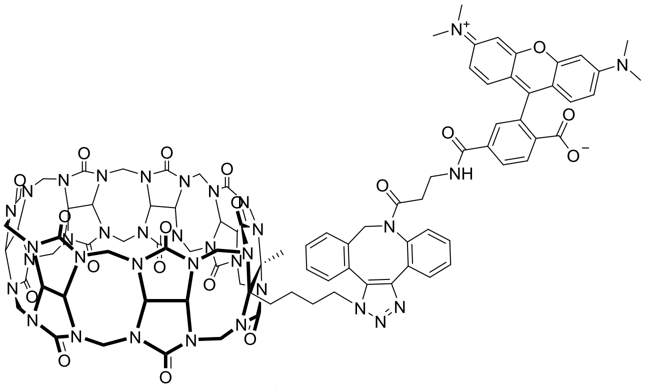

**C2.15**

**Figure 53.** Chemical structure of the covalent linked unimolecular CB7-tetramethyl rhodamine chemosensor **C2.15**.

A novel concept to overcome the negative impact of salts on the detection of amino acids was introduced by the Hof group. A fluorescent calix[4]arene-type chemosensor (**C2.16**) that forms dimers in aqueous media, leading to emission quenching, was utilized (Figure 54).[275] The authors showed that the strong binding guest trimethyllysine disrupts the dimer and thus restores the emission, while lysine itself shows only a weak interaction. Importantly, the dimerization is not affected by salts, and thus the chemosensors retain their sensing performance in physiological buffers. It was possible to successfully apply the "DimerDye Disassembly Assay" (DDA) to monitor the activity a methyltransferase under physiological conditions in real time. The DDA approach offers an interesting alternative for monitoring enzymatic methylation of Lys residues over previous assays that were limited to minimal buffers[215,217] and over commercial assays that are limited to end-point measurements requiring time consuming sample post-treatment steps.[275] A similar concept was later successfully applied by the same group to the detection of illicit drugs in saliva;[276] see Figure 213 in section 9.1 for more details.

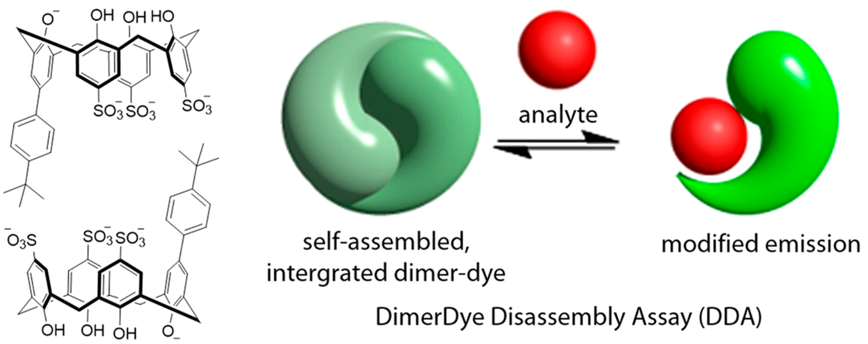

**C2.16**

**Figure 54.** Chemical structure of the calix[4]arene-type chemosensor **C2.16** and the binding scheme of DDA. Reproduced with permission from ref 275. Copyright 2014 American Chemical Society.

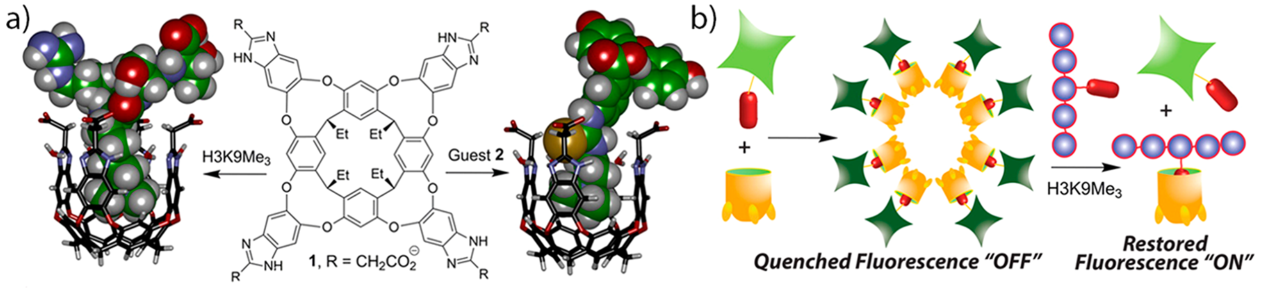

**C2.17**

**Figure 55.** (a) Chemical structure of **C2.17** and models of host−guest complexes. (b) Scheme of the aggregation-based sensing system in analogy to **C2.17**. Adapted with permission from ref 277. Copyright 2014 American Chemical Society.

Hooley, Zhong, and coworkers developed a conceptually related system for detecting trimethylated peptides as well as trimethyllysine and the determination of histone demethylase activity.[277] Their negatively charged cavitands (**C2.17** in Figure 55) show a binding preference for positively charged guests and form aggregates in 1× PBS, pH 7.4, in the presence of fluorophores that carry a trimethylammonium side chain. The aggregates, which show quenched emission, disrupt upon binding of competitive guests such as histone peptides carrying a trimethyllysine residue. This assay was found to be salt tolerant, and control over the aggregation can be achieved by addition of chaotropic anions.

Recently, Kursunlu and coworkers introduced a pillar[5]-arene chemosensor that features 10 pendant BODIPY groups (Figure 56).[278] The chemosensor **C2.18** displayed an emission enhancement upon binding to asparagine in 50% DMF in water, while 12 other tested amino acids did not provide a signal change in the blue emission channel. The host displayed a surprisingly high binding affinity for asparagine, $K_a = 2.5 \times 10^8$ $M^{-1}$, suggesting that improved pillar[*n*]arene derivatives may become viable for the detection of amino acids in aqueous media.

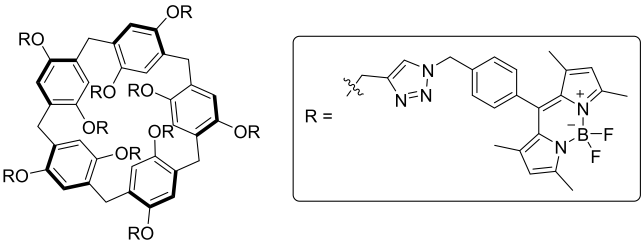

**C2.18**

**Figure 56.** Chemical structure of chemosensor **C2.18**.

Cyclodextrins (CDs), particularly dye-tethered cyclodextrins as unimolecular chemosensors,[279−281] are also attractive for amino acid sensing. Unlike most synthetic hosts, cyclodextrins are inherently chiral and therefore can be used for chiral discrimination of enantiomeric amino acids and their derivatives. However, the chiral discrimination factors of the shape-flexible CDs are rather low, and typically multiple molecular recognition events are required to achieve a practical chirality sensing method. This occurs when separating chiral substances with cyclodextrin-functionalized stationary phases through chromatographic methods.

Inoue, Yang, and coworkers have overcome this problem by introducing an enantiomeric helicene that is conformational rigid, axial chiral, and fluorescent to the primary rim of $\beta$-CD (Figure 57).[282] The resulting diastereomeric $\beta$-CD−helicene conjugate (**C2.19**) did not only show a fluorescence response upon binding of amino acids but was also capable of distinguishing the L- and D-form of hydrophobic amino acids with high discrimination factors, *e.g.*, $K_a = 1.2 \times 10^4$ $M^{-1}$ and $1.0 \times 10^3$ $M^{-1}$ for L-Leu and D-Leu, respectively, and $K_a = 3.6 \times 10^2$ $M^{-1}$ and $4.2 \times 10^3$ $M^{-1}$ for L-Trp and D-Trp, respectively, in aqueous media at pH 7.3. Corradini and coworkers have prepared improved cyclodextrin-based chirality chemosensors (**C2.20** in Figure 57b) by introducing an additional amino acid binding motif, *i.e.*, a metal-binding site on the tether that connects the fluorescent indicator dye.[283] In the presence of $Cu^{II}$ ions, the chiral host and amino acid are interacting with each other through an additional metal-coordination binding motif. By assessing the different binding affinities of the chiral analytes to the chiral host, the authors were able to distinguish enantiomeric amino acids from each other through fluorescence-based titrations. Furthermore, the applicability of the assay to the microwell plate format was demonstrated, where the enantiomeric excess of valine and proline samples was determined in the submillimolar concentration regime.

The coordination of carboxylates by $Cu^{II}$ centers was utilized by the Huang group to arrive at a tweezer-like chemosensor (**C2.21** in Figure 58) that contains two anthracenyl moieties as signal transduction units.[284] Upon carboxylate binding, the emission quenching behavior of the $Cu^{II}$ center is reduced and therefore, the emission of the chemosensor is enhanced. This chemosensor can be used for the detection of alanine, aspartate, and glutamate, and the dipeptide Phe-Gly, each of which show affinities in the millimolar range in mixed aqueous organic media (50% MeOH in Tris buffer, pH 7.4). Moreover, a high affinity discrimination factor of ∼10 was found between L- and D-mandelate with this chiral chemosensor.

### 2.3.1. Selective Sensing of Amino Acids by Metal Complex-based Chemosensors.

*2.3.1.1. Metal Complex-based Chemosensors for Histidine.* Some amino acids and their derivatives can be selectively targeted by metal complex-based chemosensors. For instance, histidine contains nitrogen atoms that are part of a heterocyclic aromatic ring and which therefore possess unique metal-binding properties amongst the class of amino acids. Inspired by the wide occurrence of the [$His_2ZnCys_2$] binding motif in zinc finger proteins,[285−288] the affinities of $Zn^{II}$ centers for histidine have been exploited in the design of chemosensors in a biometric fashion. The chemosensors discussed within this section are summarized in Table 5.

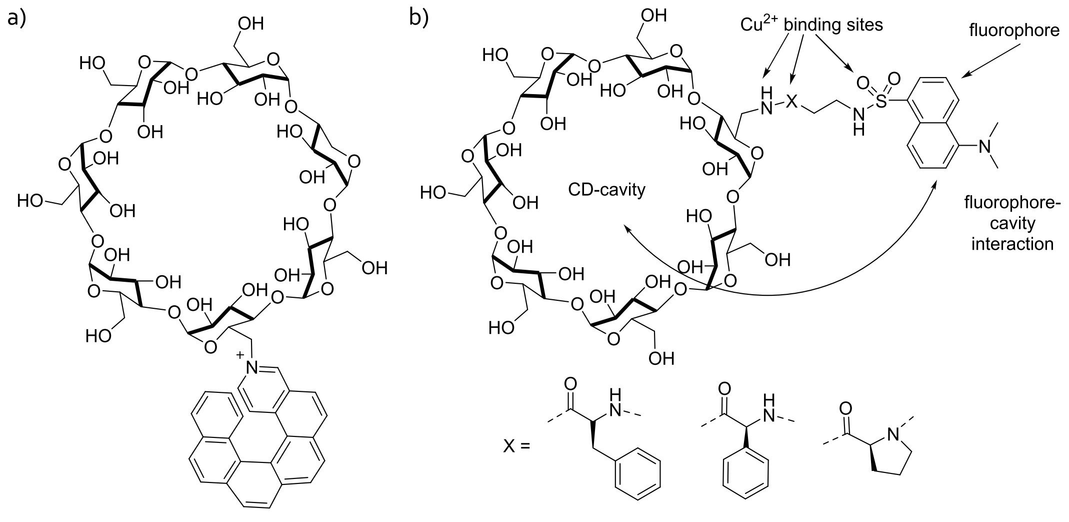

**C2.19** **C2.20**

**Figure 57.** (a) Chemical structure of chemosensor **C2.19**. (b) General scheme of enantioselective fluorescent cyclodextrins showcased for chemosensor **C2.20**.

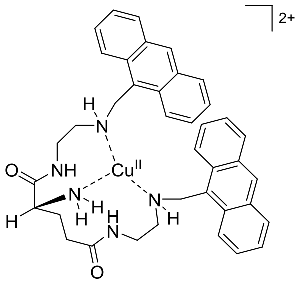

**C2.21**

**Figure 58.** Chemical structure of copper containing anthracene-functionalized chemosensor **C2.21**.

In 2004, Yang and coworkers described a zinc porphyrin complex with a covalently attached pyrene functionality as a signal transducer.[289] The complex **C2.22** in Figure 59 was immobilized on plasticized polyvinyl chloride membranes, which then were successfully used for histidine detection in aqueous media. In the presence of the target analyte, two equivalents of such porphyrin complexes were brought in close spatial proximity through the bridging function of histidine. This can be easily observed through the emerging pyrene excimer emission. The sensor membrane can be used for determining histidine in the submicromolar to millimolar concentration regime and showed a high selectivity over other amino acids. Pleasingly, adverse binding by potentially Zn$^{II}$ binding anions, such as isothiocyanate, fluoride, chloride, nitrite, sulfate, and salicylate, were not detected. In fact, the authors demonstrated that blood serum levels of histidine can be reliably measured with their sensor. The sensor membrane was found to be washable and reusable.

Another histidine-selective chemosensor (**C2.23**) was prepared by Yu, Pu, and coworkers in 2013, which complements other previously reported zinc complexes for histidine sensing.[290] The authors combined a crown ether moiety and a terpyridine unit to provide two binding stations for Zn$^{II}$ (Figure 60). As a result of the simultaneous binding of the heterocyclic "*N*", the $-NH_2$ and the $-COO^-$ moieties of the target analyte, this system selectively responded to micromolar concentrations of histidine in 25 mM HEPES containing 1% THF, pH 7.35, with a strong emission enhancement, while all other proteinogenic amino acids give no response under the same conditions. It is noteworthy that neither N-protected and O-protected histidine nor imidazole and derivatives also caused any fluorescence response. However, it can be expected that nucleosides are cross-reactive with **C2.23** because structurally analogous chemosensors, *e.g.*, **C6.4** in Figure 162 in section 6, were utilized for adenosine triphosphate (ATP) detection.

Other researchers put their focus on Cu$^{II}$ ions to form chelate complexes with histidine. For example, two structurally related coumarin-based dyes have been introduced in consecutive years (Figure 61).[291,292] Both dyes feature a metal-ion binding station and experience emission quenching upon Cu$^{II}$ binding. Such dyes can thus also be utilized for the detection of Cu$^{II}$ ions. In the presence of histidine, the emission intensity of both histidine chemosensors **C2.24** and **C2.25** is restored because the target analyte competitively binds Cu$^{II}$ ions. Chemosensor **C2.24** was developed by Li, Yu, and coworkers for the detection of histidine in the low micromolar concentration regime with 0.5% DMSO in 20 mM HEPES buffer, pH 7.4. **C2.24** was found to be unresponsive to all amino acids but histidine and cysteine, even if they were added at 100× molar excess. To a certain extent, this chemosensor can also be used to distinguish His from Cys, as the latter only gave a modest emission enhancement. Indeed, the authors also succeeded in the parallel quantification of His concentration in human urine and fetal calf serum.[291] The analogous chemosensor **C2.25** introduced by Chan, Leung, and coworkers showed similar sensitivity and selectivity for histidine detection. It is noteworthy that the authors demonstrated that biothiols such as Cys also cause an emission enhancement due to their binding to Cu$^{II}$ ions.[292] This system has been successfully utilized for monitoring of intracellular histidine in human glioblastoma cells. Conceptually related systems that operate through histidine-triggered release of Cu$^{II}$ ions have been reported by others, *e.g.*, Chattopadhyay, Das, and coworkers,[293] and the Li group.[294] Likewise, these systems displayed cross-reactivities with other thiols.

**Table 5. Summary of Chemosensors for Amino Acids (LOD, Limit of Detection)**

| chemosensor | media | concentration range | ref |
|---|---|---|---|
| Amino Acids Analyte | | | |
| **C2.1** | water | 25 mM | 270 |
| **C2.10**[i,j] | 10 mM sodium phosphate buffer, pH 7.0 | mM range | 234 |
| **C2.11**[f,j] | water or low salt buffer, *e.g.*, 10 mM phosphate buffer, pH 7.0 | $\mu$M range | 265 |
| **C2.12**[j] | water | $\mu$M range | 267 |
| **C2.13**[j] | 10 mM phosphate buffer, pH 4.0/pH 4.5/pH 8.0 | $\mu$M range | 222 |
| **C2.15** | 10 mM sodium phosphate buffer, pH 7.4 | mM range | 273 |
| **C2.19** | aq media, pH 7.3 | mM range | 282 |
| **C2.20** | 100 mM sodium borate buffer, pH 7.0 | $\mu$M range | 283 |
| Alanine (Ala) Analyte | | | |
| **C2.21** | 50% MeOH in Tris buffer, pH 7.4 | 0−2.0 mM | 284 |
| Arginine (Arg) Analyte | | | |
| **C2.5**[a] | water, pH 7.0 | 0−500 $\mu$M | 234 |
| **C2.9**[b] | water | $\mu$M range | 246 |
| **C2.32** | 10 mM HEPES, pH 7.4 | 10 $\mu$M | 306 |
| Aspartate (Asp) Analyte | | | |
| **C2.21** | 50% MeOH in Tris buffer, pH 7.4 | 0−2.0 mM | 284 |
| **C2.31**[c] | 50% MeOH in 10 mM HEPES, pH 7.4 | $\mu$M range | 305 |
| Asparagine (Asn) Analyte | | | |
| **C2.18** | 50% DMF in water | $\mu$M range | 278 |
| Bovine Serum Albumin (BSA) Analyte | | | |
| **C2.3** | water | 0−250 $\mu$M | 232 |
| **C2.32** | 10 mM HEPES, pH 7.4 | 10 $\mu$M;<br>LOD, 15 nM | 306 |
| Glutamate (Glu) Analyte | | | |
| **C2.21** | 50% MeOH in Tris buffer, pH 7.4 | 0−2.0 mM | 284 |
| Histidine (His) Analyte | | | |
| **C2.5**[a] | water, pH 7.0 | 0−1.0 mM | 234 |
| **C2.22** | 60% MeOH in water; blood serum | sub-$\mu$M−mM;<br>LOD, 0.13 $\mu$M | 289 |
| **C2.23** | 1% THF in 25 mM HEPES, pH 7.4 | 0.8−8.0 $\mu$M | 290 |
| **C2.24**[c] | 0.5% DMSO in 20 mM HEPES buffer, pH 7.4; human urine; fetal calf serum | 2.0−60 $\mu$M | 291 |
| **C2.25**[c] | 20% MeCN in 20 mM HEPES buffer, pH 7.4 | 0−125 $\mu$M | 292 |
| **C2.26**[d] | 25 mM HEPES buffer, pH 7.4 | sub-mM | 295 |
| **C2.27** | 50 mM HEPES buffer, pH 7.0 | 0−4.0 $\mu$M | 297 |
| **C2.28** | 1× PBS; cell homogenate in 10 mM PBS, pH 6.8 | 0.5−100 $\mu$M;<br>LOD, 76 nM | 296 |
| **C2.29** | 40% EtOH in 50 mM HEPES, pH 7.2; HeLa cells | mM range | 298 |
| **C2.30a** | HEPES buffer, pH 7.7 | $\mu$M range | 304 |
| **C2.30b** | HEPES buffer, pH 7.7 | $\mu$M range;<br>LOD, 0.3 $\mu$M | 304 |
| Insulin Analyte | | | |
| **C2.1** | 10 mM sodium phosphate buffer, pH 7.0 | $\mu$M range | 211 |
| Lysine (Lys) Analyte | | | |
| **C2.5**[a] | water, pH 7.0 | 0−1.0 mM | 234 |
| **C2.9**[b] | water | $\mu$M range | 246 |
| Lysine (Lys) Analyte | | | |
| **C2.2**[e] | 10 mM ammonium acetate buffer, pH 6.0 | $\mu$M range | 226 |
| **C2.6/C2.7** | phosphate buffer, pH 6.0 | 50 $\mu$M | 236 |
| Trimethyllysine Analyte | | | |
| **C2.16** | 100 mM phosphate buffer, pH 7.4 | $\mu$M range | 275 |
| **C2.17** | 1× PBS (10 mM phosphate buffer containing 150 mM NaCl), pH 7.4 | $\mu$M range | 277 |
| Methionine (Met) Analyte | | | |
| **C2.6/C2.7** | phosphate buffer, pH 6.0 | 50 $\mu$M | 236 |
| Ornithine Analyte | | | |
| **C2.5**[a] | water, pH 7.0 | 0−1.0 mM | 234 |
| Peptide Thr-Gly-Ala-Phe-Met-NH$_2$ Analyte | | | |
| **C2.1** | 10 mM ammonium phosphate buffer, pH 7.2 | 0−55 $\mu$M | 221 |
| PeptidePhe-Gly-Gly Analyte | | | |
| **C2.15** | 10 mM sodium phosphate buffer, pH 7.0 | 0−8.5 $\mu$M | 273 |
| Peptide Phe-Gly Analyte | | | |
| **C2.21** | 50% MeOH in Tris buffer, pH 7.4 | 0−2.0 mM | 284 |
| Phenylalanine (Phe) Analyte | | | |
| **C2.4**[f] | 50 mM sodium acetate buffer, pH 4.7 | $\mu$M−low mM | 233 |
| **C2.8**[b] | water | $\mu$M range | 246 |
| Phosphatidyl-serine Analyte | | | |
| **C2.33** | cell surface | | 307 |
| Proline (Pro) Analyte | | | |
| **C2.20** | 100 mM sodium borate buffer, pH 7.0 | $\mu$M range | 283 |
| Tryptophan (Trp) Analyte | | | |
| **C2.4** | 50 mM sodium acetate buffer, pH 4.7 | $\mu$M−low mM | 233 |
| **C2.8** | water | $\mu$M range | 246 |
| **C2.11**[h] | water; low salt buffer, *e.g.*, 10 mM phosphate buffer, pH 7.0 | $\mu$M range | 265 |
| **C2.14**[h] | 5 mM Sodium phosphate buffer, pH 7.4 | 50 $\mu$M | 272 |
| **C2.19** | aq media, pH 7.3 | 0−4.0 mM | 282 |
| Tyrosine (Tyr) Analyte | | | |
| **C2.4**[g] | 50 mM sodium acetate buffer, pH 4.7 | $\mu$M−low mM | 233 |
| Valine (Val) Analyte | | | |
| **C2.20** | 100 mM sodium borate buffer, pH 7.0 | $\mu$M range | 283 |

[a] Eu$^{III}$ required for quantifiable emission change upon guest binding. Also detects putrescine, cadaverine, agmatine and histamine. [b] Also detects derivatives of the analyte. Detects Phe, Val *etc.* with $K_a$ one order of magnitude smaller. [c] Detects also Cys, Hcys, GSH, NAC, but these interferants can be eliminated by N-ethylmaleimide as biothiol scavenger. [d] Cross-reactivity with Cys. [e] Enzymatic assay with cadaverine as targeted product. Decarboxylation of His, Arg, Tyr, Trp and ornithine were also investigated. [f] Trp and derivatives detected during various enzymatic reactions. [g] Responds to all CB7 binders such as Lys, Phe and derivatives as well as neurotransmitters and nucleobases. [h] Cross-reactivity with tryptamine. [i] Detects also short peptide sequences. [j] See Figure 51 for other ABA reporter dyes.

An alternative copper-based design has been pursued by Yu, Pu, and coworkers that reported the simple coordination complex terpyridine−Cu$^{II}$Cl$_2$ as a chemosensor (**C2.26** in Figure 61c) for histidine (and cysteine).[295] This system was proposed to associatively bind His without displacement of the Cu$^{II}$ ions, giving rise to a remarkable 1000-fold emission enhancement. The binding affinity of the chemosensor for histidine was reported as $K_a = 9 \times 10^3$ M$^{-1}$ in 25 mM HEPES

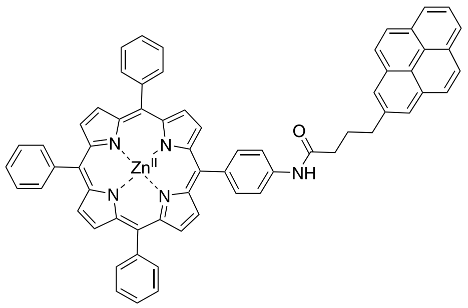

**C2.22**

**Figure 59.** Chemical structure of the zinc porphyrin chemosensor **C2.22**.

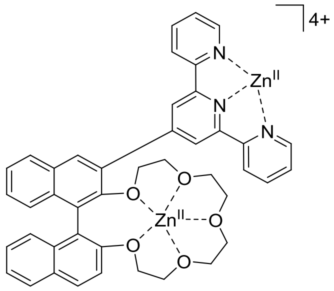

**C2.23**

**Figure 60.** Chemical structure of histidine selective chemosensor **C2.23**.

buffer, pH 7.4, which restricts the sensitivity of the assay to the submillimolar concentration regime. Additional practical challenges are the cross-reactivity for cysteine and the somewhat practical limiting short excitation wavelength (298 nm) of the chemosensor.

The His-coordination ability of Cu$^{II}$-bound chemosensors was utilized by the Fabbrizzi group, who investigated the complexation of amino acids by a dimetallic cyclophane, *e.g.*, by **C2.27**.[297] It was demonstrated that an emission turn-on response can be achieved through involving eosin Y as an indicator dye (Figure 62a). Importantly, while the dimetallic cyclophanes bind a wide range of amino acids, histidine stood out as the strongest binder ($K_a \geq 10^7$ M$^{-1}$ in 50 mM HEPES buffer, pH 7.0). Therefore, it was possible to tune the selectivity of the chemosensing ensemble exclusively to His by using the strongly binding indicator dye eosin Y ($K_a \sim 10^7$ M$^{-1}$) that can only be displaced by His but not by other, more weakly binding amino acids. However, the structural similarity of **C2.27** to a nucleoside chemosensor (**C6.6** in Figure 164 in section 6) again suggests a possible cross-reactivity.

An unusual approach for histidine sensing has been proposed by Lin, Chen, and coworkers, who exploited the catalytic function of copper ions for alkyne-azide click reactions.[296] Specifically, an azide-functional coumarin dye and a small molecule alkyne are added to the sample solution, as well as Cu$^{II}$ salt and ascorbate. The resulting chemosensing mixture is herein labelled as **C2.28**. If no Cu$^{II}$-binding species is present in the sample solution, an emission turn-on response is observed as the azide-functional coumarin dye is catalytically converted into a fluorescent compound. Conversely, if histidine is present, the Cu$^{II}$-ions are sequestered, and the catalytic reaction does not take place (Figure 62b). The authors succeeded in determining histidine in the lower $\mu$M regime with an estimated LOD of 76 nM in 1× PBS and in cellular homogenate.

It appears that most copper-based chemosensors for histidine are cross-reactive towards bio-thiols,[291−295,298,299] which limits their use for cell imaging applications due to the relatively high concentrations of cysteine (Cys, about 100

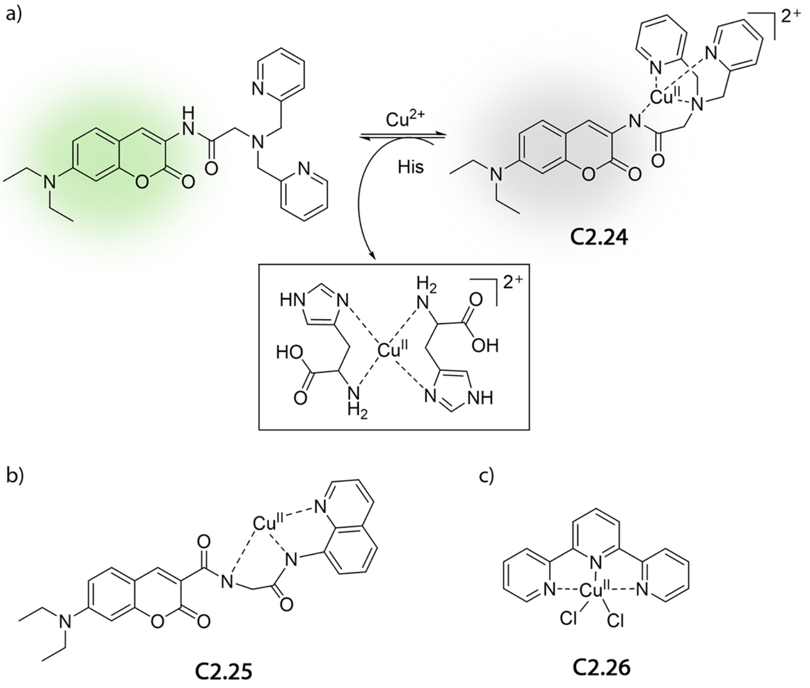

**Figure 61.** (a−c) Three different coumarin-based Cu$^{II}$ binding chemosensors (**C2.24**−**C2.26**) for the detection of histidine that operate through a competitive binding mechanism with emission-quenching Cu$^{II}$ ions. (a) Adapted with permission from ref 291. Copyright 2013 The Royal Society of Chemistry.

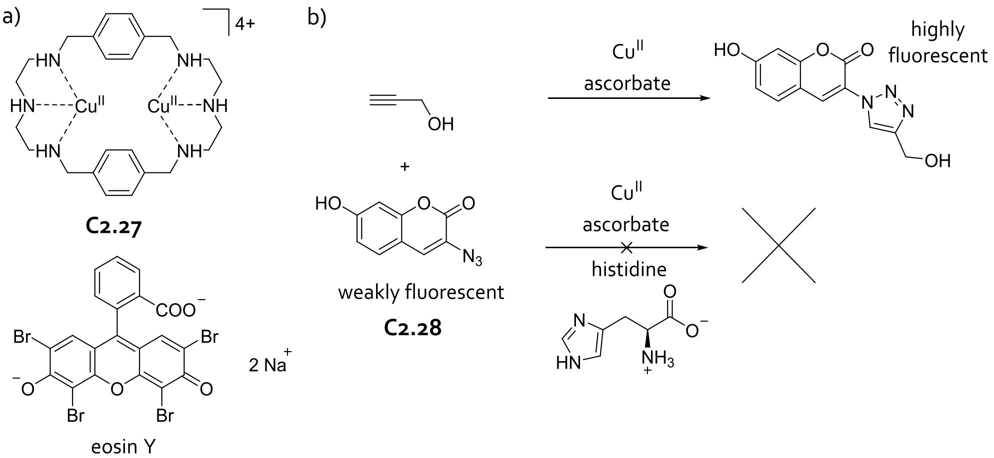

**Figure 62.** (a) Chemosensing ensemble **C2.27** utilized for the selective detection of histidine obtained by combining $Cu^{II}$-bound paracyclophanes and eosin Y as an indicator dye. (b) Schematic representation of the sensing mechanism for histidine with the sensing ensemble **C2.28** in the presence of copper ascorbate. Adapted with permission from ref 296. Copyright 2012 Elsevier BV.

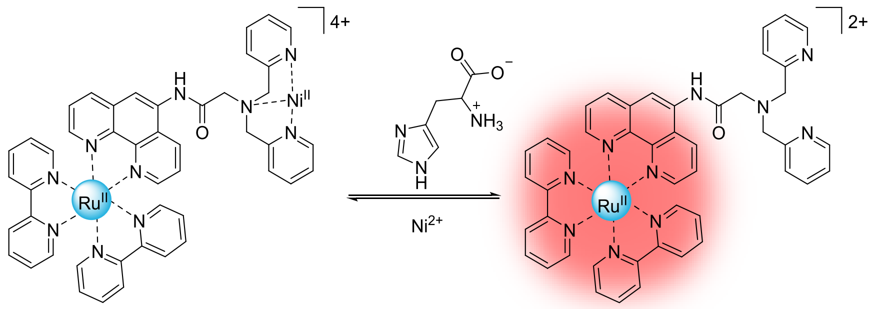

**C2.29**

$[Ru(bpy)_2(phen\text{-}dpa)]^{2+}$

**Figure 63.** Schematic representation of the emission turn-on indicator displacement assay for the detection of histidine with a heterobimetallic ruthenium$^{II}$–nickel$^{II}$ complex through competitive binding of $Ni^{II}$ ions.

μM), reduced glutathione (GSH, in mM concentrations), and thiol-functional proteins found inside living cells.

In an effort to arrive at a chemosensor useful for histidine imaging in live systems, Ye and coworkers proposed the use of $Ni^{II}$-centers as binding motifs.[298] Indeed, nickel ions as well as later discussed nanoparticles are widely being exploited in the His-tag technology for protein purification and labeling.[300−303] The authors attached a $Ni^{II}$ targeting motif to a $[Ru^{II}(bpy)_2(phen\text{-}dpa)]$ (bpy = bipyridine, dpa = dipicolylamine, phen = phenantroline) complex, whose phosphorescence was quenched upon binding of a paramagnetic $Ni^{II}$ ion (Figure 63).[298] This dimetallic chemosensor (**C2.29**) responded to the presence of micromolar concentrations of histidine with an emission enhancement at 603 nm on account of the competitive removal of the $Ni^{II}$ quencher, which is strongly complexed by histidine in 40% EtOH in 50 mM HEPES, pH 7.2. Remarkably, other potential competitors such as the biothiols Cys, GSH, and Hcys as well as various anions, ascorbic acid, DNA, BSA, and 12 tested amino acids, did not trigger a phosphorescence response. Cell imaging results demonstrated that the chemosensing ensemble is membrane permeable and that it can be applied for visualizing histidine in live cells. The utility of the system was further highlighted by employing it for phosphorescence imaging of histidine in larval zebrafish and *Daphnia magna*.

A vitamin B6 derived ligand that can efficiently bind to $Al^{3+}$ ions ($K_a = 4 \times 10^5$ $M^{-1}$ in HEPES buffer, pH 7.7) was developed by Oliveira, Lodeiro, and coworkers (Figure 64).[304] Interestingly, subsequent binding of two equivalents of histidine results in a strong additional 100× emission enhancement, making this system a promising emission turn-on chemosensor for this amino acid. The authors also reported that even in the absence of $Al^{3+}$, the ligand behaves as a chemosensor (**C2.30a**) and responds with emission turn-on to the presence of histidine, albeit with a lower signal enhancement factor. A detection limit of 300 nM histidine was found with **C2.30a** in HEPES buffer, pH 7.7. The authors also discussed the high selectivity of the $Al^{3+}$-bound chemosensor **C2.30b** for histidine over other proteogenic amino acids and

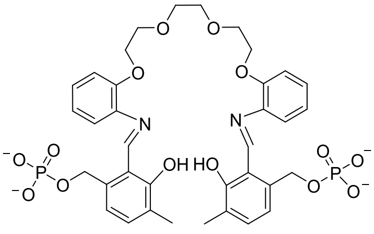

ligand **C2.30a**
ligand + $Al^{3+}$ **C2.30b**

**Figure 64.** Chemical structure of chemosensor **C2.30**.

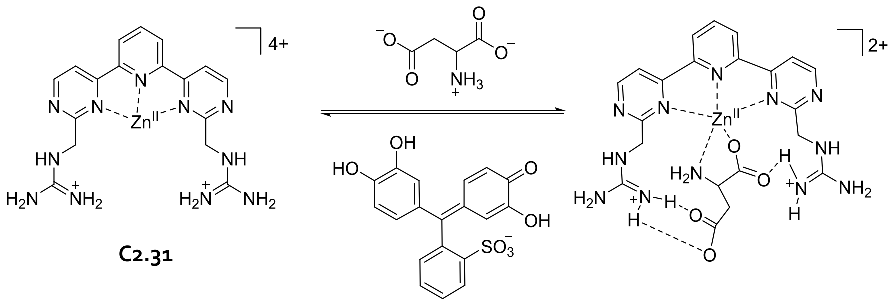

**Figure 65.** Schematic representation of the chemosensing ensemble **C2.31** composed of a guanidinium-functional Zn$^{II}$ complex and the indicator dye pyrocatechol violet for the (selective) detection of the amino acid aspartate in mixed organic−aqueous media.

demonstrated its applications for histidine detection in human urine.

*2.3.1.2. Metal Complex-based Chemosensors for Aspartate, Arginine, and Phosphatidyl-serine.* Besides the already discussed selective sensing strategies for histidine and thiols, several other amino acids can be detected through their metal-ion coordinating ability.

An aspartate-selective chemosensing ensemble (**C2.31**) has been introduced by the Anslyn group, which capitalized on the cooperative chelation between a Zn$^{II}$ complex and amino acids that are bound *via* their carboxylate and amine functionalities (Figure 65).[305] To introduce a binding selectivity for aspartate, positively charged guanidinium moieties were installed in strategic positions on the receptor scaffold. Moreover, the indicator dye pyrocatechol violet was introduced to furbish an easily quantifiable ratiometric absorbance signal response through dye displacement upon addition of the target analytes. Pleasingly, this system showed the anticipated selectivity for aspartate over other amino acids, including glutamate in 50% MeOH in 10 mM HEPES, pH 7.4 ($K_a$ = 1.5 × $10^5$ $M^{-1}$ for aspartate and $K_a$ ~ $10^4$ $M^{-1}$ for Phe, Val, Gly, Asn, Glu, and succinic acid). While these results were instructive and promising in a fundamental sense, future research is needed to make this system applicable for aspartate detection in pure aqueous media and biofluids.

By attaching a crown ether moiety to a Zn$^{II}$-terpyridine complex, Wu and coworkers arrived at a chemosensor (**C2.32**) that shows a selective hypochromic fluorescence response for arginine in 10 mM HEPES, pH 7.4 (Figure 66).[306] The authors reasoned that the combination of H-bonds, electrostatic, and van der Waals forces caused the observed binding selectivity. It was found that other amino acids, including lysine, and the arginine-derived nonproteinogenic amino acid citrulline, do not cause a noticeable change of the emission properties of the chemosensor. The sensitivity of the chemosensor is limited to the submillimolar range because the binding affinity of $K_a$ = 1.8 × $10^4$ $M^{-1}$ in HEPES buffer is only modest. Moreover, it has to be assumed that the performance of the chemosensor is adversely affected by $Na^+$ and $K^+$ ions present in biofluids, which competitively bind the crown ether unit. Nevertheless, this system showed promising results for the detection of the arginine- and His-rich protein BSA in HEPES buffer.

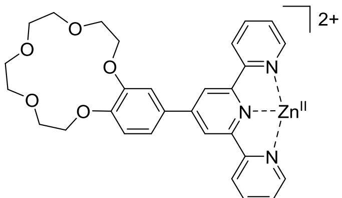

**C2.32**

**Figure 66.** Chemical structure of chemosensor **C2.32**.

Artificial binders that are covalently connected to an indicator dye can serve as dilution-stable, unimolecular chemosensors. For example, Jolliffe and coworkers developed a coumarin labelled fluorogenic chemosensor **C2.33** that can be utilized for recognizing and detecting phosphatidylserines on cell surfaces through an intramolecular indicator displacement mechanism (Figure 67).[307] The chemosensor design capitalized on the binding preference of Zn$^{II}$ ions for "hard" anions, *e.g.*, carboxylates and phosphates. The use of an appropriately designed spacer ensured that the binding affinity is maximized for the phosphatidyl serine target analyte.

## 2.4. Nanosensors for Amino Acids and Proteins

Menon and coworkers reported the use of *p*-sulfonatocalix[4]arene thiol-functionalized gold nanoparticles (AuNPs) for fluorescence-based detection of the basic amino acids lysine, arginine, and histidine in phosphate buffered solution at $\mu$M concentrations (**N2.1** in Figure 68).[308] At physiological pH, protonated amino groups of the analytes bind *via* electrostatic interactions with the negatively charged *p*-sulfonatocalix[4]arene moieties. In the case of histidine, additional host−guest interactions came into play when binding to **N2.1**, which were mediated by the imidazole moiety. After binding with amino acids, the electrostatic repulsive forces between the particles decreased, which was concluded from the distinct color change in the dispersion of **N2.1** as the surface plasmon resonances changed upon aggregation. The degree of aggregation was measured by UV−vis absorption spectroscopy and correlated with the amount of basic amino acid in solution. The authors showed that other amino acids (*e.g.*, Gly, Ala, Leu, Val, Pro, Ser, Asp, and Glu) also triggered a colorimetric response. All nanosensors discussed within this section are summarized in Table 6.

Quantum dots (QDs) are characterized by high fluorescence quantum yields, size dependent emission wavelengths, and good resistance against photobleaching, which are desirable properties for the development of new fluorescent nanosensors.[310] Willner and coworkers reported the preparation of *β*-cyclodextrin (*β*-CD) decorated Se/ZnS QDs for enantioselective and fluorescence-based detection of L-tyrosine ($K_a$ = 2.2 × $10^3$ $M^{-1}$) and L-phenylalanine ($K_a$ = 3.05 × $10^3$ $M^{-1}$) in 100 mM phosphate buffer, pH 10.3, at $\mu$M concentrations (**N2.2** in Figure 69).[309] Upon light excitation of QDs, efficient energy transfer occurs from the nanoparticle to the host-bound rhodamine B dye, causing its sensitized emission, while particle

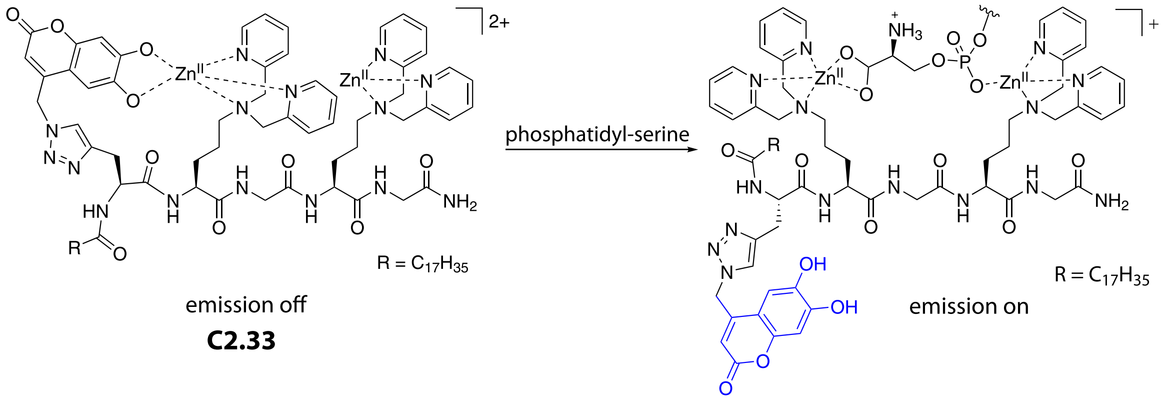

**Figure 67.** Schematic representation of chemosensor **C2.33** upon reaction with phosphatidyl-serine.

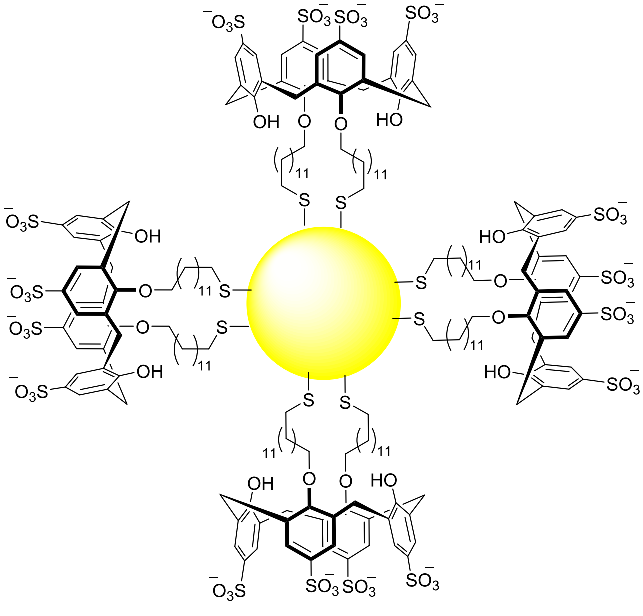

**N2.1**

**Figure 68.** *p*-Sulfonatocalix[4]arene-functionalized plasmonic AuNP (**N2.1**) for the detection of basic amino acids at $\mu$M concentration in PBS, pH 7.0.

emission is quenched. However, in the presence of aromatic L-amino acids, the rhodamine dye is displaced from the macrocyclic host by the stronger binding amino acid, resulting in the increase of the fluorescence of the QD. Further examples of enantioselective detection using CD-functionalized QDs have been reported for the detection of tyrosine, methionine, and histamine.[311,312]

Although QDs possess exquisite photophysical properties to be used for the preparation of fluorescent-based nanosensors, they can cause toxicity issues when applied for *in vitro* or *in vivo* application.[313] However, the toxicity of QDs can be reduced by building a biocompatible and protective shell around the particles, which prevents unwanted metal ion dissolution into biological environments. Tang, Liu, Tang, and coworkers developed $\beta$-CD functionalized and silica coated QDs for the enantioselective detection of His in PBS at $\mu$M concentrations (**N2.3** in Figure 70).[312] Upon addition of L-His to a dispersion of **N2.3**, an increased fluorescence emission intensity was observed, whereas the addition of D-His resulted in a much lower fluorescence enhancement. This enantioselective response was explained by the preferred binding of L-His to the $\beta$-CD moieties. It has been speculated that the observed luminescence enhancement after His binding is caused by rigidochromic effects. Besides the beneficial biological properties of a silica shell around QDs, coating of a nanoparticle also facilitates further surface functionalization *via* simple alkoxy-silane chemistry. For instance, other silica-based nanomaterials for the detection of amino acids were prepared from epitope-imprinted mesoporous silica particles[314] or molecularly imprinted silica particles.[315]

### Table 6. Summary of Nanosensors for Amino Acids and Proteins (LOD, Limit of Detection)

| nanosensor | media | concentration range | ref |
|---|---|---|---|
| | Arginine (Arg) Analyte | | |
| **N2.1** | PBS, pH 7.4 | 0–100 $\mu$M; LOD, 4.0 $\mu$M | 308 |
| | Albumin (HSA, BSA, MSA) Analyte | | |
| **N2.4** | 1× PBS, pH 7.0 | 0–100 mg $L^{-1}$ | 316 |
| | urine samples | 0–400 mg $L^{-1}$ | |
| | Cysteine (Cys) Analyte | | |
| **N2.6** | water | 0–100 $\mu$M in water; LOD, 150 nM in water | 323 |
| | artificial serum samples | 100 $\mu$M in serum | |
| | Histidine (His) Analyte | | |
| **N2.1** | PBS, pH 7.4 | 0–75 $\mu$M; LOD, 2 $\mu$M | 308 |
| **N2.3** | PBS, pH 7.7 | 0–60 $\mu$M for D-His; 0–20 $\mu$M for L-His | 312 |
| | Lysine(Lys) Analyte | | |
| **N2.1** | PBS, pH 7.4 | 0–100 $\mu$M; LOD, 1.0 $\mu$M | 308 |
| | Tyrosine(Tyr) Analyte | | |
| **N2.2**[a] | 100 mM phosphate buffer, pH 10.3 | 0–500 $\mu$M | 309 |
| | Phenylalanine (Phe) Analyte | | |
| **N2.2**[a] | 100 mM phosphate buffer, pH 10.3 | 0–500 $\mu$M | 309 |
| | Thrombin Analyte | | |
| **N2.5** | 25 mM HEPES buffer, pH 7.4 | 0–2.0 $\mu$M; LOD, 25 nM | 318 |

[a] Cross-reactivity with histamine.

Carbon-based nanomaterials such as single-walled carbon nanotubes (SWCNTs) are attractive candidates for sensing applications because they can serve as NIR-emitters which have good transparency to biological tissues. The optical properties of such fiber-like structures strongly depend on their surface (corona) composition. The use of polymer-functionalized SWCNTs for the detection of albumin in urine samples has been recently reported by Heller and coworkers (**N2.4** in

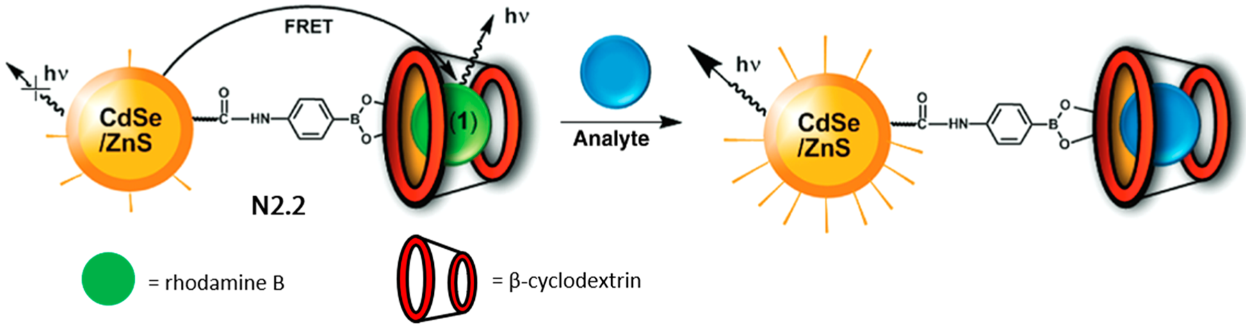

**Figure 69.** Core-shell quantum dots (**N2.2**) for enantioselective and fluorescence-based detection of tyrosine and phenylalanine in 100 mM phosphate buffer, pH 10.3. Reproduced with permission from ref 309. Copyright 2009 American Chemical Society.

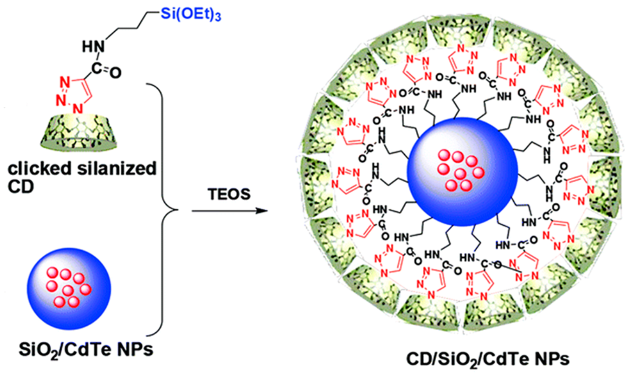

**N2.3**

**Figure 70.** Schematic representation of the preparation of *β*-CD-functionalized and QD-doped silica particles (**N2.3**) enabling fluorescence-based detection of L-His in PBS, pH 7.7, at *μ*M concentrations. Adapted with permission from ref 312. Copyright 2016 The Royal Society of Chemistry.

Figure 71).[316] In this example, the authors functionalized SWCNTs with various polycarbodiimide polymers that have polyethylene glycol and amine moieties. These functional groups are thought to bind human albumin through electrostatic and hydrophobic interactions. Once albumin interacted with the polymer layer, a hypsochromic shift in the emission of **N2.4** emission was observed, which was attributed to the previously described solvatochromic behavior of SWCNTs[317] and was used for protein quantification. The sensitivity obtained for albumin detection in urine samples (3 mg $L^{-1}$) was comparable to commercial immunoturbidimetry assays used in clinics (1 mg $L^{-1}$), indicating the potential of **N2.4** as a functional sensor for detection of microalbuminuria.

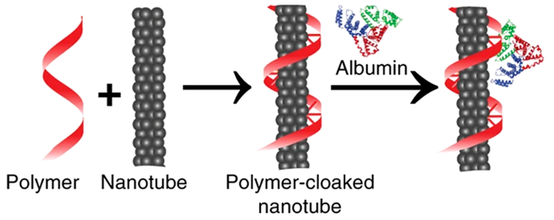

**N2.4**

**Figure 71.** Polymer modified single-walled carbon nanotubes (**N2.4**) used for the detection of albumin in 1× PBS and urine samples. Adapted with permissions from ref 316. Copyright 2019 Springer Nature.

König and coworkers designed phospholipid-based vesicles with thrombin-binding aptamers and fluorescent dyes embedded in the membrane (**N2.5** in Figure 72).[318] These vesicles have been successfully applied for fluorescence-based detection of thrombin at *μ*M concentrations in 25 mM HEPES buffer, pH 7.4. Proteins present in the sample bind to the aptamer moiety, resulting in an increase of emission from the receptor dye (pyrene or rhodamine dye derivatives). The increase in fluorescence was explained by the conformational change of the aptamer upon protein binding. The use of vesicle presents a useful strategy when multifunctional nanoparticles need to be prepared for sensing and drug delivery applications.[319,320] Nevertheless, a main disadvantage of phospholipid-based vesicles is their insufficient shelf-stability. Covalently cross-linked polymersomes[321] or more stable vesicular structures, such as quatsomes,[322] may be suitable alternatives.

Metal–organic frameworks (MOFs) are micro- to mesoporous crystalline materials that are composed of metal ion (clusters) and organic ligands as the building blocks. Lanthanide-MOFs are interesting nanoparticles for the preparation of fluorescence-based sensors due to their high stability and monochromaticity of emission.[324] Yang, Fan, and coworkers recently reported the preparation of a novel and fluorescent anionic MOF, $[[Eu_2K(bpda)_4(C_2H_5OH)]\cdot(H_3O)\cdot(H_2O)_x]_n$ (bpda = 2,2′-bipyridine-6,6′-dicarboxylic acid), for the detection of cysteine in water and artificial blood samples at *μ*M concentrations (**N2.6** in Figure 73).[323] The $[Eu(bpda)_2]^-$ subunits were linked through $K^+$ cations forming **N2.6**. When the MOF is immersed in $Fe^{3+}$ solutions, its emission is efficiently quenched due to the adsorption of iron cations in the porous framework, where they quench the lanthanide luminescence *via* electron transfer processes. However, when cysteine was added, it promoted the depletion of ferrous ions from the MOF, restoring its fluorescence properties. The authors showed that other possible interfering species (*e.g.*, $Na^+$, $K^+$, $Cl^-$, $PO_4^{2-}$, GSH, His, Lys, glucose, dopamine, phenylalanine, and ascorbic acid) did not affect the performance of **N2.6**.

Other systems for protein detection using nanosensors have been demonstrated with array-based sensing platforms ("chemical nose/tongue") in which multiple sensing elements on the surface of the nanoparticles, *i.e.*, fluorescent dyes[325] or proteins,[326] interact with the target analytes to produce a unique pattern of optical response that enable analyte identification. This approach offers unique opportunities compared to highly specific sensing elements such as antibodies, as these relatively simple cross-reactive arrays

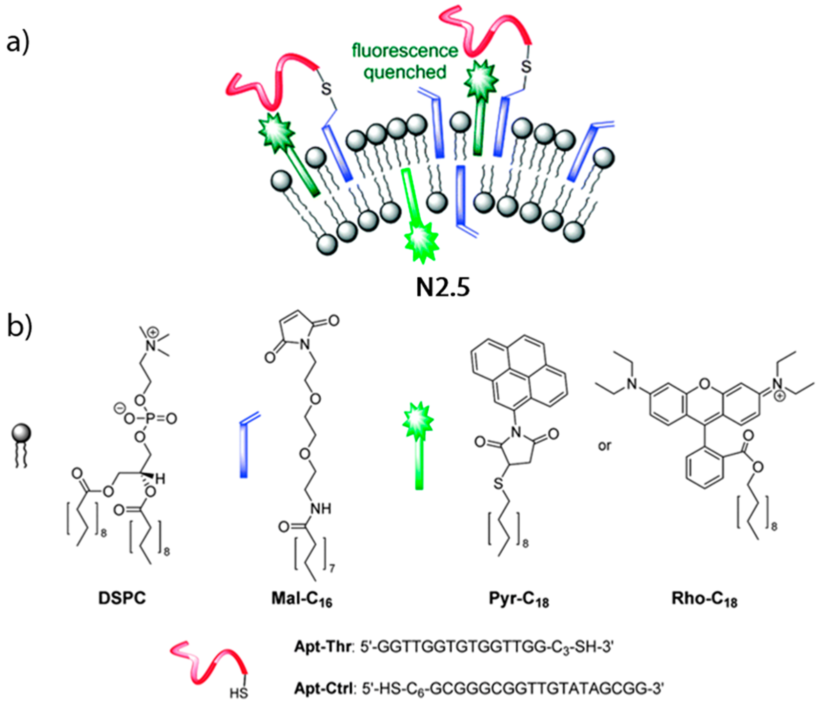

**Figure 72.** (a) Fluorescent vesicles (**N2.5**) used for the detection of thrombin in buffered solutions. (b) Chemical structures of vesicle components. Reproduced with permission from ref 318. Copyright 2014 The Royal Society of Chemistry.

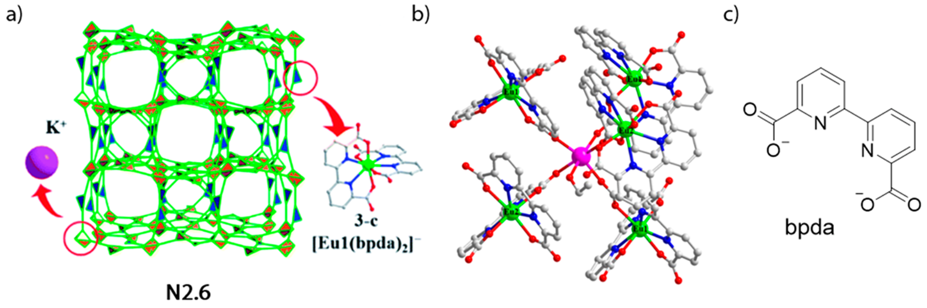

**Figure 73.** (a) Schematic representation of the luminescent anionic MOF containing the luminescent $[Eu(bpda)_2]^-$ subunits linked to $K^+$ ions (**N2.6**). (b) Crystal structure of **N2.6**. Reproduced with permission from ref 323. Copyright 2020 The Royal Society of Chemistry. (c) Chemical structure of the organic ligand 2,2′-bipyridine-6,6′-dicarboxylate (bpda).

provide unique opportunities for identifying changes in complex biological mixtures. Notable work on the development of nanoparticle-based "chemical noses" has been reported by the Rotello group,[325,327,328] which showed that these array-based sensors excel at discriminating small changes in complex mixtures and represent promising systems that can serve as new tools for future sensing technologies. Because the topic of array-based sensors with "chemical noses" has already been extensively covered in the literature, we refer the reader to these reviews for a detailed presentation on this type of array-based nanosensors.[329,330]

To evaluate the current state-of-the-art of probes, chemosensors, and nanosensors for potential applications in molecular diagnostics of amino acids, peptides, and proteins, Table 7 lists the typical concentration of amino acid occurrence in biofluids. By now, there is a range of systems available that are operational in water, buffers, or even biofluids, with affinities and sensitivity high enough to warrant a practical application. However, a major limitation appears to be the lack of selectivity, which still hampers the use of such systems for single- or multiparameter diagnostics.

## 3. AMINES (OTHER THAN AMINO ACIDS)

Polyamines are a class of natural and synthetic organic amines with at least two or more amino groups and exist as polycationic species at physiological pH (Figure 74). Endogenously, polyamines are synthesized from ornithine by the activity of ornithine decarboxylase, resulting in the formation of putrescine, the building block for further biosynthesis of other polyamines such as spermidine and spermine.[343] Because of their positive charge, polyamines can interact with negatively charged biomolecules such as DNA, RNA, and proteins through electrostatic interactions. Therefore, this class of amines is involved in many biological processes, most of which are related to cell growth, survival, and proliferation.[344,345] At normal concentrations, some polyamines have cardioprotective and neuroprotective effects, improve age-related metabolic decline, and stimulate immune surveillance against cancer.[346,347] Furthermore, other types of polyamines such as cadaverine and agmatine are produced by microorganisms that play an important role in the human microbiome.[345,348−350] As major components of the polyamine

Table 7. Summary of the Normal Concentration Range of Amino Acids in Biofluids[a]

| concentration range | media | ref |
|---|---|---|
| L-Alanine (Ala) Analyte | | |
| 259−407 μM | blood | 331 |
| 7.10−43.0 μmol/mmol creatinine = 71.0−430 μM | urine | 50 |
| 10.9−17.1 μM | saliva | 332 |
| L-Arginine (Arg) Analyte | | |
| 100−160 μM | blood | 333 |
| 3.80−18.6 μmol/mmol creatinine = 38.0−186 μM | urine | 50 |
| 5.20−9.80 μM | saliva | 332 |
| L-Asparagine (Asn) Analyte | | |
| 16.4−57.2 μM | blood | 334 |
| 3.00−26.0 μmol/mmol creatinine = 30.0−260 μM | urine | 50 |
| 0.76−3.48 μM | saliva | 335 |
| L-Aspartic Acid (Asp) Anayte | | |
| 14.8−27.0 μM | blood | 333 |
| 0.43−0.82 μmol/mmol creatinine = 4.30−8.20 μM | urine | 336 |
| 13.9−52.7 μM | saliva | 62 |
| L-Glutamine (Gln) Analyte | | |
| 400−587 μM | blood | 333 |
| 19.1−77.9 μmol/mmol creatinine = 191−779 μM | urine | 50 |
| 4.80−68.4 μM | saliva | 337 |
| L-Glutamic Acid (Glu) Analyte | | |
| 9.00−39.0 μM | blood | 331 |
| 3.30−18.4 μmol/mmol creatinine = 33.0−184 μM | urine | 50 |
| 11.2−16.0 μM | saliva | 332 |
| Glycine (Gly) Analyte | | |
| 224−436 μM | blood | 333 |
| 24.0−128 μmol/mmol creatinine = 0.24−1.28 mM | urine | 50 |
| 1.00−472 μM | saliva | 338 |
| L-Histidine (His) Analyte | | |
| 116−170 μM | blood | 333 |
| 17.0−90.0 μmol/mmol creatinine = 170−900 μM | urine | 50 |
| 7.00−9.40 μM | saliva | 332 |
| L-Isoleucine (Ile) Analyte | | |
| 30.0−108 μM | blood | 339 |
| 0.50−2.7 μmol/mmol creatinine = 5.0−27 μM | urine | 50 |
| 0.40−10.4 μM | saliva | 332 |
| L-Leucine (Leu) Analyte | | |
| 98.0−148 μM | blood | 331 |
| 1.40−2.30 μmol/mmol creatinine = 14.0−23.0 μM | urine | 336 |
| 4.00−12.2 μM | saliva | 332 |
| L-Lysine (Lys) Analyte | | |
| 184−216 μM | blood | 340 |
| 3.70−51.3 μmol/mmol creatinine = 37.0−513 μM | urine | 50 |
| 4.60−15.0 μM | saliva | 332 |
| L-Methionine (Met) Analyte | | |
| 21.0−29.0 μM | blood | 331 |
| 0.70−2.70 μmol/mmol creatinine = 7.00−27.0 μM | urine | 341 |
| 2.90−14.7 μM | saliva | 62 |
| L-Phenylalanine (Phe) Analyte | | |
| 50.0−107 μM | blood | 333 |
| 5.00−11.3 μmol/mmol creatinine = 50.0−113 μM | urine | 50 |
| 7.50−14.1 μM | saliva | 332 |
| L-Proline (Pro) Analyte | | |
| 133−263 μM | blood | 333 |
| 410−660 nmol/mmol creatinine = 4.10−6.60 μM | urine | 336 |
| 1.50−21.3 μM | saliva | 332 |
| L-Serine (Ser) Analyte | | |
| 133−186 μM | blood | 333 |
| 10.4−35.8 μM μmol/mmol creatinine = 104−358 μM | urine | 50 |
| 9.50−12.1 μM | saliva | 332 |
| L-Threonine(Thr) Analyte | | |
| 87.0−167 μM | blood | 333 |
| 6.40−25.2 μmol/mmol creatinine = 64.0−252 μM | urine | 50 |
| 0.10−7.30 μM | saliva | 332 |
| L-Tryptophan (Trp) Analyte | | |
| 45.0−64.0 μM | blood | 333 |
| 2.10−9.30 μmol/mmol creatinine = 21.0−93.0 μM | urine | 50 |
| 0−1.00 μM | saliva | 342 |
| L-Tyrosine (Tyr) Analyte | | |
| 45.0−64.0 μM | blood | 333 |
| 6.10−23.0 μmol/mmol creatinine = 61.0−230 μM | urine | 50 |
| 11.0−18.0 μM | saliva | 332 |
| L-Valine (Val) Analyte | | |
| 150−273 μM | blood | 333 |
| 2.70−9.80 μmol/mmol creatinine = 27.0−98.0 μM | urine | 50 |
| 1.90−20.7 μM | saliva | 332 |

[a] Urinary analyte concentrations were converted assuming a representative creatinine level of 10 mmol/L.

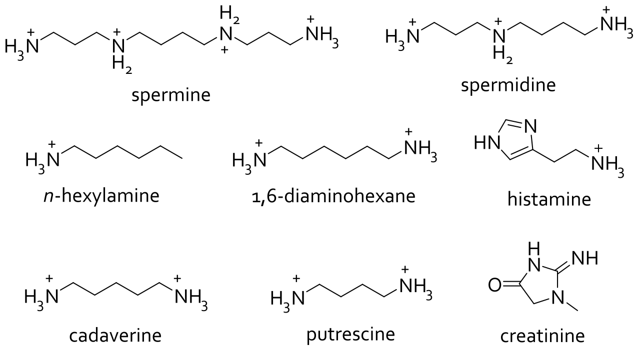

**Figure 74.** Chemical structures of selected amines and polyamines. Note: at physiological pH in biofluids, amines are (partially) protonated.

metabolic pathway, putrescine, spermidine, and spermine can be linked to many diseases such as cystic fibrosis,[351] stroke,[352−354] renal failure,[354,355] Parkinson's disease,[356] as well as heart failure[357] and cardiac infarction.[357,358] For example, a significant decrease in spermidine and spermine levels alongside with an increased putrescine level was observed in the plasma of stroke patients within the first 20 days after their stroke.[352] Impaired polyamine and arginine metabolism were found in humans with mild cognitive impairments (MCIs) and Alzheimer's disease (AD).[359−361] For example, spermidine levels in plasma were lower in both groups of MCIs and AD patients compared to the healthy group, and the concentration of spermine was increased in the MCI group but decreased in the subgroups of MCIs patients who transitioned to AD.[361] In addition, high polyamine levels are usually found in cancer cells,[347,362,363] and their urinary and plasma concentrations may be useful markers of cancer.[364−368] For example, urinary diacetylspermine has been identified as a biomarker for lung and ovarian cancer.[369−372] Importantly, diacetylspermine in urine can be a more sensitive marker for various cancers in humans than commonly used biomarkers and can be used to identify colorectal or breast cancers at an early stage.[347] With the exception of aromatic amine neurotransmitters, an important class of analytes highlighted in section 4, biogenic amines are often formed as product of a catabolic pathway and, at elevated concentrations, can be harmful to many organisms, including human beings. Indeed, biogenic amines such as putrescine and cadaverine are known food spoilage indicators and highly toxic in larger quantities (Figure 74).[373,374] The offensive odor that many amines display is in fact a universal indicator for danger arising from the exposure to amines. Likewise, many stimulating or hallucinogenic drugs and neurotoxic substances are amines, for instance, ephedrine or tryptamine and its derivatives, *e.g.*, 5-MeO-*N*,*N*-diisopropyltryptamine.[375] In general, for psychedelic drugs, achieving a good detection limit is of high priority (∼ng drug per mL biofluid), explaining why contemporary analytical methods are based on LC-MS coupled formats.[376] In comparison, the detection of biogenic ubiquitous amines is less challenging because they naturally occur in the micromolar to millimolar concentration range in cells and biofluids.[377] In this review, we focus our attention on probes and chemosensors which are somewhat selective for amines over amino acids. As before, we restrict our attention in this review toward the detection of analytes in aqueous media and biofluids. The molecular probes, chemosensors, and nanosensors discussed within this section are summarized in Table 8 −10.

**Table 8. Summary of the Molecular Probes for Amines (LOD, Limit of Detection)**

| probe | media | concentration range | ref |
|---|---|---|---|
| | | Amines Analyte | |
| **P3.4**[a] | 10% THF in water | $\mu$M range; LOD, 75 $\mu$M (propylenediamine) | 393 |
| | | Cadaverine Analyte | |
| **P3.1** | 6.0 mM SDS in 50 mM HEPES buffer, pH 7.4 | $\mu$M range | 378 |
| | | Creatinine Analyte | |
| **P3.3** | 0.5% MeCN in 10 mM PBS, pH 7.2; human blood serum | 1−300 $\mu$M; LOD, 0.3 $\mu$M | 367 |
| | | Histamine Analyte | |
| **P3.1** | 6.0 mM SDS in 50 mM HEPES buffer, pH 7.4 | 0.1−1.2 mM | 378 |
| | | *n*-Hexylamine Analyte | |
| **P3.2** | 50% dioxane in water | 0−400 $\mu$M | 379 |
| | | Putrescine Analyte | |
| **P3.1** | 6.0 mM SDS in 50 mM HEPES buffer, pH 7.4 | $\mu$M range | 378 |
| | | Spermine Analyte | |
| **P3.1** | 6.0 mM SDS in 50 mM HEPES buffer, pH 7.4 | $\mu$M range | 378 |
| | | Spermidine Analyte | |
| **P3.1** | 6.0 mM SDS in 50 mM HEPES buffer, pH 7.4 | $\mu$M range | 378 |
| | | Tryptamine Analyte | |
| **P3.1** | 6.0 mM SDS in 50 mM HEPES buffer, pH 7.4 | $\mu$M range | 378 |
| | | Tyramine Analyte | |
| **P3.1** | 6.0 mM SDS in 50 mM HEPES buffer, pH 7.4 | $\mu$M range | 378 |

[a] *n*-Butylamine, *tert*-butylamine, benzylamine, cyclohexylamine, ethylenediamine, propylenediamine, cadaverine, morpholine, ephedrine, 4-aminopyridine, and ethanolamine can be distinguished from each other by the sensor array **P3.4**.

**Table 9. Summary of the Chemosensors for Amines**

| chemosensor | media | concentration range | ref |
|---|---|---|---|
| | Cadaverine Analyte | | |
| **C3.5** | water, pH 4.0 or 7.0 | 0−4.0 $\mu$M | 401 |
| | Creatinine Analyte | | |
| **C3.6** | aq $CH_2Cl_2$ | 0−10 mM | 404 |
| | Putrescine Analyte | | |
| **C3.5** | water, pH 4.0 or 7.0 | 0−4.0 $\mu$M | 401 |
| | Spermine Analyte | | |
| **C3.1** | 800 $\mu$M MOPS buffer, pH 7.0 | 0−400 nM | 394 |
| **C3.2** | 330 $\mu$M POC12 in water | 20−100 $\mu$M;<br>LOD 4.7 $\mu$M | 395 |
| **C3.3**[a] | 10 mM HEPES buffer, pH 7.4; artificial urine | 0−100 $\mu$M;<br>LOD 600 nM | 396 |
| **C3.4** | borate buffer, pH 8.5 | 0−3.0 $\mu$M | 400 |

[a] Spermidine gives a (much) weaker response.

### 3.1. Molecular Probes for Amines (Other than Amino Acids)

In the previous section, we have described probes for the detection of amino acids, such that we herein focus on probes that selectively detect amines.

In 2011, Severin and coworkers demonstrated that an aldehyde-containing coumarin probe (**P3.1** in Figure 75) selectively reacts with primary biogenic amines, such as spermine, spermidine, cadaverine, tryptamine, tyramine, and histamine, in 50 mM HEPES buffer, pH 7.4, that contains sodium dodecyl sulfate (SDS) as the surfactant.[378] Probe **P3.1** provided ratiometric changes in the absorbance spectra (350−500 nm) for most amines and a fluorescence turn-on response through the formation of a set of different products, including enamines and imines. Notably, the tested amino acids, glycine (Gly), histidine (His), cysteine (Cys), glutamic acid (Glu), and $\gamma$-aminobutyric acid (GABA) showed a much weaker response, possibly because the negatively charged SDS micelles prevent their encounter with the probe through charge repulsion. While the assay can detect amines in the micromolar concentration range, its prolonged reaction time of hours and need for high temperature around 50°C limits its utility, *e.g.*, for practical diagnostic purposes.

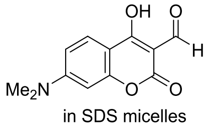

**P3.1**

**Figure 75.** Chemical structure of **P3.1**.

Wang, Cao, and coworkers recently showcased a nanoaggregate forming probe (**P3.2**) that responds to amines by bond detachment of, *e.g.*, B−N bonding motifs, and uncaging of fluorophores (Figure 76).[379] Probe **P3.2** was found to be particularly reactive towards primary amines with a reaction rates in the following order *n*-hexylamine >1,6-hexylenediamine ≫ spermine and spermidine in 50% dioxane in water. The authors also demonstrated that food spoilage, *e.g.*, of shrimps, can be monitored when **P3.2** is deposited on filter strips.

Creatinine, which is shown in Figure 77, is an aminofunctional heterocyclic compound that is produced in the organism

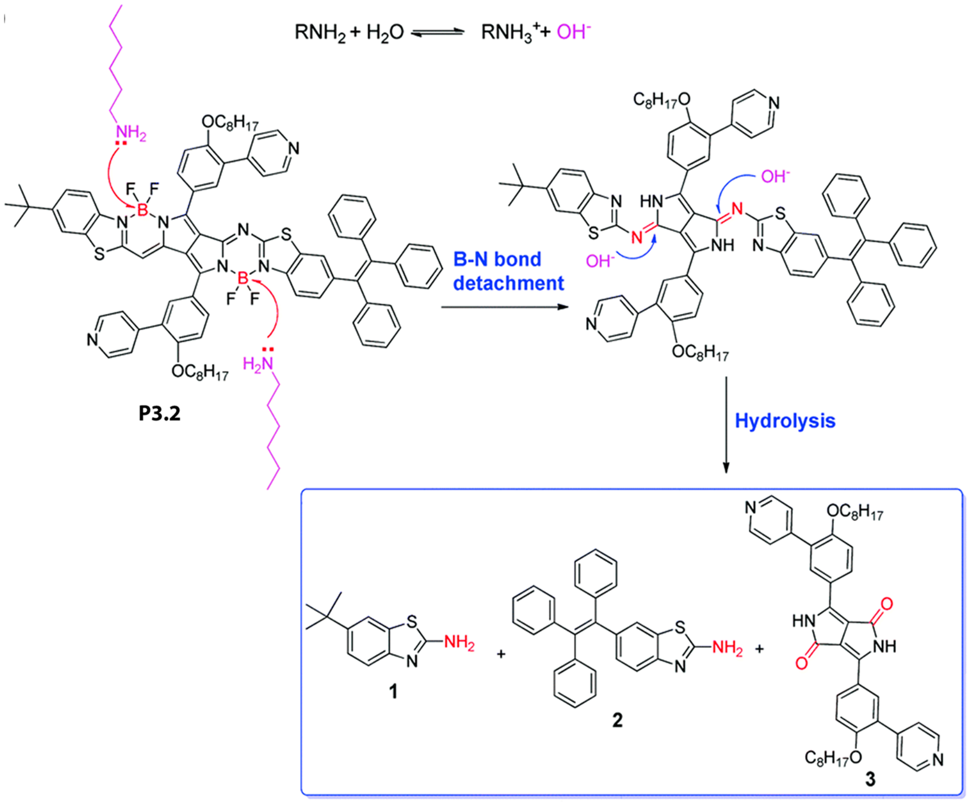

**Figure 76.** Reaction mechanism between **P3.2** and *n*-hexylamine. Reproduced with permission from ref 379. Copyright 2019 The Royal Society of Chemistry.

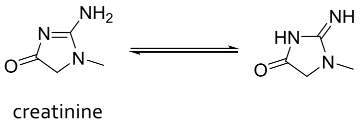

**Figure 77.** Chemical structure of creatinine and its tautomeric equilibrium.

through a reaction involving creatine phosphate and adenosine triphosphate (ATP). In healthy individuals, creatinine is mainly removed from the blood by the kidneys, and little to no tubular reabsorption occurs. Thus, elevated blood creatinine concentrations are an important kidney dysfunction indicator. Creatinine levels are also routinely checked in urine, and urinary biomarkers are frequently reported as a normalized ratio to urinary creatinine concentration to compensate for variations in urine volumes.[380] Creatinine can be detected by a long known colorimetric assay, the Jaffe reaction first introduced in 1886, which is based on the reaction of creatinine with alkaline picrate that yields an orange-red complex in alkaline medium within a few minutes of assay time. However, neither the exact structure of the formed product is clear nor is the reaction selective. It has been reported that various in biomedia omnipresent compounds such as glucose,[381] ketone bodies,[382] or bilirubin[383] produce a Jaffe-like chromophore that can interfere with creatinine quantification. These problems are particularly pronounced for creatinine determinations in blood serum. In urine, the Jaffe method is less prone to interferences due to the high abundance of creatinine and the lower number of interfering chromogens in this biofluid. Alternative methods for creatinine determination in blood (and urine) are therefore still on demand. Nowadays laboratories also routinely apply enzymatic assay kits with creatininase or creatinine deaminase[384−387] as well as GC-MS, LC-MS, and HPLC[388,389] for quantitative analysis of creatinine.[390,391]

In 2016, a fluorescence turn-on probe was disclosed by the Dhara group that is applicable for the selective detection and quantification of creatinine in 10 mM PBS and biofluids.[367] The authors exploited the metal-coordinating property of creatinine, which was found to displace “Pd” from the ethylene−diamine binding station that was installed to a naphthalimide core (Figure 78). Displacement of the emission quencher caused a 27-fold increase in the fluorescence

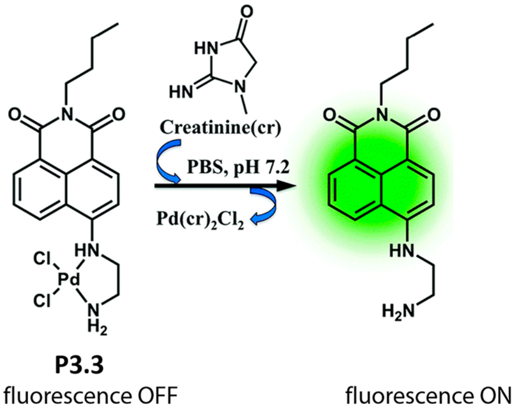

**Figure 78.** Proposed mechanism for the emission-based creatinine detection by an IDA-type metalorganic probe (**P3.3**). Reproduced with permission from ref 392. Copyright 2016 The Royal Society of Chemistry.

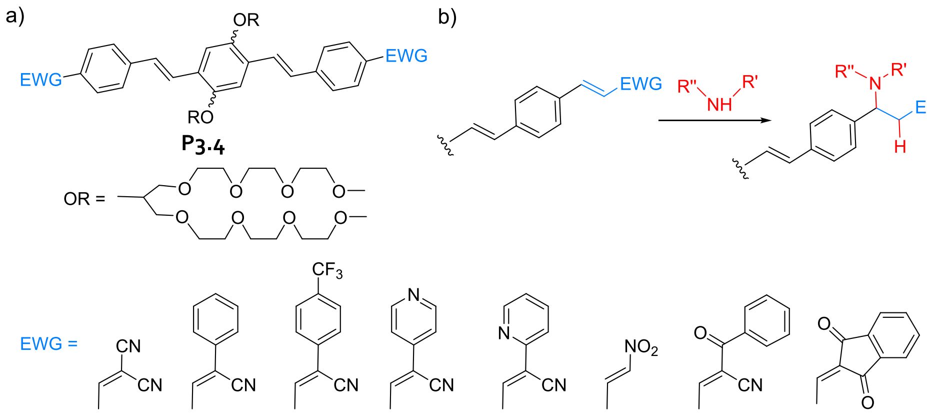

**Figure 79.** (a) Chemical structure of sensor array **P3.4** and (b) reaction of probe **P3.4** with an amine (EWG = electron withdrawing group). Adapted with permission from ref 393. Copyright 2015 American Chemical Society.

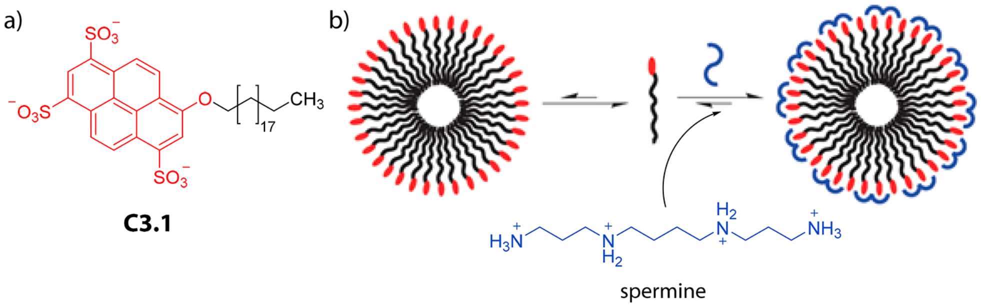

**Figure 80.** (a) The chemical structure of chemosensor **C3.1**. (b) Proposed mechanism of spermine detection with self-assembled chemosensor **C3.1**. Adapted with permission from ref 394. Copyright 2012 The Royal Society of Chemistry.

intensity of the probe in 0.5% MeCN in 10 mM PBS, pH 7.2, at 37°C. This probe was shown to be applicable for the determination of creatinine in human blood serum. The side-by-side evaluation of the new probe-based assay and the Jaffe method for creatinine quantification in seven blood serum samples gave promising results, suggesting that **P3.3** may be applied in clinical and toxicological analysis. The probe shows wide applicable concentration range and a superior detection limit of 0.3 $\mu$M in 10 mM PBS (up to 300 $\mu$M creatinine were tested). Importantly, **P3.3** is also more selective for creatinine than the Jaffe reagent, *e.g.*, glucose is not cross-reactive with **P3.3**. However, compared to the Jaffe method, this probe-based assay requires a longer assay time as the reaction of **P3.3** with creatinine is not completed after 30 min.

A recurring theme of this review is the difficulty to distinguish structurally similar analytes from each other by means of modestly selectively artificial receptors. Again, the most prudent strategy available today appears to set up array-based sensing formats that exploit differentially selective probes. In a proof-of-concept study, Bunz and coworkers established a sensing assay for the distinction of 11 different amines through an array that was composed of six reactive probes.[393] The distyrylbenzenedialdehyde-type probes (**P3.4**) were designed to form Knoevenagel adducts with the amines in 10% THF in water and provided characteristic, analyte-indicative spectroscopic fingerprints in the emission spectra upon reaction with the amines (Figure 79). The reaction times for the different probes varied between a few minutes to nearly an hour, and the detection limit for the amines ranged from 75 $\mu$M to 7.5 mM depending on the combination of probe and amine used. The probes were typically employed at low micromolar concentrations.

## 3.2. Chemosensors for Amines (Other than Amino Acids)

Unlike reactive probes that typically target nucleophilic, deprotonated amines, many chemosensor exploit the formation of ion-pairs, charge assisted hydrogen bonds, and cation−$\pi$ interactions for the noncovalent binding of protonated amines.

Capitalizing on the molecular recognition-based selectivity enhancements in self-assembled systems, Severin and coworkers designed a charge-frustrated amphiphile with a highly fluorescent and negatively charged pyrene-1,3,6-trisulfonate head group and a hydrophobic eicosane ($-C_{20}H_{41}$) tail (Figure 80).[394] This self-assembled chemosensor **C3.1** selectively responds through emission quenching to the presence of polycationic spermine, while other biogenic amines, including spermidine, cadaverine, serotonin, as well as amino acids, *e.g.*, Cys, Lys, and Phe, provided a much weaker signal change. Spermine can be detected in the low nanomolar regime, and only 200 nM suffice for a naked-eye detection in 800 $\mu$M MOPS buffer, pH 7.0. In 2016, Xu and coworkers included a squaraine dye into a pyrene-1,3,6-trisulfonate surfactant-based assembly (**C3.2**), thereby achieving a fluorescence turn-on assay for spermine.[395] It remains to be seen if such systems can be operational in biofluids containing high millimolar concentrations of salts that may interfere with the charge-mediated recognition process between the negatively charged micelle and the polycationic analyte.

A step toward an applicable urine test for spermine, which functions as a tumor marker,[397−399] has been made by the Kim group, establishing analyte-directed formation of emissive

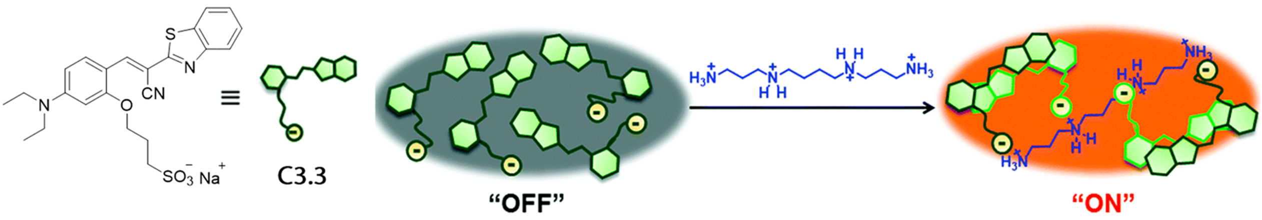

**Figure 81.** Schematic representation of a fluorescent turn-on sensing mechanism for polyamine cations using anionic chemosensor **C3.3**. Adapted with permission from ref 396. Copyright 2016 The Royal Society of Chemistry.

excimers in the presence of polyamines, particularly spermine.[396] The emission turn-on probe (**C3.3** in Figure 81) was operational in 10 mM HEPES, pH 7.4, and in artificial urine. Its spermine detection limit of 0.6 $\mu$M makes it potentially suitable for diagnostic applications.

Sulfonatocalix[*n*]arenes can be used for the detection of amines in aqueous media and show respectable binding affinities for amines. One representative example of an emissive *p*-sulfonatocalix[4]arene that can be used for the micromolar detection of spermine in borate buffer at pH 8.5 was introduced by the Geremia group.[400] The authors found that 2:1 and 1:1 calixarene•spermine complexes are formed, both showing only a slight emission quenching. However, when a tetracationic porphyrin was added to **C3.4** as a signal modulator, the fluorescence titration curve became significantly steeper upon spermine addition, enhancing the sensitivity of the assay (Figure 82).

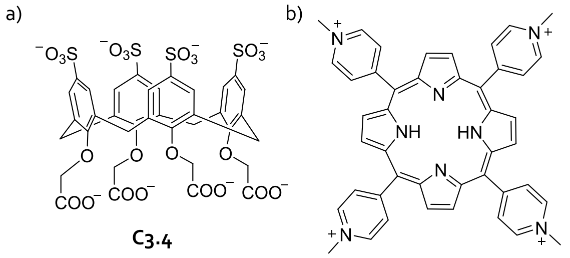

**Figure 82.** Chemical structures of (a) a *p*-sulfonatocalix[4]arene-based chemosensor (**C3.4**) and (b) a tetracationic porphyrin that can be used to modulate the sensitivity of chemosensor **C3.4** for the target analyte spermine.

Cucurbit[*n*]uril-based host–guest chemistry can be exploited for the detection of biogenic amines through IDA. For instance, a complex of CB6 as host with a chromophoric aminonaphthalimide–putrescine conjugate was reported by the Pischel group (**C3.5** in Figure 83). The detection of low micromolar concentrations of biogenic amines, *i.e.*, putrescine and cadaverine, at slightly acidic or under physiological pH was possible.[401]

Moreover, a recent example reported by Biedermann, Hirtz, and coworkers showed that CB*n*-based microarrays can be used for multiplex and highly sensitive detection of biogenic amines, *e.g.*, spermine, cadaverine, and amantadine, in dry air state and microfluidic channel. By this design, nM concentration regimes of cadaverine can be detected.[402] However, as it was pointed out before, the competitive binding of other metabolites and metal cations to the host always needs to be considered when attempting to extend CB*n*-based assays to applications in biofluids.

It is noteworthy that chirality sensing of amines is not directly possible with CB*n*-based chemosensors in an IDA format because CB*n* macrocycles are achiral. Isaacs and coworkers made a step towards chirality sensing of amines by preparing a chiral *nor-seco*-cucurbit[6]uril derivative as a racemic mixture that showed diastereoselective recognition of chiral amino acids and amines (see Figure 84).[403] Moderate to good levels of diastereoselectivity towards Phe (88:12), and its derived amino alcohol (*S*)-2-amino-3-phenylpropanol (76:24) were deduced from $^1$H NMR experiments in $D_2O$. Interestingly, it was even possible to distinguish between the enantiotopic groups of the *meso*-compound (1*R*,2*S*)-1,2-diphenylethane-1,2-diamine (74:26). When (chiral) indicator dyes become available for this host, it may find future use for absorbance or fluorescence-based sensing of chiral amines in aqueous media.

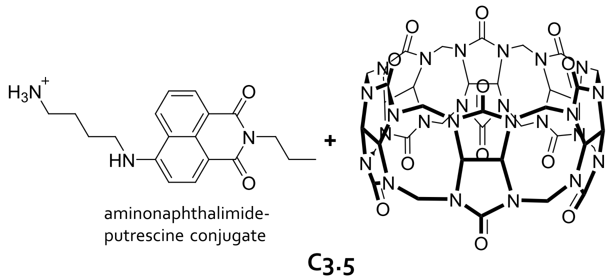

**Figure 83.** A fluorescent indicator dye that in combination with the host CB6 can be used as a chemosensing ensemble (**C3.5**) for the detection of biogenic amines in aqueous media.

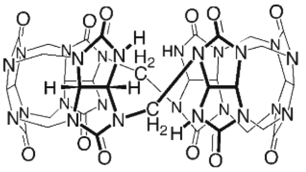

**Figure 84.** Chiral host *nor-seco*-cucurbit[6]uril diastereoselectively recognizes some chiral amines in aqueous media.

Notable efforts were also made to develop chemosensors for the detection of creatinine in aqueous media. The design of receptors that can strongly bind creatinine in water is a challenge due to the high hydrophilicity of the target analyte. A possible work-around was presented by the Bell group, who designed a hydrogen-bonding receptor **C3.6** which is capable of binding creatinine in chlorinated organic solvents that were saturated with water.[404] Under such conditions, the binding affinity was relatively strong, *i.e.*, $K_a = 2 \times 10^6$ $M^{-1}$ in aq $CHCl_3$. The unique color signal response upon binding the target analyte was proposed to stem from an intramolecular proton shift from one end of the receptor to the other; see Figure 85 for a schematic depiction of the binding mechanism. The system was found to be selective for creatinine relative to

Table 10. Summary of the Nanosensor for Amines (LOD, Limit of Detection)

| nanosensor | media | concentration range | ref |
|---|---|---|---|
| | Cadaverine Analyte | | |
| **N3.10**[a] | water | 3 μM−1 mM; LOD, 4 μM | 417 |
| **N3.11**[b] | water | 10 μM−1 mM; LOD, 13 μM | 417 |
| | Creatinine Analyte | | |
| **N3.13** | water, pH 5.0; artificial and real urine samples | 15−35 μM; LOD, 19 nM | 419 |
| **N3.14** | phosphate buffer, pH 7.0; blood samples; cerebrospinal fluid | 0.01−1 μM in buffer; LOD 8.4 μM in buffer | 421 |
| **N3.15** | phosphate buffer, pH 9.0; blood samples | 20−520 μM; LOD, 2 nM | 423 |
| **N3.16** | 10 mM NaOH solution, pH 12.0 | 0−12 μM; urine samples[a] | 424 |
| **N3.17** | 100 mM citrate buffer, pH 7.4<br>urine samples | 1.0−120 μM in buffer; LOD, 70 nM in buffer<br>8.3−9.4 μM in urine samples | 425 |
| **N3.18**[c] | water; artificial urine | μM range; LOD, 42−530 nM | 428 |
| **N3.19** | 10 mM phosphate buffer, pH 6.0; diluted serum[5] and urine samples | 0.05−200 μM (LOD, 4.7 nM) | 429 |
| | Diamino-benzenes/Phenylene-diamines Analyte | | |
| **N3.1**[d] | water, pH 6.1 | 0−100 μM for *m*-isomer; LOD, 1 μM for *m*-isomer<br>0−80 μM for *p*-isomer; LOD, 4 μM for *p*-isomer | 407 |
| **N3.2** | water | 1 μM−1 mM; LOD, 50 μM | 408 |
| | Methylamine Analyte | | |
| **N3.3** | water | 0.3 mM | 409 |
| | *n*-Heptylamine Analyte | | |
| **N3.12** | water, pH 7.0−10.0 | mM range | 418 |
| | *n*-Nonylamine Analyte | | |
| **N3.12** | water, pH 7.0−10.0 | mM range | 418 |
| | *n*-Octylamine Analyte | | |
| **N3.12** | water, pH 7.0−10.0 | mM range | 418 |
| | Spermine Analyte | | |
| **N3.4** | 0−100 mM NaCl in 10 mM HEPES buffer, pH 7.4; artificial urine | 0−200 μM | 410 |
| **N3.5** | 1× PBS, pH 6.0; serum and urine | 0−130 μM; LOD, 130 pM | 411 |
| **N3.7** | 1% DMF in water, pH 6.0−11.0; mushroom samples; meat samples | 0−2.6 μM; LOD, 36.2 nM | 414 |
| **N3.8** | 20 mM HEPES buffer, pH 7.4; urine samples; blood samples | μM range; LOD, 6 μM in buffer; 3−100 μM in biofluids | 415 |
| **N3.9** | 10 mM HEPES buffer, pH 8.0; meat samples | 0−1 μM in buffer; LOD, 76 nM in buffer | 416 |
| | Spermidine Analyte | | |
| **N3.4** | 0−100 mM NaCl in 10 mM HEPES buffer, pH 7.4; artificial urine | 0−200 μM | 410 |
| **N3.5** | 1× PBS, pH 6.0 | 0−100 μM; LOD, 636 pM | 411 |
| **N3.6** | water | 10 nM−100 μM | 412 |
| **N3.7** | 1% DMF in water, pH 6.0−11.0; mushroom samples; meat samples | 0−2.2 μM; LOD, 35 nM | 414 |
| **N3.8** | 20 mM HEPES buffer, pH 7.4; urine samples; blood samples | μM range in buffer; LOD, 6 μM in buffer; 3−100 μM in biofluids | 415 |

[a] Cross-reactivity with 4,4′-oxydianiline. [b] Cross-reactivity with 4,4′-oxydianiline and dopamine. [c] LOD wither determined by UV-Vis spectroscopy or for diluted synthetic urine samples with SERS.[2] Serum samples have been treated with MeCN for protein removal. [d] Other aromatic amines such as nitroaniline, chloroaniline, toluidine, and aniline did not lead to a detectable signal change.

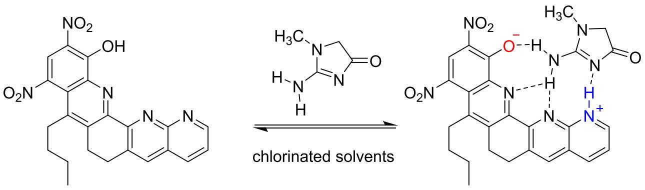

**C3.6**

**Figure 85.** Schematic representation of creatinine binding with chemosensor **C3.6**.

sodium, potassium, and ammonium ions. However, the suggested perspective on a potential applicability of the chemosensor in blood serum appears difficult and was not reached yet. In general, the transfer of binding principles developed and tested in organic solvents or aqueous-organic solvent mixtures to pure water, saline buffers, or biofluids has often proven to be a challenging obstacle.[16,405] Recently, Pischel, Ballester, and coworkers introduced calix[4]pyrrole phosphonate-cavitands as receptors for the detection of creatinine through an indicator displacement assay in chloroform ($K_a \sim 4 \times 10^5$ M$^{-1}$).[406] It remains to be seen if this new design is applicable for chemosensors that are operational in aqueous media and biofluids.

### 3.3. Nanosensors for Amines (Other than Amino Acids)

Li and coworkers prepared *p*-sulfonatocalix[6]arene-modified gold nanoparticles (**N3.1** in Figure 86), which were used as colorimetric nanosensors for the selective detection of constitutional isomers of diaminobenzenes at μM concentrations in water, pH 6.1.[407] Upon addition of ethanolic solutions of *meta*- or *para*-diaminobenzene to aqueous dispersions of **N3.1**, a distinct color change from red to blue occurred, which was attributed to the nanoparticle aggregation. No changes were observed in the presence of *ortho*-

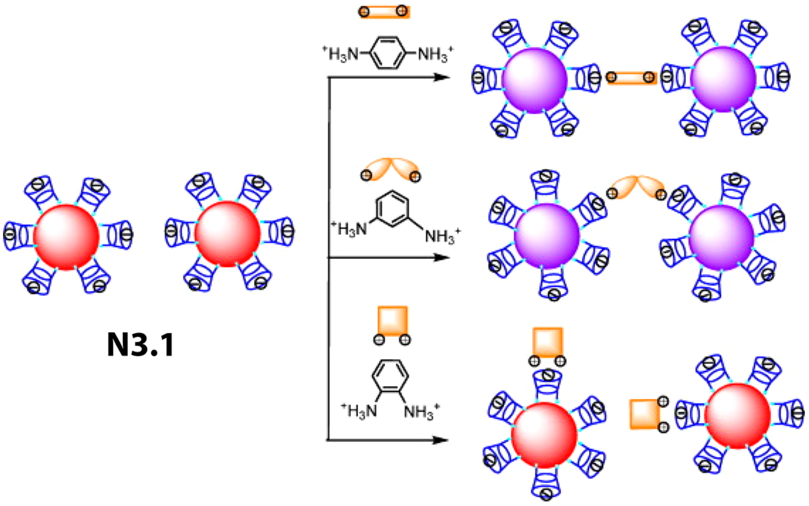

**Figure 86.** *p*-Sulfonatocalix[6]arene-modified gold nanoparticles **N3.1** used for colorimetric detection of diaminobenzene isomers at μM concentrations in water. Reproduced with permission from ref 407. Copyright 2009 Elsevier BV.

diaminobenzene. The distinct color response can be explained by host−guest interactions that preferentially occur between *p*-sulfonato[6]calix-arenes and *m*- as well as *p*-diaminobenzenes, causing a change in the plasmon resonance. These isomers crosslink the nanoparticles by forming supramolecular bridges between the particles. The selectivity of **N3.1** was investigated against other aromatic amines, such as nitroaniline, chloroaniline, toluidine, and aniline, which did not trigger particle aggregation due to weaker interactions with *p*-sulfonatocalix[6]arenes.

More recently, a colorimetric-based nanosensor (**N3.2** in Figure 87) with structural isomer selectivity towards phenylenediamines was reported by Zou and coworkers using β-cyclodextrin (β-CD)-functionalized silver nanoparticles.[408] The authors were able to distinguish all three different isomers, *i.e.*, *o*-, *m*-, and *p*-phenylenediamine by examining distinct color changes induced by each of the isomers. As depicted in Figure 87, the different color outcome was attributed to specific NP aggregations based on different degrees of host−guest interactions for each isomer-β-CD-combination. For example, the addition of *p*- and *m*-phenylenediamine resulted in a color change from the initial red appearing particle dispersion to black and magenta, respectively. The *ortho*-isomer gave slightly orange-colored dispersions. Constitutional isomers of phenylenediamines were detected spectroscopically with moderate detection limits in water (LOD, 50 μM).

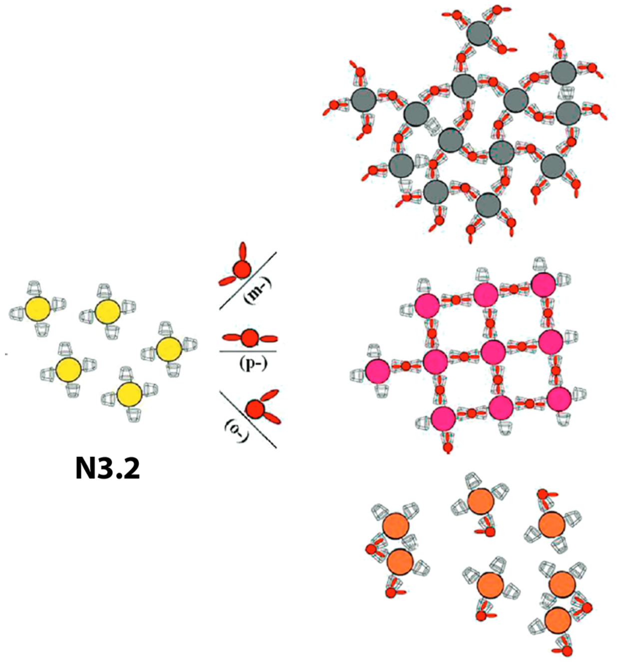

**Figure 87.** β-CD-functionalized silver nanoparticles **N3.2** used for the selective detection of phenylenediamine isomers in water. Adapted with permission from ref 408. Copyright 2010 American Chemical Society.

A unique approach for the colorimetric detection of small organic amines was reported by Corma, García, and coworkers, who prepared a supramolecular inclusion complex between a gold nanoparticle (AuNP) or Au clusters and the macrocyclic host cucurbit[7]uril (CB7, **N3.3** in Figure 88).[409] The encapsulation of approximately 1 nm-sized AuNPs in CB7 was achieved by gas-phase adsorption of gold atoms into cucurbit[7]uril powders, and the successful formation of the inclusion complex was deduced by absorption and energy electron loss spectroscopy. Colorimetric detection of amines with **N3.3** was carried out by absorption measurements. **N3.3** responds with large changes in the plasmonic energies, and therefore in the absorption of the nanoparticles as the amines

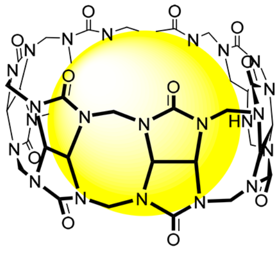

**N3.3**

**Figure 88.** Schematic representation of the supramolecular inclusion complex **N3.3** of a AuNPs and cucurbit[7]uril (CB7) used for the colorimetric detection of small aliphatic amines in water.

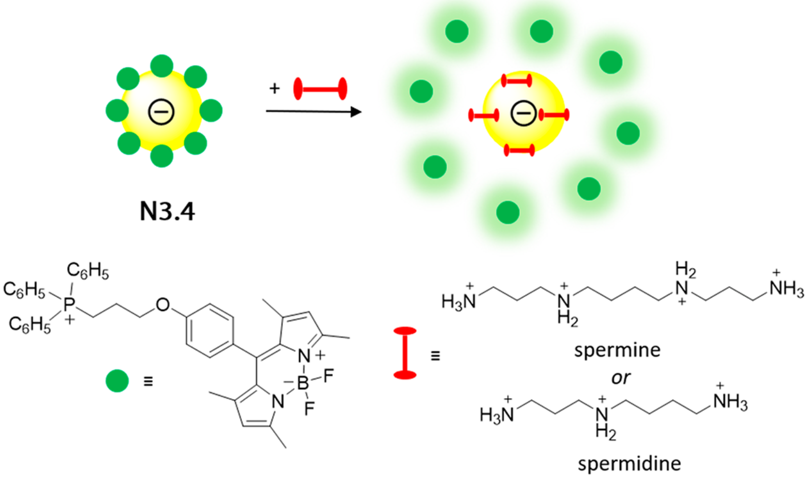

Figure 89. BODIPY-functionalized AuNPs (**N3.4**) used for fluorescent turn-on detection of spermine and spermidine in 10 mM HEPES buffer, pH 7.4, at $\mu$M concentrations.

displace the gold nanoparticle from the cavity of the macrocycle. The authors demonstrated that the displacement of gold nanoparticles occurred with methylamine but not with triphenylamine, indicating the sensor size selectivity towards small and sterically simple amines. Methylamine can be detected at concentrations of about 0.3 mM in water.

A sensitive fluorescence turn-on nanosensor for the detection of biologically active polyamines in 10 mM HEPES buffer, pH 7.4, was reported by Kim and coworkers.[410] The citrate-capped and BODIPY-functionalized gold nanoparticles (**N3.4** in Figure 89) showed quenched BODIPY emission due to an energy transfer processes between the plasmonic nanoparticle and the dye. The selectivity of the nanosensor towards spermidine and spermine over primary alkylamines can be rationalized by the stronger electrostatic interactions of the negatively charged nanoparticles with polyamines than with monoamines.

Kailase and coworkers reported the use of gold nanoparticles doped with oxidized tyrosine for the colorimetric detection of spermine and spermidine at $\mu$M and nM concentrations in 1× PBS, pH 6.0, and in biological samples (**N3.5** in Figure 90).[411] The electrostatic interaction of the negatively charged **N3.5** with polyamines leads to the formation of large **N3.5**-amine aggregates. These aggregates exhibit a bathochromic shift in their SPR absorption band compared to non-aggregated **N3.5**, such that a visible color change from originally blue to red is observed as the aggregates absorb red light. Moreover, quantitative polyamine detection was also demonstrated by fluorescence spectroscopy. The authors showed that the presence of several (alkali) metals, halogen anions, as well as biological relevant amines and amino acids, urea, and heparin did not affect the performance of **N3.5**. It was therefore possible to determine spermine and spermidine in spiked serum and urine samples with good recoveries (>99%).

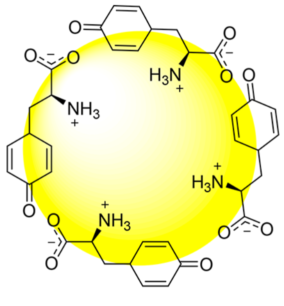

**N3.5**

Figure 90. Oxidized tyrosine-doped gold nanoparticles **N3.5** used for colorimetric detection of the biogenic polyamines spermidine and spermine at nM and $\mu$M concentrations in PBS and biological samples.

Smartphone-based and femtomolar detection of spermidine in Milli-Q water was recently reported by Chandran, Ramamurthy, and coworkers through the analysis of surface plasmon coupled emissions (SPCE) of rhodamine using gold-silica nanohybrids (AuSils) as spacers (**N3.6** in Figure 91).[412]

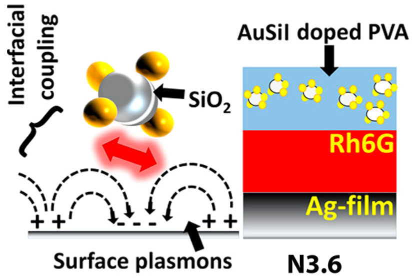

**N3.6**

Figure 91. Surface plasmon coupled emission-based detection of spermidine at fM concentrations in water using silica gold nanohybrid particles (**N3.6**). Reproduced with permission from ref 412. Copyright 2020 American Chemical Society.

In this example, a newly SPCE device with reverse Kretschmann configuration[413] was developed with which SPCE emissions were analyzed by using an extended cavity interface. To prepare the plasmonic and amine responsive device, poly(vinyl alcohol) dispersions of AuSils were deposited on a rhodamine-coated silver substrate. The treatment of such films with aqueous solutions of spermidine led to an 88-fold increase (compared to untreated films) in SPCE fluorescence of rhodamine. The increase in SPCE emission was explained by the ability of polyamines to coordinate and crosslink AuSils and therefore trigger interparticle aggregation on films, ultimately shortening

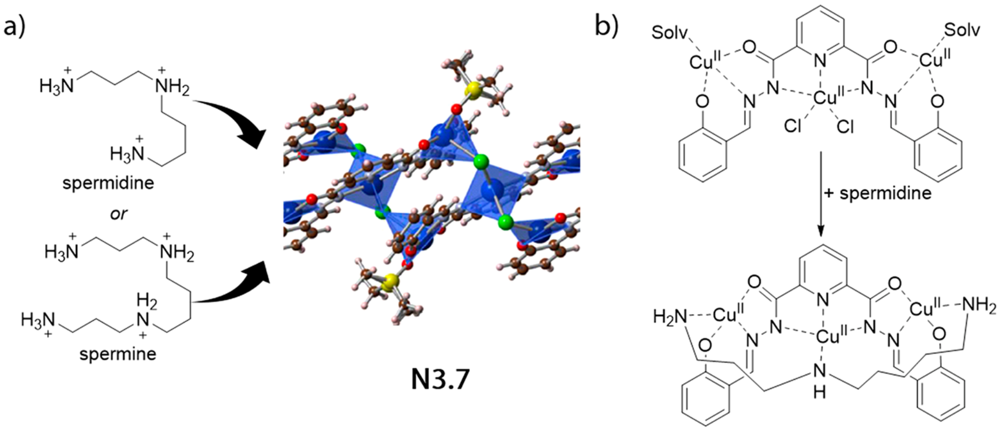

**Figure 92.** (a) Polyamines such as spermine and spermidine diffuse into the pores of Cu$^{II}$ complex-based nanoparticles (**N3.7**). (b) Polyamines displace the solvent from the Cu$^{II}$ centers, changing the photophysical properties of **N3.7** and allowing the detection of spermine and spermidine at nM concentrations in water. Adapted with permission from ref 414. Copyright 2017 American Chemical Society.

intraparticle distances and creating optimal plasmonic hotspots for rhodamine. The modulation in the fluorescence was recorded using a smartphone camera, and color processing was analyzed using a smartphone application. Other biogenic polyamines such as cadaverine and putrescine did not significantly increase the sensor response. However, spermine was found to produce an SPCE emission signal, but it was orders of magnitude lower (the relative emission compared to spermidine is only about 25%). The authors attributed the lower signal intensities of spermine to excessive clustering of AuSil due to the increased amount of −NH functionalities in spermine compared to spermidine. To evaluate the full potential of **N3.6** for polyamine detection in a more realistic scenario, future performance studies of **N3.6** will need to include biofluids, as cations or other positively charged species in such fluids might lead to clustering of AuSils, which would cause adverse signal interference.

Nanometer-sized aggregates, composed of trinuclear Cu$^{II}$ complexes, were used by Kaur and coworkers for colorimetric detection of spermine and spermidine at nM detection in water (**N3.7** in Figure 92).[414] The nanosensors showed a characteristic enhanced fluorescence compared to the monomer dissolved species due to the aggregation-induced emission enhancement (AIE). When polyamine solutions were added to dispersions of **N3.7** in water (pH 6.0−11.0), a significant change in UV−vis absorption spectra and decreasing fluorescence intensities were observed. The change in photophysical properties was caused by the diffusion of polyamines into the pores of the nanoparticles (Figure 92a), where they change the coordination sphere of Cu$^{II}$ by displacing solvent molecules (Figure 92b).

A fluorescent nanosensor for the $\mu$M detection of biogenic polyamines in 20 mM HEPES buffer, pH 7.4, blood and urine samples was reported by Ganguly, Chatterjee, and coworkers (**N3.8** in Figure 93).[415] In this work, the authors used emissive 3-((7-hydroxy-4-methylcoumarin)-methylene)-aminophenylboronic acid-doped agarose nanoparticles, which showed increased fluorescence intensity in the presence of the polyamines spermine and spermidine. The enlarged photoluminescence quantum yield was attributed to the formation of complexes with H-bonding interactions between ammonium groups, imines, and boronic acids. The authors showed that **N3.8** is not adversely affected by other biomolecules, *e.g.*, nucleobases, sugars, metal cations, and inorganic anions. In spiked urine and blood serum samples, **N3.8** was able to detect spermine with a linear signal response of 3−100 $\mu$M. There was a good correlation with spermine concentrations obtained from HPLC. Other biorelevant molecules, *i.e.*, adenine, thiamine, uracil, cytosine, guanine, and several cations and sugars, did not cause any interferences in HEPES buffer.

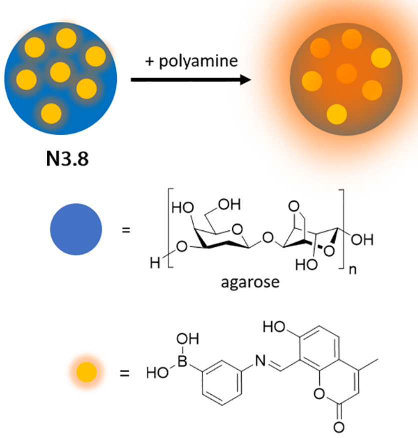

**Figure 93.** 3-((7-Hydroxy-4-methylcoumarin)methylene)-aminophenylboronic acid-doped agarose nanoparticles (**N3.8**) used for the detection of spermine and spermidine in HEPES buffer, blood, and urine samples at $\mu$M concentrations.

Recently, Huan, Lan, Song, and coworkers reported the use of carbon dots and cadmium telluride quantum dots (CdTe QDs) for the emission-based ratiometric detection of spermine in 10 mM HEPES buffer, pH 8.0, and pork meat samples at $\mu$M concentrations (**N3.9**).[416] The characteristic red fluorescence of CdTe was effectively quenched by samples which contained spermine, whereas the blue fluorescence of carbon dots remained unaltered, enabling ratiometric detection. The particles can be deposited on paper stripes *via* a simple impregnation procedure, retaining their characteristic fluorescent response to polyamines. The change in the photoluminescence properties of **N3.9** in the presence of spermine was attributed to the formation of multiple hydrogen bonds and strong electrostatic interaction between the analyte and the CdTe QDs.

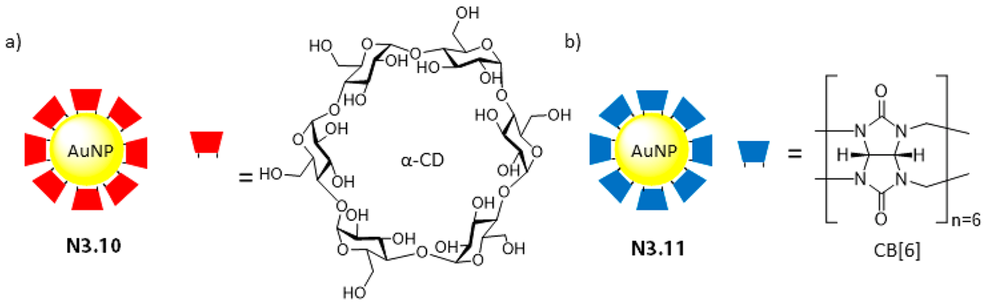

**Figure 94.** (a) $\alpha$-cyclodextrin (**N3.10**) and (b) CB6 (**N3.11**) functionalized gold nanoparticles used for colorimetric detection of cadaverine in water samples at $\mu$M concentrations.

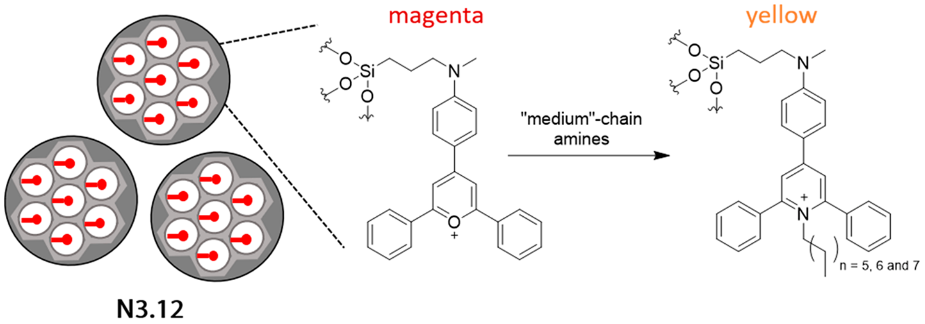

**Figure 95.** 2,4,6-Triphenylpyrylium-functionalized and hexamethyldisilazane surface passivated mesoporous silica nanoparticles (**N3.12**) used for colorimetric detection of aliphatic amines in water (pH 7.0−10.0).

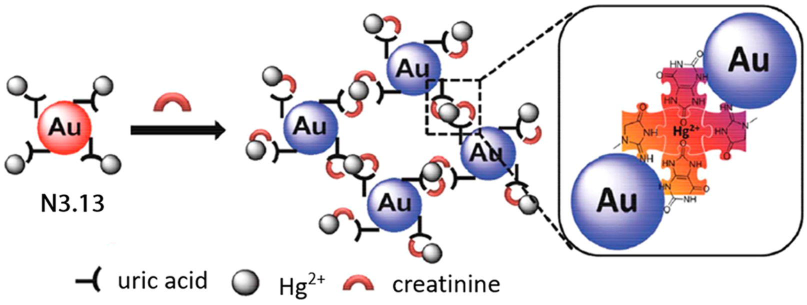

**Figure 96.** Uric acid-functionalized and $Hg^{2+}$-doped gold nanoparticles (**N3.13**) aggregate in the presence of creatinine, allowing for its detection at $\mu$M concentrations in water, pH 5.0, in artificial urine and in real urine. Reproduced with permission from ref 419. Copyright 2015 Wiley-VCH.

Quintana and coworkers prepared $\alpha$-cyclodextrin ($\alpha$-CD) and cucurbit[6]uril (CB6) decorated gold nanoparticles for the colorimetric sensing of $\mu$M concentrations of cadaverine in water (**N3.10** and **N3.11** in Figure 94).[417] The analyte was detected by the formation of host−guest complexes, which triggered interparticle crosslinking and aggregation, resulting in a color change of the nanoparticle dispersion. While the interaction of CB6 with polyamines is known for its high affinity,[233,234] it is curious that $\alpha$-CD functionalized **N3.10** also responded to polyamines despite the only weak inclusion complex formation of CDs with positively charged guests. Although simple to use, both **N3.10** and **N3.11** require long assay times (approx. 4 h) for reaching acceptable detection limits. The nanosensor **N3.10** was reported to show cross-reactivity with 4,4′-oxydianiline, whereas **N3.11** reacted with 4,4′-oxydianiline and dopamine.

Martinez-Máñez and coworkers utilized mesoporous silica particles covalently functionalized with the fluorescent amine-probe 2,4,6-triphenylpyrylium (**N3.12** in Figure 95) for the detection of aliphatic amines in water (pH 7.0−10.0).[418] The hydroxyl groups present on the surface of the nanoparticles were derivatized with hexamethyldisilazane to increase the long-term stability of silica nanoparticles in aqueous solutions. In the presence of primary amines, aqueous dispersions of **N3.12** produced a distinct color change from magenta to yellow, which was attributed to the ability of amines to form a pyridinium adduct with 2,4,6-triphenylpyrylium. Remarkably, the change in color was only observed for amines with medium chain length, such as *n*-heptylamine, *n*-octylamine, and *n*-nonylamine. This selectivity was explained by the hydrophobic nature of the particle, which makes it unfavorable for hydrophilic short-chain amines to diffuse towards reporter dyes located in the pores of **N3.12**. Likewise, the reaction of the long-chain amines *n*-undecane- and *n*-dodecylamine with **N3.12** was prevented for steric reasons. The authors reported the possibility to detect medium-chain amines in water at mM concentrations by correlating the change in color recorded *via* UV−vis absorption spectroscopy.

Peng, Cheng, and coworkers reported a colorimetric-based detection method for creatinine at $\mu$M concentrations in water, pH 5.0, artificial urine, and real urine samples using uric acid functionalized and $Hg^{2+}$-doped gold nanoparticles (**N3.13** in

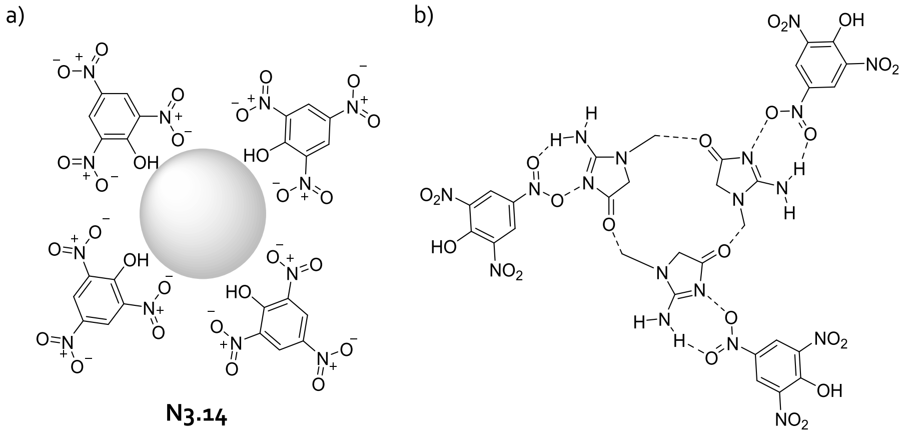

**Figure 97.** (a) Picric acid-functionalized gold nanoparticles (**N3.14**) used for colorimetric detection of creatinine in phosphate buffer, pH 7.0, and human serum at $\mu$M concentrations. (b) Interaction between picric acid and creatinine.

Figure 96).[419] The design of their nanosensor is based on a system previously reported by the same group, in which the authors found that uric acid and creatinine can adsorb on the surface of gold when $Hg^{2+}$ cations are added to the system.[420] Although **N3.13** formed stable colloidal dispersions in aqueous dispersions, additions of creatinine triggered the aggregation of the particles, as observed by a visible color change of the dispersion from red to blue due to a change in the plasmonic surface resonance energies. The aggregation of **N3.13** in the presence of creatinine was explained by its ability to coordinate with both $Hg^{2+}$ cations and uric acid, forming a stable molecular bridge between the particles. The authors also showed that their nanosensor is selective for creatinine over metal cations or inorganic anions.

In the same year, Menon and coworkers designed a picric acid-capped silver nanoparticle (**N3.14** in Figure 97) for the detection of creatinine at $\mu$M concentrations in phosphate buffer, pH 7.0, blood samples, and cerebrospinal fluid samples.[421] Creatinine interacts with the nitro group of picric acid on **N3.14** *via* H-bond interaction, triggering the aggregation of the particles, and the color of the particle dispersion changed from initially yellow to orange (Figure 97b). It was shown that the selectivity of **N13.4** is not affected by other inorganic anions (*e.g.*, $Br^-$, $SO_4^{2-}$), metal cations (*e.g.*, $Fe^{3+}$, $Ca^{2+}$, $Zn^{2+}$, $Na^+$), or bilirubin. The performance of the nanosensor was tested in the analysis of three different types of spiked human serum (*e.g.*, icteric blood, hemolyzed blood, and normal blood) and spiked cerebrospinal fluid with recoveries in the range of 96.7−99.9%.

The combination of the unique optical, electronic, and catalytic properties of hybrid metal quantum clusters with the inherent biological properties of proteins make protein-noble metal nanoclusters promising candidates for various biomedical applications such as imaging, sensing, delivery, and therapeutics.[422] For example, Joseph and coworkers reported a hybrid nanoparticle composed of multiple gold quantum clusters (about 25 Au atoms, as detected by fluorescence spectroscopy) in a stabilizing gluten shell functionalized with picric acid (**N3.15** in Figure 98).[423] The typical red fluorescence of gold nanoclusters is quenched due to electron transfer processes with picric acid, while the presence of creatinine restored fluorescence (61% recovery of fluorescence), as creatinine displaced the fluorescence quencher from the surface of **N3.15** in phosphate buffer, pH 9.0. The selectivity of the sensor was tested with biomolecules (*e.g.*, monosaccharides, amino acids, urea), inorganic anions (*e.g.*, $NO_3^-$, $SO_4^{2-}$, $S_2^-$, $PO_4^{3-}$, $F^-$, $I^-$, $CH_3COO^-$, and $CO_3^{2-}$), or metal cations (*e.g.*, $Fe^{3+}$, $Mg^{2+}$, $Zn^{2+}$, $Na^+$), which did not affect the properties of **N3.15**. As such, **N3.15** enabled fluorescence-based detection of creatinine in phosphate buffer, pH 9.0, and spiked blood samples.

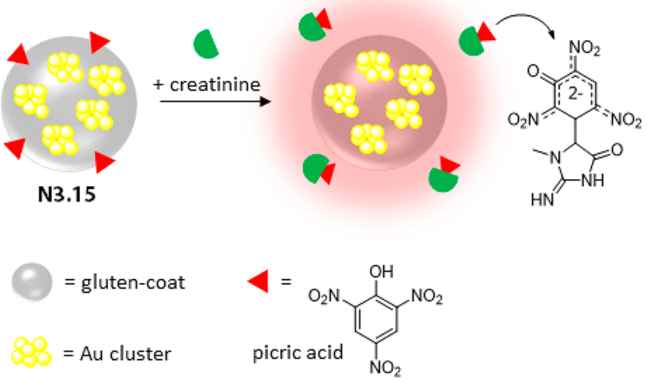

**Figure 98.** Gluten-coated and picric acid-functionalized gold nanoclusters (**N3.15**) allow fluorescence turn-on detection of creatinine in phosphate buffer, pH 9.0, and blood samples at $\mu$M concentrations.

Blackburn and coworkers reported the use of plasmonic silver nanoparticles (AgNPs) for the detection of creatinine in 10 mM NaOH, pH 12.0, and basic human urine samples (**N3.16** in Figure 99).[424] Creatinine-dependent aggregation of citrate-capped silver nanoparticles was visualized by the color change of a particle dispersion from yellow to black, and the degree of aggregation was correlated with the amount of creatinine. The authors proposed that the aggregation of **N3.16** in alkaline media is triggered by the formation of a stable H-bonded network between the carbanion/oxoanion amino tautomers of creatinine and the negatively charged carboxylate groups of citrate-capped silver nanoparticles. The authors further tested the selectivity of their nanosensor. Fortunately, metal cations (*e.g.*, $Na^+$, $K^+$, $Ca^{2+}$, $Zn^{2+}$, $Fe^{2+}$, and $Fe^{3+}$) or biomolecules (*e.g.*, ascorbic acid, glucose, glutamic acid, urea, glycine, and uric acid), did not cause interferences for creatinine detection.

Delgado-Lòpez, Ramírez-Rodríguez, and coworkers recently reported a fluorescence-based nanosensor composed of

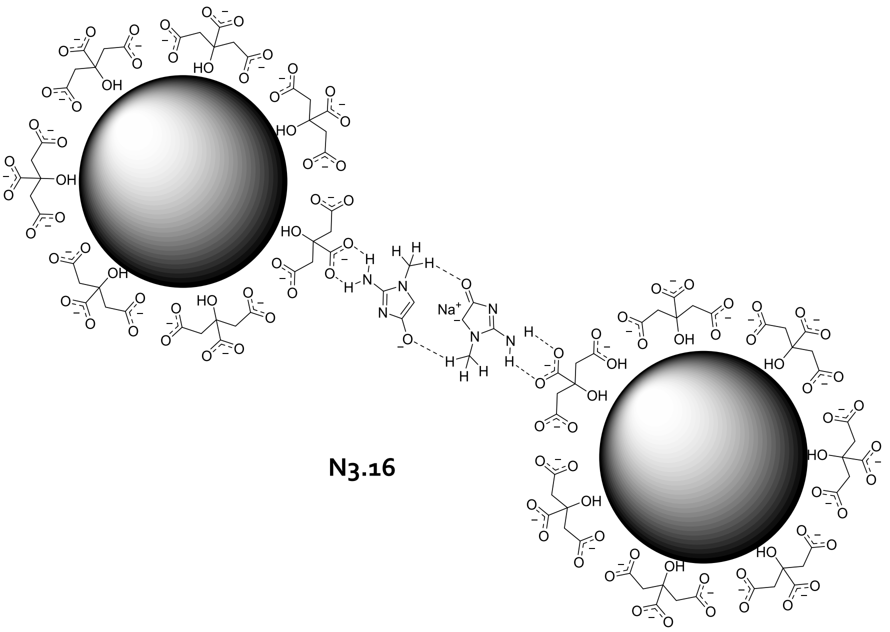

**N3.16**

**Figure 99.** Citrate-capped AgNPs (**N3.16**) form a stable H-bonding network with creatinine allowing for its colorimetric detection in 10 mM NaOH, pH 12.0, and in basic urine samples at $\mu$M concentrations.

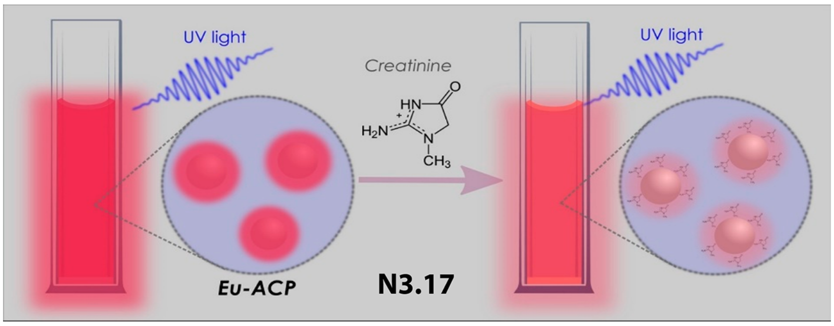

**Figure 100.** Europium-doped amorphous calcium phosphate nanoparticles **N3.17** enable fluorescence turn-off detection of creatinine at $\mu$M concentration in citrate buffer and urine samples. Reproduced with permission from ref 425. Copyright 2020 Elsevier BV.

europium-doped amorphous calcium phosphate nanoparticles (**N3.17** in Figure 100) that allows for $\mu$M detection of creatinine in 100 mM citrate buffer, pH 7.4, and human urine samples.[425] Luminescent inorganic nanoparticles such as lanthanide-based nanophosphors are attractive candidates to serve as novel nanosensors. Characteristic for them are long luminescence lifetime, high luminescence quantum yield, sharp emission bands, and good resistance to photobleaching.[426] In this work, the authors observed that the characteristic fluorescence emission of the nanoparticles ($\lambda_{ex}$ = 390 nm, $\lambda_{em}$ = 600 nm) was increasingly quenched by addition of creatinine. The observed fluorescence quenching was attributed to the presence of creatinine acting as a primary internal filter.[427] As such, the decrease in emission intensities was successfully correlated to the amount of creatinine present in citrate buffer and spiked human urine samples with good recovery ranges (~98 %).

Recently, Lee and coworkers reported the use of plasmonic nanocomposites of CB7 and citrate-capped AuNPs as nanocomposites (**N3.18** in Figure 101) for both colorimetric and quantitative surface-enhanced Raman spectroscopy (SERS)-based detection of creatinine in water and synthetic urine at sub-$\mu$M concentrations.[428] In this approach, the authors utilized the complexation of creatinine by CB7 in aqueous solution. The addition of AuNPs caused nanoparticle aggregation due to the adsorption of the CB7−creatinine complex on the AuNP surface, reducing the negative surface

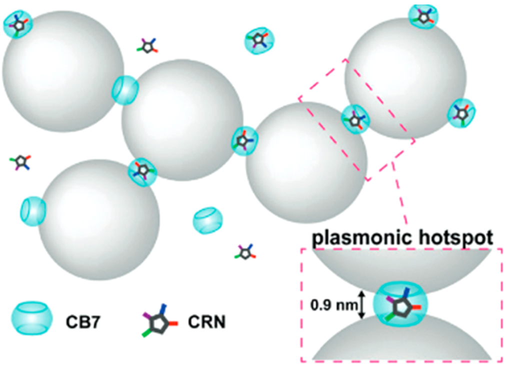

**N3.18**

**Figure 101.** Plasmonic nanocomposites (**N3.18**) of cucurbit[7]uril (CB7) and citrate-capped gold AuNPs for creatinine detection. Reproduced with permission from ref 428. Copyright 2020 The Royal Society of Chemistry.

charges which are required for colloidal stability. A dispersion of aggregated nanoparticles was analyzed by UV−vis absorbance spectroscopy because aggregation involves a shift in the surface plasmon absorption band of the nanoparticles, allowing for a simple colorimetric-based quantification of creatinine (LOD: 530 nM in water). Moreover, highly sensitive SERS measurements were carried out in the absence and presence of creatinine. In fact, with SERS, an LOD of 42 nM in water and 111 nM in spiked artificial urine samples was achieved.

A turn-on fluorescence sensor for creatinine based on quinoline-modified metal−organic framework (MOF) was recently reported by Jia and coworkers (**N3.19** in Figure 102).[429] The authors prepared amino-modified UiO-66 MOFs, which were subsequently post-synthetically modified using 8-hydroxy-2-quinolinecarboxaldehyde as a ligand that provides abundant metal coordination sites for $Al^{3+}$-doping. The fluorescence of the MOF was significantly quenched by $Al^{3+}$, while in the presence of creatinine, the fluorescence of the MOF nanoparticles was restored. The authors explained this effect by the ability of creatinine to form stable coordination complexes with $Al^{3+}$, thus displacing the fluorescence quencher from **N3.19**. Other biorelevant molecules such as cysteine, glycine, aspartic acid, glucose, dopamine, ascorbic acid, uric acid, urea, bilirubin, or inorganic cations, *e.g.*, $Na^+$, $K^+$, and $Mg^{2+}$, did not cause a strong emission response. Finally, the authors successfully demonstrated that their nanosensor can determine creatinine in diluted spiked serum (recovery ∼99%) and spiked urine samples (recovery ∼98%) at μM concentrations.

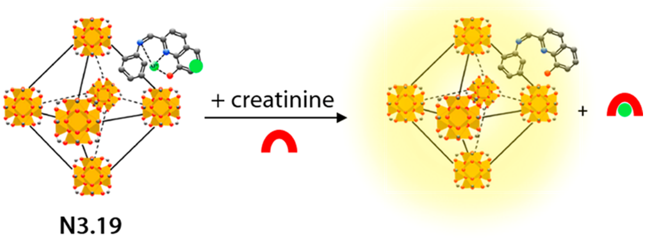

**Figure 102.** 8-Hydroxy-2-quinolinecarboxaldehyde and $Al^{3+}$ cations doped UiO-66 MOFs (**N3.19**) allow for fluorescence-based detection of creatinine (μM concentrations) in PBS, diluted urine, and serum samples.

A considerable number of both probes and chemosensors has already been developed that detect amines through their nucleophilic reactivity or by their positive charge that biogenic amines adopt under physiological conditions through protonation. Furthermore, nonprotonated amines are excellent electron donors, enabling their detection through photoinduced electron transfer (PET) quenching.[430] Such a design motif has been widely used to detect small molecule amines from the gas phase, *e.g.*, in combination with emissive conjugated polymers, for which several excellent literature sources can be consulted.[431−434] It is worth pointing out that many powerful probes and chemosensors for amines that are operational in organic solvents have already been reported, for instance, by the Wolf group.[435−440] Intuitively, aforementioned amine-reactive probes such as ninhydrin can react with amines in general, even though this was not expected by the time ninhydrin was first described for amino acid detection.[93−95] Very recently, Wolf and coworkers demonstrated that the chiral chromophoric adduct formed under mild conditions from the reaction of chiral amines with ninhydrin can be used for chirality sensing of the nonchromophoric amine analytes in a practically convenient and inexpensive method.[436] We would like to refer the reader to the original literature and reviews[21,441] as we focus herein on those systems that operate in aqueous media. In fact, it is rather challenging to design simple probes and chemosensors that only recognize amines but not amino acids, but several sophisticated systems have appeared that can achieve that goal.

Similar to the findings for amino acids, comparison of the sensitivity needs for amine detection in biofluids (low micro- to submicromolar concentration range, see Table 11), and the achievements that have been made with probes, chemosensors and nanosensors are rather promising (Table 8−10), albeit in some cases further improvements are still needed to reach the submicromolar concentration range. Curiously, mostly spiked blood serum or urine samples were analyzed, pointing to potential matrix-effect problems with real biofluids obtained from different patients. Standing problems are likely again caused by the lack of selectivity of artificial chemosensing systems limiting the utility of the probes, chemosensors, and nanosensors for sensing absolute amine concentrations in real biofluid samples.

**Table 11. Summary of the Normal Concentration Range of the Amines in Biofluids**[a]

| concentration range | media | ref |
|---|---|---|
| Cadaverine Analyte | | |
| 10.0−820 nmol/mmol creatinine = 0.10−8.20 μM | urine | 442 |
| 250−390 nM | human serum | 443 |
| Creatinine Analyte | | |
| 8.40−12.4 mM | urine | 50 |
| 1.60−8.19 μM | saliva | 62 |
| 60.0−120 μM | plasma | 444 |
| Histamine Analyte | | |
| 10.0−100 nmol/mmol creatinine = 0.10−1.00 μM | urine | 50 |
| 0.0−7.6 μM | saliva | 62 |
| 0.3−1.0 μM | whole blood | 445 |
| 0.5−1.8 nM | plasma | 444 |
| Putrescine Analyte | | |
| 0.08−1.06 μmol/mmol creatinine = 0.80−10.6 μM | urine | 442 |
| 25.0−250 μM | saliva | 62 |
| 458−518 nM | human serum | 443 |
| 150−330 nM | blood | 446 |
| Spermidine Analyte | | |
| 10−90 nmol/mmol creatinine = 100−900 μM | urine | 442 |
| 0.0−10 μM | saliva | 62 |
| 276−296 nM | human serum | 443 |
| Spermine Analyte | | |
| 10.0−230 μmol/mmol creatinine = 0.1−2.8 μM | urine | 442 |
| 0.0−1.3 μM | saliva | 62 |
| 165−185 nM | human serum | 443 |

[a] Urinary analyte concentrations were converted assuming a representative creatinine level of 10 mmol/L.

## 4. NEUROTRANSMITTERS

Neurotransmitters (NTs) are a class of chemical messenger molecules found in living organisms that are typically secreted by nerve cells to trigger important signaling processes, making them essential for almost all vital functions.[447] NTs affect the electrical excitability of a neuron, increasing or decreasing the likelihood that the cell will generate an action potential. Therefore, their abnormal concentration fluctuations are causes or markers of diseases.[448−450] For example, abnormalities in cholinergic, catecholaminergic (noradrenergic, dopaminergic), and serotonergic (5-HT) transmission patterns are linked to depression, anxiety, and even bipolar disorders.[451−454] A well-known example of a disease caused by inhibition of the dopaminergic system and characterized by a disturbed dopamine/acetylcholine balance is Parkinson's disease.[455] Therefore, it is not surprising that known NT precursors are being considered for the treatment of this disease. For example, oral doses of L-3,4-dihydroxyphenylalanine (L-DOPA) are administered as Parkinson's medication, which is converted into dopamine in the brain.[456,457] Anomalies in the bodies catecholamine concentrations have been associated with diseases such as Alzheimer's disease and the presence of tumors.[458−460] For example, elevated NT levels are found in pheochromocytoma,[461,462] a type of tumor that grows in the adrenal glands and produces an excess of catecholamines. Furthermore, it has been suggested that abnormal catecholamine concentrations found in the urine of neuroblastoma patients can provide some information regarding the prognosis of this aggressive cancer of the nervous system.[463,464]

Other common diseases, besides neurological disorders and tumors, that are associated with abnormal neurotransmitter levels, making them important biological markers of disease, include irritable bowel syndrome and sudden infant death syndrome.[465−472] Additionally, factors such as infections in the body or stress can alter catecholamine levels.[473,474] Serotonin and melatonin are indole-based NTs that are essential to the human body as they are involved in a variety of functions, including (infant) development, cardiovascular function, cognition, and mood[475−478] as well as day−night rhythm[479] and timing for the endogenous circadian system that modulates memory processes.[480] Abnormal concentrations of such neurotransmitters in biofluids may serve as markers of severe neurological and psychiatric disorder and of suboptimal drug dosing for the treatment of these diseases, *e.g.*, drugs that target serotonin receptors.[481] Figure 103 shows some selected examples of small, important NTs such as dopamine and serotonin and their functional groups that can serve as chemical anchors/recognition motifs for the development of probes, chemosensors, and nanosensors.

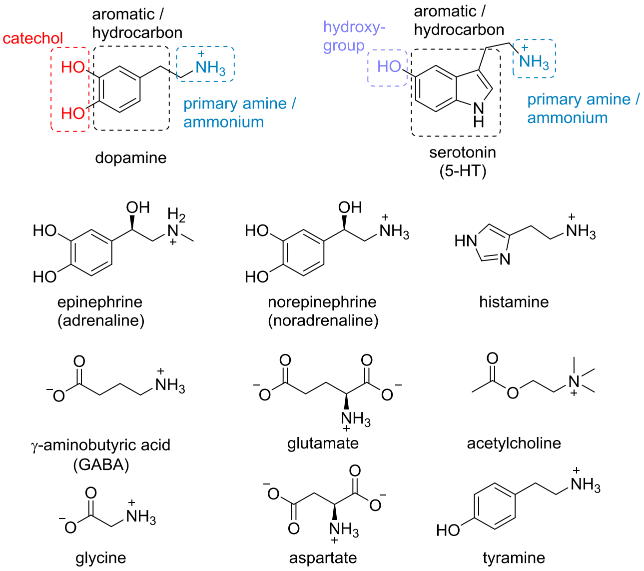

**Figure 103.** Selected examples of important neurotransmitters (NTs). Possible chemical anchors/molecular recognition motifs that can be targeted by probes, chemosensors, and nanosensors are indicated for dopamine and serotonin.

## 4.1. General Approaches for Neurotransmitter Detection

Continuous efforts are devoted to the development of simple, cost-effective, and easy to use sensing methods that are applicable to amino acid-derived neurotransmitters. Neurotransmitter sensing in clinical diagnostics currently relies on antibody-based immunoassays[482] or instrumental analytical methods, such as coupled HPLC-MS measurements, and therefore remains applicable only to specialized diagnostic laboratories. Moreover, natural receptor-based fluorescent protein mutants have been developed for the detection and imaging of neurotransmitters,[483,484] but their large-scale preparation is expensive and their handling cumbersome. Another common strategy for the detection of dopamine and some other electron-rich NTs, *e.g.*, glutamate, is the use of electrochemical biosensors, however, this is out of the scope of this review. For electrochemical-based detections of neurotransmitters, we refer the reader to the recently published review by Slaughter and coworkers.[485] For less electron-rich aromatic amino acid-derived neurotransmitters such as serotonin, or the electron-poor histamine, electrochemical sensing methods are less attractive, and therefore molecular probes, chemosensors, and nanosensors are even more sought-after alternatives.

The primary or secondary amino group of neurotransmitters are usually targeted as the main recognition point in contemporary designs of molecular probes and chemosensors. For instance, probes typically operate by exploiting the high nucleophilicity of unprotonated $-NH_2$ moieties, while chemosensors often establish ion pair bonding or charge-assisted hydrogen bonding motifs with $-NH_3^+$ groups found in the physiological form of amine neurotransmitters. Additional functional moieties such as aromatic residues, *e.g.*, found in catecholamine neurotransmitters, and carboxylate groups as can be found in glycine, aspartate, glutamate, and GABA, are recognition motifs that can be addressed to enhance the binding affinity and selectivity of the chemosensor or probe.

## 4.2. Molecular Probes for Neurotransmitters

Aldehyde groups and arylboronic acids have attracted much attention in the development of probes/chemosensors for catechol-type neurotransmitters. Aldehyde groups condense with amines under imine-bond formation. Arylboronic acids have the unique feature to form reversible covalent complexes with 1,2- or 1,3-substituted Lewis base donors, *e.g.*, hydroxyl- or aminofunctional groups.[486] All molecular probes discussed within this section are summarized in Table 12.

Glass and coworkers reported several probes, *e.g.*, **P4.1** and **P4.2**, that target catecholamine neurotransmitters (Figure 104a). These probes possess an aldehyde functionality that condenses with amines to form imine bonds.[487,488] Additionally, probe **P4.2** has a boronic acid moiety that reacts with aromatic 1,2-diols to yield boronic esters. Because of the interplay of two recognition units, the probes selectively bind catecholamines with a primary amino group, such as norepinephrine, whereas other biogenic amines, *e.g.*, glutamate, or secondary amine neurotransmitters, such as epinephrine,

Table 12. Summary of the Molecular Probes for Neurotransmitters

| probe | media | concentration range | ref |
|---|---|---|---|
| | L-DOPA Analyte | | |
| **P4.3** | 100 mM MOPS, pH 7.2 | mM range | 488 |
| | Dopamine Analyte | | |
| **P4.1**[a] | 1% MeOH in 25 mM HEPES containing 50 mM $Na_2S_2O_3$, pH 7.4 | 0−40 mM | 488 |
| **P4.2**[a] | 50 mM $Na_2S_2O_3$ in 25 mM HEPES, pH 5.0 | 0−40 mM | 487 |
| **P4.4**[b] | 50% MeOH in 50 mM HEPES buffer, pH 7.4 | 0−2.7 mM | 490 |
| **P4.4**[b] | MeOH | 0−2.7 mM | 490 |
| **P4.5**[b] | 50% MeOH in 50 mM HEPES buffer, pH 7.4 | 0−2.7 mM | 490 |
| **P4.5**[b] | MeOH | 0−2.7 mM | 490 |
| **P4.6** | 100 mM $NaH_2PO_4$, pH 7.0 | 0−20 mM | 491 |
| **P4.7** | 100 mM $NaH_2PO_4$, pH 7.0 | 0−20 mM | 491 |
| | Epinephrine (Adrenaline) Analyte | | |
| **P4.1**[a] | 1% MeOH in 25 mM HEPES containing 50 mM $Na_2S_2O_3$, pH 5.0 | 0−40 mM | 488 |
| **P4.4**[b] | 50% MeOH in 50 mM HEPES buffer, pH 7.4 | 0−2.7 mM | 490 |
| **P4.4**[b] | MeOH | 0−2.7 mM | 490 |
| **P4.5**[b] | 50% MeOH in 50 mM HEPES buffer, pH 7.4 | 0−2.7 mM | 490 |
| **P4.5**[b] | MeOH | 0−2.7 mM | 490 |
| **P4.6** | 100 mM $NaH_2PO_4$, pH 7.0 | 0−20 mM | 491 |
| **P4.7** | 100 mM $NaH_2PO_4$, pH 7.0 | 0−20 mM | 491 |
| | Norepinephrine (Noradrenaline) Analyte | | |
| **P4.1**[a] | 1% MeOH in 25 mM HEPES containing 50 mM $Na_2S_2O_3$, pH 5.0 | 0−40 mM | 488 |
| **P4.2**[a] | 50 mM $Na_2S_2O_3$ in 25 mM HEPES, pH 5.0 | 0−40 mM | 487 |
| **P4.6** | 100 mM $NaH_2PO_4$, pH 7.0 | 0−20 mM | 491 |
| **P4.7** | 100 mM $NaH_2PO_4$, pH 7.0 | 0−20 mM | 491 |

[a] Glutamate is weakly bound ($K_a$ at least one order of magnitude lower). [b] Catechol and aromatic amino acids, *i.e.*, L-Phe, L-Tyr, or L-Trp, possess a similar binding strength.

form no or much weaker adducts. Therefore, the aldehyde−boronic acid-based probe **P4.2** can be used for staining of norepinephrine-enriched chromaffin cells and was shown to be functional in living and fixed secretory cells.[388] To date, one remaining drawback for the use of such probes in diagnostic or imaging applications is their shortcoming in quantitative neurotransmitter sensing.

Likewise, other researchers, *e.g.*, Coskun and Akkaya, or Schrader and coworkers, incorporated boronic acids as recognition motifs into fluorescent probes, resulting in the probe structures presented in Figure 104. Similarly to probe **P4.2**, probe **P4.3** also shows binding affinities for various catecholamines with $K_a$ values in the order of $10^3$ $M^{-1}$ in water,[489] whereas probe **P4.4** and **P4.5** display similar binding strengths to catecholamines in 50% MeOH.[490] Interestingly, the additional aldehyde group, which is present in **P4.5** but not in **P4.4**, did not significantly affect the binding properties and affinities of the probe. A potential drawback for the boronic acid recognition motif is the pH dependency of the reversible bond formation between the boronic acid and the catechol. The competing equilibria of the boronated species occurs near physiological pH. Additionally, boronic acids are known to bind unselectively all 1,2-diols, *e.g.*, diol-decorated carbohydrates such as fructose (see section 5 in this review). Schrader and coworkers developed two acyclic phosphonate−boronate compounds (probe **P4.6** and **P4.7**),[491] but unfortunately, the anticipated improvement *via* installation of the additional bisphosphonate recognition elements was not investigated. Indeed, counterintuitively, the design turned out to yield lower binding affinities for catecholamines compared to the other, simpler boronate-based receptors. However, at least **P4.6** and **P4.7** offer a good selectivity against non-catechol species.

### 4.3. Chemosensors for Neurotransmitters

Host−guest systems using macrocycles such as cucurbit[*n*]urils (CB*n*), *p*-sulfonatocalix[*n*]arenes (Cx*n*), or cyclodextrins (CDs) can provide good affinities for neurotransmitters such as serotonin, dopamine, and structurally similar NTs. The chemosensors discussed within this section are summarized in Table 13. For serotonin, which is an important neurotransmitter connected to depression or certain tumors, Koner and coworkers recently published a supramolecular study regarding the encapsulation of serotonin to CB7.[492] However,

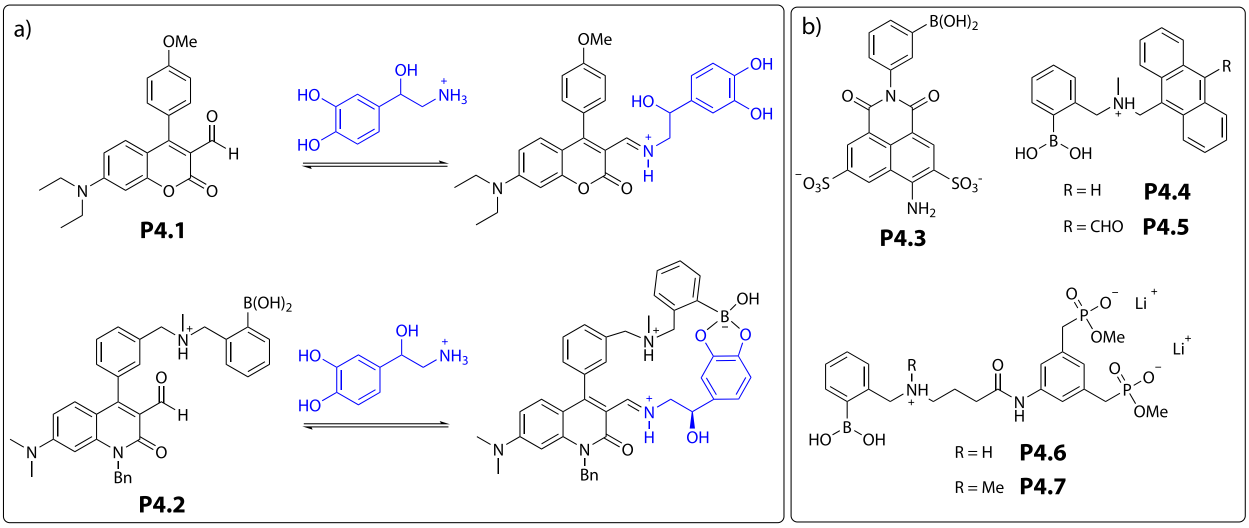

**Figure 104.** (a) Synthetic probes (**P4.1** and **P4.2**) with aldehyde and boronic acid functional groups that can be used for the selective detection of primary amine catecholamines. (b) Chemical structures of other catecholamine probes (**P4.3**−**P4.7**) that feature a boronic acid recognition motif.

**Table 13. Summary of the Chemosensors for Neurotransmitters**

| chemosensor | media | concentration range | ref |
|---|---|---|---|
| Acetylcholine Analyte | | | |
| **C4.4**[a] | 10 mM zodium phosphate buffer, pH 8.0 | 0–40 μM | 496 |
| **C4.5**[b] | PBS, pH 7.2 | 0–16 mM | 498 |
| Amphetamine Analyte | | | |
| **C4.10** | 1× PBS, pH 7.4 | 1.0 pm–1.0 μM | 505 |
| Dopamine Analyte | | | |
| **C4.1** | water | 0–600 μM | 493 |
| **C4.3**[c] | 50 mM NaOAc, pH 4.7 | 0–290 μM | 233 |
| Histamine Analyte | | | |
| **C4.6**[d] | 1× PBS, pH 7.4 | 1.0–5.0 μM | 501 |
| **C4.8** | 1 mM HBSS | 0–2.0 mM | 503 |
| **C4.9**[e] | 1× DPBS | 0–1.0 mM | 504 |
| Methamphetamine Analyte | | | |
| **C4.10** | 1× PBS, pH 7.4 | 1.0 pm–1.0 μM | 505 |
| Tyramine Analyte | | | |
| **C4.7**[f] | water | 0.8–100 μM | 502 |
| γ-Hydroxybutyric acid (GHB) Analyte | | | |
| **C4.2** | water | 230 μM | 494 |

[a] Can be used in an enzymatic tandem assay with choline (0–75 μM). [b] Choline interferes, other NTs or amino acids do not interfere. [c] Catechol is binding with a similar binding affinity as well as other aromatic amino acids, *i.e.*, L-Phe, L-Tyr, or L-Trp. [d] Cadaverine as interferent. [e] Cu-complex, interferents: Glu, GHS, Gly, dopamine. Not interfering: cadaverine, GABA, putrescine, serotonin. Ni-complex, not interfering: cadaverine, GABA, putrescine, serotonin, Glu, GHS, Gly. [f] Glycine, glutamate, serine, aspartate, ACh, choline, arginine, guanidinium hydrochloride, melatonin, and dopamine are by at least an order of magnitude in $K_a$ weaker binders.

CB7 and the other aforementioned hosts are spectroscopically silent and thus must be used in combination with dyes to furbish IDA, GDA, or ABA type assays for practical sensing considerations.

Ternary complexes with CB8 have been used for neurotransmitter detection in water and low salt buffers. For example, Scherman and coworkers described the detection of dopamine in the presence of epinephrine and norepinephrine with the help of PDI as reporter dye and CB8 as the host (**C4.1** in Figure 105).[493] A detection limit below 2 × $10^{-5}$ M in water was reported, and assay times of 5–10 min without the need of presampling or functionalization steps were reached. For dopamine, binding affinities ≥$10^5$ $M^{-1}$ to **C4.1** were found even in the presence of ascorbic acid, which is a major interferent in the electrochemical detection of dopamine.

γ-Hydroxybutyric acid (GHB), a precursor to the neurotransmitter γ-aminobutyric acid (GABA), is one of the most dangerous illicit drugs of abuse today. Garcia and coworkers combined four common fluorescent tricyclic cationic dyes with CB7 and CB8 as hosts, reporting the successful preparation of chemosensor arrays (**C4.2** in Figure 106) based on colorimetric- as well as emission-based detection mode.[494] Upon addition of a co-solvent such as acetone, which has been shown to be an essential component in reducing solvation effects that interfere with the interaction between **C4.2** and GHB, the detection of the target drug was possible in the concentration range of $10^{-3}$ M even by naked eye.

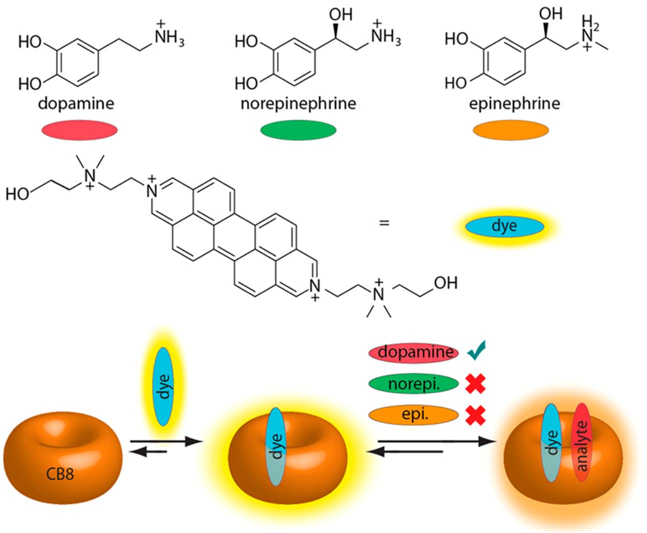

**C4.1**

**Figure 105.** Schematic representation of the selectivity of PDI•CB8 (**C4.1**) towards dopamine in the presence of other catecholamine neurotransmitters, *i.e.*, epinephrine and norepinephrine. Adapted with permission from ref 493. Copyright 2013 Taylor & Francis.

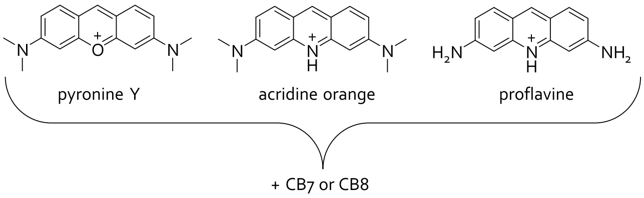

**C4.2**

**Figure 106.** Schematic representation of a chemosensing ensemble (**C4.2**) based on a combination of fluorescent dyes and cucurbit[*n*]urils.

Issacs and coworkers transformed the small and spectroscopically silent CB-homologue CB6 into a fluorescent chemosensor (**C4.3**) by incorporating chromophoric and emissive (bis)phthalhydrazines into the walls of the macrocycle (Figure 107).[233] With the help of **C4.3**, neurotransmitters, aromatic nitro compounds, amino acids, dyes, and other size-fitting species can be detected. For dopamine, a binding affinity of $K_a$ = 7.1 × $10^4$ $M^{-1}$ was found in 50 mM NaOAc, pH 4.7, which is slightly lower than that for catechol ($K_a$ = 2.9 × $10^5$ $M^{-1}$). As previously discussed, no analyte specific detection can be reached with cucurbit[*n*]urils due to their promiscuous binding properties.

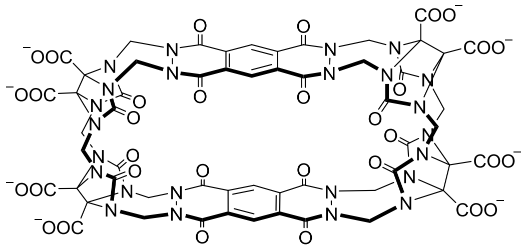

**C4.3**

**Figure 107.** Chemical structure of a fluorescent CB6 derivative (**C4.3**).

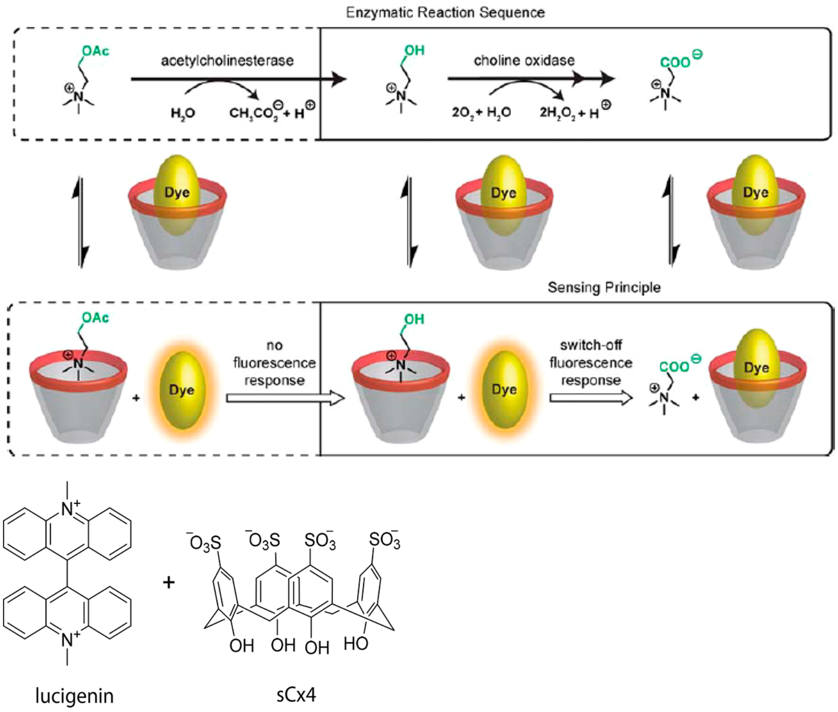

**C4.4**

**Figure 108.** Schematic representation of reactions catalyzed by acetylcholinesterase and choline oxidase and the corresponding (enzyme-coupled) tandem assay with chemosensor **C4.4** consisting of lucigenin and sCx4. Reproduced with permission from ref 217. Copyright 2011 The Royal Society of Chemistry.

Utilizing *p*-sulfonatocalixarenes (sCx4) as a high-affinity host for choline and acetylcholine ($K_a \sim 10^5$ $M^{-1}$), Nau, Liu, and coworkers developed a supramolecular tandem assay for these neurotransmitters. Their assay made use of the chemosensing ensemble **C4.4** that generates a fluorescence signal through the IDA mechanism.[46,495] Importantly, enzymes were used to achieve high selectivity (Figure 108), and the authors successfully extended their approach towards the monitoring of enzymatic reactions of acetylcholinesterase and choline oxidase, which catalyze the hydrolysis of acetylcholine to choline and the oxidation of choline to betaine. The system is based on the strong static fluorescence quenching of the sCx-complexed lucigenin.[217,496] Extending their studies on **C4.4** as chemosensor, Nau and coworkers showcased in 2015 the first indicator displacement assay inside living V70 and CHO cells. A fluorescence turn-on response of the intracellular chemosensors was observed as the added choline, acetylcholine, or protamine translocated into the cells.[219] So far, the assay can only be used semiquantitatively, as acetylcholine and choline are not distinguishable by the chemosensor, whereas protamine and betaine can be distinguished from the two aforementioned analytes by their characteristic binding affinities. Shoeib and coworkers used sCx4, taking advantage of its relatively strong binding affinity in the $10^4$–$10^5$ $M^{-1}$ range for these and other structurally related analytes, to prepare a direct binding assay. Absorbance-based detection of L-carnitine and choline was possible due to the strong change in the absorbance signal upon binding of sCx4 to the analytes.[497] The authors compared the performance of their chemosensor to the official U.S. Pharmacopeia method and found linear ranges within 10–160 μM for choline and 10–180 μM for L-carnitine.

Jin and coworkers detected acetylcholine by utilizing sCx8●rhodamine 800 complexes (**C4.5**) as IDA-type chemosensors that feature a desirable near-infrared fluorescence response (Figure 109).[498] The authors found a respectable selectivity for acetylcholine over dopamine, GABA, glycine, and L-aspartate; the former binds with an association constant of $K_a = 6.0 \times 10^3$ $M^{-1}$ in PBS, pH 7.2.

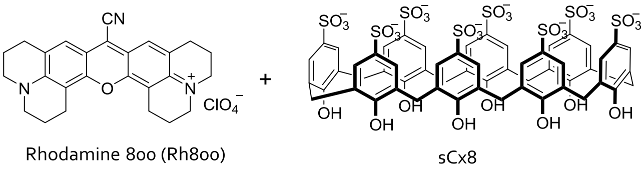

**C4.5**

**Figure 109.** Chemical structures of the discussed fluorescent dye and *p*-sulfonatocalixarenes (sC*xn*).

Histamine is another important neurotransmitter and is connected to allergies caused by histamine intolerance.[499] This circumstance makes its detection in blood or in food products important to identify potential risk factors. Amorim and coworkers recently reported a new histamine-selective electrode based on CB6 as ionophore and a polymeric membrane.[500] Moreover, 2-nitrophenyl octyl ether was used as a solvent mediator, and potassium tetrakis(4-chlorophenyl)-borate functioned as anionic additive. The addition of multiwalled carbon nanotubes as electrical conductors in the membrane extended the lifetimes of the electrodes, shortened the response times, and enabled a detection limit of 100 nM for histamine. Therefore, the assay becomes attractive for applications in biofluids.

Abd Karim and coworkers prepared zinc$^{II}$ salphen complexes (**C4.6** in Figure 110) that showed fluorescence increase in the presence of histamine.[501] The enhancement is ascribed to the electron transfer from histamine to the Zn$^{II}$ metal center. **C4.6** was immobilized on silica microparticles, thereby achieving histamine detection in PBS, pH 7.4, with a linear working concentration range of $10^{-11}$−$10^{-6}$ M. The system showed selectivity for histamine and cadaverine over other amines, such as 1,2-phenylenediamine, triethylamine, and trimethylamine. The authors also demonstrated the detection of histamine in spiked shrimp samples and reported 90−96% accuracy.

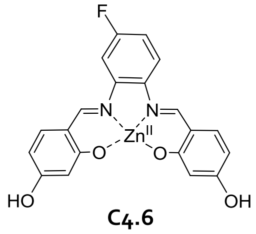

**C4.6**

**Figure 110.** Chemical structure of the Zn$^{II}$ salphen complex (**C4.6**).

There are only a few studies that addressed tyramine as neurotransmitter. Mohanty and coworkers developed a tyramine chemosensor based on sulfobutylether-β-cyclodextrin and thiazole orange (**C4.7**). This chemosensor was found to be selective for tyramine compared to other aminofunctional neurotransmitters such as dopamine or melatonin (Figure 111). In artificial mixtures of 11 amino-type analytes, a significant fluorescence quenching (52%) was observed only in the presence of tyramine, whereas in the absence of tyramine, only about 20% quenching of the **C4.7** emission occurred in water.[502] Interestingly, a good performance of **C4.7** was witnessed even after several heating and cooling cycles, indicating a high robustness of the chemosensor.

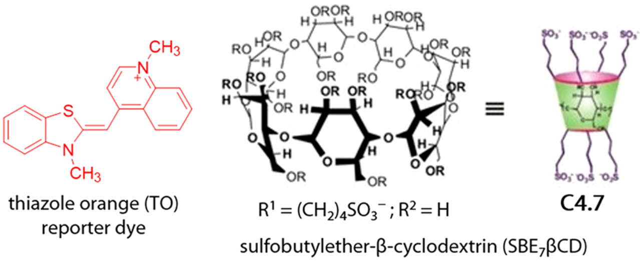

**Figure 111.** Schematic representation of the chemosensing ensemble (**C4.7**) composed of a functionalized, negatively charged β-CD host and thiazole orange as a fluorescent reporter dye. Reproduced with permission from ref 502. Copyright 2019 Wiley-VCH.

Additionally, the binding affinity of histamine for transition metals has been exploited to prepare fluorescence turn-on chemosensors that operate through the competitive binding of metal ions to histamine and the corresponding release of these emission quenchers from their dye−metal complexes. In this way, Ojida and coworkers were able to detect high micromolar concentrations of histamine with Co$^{II}$ complex of a cyanine dye (**C4.8**) in Hank's balanced salt solutions (HBSS = sodium bicarbonate buffer, Figure 112).[503] Similarly, Imato and coworkers detected histamine in living cells (RAW264 cells) that were washed with Dulbecco's PBS (1× DPBS) and then treated with chemosensor **C4.9**, which holds Nile Red as dye and a Ni$^{II}$−iminodiacetic acid complex as the histamine binding site.[504] They investigated also various other metal ions, *e.g.*, Co$^{II}$, Cu$^{II}$, Fe$^{II}$, and Zn$^{II}$, out of which the fluorescence response for the Cu$^{II}$ and Ni$^{II}$ complexes were by far the largest. Moreover, the Ni$^{II}$ complex showed an astonishing selectivity for histamine over a wide range of biogenic amines, whereas the Cu$^{II}$ complex was less selective. Importantly, functionalized variants of the chemosensors can be anchored in cell membranes and retain their sensing functionality. Thus, the degranulation of histamine from mast cell granules was monitorable by fluorescence microscopy in real time. Conceptually related approaches for the detection of the amino acid histidine are presented in section 2.3.1.1 of this review.

Recently, Hwang, Oh, Kim, and coworkers exploited the high binding affinity of CB7 for amphetamine-type stimulants (ATS) through an organic transistor setup where functionalized CB7 macrocycles were deposited *via* spin-coating on surfaces of water-stable semiconducting polymers (**C4.10** in Figure 113).[505] An impressive picomolar detection limit for amphetamines was reported in buffers, while a nanomolar detection limit was achieved in spiked urine.

In short summary, the development of robust and fast responding probes and chemosensors for neurotransmitters could open exciting new possibilities for home-use and point-of-care diagnostics that cannot be realized with existing technologies.[21,506] We hope that the discussed design strategies inspire the reader to tackle the challenging task of constructing practically applicable chemosensors for neurotransmitters.

### 4.4. Nanosensors for Neurotransmitters

Gold nanoparticles (AuNPs) are particularly attractive for the development of nanosensors because their surface can be readily functionalized with molecular recognition units for neurotransmitters. For instance, boronic acids, aromatic aldehydes, carboxylic acids, or succinimide esters were installed on the surface of AuNPs for targeting catechol deriva-

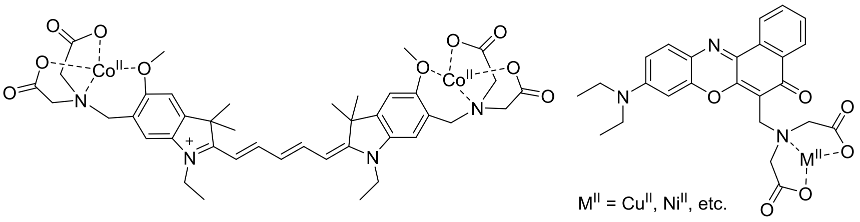

**C4.8**

**C4.9**

**Figure 112.** Chemical structures of the cyanine-based chemosensor (**C4.8**) and the Nile Red-based chemosensor (**C4.9**) for histamine detection.

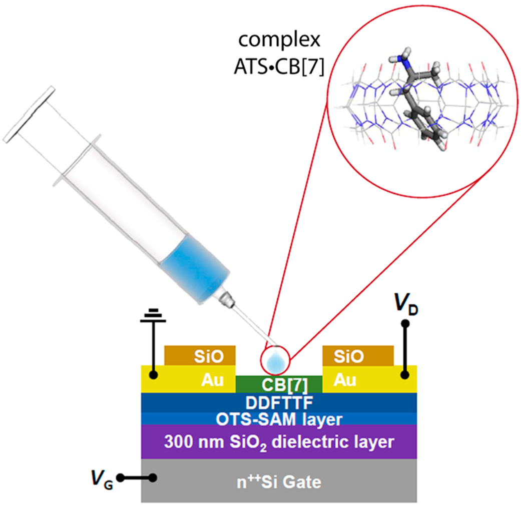

**C4.10**

**Figure 113.** Schematic representation of the top-contact OFET drug sensor platform (**C4.10**) based on the supramolecular complex of CB7 and amphetamine-type stimulants (ATS). Adapted with permission from ref 505. Copyright 2017 Elsevier BV.

tives.[507−511] AuNPs, which are plasmonic nanoparticles, possess distinct spectroscopic properties, *e.g.*, absorption of light, due to the existence of surface plasmon resonances (SPRs).[512] Colorimetric nanosensors for neurotransmitters can be prepared by using boronic acid functionalized AuNPs, as the SPRs strongly depend on the aggregation/disaggregation of the nanoparticles in the presence/absence of catecholamines, *e.g.*, dopamine. The resulting change in SPRs upon interaction of the AuNP-based nanosensors with analytes can be easily detected by spectroscopic methods, *e.g.*, UV−vis spectroscopy. The nanosensors discussed within this section are summarized in Table 14.

The detection of norepinephrine at $\mu$M concentrations in 10 mM phosphate buffer, pH 6.5, and spiked urine samples was described by Martínez-Máñez and coworkers.[508] In this work, AuNPs were functionalized with 4-mercaptophenylboronic acids (MBA) and 4-(liponyloxy)benzaldehydes that allow for norepinephrine binding, leading to nanosensor aggregation (**N4.1** in Figure 114). This caused a spectroscopically measurable shift in the SPR absorption energies of the system that was dependent on the analyte concentration. The authors showed that no colorimetric response was observed in the presence of L-Tyr, Lys, glucose, uric acid, glutamic acid, and 5-hydroxyindoleacetic acid (main degradation product of serotonin found in urine).

Following a similar strategy, Tian and coworkers described the preparation of MBA and dithiobis(succinimidylproprionate) (DSP) functionalized AuNPs (MBA-DSP-AuNPs, **N4.2**),[510] which allowed for nM detection of dopamine in water. Dopamine added to dispersions of **N4.2** caused crosslinking of the AuNPs and therefore triggered their aggregation. The amount of dopamine present in the sample was determined *via* absorption spectroscopy. In another example, Chen and coworkers reported the use of citrate-capped AuNPs (**N4.3**) in combination with melamine for colorimetric-based detection of dopamine in Tris-HCl buffer and spiked serum at nM concentrations.[513] For nanosensor **N4.3**, the authors found that melamine triggered aggregation only when dopamine was present in particle dispersions. As a

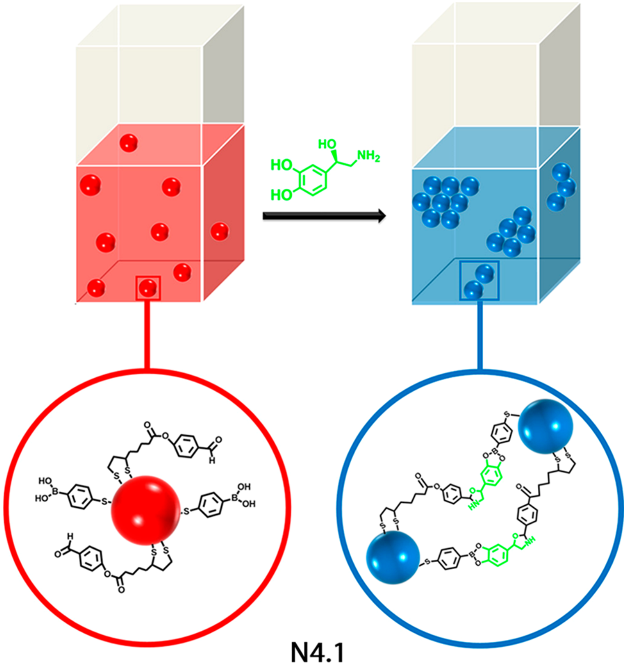

**N4.1**

**Figure 114.** Schematic representation of the colorimetric detection of norepinephrine using aldehyde and phenylboronic acid functionalized AuNPs (**N4.1**) in phosphate buffer at $\mu$M concentrations. Reproduced with permission from ref 508. Copyright 2019 American Chemical Society.

result, a clear color change of the particle dispersion from red to blue was observed and correlated with the amount of dopamine added to the sample. The mechanism of particle aggregation was explained by the ability of melamine to crosslink AuNPs that adsorbed dopamine on their surface *via* H-bond interactions.

In addition to the functionalization of AuNPs with small molecules, aptamers have been used in combination with plasmonic particles and were successfully applied for colorimetric-based detection of dopamine at $\mu$M concentrations (**N4.4−N4.6**).[514−516] For example, Kelley-Loghnane and coworkers used aptamer-functionalized AuNPs (**N4.7**), which allowed for selective serotonin detection in PBS containing 1 mM $MgCl_2$ and fetal bovine serum at $\mu$M concentrations with rapid readouts (within 5 min).[517] Despite the improved selectivity and good sensitivity for serotonin, *e.g.*, over 5-hydroxyindoleacetic acid, the aptamer functionalized nanosensors suffered from a low stability over time when stored at room temperature, which was attributed to DNA degradation. Fortunately, the aptamer functionalized AuNPs remained functional for a few weeks when stored at 4°C.

An alternative approach for colorimetric-based sensing with AuNPs was reported by Mancin, Gabrielli, and coworkers, who described a unique $^{19}$F NMR spectroscopy-based displacement assay for the detection of dopamine at $\mu$M concentrations (**N4.8** in Figure 115).[518] To this end, the authors coated AuNPs with thioundecyl-D-glucopyranosides, which are capable of adsorbing a $^{19}$F NMR active indicator. In this nanoparticle-bound state, the indicator provided only broad $^{19}$F NMR signals. Upon addition of dopamine to **N4.8**, sharper and more intense $^{19}$F NMR signals were observed as the indicator was no longer subjected to prolonged relaxation times upon displacement from the nanosensor surface.

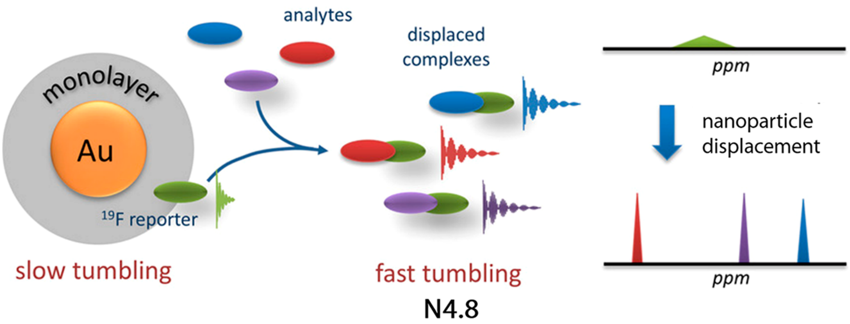

**Figure 115.** Schematic representation of the working principle of $^{19}$F NMR spectroscopy-based IDA for the detection of dopamine (**N4.8**). Reproduced with permission from ref 518. Copyright 2018 Wiley-VCH.

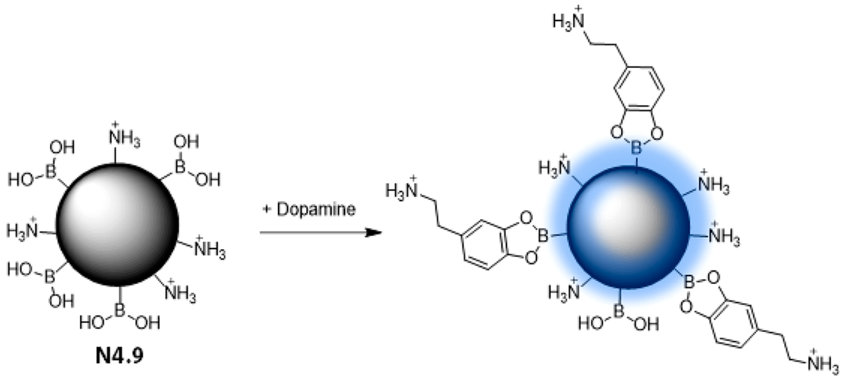

**Figure 116.** Bifunctional carbon dots (**N4.9**) bearing boronic acid and amino groups are used for the detection of dopamine in water and serum samples down to nM concentrations.

Carbon dots (C-dots) have attracted attention for the preparation of fluorescence-based nanosensors because of their good dispersibility in aqueous media, simple preparation, and outstanding fluorescence properties, such as excitation-wavelength-dependent emission color and excellent photostability.[519,520] Zhou, Shen, and coworkers developed bifunctional fluorescent C-dots bearing boronic acid and amino groups (**N4.9** in Figure 116) and used these for molecular recognition-based dopamine detection in water.[521] Interestingly, the fluorescence intensity of the C-dots increased in the presence of dopamine and was directly dependent on the analyte concentration, whereas other compounds (*e.g.*, glucose, ascorbic acid, levulose, maltose, and cysteine) caused no change in fluorescence. Therefore, fluorescence measurements were performed to detect dopamine in human serum samples (nM concentrations) using the standard addition method and recoveries of approximately 99% were reported. While not tested, it is likely that also other catecholamines, *e.g.*, (nor)epinephrine are detectable by **N4.9**.

$Fe^{3+}$-doped carbon dots for neurotransmitter detection were recently introduced by Qu and coworkers (**N4.10** in Figure 117).[522] The authors demonstrated the detection of dopamine in a linear concentration range of 0.1−10 $\mu$M (LOD: 68 nM) in 10 mM HEPES buffer, pH 7.0. The carbon dots were prepared by a hydrothermal synthesis protocol with (partially) oxidized catechol groups on the surface. It was observed that the fluorescence of the carbon dots was quenched when $Fe^{3+}$ cations were added to the particle dispersion, which can be explained by their participation in nonradiative electron transfer processes from the excited state of the C-dots. In addition, the authors argued that part of the fluorescence quenching may be causes by the ability of $Fe^{3+}$ to oxidize remaining catechol groups of the C-dots to quinones, which also participate in nonradiative electron transfer processes. However, when dopamine was present in the samples, the fluorescence of the nanosensor was restored, which the authors attributed to the reduction of $Fe^{3+}$ to $Fe^{2+}$ (and the reduction of quinones to catechols) by dopamine.[523] It remains a point of interest if other reducing analytes are cross-reactive with **N4.10**.

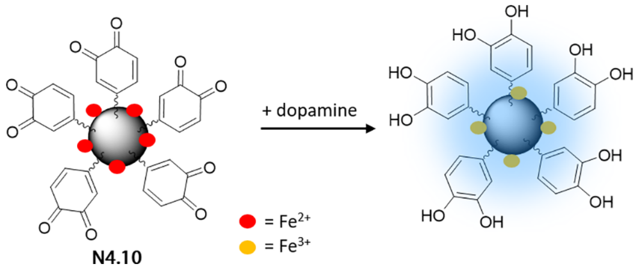

**Figure 117.** $Fe^{3+}$-doped carbon dots (**N4.10**) for fluorescence-based detection of dopamine at nM concentrations in HEPES buffer.

Kaifer and coworkers prepared silica nanoparticles functionalized with the electron-deficient dicationic 2,7-diazapyrenium (DAP) dye, which were used in combination with cucurbit[8]uril (CB8, **N4.11** in Figure 118) for the detection of the electron-rich neurotransmitter dopamine and catechol in phosphate buffer containing 100 mM NaCl, pH 7.0.[263] The fluorescence intensity of the DAP is strongly reduced in the presence of dopamine and CB8 due to the formation of the ternary CB8-DAP-dopamine inclusion complex (Figure 118a).

Competitive binding assays based on magnetic resonance imaging (MRI) using superparamagnetic iron oxide nano-

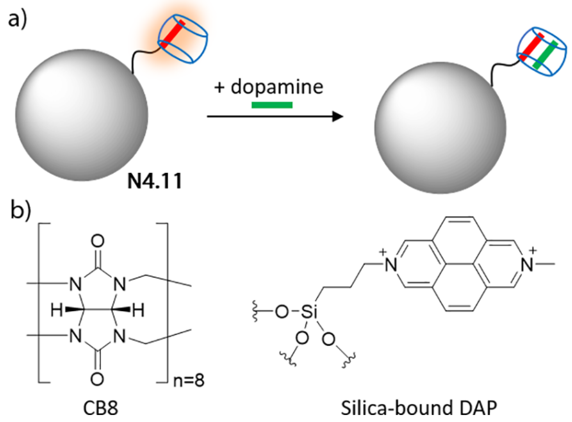

**Figure 118.** (a) Schematic representation of 2,7-diazapyrenium (DAP) functionalized silica nanoparticles (**N4.11**) for the fluorescence-based detection of dopamine in phosphate buffer containing 100 mM NaCl, pH 7.0. (b) Chemical structures of CB8 and silica-bound DAP.

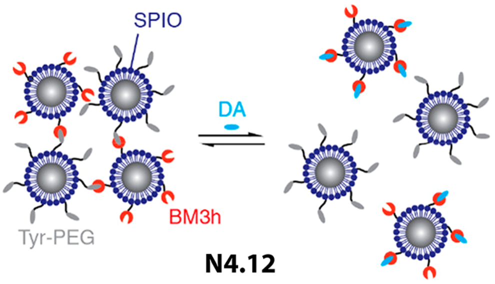

**Figure 119.** Bacterial cytochrome P450-BM3 heme domain protein- or tyramine-functionalized superparamagnetic iron oxide nanoparticles (SPIOs, **N4.12**) used for MRI-based detection of dopamine and serotonin in PBS at $\mu$M concentrations. Reproduced with permission from ref 524. Copyright 2019 American Chemical Society.

particles (SPIOs) (**N4.12** in Figure 119) have been reported by Jasanoff and coworkers for the detection of dopamine and serotonin.[524] Because of the high sensitivity of MRI-based techniques, even subnanomolar particle concentrations were effective for neurotransmitter detection. The authors used two types of SPIOs that were functionalized either with bacterial cytochrome P450-BM3 heme domain proteins (BM3h) or tyramine. A 1:1 mixture of these particles aggregated due to the binding of BM3h with tyramine, causing a darkening of the MRI signal. In the presence of the neurotransmitters, and due to their stronger affinity towards BM3h, the particle clusters were disrupted concomitant with a whitening of the MRI signal. This displacement-based assay allowed for $\mu$M dopamine detections in PBS and more importantly in rat brains, showcasing its good sensibility and robustness for potential *in vivo* applications. By varying the surface functionalization of the SPIOs, the authors also achieved the detection of serotonin.

Luminescence-based detection methods using near infrared (NIR) light ($\lambda$ = 800−2000 nm) are of special interest because tissues have good transparency to this wavelength region. Single-walled carbon nanotubes (SWCNTs) are important NIR emitters which have been used by Strano and coworkers for the detection of dopamine in 10 mM PBS, pH 7.4 (**N4.13** in Figure 120).[525] The authors described the preparation of a fluorescence turn-on nanosensor using single-stranded DNA (ssDNA, composed of 15 repeating units of guanine and thymine $(GT)_{15}$) functionalized SWCNT that exhibit enhanced NIR fluorescence in the presence of dopamine. This increase in fluorescence was attributed to the interaction of dopamine with the nanosensor, mediated by $\pi-\pi$ interactions, resulting in partial removal of ssDNA and displacement of quenching species such as solvent molecules from the surface of the SWCNTs. Noteworthy, control experiments showed that the emission enhancement was not generated by nanoparticle-mediated redox reactions. The authors showcased that epinephrine, norepinephrine, L-3,4-dihydroxyphenylalanine, and 3,4-dihydroxyphenylacetic acid also cause similar fluorescence responses and are therefore potential target analytes but also interferents.

The detection of dopamine at $\mu$M concentrations in 20 mM PBS, pH 7.4, and within cells with minimal interference from matrix components has been reported by Shen and coworkers.[526] The nanoparticles used in their study consisted of a fluorescent fluorenylbenzothiadiazole polymer core and a polyethylene glycol (PEG) shell, which ensured colloidal stability and reduced the immunogenic response after injection into living organisms. To provide the nanoparticles with dopamine-recognizing functional groups, additional arylboronic acids (PBAs) were integrated into the final particle structure (**N4.14** in Figure 121). In the presence of dopamine, emission quenching of the fluorescent core occurred, which was attributed to a dopamine-mediated photoinduced charge transfer process. The selectivity of **N.14** toward dopamine was confirmed, and other biomolecules (*e.g.*, ascorbic acid, tyramine, tyrosine, epinephrine (100 nM), or norepinephrine (100 nM)) did not quench the fluorescence. The particles were further investigated for *in vivo* application due to their apparent selectivity for dopamine at typical concentrations found in the brain of some mammals (0.1−1.0 $\mu$M).[527] For this purpose, **N4.14** was microinjected into brain ventricles of fish larvae, and the fluorescence intensities of the nanosensor decreased when exogenous dopamine was injected into the brain.

Pan and coworkers described the preparation of a molecularly imprinted nanoparticle-based assay strip for the detection of dopamine in 20 mM PBS, pH 7.4, and spiked urine samples from nM to $\mu$M concentrations.[528] To this end,

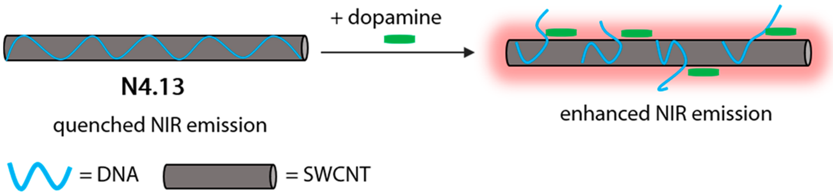

**Figure 120.** ssDNA functionalized SWCNTs (**N4.13**) used for fluorescence-based detection of dopamine at $\mu$M concentrations in PBS.

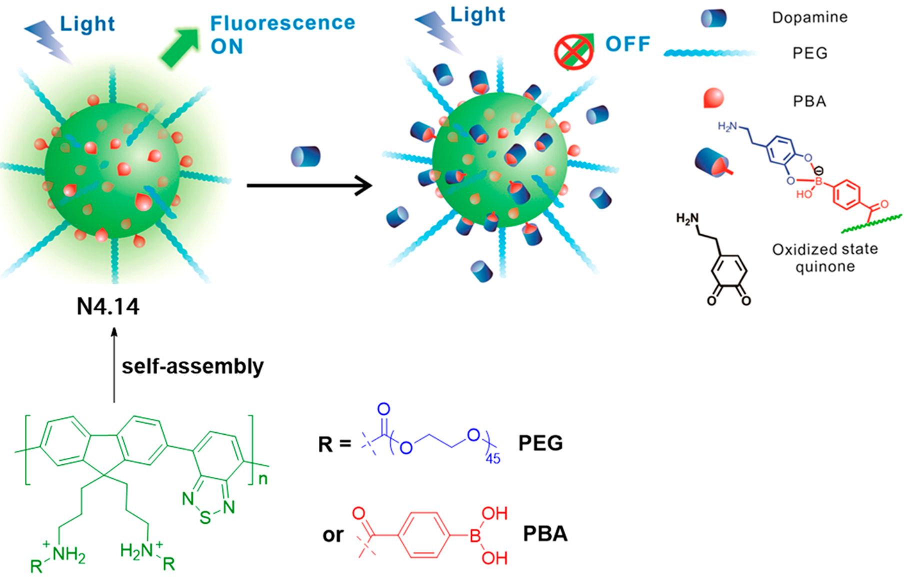

**Figure 121.** Biocompatible polymeric nanoparticles **N4.14** allow for fluorescence turn-off detection of dopamine at $\mu$M concentrations in 20 mM PBS, pH 7.4. Reproduced with permission from ref 526. Copyright 2015 American Chemical Society.

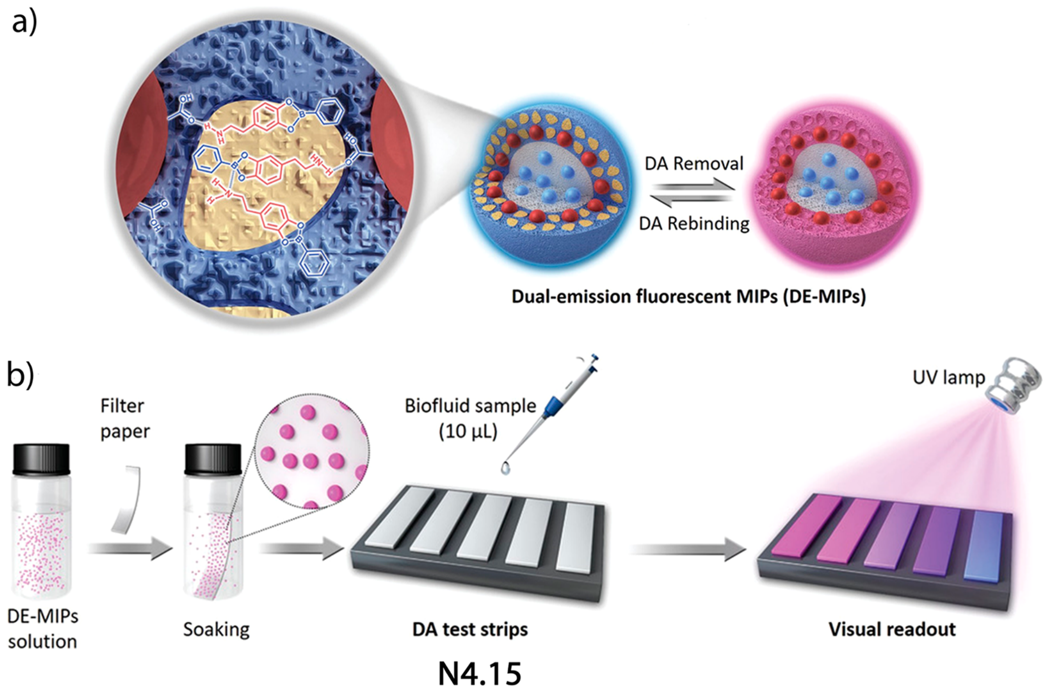

**Figure 122.** (a) Schematic representation of core−shell particles **N4.15** used for fluorescence-based detection of dopamine in PBS and human serum at nM and $\mu$M concentrations. (b) Paper strips were impregnated with **N4.15** by a soaking procedure and used for biofluid analysis. Reproduced with permission from ref 528. Copyrights 2019 Wiley-VCH.

the authors prepared core−shell particles in which the core consisted of blue-emitting quantum dots (QDs), while the shell consisted of a molecularly imprinted polymer in which red-emitting CdTe QDs were immobilized (**N4.15** in Figure 122). Dopamine spontaneously bound to the imprinted shell of the particles, resulting in a quenched red emission from the CdTe QDs *via* energy transfer processes. No comparable response was observed with catechol, gallate, quinone, glutamic acid, and $\gamma$-aminobutyric acid, whereas levodopa and norepinephrine yielded weak fluorescence quenching. Furthermore, the authors immobilized the nanoparticles by a simple impregnation procedure, obtaining paper-based test strips capable of detecting dopamine in human serum at nM concentrations. Besides the aforementioned nanoparticle and also other hard matter-based nanoparticles such as upconverting nanoparticles (**N4.16**−**N4.19**),[529−532] carbon dots (**N4.120**−**N4.23**),[533−536] quantum dots (**N4.24**−**N4.28**),[537−541] silicon nanoparticles (**N4.29**),[542] metal−organic frameworks (**N4.30**),[543] and silica-based nanoparticles (**N4.31**−**N4.33**)[544−546] have been reported for sensing of neurotransmitters.

A new and modular receptor design strategy based on microporous hybrid zeolite receptors (**N4.34** in Figure 123) was recently described by us. The detection of the neuro-

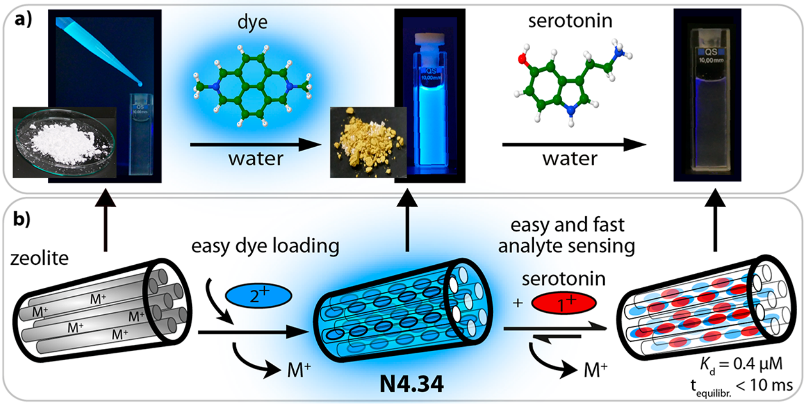

**Figure 123.** Schematic representation of preparation and sensing with reporter dye-loaded zeolite-based chemosensors (**N4.34**). Adapted with permission from ref 547. Copyright 2021 Wiley-VCH.

transmitters serotonin and dopamine (amongst others) was possible in buffers and real biofluids.[547] Serotonin and dopamine were shown to bind in the reporter dye-loaded pores of the ZARs (= zeolite-based artificial receptors), exploiting both the nonclassical hydrophobic effect and direct noncovalent recognition motifs. Evidence for this unprecedented binding mechanism was obtained by in-depth photophysical and calorimetric experiments in combination with full atomistic modeling. In addition, **N4.34** was shown to be applicable for label-free monitoring of important enzymatic reactions, (two-photon) fluorescence imaging, and high-throughput diagnostics in biofluids such as urine, neurobasal medium, and human serum. The presence of epinephrine, cadaverine, ascorbic acid, tyramine, histamine, 5-hydroxytryptophan, indole, octopamine, phenethylamine, $TrpNH_2$, tryptamine, and L-tryptophan did not interfere with the detection of serotonin or dopamine.

The comparison of the diagnostic or biological sensitivity needs for neurotransmitter detection and the current key parameters achieved by probes, chemosensors, and nanosensors reveals some standing limitations. While neurotransmitters can be found locally in millimolar concentrations near their site of action (*e.g.*, synaptic cleft), their bulk occurrence in readily accessible biofluids such as urine and blood serum are much lower (micromolar to nanomolar concentration range, see Table 15). With the exception of redox-reaction-based nanosensors for dopamine, other molecular-recognition-based systems usually still fall short in terms of sensitivity (Tables 12−14). Even more challenging is the selective detection of neurotransmitters in real biofluids, where a large excess of other potential interferents, *e.g.*, amino acids and amines, can be found. It appears that most probes, chemosensors, and nanosensors reported so far are not directly applicable for neurotransmitter detection in biofluids and that alternative receptor design strategies may be needed to close the performance gap. The use of ZARs (**N4.34**) may be one promising avenue to consider.

## 5. CARBOHYDRATES

Carbohydrates are compounds containing polyhydroxy aldehydes or ketones, which can be subdivided into mono-, di-, oligo-, and polysaccharides and are involved in a variety of biological processes. They are an important energy source and storage (glycogen or starch) for all living organisms, are mediators of cell−cell or cell-pathogen recognition,[559,560] and are part of the structural framework of RNA and DNA. A variety of diseases such as infections, cancer, inflammation, cardiovascular malfunctions, and many more can be correlated to carbohydrate-based biomarkers. Fructose, for example, is a highly lipogenic sugar present in processed food. Its excessive consumption is directly linked to numerous diseases such as obesity, hypertension, the metabolic syndrome, type 2 diabetes, and kidney disease.[561−564] In addition to diabetes, glucose and its metabolites play a role in the aging process in the pathophysiology of nonalcoholic fatty liver disease and in the signaling processes of some cancers.[565−568] Sialic acids, a class of $\alpha$-keto acid sugars, are known to mediate or modulate a variety of physiological and pathological processes. For example, the density of sialic acids in glomerular basement membrane appears to be critical for maintaining the normal filtering functions of the kidneys, which is why they are considered as markers for many diseases, including cardiovascular diseases,[569,570] inflammatory skin diseases,[571] and coronary heart diseases.[572] Besides, the polysaccharide heparin remains the most widely used anticoagulant and antithrombotic agent for the treatment of cardiovascular and cerebrovascular, pulmonary and renal diseases, and cancer.[573,574] Therefore, the detection of carbohydrates is of great interest for the development and improvement of diagnostics and therapeutics.[575,576] For more details about carbohydrates and their metabolism, we refer the interested readers to literature reviews.[577−580] Figure 124 shows a representative selection of important carbohydrates with their chemical structures.

In recent years, carbohydrate sensing has become an important field of research in which the use of probes and chemosensors has become indispensable. However, there are two main challenges to enable effective recognition of different carbohydrates in aqueous solution. Firstly, binding selectivity amongst the different carbohydrates is difficult to achieve as they do not differ in any structural motifs except for their size (mono- *vs* di-/polysaccharides) and their configuration at the stereocenters. Secondly, carbohydrates are usually highly solvated in aqueous solution, making it difficult for artificial receptors to overcome those "solvent barriers" and bind to the carbohydrate. The importance of carbohydrate sensing for diagnostics and therapeutics has caused a major push towards the development of artificial sensors and probes, where the hydroxyl groups of the carbohydrates are the easiest targetable functional groups. In nature, carbohydrate recognition is

### Table 14. Summary of the Nanosensors for Neurotransmitters (LOD, Limit of Detection)

| nanosensor | media | concentration range | ref |
|---|---|---|---|
| | Acetylcholine Analyte | | |
| **N4.24** | PBS, pH 7.4 | mM range | 537 |
| | Dopamine Analyte | | |
| **N4.2** | water | 20–160 nM; LOD, 0.5 nM | 510 |
| **N4.3** | 10 mM Tris-HCl buffer, pH 7.0 | 33 nM–3.33 mM | 513 |
| **N4.4** | 100 mM PBS, pH 7.0 | 0.5–5.4 $\mu$M | 514 |
| **N4.5** | 30 mM PBS containing $MgCl_2$; human serum samples | $\mu$M range; LOD, 79 nM | 515 |
| **N4.8** | 0.001% NaOD in DMSO-$d_6$ | 0–200 $\mu$M; LOD, 20 $\mu$M | 518 |
| **N4.9** | water<br>human serum | 0–1.0 $\mu$M in water<br>10–100 nM in serum | 521 |
| **N4.10** | 10 mM HEPES buffer, pH 7.0 | 0.1–100 $\mu$M; LOD, 68 nM | 522 |
| **N4.11** | 100 mM NaCl in phosphate buffer, pH 7.0 | 0–1.0 mM | 263 |
| **N4.12** | PBS, pH 7.4 | $\mu$M range | 524 |
| **N4.13** | 10 mM PBS, pH 7.4 | $\mu$M range; LOD, 11 nM | 525 |
| **N4.14** | 20 mM PBS, pH 7.4<br>in cells and fish larvae brains | 0.0025–10.0 $\mu$M in PBS<br>0–10 $\mu$M in biosamples | 526 |
| **N4.15** | 20 mM PBS, pH 7.4<br>serum samples | $\mu$M range; LOD, 100 nM in buffer<br>0–600 nM in serum; LOD, 100 nM in serum | 528 |
| **N4.16** | 2.5 mM Tris-HCl buffer, pH 8.5 | 0–20 $\mu$M; LOD, 30 nM | 529 |
| **N4.17** | 100 mM PBS, pH 7.4 | 0–20 $\mu$M | 530 |
| **N4.18** | *in vitro* neuronal cells | pM range | 531 |
| **N4.19** | Tris-HCl buffer, pH 8.5; urine samples | 0–300 $\mu$M in buffer; LOD, 1.62 $\mu$M in buffer | 532 |
| **N4.20** | 50 mM phosphate buffer, pH 6.8 | $\mu$M range | 533 |
| **N4.21** | 5 mM PBS, pH 7.5 | nM range | 534 |
| **N4.22** | water, pH 10.0; urine samples | nM range | 535 |
| **N4.23** | PBS; blood samples | nM range | 536 |
| **N4.25** | 10 mM phosphate buffer, pH 7.4 | $\mu$M range | 538 |
| **N4.26** | 10 mM PBS, pH 8.0 | 0.15–3.0 $\mu$M | 539 |
| **N4.27** | water | $\mu$M range | 540 |
| **N4.28** | 10 mM PBS, pH 8.0 | $\mu$M range | 541 |
| | Dopamine Analyte | | |
| **N4.29** | 10 mM Tris-HCl, pH 6.5; synthetic urine | 0.005–10 $\mu$M | 542 |
| **N4.31** | PBS, pH 7.4 | at 30 $\mu$M | 544 |
| **N4.32** | 10 mM PBS, pH 7.4 | 0.1–200.0 $\mu$M | 545 |
| **N4.33** | 10 mM PBS, pH 7.4 | nM range | 546 |
| **N4.34**[a] | water; 10 mM HEPES buffer, pH 7.2<br>10 mM sodium phosphate buffer, pH 7.0<br>1× PBS, pH 7.0<br>human urine containing 50% HEPES; pH 7.2<br>human serum containing 50% HEPES, pH 7.2<br>neurobasal medium | $\mu$M range | 547 |
| | Norepinephrine Analyte | | |
| **N4.1** | 10 mM phosphate buffer, pH 6.5<br>artificial urine | 0–1.0 $\mu$M; LOD, 70 nM<br>LOD, 90 nM in synthetic urine | 508 |
| **N4.34**[a] | water; 10 mM HEPES buffer, pH 7.2<br>10 mM sodium phosphate buffer, pH 7.0; 1× PBS, pH 7.0 | $\mu$M range | 547 |
| | Serotonin Analyte | | |
| **N4.7** | 1 mM $MgCl_2$ in 0.125× PBS | 750 nM–2.5 $\mu$M; LOD, 300 nM | 517 |
| **N4.12** | PBS, pH 7.4; serum samples | $\mu$M range | 524 |
| **N4.30** | water, pH 7.0 | 0–40 $\mu$M; LOD, 0.66 $\mu$M | 543 |
| **N4.34**[a] | water; 10 mM HEPES buffer, pH 7.2<br>10 mM sodium phosphate buffer, pH 7.0<br>1× PBS, pH 7.0<br>human urine containing 50% HEPES; pH 7.2<br>human serum containing 50% HEPES, pH 7.2<br>neurobasal medium | $\mu$M range | 547 |

[a] Epinephrine, cadaverine, ascorbic acid, tyramine, histamine, 5-HTP, indole, octopamine, phenethylamine, TrpNH2, tryptamine, L-Trp, and tyramine were also tested.

moderated by a variety of protein classes of which lectins are most intensively studied.[581−583] These proteins are used as model systems to guide the design of artificial chemosensors for effective carbohydrate recognition in aqueous media using noncovalent interactions, such as hydrogen bonding. In contrast, molecular probe-based approaches aim for covalent bond formation usually with the hydroxyl groups of the carbohydrates. Moreover, the aldehyde moiety of reducing sugars can be exploited for carbohydrate detection. Both methodologies will be described in the following sections.

### 5.1. Molecular Probes for Carbohydrates

In the early days of chemistry, (reducing) carbohydrates were detected through their reaction with copper salts, which leads to the appearance of a blue color. During this so-called Fehling's test, the aldehyde group of the acyclic sugar is oxidized to yield an acid.[584] Another common method for the sugar detection uses the Tollens' reagent, where silver nitrate is reduced to elemental silver. These methods can be considered as the first practically useful probes for saccharides.[585]

Molecular probes based on boronic acids have been developed as attractive options to sense carbohydrates over the past decades. The operating mode of most probes is based on the reversible covalent interaction of boronic acids with diols forming five- or six-membered cyclic esters, first studied by Lorand and Edwards using phenylboronic acids.[586] Because several detailed reviews have already been published in the past years covering the broad outline of probes for carbohydrate detection,[587−590] we provide here only a summary of recent reports for carbohydrates sensing in aqueous media from the year 2000 onwards.

The reaction of a boronic acid and a 1,2-diol is an equilibrium-based process in aqueous media (Figure 125). The

**Table 15. Summary of the Normal Concentration of Neurotransmitters in Biofluids**[a]

| concentration range | media | ref |
|---|---|---|
| Acetylcholine Analyte | | |
| 3.4−14.2 μM | saliva | 62 |
| 0.2−1.3 μM | blood | 548 |
| 2.57−5.81 μmol/mmol creatinine = 25.7−58.1 μM | urine (>50 years old, females) | 549 |
| 1.8−6.6 μmol/mmol creatinine = 17.8−65.7 μM | urine (> 50 years old, males) | 549 |
| Aspartate Analyte | | |
| 3.5−21.8 μmol/mmol creatinine = 35−218 μM | urine | 50 |
| 13.9−52.7 μM | saliva | 62 |
| 7.0 μM | serum | 550 |
| 4.0−8.6 μM | human plasma | 551 |
| Dopamine Analyte | | |
| 0.2−0.7 μmol/mmol creatinine = 2.0−7.0 μM | urine | 50 |
| 150−290 nmol/mmol creatinine = 1.5−2.9 μM | urine | 552 |
| 8.0−9.0 nM | human plasma | 553 |
| Epinephrine Analyte | | |
| 4.7−5.7 nmol/mmol creatinine = 47−57 nM | urine | 554 |
| 0.36−0.56 nM | human plasma | 553 |
| GABA Analyte | | |
| 2.7−3.3 μmol/mmol creatinine = 27−33 μM | urine | 50 |
| 85.0−135 nM | human plasma | 555 |
| Glutamate Analyte | | |
| 3.30−18.4 μM/mM creatinine = 33.0−184 μM | urine | 50 |
| 12−40 μM | human plasma | 556 |
| Glycine[b] Analyte | | |
| 44.0−300 μmol/mmol creatinine = 0.44−3.00 mM | urine | 50 |
| 34.0−230 μM | saliva | 62 |
| ∼92 μM | serum | 550 |
| 155−270 μM/L plasma | human plasma | 556 |
| Histamine Analyte | | |
| 0−7.5 μM | saliva | 62 |
| 10−100 nmol/mmol creatinine = 0.3 (0.1−1.0) μM | urine | 50 |
| 0.3−1.0 μM | whole blood | 445 |
| 0.49−1.8 nM | plasma | 444 |
| Norepinephrine Analyte | | |
| 3.40−33.6 μmol/mmol creatinine = 34.2−336 μM | urine | 557 |
| 1.52−1.76 nM | human plasma | 553 |
| Serotonin Analyte | | |
| 40.0−120 nmol/mmol creatinine = 0.4−1.2 μM | urine | 50 |
| 80.0−750 nM | human plasma | 551 |
| Tyramine Analyte | | |
| 200−275 nmol/mmol creatinine = 0.20−2.75 μM | urine | 558 |

[a] Urinary analyte concentrations were converted assuming a representative creatinine level of 10 mmol/L. [b] Wide range of concentrations reported.

addition of water (or $OH^-$) to the boronic acid leads to the formation of the tetravalent boronate anion ($K_{tet}$), which can then form three covalent bonds in a $sp^2$-type geometry. Besides that, the boron center acts as a Lewis acid and can form covalent bonds with a $sp^3$-type geometry ($K_{trig}$) with the diol. Consequently, for the calculation of the binding constant ($K_a$), both processes should be considered. Fortunately, Wang and coworkers established a method that allows to determine $K_a$, $K_{tet}$, and $K_{trig}$ through titrations at different pH values.[591,592]

The reversible and relatively fast-equilibrating dynamic covalent boronic acid−diol interaction renders boronic acids and their derivatives attractive probes for the detection of carbohydrates in aqueous media. The binding strength of boronic acids to carbohydrates depends on the orientation of the target analytes' hydroxyl groups, which enables a differentiation between various carbohydrates. Besides, there is a remarkable difference of the binding affinities for monosaccharides between mono- and diboronic acids. Monoboronic acids tend to show a higher selectivity for fructose over glucose, as fructose interacts only with one boronic acid group. Conversely, diboronic acids show increased selectivity towards D-glucose because α-D-glucofuranose can bind two boronic acid groups.[586,593] The selective sensing of D-glucose in biofluids (mainly blood) is of special interest because D-glucose plays an important role in biological processes and is used as an indicator parameter for diabetic patients. This might be the reason why many more probes have been developed for D-glucose compared to other saccharides so far. All molecular probes, chemosensors, and nanosensors discussed within this section are summarized in Tables 16−18.

### 5.2. Molecular Probes for D-Glucose and Other Saccharides

A variety of molecular probes has been designed for selective D-glucose sensing, and among these a fluorescence-based signal transduction is commonly used. For example, the boronic acid moiety can be combined with different fluorophores, resulting in a fast and easy to detect emission change. The first fluorescence-based D-glucose probes were introduced by the groups of Czarnik and Shinkai in the 1990s, each using an anthracene moiety as the fluorophore.[593−595]

James and coworkers showed a new design of a molecular probe bearing two phenylboronic acid groups in combination with a pyrene group and alkyl linkers. By varying the alkyl linker length from $n = 3$ to $n = 8$, the authors demonstrated that the hexamethylene-linked probe **P5.1** provides optimal D-glucose sensitivity and selectivity over D-galactose, D-mannose, and D-fructose in phosphate buffer (52% MeOH).[597] In 2010, the influence of the fluorophore, *e.g.*, pyrene, anthracene, and naphthalene, and of the geometry of the two boronic acid linkers on the selectivity for D-glucose over several monosaccharides was studied by a variety of probes, *e.g.*, **P5.2** and **P5.3**. Fluorescence titration experiments showed that the affinity for D-glucose is highly influenced by the chemical nature of the probe. In addition, the structures of the complexes formed were studied using CD spectroscopy. All six probes were found to be D-glucose selective (Figure 126).[596]

The fluorescence enhancement of the *o*-aminomethylphenyl boronic acid probes upon carbohydrate binding is widely believed to be caused by turning off the PET quenching after boronic acid−sugar complexation. However, the groups of Larkin and Anslyn suggested an alternative explanation that they deduced from the investigation of the photophysical behavior of probe **P5.4** upon its binding to fructose in water containing 33% MeOH and upon the subsequent addition of 50 mM NaCl (Figure 127).[598] The observed increase in emission intensity upon fructose addition was attributed to

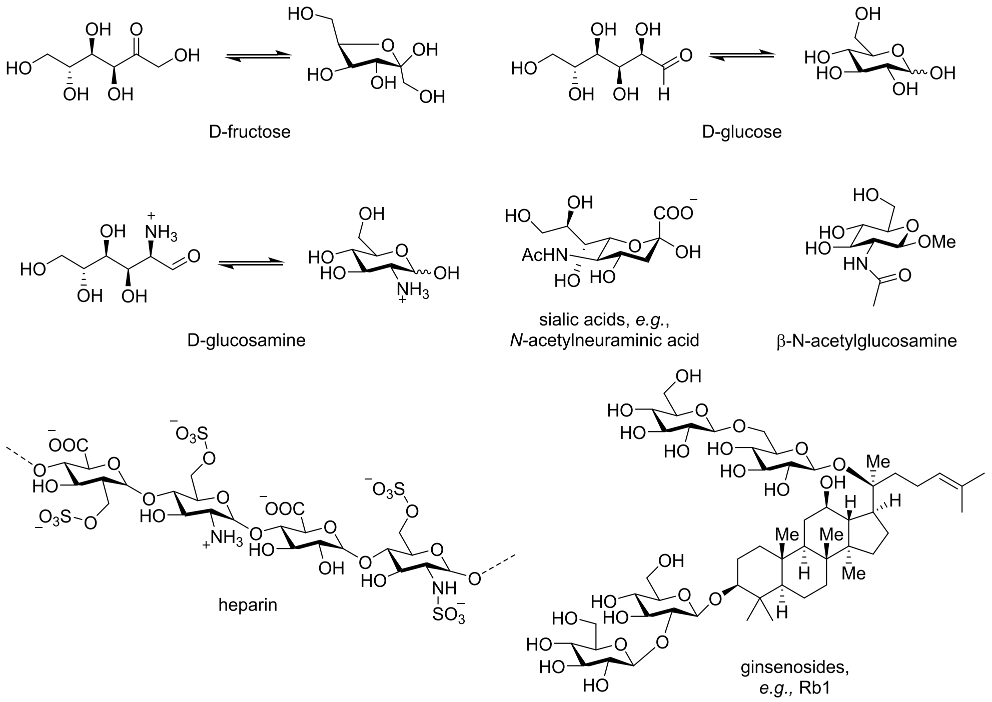

**Figure 124.** Chemical structures of selected carbohydrates.

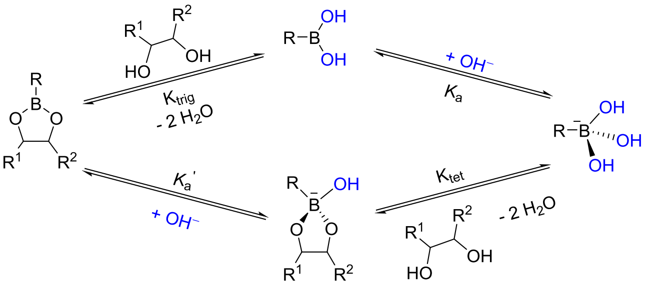

**Figure 125.** Thermodynamic cycle of the reversible transformation of boronic acids with 1,2-diols to boronic esters.

disaggregation of probe **P5.4**. Later, the authors put forward the so-called "loose bolt effect" internal conversion mechanism for explaining the emission enhancement of probe **P5.5** upon its interaction with fructose.[599]

In 2002, Wang and coworkers developed a fluorescent diphenylboronic acid-based probe (**P5.6** in Figure 128) bearing two symmetrical arranged anthracene groups that showed a high affinity for D-glucose ($K_a$ = 1472 $M^{-1}$) in 50% MeOH in 100 mM phosphate buffer, pH 7.4, with 43- and 49-fold selectivity for glucose over fructose and galactose, respectively.[600] The functionalization of this probe with an electron-withdrawing cyano group (**P5.7**) or nitro group (**P5.8**) at the phenylboronic acid moiety resulted in an even higher apparent binding constant for D-glucose ($K_a$ = 2540 $M^{-1}$ and $K_a$ = 1810 $M^{-1}$), whereas the fluorinated probe (**P5.9**) showed a lower affinity ($K_a$ = 630 $M^{-1}$). In contrast, the selectivity between glucose and fructose was reduced for all three derivatives compared to the parent probe.[601]

In 2009, the groups of Barwell and James presented another approach towards D-glucose selective sensing. They designed a molecular tweezer-type probe (**P5.10**), which showed an almost equal binding affinity for D-glucose and D-fructose ($K_a$ = 2850 $M^{-1}$ and $K_a$ = 2660 $M^{-1}$) in phosphate buffer containing 52% MeOH. Nevertheless, the two analytes were distinguished from each other as exclusively D-glucose opens the tweezer by forming a 1:1 complex with the boronic acid moieties, causing a quenching of the pyrene excimer emission. In contrast, D-fructose yields a 1:2 complex without disrupting the pyrene excimer emission (Figure 129).[602]

Another fluorescent molecular probe that uses both an aldehyde and a boronic acid binding motif was developed by Glass and coworkers in 2015.[603] The boronic acid-containing coumarin aldehyde **P5.11** exhibits a remarkable glucosamine selectivity over several structurally similar biomolecules in 25 mM HEPES buffer, pH 7.4, containing 120 mM NaCl (Figure 130). D-Glucosamine is one of today's most common nutraceutical products, used to treat osteoarthritis and often administered as a dietary supplement, although the efficiency of such treatments remains debated.[604,605] For glucosamine, a high binding affinity with **P5.11** ($K_a$ = 4100 $M^{-1}$) concomitant with a strong fluorescence enhancement was observed, which can be traced back to its "dual" functionality, as it binds with both the boronic acid and the aldehyde group in a cooperative manner. The fluorescence increase is explained by the reversible iminium formation of the primary amine with the aldehyde group of **P5.11**, which induced an ICT of the coumarin and caused a large red-shift in the excitation spectrum. Accordingly, glucose showed almost no fluorescence change and only a low binding constant, as it lacks an amine group. Notably, norepinephrine, which also features amine and diol groups, is for steric reasons only bound *via* its amine functionality to **P5.11** and shows a similar low binding constant as glucose.

The administration of heparin, an anticoagulant, is a common medical treatment of heart attacks, angina pectoris, and other cardiovascular dysfunctions, which makes its monitoring important to adjust the treatment. Heparin is a highly negatively charged oligosaccharide consisting of repeating disaccharide units of 1 → 4 linked sulfated iduronic

### Table 16. Summary of Molecular Probes for Carbohydrates Sorted by Analytes (LOD, Limit of Detection)

| probe | media | concentration range | ref |
|---|---|---|---|
| | D-Fructose Analyte | | |
| **P5.21** | 1 mM sodium phosphate buffer, pH 9.0 | 0.1–100 mM | 617 |
| **P5.22** | 1 mM sodium phosphate buffer, pH 9.0 | 0.1–100 mM; LOD, 200 $\mu$M | 617 |
| **P5.4** | 50 mM NaCl in 33% MeOH in water | 0–32 mM | 598 |
| **P5.5** | water | 0–100 mM | 599 |
| | D-Glucose Analyte | | |
| **P5.1**[a] | 52% MeOH in phosphate buffer, pH 8.2 (10 mM KCl, 2.75 mM $KH_2PO_4$, 2.75 mM $Na_2HPO_4$) | 0–100 mM | 597 |
| **P5.2** | 52% MeOH in phosphate buffer, pH 8.2 (10 mM KCl, 2.75 mM $KH_2PO_4$, 2.75 mM $Na_2HPO_4$) | 0–100 mM | 596 |
| **P5.3** | 52% MeOH in phosphate buffer, pH 8.21 (10 mM KCl, 2.75 mM $KH_2PO_4$, 2.75 mM $Na_2HPO_4$) | 0–100 mM | 596 |
| **P5.6** | 50% MeOH in 100 mM phosphate buffer, pH 7.4 | 0–100 mM | 600 |
| **P5.7** | 50% MeOH in 100 mM phosphate buffer, pH 7.4 | 0–10 mM | 601 |
| **P5.8** | 50% MeOH in 100 mM phosphate buffer, pH 7.4 | 0–20 mM | 601 |
| **P5.9** | 50% MeOH in 100 mM phosphate buffer, pH 7.4 | 0–20 mM | 601 |
| **P5.10**[b] | 52% MeOH in phosphate buffer, pH 8.2 (10 mM KCl, 2.75 mM $KH_2PO_4$, 2.75 mM $Na_2HPO_4$) | 0–100 mM | 602 |
| **P5.15** | 100 mM NaCl in water containing 1% DMSO, pH 10.0 | mM range | 610 |
| **P5.16** | 1% DMSO in carbonate buffer, pH 10.5; artificial urine | mM range | 609 |
| **P5.17** | 2% or 10% DMSO in carbonate buffer, pH 10.0; artificial urine | 0–10 mM in buffer; mM range in urine | 614 |
| **P5.18** | 50 mM phosphate buffer; 52% MeOH in 50 mM phosphate buffer; 1× PBS | $\mu$M–mM range | 615 |
| **P5.19** | 50 mM phosphate buffer; 52% MeOH in 50 mM phosphate buffer; 1× PBS | $\mu$M–mM range | 615 |
| **P5.20** | 50 mM phosphate buffer; 52% MeOH in 50 mM phosphate buffer; 1× PBS | $\mu$M–mM range | 616 |
| **P5.23** | 50 % EtOH in PBS; whole blood | 200 $\mu$M–200 mM | 618 |
| **P5.24** | 2% MeOH in 50 mM carbonate buffer, pH 10.0 | mM range | 619 |
| **P5.26** | 150 mM PBS, pH 7.4 | 0–100 mM | 621 |
| **P5.27** | *in vivo* (intravascular) | 40–400 mg $dL^{-1}$ | 17 |
| **P5.28** | *in vivo* (intravascular) | 40–400 mg $dL^{-1}$ | 18 |
| | Glucosamine Analyte | | |
| **P5.11** | 120 mM NaCl in 25 mM HEPES buffer, pH 7.4 | 0–2.0 mM | 603 |
| | Mono-/disaccharide Analyte | | |
| **P5.25**[c] | 50 mM HEPES buffer, pH 7.4 | 0–1.0 M | 620 |
| | Heparin | | |
| **P5.12**[d] | 50% MeOH in HEPES buffer, pH 7.4 | 0–1.75 mM | 606 |
| **P5.13**[e] | 10 mM HEPES buffer, pH 7.4 | 0–10 $\mu$M | 607 |
| | human serum | 0–4.0 $\mu$M | |
| **5.14** | 25 mM HEPES buffer, pH 7.1 | 0–3.0 $\mu$M | 608 |

[a] Galactose and fructose show also small binding affinities, depending on the length of the alkyl chain.[597] [b] Binds also fructose with similar $K_a$ but only glucose causes emission quenching. [c] Various saccharides tested. [d] Binds chondroitin-4-sulfate and heparin disaccharide I–S with binding affinities of one magnitude smaller than heparin. [e] Can be recovered by protamine addition.

### Table 17. Summary of Chemosensors for Carbohydrates Sorted by Analytes

| chemosensor | media | concentration range | ref |
|---|---|---|---|
| | D-Glucose Analyte | | |
| **C5.2** | 100 mM phosphate buffer, pH 7.1 | 0–80 mM | 582 |
| **C5.3**[a] | water;10 mM phosphate buffer, pH 7.4; human serum | mM range | 629,630 |
| | Heparin Analyte | | |
| **C5.4** | 150 mM NaCl in 10 mM Tris-HCl buffer | 0–100 $\mu$M | 631 |
| **C5.5** | 5 mM HEPES buffer, pH 7.4; 1% FBS serum | 0–2 $\mu$g $mL^{-1}$ | 632 |
| | Me-*β*-*N*-acetyl-glucosamine Analyte | | |
| **C5.1**[a] | $D_2O$ | high mM range | 628 |

[a] Binds also several other saccharides but with lower affinity.

### Table 18. Summary of Nanosensors for Carbohydrates Sorted by Analytes (LOD, Limit of Detection)

| nanosensor | media | concentration range | ref |
|---|---|---|---|
| | D-Glucose Analyte | | |
| **N5.2** | 100 mM phosphate buffer, pH 7.4 | 0–200 mM; LOD, 0.06 mM | 634 |
| **N5.3** | 100 mM PBS, pH 8.0; urine samples | 0–2.0 mM in buffer; LOD, 10 $\mu$M; 250–1500 $\mu$M in urine | 636 |
| **N5.4** | 100 mM PBS, pH 7.4; blood samples | 0–210 $\mu$M; LOD, 1.7 $\mu$M | 637 |
| **N5.5** | water; serum samples, pH 9.0 | 32 $\mu$M–2.0 mM; LOD, 8 $\mu$M | 638 |
| **N5.6** | water, pH 9.0; human serum samples, pH 9.0 | 3 $\mu$M–3.0 mM; LOD, 0.8 $\mu$M | 639 |
| **N5.7** | PBS, pH 7.4 | mM range | 640 |
| | Ginsenosides, *e.g.*, Rb1 Analyte | | |
| **N5.8** | 67 mM PBS, pH 7.1 | mM range | 641 |
| | Sialic Acid Analyte | | |
| **N5.1** | 5 mM phosphate buffer, pH 5.6; human serum samples | 50–900 $\mu$M in buffer; LOD, 35 $\mu$M; 300–500 $\mu$M in serum | 633 |

acid and sulfated glucosamine. Anslyn and coworkers reported molecular probe **P5.12** for the colorimetric detection of heparin within a preorganized macrocyclic cavity (Figure 131).

The binding of heparin to **P5.12** compared to structurally similar polysaccharides such as hyaluronic acid was studied in an IDA format in HEPES buffer, pH 7.4, containing 50% MeOH. A strong alteration of the absorbance spectrum, *i.e.*, a signal decrease at 430 nm and a signal increase at 526 nm, was reported when using pyrocatechol violet as the indicator dye. The binding constant for heparin was determined to be $K_a$ = 7100 $M^{-1}$.[606] It is noteworthy that the binding is not only mediated by the reversible boronic ester formation but also by ion pairing between the ammonium, carboxylate, and sulfate moieties of heparin. To make the molecular probe applicable in biological media, Anslyn and coworkers incorporated a fluorescent scaffold into probe **P5.13** (Figure 131), which thus can be used in a direct binding assay in crude serum.[607] Indeed, a calibration curve in the clinical relevant concentration range (0.08–3.2 $\mu$M) for unfractionated heparin and for low-molecular-weight heparin was obtained. Probe **P5.13** showed a significantly enhanced affinity and selectivity for heparin in 10 mM HEPES buffer, and the binding constant of **P5.13** for UFH was determined to be $K_a$ = 1.4 × $10^8$ $M^{-1}$, which is $10^4$ times higher than that of probe **P5.12**.

The Schrader group combined dynamic covalent binding and noncovalent binding motifs for selective sensing of heparin.[608] The fluorescent copolymer (**P5.14** in Figure 132)

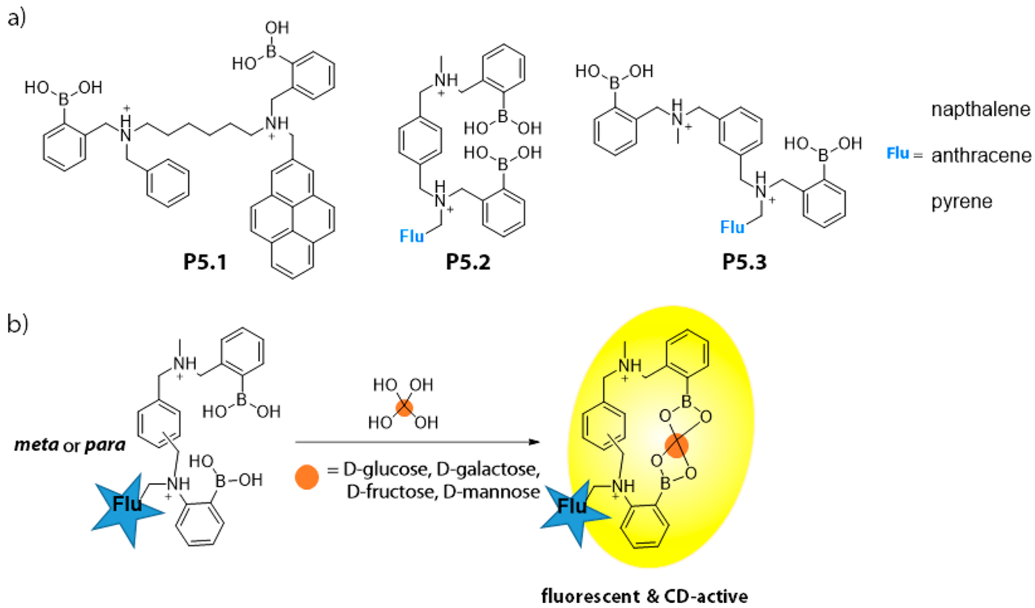

**P5.1** **P5.2** **P5.3**

**Figure 126.** (a) Chemical structures of the D-glucose-sensing probes **P5.1**−**P5.3**. (b) Schematic representation of the binding of a saccharide to the molecular probes **P5.2** and **P5.3**. Adapted with permission from ref 596. Copyright 2002 The Royal Society of Chemistry.

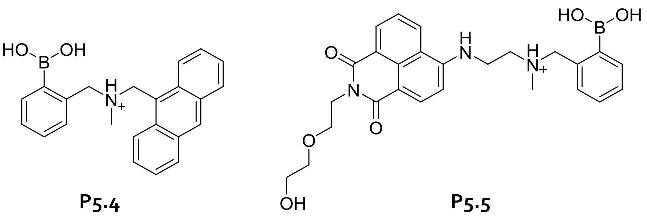

**P5.4** **P5.5**

**Figure 127.** Chemical structures of probe **P5.4** and **P5.5**.

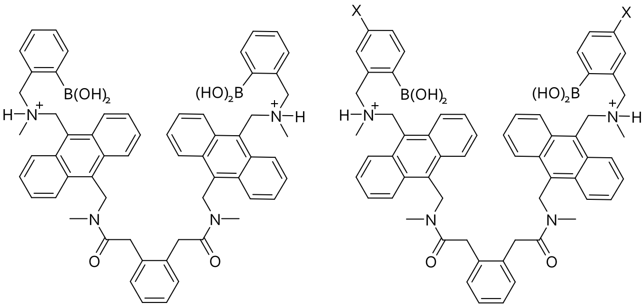

**P5.6**

**P5.7** X = CN
**P5.8** X = $NO_2$
**P5.9** X = F

**Figure 128.** Chemical structures of probes **P5.6**−**P5.9**.

contained binding sites tailored for recognizing sulfated carbohydrates and allowed for specific detection of heparin in 25 mM HEPES buffer, pH 7.1, with a remarkably high sensitivity (30 nM heparin).

Hayashita and coworkers have shown that a phenylboronic acid azoprobe/$\gamma$-CD complex (**P5.15** in Figure 133a) exhibited a high D-glucose selectivity by forming a 2:1 complex with an apparent binding constant of $K_a = 3.0 \times 10^7$ $M^{-2}$ in water containing 1% DMSO and 100 mM NaCl, pH 10.0. Interestingly, a dye analogue which lacked the benzamide spacer showed no response to D-glucose.[610] Following a similar supramolecular design idea, Jiang and coworkers developed a 2:2 stilbeneboronic acid−$\gamma$-cyclodextrin ensemble (**P5.16**), which allowed for the selective detection of D-glucose over fructose and other monosaccharides in 1% DMSO in carbonate buffer, pH 10.5, and even in artificial urine samples at sub-mM levels (Figure 133b).[609] The combination of boronic acid-based carbohydrate recognition with cyclodextrin-based host−guest chemistry could have several advantages, for instance, ensuring water solubility of the probe that is often limiting for unmodified phenylboronic acids. Moreover, the noncovalent binding of dye molecules opens new possibilities for the fine-tuning of the probe. Therefore, several probes using such boronic acid/cyclodextrin combinations for saccharide detection have been reported within the last few years.[611−613]

A "light-up" molecular probe (**P5.17**) with a high specificity for D-glucose was developed by Sun, Tang, and coworkers.[614] Advantages of the probe are its simple preparation and the strong fluorescence enhancement caused by the aggregation of bisboronic acid tetraphenylethylene fluorogenes. Binding of D-glucose to the boronic acid moieties led to the formation of linear oligomers that restricted the intramolecular rotation of the tetraphenylethylene moiety (rigidochromic effect), causing a fluorescence turn-on response. The specificity of **P5.17** for D-glucose was verified by investigating other monosaccharides, *e.g.*, D-fructose, D-mannose, and D-galactose, as potential interferents. Only with D-glucose, a fluorescence increase was observed in carbonate buffer, pH 10.5, containing 2% DMSO, which was explained by the fact that only D-glucose possesses *cis*-diol units that are essential for the oligomerization to occur. The authors showed that the probe can be applied for the detection of D-glucose in artificial urine at millimolar concentrations (Figure 134).

Hansen and coworkers examined the binding properties of three BODIPY-containing probes (**P5.18**−**P5.20** in Figure 135) towards D-glucose in several buffers such as 50 mM phosphate buffer, methanolic buffer, and 1× PBS.[615,616] The binding affinity of the fluorinated probes toward D-glucose was independent of the used buffers. In contrast, the binding affinity for unsubstituted and methylated probes were significantly reduced in buffered solutions ($K_a$ < 2 $M^{-1}$ in

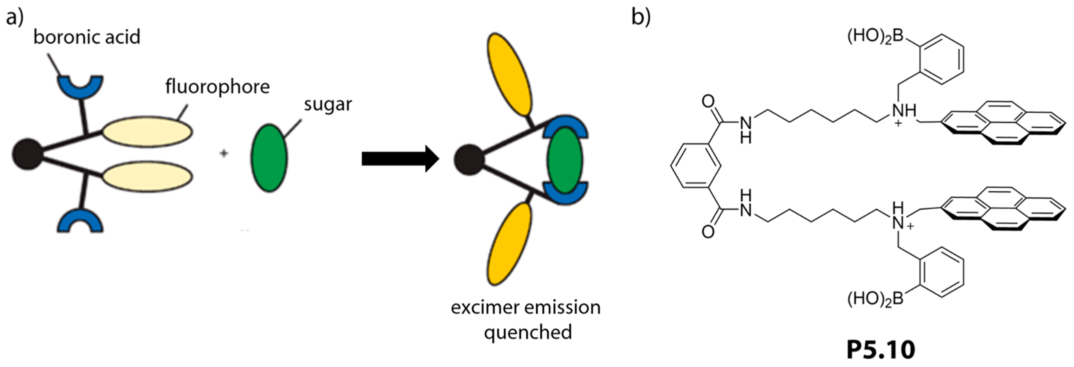

**Figure 129.** (a) Schematic representation showing the binding of D-glucose and D-fructose to a molecular tweezer. (b) Chemical structure of molecular probe **P5.10**. Adapted with permission from ref 602. Copyright 2009 The Royal Society of Chemistry.

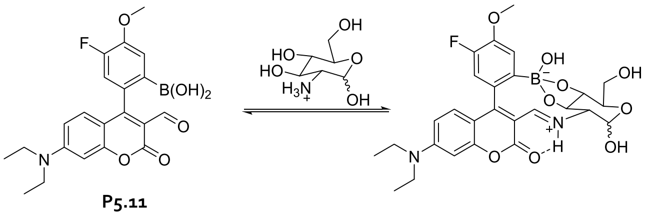

**Figure 130.** Schematic representation of the binding event of D-glucosamine to probe **P5.11**, causing a fluorescence turn-on.

saline and phosphate buffer; $K_a$ = 1 $M^{-1}$ in methanolic phosphate buffer). The fluorinated BODIPY-probe **P5.18** displayed a strong binding affinity towards D-glucose ($K_a$ = 5.8 × $10^5$ $M^{-1}$). Because of its high robustness in several buffers and its high $K_a$ value sufficient for D-glucose detection at physiological relevant concentration ranges, the use of **P5.18** may be promising for D-glucose-monitoring in human blood.

Qin and coworkers synthesized an unsymmetrical BODIPY derivative *via* a Knoevenagel condensation reaction to achieve an emission shift towards higher wavelengths.[617] The obtained phenylboronic acid-BODIPY probe (**P5.21** in Figure 136) showed a binding affinity of $K_a$ = 55 $M^{-1}$ toward D-fructose in 1 mM phosphate buffer, pH 9.0, but did not challenge the performance of the unsubstituted probe **P5.22**, which offered a higher binding affinity towards D-fructose ($K_a$ = 297 $M^{-1}$) and was therefore selected for the application in polymeric optodes. The generated optodes showed a reasonable selectivity for D-fructose over D-glucose and D-galactose in the concentration range of 0.1−100 mM, with a D-fructose detection limit of 200 μM in 1 mM sodium phosphate buffer, pH 9.0.

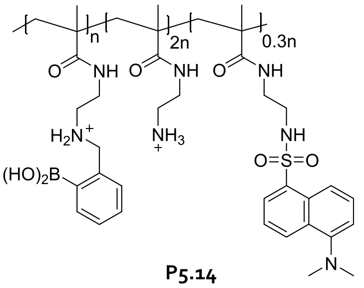

**Figure 132.** Chemical structure of the copolymer-based probe **P5.14**.

A redox-reaction-based approach for D-glucose sensing was introduced in 2015 by Qin, Jiang, and coworkers. The fluorescence probe (**P5.23**) was obtained by the combination

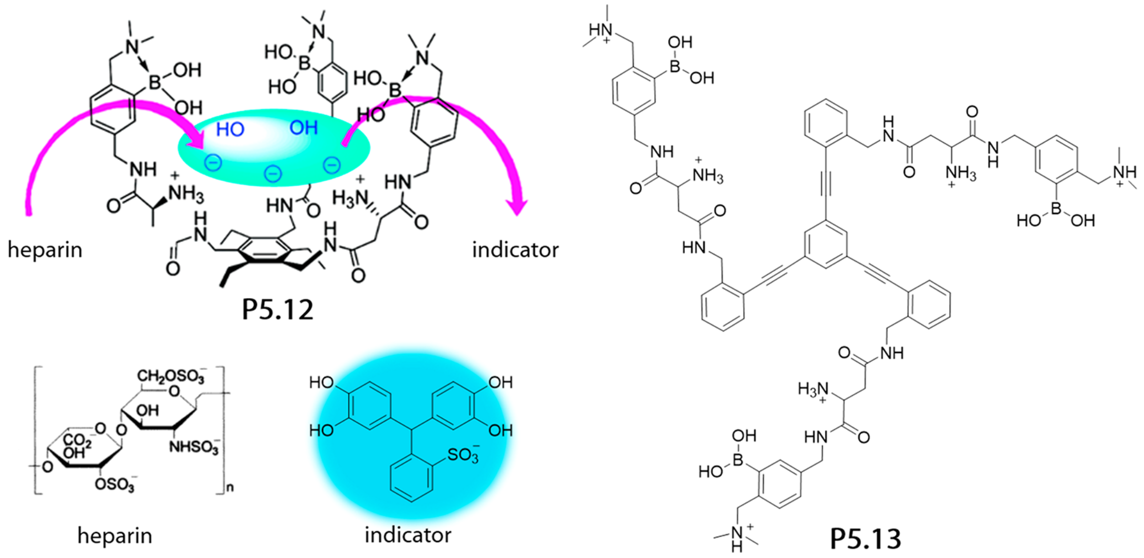

**Figure 131.** Schematic representation of heparin binding to probes **P5.12** and **P5.13**. While probe **P5.12** operates through an IDA mechanism, probe **P5.13** is inherently fluorescent and can be used in a DBA. Adapted with permission from ref 606. Copyright 2002 American Chemical Society.

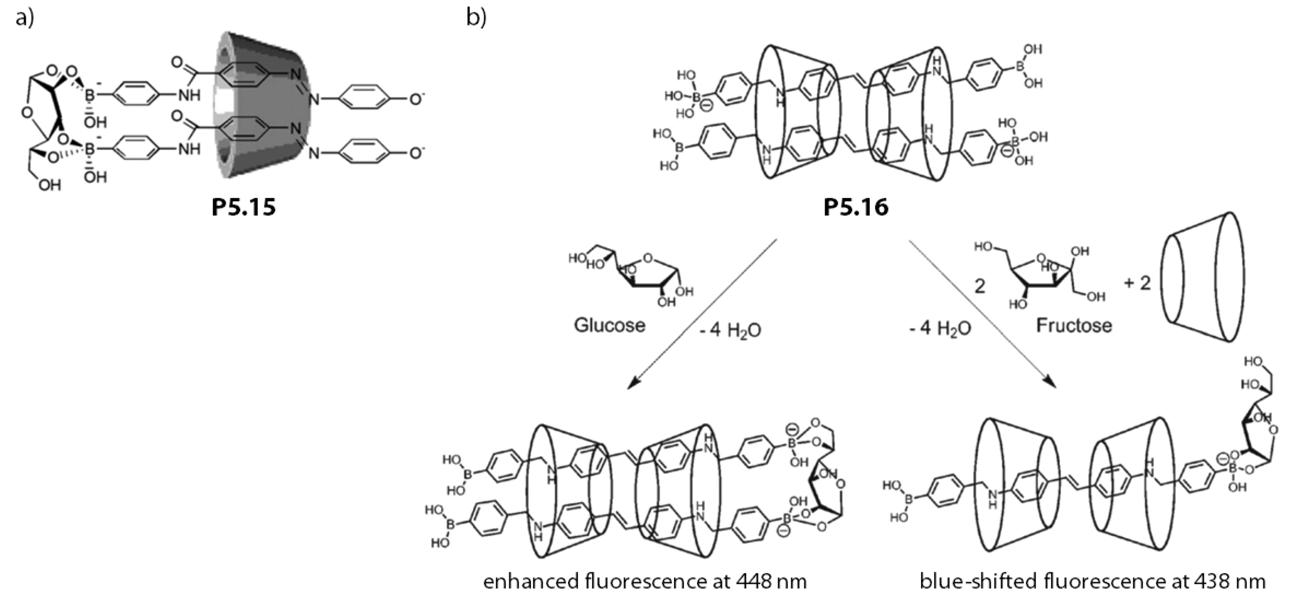

**Figure 133.** (a) Chemical structure of D-glucose sensing with probe **P5.15**. (b) Interaction of probe **P5.16** (2:2 complex) with D-glucose and D-fructose. Adapted with permission from refs 609 and 610. Copyrights 2009 and 2012 The Royal Society of Chemistry.

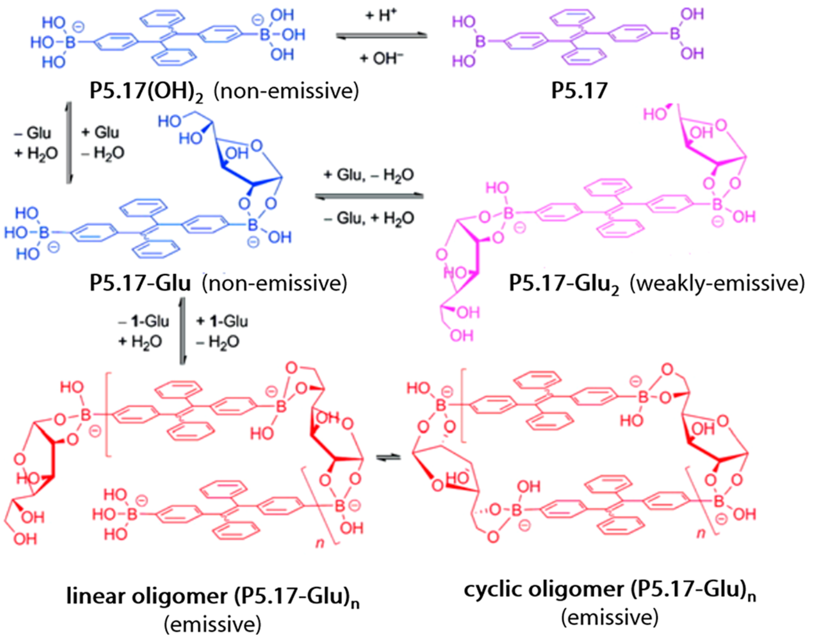

**Figure 134.** Proposed mechanism for the D-glucose-specific sensing with probe **P5.17**. Adapted with permission from ref 614. Copyright 2010 American Chemical Society.

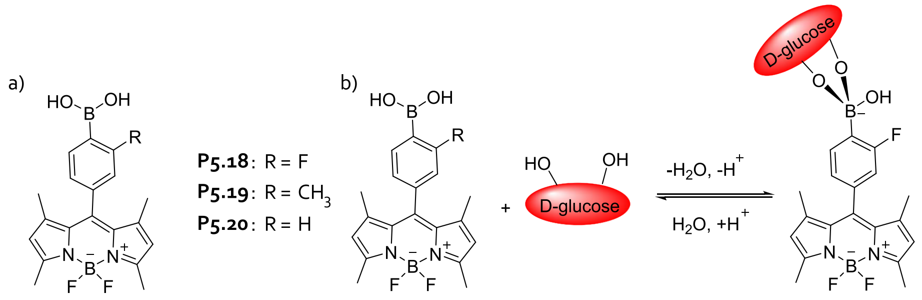

**Figure 135.** (a) Chemical structures of the probes **P5.18**−**P5.20**. (b) Proposed binding mechanism for D-glucose binding of probe **P5.18**, causing an emission turn-on response. Adapted with permission from ref 615. Copyright 2013 Elsevier BV.

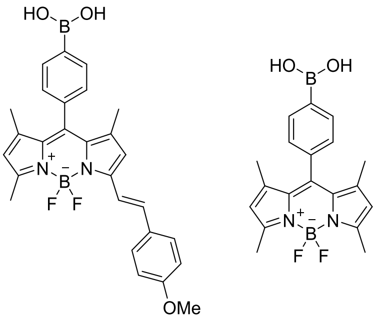

**P5.21** **P5.22**

**Figure 136.** Chemical structures of probes **P5.21** and **P5.22**.

of an azaBODIPY dye with two phenylboronic acid groups (Figure 137). The detection of D-glucose was possible due to the enzymatic reaction of glucose oxidase, in which D-glucose was converted into gluconolactone. The released hydrogen peroxide led to the transformation of the phenylboronic acid moiety into phenolic groups, resulting in a red-shift of the emission from 682 to 724 nm. D-Glucose was successfully detected with high selectivity in a concentration range from 0.2 to 200 mM in PBS, pH 7.4, containing 50% EtOH. In addition, the authors successfully immobilized the probes into a thin polymer layer and were able to determine D-glucose concentrations in 40-fold diluted whole blood samples from sheep.

In 2013, Jiang, James, and coworkers developed the fluorescent probe **P5.24** composed of an amphiphilic monoboronic acid with a pyrene fluorophore, which allowed for the sensitive and selective ratiometric sensing of D-glucose in aqueous media.[619] D-Glucose sensing was performed in the presence of fructose and gave excellent selectivity results. Even though **P5.24** bound both monosaccharides, only D-glucose offered a dual binding motif to **P5.24**, which caused the formation of aggregates in which the pyrene moieties came in close proximity and displayed excimer emission. The binding constants for D-glucose with probe **P5.24** were reported as $K_a = 1.4 \times 10^3\ \text{M}^{-1}$ and $1.9 \times 10^6\ \text{M}^{-2}$ (assuming 1:2 binding) in 50 mM carbonate buffer, pH 10.0, containing 2% MeOH (Figure 138).

A pattern-recognition-based sensing strategy, which used functional polymers for D-glucose detection in 50 mM HEPES buffer, pH 7.4, was introduced by the group of Bonizzoni in 2019. Polymeric poly(methacrylic acid) (PMAA) was doped with acrylamido phenylboronic acid (AAPBA) moieties to yield a water-soluble copolymer (PMAA-*co*-AAPBA) that acted as a supramolecular probe (**P5.25** in Figure 139) for carbohydrates. Hematoxylin served as an indicator dye that was displaced by the carbohydrates tested, as could be readily witnessed by the resulting absorbance enhancement. With **P5.25**, it was possible to distinguish both mono- and disaccharides, *e.g.*, glucose, fructose, and galactose, through an array-based sensing protocol in which absorbance, steady-state fluorescence intensity, and anisotropy were recorded.[620]

Incorporation of boronic acid-based probes within hydrogels was carried out by the groups of Butt and Elsherif in 2018.[621] The authors aimed to develop an optical D-glucose sensor that can be integrated into contact lenses. Therefore, a holographic-diffuser structure was imprinted on a phenylboronic acid motif, which was present in a hydrogel (**P5.26**). When the hydrogel films were soaked in solutions of D-glucose in 150 mM PBS, pH 7.4, swelling occurred, and the degree of swelling was found to be glucose concentration dependent. The swelling reversibly altered the focal length of the optical system, which was determined by measuring the intensity of the light passing through this device (Figure 140). As such, it was possible to detect the D-glucose in the concentration range of 0 to 100 mM. In addition, the authors showed that their glucose-sensing contact lenses also capture the analyte when placed on an artificial eye, suggesting that this approach can be developed into a practical sensor for noninvasive D-glucose level monitoring.

Practical (invasive) glucose sensors that have already found clinical and daily point-of-care use have been independently developed by Senseonics and GlySure Ltd.

The Eversense system is used for the detection of glucose through an implantable sensor.[17] This system is constituted of fluorescent *o*-amino-methylphenylboronic acids functioning as glucose-selective turn-on probes and was developed by James, Sandanayake, and Shinkai.[17,593,595] In the sensor design, probe **P5.27** is immobilized on poly(2-hydroxyethyl methacrylate) hydrogels and integrated into an implantable poly(methyl methacrylate) (PMMA) capsule, which also contains a light-emitting diode for excitation and two photodiodes for fluorescence signal read-out. This so-called "microfluorometer" is depicted in Figure 141a. In the absence of glucose, the fluorescence of **P5.27** is quenched, possibly due to an intermolecular PET process (Figure 141b). When glucose is present, it reversibly binds with boronic acids and causes

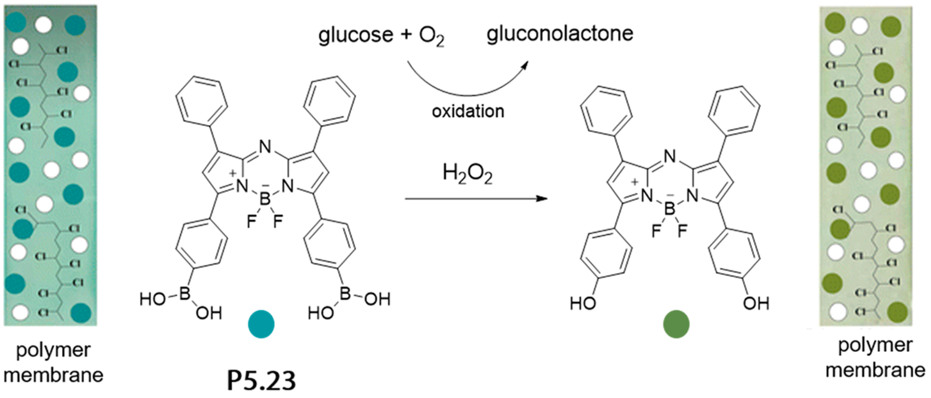

**Figure 137.** Detection mechanism of D-glucose with the azaBODIPY modified probe **P5.23**. Adapted with permission from ref 618. Copyright 2015 American Chemical Society.

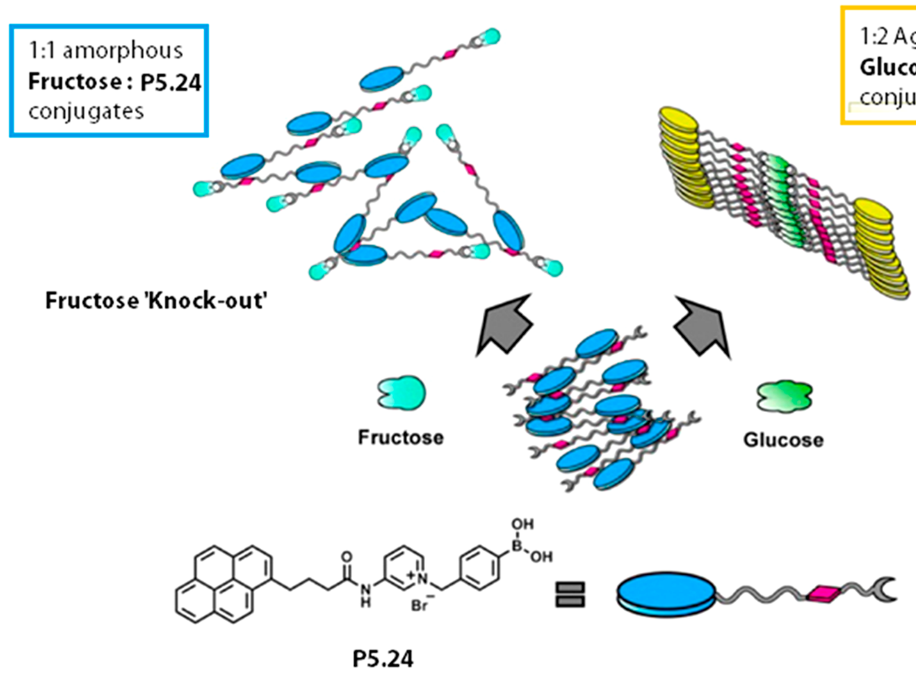

**Figure 138.** Schematic representation of the 1:1 fructose complex and the 1:2 glucose aggregate formed with **P5.24.** Adapted with permission from ref 619. Copyright 2013 American Chemical Society.

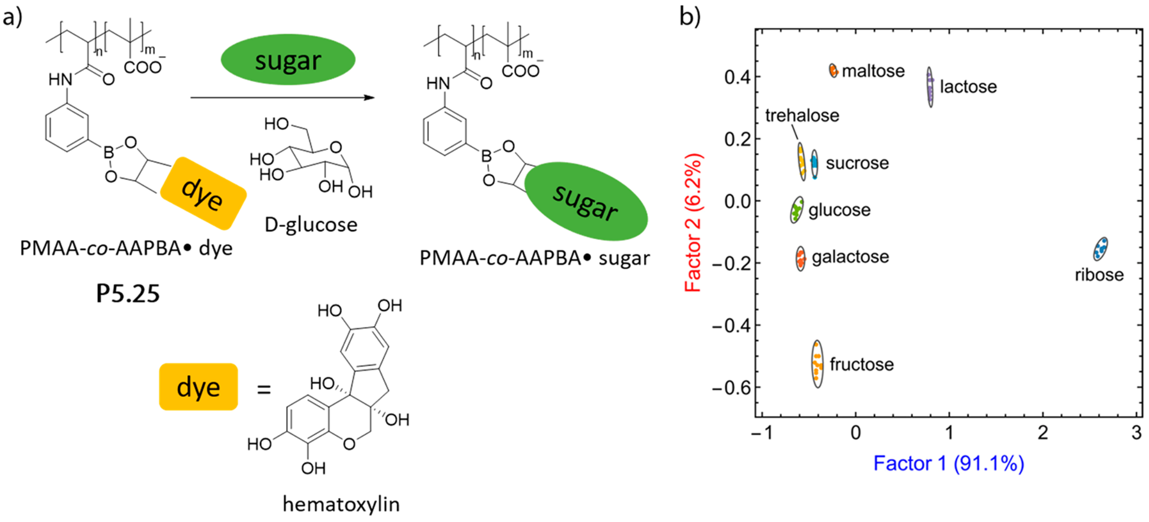

**Figure 139.** (a) Schematic representation of probe **P5.25** that releases the indicator dye hematoxylin upon D-glucose binding. (b) Linear discriminant analysis (LDA) score plot of the interaction of **P5.25** with several different mono- and disaccharides in 50 mM HEPES buffer, pH 7.4. Adapted with permission from ref 620. Copyright 2019 American Chemical Society.

fluorescence increase until all indicator binding sites are occupied. Finally, the recorded emission intensities are converted into an electromagnetic signal and sent to external devices such as smartphones or personal computers for further processing and user interaction. The Eversense system allows for dynamic subcutaneous glucose monitoring (every 5 min) within a concentration range of 40 to 400 mg $dL^{-1}$.

The GlySure Ltd. system developed by Arimori, Frimat, and James in collaboration with Beckman and Coulter is based on hydrogel-immobilized, fluorescent *o*-aminomethylphenylboronic acids (**P5.28** in Figure 142).[597,622] This system enables intravascular glucose monitoring through a disposable glucose sensor that is inserted in a central venous catheter. Analogous to the previous example, the emission of the probe is enhanced in the presence of glucose, which can be dynamically detected in the physiologically relevant concentration range of 40−400 mg $dL^{-1}$.

### 5.3. Chemosensors for Carbohydrates

Although the molecular probes dominate in the field of carbohydrate sensing, there are also many different chemosensors that have been reported for carbohydrate detection. Carbohydrate complexation by chemosensors mainly exploits dispersive interactions and hydrogen bonds as recognition motifs. Especially, the CH−$\pi$ interactions are considered to be of importance for carbohydrate recognition in water as they amplify the hydrophobic effect.[623]

Several synthetic lectins were developed in the past years with promising results towards carbohydrate sensing. The first

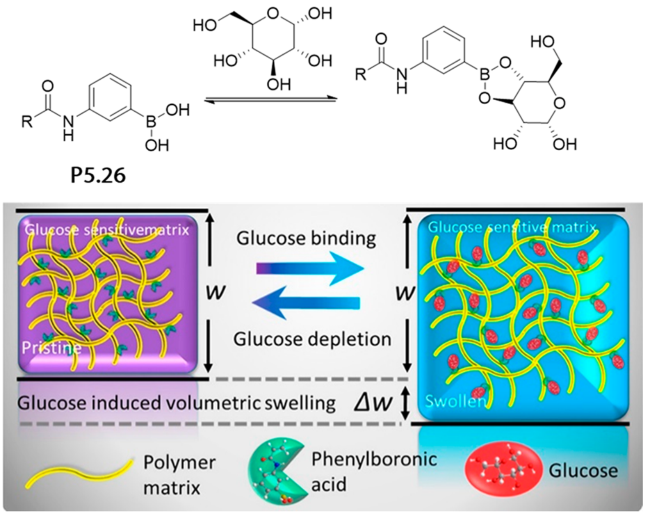

**P5.26**

**Figure 140.** Schematic representation of D-glucose binding to the phenylboronic acid-based hydrogel matrix **P5.26** and resulting swelling of the hydrogel matrix. Adapted with permission from ref 621. Copyright 2019 American Chemical Society.

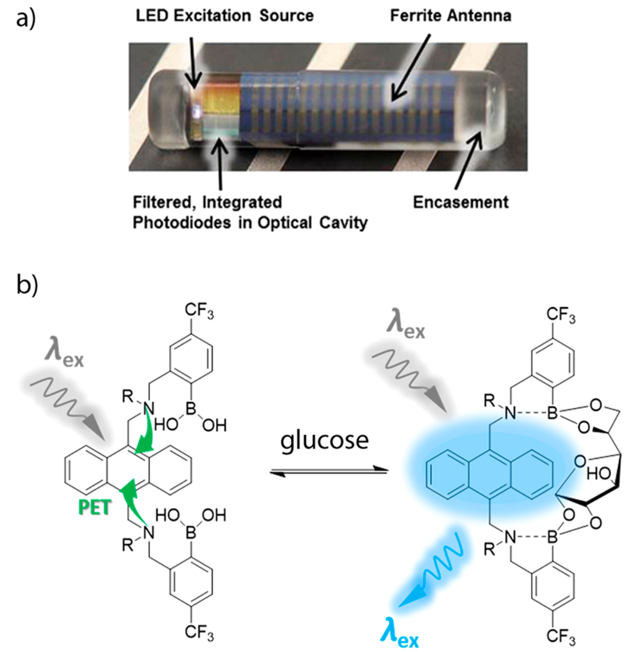

**P5.27**

**Figure 141.** (a) Photograph of the sensor device developed by Senseonics. (b) Schematic representation of the glucose sensing mechanism for probe **P5.27**. Adapted with permission from ref 17. Copyright 2014 Elsevier BV.

lectin-based artificial receptors for D-glucose were designed according to a temple-like structure (Figure 143), consisting of apolar top and bottom panels and two to four polar pillars.[624] This design was inspired by the assumption that D-glucose will form an inclusion complex, where its polar groups point equatorially towards the pillars, whereas its C−H groups point axially towards the aromatic "lids" of the temple structure.[625,626]

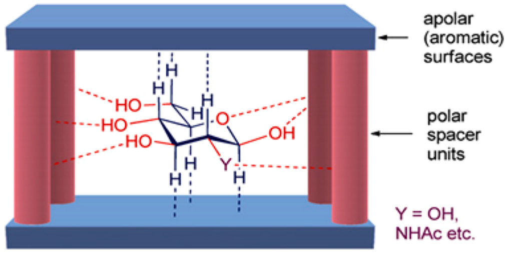

**Figure 143.** Schematic representation of the temple design for synthetic lectins. Reproduced with permission from ref 624. Copyright 2019 Wiley-VCH.

Davis and coworkers developed a tricyclic polyamide cage (**C5.1** in Figure 144), which was able to bind carbohydrates in water with good selectivity but low affinities.[627] Contrary to the observed weak binding of D-glucose ($K_a$ = 9 $M^{-1}$), the anomeric methylated $\beta$-$N$-acetylglucosamine showed a binding constant of $K_a$ = 630 $M^{-1}$ with this receptor in $D_2O$.[628]

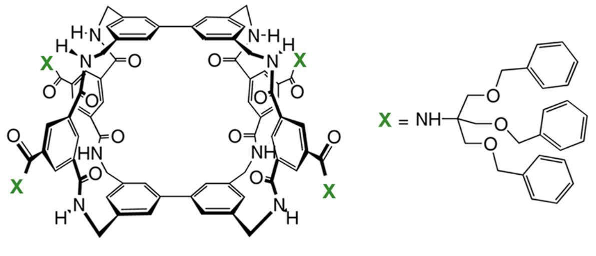

**C5.1**

**Figure 144.** Chemical structure of the macrotricyclic chemosensor **C5.1**. Adapted with permission from ref 627. Copyright 2005 Wiley-VCH.

In 2012, a "simple" glucose chemosensor **C5.2** was reported that was not only synthetically accessible in fewer steps but that also featured a fluorophore unit which allowed for the direct monitoring of D-glucose binding. The reported affinity of **C5.2** for D-glucose, $K_a$ = 56 $M^{-1}$, was sufficient for D-glucose sensing at mM concentrations in phosphate buffer, pH 7.1 (Figure 145).[582] This chemosensor also showed a respectable

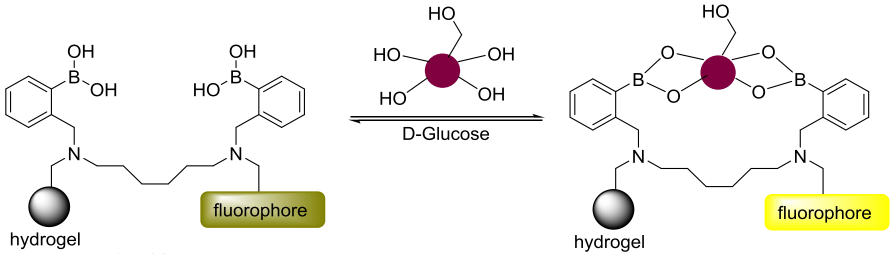

**P5.28**

**Figure 142.** Schematic representation of glucose sensing with probe **P5.28**.

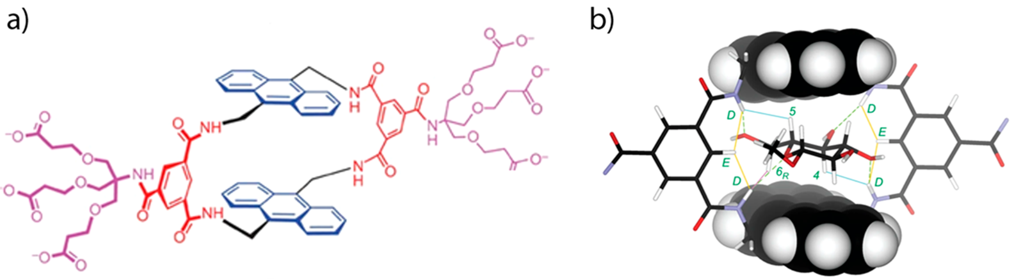

**C5.2**

**Figure 145.** (a) Chemical structure of the monocyclic lectin-based chemosensor **C5.2**. (b) 3D structure for the complex of **C5.2** with methyl-$\beta$-D-glucoside. Reproduced with permission from ref 582. Copyright 2012 Springer Nature.

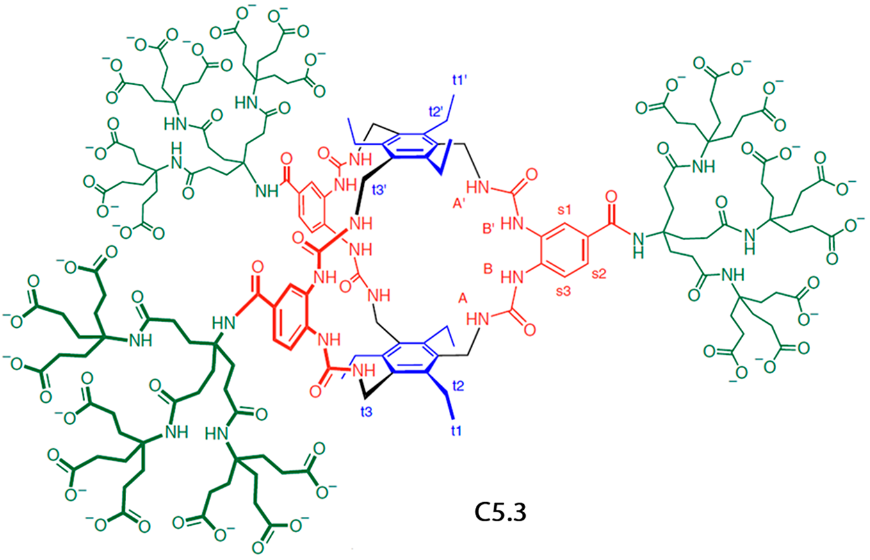

**C5.3**

**Figure 146.** Chemical structure of chemosensor **C5.3**. Reproduced with permission from ref 629. Copyright 2018 Springer Nature.

selectivity for glucose over other common monosaccharides such as galactose (factor 50 in $K_a$).

Recently, another lectin mimicking chemosensor (**C5.3** in Figure 146) was reported by the Davis group, showing a remarkable high binding affinity of $K_a = 1.8 \times 10^5$ $M^{-1}$ for D-glucose in $D_2O$, which is comparable to the binding strength of natural lectin proteins.[629] The bicyclic structure consists of hydrophobic triethylmesitylene roof and floor panels, enabling CH−$\pi$ interactions with D-glucose, and urea moieties that provide several contact points for polar interactions and hydrogen bonding. The periphery nonacarboxylates ensure the solubility of the chemosensor in water. Because of its unique structure, D-glucose with its all-equatorial hydroxy groups can fit well into the cavity, resulting in a high selectivity of this chemosensor for D-glucose over other monosaccharides. Besides, it should be noted that molecules other than carbohydrates do not bind at all. The applicability of this chemosensor to the selective D-glucose detection in aqueous phosphate buffer and human serum was demonstrated.[630]

The sensing of oligo- or polysaccharides, such as heparin, typically relies on a complete different chemosensor design principle: Usually the chemosensor intercalates into the heparin structure causing aggregation. Smith and coworkers developed a heparin responsive chemosensor persisting of an arginine-functionalized thionine (**C5.4** in Figure 147), called Mallard Blue.[631] This chemosensor showed an absorbance decrease in the wavelength region from 550 to 650 nm upon binding of heparin in 10 mM Tris buffer containing 150 mM NaCl. Mallard Blue did not show a significant response to other glycosaminoglycans such a hyaluronic acid. Thus, selective heparin sensing was even possible in 100% human or horse serum, which is not feasible with other common heparin binding dyes such as azure A.

Kanvah and coworkers developed the water-soluble dicationic chemosensor **C5.5** (Figure 148) consisting of a pyridinium acceptor and a (diethylamino)coumarin donor. **C5.5** showed an outstanding fluorescence selectivity and

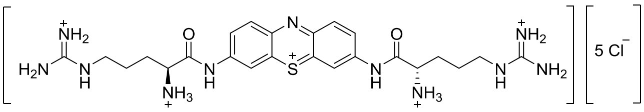

**C5.4**

**Figure 147.** Chemical structure of Mallard Blue **C5.4**.

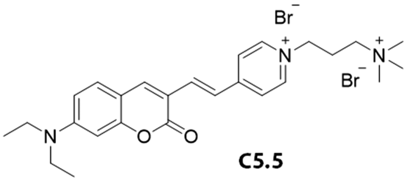

**C5.5**

**Figure 148.** Chemical structure of chemosensor **C5.5**.

sensitivity towards heparin over its analogues. The binding of heparin to **C5.5** led to a decrease of both the absorption and the emission intensity in HEPES buffer. Besides that, the detection of heparin in 1% FBS serum was successful, giving a (extrapolated) detection limit of 150 nM.

### 5.4. Nanosensor for Carbohydrates

Most nanoparticle-based sensors for the detection of carbohydrates rely on electrochemical or enzymatic reactions. Examples in which nanoparticles were functionalized with molecular probes or chemosensors are relatively rare. One prominent strategy for the detection of carbohydrates is based on phenylboronic acid functionalized nanoparticles. For example, Rujiralai and coworkers reported the preparation of 3-aminophenylboronic acid functionalized AuNPs for the selective detection of sialic acid at nM to $\mu$M concentrations in 5 mM phosphate buffer, pH 5.6, and spiked serum samples (**N5.1** in Figure 149).[633] The boronic acid moieties of **N5.1** preferentially reacted with the diol groups of sialic acid, causing aggregation of **N5.1** that altered the surface plasmon resonance absorption bands and therefore provided a readily measurable absorbance signal read out. No interferences with other sugars such as glucose, fructose, galactose, mannose, sucrose, lactose, or maltose were observed and good recoveries (>97%) in spiked serum samples were reported.

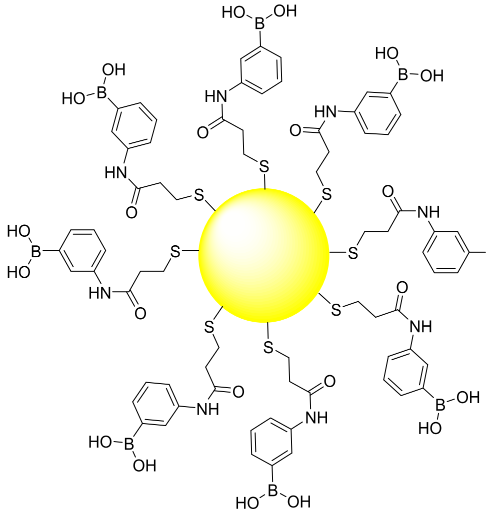

**N5.1**

**Figure 149.** Phenylboronic acid functionalized AuNPs (**N5.1**) for nM−$\mu$M detection of sialic acid in 5 mM phosphate buffer, pH 5.6, and serum samples.

Graphene quantum nanodots (GQDs) are nanoparticles with a diameter typically smaller than 100 nm. Their photophysical properties can be controlled through heteroatom doping, surface functionalization, or size tuning.[635] Detection of glucose in the mM concentration regime in 100 mM phosphate buffer, pH 7.4, using boronic acid-functionalized boron-doped GQDs (**N5.2** in Figure 150) was reported by Qiu and coworkers.[634] Because of the boronic acid moieties, the nanosensor aggregated in the presence of glucose, which served as a molecular bridge between the particles. The aggregation process reduced nonradiative relaxation processes, which in turn led to the formation of aggregation-induced emission.

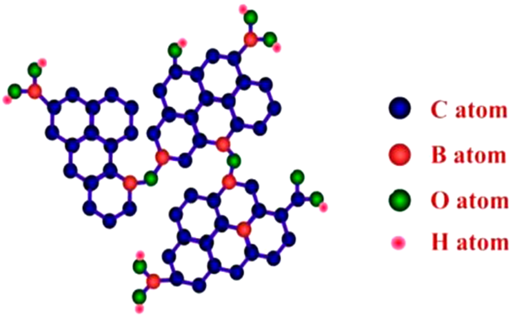

**N5.2**

**Figure 150.** Boronic acid functionalized boron-doped graphene quantum nanodots (**N5.2**) used for the detection of glucose in phosphate buffer. Reproduced with permission from ref 634. Copyright 2014 American Chemical Society.

A ratiometric nanosensor for the detection of glucose was recently reported by Zou, Li, and coworkers (**N5.3** in Figure 151). The nanosensor was based on boronic acid functionalized carbon dots (C-dots) and utilized synchronous fluorescence quenching as well as resonance light scattering (RLS) enhancement for detection.[636] In this example, 3-aminophenyl boronic acid and sodium citrate were used as precursor materials for the preparation of the C-dots *via* a "synthesis-modification integration" strategy. Under the assay conditions, the *cis*-diols of glucose reacted with the boronic acids upon particle aggregation. Thereby, the emission of the nanosensor was quenched, while a pronounced RLS enhancement was observed. Ratiometric sensing of glucose at $\mu$M concentrations was achieved in 100 mM PBS, pH 8.0, and spiked urine samples (recovery <98 %). The authors showed that **N5.3** is selective for glucose, as fluorescence quenching and RLS enhancement were negligible for fructose, maltose, lactose, and sucrose. Recently, Das and coworkers reported the use of phenylboronic acid functionalized C-dots (**N5.4**) for the detection of glucose in 100 mM PBS and in blood samples at $\mu$M concentrations (**N5.4** in Figure 151).[637] The detection mechanism is presumably similar to the one described for **N5.3**. This fluorescence turn-off nanosensor was successfully employed to detect glucose with minimal interference from other biomolecules. The authors also achieved immobilization of the boronic acid functionalized C-dots on paper, allowing for paper strip-based sensing.

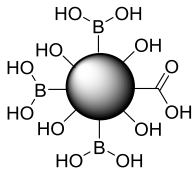

**N5.3 / N5.4**

**Figure 151.** Schematic representation of boronic acid functionalized carbon dots **N5.3** and **N5.4**.

Salimi and coworkers reported the use of a smartphone-assisted glucose detection at $\mu$M concentrations in water and blood samples using boronic acid functionalized C-dots (**N5.5** in Figure 152).[638] The nanosensor **N5.5** was prepared from 4-carboxyphenylboronic acid, *o*-phenylenediamine, and rhodamine B and showed a remarkably strong emission quantum yield (46%). Again, the presence of glucose triggered the

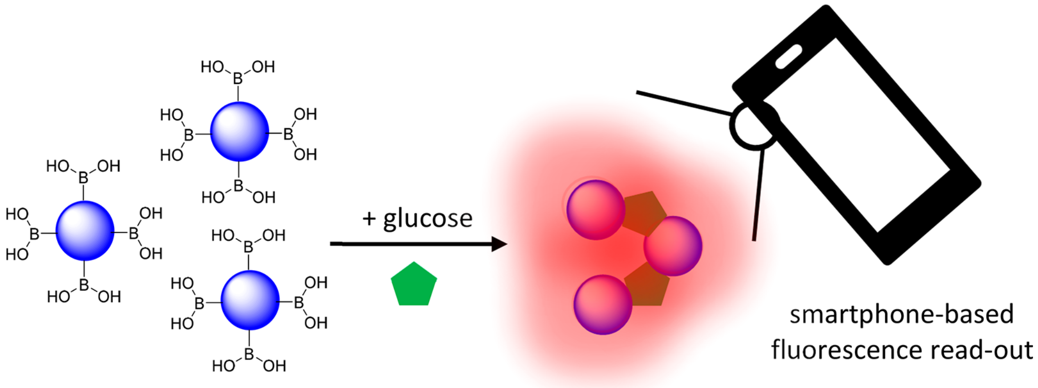

**N5.5**

**Figure 152.** Boronic acid functionalized C-dots (**N5.5**) used for smartphone-assisted $\mu$M glucose detection in water and in human blood samples.

aggregation of the particles and, as a result, increased C-dot and rhodamine emissions were observed and used to quantify the glucose concentrations. Specifically, two wavelengths were recorded simultaneously with both emission intensities increasing as the analyte was bound to the boronic acid moieties of **N5.5**. The corresponding colored images were processed with an RGB color model-based application of a smartphone. Importantly, other biomolecules and metal cations (*e.g.,* GSH, dopamine, uric acid, catechol, fructose, maltose, Ala, Arg, Cys, Hcys, Thr, Pro, Ser, $Na^+$, $K^+$, $Mg^{2+}$, and $Ca^{2+}$) did not affect the performance of **N5.5**. The results obtained from spiked blood samples (recoveries >99%) agreed well with quantitative measurements with a standard blood glucose meter, as it is used in hospitals.

Besides carbon-based nanosensors for the detection of carbohydrates, several polymeric probes have been investigated during the last years. In 2017, Wang and coworkers reported the use of a sandwich boronated affinity sorbent assay (SBASA) to sense glucose at $\mu$M concentrations in aqueous solutions, pH 9.0, and serum samples using boronic acid composite materials (**N5.6** in Figure 153).[639] The polymer was prepared by polymerizing boronic acid-terminated 9-anthracene methyl acrylate and methyl methacrylate *via* atom transfer radical polymerization (ATRP), using a phenylboronic acid-labeled initiator. The boronic acid functionalized nanoparticles bind to glucose by forming boronic acid ester linkages and when the fluorescent polymer is subsequently added, it can react with the residual sugar diols, forming a nanoparticle–sugar polymer composite. The composite recovered, *e.g.,* centrifugation, and after hydrolysis of the boric acid ester bonds, the fluorescent polymer dissolves and its emission can be measured and correlated to the amount of glucose present in the original samples. The recoveries in spiked serum samples ranged from 90.5–100.0% with a relative standard deviation of 1.2–3.8%. Overall, these aggregation-based systems appear to be mechanistically robust and selective for glucose (as other saccharides do not contain multiple *cis*-diols and therefore do not act as particle connectors), but the lack of reversibility likely makes them unsuitable for dynamic monitoring of glucose levels.

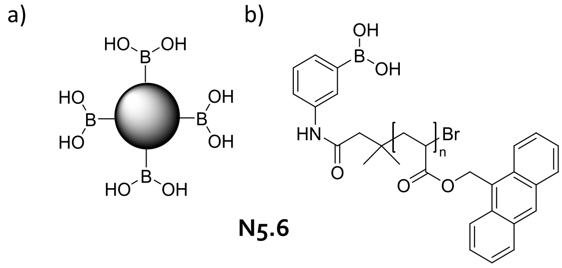

**Figure 153.** (a) Schematic representation of boronic acid-functionalized carbon-based nanoparticles used in combination with the 9-anthracene methyl acrylate polymer (**N5.6**) for fluorescence-based glucose detection in water at $\mu$M concentrations. (b) Chemical structure of the 9-anthracene methyl acrylate polymer.

Théato and coworkers prepared glucose-responsive polymeric micelles formed by diol-mediated self-assembly between a phenylboronic acid-based polymer and a diol-functionalized polymer. The resulting micelles were doped with the diol-functional dye alizarin red S in order to form nanosensors (**N5.7** in Figure 154a) that operate in an IDA fashion.[640] Aqueous dispersions of **N5.7** were initially fluorescent due to the presence of boronic acid-bound alizarin red S (Figure 154b). However, the dye was displaced from **N5.7** in the presence of glucose, leading to a readily observable emission decrease.[592] The authors demonstrated glucose detection at mM concentrations in PBS, pH 7.4.

A series of amphiphilic fluorescent molecules based on tetraphenylethylene (TPE) units, *e.g.,* TPE4S and TPE4L (Figure 155), was prepared by Xing and coworkers. The amphiphilic TPEs spontaneously self-assemble into weakly emissive fluorescent organic nanoaggregates (FONs) in water.[641] **N5.8** was used for the detection of ginsenosides at mM concentrations in 67 mM PBS, pH 7.1. It was observed that the presence of glycosylated ginsenosides triggered the formation of new and highly emissive vesicle-like structures and **N5.8**. This was explained by the ability of the glycosylated ginsenosides to displace the carbohydrate-based interactions between molecules of **N5.8** by forming new and stronger bonds. The observed fluorescence enhancement was attributed to aggregation-induced fluorescence enhancement (AIE) of the TPE units in the densely packed vesicular structure. The TPE4S amphiphile that contains four negatively charged sialic acid units and that is surrounded by the TPE units showed the highest fluorescence enhancement in the presence of polyglycosylated ginsenosides (*e.g.,* RB1 in Figure 124). In contrast, no fluorescence enhancement was observed when TPE4L was used, which was attributed to the inability of glycosylated ginsenosides to interfere with the intermolecular carbohydrate interactions of this TPE-based amphiphile (the

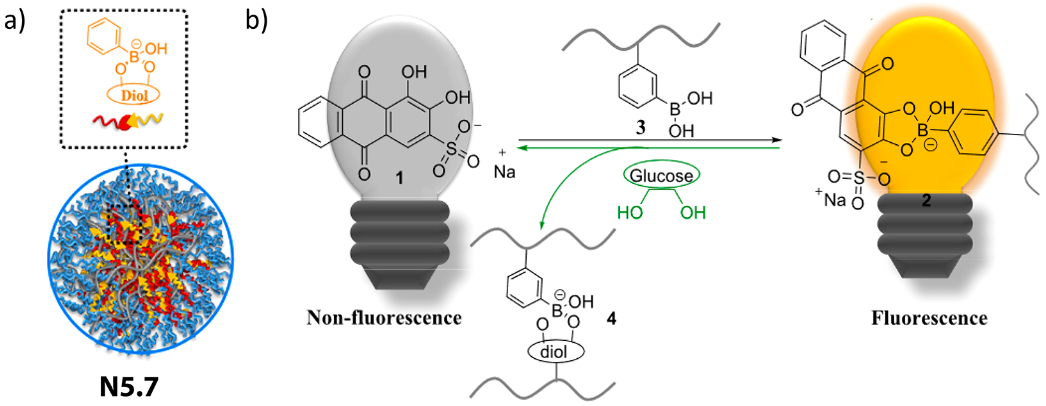

**Figure 154.** (a) Phenylboronic acid-based micelles doped with alizarin red S (**N5.7**) can be used for the detection of glucose in PBS at mM concentrations. (b) Schematic representation of a proposed mechanism of the fluorescence-based detection of glucose with **N5.7**. Reproduced with permission from ref 640. Copyright 2019 American Chemical Society.

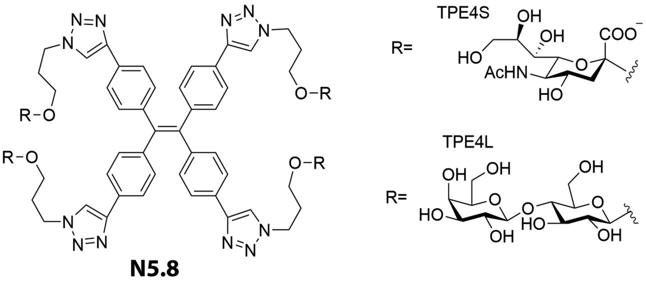

**Figure 155.** Chemical structure of tetraphenylethylene-based amphiphilic molecules (TPE4S and TPE4L) used for the preparation of the fluorescent organic nanoparticles **N5.8**. Adapted with permission from ref 641. Copyright 2020, Wiley-VCH.

strong intermolecular carbohydrate interactions between TPE4L molecules were also confirmed by their low critical micelle concentration (CMC) values when forming weakly emitting aggregates). Finally, TPE4S was observed to be more selective toward ginsenosides containing three or more glycosyl units, indicating preferential formation of emitting vesicles when a larger number of carbohydrate interactions are present.

In summary, a variety of boronic acid-based molecular probes and nanosensors, as well as lectin-inspired chemosensors (temple design), were developed for sensing carbohydrates. Many of the advanced systems show good selectivity and affinity for certain carbohydrates, such as glucose, fructose, or heparin, and are operational in water and biofluids. Some have already reached the sensitivity as well as selectivity required for practical use, *e.g.*, compare the tabulated data in Table 16–18 for the key parameters of synthetic probes, chemosensors, and nanosensors, with the typical concentration range of carbohydrates in biofluids (Table 19). Amongst the different carbohydrates, glucose is the most targeted analyte, and (implantable) glucose sensor devices have transitioned into clinical routines and daily point-of-care use. The development of medically applicable artificial receptors for glucose sensing is certainly one of the biggest achievements made by analytical supramolecular chemistry so far. For comparison, detecting fructose selectively at the medically relevant micromolar concentration range in the presence of glucose will likely remain very challenging by the current probe, chemosensor, and nanosensor designs. It will be interesting to see if analogous concepts also succeed in targeting other sugars and oligosaccharides that are of diagnostic relevance.

### Table 19. Summary of the Normal Concentration of Carbohydrates in Biofluids[a]

| concentration range | media | ref |
|---|---|---|
| D-Fructose Analyte | | |
| 28–34 μM | blood | 642 |
| 15–61 μM (daily excretion) | urine | 643 |
| D-Glucose Analyte | | |
| 4.9–6.9 mM | urine | 644 |
| 10.3–56.7 μmol/mmol creatinine = 103–567 μM | blood | 645 |
| D-Glucosamine Analyte | | |
| 0–0.6 μM | urine | 646 |
| 1.45 μmol/mmol creatinine = 145 μM | blood | 647 |
| Heparin Analyte | | |
| 3.56–6.82 μM | blood | 648 |
| Sialic Acid Analyte | | |
| 0–1.66 μM | urine | 642 |
| 8.56–84.6 μmol/mmol creatinine = 85.6–846 μM | blood | 649 |

[a] Urinary analyte concentrations were converted assuming a representative creatinine level of 10 mmol/L.

## 6. NUCLEOTIDES, NUCLEOSIDE PHOSPHATES, AND OLIGONUCLEOTIDES

Nucleosides are biomolecules essential for metabolic and anabolic processes in all known living organisms and have an impact on cell homeostasis and epigenetic plasticity.[650−654] For example, they are important cofactors for biochemical reactions such as acylation and redox reactions, which influence cellular signaling pathways[655] and are also essential for the energy regulation of cells.[656] Information on abnormal concentrations of nucleosides in biological fluids can provide insights into pathophysiological conditions such as inflammation, hypoxia, and cancer.[657,658] For instance, elevated levels of nucleosides have been found in the urine of patients with AIDS;[659] leukemia;[657,660] lung, liver,[665] or breast cancer;[661−663] a lymphoma or renal cell carcinoma;[664] and Hodgkin's disease.[666] Given that nucleic acids and oligonucleotides are released into the blood by apoptotic and necrotic cells,[667] their elevated levels in the blood can indicate a variety of pathologic processes, including malignant and benign lesions,[668] inflammatory diseases,[669] and trauma.[670] Furthermore, nucleic acids present in biofluids are important markers

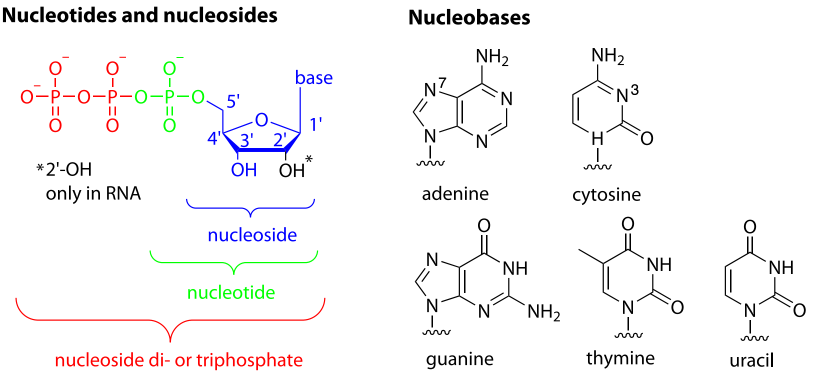

**Figure 156.** Chemical structures of the most common nucleotides, nucleosides, and nucleobases.

of viral infections.[671−673] Aside from their function as biomarkers for diseases, nucleotides, nucleosides, and their derivatives are also used as drugs to treat cancer[674,675] and viral infections.[676] Regarding their use as new therapeutic agents, they have become extremely attractive for oligonucleotide-based therapeutics, e.g., as antisense oligonucleotide (ASO)-based therapies.[677,678] ASOs are oligonucleotides that can potentially repair abnormal genetic alterations, thereby restoring a normal physiological situation in the body. For the success of future ASO-based therapies, it is important to be able to characterize the underlying distribution of oligonucleotide species in biological fluids. Before introducing the reader to the principles of detection of nucleotides, nucleosides, nucleoside phosphates, and nucleic acids (DNA and RNA), it is convenient to briefly recall the standard nomenclature and structural properties of this class of compounds. Nucleosides are composed of a nucleobase (adenine, guanine, cytosine, thymine, and uracil) and a ribose unit (in the case of RNA) or 3′-deoxy ribose (in the case of DNA, Figure 156). Nucleotides are derived from nucleosides and have an additional phosphate group at the 5′-position of the sugar moiety. Nucleosides with two or three phosphates are referred to as nucleoside di- or triphosphates or more generally as nucleoside phosphates. Oligonucleotides are short strands of DNA and RNA (nucleic acids) and are defined by the sequence of nucleotides linked by phosphodiester bonds. Oligonucleotides and nucleic acids can bind to their respective complementary counterparts in a sequence-specific manner to form double helixes of DNA or RNA.

## 6.1. General Approach for Nucleotide, Nucleoside Phosphates, and Oligonucleotide Detection

Nucleotides are negatively charged in aqueous solutions (pH ∼ 7.0) due to the strongly acidic nature of the phosphate groups ($pK_a \sim 1{-}2$). The aromatic purine- and pyrimidine-based nucleobases remain noncharged at neutral pH values and thus have hydrophobic character. The nucleobases are responsible for the distinct self-assembly properties of oligomeric nucleotides into double stands, such as DNA, and are mediated *via* Watson−Crick base-pairing (H-bonds between complementary nucleobases) and $\pi-\pi$ stacking interactions.[679] Nucleobases can coordinate to soft cations. For example, the N3 atom of cytosine ($pK_a = 4.2$ of its conjugate acid) is a "soft" center and capable of coordinating "soft" metal cations (*e.g.*, $Ag^+$ and $Hg^{2+}$ cations), while the nitrogen atom N7 of adenine and guanine is known to coordinate "soft" (*e.g.*, $Pt^{2+}$ and $Pd^{2+}$) and "hard" (*e.g.*, $Cu^{2+}$ and $Zn^{2+}$) metal cations.[680] The sugar moiety represents a functional building block that can be used to distinguish DNA from RNA. The ribose present in RNA contains a targetable 1,2-diol group; in the case of DNA, the 2′-hydroxyl group is absent. Considering these different chemical properties, molecular probes and chemosensors selective for RNA or DNA can be designed by capitalizing on electrostatics, H-bonding, $\pi-\pi$-stacking, the presence of 1,2-diols, and metal complexation interaction motifs.

Nucleosides and oligonucleotides are typically separated by chromatographic or electrophoretic separation methods and detected by mass spectrometry. In addition, chemiluminescence-based chemical kits for the detection of nucleosides and nucleoside derivatives (*e.g.*, nicotinamide adenine dinucleotide, NADH)[681,682] are commercially available. These chemiluminescence-based probes rely on enzymatic or chemical transformations and are beyond the scope of this review. In the following sections, we present molecular probes, chemosensors, and nanosensors that have been recently published and were used for the detection of nucleosides, nucleotides, oligonucleotides, and DNA in aqueous solutions and biological fluids (see also Tables 20−22). We highlight contemporary examples and challenges in the development of new hosts for this class of compounds. In addition, we would like to refer the reader to the recently published review by Ahn and coworkers regarding the use of small-molecule probes for the detection of adenosine triphosphate specifically within cells and tissues.[683]

**Table 20. Summary of Molecular Probes for Nucleosides**

| probe | media | concentration range | ref |
|---|---|---|---|
| | Adenosine Triphosphate (ATP) Analyte | | |
| **P6.1** | 0.1% DMSO in 10 mM PBS, pH 7.4 | 0.5−15 mM in buffer; LOD, 33 $\mu$M in buffer | 689 |
| | neuronal cells | mM range in neuronal cells | |
| **P6.2** | 10% EtOH in 25 mM HEPES buffer, pH 7.4 | 0−10 mM in buffer | 690 |
| | HeLa cells | mM range in HeLa cells | |
| **P6.3** | 60% glycerol in Krebs buffer, pH 7.8 | 0−10 mM in buffer | 691 |
| | HeLa and COS cells | mM range in cells | |

## 6.2. Molecular Probes for Nucleoside Phosphates and Their Structurally Related Derivatives

Rhodamine dyes are attractive molecules for the design of fluorescence turn-on probes because they can exist either in a non-fluorescent closed ring structure or in a strongly emitting open-ring form (Figure 157). Adoption of the open-ring

### Table 21. Summary of Chemosensors for Nucleotides (LOD, Limit of Detection)

| chemosensors | media | concentration range | ref |
|---|---|---|---|
| | Adenosine Triphosphate (ATP) Analyte | | |
| **C6.1** | 5 mM Tris-acetate buffer, pH 7.6 | 0 and 5 $\mu$M tested | 692 |
| **C6.3** | 10% DMSO in 10 mM Tris buffer, pH 7.0 | 0–3.0 mM | 696 |
| **C6.4** | 0.5% DMSO in 10 mM HEPES buffer, pH 7.4; melanoma cells | 0–22.5 $\mu$M in buffer $\mu$M, range in cells | 697 |
| **C6.5** | 100 mM HEPES buffer, pH 7.4 | 0–100 $\mu$M | 698 |
| **C6.6** | 50 mM HEPES buffer, pH 7.0 | 1.0–10 $\mu$M | 702 |
| **C6.7** | water; human serum samples | $\mu$M range | 703 |
| **C6.8** | 10 mM HEPES buffer, pH 7.4 | $\mu$M range | 704 |
| **C6.9** | 20 mM Sodium phosphate-buffered $D_2O$, pD 7.4 | mM range | 708 |
| **C6.10** | 1 mM Tris buffer, pH 4.5–7.0 | $\mu$M range | 709 |
| **C6.11** | 32 mM phosphate buffer containing 50 mM NaCl, pH 7.4 | $\mu$M range | 710 |
| **C6.12** | water | $\mu$M range | 711 |
| **C6.15** | 10 mM HEPES buffer, pH 7.0 | 1.0 mM | 716 |
| | Adenosine Diphosphate (ADP) Analyte | | |
| **C6.5** | 100 mM HEPES buffer, pH 7.4 | 0–100 $\mu$M | 698 |
| **C6.8** | 10 mM HEPES buffer, pH 7.4 | $\mu$M range | 704 |
| **C6.9** | 20 mM sodium phosphate buffered $D_2O$ | mM range | 708 |
| **C6.15** | 10 mM HEPES buffer, pH 7.0 | 1.0 mM | 716 |
| | Adenosine Monophosphate (AMP) Analyte | | |
| **C6.8** | 10 mM HEPES buffer, pH 7.4 | $\mu$M range | 704 |
| **C6.15** | 10 mM HEPES buffer, pH 7.0 | 1.0 mM | 716 |
| | dsDNA Analyte | | |
| **C6.19** | water | 0–2.0 $\mu$g mL$^{-1}$ | 730 |
| **C6.20** | 10 mM ammonium phosphate buffer, pH 7.2 | 0–26 mM; LOD, 78 $\mu$M | 731 |
| | Guanosine Triphosphate Analyte | | |
| **C6.13** | 40 mM MOPS buffer, pH 7.0; artificial plasma;<br>urine samples | 0–510 $\mu$M in buffer<br>$\mu$M-range in plasma and urine | 712 |
| **C6.14** | 10 mM phosphate buffer, pH 7.4; serum samples | 0–1.6 mM | 715 |
| **C6.15** | 10 mM HEPES buffer, pH 7.0 | 1.0 mM | 716 |
| | G4-Quadruplex Analyte | | |
| **C6.16** | K-100 buffer (10 mM $LiAsMe_2O_2$, 100 mM KCl), pH 7.2 | 0–15 $\mu$M | 727 |
| **C6.18** | 50 mM Tris-HCL buffer containing 50 mM NaCl/KCl, pH 7.4 | 8 and 10 $\mu$M tested | 729 |
| | Nucleosides Analyte | | |
| **C6.2** | aq solutions and cells | $\mu$M range | 694,695 |
| | Polymorph DNA Analyte | | |
| **C6.17** | 20 mM Tris-HCl buffer containing 200 mM KCl and 10 mM $MgCl_2$, pH 7.4<br>1× NASAB buffer (Tris-HCl buffer, pH 8.5, $MgCl_2$, KCl, DTT, and DMSO) | nM range<br>LOD, 0.44 nM | 728 |
| | Uridine Triphosphate (UTP) Analyte | | |
| **C6.9** | 20 mM sodium phosphate buffered $D_2O$, pD 7.4 | mM range | 708 |

### Table 22. Summary of Nanosensors for Nucleotides

| nanosensors | media | concentration range | ref |
|---|---|---|---|
| | Adenosine Triphosphate (ATP) Analyte | | |
| **N6.1** | 100 mM HEPES buffer, pH 7.4 | 0–333 $\mu$M | 733 |
| **N6.2** | 25 mM HEPES buffer, pH 7.4 | 0–30 $\mu$M | 735 |
| **N6.3** | $D_2O$ | $\mu$M range | 736 |
| | Guanosine Triphosphate (GTP) Analyte | | |
| **N6.2** | 25 mM HEPES buffer, pH 7.4 | 0–30 $\mu$M | 735 |

structure is promoted by the presence of nucleoside triphosphates that preferentially bind the polar open form through electrostatic interactions and H-bonds. Moreover, nucleoside triphosphate binding stabilizes the polar transition state of the ring-opening reaction and minimizes the energy barrier required for the reaction to proceed.[684] Depending on the design of the rhodamine B dye, this reaction requires seconds to several minutes (*e.g.*, 40 min). Several newly developed fluorescent molecular probes for nucleoside triphosphates feature amino-functionalized rhodamine dyes suitable for fluorescent turn-on detection in live-cell imaging.[685–690]

A recent example using a rhodamine-based fluorescence turn-on probe (**P6.1** in Figure 158) for the detection of adenosine triphosphate (ATP) and reactive oxygen species (ROS) was reported by Tian and coworkers.[689] **P6.1** combined two dye moieties: firstly, an ATP-responsive spirolactam-rhodamine group and secondly a ROS responsive naphthalimide-based boronic ester moiety. **P6.1** was shown to be functional in 10 mM PBS, pH 7.4, but also in a zebrafish animal model. The binding of **P6.1** to ATP resulted in an enhanced emission of the probe, which can be explained by the subsequent formation of the fluorescent open-ring form of rhodamine. Moreover, the naphthalimide moiety undergoes a ROS-induced cleavage of the phenylboronic ester moiety concomitant with a fluorescent emission enhancement.

In the same year, Yuan and coworkers described a Förster resonance energy transfer (FRET)-based detection principle for the intracellular detection of ATP at mM concentrations in 25 mM HEPES buffer containing 10% EtOH, pH 7.4 (**P6.2** in

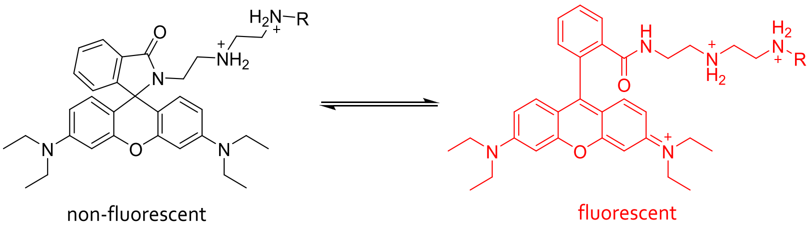

**Figure 157.** Chemical structure of the amino-bearing rhodamine B spirolactam that undergoes environment-responsive ring-opening/-closure, alternating between a nonemissive and an emissive state.

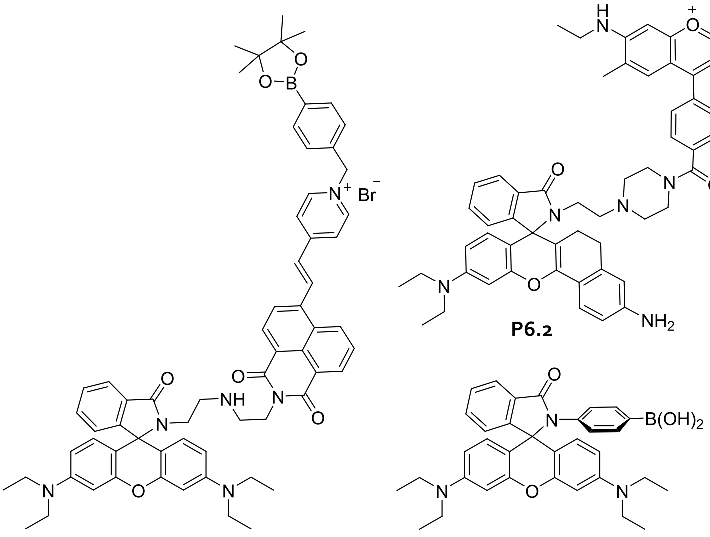

**P6.1** **P6.2** **P6.3**

**Figure 158.** Chemical structures of probes **P6.1**−**P6.3** used for the detection of ATP.

Figure 158).[690] The authors used a far-red emitting, two-photon excitable fluorophore (ACFPN) as the FRET-acceptor, while the rhodamine moiety served as FRET-donor unit. Additionally, **P6.2** featured a piperazine unit that can bind ATP *via* H-bonding interactions. As in the aforementioned example, ring opening of the nonfluorescent spirolactam of **P6.2** occurred in the presence of ATP at mM concentrations, leading to the formation of the fluorescence-active derivative of rhodamine (response time: 8 min). The authors demonstrated the applicability of **P6.2** for ATP imaging in living cells.

An alternative ATP detection approach targeting the 1,2-diol functionality on the ribose building block of ATP was reported by Chang, Yuan, and coworkers (**P6.3** in Figure 158).[691] In their design, a boronic acid moiety was introduced to allow for covalent conjugation of the probe with ATP by forming boronic esters. Again, ATP binding results in the formation of the emissive open ring structure of rhodamine, leading to a fluorescence enhancement (response time approximately 20 s). The detection of ATP at millimolar concentrations was achieved with **P6.3** in Krebs buffer, pH 7.8, containing 60% glycerol, and within cells.

Despite the unique fluorescence turn-on features of the above-mentioned molecular probes, nucleoside biomarker analysis generally requires detection limits below the mM concentration range. The following subsection describes recently reported chemosensors that can be used for $\mu$M detection of nucleotides and analogous structures.

### 6.3. Chemosensors for Nucleotides, Nucleoside Phosphates, and Oligonucleotides

An early example of a luminescent chemosensor for the detection of ATP and NADPH at $\mu$M concentrations was reported by Lehn and coworkers (**C6.1** in Figure 159).[692] This acridine-functionalized aza-crown-based chemosensor showed a good selectivity for ATP ($K_a$ = 7 × $10^7$ $M^{-1}$) over other nucleoside phosphates (*e.g.*, CTP, GTP, UTP, ADP, and AMP) in 5 mM Tris-acetate buffer, pH 7.6, which was rationalized by the stronger electrostatic attraction between the triphosphate chain of ATP and the polyammonium moiety of **C6.1**. The detected fluorescence enhancement upon target analyte binding was attributed to stacking interactions between the acridine moiety of the chemosensor and adenine. The binding preference for NADPH ($K_a \geq 7 \times 10^8$ $M^{-1}$) over

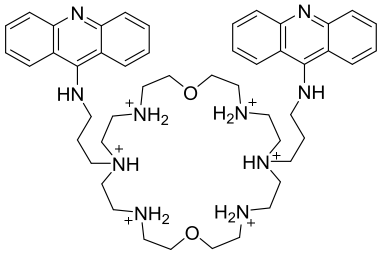

**C6.1**

**Figure 159.** Chemical structure of an acridine-functionalized aza-crown (**C6.1**) that can be used for the selective detection of NADPH and ATP.

NADH likely stems from electrostatic effects. The authors also demonstrated selective binding of **C6.1** to specific polybase pair sequences. Soon after, Martínez-Máñez and coworkers reported the use of ruthenium$^{II}$ complexes, linked to a cyclam−Cu$^{II}$ complex, for the detection of nucleosides *via* fluorescence spectroscopy measurements.[693]

Commercially available chemosensors for the detection of vesicular-bound ATP are often based on acridine-type fluorescent dyes, *e.g.*, quinacrine (**C6.2** in Figure 160).[694,695]

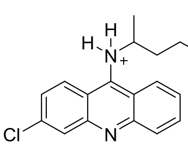

**C6.2**

**Figure 160.** Chemical structure of quinacrine (**C6.2**) that is commercially available for the detection of polynucleotides in aqueous solutions.

Quinacrine exists as a dicationic species under physiological conditions and thus effectively binds to polynucleotides *via* electrostatic interactions in aqueous solutions. An enhanced fluorescent emission is typically observed upon binding to nucleosides, and as such, quinacrine can be used for nonselective detection of nucleosides and DNA at $\mu$M concentrations.

A recent example for the detection of ATP from $\mu$M up to mM concentrations in 10 mM Tris buffer, pH 7.0, containing 10% DMSO, was described by Anzenbacher Jr. and coworkers (**C6.3** in Figure 161).[696] In their design, a bisantrene derivative that featured two imidazolium hydrazone moieties allowed for the selective complexation of ATP mediated by electrostatic and H-bonding interactions. The simultaneously arising $\pi-\pi$ interactions between the bisantrene moieties and adenine led to a chelation-enhanced fluorescence response of the chemosensor **C6.3**. The binding constants derived from fluorescence titrations in Tris buffer containing 10% DMSO were $1.3 \times 10^3$ $M^{-1}$ and $1.0 \times 10^2$ $M^{-1}$ for ATP and ADP, respectively. **C6.3** preferentially binds ATP over other nucleoside triphosphates; for instance affinities of $K_a = 3.8 \times 10^2$ $M^{-1}$ (UTP) and $K_a = 1.1 \times 10^2$ $M^{-1}$ (CTP) were reported. The authors also verified that other anions, such as $F^-$, $Cl^-$, $H_2PO_4^-$, or $HP_2O_7^{3-}$, did not interfere with the ATP sensing mechanism.

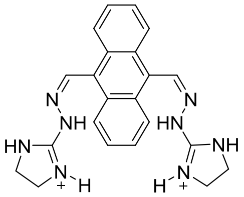

**C6.3**

**Figure 161.** Chemical structure of bisantrene-based chemosensor (**C6.3**) used for selective fluorescence-based detection of ATP at $\mu$M concentrations in Tris buffer.

Metal complexes based on divalent zinc cations have been successfully developed for the selective detection of nucleoside phosphates. For instance, Yoon, Park, and coworkers utilized a terpyridine−Zn$^{II}$ complex possessing hydrophilic polyether chains as a chemosensor for $\mu$M detection of ATP in 10 mM HEPES buffer, pH 7.4, and in cells (**C6.4** in Figure 162).[697] In buffered solutions and in the absence of ATP, the fluorescence of **C6.4** was quenched due to the formation of nonemissive aggregates. The terpyridine moiety of **C6.4** efficiently coordinates to the phosphate groups of ATP, resulting in disaggregation and consequential emission intensity increase. The selectivity of **C6.4** against other anions (*e.g.*, pyrophosphate, $Br^-$, $CH_3COO^-$, $ClO_4^-$, $F^-$, $H_2PO_4^-$, $HSO_4^-$, $I^-$, $Cl^-$, $N_3^-$, $NO_3^-$, $PO_4^{3-}$, and $SCN^-$) was tested, and it was observed that (only) pyrophosphate yields a strong fluorescence response which can potentially interfere with the detection of ATP. Note that **C6.4** is likely cross-reacting with the amino acid histidine because "His-selective" chemosensor **C2.23** (Figure 60 in section 2) features similar binding motifs.

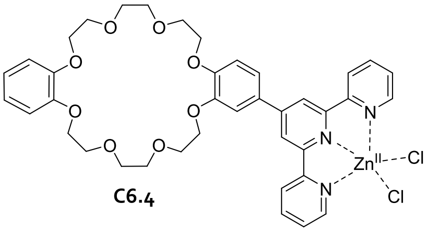

**C6.4**

**Figure 162.** Chemical structure of terpyridine-based chemosensor (**C6.4**) that is applicable for $\mu$M detection of ATP in HEPES buffer solutions.

In addition to the propensity of the aromatic N-atoms of nucleosides to coordinate with "soft" metal centers, oxygen atoms of phosphates can participate in the coordination of "hard" lanthanide cations.[699,700] Because lanthanide ions have relatively low absorption cross sections, their inherent luminescence properties are relatively uninteresting for sensing applications. However, the binding of nucleosides to certain lanthanide complexes results in the formation of antenna systems that allow for efficient energy transfer from the ligand to the metal center, thus enabling efficient fluorescence-based detection.[700] Shuvaev, Parker, and coworkers first reported the possibility of determining the ADP/ATP ratio by measuring the circularly polarized luminescence (CPL)[701] generated upon binding of the bimetallic zinc−europium complex (**C6.5**) to ATP or ADP (Figure 163).[698] Interestingly, the resulting CPL signal of the ADP-bound complex (log $K_a \approx 4.8$ assuming a 1:1 binding model) had an opposite sign compared to that of the ATP-bound complex (log $K_a \approx 4.7$ assuming a 1:1 binding model) despite their similar binding affinity. This can be explained by a different coordination mode of the analytes with the chemosensor (Figure 163). Thus, the nucleoside ratio was successfully determined by analyzing the intensity of the total CPL signal obtained from a mixture of the nucleosides at $\mu$M concentrations in 100 mM HEPES buffer, pH 7.4.

Taglietti and coworkers reported an IDA-based chemosensor using a dicopper(II)-polyaza-macrocyclic host and an indicator dye (*e.g.*, the rhodamine derivative 6-TAMRA) for the detection of ATP at $\mu$M concentrations in 50 mM HEPES buffer, pH 7.0 (**C6.6** in Figure 164).[702] Effective indicator displacement occurred in the presence of ATP due to the high affinity of the macrocycle for this target nucleoside triphosphate (log $K_a = 8.0 \pm 0.2$ for the 1:1 adduct). Through the displacement of the dye, the emission intensity increased proportionally to the concentration increase of ATP in solution. Unfortunately, it was found that similar fluorescence

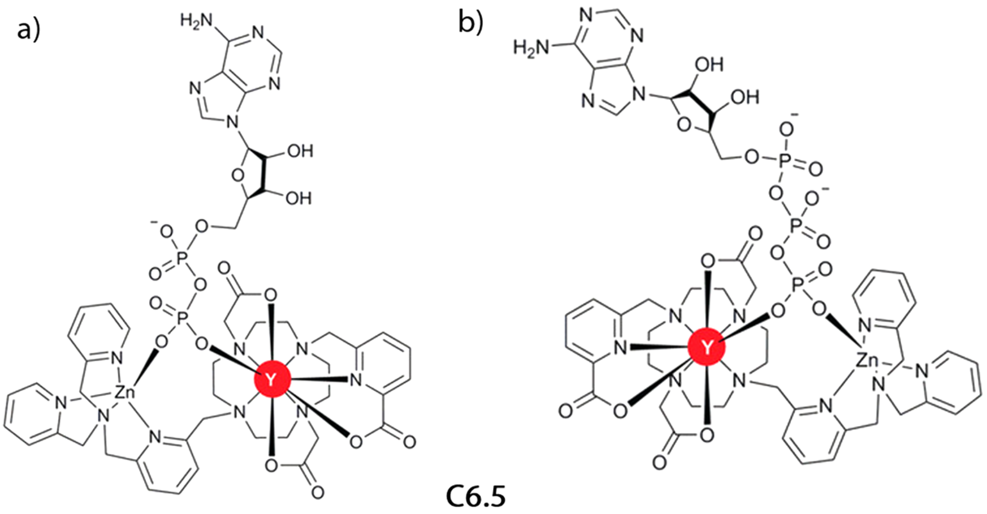

**Figure 163.** Structure of the complex of chemosensor **C6.5** with (a) ADP and (b) ATP (Y = $Eu^{III}$). Reproduced with permission from ref 698. Copyright 2018 Wiley-VCH.

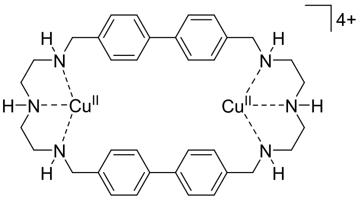

**C6.6**

**Figure 164.** Chemical structure of $dicopper^{II}$ polyazamacrocyclic receptor (**C6.6**) used for IDA-based detection of ATP ($c = 10^{-6}$–$10^{-5}$ M) in HEPES buffer solutions.

responses were obtained with ADP (log $K_s = 7.4 \pm 0.2$), AMP (log $K_s = 5.3 \pm 0.2$), and pyrophosphate anions (log $K_s = 7.3 \pm 0.2$), indicating the limitations of this chemosensor when it comes to the selective detection of ATP. Moreover, the structural similarity of this chemosensor to histidine chemosensor **C2.27** (Figure 62 in section 2) suggests a possible cross-reactivity.

More recently, Singh and coworkers reported the use of a sulfated *β*-cyclodextrin combined with $Zn^{2+}$ and the indicator dye thioflavin T as a fluorescence turn-on chemosensor ensemble for ATP detection (**C6.7** in Figure 165).[703] $Zn^{2+}$ binds strongly to the negatively charged sulfate groups of the cyclodextrin derivative and prevented the binding of thioflavin to the macrocycle. However, when ATP was added to a solution of the chemosensor ensemble in water, it efficiently captured the metal cations from the sulfonated cyclodextrin. This allowed for the formation of an inclusion complex of **C6.7** with the positively charged thioflavin dye, which subsequently led to an emission intensity increase. The authors were able to detect ATP at *μ*M concentrations in water and in diluted ATP-spiked human serum samples. However, the chemosensor also showed a fluorescence response in the presence of pyrophosphate, ADP, and histidine, indicating its limited selectivity.

A bisquinoline-functionalized *β*-cyclodextrin was recently introduced by Borovkov, Wu, Yang, and coworkers for colorimetric detection and discrimination of AMP, ADP, and ATP at *μ*M concentrations in 10 mM HEPES buffer, pH 7.4.[704] Although nucleoside phosphates generally have weak binding affinities to *β*-cyclodextrins ($K_a \approx 40$ $M^{-1}$),[705,706] functionalization of CDs with cationic amino groups on the

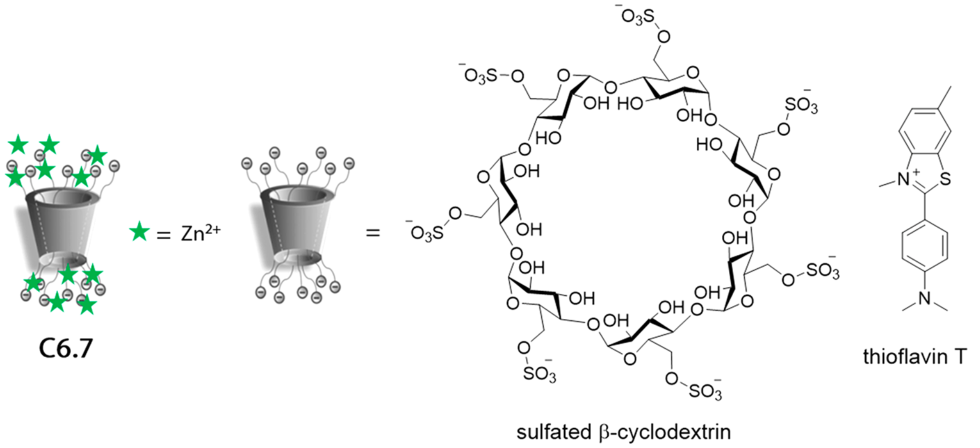

**Figure 165.** Schematic representation of a sulfated *β*-cyclodextrin that is combined with $Zn^{2+}$ and the indicator dye thioflavin T to furbish fluorescence turn-on chemosensor ensemble (**C6.7**) for the detection of ATP in water and human serum samples at *μ*M concentrations. Adapted with permission from ref 703. Copyright 2020 The Royal Society of Chemistry.

primary side of the cyclic oligosaccharide framework has been shown to largely increase binding strength ($K_a$ of methyl-amino-$\beta$-cyclodextrin with AMP and ATP are $1.3 \times 10^5$ and $3.1 \times 10^6$ $M^{-1}$, respectively).[707] As shown in Figure 166, a

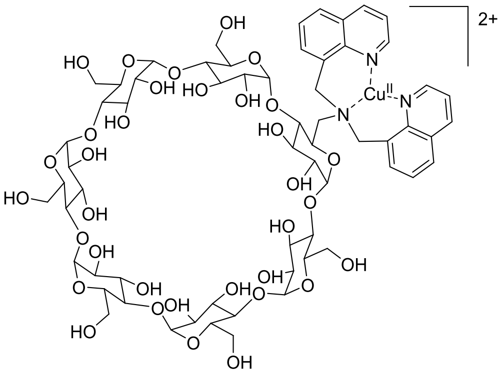

**C6.8**

**Figure 166.** Chemical structure of quinoline-functionalized $\beta$-cyclodextrin Cu$^{II}$-complex (**C6.8**) used for the detection of AMP, ATP, and ADP in HEPES buffer at $\mu$M concentrations.

fluorescent, dicationic [Cu$^{II}$-bisquinoline] complex (**C6.8**) was prepared that forms inclusion complexes with adenosine mono-, di-, or triphosphates that can be distinguished from each other by their photophysical properties. For instance, binding of AMP to **C6.8** resulted in an increase in the absorption maximum accompanied by a blue shift ($\Delta\lambda_{em}$ = 50 nm) emission quenching. In this case, the phosphate backbone of the nucleosides is assumed to interact with the metal center present in **C6.8**, while the ribose moiety is engulfed within the cavity of the $\beta$-cyclodextrin. In contrast, the complexes of **C6.8** with ADP and ATP displayed a small hypochromic effect in the absorption spectra and an enhanced fluorescence emission at 427 nm ($\lambda_{ex}$ = 315 nm).

The importance of positively charged moieties for the detection of nucleoside phosphates was recently illustrated by Issacs and coworkers.[708] In their work, an acyclic and positively charged CB*n*-type molecular container (**C6.9** in Figure 167) was prepared, which is able to bind various nucleoside phosphates ($K_a \approx 10^3$ $M^{-1}$ for ATP, UTP, and ADP measured in 20 mM sodium phosphate-buffered $D_2O$, pD 7.4) due to combination of aromatic moieties and electrostatic interactions.

Other positively charged chemosensors designed to promote nucleoside phosphate binding are depicted in Figure 168. For example, Bencini and coworkers reported positively charged phenanthroline-based polyamine receptors (**C6.10** in Figure 168a) that featured binding interactions with nucleoside triphosphates with decreasing strength in the order ATP ≥ GTP < TTP < CTP in 1 mM Tris-buffer, pH 6.0.[709] ATP engages in stronger $\pi-\pi$ stacking and electrostatic interactions with **C6.10**, leading to a strong binding affinity, *i.e.*, $K_a \approx 10^9$ $M^{-1}$ for the [H6**C6.10**(ATP)]$^{2+}$ complex. Upon binding of ATP, the initial emission of **C6.10** was quenched due to the occurrence of photoinduced electron transfer (PET) between the adenine moiety and the excited phenanthroline dye. It was shown that $\mu$M concentrations of ATP can be detected by chemosensor **C6.10**.

Lara and coworkers uncovered that cyclophane-type macrocycles that are functionalized with two anthraquinone groups (**C6.11** in Figure 168b) can associate with nucleoside phosphates with increasing binding strength in the order AMP < ADP < ATP.[710] The main forces stabilizing the complexes are believed to be the result of ion pairing, stacking, and hydrophobic interactions. A hypochromic effect in the absorbance spectra of the chemosensor was observed upon nucleoside binding and was used to quantify nucleosides in 32 mM PBS, pH 7.4, at $\mu$M concentrations.

Polycationic pyrenophanes capable of binding nucleoside triphosphates in deionized water (**C6.12** in Figure 168c) were described by Inouye and coworkers.[711] For instance, a strong association complex ($K_a = 1.0 \times 10^6$ $M^{-1}$) is formed between ATP and **C6.12**, while nucleoside mono- and diphosphates are much more weakly bound ($K_a \approx 6 \times 10^3$ $M^{-1}$). ATP can be detected at $\mu$M concentrations by recording the absorption changes and the quenching of the excimer emission of the chemosensor **C6.12**. Unfortunately, selective detection of ATP over GTP and TTP was not possible due to the similar binding affinities of **C6.12** for such substrates.

While most researchers focus on the development of chemosensors for ATP, complementary systems for the detection of other nucleoside triphosphates are also needed. In this respect, the recently published work by Dorazco-González and coworkers reported an important advance in the field by introducing dinuclear Zn$^{II}$-dipicolylamine (Zn$^{II}$-dpa) complexes that can be used for the selective detection of GTP at $\mu$M concentrations in 40 mM MOPS buffer, pH 7.0, and artificial biological fluids (**C6.13** in Figure 169).[712] Although some Zn$^{II}$−dpa complexes have been reported for the detection of phosphates and AMP,[713,714] the rationally designed asymmetric Zn$^{II}$−dpa complex **C6.13** allowed for selective GTP binding over other nucleosides in water and artificial biological fluids. Addition of GTP to **C6.13** resulted in a strong binding ($K_a = 10^6$ $M^{-1}$ for a 1:1 complex) and in near-quantitative emission quenching ($\lambda_{ex}$ = 325 nm, $\lambda_{em}$ = 410 nm). It is assumed that the GTP coordinates *via* its N7

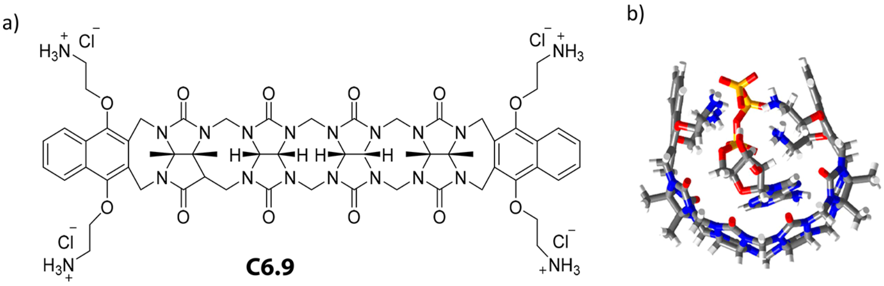

**C6.9**

**Figure 167.** (a) Chemical structure of acyclic and positively charged CB*n*-type chemosensor (**C6.9**). (b) 3D rendering of an acyclic and positively charged CB*n*-analogue that is bound to ATP. Reproduced with permission from ref 708. Copyright 2016 Taylor & Francis.

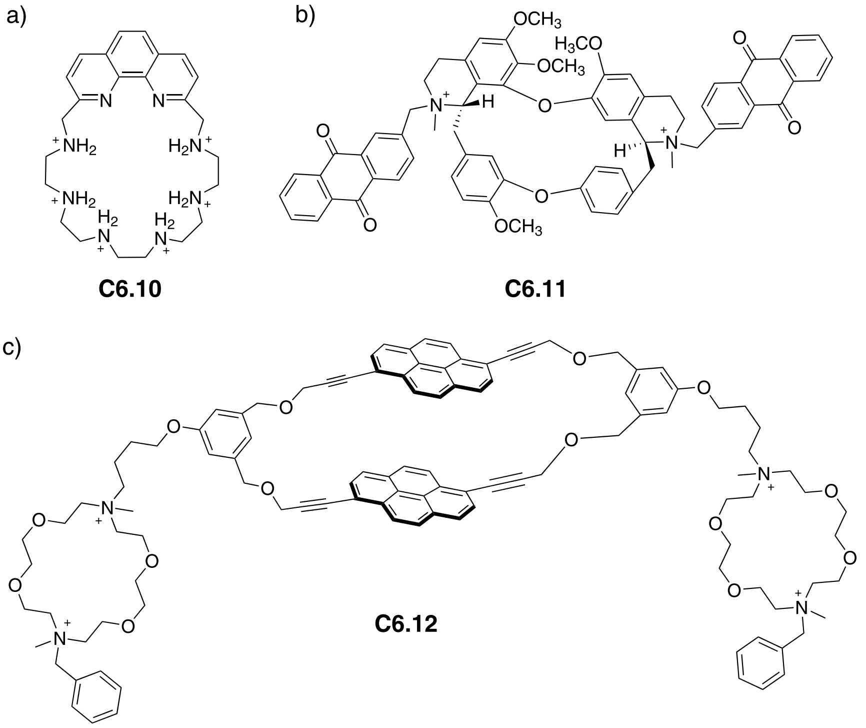

**C6.10** **C6.11** **C6.12**

**Figure 168.** Chemical structures of positively charged chemosensors used for the detection of nucleosides. (a) Phenanthroline-based polyamine receptor **C6.10**. (b) Anthraquinone-functionalized tetrandrine derivative **C6.11**. (c) Polycationic pyrenophane-based chemosensor **C6.12**.

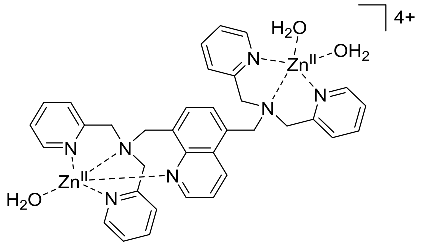

**C6.13**

**Figure 169.** Chemical structure of dinuclear Zn$^{II}$−dipicolylamine (Zn$^{II}$−dpa) complex (**C6.13**) that can be used for the selective detection of GTP.

guanosine atom to one Zn$^{II}$ center of **C6.13**, while the other Zn$^{II}$ center interacts with the phosphate groups of GTP. The authors explained the selectivity of their chemosensor for GTP over ATP by the higher energetic cost of desolvating ATP and by the asymmetric structure of **C6.13.**

A host−guest system for the selective detection of GTP at mM concentrations in 10 mM phosphate buffer, pH 7.4, and biofluids was reported by Ramaiah and coworkers, where 8-hydroxypyrene-1,3,6-trisulfonic acid (HPTS) was used as an indicator dye (**C6.14** in Figure 170).[715] In the presence of GTP, HPTS was displaced from the cyclophane host, thus resulting in a 150-fold emission enhancement. The fluorescence response of **C6.14** towards AMP, ADP, CTP, and UTP was negligible, but a 50-fold fluorescent enhancement was observed when ATP or ITP were added to the chemosensor, indicating its cross-reactivity for such nucleosides.

Recently, Butler and coworkers prepared Eu$^{III}$- and Tb$^{III}$-based anion receptors that enabled fluorescence-based detection of eight nucleoside phosphate anions in an array-based assay design, taking advantage of the multiple emission bands and long emission lifetimes associated with luminescent lanthanide complexes (**C6.15** in Figure 171).[716] The authors showed that the relative position of the quinoline groups on the macrocycle significantly affected the stability of the host−anion complex. In addition, the anion affinity was increased by incorporating H-bond donors into the quinoline moiety. The nucleoside phosphates ATP, ADP, AMP, cAMP, GTP, GDP, GMP, and pyrophosphate were distinguished by principal component analysis using variations in the emission bands and fluorescence lifetimes of four Eu$^{III}$ complexes in 10 mM HEPES buffer, pH 7.0, at mM concentrations.

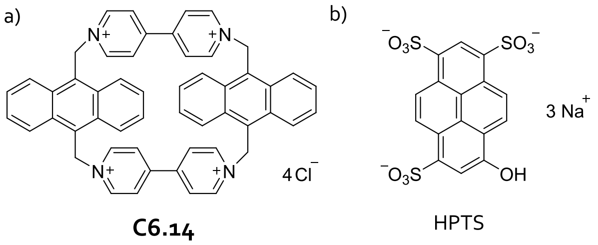

**C6.14** HPTS

**Figure 170.** (a) Cyclophane-based chemosensor (**C6.14**) and (b) indicator dye 8-hydroxypyrene-1,3,6-trisulfonic acid (HPTS) used for IDA-based detection of GTP.

Commercially available dyes are widely used for quantitative analysis of DNA (*e.g.*, for staining in electrophoresis gels), and selected examples are shown in Figure 172.[717−721] Because of their cationic and aromatic nature, these dyes can interact with the negatively charged phosphodiester backbone and intercalate between the nucleobases of DNA. Such fluorescent dyes can be used to detect picograms of DNA but lack sequence selectivity and can only be applied for double-stranded DNA. Because of the importance of selective probes and sensors, the following examples describe newer systems that have an additional degree of structural selectivity, *e.g.*, toward

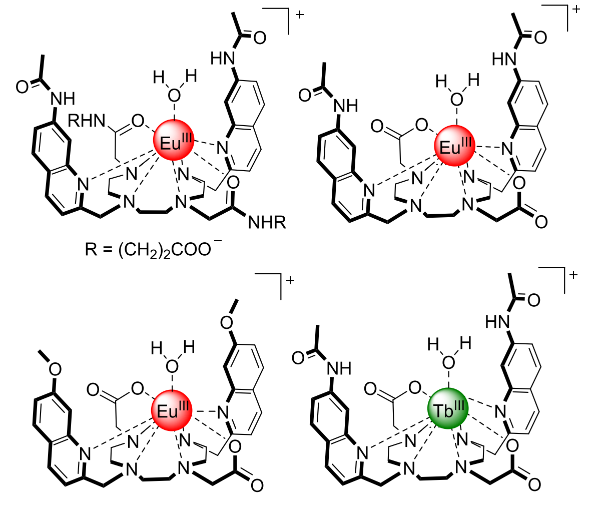

**C6.15**

**Figure 171.** Chemical structures of selected Eu$^{III}$- and Tb$^{III}$-based anion receptors used in an array-based assay design for fluorescence-based nucleoside phosphate detection at mM concentration in 10 mM HEPES buffer, pH 7.0. Adapted with permission from ref 716. Copyright 2020 The Royal Chemical Society.

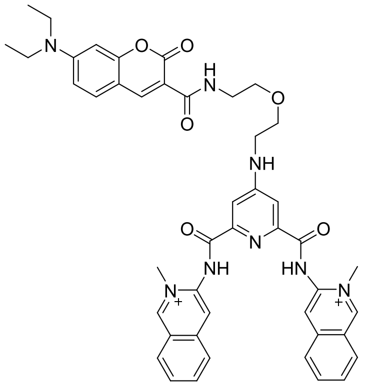

**C6.16**

**Figure 173.** Chemical structure of a bis(quinolinium)-pyridodicarboxamide (PDC)-based fluorescent chemosensor (**C6.16**) for the selective G4 staining of DNA.

secondary DNA structures, specific base sequences in DNA, or the ability to distinguish single-stranded DNA from double-stranded DNA.

G-Quadruplexes (G4) are secondary DNA structures formed by guanine-rich sequences in DNA and are known to play a role in vertebrate transcription processes.[722−726] Therefore, the realization of chemosensors that can detect such secondary structures is of great interest. For example, a fluorescence turn-on chemosensor (**C6.16** in Figure 173) that allows for the detection of G4 at $\mu$M concentrations in buffered solution (K-100 buffer containing 10 mM LiAs-$Me_2O_2$, 100 mM KCl, pH 7.2) and serum samples was reported by Granzhan and coworkers.[727] In this work, the authors prepared a fluorescent chemosensor composed of the G4 targeting bis(quinolinium) pyridodicarboxamide (PDC) unit and the fluorophore coumarin. Because of its aromaticity and size-matching shape, PDC strongly interacts with the surfaces of G4 units *via* $\pi-\pi$ interactions. Consequently, the intramolecular PET processes between PDC and coumarin moieties were disrupted, leading to the observed increased emission intensity upon quadruplex addition.

Gerasimova, Kolpashchikov, and coworkers recently reported the combined use of two single-stranded DNA (ssDNA) and the dye dapoxyl-F (**C6.17** in Figure 174a) for single-nucleotide polymorphism detection at nM concentrations. The sensing experiments were carried out in 20 mM Tris-HCl containing 200 mM KCl and 10 mM $MgCl_2$, pH 7.4,

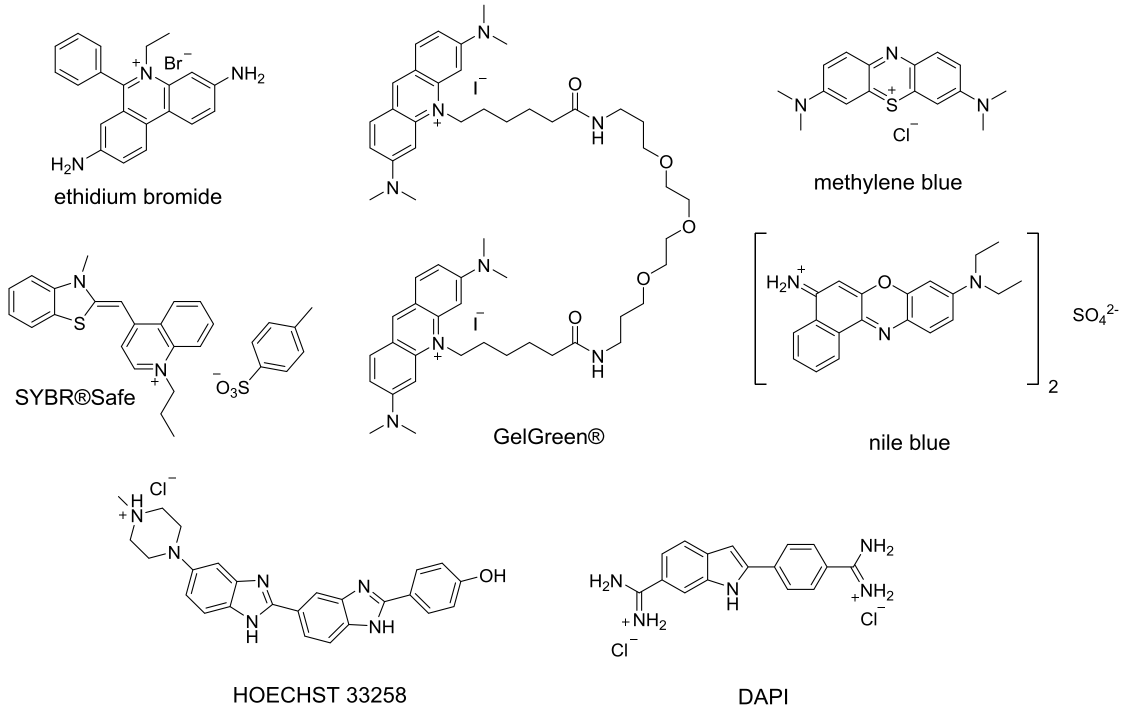

**Figure 172.** Chemical structures of DNA-staining dyes used in commercially available assays.

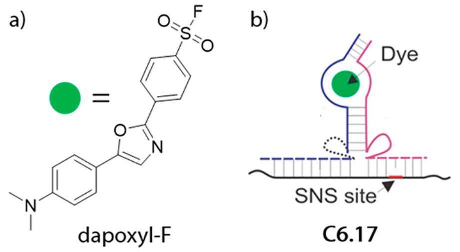

**Figure 174.** (a) Chemical structure of a dapoxyl-dye used in combination with aptamer strands (**C6.17**) for the detection of DNA polymorphism. (b) Two ssDNA strands (blue and purple) bind a target sequence (black) to form a high affinity "binding pocket" for the dye. Adapted with permission from ref 728. Copyright 2019 American Chemical Society.

or 1× NASAB buffer, pH 8.5.[728] The two ssDNA strands hybridize to their specific oligonucleotide sequence found in DNA samples, forming a "binding pocket" for dapoxyl-F (Figure 174b). This fluorescence turn-on assay allows for the detection of single nucleobase mutations of DNA polymorphs.

Mohanty, Pradeepkumar, Bhasikuttan, and coworkers showed that thioflavin T (**C6.18** in Figure 175) selectively binds to G4-units in dsDNA when working in 50 mM Tris-HCl buffer containing 50 mM KCl, pH 7.4.[729] The authors observed that upon binding to G4 units, the fluorescence emission intensities of **C6.18** increased 2000-fold, whereas only a 250-fold increase was observed while binding to other DNA forms, allowing for $\mu$M detection of G4 units in DNA. The chemosensor **C6.18** not only showed a satisfactory binding affinity for G4 units in dsDNA ($K_a = (3.8 \pm 0.4) \times 10^5$ $M^{-1}$ for the 1:1 adduct in Tris-HCl buffer containing 50 mM KCl, pH 7.4) but was also shown to induce quadruplex folding in ssDNA. It was hypothesized that the most likely binding mode for **C6.18** is end-stacking interaction with G4, resulting in a structure planarization and marked fluorescence increase.

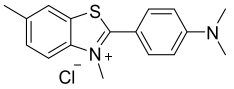

**C6.18**

**Figure 175.** Chemical structure of thioflavin T (**C6.18**).

Tang, Meng, Luo, and coworkers reported the use of a triphenylamine-based chemosensor (**C6.19** in Figure 176), which has different luminescence properties in the presence of dsDNA and ssDNA.[730] **C6.19** interacted with dsDNA *via* electrostatic interactions and was eventually bound to the grooves of DNA, experiencing a structural stiffening that increased its fluorescence quantum yield (rigidochromic effect). In addition, a significant shift in the fluorescence emission wavelength of **C6.19** from red to green was observed, which was explained by a conformational twist of **C6.19**. Because ssDNA lacks grooves, **C6.19** remains weakly red-emissive when interacting with ssDNA. The authors were able to detect selectively dsDNA at $\mu$M concentrations in water. Additionally, the chemosensor was successfully applied for the detection of DNA damage caused by UV-light irradiation of blood samples.

Nau, Hennig, and coworkers reported the detection of dsDNA with the use of a host–guest Förster resonance energy transfer (FRET)-based pair formed by carboxyfluorescein-labelled CB7 (acceptor) and the fluorescent dye DAPI (donor, Figure 177a).[731] When DNA samples were added to a solution of **C6.20**, DAPI dissociated from CB7 due to its stronger affinity for the minor groove of DNA (Figure 177b). Upon relocation of DAPI, the FRET signal from **C6.20** significantly decreased and a new fluorescence emission band from DNA-bound DAPI arose. By analyzing the ratio of these two emissions intensities, the authors successfully detected sperm DNA at $\mu$M concentrations (LOD, 78 $\mu$M) in 10 mM ammonium phosphate buffer, pH 7.2.

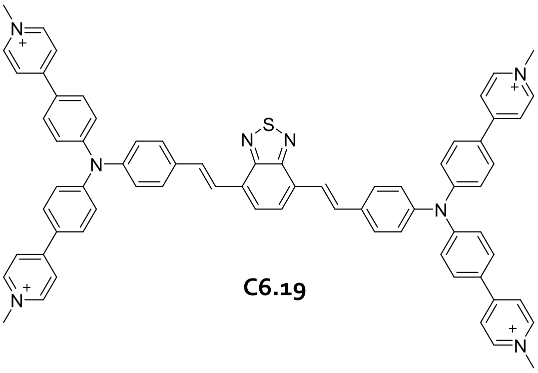

**Figure 176.** Structure of triphenylamine-based chemosensor (**C6.19**) for simple fluorescence-based detection of dsDNA at $\mu$M concentrations in water.

For more details on similar concepts for DNA detection, we refer the interested reader to the recently published review by Berdnikova and Chernikova.[732]

### 6.4. Nanosensors for Nucleoside Phosphates and Oligonucleotides

Schmidt and coworkers reported dual fluorescent silica particles for ratiometric fluorescence turn-on detection of ATP at $\mu$M concentrations in 100 mM HEPES buffer, pH 7.4 (**N6.1** in Figure 178).[733] The core of the silica particles was functionalized with the reference dye rhodamine, whereas the surface of the particles was grafted with fluorescent naphthalimide-based dipicolylamine $Zn^{II}$-indicator complexes (ndp–$Zn^{II}$). The emission intensity of the surface-bound ndp–$Zn^{II}$ increased upon analyte binding, while the signal of the reference dye remained almost unaffected (around 11% when compared to the fluorescence of the indicator dye). The authors concluded that the phosphate group of ATP coordinates to the $Zn^{II}$ center weakening the $Zn^{II}$–NH interaction.[734] When the indicator dye was covalently linked on the surface of the particles, it showed a lower binding affinity for ATP ($K_a = 3.3 \times 10^3$ $M^{-1}$) compared to ndp–$Zn^{II}$ in solution ($K_a = 5.0 \times 10^5$ $M^{-1}$), possibly due to steric hindrance reducing the $\pi$–$\pi$ stacking interaction between ATP and the dye. In addition to ATP, **N6.1** responded to GTP, UTP, and CTP, indicating a cross-reactivity for other nucleoside phosphates. The authors were able to show that **N6.1** is internalized in cells without exerting cytotoxic effects. Vesicle-based nanosensors for the detection of nucleosides were developed by König and coworkers.[735] The authors embedded amphiphilic indole-functionalized binuclear zinc–cyclen complexes ($Zn_2Trp$) and $Tb^{III}$ diethylenetriaminepentaacetic acid (DTPA)-based (Tb-1) emitters into the membrane of phospholipid vesicles (**N6.2** in Figure 179). Nucleoside binding to $Zn_2Trp$ reduces the donor-dye ability to sensitize the emission of the lanthanide due to spatial separation. The

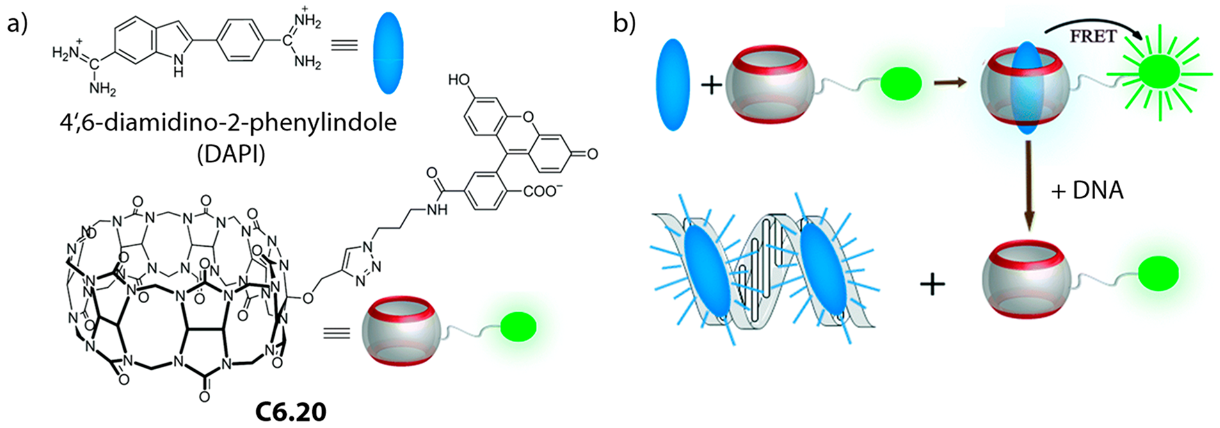

**Figure 177.** (a) Chemical structures of a carboxyfluorescein-labelled cucurbit[7]uril and the dye DAPI. (b) Schematic illustration of a DNA chemosensing ensemble featuring FRET. Reproduced with permission from ref 731. Copyright 2019 The Royal Society of Chemistry.

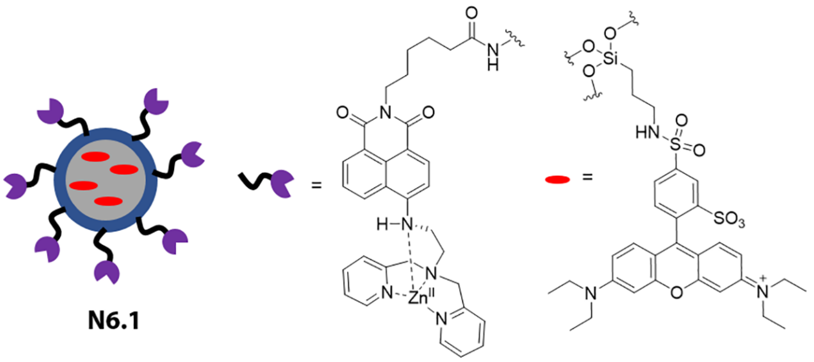

**Figure 178.** Schematic representation of dual fluorescent silica nanoparticles (**N6.1**) used for fluorescence-based detection of ATP at $\mu$M concentrations in aqueous buffers.

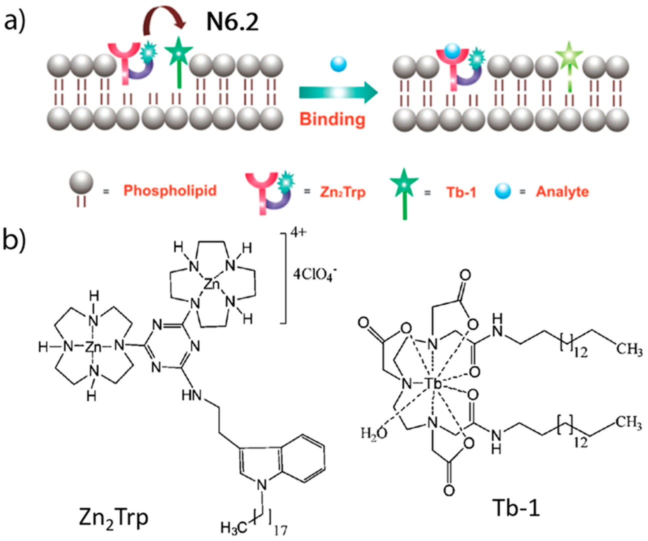

**Figure 179.** (a) Schematic representation of the sensing mechanism for nucleotides by nanosensor **N6.2** in HEPES buffer at micromolar concentrations. (b) Chemical structures of $Zn_2$Trp and Tb-1 used in the sensing system. Adapted with permission from ref 735. Copyright 2013 The Royal Society of Chemistry.

authors successfully detected nucleoside triphosphates at $\mu$M concentrations in 25 mM HEPES buffer, pH 7.4, and further showed that the performance of **N6.2** remains unaffected in the presence of monovalent and divalent anions such as $Cl^-$, $Br^-$, $AcO^-$, and $CO_3^{2-}$.

Nitschke and coworkers developed water-soluble, tetrahedral cage-like structures formed by fluorescent triazatriangulenium ($TATA^+$) panels linked through their vertices by complexation of $Zn^{II}$ cations (**N6.3** in Figure 180).[736] Because of the cationic nature of $TATA^+$, a positively charged interior space is formed that can interact with negatively charged guest molecules. For example, the cage was shown to favor binding of large inorganic anions (*e.g.*, $Mo_6O_{19}$) over smaller anions (*e.g.*, $BF_4^-$, $ClO_4^-$, $TfO^-$), suggesting that both electrostatic and size complementarity between the host's cavity and the

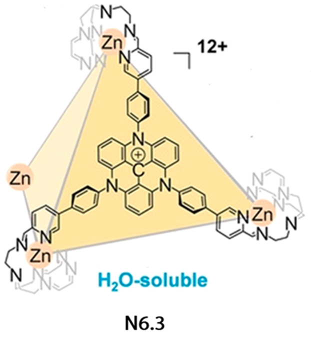

**Figure 180.** Chemical structure of the triazatriangulenium ($TATA^+$)-$Zn^{II}$ cage (**N6.3**) used for fluorescence-based detection of nucleoside phosphates at $\mu$M concentrations in deuterated water. Adapted with permission from ref 736. Copyright 2019 Wiley-VCH.

guest are required for complexation. **N6.3** was used for the μM detection of ATP ($K_a$ = 1.8 × $10^3$ $M^{-1}$ in $D_2O$), AMP ($K_a$ = 1.3 × $10^2$ $M^{-1}$ in $D_2O$) and GMP ($K_a$ = 1.0 × $10^3$ $M^{-1}$ in $D_2O$), whereas the non-charged adenosine, guanosine, and uridine are not bound.

In summary, probes based on amino-modified rhodamine derivatives provide unique fluorescence turn-on properties that can be used for the detection of nucleoside phosphates but have not yet achieved the selectivity needed for routine use in diagnostics of complex biofluids such as saliva, urine, and blood. The same applies for the design of chemosensors, which ideally should be selective for mono-, di-, and triphosphate nucleosides in addition to the ability of discriminating between different nucleosides such as ATP and GTP. While the medically relevant concentration range of ATP detection in blood (millimolar, see Table 23) has been reached by the reported molecular probes, chemosensors, and nanosensors (Table 20−22), their practically preferred application in readily accessible biofluids such as saliva still requires improvements in terms of binding strength and sensitivity to be reliably used in the submicromolar nucleotide concentration range.

**Table 23. Summary of the Normal Concentration Range of Nucleotides in Biofluids**

| concentration range | media | ref |
|---|---|---|
| Adenosine Triphosphate (ATP) Analyte | | |
| 1.50−4.90 mM | blood | 741 |
| 370−670 nM | saliva | 742 |
| Adenosine Monophosphate (AMP) Analyte | | |
| 100−430 nM | saliva | 335 |
| Circulating Free DNA Analyte | | |
| 9.80−18.0 ng/mL | blood | 743 |
| Guanosine Triphosphate (GTP) Analyte | | |
| 49.0−63.0 μM | blood | 642 |
| 1.80−1.86 μM | cerebrospinal fluid | 744 |
| Uridine Triphosphate (UTP) Analyte | | |
| 0.39−1.69 μM | saliva | 62 |

Some promising chemosensors, such as supramolecular complexes with the small molecules thioflavin T or dapoxyl dyes, have been successfully used to selectively detect DNA polymorphism or secondary structures within DNA samples (*e.g.*, G4 quadruplexes). Compared to many chemosensors and probes currently being explored for the detection of nucleoside phosphates and DNA, the number of nanosensors reported in the literature for nucleotide detection is relatively small, which may encourage the development of other nanomaterials in this direction. The fact that there are only a few examples of nanosensors may be due to the successful and promising alternatives based on aptamer- and ssDNA-functionalized nanoparticles through DNA nanotechnology. We did not cover these technologies in this review, as they are comprehensively covered elsewhere.[737−740]

## 7. CARBOXYLATES

Carboxylic acids are organic compounds with one or more −COOH groups bonded to a hydrocarbon residue. Because of their acidity, carboxylic acids are partially deprotonated at physiological pH values and are present in the form of their conjugated bases, known as carboxylates. The negative charge in carboxylates is distributed over three atoms (−COO) and carboxylates are generally well solvated in water (see Figure 181). Carboxylates are widely distributed in nature and are intermediates of the Krebs cycle, the key metabolic pathway that links carbohydrate, fat, and protein metabolism and is

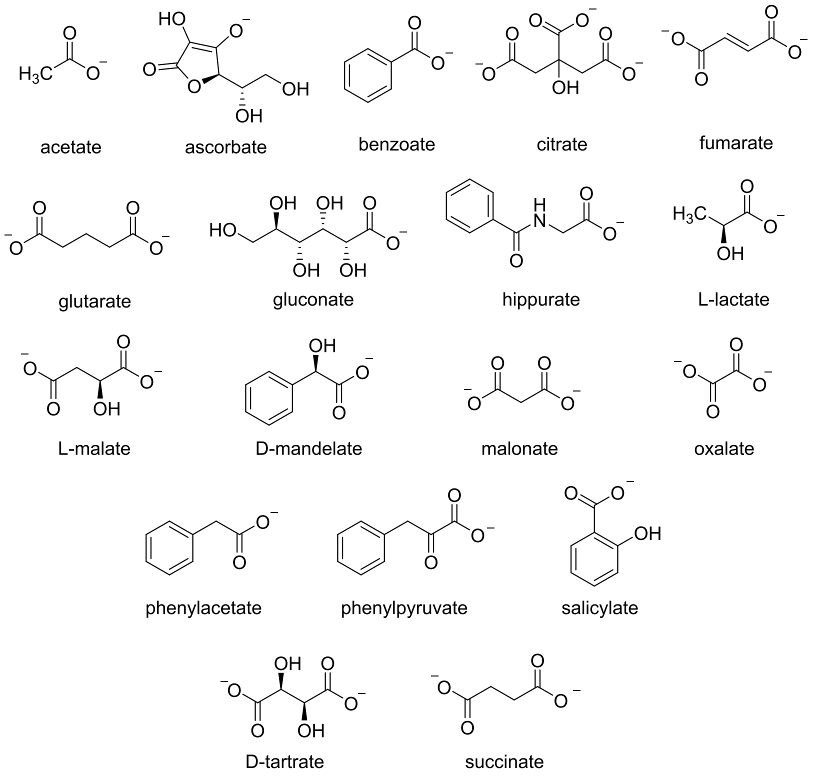

**Figure 181.** Chemical structures of carboxylates.

used by all aerobic organisms for energy production.[745] Abnormal concentrations of carboxylates in various biofluids have been repeatedly shown to be associated with diseases. For example, scurvy is caused by a severe deficiency of ascorbic acid (vitamin C), *i.e.*, the concentration of ascorbate in serum is less than 12 $\mu$mol/L.[746−750] In addition, there is evidence that low ascorbate levels can be associated with diseases such as coronary vascular diseases, diabetes, and strokes.[750] Moreover, it was found that the level of citrate is a potential marker for prostate cancer tissue because malignant prostate tissue has a significantly lower level of citrate compared to healthy tissue or its premalignant state.[751−758] Lactate is the end product of the anerobic glycolysis and is formed during physical stress, such as strenuous exercise, in rather high concentrations up to 20 mM.[759] Detection of lactate in the blood is of great importance because sustained hyperlactatemia ($c_{\text{lactate}} > 6.5$ mM) can be associated with several disorders such as sepsis or trauma.[760−762] Hippurate, a harmful uremic toxin, is involved in a variety of pathological conditions, such as neurological disorders, chronic kidney diseases, and some cancers.[763−766] For example, elevated hippurate levels are found in the serum of patients with uremia, a condition in which elevated blood urea levels are a result of inadequate kidney function.[763] Recently, hippuric acid was confirmed to be significantly associated with left ventricular hypertrophy, which is one of the most common cardiac abnormalities in patients with end-stage renal disease.[767] Besides hippurate, gluconate and gluconolactone are carboxylates that are involved in chemical homeostasis and were found to have antioxidant properties.[768] Although gluconate metabolism is relatively unexplored in terms of its potential role in disease development and indication, there are several reports linking lower plasma gluconate levels to Alzheimer's disease and increased oxidative stress.[769,770] Furthermore, gluconate is not only a relevant biomarker for diseases but is also used as a drug, *e.g.*, in the form of iron gluconate complexes for the treatment of anemic pediatric patients with end-stage renal disease undergoing hemodialysis.[771,772] Interestingly, gluconate may be considered as a potential candidate for cancer treatment, as it blocks citrate transport into cancer cells, thus resulting in decreased tumor growth.[773] It has been reported that salicylate levels found in serum samples may be associated with Reye's syndrome, a rare but serious condition that causes swelling in the liver and brain.[774,775] Synthetic carboxylates such as aspirin or ibuprofen are nonsteroidal anti-inflammatory drugs (NSAIDs) and are commonly used to treat rheumatic diseases.[776] However, overdosage of such NSAIDs can lead to microvesicular steatosis of the liver,[774] and their concentration levels in biological fluids are important indicators of misuse or incorrect dosing of these drugs. A closer insight into drug sensing is given in section 9.

Looking at the overview of common metabolites in urine (see Figure 4), it is evident that in addition to zwitterionic amino acids, negatively charged carboxylates are frequently found in this biofluid and as such represent attractive target metabolites for the development of molecular probes and chemosensors for diagnostic applications. Although there are some promising chemo- and nanosensors described in the following section, it should be noted that the detection of carboxylates in aqueous media appears to be a more difficult task than, for example, the detection of amines or thiols.

## 7.1. Molecular Probes for Specific Carboxylates

As for their chemical reactivity, carboxylates are "hard" nucleophiles and are much less nucleophilic in aqueous media than, for example, amines and thiols. As such, they do not easily engage in Michael-type addition reactions with C=C-EWG moieties (= Michael acceptors). For quantitative nucleophilicity scales, see for instance the extensive work of the Mayr group and their online database for reactivity parameters.[777−781] Additionally, carboxylates form much weaker metal−ligand complexes in aqueous media with appropriate metal centers than for instance thiols, which presents a challenge for designing metal-based probes.

Given the difficulties in designing covalent bond-like binding motifs for carboxylates, it is not surprising that only a handful of probes capable of targeting these analytes in aqueous media have been reported to date. The probes and chemosensors discussed within this section are summarized in Table 24. In 2004, Anslyn and coworkers demonstrated that the binding of $\alpha$-hydroxy acids to boronic acids can be used for setting up an indicator displacement assay (IDA, **P7.1** in Figure 182) that allowed for the detection and quantification of these particular class of carboxylates in the millimolar concentration range in 10 mM HEPES buffer containing 75% MeOH, pH 7.4. The use of chiral boronic acids as the binding motif made chirality sensing and the determination of enantiomeric excess of $\alpha$-hydroxy acids possible.[782]

**Table 24. Summary of Molecular Probes for Carboxylates (LOD, Limit of Detection)**

| probe | media | concentration range | ref |
|---|---|---|---|
| | Ascorbate Analytes | | |
| **P7.5** | 1% DMSO in 100 mM PBS, pH 7.4; blood plasma | 0.13−8.0 $\mu$M; LOD, 9.7 nM | 787 |
| **P7.6** | vitamin drinks and orange juices | 0.1−2.0 mM; LOD, 14 $\mu$M | 788 |
| **P7.7** | 50 mM PBS, pH 7.0; human blood serum | 80 nM−50 $\mu$M; LOD, 20 nM | 789 |
| **P7.8** | Tris-HCl buffer, pH 7.1 | LOD, nM range | 790 |
| | $\alpha$-Hydroxy Acetates (Lactate, Mandelate) Analytes | | |
| **P7.1** | 75% MeOH in 10 mM HEPES, pH 7.4 | mM range | 782 |
| | Sugar Acetates (Gluconate, Glucarate) Analytes | | |
| **P7.2** | 50% MeOH in water containing 50 mM NaCl, pH 5.6−8.3 | $\mu$M range | 783 |
| | Lactate Analytes | | |
| **P7.3** | 52% MeOH in phosphate buffer, pH 7.4 | 0−300 mM | 784 |
| **P7.4** | 52% MeOH in phosphate buffer, pH 7.4 | 0−300 mM | 784 |

In the same year, the James group reported axially chiral binaphthol derivatives that featured two boronic acids moieties as recognition motifs for $\alpha$-hydroxy acid-based analytes (**P7.2** in Figure 183).[783] Uniquely, the two enantiomers of the probe responded differently, one with fluorescence increase and the other with fluorescence decrease, to the presence of the chiral target analyte enantiomers, *e.g.*, tartaric acid. Additionally, the probes were used for the emission-based detection and chirality sensing of sugar acids such as glucaric acid, gluconic acid, and glucuronic acid in aqueous organic media (50 mM NaCl in water containing 50% MeOH, pH 5.6−8.3) in the micromolar concentration range.

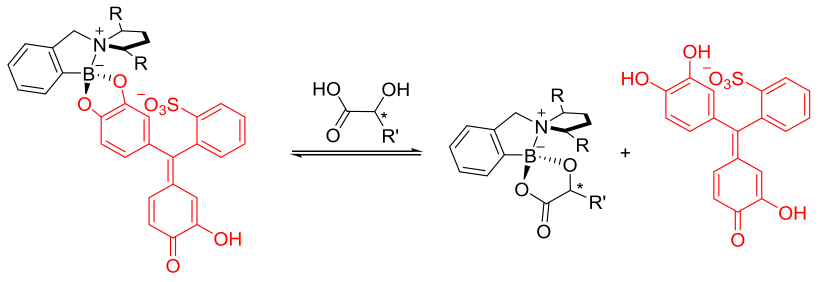

**P7.1**

**Figure 182.** Schematic representation of the boronic-acid-based IDA-type probe **P7.1** for the detection of $\alpha$-hydroxy acids in organic aqueous media at mM concentrations. Adapted with permission from ref 782. Copyright 2004 American Chemical Society.

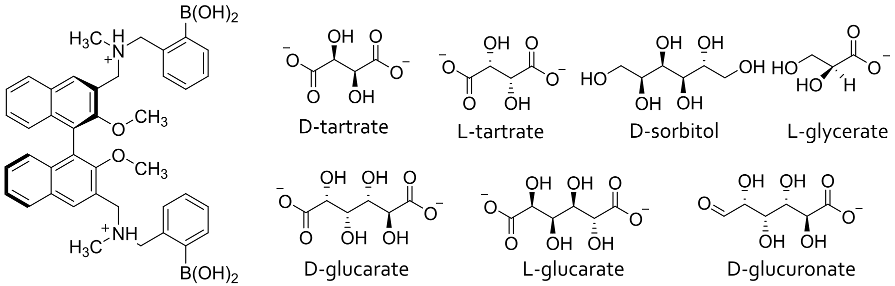

**P7.2**

**Figure 183.** Chemical structure of a boronic acid-based fluorescent probe (**P7.2**; (*R*)-enantiomer shown) for the enantioselective detection of tartaric acid and sugar acids in aqueous organic media at $\mu$M concentrations.

BODIPY-based boronic acid probes (**P7.3** and **P7.4** in Figure 184) were introduced by Christensen and coworkers for the detection of lactate at physiological pH.[784] The probes **P7.3** and **P7.4** showed high selectivity for lactate in 25 mM phosphate buffer, pH 7.4, containing 52% MeOH with binding affinities of $K_a = 1.7 \times 10^5\ M^{-1}$ and $1.6 \times 10^5\ M^{-1}$, respectively, allowing for its mM detection. The authors showed that the binding of lactate caused an emission enhancement, whereas no fluorescence response was observed for non-$\alpha$-hydroxy acids, *e.g.*, glucose, fructose, and mannose. However, **P7.3** and **P7.4** were shown to also bind, although to a lesser extent, to L-malate and L-ascorbate, indicating potential cross-reactivity with other $\alpha$-hydroxy acids.

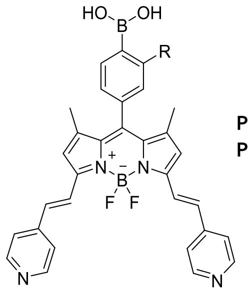

**P7.3:** R = H
**P7.4:** R = F

**Figure 184.** Chemical structure of the BODIPY-based boronic acid probes **P7.3** and **P7.4** for the detection of lactate in 25 mM phosphate buffer containing 52% MeOH, pH 7.4.

Ascorbic acid is a particular lactone-functional metabolite for which a redox chemistry coupled detection strategy can be exploited due to its reducing properties. Several researchers have successfully capitalized on the finding that nitroxides can be reduced by ascorbic acid.[785,786] Nitroxides quench the emission of various fluorescent dyes by electron transfer from the nitroxide to the fluorophore. However, in the presence of reducing agents that convert the nitroxide to hydroxylamine, the quenching mechanism is interrupted. Starting from this principle, ascorbate selective probes were successfully designed through tailoring of the substituents on the nitroxide moiety, and a proper choice of the attached fluorophore.

For instance, Fukuzumi, Yamada, and coworkers developed a Nile blue nitroxide conjugate that was successfully used for fluorescence turn-on detection and quantification of ascorbic acid in 100 mM PBS containing 1% DMSO, pH 7.4, and in diabetic rat plasma (**P7.5** in Figure 185).[787] With this probe, a low detection limit of 9.7 nM for ascorbic acid was achieved,

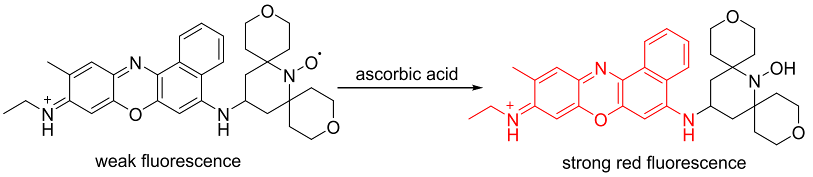

**P7.5**

**Figure 185.** Emission turn-on sensing of ascorbic acid with the Nile blue nitroxide conjugate (**P7.5**) in 100 mM PBS containing 1% DMSO, pH 7.4.

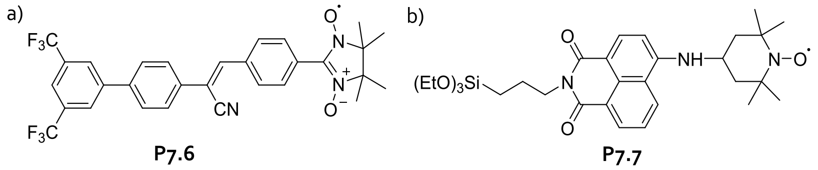

**Figure 186.** (a) Chemical structure of nitroxide-based fluorescent probe **P7.6** that is appliable for the detection of ascorbic acid in fruit juices (LOD, 14 μM). (b) Chemical structure of naphthalene imide-nitroxide probe **P7.7** that can be used for the detection of ascorbic acid at nM to μM concentrations in 50 mM PBS, pH 7.0.

**Table 25. Summary of Chemosensors for Carboxylates (LOD, Limit of Detection)**

| chemosensor | media | concentration range | ref |
|---|---|---|---|
| Aromatic Carboxylates, *e.g.*, Salicylate, Analytes | | | |
| **C7.12** | Tris buffer containing 100 mM TMACl, pH 7.4 | sub-mM range | 802 |
| | HEPES buffer containing 100 mM TMACl, pH 7.4 | | |
| Carboxylates, *e.g.*, Aliphatic and Aromatic Carboxylates Analytes | | | |
| **C7.14** | borate buffer, pH 7.0; human urine samples | 0.1−1.0 mM | 805 |
| Dicarboxylates, *e.g.*, Malonate Analytes | | | |
| **C7.1**[a] | 10 mM Tris buffer, pH 7.5; | 0−480 μM | 795 |
| Nonsteroidal Anti-inflammatory Drugs (NSAIDs) Analytes | | | |
| (**C7.4−7.11**) chemosensor array | water, pH 8.5 | μM range; LOD, 0.33 μm | 800 |
| Oxalate Analytes | | | |
| **C7.13** | 10% EtOH in 10 mM Tris-HCl, pH 7.0 | 0−120 μM; LOD, 3.0 μM | 804 |
| Phenylpyruvate Anayte | | | |
| **C7.3** | 50 mM acetate buffer, pH 5.8 | 1.0−20 μM; LOD, 1.0 μM | 799 |
| | artificial urine | 2.7−60.0 μM; LOD, 2.7 μM | |
| (*S*,*S*)-Tartrate Analyte | | | |
| **C7.2** | 5 mM Tris buffer, pH 7.0 | log $K_a$ = 5.8 | 796 |

[a] Glutamate and aspartate did not cause an emission signal change.

requiring approx. 20 min of reaction time. It was shown that blood plasma from healthy and diabetic rats can be readily distinguished which was further corroborated by HPLC analysis.

Similarly, the Park group introduced a nitroxide-based fluorescent probe (**P7.6** in Figure 186) for the detection of ascorbic acid (LOD, 14 μM) that provided a dual electron spin resonance (ESR) response.[788] With the use of **P7.6**, the authors were able to detect ascorbic acid in fruit juices even in the presence of other biologically relevant reducing agents such as thiols and nicotinamide adenine dinucleotide (NADH). Previously, Du, Xiao, and coworkers have demonstrated that the detection of ascorbic acid in 50 mM PBS, pH 7.0, human blood serum and cell lysates can be achieved with a naphthalene imide−nitroxide conjugate (**P7.7** in Figure 186) that features an additional alkoxysilane moiety to increase its hydrophilicity.[789] The authors found a linear emission response of **P7.7** in the ascorbate concentration range of 80 nM to 50 μM and estimated a detection limit of about 20 nM in PBS. In addition, **P7.7** was not affected by other biologically occurring reducing agents such as glutathione. Wang and coworkers used the quenching of hyperbranched conjugated polyelectrolytes by Cu$^{2+}$ ions for the design of the fluorescent turn-on probe **P7.8**.[790] In the presence of ascorbate, Cu$^{2+}$ is reduced to Cu$^{+}$, and thereby becomes a much less efficient emission quencher of the hyperbranched conjugated polyelectrolyte. This system displays a nanomolar detection limit for ascorbate in Tris-HCl buffer, pH 7.1.

## 7.2. Chemosensors for Carboxylates

Comparatively more chemosensors than probes are known for the detection of carboxylates in aqueous media, even though their range of application is still limited. In a popular design strategy, multiple positively charged binders (*e.g.*, macrocyclic hosts) are constructed to form several charge-assisted hydrogen bonding contacts with the negatively charged carboxylate target analytes. However, many of the concave, macrocyclic hosts, *e.g.*, cucurbit[*n*]urils and pillar[*n*]arenes, which are known to have record binding affinities for neutral or positively charged guests, are comparably weak binders for anionic species because their cavity interiors display a compressed electron distribution and a negative electrostatic potential.[187,261,791,792] Gibbs and coworkers have shown that, despite unfavorable electrostatic contributions, deep cavitands are efficient anion binders, especially for chaotropic anions such as PF$_6^-$, driven by the effects of counter cations and the solvation of "empty" hosts.[792−794] Unfortunately, the rather kosmotropic carboxylates are also not bound by this enveloping host family in an efficient manner. Promising chemosensor designs for the detection of carboxylates discussed in this section are summarized in Table 25.

For instance, Glass and coworkers developed a pinwheel-shaped chemosensor (**C7.1**) that featured four guanidinium moieties strapped to a rigid but rotationally flexible aromatic scaffold (Figure 187).[795] In addition, two anthryl units were tethered to the chemosensor as fluorescent reporter groups. Upon binding with dicarboxylates such as malonate, **C7.1** twists around its axis and adopts a conformation with a restricted rotation. This brings the anthryl units in close spatial contact, resulting in a characteristic fluorescence response. In contrast, **C7.1** did not show this type of emission change in the presence of monocarboxylates such as acetate, which were probably bound to the chemosensor but did not promote an alteration of this conformation. **C7.1** is capable of complexing two dicarboxylates cooperatively, with Hill coefficients around 1.7−2.0 and ternary affinity constants of $10^6$−$10^9$ M$^{-2}$ in 10 mM Tris buffer, pH 7.5, or 10 mM sodium acetate buffer. For instance, **C7.1** can be used for emission-based sensing of oxalate, malonate, succinate, maleate, fumarate, glutarate, and phthalate at μM concentrations. In contrast, the dicarboxylates glutamate and aspartate provided no change in the emission signal, which the authors attributed to the inability to induce a rotationally restricted binding conformation in **C7.1**.

In section 7.1, we had showcased the work from the James group on the design of chiral, binaphthol-based probes for α-hydroxy acids.[783] Utilizing a similar design idea, Bencini, Lippolis, Pasini, and coworkers developed an enantioselective

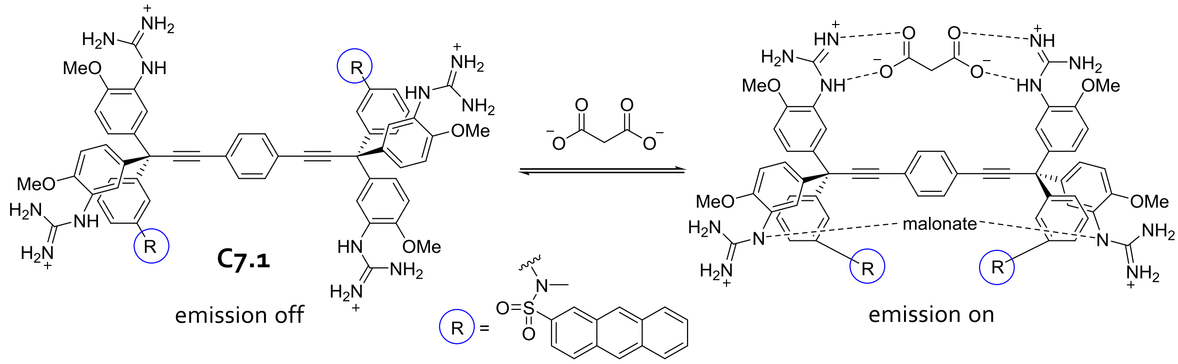

**Figure 187.** Fluorescent pinwheel-shaped chemosensor **C7.1** allows for the cooperative recognition and selective sensing of dicarboxylates in Tris- or sodium acetate buffer at $\mu$M concentrations. Adapted with permission from ref 795. Copyright 2002 American Chemical Society.

chemosensor (**C7.2** in Figure 188) for (*S*,*S*)-tartaric acid in 5 mM Tris buffer, pH 7.0, by attaching two polyamine moieties ([9]ane$N_3$ azacrown ethers) to a chiral binaphthol scaffold.[796] The affinity of the deprotonated state of **C7.2** for (*S*,*S*)-tartaric acid was reported as log $K_a$ = 5.8, which is much higher than that for *meso*-tartrate (log $K_a$ = 3.8), (*R*,*R*)-tartrate (log $K_a$ = 3.1), or other dicarboxylates such as succinate (log $K_a$ = 3.7) and fumarate (log $K_a$ = 2.7); all values were obtained in 100 mM $NMe_4Cl$ solution. In addition, it was demonstrated that **C7.2** does not or only weakly responds to maleate and lactate. The authors concluded that analyte binding causes the observed emission enhancement and spectral red-shift through assisting an excited-state intramolecular proton transfer (ESIPT)[797,798] of the binaphthol chromophore.

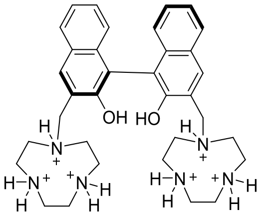

**C7.2**

**Figure 188.** Aza-crown ether substituted binaphthol (**C7.2**) used for enantioselective and fluorescence-based detection of (*S*,*S*)-tartaric acid in 5 mM Tris buffer, pH 7.0.

General binders for carboxylates, including monocarboxylates, were recently introduced by the Jiang group (Figure 189),[799] extending the design of molecular tubes introduced by Glass and coworkers (see section 8.1). These protonatable, dicationic naphthotubes (**C7.3a** and **C7.3b** in Figure 189b) bind both aromatic and aliphatic carboxylates with binding affinities ranging from $10^2$ to $10^5$ $M^{-1}$ in acetate buffer (50 mM, pH 5.8). Complexation of carboxylates can be easily monitored by fluorescence spectroscopy because the fluorescence emission from the naphthotubes is quenched upon binding of the analyte. For example, **C7.3b** possessed a high binding affinity for phenylpyruvic acid ($K_a \approx 1.3 \times 10^4$ $M^{-1}$) and was successfully used for its detection at $\mu$M concentrations in acetate buffer, pH 5.8. The formation of a buried salt bridge and the contributions of cavity water release most likely explain why this chemosensor class shows these relatively high affinities and markedly exothermic binding characteristics ($\Delta H \approx -15$ to $-35$ kJ $mol^{-1}$), despite the presence of potentially competing buffer anions. In addition, the complexation of chiral carboxylates has been found to produce analyte-indicative induced circular dichroism (ICD) signals, which can be used for both analyte identification and chirality detection (determination of *ee*% values).

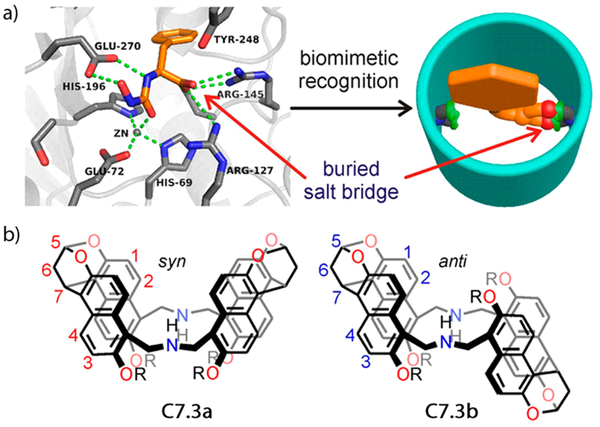

**Figure 189.** (a) Protonatable molecular tubes forming buried salt-bridges are general binders for carboxylates in aqueous buffers, providing emission quenching and induced circular dichroism signals (for chiral analytes) as optical readout. (b) Chemical structures of amine naphthotubes (**C7.3a** and **C7.3b**). Reproduced with permission from ref 799. Copyright 2020 Wiley-VCH.

Nevertheless, the direct use of the aforementioned dicationic carboxylate binders for diagnostic applications is hampered by their low binding selectivity. However, carboxylate sensing and differentiation is possible by combining multiple chemosensors through the use of chemosensor arrays and pattern recognition analysis, as it was demonstrated by the Anzenbacher Jr. group in 2013 (Figure 190).[800] In their design, calix[4]pyrroles were functionalized with different fluorophores to yield the anion-binding chemosensors (**C7.4**−**C7.11**), which typically respond with an analyte-dependent change in their emission spectrum (color) upon complex formation (Figure 190a). The characteristic fluorescence response is the result of an intramolecular partial charge transfer (IPCT) process modulated by the hydrogen bonding interaction of the anionic analyte with the protonated pyrrole moiety of the receptor and transmitted through the −CH═CH− linker to the reporter dye (Figure 190b). The authors demonstrated that this fortunate circumstance allows for distinguishing different carboxylates at micromolar concentrations in water, pH 8.5, from each another. In addition, a tripodal, turn-on fluorescent chemosensor (**C7.11** in Figure 190a) prepared from (2,4,6-triethyl-

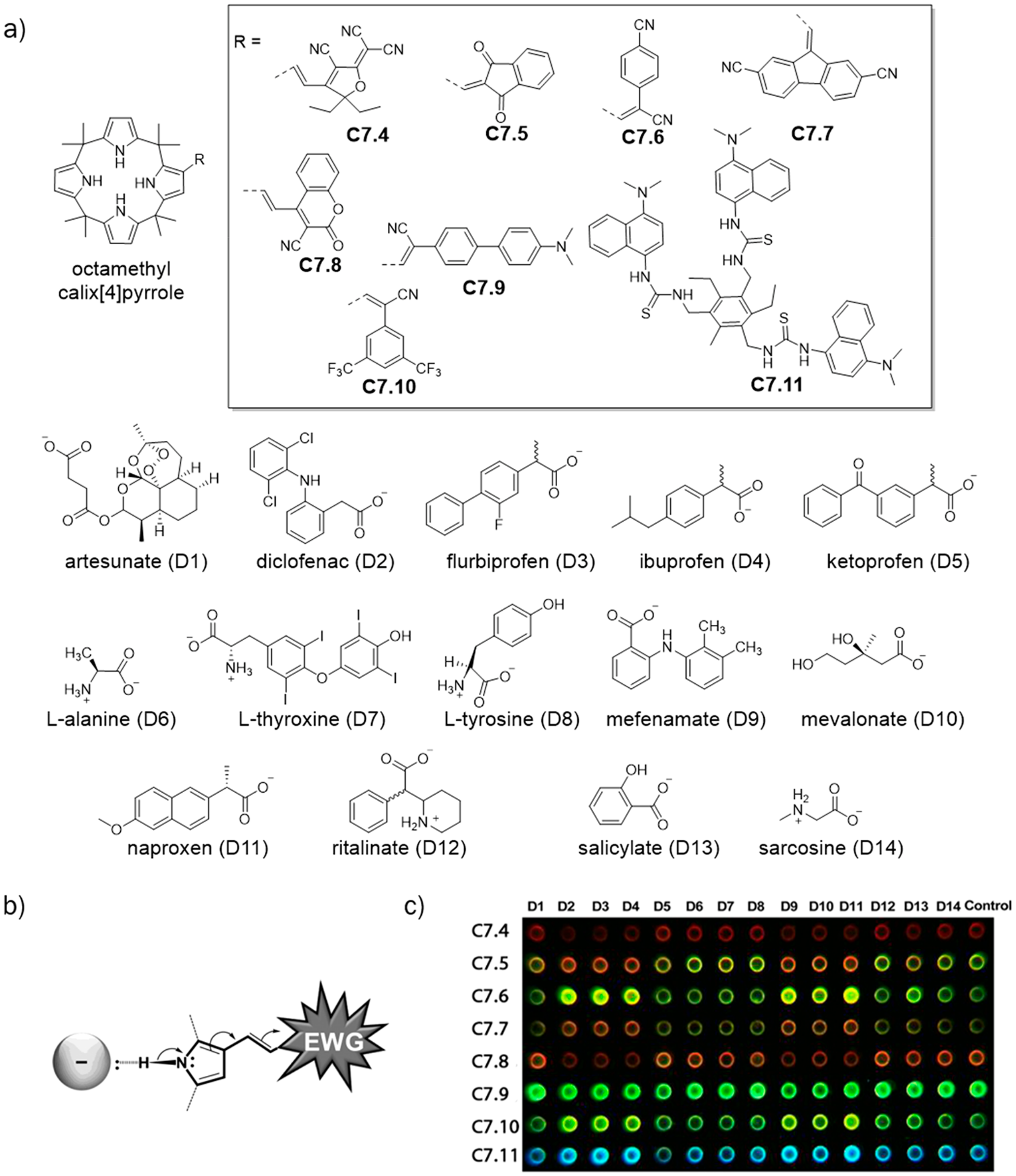

**Figure 190.** (a) Chemical structures of dye-substituted calix[4]pyrroles **C7.4**−**C7.11** which function as fluorescent chemosensors for aliphatic and aromatic carboxylates in pure aqueous media. (b) Analyte-indicative modulation of emission spectra occurs *via* intramolecular partial charge transfer (IPCT) and allows for fluorescence-based discrimination of different carboxylates from each other. (c) Fluorescence responses of the chemosensor array to the presence of carboxylates D1− D14 (1 mM in water at pH 8.5, 200 nL). Adapted with permission from ref 800. Copyright 2013 American Chemical Society.

1,3,5-trimethylamino)benzene was described for the detection of aliphatic carboxylates in the presence of other anions. However, **C7.11** also responded with an emission change to phosphate anions, which can therefore interfere with the selective detection of aliphatic carboxylates. Nevertheless, by using both colorimetric and fluorometric response of **C7.4**−**C7.11**, and by using an array-based sensing format (Figure 190c), the authors were capable to distinguish 14 different carboxylates from each other, even in the complex biofluid urine that contains several potentially interfering (inorganic) anions (Figure 190c). Small sample volumes of 200 nanoliters with typically 500 $\mu$M analyte concentration were sufficient, and even semiquantitative identification of six nonsteroidal anti-inflammatory drugs (diclofenac, flurbiprofen, ibuprofen, salicylic acid, ketoprofen, and naproxen) was possible at concentrations of 0.5−100 ppm. This example is an important proof-of-concept that array-based assays can also be developed for quantitative sensing, a task that has often proven to be a real challenge for differential sensing methods.

Recently, the Bunz group reported a fluorescence sensor array ("chemical tongue"), consisting of 11 components, for distinguishing 21 benzo- and phenylacetic acid derivatives from

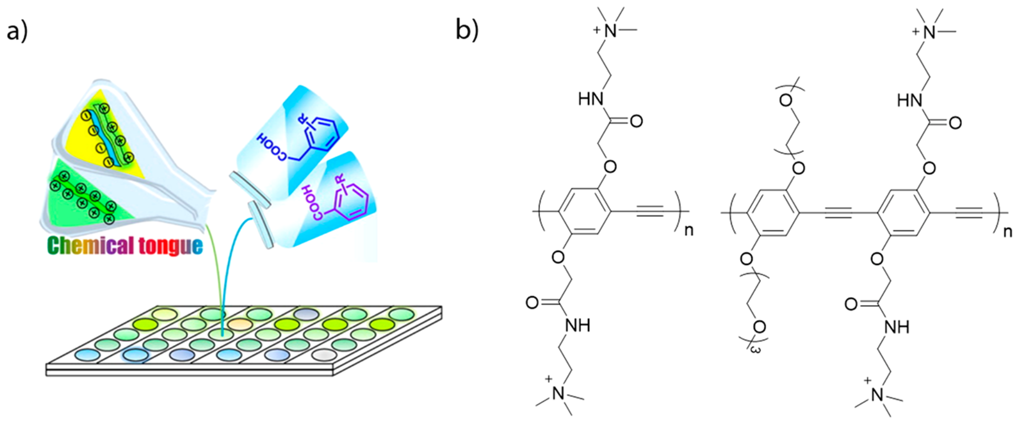

**Figure 191.** (a) Fluorescence sensor array ("chemical tongue") reported by the Bunz group. (b) Chemical structure for one type of positively charged poly($p$-arylene ethynylene)s used in this assay. Adapted with permission from ref 801. Copyright 2016 American Chemical Society.

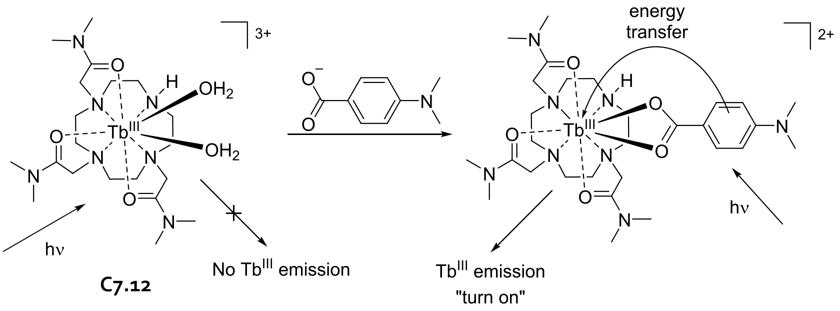

**Figure 192.** Formation of a luminescent ternary complex upon the reaction of the Tb$^{III}$-complex **C12.7** with an aromatic carboxylate that serves as an antenna ligand.

each other with high reliability (>99%) in buffered solution at pH 7.0 and pH 13.0 (Figure 191).[801] This sensor array consisted of four fluorescent poly($p$-arylene ethynylene)s (see Figure 191b for an example polymer) that produced an analyte-dependent fluorescence response in the presence of aromatic carboxylates, allowing for mM detection. Through a linear discriminant analysis (LDA), the authors were able to distinguish between hydroxy substituted, iodine- and amino-substituted benzoic acids as well as phenyl acetic acid analytes, respectively.

Alternative chemosensor designs for the detection of carboxylic acids involve the use of metal complexes that directly coordinate carboxylates. For example, Gunnlaugsson and coworkers reported the use of cyclam–Tb$^{III}$ complexes (**C7.12** in Figure 192) for fluorescence turn-on detection of aromatic carboxylates (*e.g.*, aspirin) at sub-mM concentrations in both 100 mM Tris and HEPES buffer, both enriched with 100 mM TMACl, pH 7.4.[802] Coordination of the carboxylate to the Tb$^{III}$ metal center of **C7.12** resulted in increased fluorescence intensities of the lanthanide, as coordination displaced labile water ligands in favor of analytes that can act as antenna ligands. It is noteworthy that analogue Eu$^{III}$-based chemosensors do not respond to aromatic carboxylates, probably due to their weaker affinity. We invite the reader to consult the comprehensive study published in 2002 by the Gunnlaugsson group for a more detailed description of the binding and signal transduction mechanism.[803]

Alkyne-conjugated carboxamidoquinolines (**C7.13** in Figure 193) were prepared by Qian, Zhu, and coworkers for ratiometric fluorescent detection of oxalate at $\mu$M concentrations (LOD, 3 $\mu$M) in 10 mM Tris-HCl buffer containing 10% EtOH, pH 7.0.[804] In this design, the simultaneous involvement of two strategically placed Zn$^{II}$ metal centers in the coordination of the two carboxylate moieties of the target analyte makes the probe sensitive and selective enough for oxalate sensing and imaging in living cells. **C7.13** responded with emission quenching (about 80 %) in the presence of oxalate, while for other carboxylic acids (*e.g.*, formic acid, acetic acid, malonic acid, succinic acid, adipic acid, and phthalic acid) and inorganic anions (*e.g.*, $PO_4^{3-}$, $HPO_4^{2-}$, and $H_2PO_4^{-}$), only 20% emission quenching was observed.

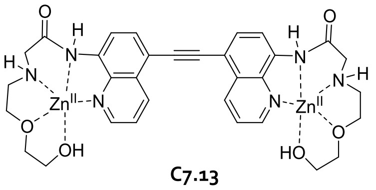

**C7.13**

**Figure 193.** Chemical structure of the alkyne-conjugated carboxamidoquinoline chemosensor (**C7.13**) used for the detection of oxalate in Tris buffer at $\mu$M concentrations.

Selective sensing is an important practical hurdle also for the design of metal-based carboxylate chemosensors. Khajehsharifi and coworkers reported the preparation of an array-based indicator displacement assay (**C7.14** in Figure 194) that allowed for the discrimination of 11 biologically relevant carboxylates from each other.[805] The assay involves chromophoric metal–ligand complexes that spontaneously formed from the pairwise combination of four metal cations ($Cu^{2+}$, $Fe^{2+}$, $Fe^{3+}$, and $V^{4+}$) and two metal-coordinating indicator dyes (pyrocatechol violet and eriochrome cyanine R). The final

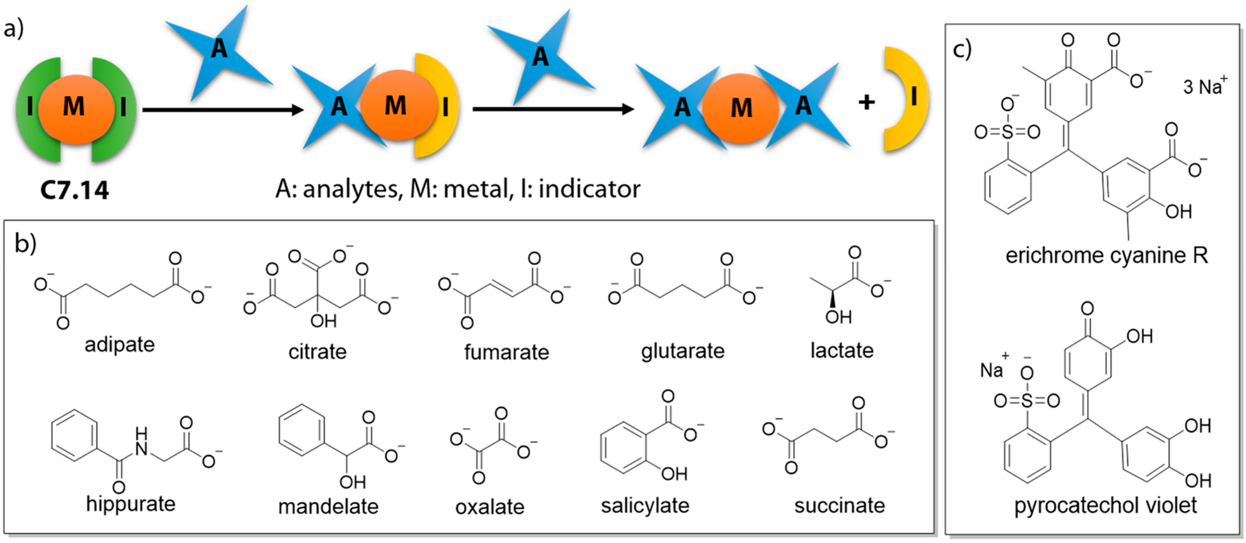

**Figure 194.** (a) A metal-complex based indicator displacement assay (**C7.14**) for the array-based sensing of 11 biologically relevant carboxylates, which are shown in (b), in borate buffer and in human urine. Indicator dyes are shown in (c). Adapted with permission from ref 805. Copyright 2017 Elsevier BV.

assay was operational in the submillimolar concentration range in borate buffer, pH 7.0. To evaluate its potential as a sensor component for the detection of biologically relevant samples, carboxylic acids were analyzed in analyte-spiked human urine samples and 100% classification accuracy was reported.

### 7.3. Nanosensors for Carboxylates

Similar to the current situation for chemosensors and probes, carboxylate-sensing nanoparticle systems are also comparably rare. All nanosensors discussed within this section are summarized in Table 26.

Ahn and coworkers reported *o*-(trifluoroacetyl)carboxanilide (TFACA) functionalized gold nanoparticles (**N7.1** in Figure 195) for the colorimetric detection of *trans*-fumarate and discrimination from *cis*-isomer in water at mM concentrations (pH 7.8).[806] Because of the strong electron withdrawing effect exerted by the F atoms at the carbonyl group of TFACA, carboxylates can act as nucleophiles to form covalent adducts that lead to particle crosslinking and aggregation, which can be detected colorimetrically due to plasmon resonance effects.[807] The selectivity for *trans*-fumarate can be understood as follows: First, monocarboxylated analytes cannot bridge between different particles, and second, dicarboxylates such as *cis*-fumarate do not cause particle aggregation because their involvement in bridging between particles is geometrically unfavorable. It remains to be seen whether this design strategy can be applied to *trans*-fumarate sensing in biofluids and other complex mixtures. For instance, omnipresent monocarboxylates may block the TFACA probe moiety and thus prevent the desired aggregation reaction otherwise induced by the target analyte.

A different strategy to detect enantiomers of mandelic acid at $\mu$M concentrations using L-tartrate functionalized gold nanoparticles was recently reported by Li and coworkers (**N7.2** in Figure 196).[808] Here, the selective detection of L-mandelic acid versus D-mandelic acid in Britton−Robinson buffer (40 mM $H_3PO_4$, 40 mM $H_3BO_3$, 40 mM acetic acid, pH 4.0) was possible because **N7.2** aggregated only in the presence of the L-enantiomer, causing a color change from red to blue. In this scenario, crosslinking of the nanoparticles by L-mandelic acid

**Table 26. Summary of Nanosensors for Carboxylates (LOD, Limit of Detection)**

| nanosensor | media | concentration range | ref |
|---|---|---|---|
| | Acetate Analyte | | |
| **N7.5** | 500 mM Tris-HCl buffer, pH 8.0 | 0−100 mM | 812 |
| | Ascorbate Analyte | | |
| **N7.6** | 20 mM HEPES, 20 mM PBS, and 20 mM MES buffer, pH 7.4−8.3 | 0−100 $\mu$M in buffer | 815 |
| | cell lysates | LOD, 590 nM in buffer | |
| | *in vivo* imaging in mice | LOD, 2.2 $\mu$M in cell lysates | |
| **N7.7** | Briton−Robinson buffer, pH 7.0 | 2.0−12 $\mu$M;<br>LOD, 92 nM | 816 |
| **N7.8** | 10 mM PBS, pH 5.0 | 0.2−11 $\mu$M in buffer;<br>LOD, 82 nM in buffer | 817 |
| | urine samples and in cells | 0.4−5 $\mu$M in urine | |
| | Benzoate Analyte | | |
| **N7.5** | 500 mM Tris-HCl buffer, pH 8.0 | 5.0−100 mM | 812 |
| | *trans*-Fumarate Analyte | | |
| **N7.1** | water, pH 7.8 | 0.5−4.0 mM | 806 |
| | Hexanoate Analyte | | |
| **N7.4** | 1 mM HEPES buffer, pH 7.0 | mM range | 810 |
| | D-Mandelate Analyte | | |
| **N7.3** | 20% MeOH in water containing 100 $\mu$M $ZnCl_2$, pH 9.0 | 0.1−1.2 mM | 809 |
| | L-Mandelate Analyte | | |
| **N7.2** | Briton−Robinson buffer, pH 4.0 | 0−100 $\mu$M | 808 |
| | L-Malate Analyte | | |
| **N7.3** | 20% MeOH in water containing 100 $\mu$M $ZnCl_2$, pH 9.0 | 0.1−1.2 mM | 809 |
| | L-Phenylacetate Analyte | | |
| **N7.3** | 20% MeOH in water containing 100 $\mu$M $ZnCl_2$, pH 9.0 | 0.1−1.2 mM | 809 |
| | Tartrate Analyte | | |
| **N7.3** | 20% MeOH in water containing 100 $\mu$M $ZnCl_2$, pH 9.0 | 0.1−1.2 mM | 809 |
| **N7.5** | 500 mM Tris-HCl buffer, pH 8.0 | 0−100 mM | 812 |

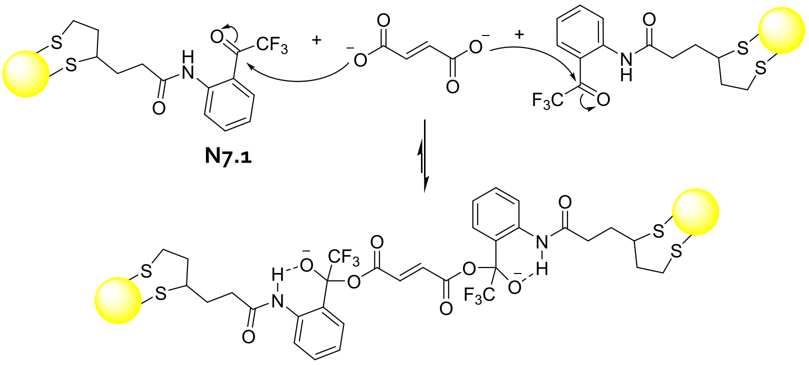

**Figure 195.** Schematic representation of *o*-(trifluoroacetyl)carboxanilide functionalized gold nanoparticles (**N7.1**) for colorimetric millimolar detection of *trans*-fumarate in water. *trans*-Fumarate reacts with *o*-(trifluoroacetyl)carboxanilide to form covalent adducts that assist to particle crosslinking and aggregation.

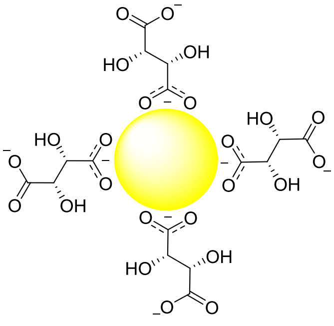

**N7.2**

**Figure 196.** Schematic representation of L-tartaric acid functionalized gold nanoparticles **N7.2** used for colorimetric and enantioselective micromolar detection of D-mandelic acid in Britton−Robinson buffer.

was proposed to occur *via* enantiospecific H-bonding interactions with nanoparticle-bound tartrates. The chiral selectivity of the nanosensor was tested with mixtures of D- and L-mandelic acid, and the colorimetric response was linearly related to the enantiomeric excess (*ee*) of L-mandelic acid, with a linear range from −100% to 100%, consistent with the HPLC results. Potential cross-reactivities were not reported such that the utility of **N7.2** for practical sensing applications remains to be explored.

An enantioselective and colorimetric nanosensor that can be used for the quantification and determination of the enantiomeric excess (*ee*) of chiral carboxylic acids (CCAs) at $\mu$M concentrations was reported by Wei and coworkers (**N7.3** in Figure 197).[809] In the presence of $Zn^{2+}$ salts, a positively charged complex is formed on the surface of the particles that acts as chiral selector for CCAs in water containing 20% MeOH and 100 $\mu$M $ZnCl_2$, pH 9.0. For example, the binding constants ($K_a$) for the positively charged $Zn^{II}$ complex and D-/L-mandelic acid enantiomers were determined to be $5.2 \times 10^7$ and $1.2 \times 10^7$ $M^{-1}$, respectively. The different binding affinities were explained by the occurrence of transient diastereomeric interactions between the chiral $Zn^{II}$ complex and CCAs, with only one enantiomeric species binding strongly to **N7.3**. The addition of D-mandelic acid reduced the positive surface charge of **N7.3** and thus triggered particle aggregation which was evident from the distinct color change of the particle dispersion.

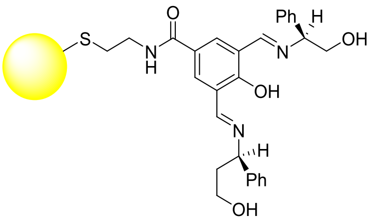

**N7.3**

**Figure 197.** Schematic representation of nanosensor **N7.3** that consist of gold nanoparticles functionalized with chiral diimine complexes. **N7.3** can be used for the enantioselective detection of chiral carboxylic acids at $\mu$M and mM concentrations in water containing 20% MeOH and 100 $\mu$M $ZnCl_2$, pH 9.0.

Martínez-Máñez, Sancenón, and coworkers prepared silica particles that have been functionalized with both chromogenic 3′,3′-dimethyl-6-nitrospiro[2*H*-1]benzopyran-2,2′-indoline (spirobenzopyran) and thiourea units (**N7.4** in Figure 198) and that were applicable for the detection of aliphatic carboxylic acids at mM concentrations in 1 mM HEPES buffer, pH 7.0.[810] Thioureas are known to be excellent

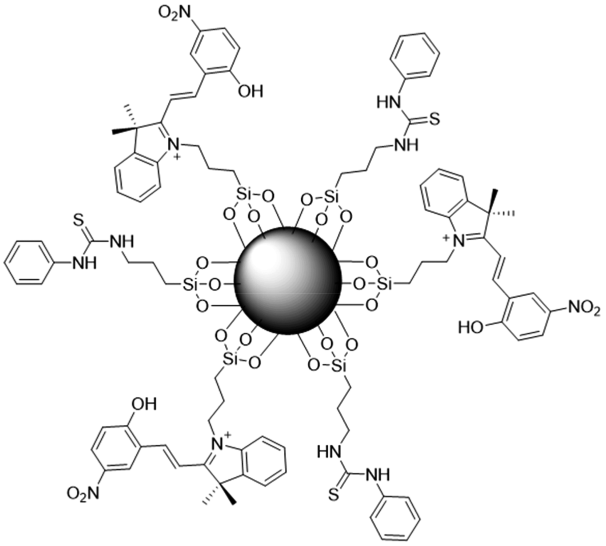

**N7.4**

**Figure 198.** Schematic representation of spirobenzopyran and thiourea functionalized silica nanoparticles (**N7.4**) that can be used for the millimolar detection of aliphatic carboxylic acids in HEPES buffer.

hydrogen bond donors, forming strong interactions with hydrogen bond acceptors, such as carboxylates.[811] Signal transduction upon analyte binding was achieved by the spirobenzopyran moiety acting as a polarity-sensitive photochromic moiety because its open and polar (merocyanine) state is destabilized upon binding of aliphatic carboxylic acids (*e.g.*, dodecanoate and hexanoate) to **N7.4**. As such, a less polar spirocyclic state is adapted in the presence of the target analyte, which can be readily monitored *via* UV−vis spectroscopy and correlated to the amount of carboxylic acids adsorbed on the surface of **N7.4**.

Morey and coworkers described a nanoparticle-based indicator displacement assay (IDA) for the mM detection of mono- and dicarboxylates (*e.g.*, acetate, tartrate, and benzoate) in 500 mM Tris-HCl buffer, pH 8.0.[812] The authors used squaramide-functionalized and oleic acid capped magnetic $Fe_2O_3$ nanoparticles, which hosted fluorescein as indicator dye (**N7.5** in Figure 199). Squaramides are one of the strongest hydrogen-bonding donors known and are therefore attractive as binding motifs for carboxylates.[813,814] Fluorescein, which has a carboxylate moiety, binds to the squaramide nanoparticle conjugate whereby its emission is quenched by energy transfer processes. When mono- or dicarboxylates were added to aqueous dispersions of **N7.5**, the indicator dye was displaced due to competitive hydrogen-bonding interaction of the analyte with squaramides. After magnetic separation of the particles, the amount of carboxylic acid can then be determined indirectly by measuring the fluorescence intensity of the remaining "free" indicator in the supernatant. Interestingly, tricarboxylic acids such as citrate or cyclohexane-tricarboxylate and other inorganic anions (*e.g.*, $Cl^-$, $Br^-$, $NO_3^-$, $PO_4^{3-}$, and $SO_4^{2-}$) did not provide a signal response. It has been reasoned that the selectivity of **N7.5** towards mono- and dicarboxylates is due to the higher probability of finding one or two rather than three squaramide residues with suitable binding conformations, causing inefficient binding of tricarboxylates.

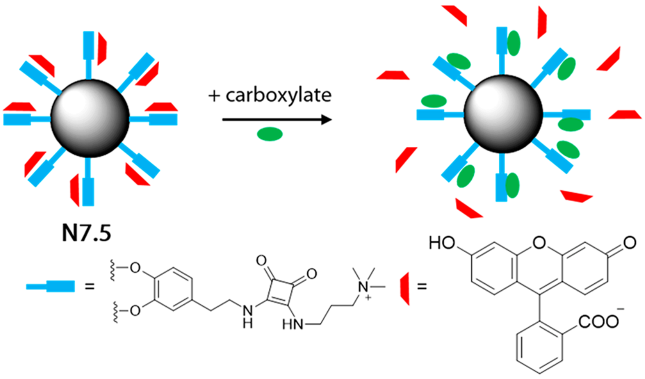

**Figure 199.** Schematic representation of squaramide functionalized iron oxide nanoparticles **N7.5** used for IDA-based detection of mono- and dicarboxylates in the mM concentration range in Tris-HCl buffer.

Similar to the probe examples presented in section 7.1, ascorbic acid can be readily detected with nanosensors by exploiting its redox properties. Tang and coworkers reported a selective nanosensor for the detection and imaging of ascorbic acid at $\mu$M concentrations in different buffer solutions, *i.e.*, 20 mM HEPES buffer, 20 mM PBS, and 20 mM MES buffer in a pH range of 7.4−8.3, cell lysates and in mice (**N7.6** in Figure 200).[815] The sensing system was prepared from persistent luminescence nanoparticles (PLNPs) composed of $Sr_2MgSi_2O_7$ : 1% $Eu^{3+}$, 2 % $Dy^{3+}$, and cobalt oxyhydroxide nanoflakes ($Co^{III}OOH$). The nanoflakes served as fluorescence quencher that engage in Förster resonance energy transfer (FRET) processes with the PLNPs. However, in solutions that contain ascorbic acid, $Co^{3+}$ cations are reduced to $Co^{2+}$, leading to nanoflake dissolution and subsequent increase emission intensity of the persistent luminescence nanoparticles (PLNPs). Fortunately, **N7.6** is not affected by other potentially interfering species (*e.g.*, $Al^{3+}$, $Mg^{2+}$, $Na^+$, $Zn^{2+}$, $Cu^{2+}$, $K^+$, $Ca^{2+}$, $Cd^{2+}$, $Co^{2+}$, NaClO, $H_2O_2$, *t*-BuOOH, hydroquinone, GSH, L-Cys, Tyr, L-Arg, Lys, Gly, Hcys, Trp, $NaHSO_3$, $NaH_2PO_2$, $H_2C_2O_4$, $NaNO_2$, and $Na_2S_2O_3$). Interestingly, the detection of ascorbic acid in cells and *in vivo* was achieved without continuous external light excitation as PLNPs have a persistent luminescence that, in principle, allows for the removal of autofluorescence and scattering of light from biological samples arising from external light excitation.

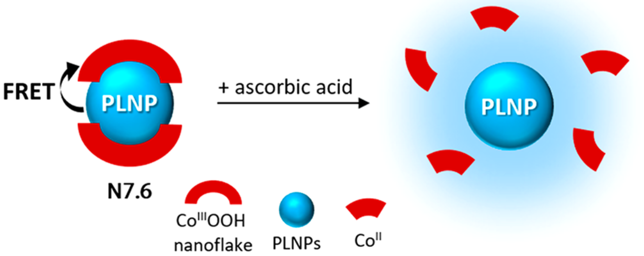

**Figure 200.** Schematic representation of persistent luminescence nanoparticles (PLNPs) that can be used in combination with fluorescence quenching oxyhydroxide nanoflakes **N7.6** for $\mu$M detection of ascorbic acid in various buffer solutions, cells, and in mice.

$Fe^{3+}$-doped carbon nanocages (CNCs, **N7.7** in Figure 201) were prepared and used as a fluorescent turn-on nanosensor for $\mu$M detections of ascorbic acid in Britton−Robinson buffer (40 mM $H_3BO_3$, 40 mM $H_3PO_4$, 40 mM AcOH, 200 mM NaOH, pH 7.0) by Zhu, Tan, and coworkers.[816] The fluorescence of CNCs was initially quenched due the participation of $Fe^{3+}$ anions in energy transfer processes. In the presence of ascorbic acid, the fluorescence intensity then increased sharply as $Fe^{3+}$ is reduced to its nonquenching $Fe^{2+}$ oxidation state. A detection range for ascorbic acid from 2 to 12 $\mu$M was stated for **N7.7** by the authors. Moreover, the nanosensor was successfully used for quantitative detection ($\mu$M range) of ascorbic acid in vitamin C tablets with minimal interference from matrix components. However, it was found that metal cations such as $Cd^{2+}$, $Hg^{2+}$, $Zn^{2+}$, $Mn^{2+}$, $Cu^{2+}$, $Mg^{2+}$,

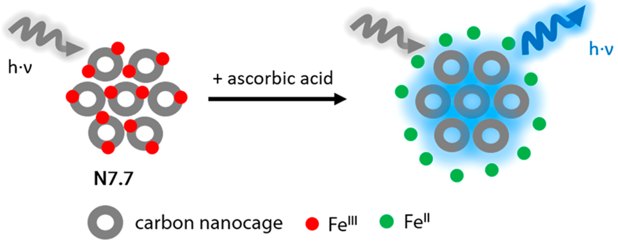

**Figure 201.** Schematic representation of $Fe^{III}$-doped carbon nanocages (**N7.7**) for fluorescence-based detection of ascorbic acid in Britton−Robinson buffer at $\mu$M concentrations.

$Co^{2+}$, and $Fe^{2+}$ can adversely affect the performance of **N7.7** as they induce moderate fluorescence quenching.

A recent nanosensor for ascorbate (**N7.8** in Figure 202) reported by Shamsipur and coworkers exploits green emitting carbon dots for the mM detection of ascorbic acid in 10 mM PBS, pH 5.0, urine samples, and in cells.[817] In this design, the emission from the nanoparticles was first quenched by doping the emissive carbon dots material with $Fe^{3+}$ ions. When $Fe^{3+}$ was subsequently reduced to $Fe^{2+}$ by the target analyte ascorbate, an increased fluorescence of **N7.8** was recorded and correlated to the concentration of the targeted analyte over a linear range from 0.2 to 11.0 μM. The authors showed that other cations such as $Na^{+}$, $Ca^{2+}$, $Ba^{2+}$, $Cu^{2+}$, $Fe^{2+}$, $Hg^{2+}$, $Zn^{2+}$, $Co^{2+}$, $Mn^{2+}$, $Ce^{3+}$, $Al^{3+}$, and $Cr^{3+}$ did not affect the performance of **N7.8**, showcasing its robustness against potential interferents.

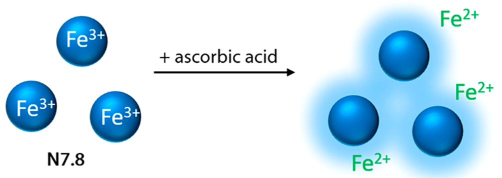

**Figure 202.** Schematic representation of the use of green emissive carbon dots (**N7.8**) for fluorescence turn-on detection of ascorbic acid in PBS, urine samples, and in cells at μM concentrations.

Carboxylates are one of the most challenging target analytes for probes, chemosensors, and nanosensors. While the detection of ascorbate (due to its redox properties) and of some chelating carboxylic acids (*e.g.*, tartrate) can be performed with good selectivity and sensitivity in aqueous media, much more advances are needed to arrive at a molecular toolbox for carboxylate recognition in biofluids. This undertaking is particularly worthwhile because many of the biorelevant metabolites present in biofluids (*e.g.*, in urine, see Figure 4 in the introduction section and Table 27 for a list of typical carboxylate concentrations in biofluids) have at least one carboxyl functionality. Improved options for carboxylate recognition may become then of great diagnostic utility, *e.g.*, for the monitoring of betaines, carnitines, short chain fatty acids, and other metabolites as indicators for cardiovascular and other diseases.[818−821]

**Table 27. Summary of the Normal Concentration of Carboxylates in Biofluids**[a]

| concentration range | media | ref |
|---|---|---|
| Ascorbate Analyte | | |
| 8.00−32.0 μM | urine | 822 |
| 4.60−78.0 μmol/mmol creatinine = 46.0−780 μM | blood | 50 |
| 590−784 nM | saliva | 823 |
| Citrate Analyte | | |
| 30.0−400 μM | urine | 824 |
| 1.82−3.62 μmol/mmol creatinine = 1.8−3.6 mM | blood | 341 |
| 18.5−38.5 μM | saliva | 62 |
| Fumarate Analyte | | |
| 0−4.0 μM | urine | 824 |
| 0.80−1.80 μmol/mmol creatinine = 8.0−18.0 μM | blood | 336 |
| 1.3−2.7 μM | saliva | 62 |
| Gluconate Analyte | | |
| 2.8−3.8 μM | | 825 |
| 8.20−26.4 μmol/mmol creatinine = 82.0−264 μM | blood | 50 |
| 21.3−69.5 μM | saliva | 62 |
| Glutarate Analyte | | |
| 0.0−1.8 μM | urine | 824 |
| 0.6−2.6 μmol/mmol creatinine = 6.0−20 μM | blood | 826 |
| 0.0−1.9 μM | saliva | 335 |
| Hippurate Analyte | | |
| 5.50−27.9 μM | urine | 827 |
| 28.0−610 μmol/mmol creatinine = 280−6100 μM | blood | 50 |
| L-Lactate Analyte | | |
| 1.4−4.6 mM | urine | 828 |
| 13.0−46.0 μmol/mmol creatinine = 130−460 μM | blood | 826 |
| 0−625 μM | saliva | 335 |
| L-Malate Analyte | | |
| 0.0−21.0 μM | urine | 824 |
| 0.7−5.3 μmol/mmol creatinine = 7.0−53 μM | blood | 826 |
| 1.7−8.7 μM | saliva | 335 |
| Malonate Analyte | | |
| 14.4−15.6 μM | urine | 829 |
| 1.2−3.1 μmol/mmol creatinine = 12−31 μM | blood | 50 |
| 0.5−1.1 μM | saliva | 335 |
| Oxalate Analyte | | |
| 2.2−4.4 μM | urine | 333 |
| 3.90−14.0 μmol/mmol creatinine = 39.0−140 μM | blood | 50 |
| Phenylacetate Analyte | | |
| 41−53 μM | urine | 830 |
| 3.3−5.1 μmol/mmol creatinine = 33−51 μM | blood | 831 |
| 47 ± 31 μM | saliva | 62 |
| Phenylpyruvate Analyte | | |
| 400−600 nM | urine | 832 |
| 50.0−670 nmol/mmol creatinine = 0.50−6.70 μM | blood | 833 |
| Succinate Analyte | | |
| 0−1 μM | urine | 834 |
| 1.1−14.5 μmol/mmol creatinine = 11−145 μM | blood | 50 |
| 2−112 μM | saliva | 338 |
| Tartrate Analyte | | |
| 1.3−46.0 μmol/mmol creatinine = 13−460 μM | urine | 826 |

[a]Urinary analyte concentrations were converted assuming a representative creatinine level of 10 mmol/L.

## 8. LIPIDS AND STEROIDS

Lipids are a broad class of amphiphilic molecules and include a variety of compounds such as fatty acids, glycerolipids, glycerophospholipids, sphingolipids, and sterols.[835] More than 850 lipids, a stunningly high number, have been identified in the human urine metabolome by instrument-based analytical methods (HPLC, MS, NMR), making it the largest class of biorelevant compounds found in this biofluid.[50,836] While most lipids only occur in trace levels, it is well accepted in the medical literature that lipids (and lipid droplets found in eukaryotic cells) are useful indicators for diseases such as tumors, inflammations, and cardiovascular diseases.[837−845] Fatty acids are a broader group of molecules that belong to the class of lipids and consist of a polar carboxyl head group linked to a saturated or unsaturated hydrophobic hydrocarbon residue. Fatty acids are an important component of a variety of cellular functions, *e.g.*, as energy substrates, components of cell structure, and signaling molecules.[846] Increased fatty acid levels in plasma, mainly due to a high-fat diet, have been confirmed to contribute to the development of several diseases such as type 2 diabetes.[847,848] Glycerophospholipids are derivatives of glycerophosphoric acid that contain at least one *O*-acyl, *O*-alkyl, or *O*-alk-1′-enyl residue attached to the glycerol

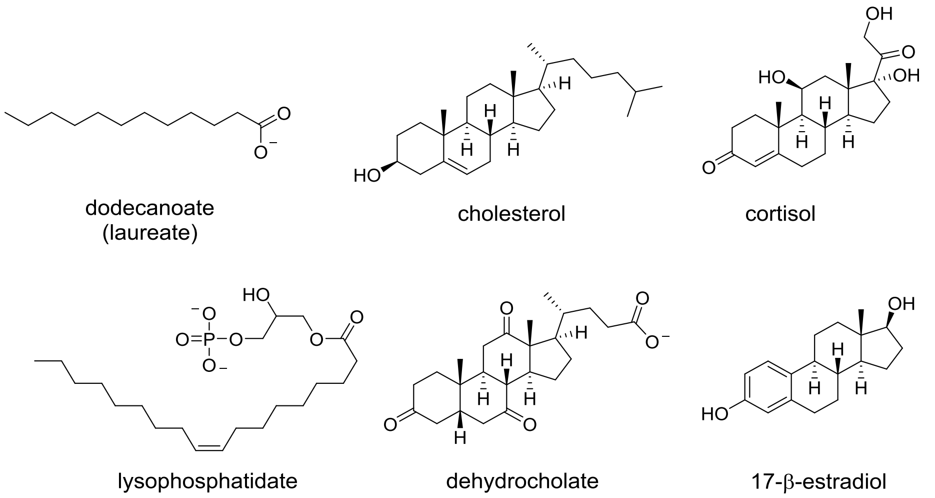

**Figure 203.** Chemical structures of representative lipids and steroids.

moiety.[849] Together with sphingolipids, a class of lipids whose backbone consists of aliphatic amino alcohols that include sphingosine, glycerophospholipids are the major structural components of cell membranes.[850−852] However, both are known to have biological activities far beyond simple structural components of single cells and are direct or precursors of signaling molecules that mediate responses to physiological signals.[853−855] Apart from this, the brain is extremely enriched with lipids, and alteration of their metabolism has been associated with many brain diseases, including neurodegenerative diseases, neurological diseases, and neuropsychiatric diseases.[856,857] Unlike phospholipids and fatty acids, steroids have a fused ring structure, and although they are not structurally closely related to other lipids, they are sometimes grouped with them because of their hydrophobic and sometimes amphiphilic character. The steroids progesterone, testosterone, and cortisone play a critical role in regulating many life processes by acting as signaling molecules in living organisms,[858] regulating vital processes such as reproduction, inflammatory responses, and gene expression.[859−861] For example, cholesterol plays a critical role in regulating inflammasome activation, and elevated cholesterol is considered an important trigger for cardiovascular disease.[862,863] Sustained stress can lead to the increase of cortisol excretion in the body, resulting in the suppression of the immune system, modulation of metabolic processes, *e.g.*, increased fatty acid and blood sugar levels, and affects the memory capacity.[864,865] In addition, steroids also play an important clinical role due to their potent anti-inflammatory and immunomodulatory properties. For example, glucocorticoids are commonly used to treat patients with rheumatoid arthritis, chronic obstructive pulmonary disease, systemic lupus erythematosus, inflammatory bowel disease, and asthma.[866,867] Steroid-mediated signaling events in living organisms involve their dynamic concentration fluctuation, typically in nM concentrations, over time. Thus, temporal information about steroid composition in biological samples is important when it comes to the diagnosis of diseases,[868,869] psychological disorders,[870,871] or the characterization of complex physiological responses such as stress.[872] Currently, standard analysis methods for steroids in biofluids are performed by using immunoassays.[873] Given the large number of lipids and their biological functions that we cannot cover herein, we instead refer interested readers to other recently published reviews on this topic.[874−877] The development of new, simple, and cost-efficient assays for the detection and imaging of lipids and steroids in biological fluids, or ideally directly *in vivo*, remains challenging and is therefore of great interest. Similar to lipids, the design of chemically reactive probes for steroidal compounds is hampered by the absence of readily targetable functional groups and their poor solubility in aqueous solutions (see Figure 203). The molecular probes, chemosensors, and nanosensors discussed within this section are summarized in Tables 28 and 29, respectively.

**Table 28. Summary of Molecular Probes and Chemosensors for Lipids**

| probe/ chemosensor | media | concentration range | ref |
|---|---|---|---|
| Dodecanoate Analyte | | | |
| **C8.2**[a] | 20 mM HPEPES, pH 8.4 | mM range | 883 |
| Lysophosphatidate Analyte | | | |
| **C8.1** | 10 mM HEPES buffer, pH 7.4 | 0−3 μM | 882 |
| Lipid Drops (LDs) Analyte | | | |
| **P8.1−P8.16**[b] | cell imaging; mice (healthy and tumor cells) | | 894898−910,912 |

[a] Other lipids are also bound, but with lower binding affinity. [b] Environmentally sensitive fluorescent probes.[894,898899−910,912]

**Table 29. Summary of Nanosensors for Steroids**

| nanosensor | media | concentration range | ref |
|---|---|---|---|
| Cholesterol Analyte | | | |
| **N8.2** | 10 mM Tris buffer, 107 mM NaCl, pH 7.4; egg yolk; human serum samples | low μM range | 916 |
| Dehydrocholinate Analyte | | | |
| **N8.1** | 5% MeOH in 10 mM Tris-HCl buffer, pH 8.0 | 1−2 mM (linear range) | 915 |
| Progesterone Analyte | | | |
| **N8.3** | 2% DMSO in 1× PBS; *in vivo* | 5−100 μM; μM range | 921 |

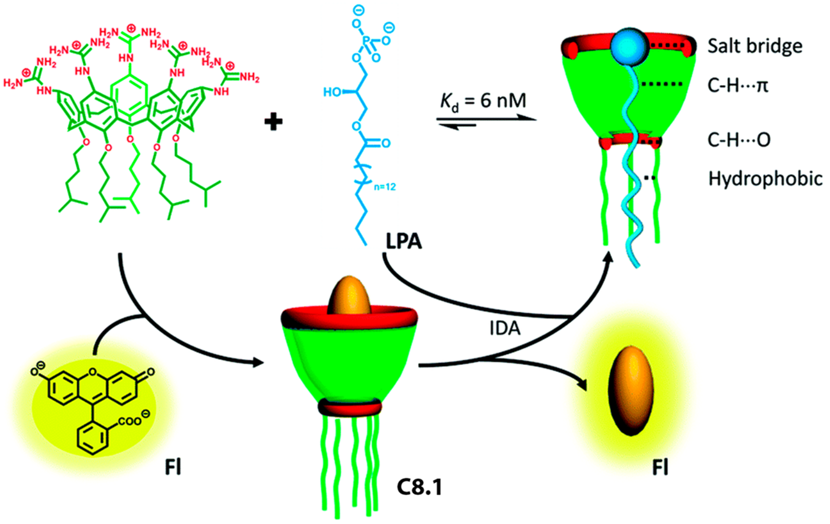

**Figure 204.** Schematic representation of the binding between the lipid lysophosphatidic acid (LPA) and a guanidinium-modified calix[5]arene (**C8.1**). Fluorescence turn-on sensing of LPA by **C8.1** is achieved with an IDA format using fluorescein as a reporter dye. Reproduced with permission from ref 882. Copyright 2018 The Royal Society of Chemistry.

## 8.1. Chemosensors and Molecular Probes for Lipids

Being hydrophobic and shape rigid, steroids are in principle excellent target analytes for macrocyclic hosts with a hydrophobic cavity. For instance, cucurbit[8]uril (CB8) was reported by Biedermann, Nau, and coworkers to be a general steroid binder with micro- to nanomolar affinities in aqueous media ($K_a \sim 10^6$ $M^{-1}$ for CB8−steroid complexes in water).[878] While this affinity is still orders of magnitude lower than that of antibodies and natural steroid receptor proteins, it is much stronger than for any other synthetic host or the carrier protein serum albumin. The smaller host homologue CB7 preferentially binds the small steroid 19-nortestosterone (also known as nandrolone), whereas larger analytes such as testosterone bind (much) more weakly to CB7. The authors showed that both CB7 and CB8 can be used as low-cost and biocompatible excipients to largely increase the solubility of steroidal substances, *e.g.*, drugs.[879] To obtain a quantifiable spectroscopic response for potential sensing applications, CB7 or CB8 can be considered with suitable indicator dyes to furbish an IDA or GDA format,[48,880] and the assay can be extended to an array-based sensing format. It has been shown that in special cases when using chromophoric hosts, such as acyclic cucurbit[*n*]urils, some of the steroids can be directly distinguished from each other by emerging spectroscopic fingerprints, *e.g.*, CD signals (see section 2.3, **C2.8** in Figure 50).[246] While the $\mu$M detection limit of CB*n*-based IDA assays for steroid sensing is in a diagnostically irrelevant range (pM to nM required), such supramolecular chemosensor assays can find direct practical use, for instance for label-free enzymatic reaction monitoring of steroidal drug interconversion in real time.[878] In another example, Hennig and coworkers demonstrated that CB8-based IDA assays can be used to monitor the depletion of steroids in bacterial cultures.[881] In this review, the focus is restricted to assays where steroids are detected *via* supramolecular interactions beyond the use of steroid recognition units of biological origins.

An important step forward for lipid sensing in blood was recently made by the Guo group that developed a guanidinium-modified calix[5]arene-based chemosensor (**C8.1** in Figure 204) for the detection of lysophosphatidic acid (LPA) at micromolar concentrations.[882] LPA is a biomarker for early diagnosis of ovarian and other gynecologic cancers and occurs for healthy individuals in a concentration range of 0.1−6.3 $\mu$M, whereas largely elevated levels (<60 $\mu$M) are found for patients suffering from these types of cancer. The target analyte is complexed by the positively charged host **C8.1** through a combination of salt bridges, C−H···$\pi$ contacts, C−H···O contacts, and the hydrophobic effect with an affinity of $K_a = 1.6 \times 10^8$ $M^{-1}$ in 10 mM HEPES buffer, pH 7.4. This binding affinity was high enough to set up a sensitive emission turn-on IDA for LPA by using fluorescein as a reporter dye ($K_a = 5.0 \times 10^6$ $M^{-1}$ for the host). Remarkably, only ATP turned out to be an even stronger competitor for the host than LPA, but all other potential binders tested, mostly organic anions, *e.g.*, other nucleoside mono- and triphosphates or aspartic acid, are much weaker binders than LPA. The authors further demonstrated that the interference of ATP can be resolved with differential sensing routines, and they successfully set up a calibration curve for the target analyte LPA in the diagnostically relevant concentration range.

Other (deep cavity) cavitands and molecular capsules[884,885] are promising host molecules for the binding of lipid acids. Nearly two decades ago, the Glass group had introduced fluorescent molecular tubes that showed respectable binding affinities to fatty acids in aqueous media, *e.g.*, $K_a = 2.7 \times 10^4$ $M^{-1}$ for dodecanoic acid in 20 mM HEPES buffer, pH 8.4 (**C8.2** in Figure 205).[883,886] The molecular tubes respond to

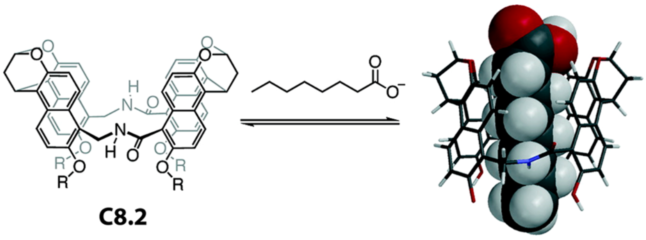

**Figure 205.** Chemical structure of a molecular tube (**C8.2**) and its binding geometry with a fatty acid. Reproduced with permission from the ref 883. Copyright 2004 American Chemical Society.

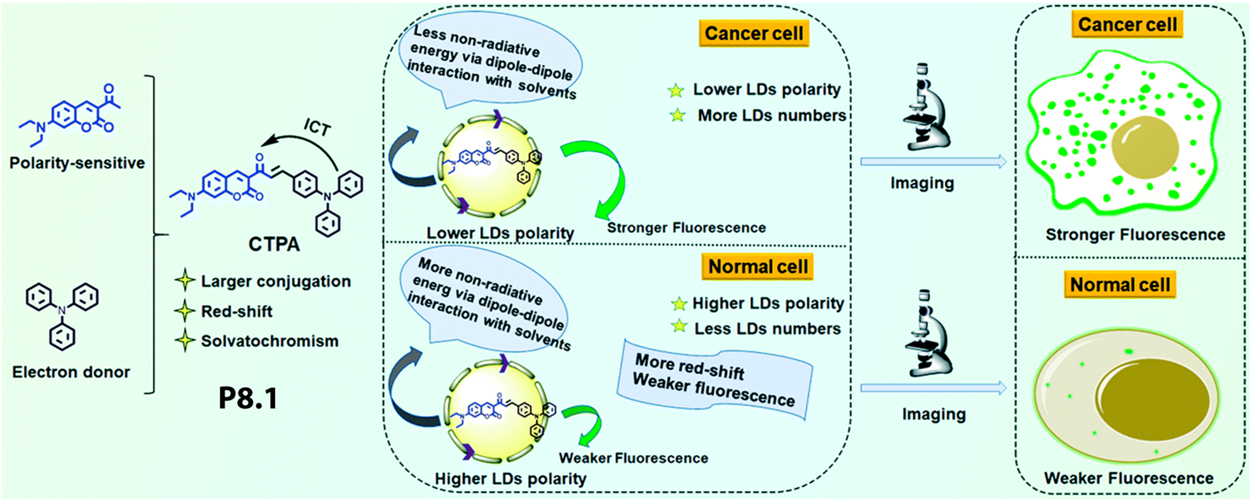

**Figure 206.** Design and use of a polarity-sensitive probe **P8.1** for lipid droplet imaging to differentiate normal from cancer cells. Reproduced with permission from the ref 894. Copyright 2018 The Royal Society of Chemistry.

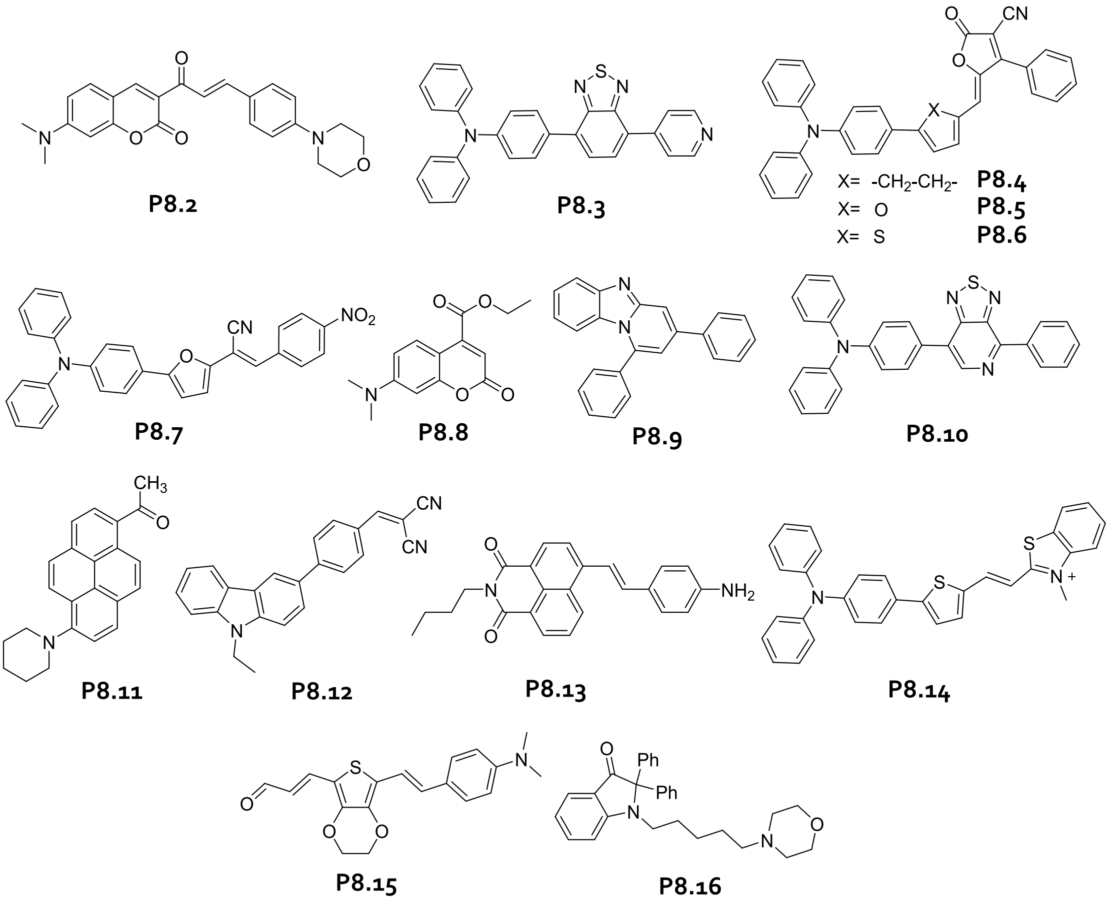

**Figure 207.** Chemical structures of probes **P8.2–P8.16** used for lipid droplet-based sensing.

guest binding with emission quenching, which in principle allows for the construction of an emission-based assay for guest detection in the millimolar concentration range. However, these hosts also strongly bind to other guests such as heptylamine ($K_a$ = 1.6 × $10^4$ $M^{-1}$),[883,886,887] and possibly many other metabolites, which likely limits their direct applicability for molecular diagnostics. Recently, the fluorescent molecular tubes experience a revival due to the contributions of the Jiang group.[888−893]

It has been experimentally confirmed, mainly by NMR, that lipid binding can also occur for molecular capsules and deep cavitands based on the resorcinarene scaffold.[885] However, because of the lack of an inherent optical response (*e.g.*, these macrocyclic phenol-type hosts are usually not emissive), one has to set up an indicator displacement assay analogous to the aforementioned report by the Guo group for the detection of lipids. The interested reader is referred to the cited review

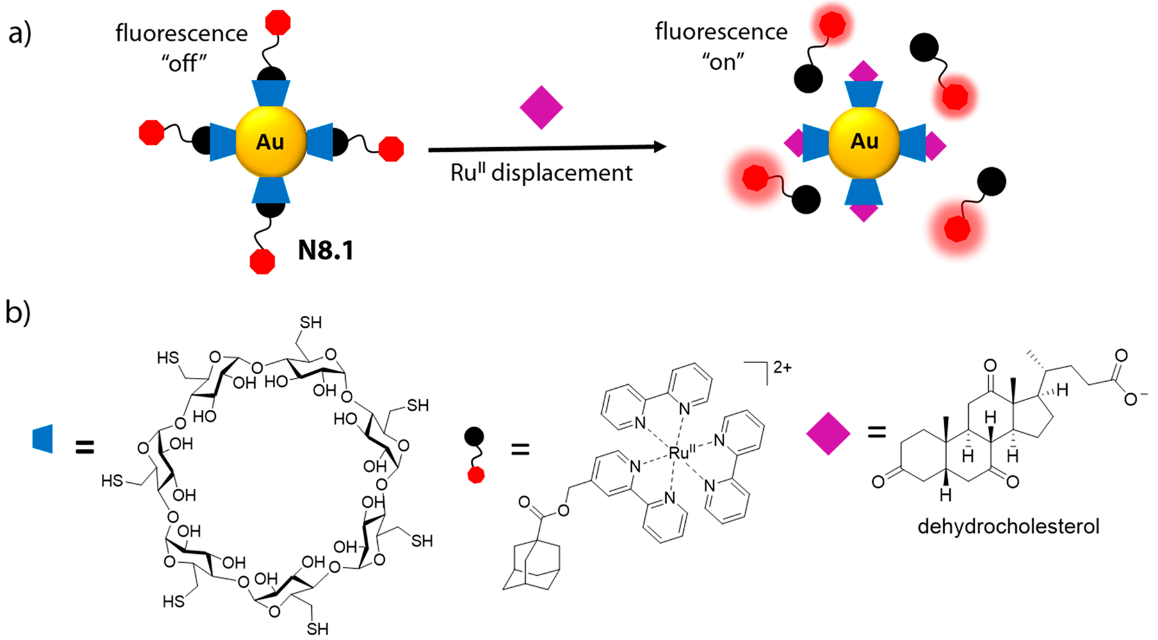

**Figure 208.** Schematic representation of the sensing mechanism for dehydrocholesterol *via* FRET using $\beta$-CD-Ru$^{II}$ host−guest complex functionalized AuNPs (**N8.1**) in 10 mM Tris-HCl buffer containing 5% MeOH, pH 8.0, at mM concentrations.

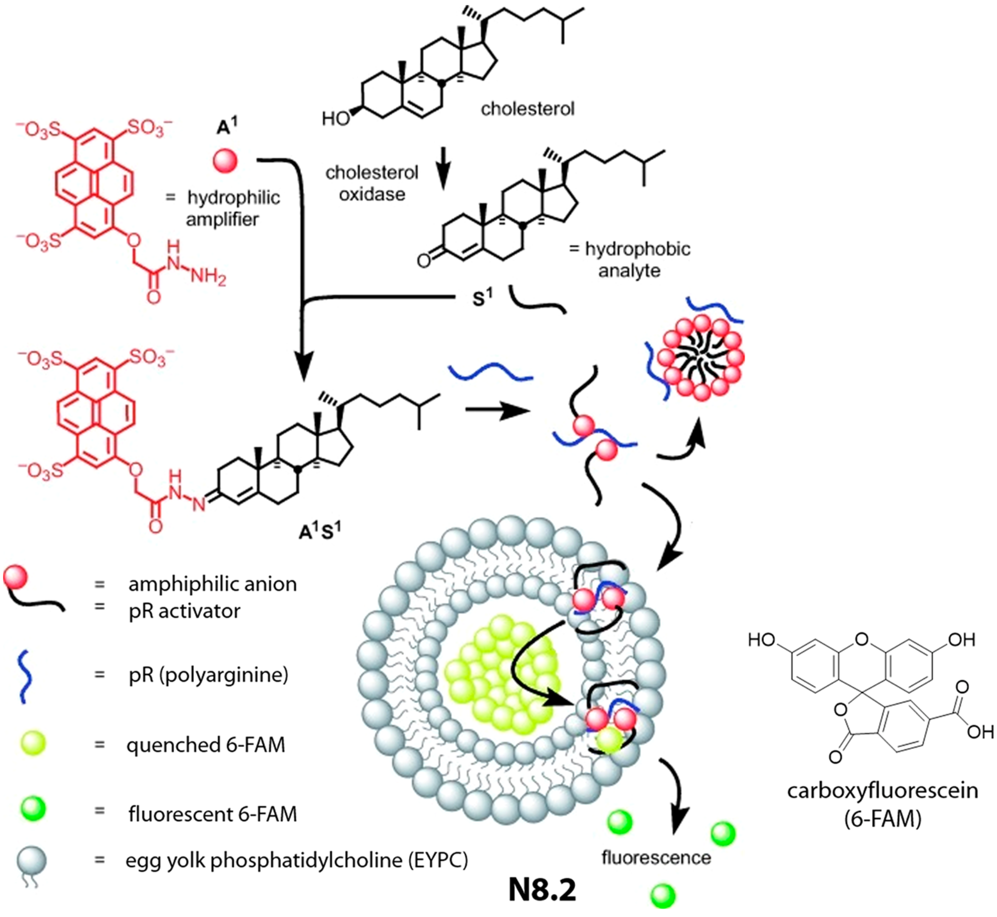

**Figure 209.** Schematic representation of the fluorescence-based detection mechanism for cholesterol using carboxyfluorescein (6-FAM)-loaded unilamellar vesicles in combination with polyarginine as the counterion transport system (**N8.2**). Reproduced with permission from ref 916. Copyright 2009 Wiley-VCH.

articles for additional information on the host−guest binding properties of cavitands.[884,885]

We would like to inform the reader now on the use of polarity-sensitive fluorescent probes that can find use for cancer diagnostics. These probes do not target single lipid molecules but rather "stain" lipid droplets that are found in eukaryotic cells, and which differ in their lipid composition, polarity, and fluidity between normal and cancerous cells.[840−842]

Environmentally sensitive fluorescent probes, such as compounds that show largely different emission spectra in apolar and polar solvents, have long been known,[895] although compounds with extraordinary structural and photophysical properties continue to emerge.[169−896,897] It is therefore not surprising that tailor-made probes can be designed for lipid droplet (LD) recognition but exciting to see that probes can readily distinguish cancerous from normal cells because the properties of LDs differ in terms of polarity, fluidity, and composition (**P8.1** in Figure 206).[894]

As exemplary reading material on polarity-sensitive fluorescent probes for lipid staining (see Figure 207 for representative dyes), we refer the reader to the recent works of Lin and coworkers (**P8.1**),[894] Fan, Dong, and coworkers (**P8.2**),[898] Liu, Tang, and coworkers (**P8.3−P8.7**),[899−901] Sun, Liu, Li, and coworkers (**P8.8**),[902] Pan, He, and coworkers (**P8.9**),[903] Zhang, Hu, and coworkers (**P8.10**),[904] Niko, Klymchenko, and coworkers (**P8.11**),[905] Lin and coworkers (**P8.12**),[906] Chang and coworkers (**P8.13**),[907] Qu, Yang and coworkers (**P8.14**),[908] Yin, Yuan, Chen, and coworkers (**P8.15**),[909] as well as by Koner and coworkers (**P8.16**).[910] Information on fluorescent probes for lipid droplet imaging can be found in a timely review written by Sessler, James, He, and coworkers.[911]

## 8.2. Nanosensors for Steroids

Signal transduction through plasmonic gold nanoparticles (AuNPs) is one popular and powerful approach for achieving colorimetric sensing as AuNPs possess distinct surface plasmon resonances (SPRs) that can be easily characterized *via* UV−vis spectroscopy and used for analyte quantification.[913,914] Furthermore, the surface of AuNPs can be easily functionalized with multiple functional groups *via* thiol chemistry, which enables the preparation of multimodal nanosensors. With this in mind, a Förster resonance energy transfer (FRET)-based nanosensor for the detection of dehydrocholic acid in 10 mM Tris-HCl buffer containing 5% MeOH, pH 8.0, was reported by Yam and coworkers (**N8.1** in Figure 208).[915] In this example, gold nanoparticles were functionalized with thiolated $\beta$-cyclodextrin ($\beta$-CD), which reversibly binds to the $Ru^{II}$−adamantane dye, resulting in its quenched fluorescence due to energy transfer processes with the plasmonic nanoparticle. However, in the presence of the steroid DHC, the $Ru^{II}$ complex is displaced from the $\beta$-CD decorated nanoparticle surface, leading to increased fluorescence intensities that allow for the quantification of DHC in the mM concentration range. Although the authors successfully described the preparation of a simple and cost-effective steroid nanosensor, the system still lacks in the sensitivity and selectivity required for practical detection of DHC in biological relevant media.

The detection of hydrophobic molecules with vesicular systems, such as pore sensors,[917,918] is particularly challenging, as the analytes tend to diffuse into the membranes and remain undetected. Matile and coworkers showed that this problem can be circumvented by applying a "reactive signal amplification strategy".[919,920] Fluorescence-based detection of cholesterol with vesicles was achieved by implementing a chemical conversion of cholesterol to the hydrazone $A^1S^1$ (amphiphilic anion or pR activator, **N8.2** in Figure 209).[916] This hydrazone then associated with polyarginine to form a polyion complex, which penetrated the vesicular bilayers of carboxyfluorescein (6-FAM)-loaded unilamellar vesicles and triggered the extravesicular transport of 6-FAM. Re-location of 6-FAM resulted in increased fluorescence intensity as it is no longer subject to strong self-quenching present inside the vesicle. The authors showed that cholesterol can be detected in 10 mM Tris buffer containing 107 mM NaCl, pH 7.4, egg yolk, and human serum samples with their approach.[916] Robust detection of cholesterol in blood samples (1.5−2.5 mg $mL^{-1}$) was possible with good reliability as confirmed by comparing the results obtained by UV−vis absorption spectroscopy (detected: 1.2 ± 0.2 mg $mL^{-1}$).

Some of the aforementioned examples still await their test for *in vivo* use, which could unleash many applications for personalized diagnostics, *e.g.*, of hormone levels. When excited by light, single-walled carbon nanotubes (SWCNTs) are near-infrared (NIR) emitters and thus especially attractive for *in vivo* applications due to the higher transparency of tissues for NIR-light compared to UV and visible light. It is known that synthetic polymers can adsorb to SWCNTs *via* $\pi$−$\pi$-stacking interactions, a phenomenon used, for example, for carbon nanotube sorting and separation.[922−927] Tailor-made polymers can be designed to target steroids, thus mediating the binding process of such analytes on the surface of SWCNTs, a concept known as corona phase molecular recognition.[928] A large step forward for steroid detection using nanosensors was recently made by Strano and coworkers, who reported the preparation of an implantable polymer-functionalized SWCNT nanosensor (**N8.3** in Figure 210).[921] In this example, progesterone- and cortisol-binding polymers were first prepared through a molecular imprinting method *via* reversible addition−fragmentation chain-transfer (RAFT) polymerization of styrene, acrylic acid, and acrylated cortisol or acrylated progesterone (Figure 210b). Once covalently linked on the surface of SWCNTs, the polymer appendages dynamically adsorb and desorb from the

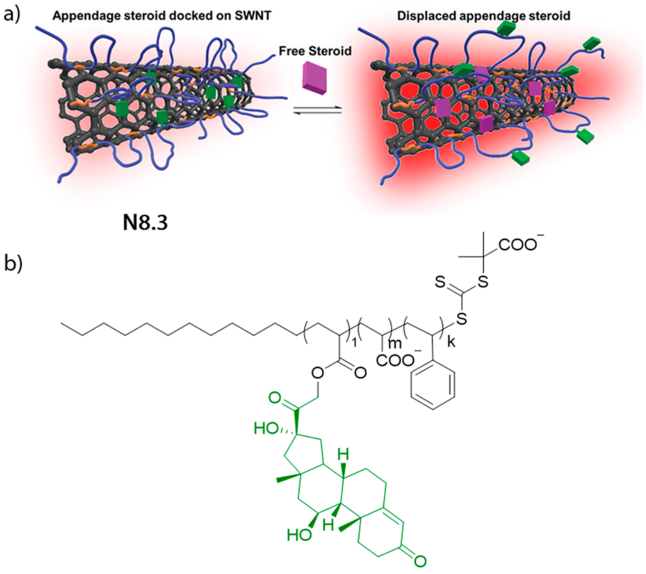

**Figure 210.** (a) Steroid-polymer-coated SWCNTs (**N8.3**) for fluorescence turn-on detection of human steroids, *e.g.*, cortisol and progesterone. Reproduced with permission from ref 921. Copyright 2020 Wiley-VCH. (b) Chemical structure of the steroid polymer.

surface of the SWCNTs, eventually forming steroid-binding cavities. Thus, when the targeted steroids are present in 1× PBS containing 2% DMSO, they displace the polymeric appendages, leading to an increased NIR emission of the SWCNTs (as the composition of the corona phase changes). In this way, the authors were able to detect progesterone at $\mu$M concentrations with good selectivity over other steroids, *e.g.*, testosterone, estradiol, cortisone, aldosterone, or corticosterone, that do not elicit a strong fluorescence enhancement of **N8.3**. In a proof-of-principle for *in vivo* applications, the authors immobilized the SWCNTs chemosensor within a hydrogel matrix in the subcutaneous space of mice and showcased the sensing of progesterone in rodents.

As mentioned above, the main obstacle to the detection of steroids using supramolecular systems is their suboptimal sensitivity for such target analytes, which makes them not yet attractive for diagnostic applications. Further, future work on the development of sensors for *in vivo* sensing of steroids is of great importance. New concepts need to be developed to minimize cross-reactivities to improve detection limits for steroids in the nano- and picomolar range in biofluids and to increase the robustness and (long-term) stability of the steroid-sensors in biological environments.

Given their medical relevance, one would naively expect that chemists have already reported several probes and chemosensors that can target lipids and thereby complement or replace instrumental analytics for lipid detection. Surely, there can be substantial health benefits, if methods become available in which the lipid metabolome can be routinely monitored by the layman at home or in point-of-care settings. However, quite the opposite is the case, and we only found a limited number of lipid-specific probes and chemosensors that have the potential to become available for sensing applications in the near future. There might be three reasons for that First, the hydrocarbon-based skeleton of lipids represents an unattractive binding motif for developing any reactive probe. Second, chemosensors may be able to efficiently bind lipids in aqueous media driven by the hydrophobic effect and dispersion interactions, yet it appears questionable how structurally closely related, *e.g.*, homologous lipids, that may have completely different biological functions and diagnostic values, can be distinguished from each other. Third, unlike amino acids and some carbohydrates, the low concentration of lipids found in biofluids and especially in urine (see Table 30 for a summary of concentrations of lipids and steroids in biofluids) requires the development of particularly sensitive detection methods, matching stringent requirements in terms of binding affinity and signal transduction capabilities. Although higher (total) concentrations of lipids are found in the blood serum, *e.g.*, currently accepted threshold levels for triglycerides and serum cholesterol are <100 mg/dL and <200 mg/dL, respectively,[929,930] and thus in the millimolar range, blood serum imposes additional challenges in terms of selectivity requirements and optical properties of the chemosensors.

Just as the detection of lipids with molecular probes and chemosensors remains a challenge, the same is true for nanosensors. Another factor impeding the development of nanosensors is that lipids themselves are in many cases essential structural components of nanosensors, *e.g.*, in liposomes[931] or nanoparticles coated with lipid layers,[932] and are therefore considered as useful building blocks rather than targetable analytes. Nanosensors for lipid detection have, to our knowledge, not yet been developed.

**Table 30. Summary of the Normal Concentration of Lipids and Steroids in Biofluids**[a]

| concentration range | media | ref |
|---|---|---|
| Cholesterol Analyte | | |
| 5.2−6.2 mM | blood | 933 |
| 9.9−20.4 mM | bile | 934 |
| Cortisol Analyte | | |
| 150−650 nM | blood | 935 |
| 1.9−14.0 nmol/mmol creatinine = 0.019−0.14 $\mu$M | urine | 936 |
| 1.1−12.7 nM | saliva | 937 |
| 17-$\beta$-Estradiol Analyte | | |
| 0.08−0.24 nM | blood (female) | 938 |
| 0.34−0.84 nmol/mmol creatinine = 3.4−8.4 nM | urine (female) | 938 |
| 0.012−0.024 nM | saliva | 937 |
| Progesterone Analyte | | |
| 16.6−53.4 nM | blood | 938 |

[a] Urinary analyte concentrations were converted assuming a representative creatinine level of 10 mmol/L.

## 9. SELECTED EXAMPLES FOR DRUG SENSING

Information about the absorption, distribution and excretion mechanisms of bioactive molecules within a living organisms is of utmost importance when it comes to the development of drugs with improved pharmacological properties.[939] Therefore, pharmacokinetic features (*e.g.*, bioavailability, circulation lifetime, and duration of action) of newly designed or discovered drugs have to be analyzed in various biological fluids as a function of time. Current standard drug analysis techniques based on immunoassays, mass spectrometry, and separation techniques, *e.g.*, chromatography, are comparably cumbersome and/or expensive to use, and therefore, synthetic and supramolecular chemists became attracted to develop molecular probes and chemosensors for the detection of drugs in biofluids. It has become apparent that the actual effectiveness of treating diseased individuals with already approved drugs can vary from patient to patient.[940,941] According to published data, current pharmaceutical treatments are not effective in 30−60% of patients, and the proportion of patients who develop adverse drug reactions may be as high as 30%.[942] The reasons for these individual variations can be diverse, *e.g.*, due to age, gender, addictions, ethnic factors, and drug-related factors (therapy with multiple drugs, concomitant diseases). To increase the efficacy of therapies or even to detect the occurrence of diseases at an early stage, more information on the presence of drugs and metabolite concentrations in biofluids will be important.[943] Patients receiving drug treatment could regularly monitor drug levels excreted in urine or saliva, which, once the data is transmitted to a physician, could offer unprecedented opportunities for personalized medical treatment. In a bold vision for the future, side effects of medications will be largely reduced when options for personal theranostics become widely available, allowing for evidence-based selection of a drug and matching of its dosage. Another topic of concern in which the detection of drugs becomes important relates to the abuse of drugs. It is a major public health problem, with fatalities attributed to overdoses numbering 7600 in the European Union[944] and 70 000 in the United States in 2017.[945] Probe- and chemosensor-based assays can become a promising, cost efficient, and facile approach for detecting illicit drugs (see Figure 211 for representative examples) in biofluids, *e.g.*, urine or saliva.

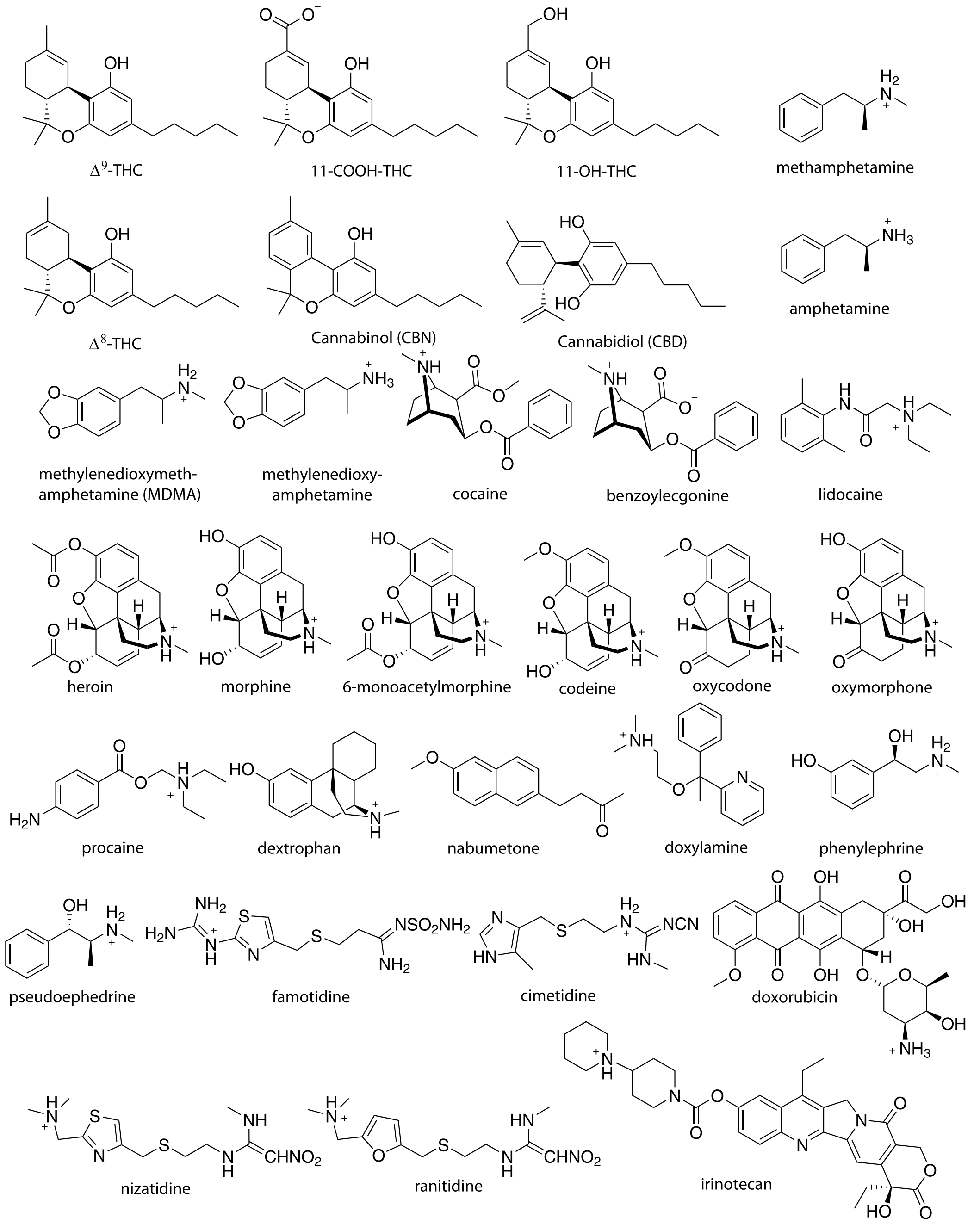

**Figure 211.** Chemical structures of selected drugs described in this section.

In the following section, we highlight a few examples of systems that appear to match already (some of) the required performance parameters for practical applications, see also Tables 31 and 32.

## 9.1. Chemosensors and Molecular Probes for Drug Sensing

The Hooley group prepared water-soluble negatively charged cavitands, which besides the detection of trimethyllysine derivatives and proteins (see section 2.3, Figure 55), were functional as sensors for cannabinols in 20 mM Tris buffer, pH 7.4, human urine, and saliva with micromolar sensitivity (**C9.1**−**C9.2** in Figure 212b).[946] Interestingly, the authors found that different cannabinoid metabolites can be distinguished from each other in urine through multivariate analysis but not in saliva. Apparently, the higher salt concentrations found in urine are less obstructive to the fluorescence-based IDA than the cationic proteins excreted in saliva. It is worth noting that the cavitand also binds strongly to steroids, including steroidal medical drugs.[947] Thus, one would need to be aware of potential false-positive results when using such host systems in routine use.

Likewise, the Hof group utilized and improved their "DimerDye Disassembly Assay" (DDA) for trimethyllysine detection (see section 2.3, Figure 54) and achieved through parallel synthesis and screening a supramolecular emission turn-on assay (**C9.3** in Figure 213) for the micromolar detection of therapeutic and illicit drugs (*e.g.*, amphetamines, cocaine, lidocaine, and nicotine) in 10 mM phosphate buffer, pH 7.4, and in saliva.[276] Although this sensing system behaves as a promiscuous binder, all 13 drugs and drug metabolites

### Table 31. Summary of Chemosensors for Drugs (LOD, Limit of Detection)

| chemosensor | media | concentration range | ref |
|---|---|---|---|
| | Amantadine Analyte | | |
| **C9.6** | 10× PBS, pH 7.4 | LOD, 67 nM (1× PBS) | 274 |
| | urine samples | μM range in urine | |
| | saliva samples | μM range in saliva | |
| | Aza-heterocyclic Compounds Analyte | | |
| **C9.8** | 0.5% P123 in 1× PBS, pH 7.4 | μM range | 184 |
| | Cannabinols[a] Analyte | | |
| **C9.1−C9.2**[b] | 20 mM Tris buffer, pH 7.4 | LOD, μM range[c] | 946 |
| | urine samples | | |
| | saliva samples | μM range in saliva | |
| | Cocaine Analyte | | |
| **C9.3**[d] | 10 mM phosphate buffer, pH 7.4; saliva | 0−240 μM (linear range); LOD, 2.7 μM | 276 |
| | Memantine Analyte | | |
| **C9.7** | 1× PBS, pH 7.4; human serum; bovine blood serum | 0−2 μM | 949 |
| | Methylenedioxy-methamphetamine (MDMA) Analyte | | |
| **C9.3**[d] | 10 mM phosphate buffer, pH 7.4; saliva | 0−240 μM (linear range); LOD, 2.7 μM; LOD, 41.2 μM | 276 |
| | Nicotine Analyte | | |
| **C9.3**[d] | 10 mM phosphate buffer, pH 7.4; saliva | 0−240 μM (linear range); LOD, 3.4 μM; LOD, 18.6 μM | 276 |
| | OTC Drugs[a] Analyte | | |
| **C9.4−C9.5** | water (pH 3.0 or pH 5.0) | μM range | 235 |

[a]The structure of the targeted analytes can be found in Figure 211. [b]The chemosensor array (**C9.1−9.2**) can differentiate six cannabinols (shown in Figure 211) by PCA analysis.[947] [c]LOD, 8.2 μM ($\Delta^9$-THC), 4.5 μM (11-OH-THC), 17.4 μM (11-COOH-THC), **C9.2** is used. [d]Chemosensor **C9.3** is a chemosensor array composed of 16 different sensors.[276]

### Table 32. Summary of Nanosensors for Drugs

| nanosensor | media | concentration range | ref |
|---|---|---|---|
| | Codeine Analyte | | |
| **N9.1** | 10 mM phosphate buffer, pH 7.0 | 30−800 nM; LOD, 9 nM | 950 |
| | urine and serum | μM range in biofluids | |
| | Doxorubicin Analyte | | |
| **N9.6** | 20 mM HEPES buffer | 0.5−50 μM | 955 |
| | serum | 0−50 μM | |
| | *in vivo* | μM range *in vivo* | |
| | Irinotecan Analyte | | |
| **N9.7** | 75% MeCN in water | 5.0−100 nM; LOD, 16 nM | 956 |
| | purified plasma | 20−200 nM in plasma | |
| | 3,4-Methylene dioxymethamphetamine (MDMA) Analyte | | |
| **N9.3** | water, pH 7.0 | LOD, 4.9 μM | 952 |
| **N9.4** | 10 mM HEPES buffer in $D_2O$, pD 7.0 | μM−mM range | 953 |
| | Morphine Analyte | | |
| **N9.1** | 10 mM phosphate buffer, pH 7.0; urine and serum | 0.07−3.0 μM; LOD, 17 nM | 950 |
| **N9.2** | water | 0.1−350 nM; LOD, 0.17 nM | 951 |
| | urine and serum | 0.5−100 nM in biofluids | |
| | Nabumetone Analyte | | |
| **N9.5** | water (10 μM NaCl) | 0−0.5 μg/L in water | 954 |
| | waste water | LOD, 0.8 nM; in water | |
| | urine | 0−0.44 μM in urine | |
| | Phenethylamine- based Drugs Analyte | | |
| **N9.4** | 10 mM HEPES buffer in $D_2O$, pD 7.0 | μM−mM range | 953 |

tested provided a distinguishable response that was assessed through multivariate analysis. Moreover, the tolerance to saliva suggests that the salivary charged proteins were not interfering with the calixarene-based chemosensing system. For comparison, sulfonated calix[4]arene (Cx4) only displayed a modest affinity for the alkaloid topotecan ($K_a$ = 1.6 × $10^3$ $M^{-1}$ in 50% MeOH aq), which is a chemotherapeutic agent.[948]

Isaacs, Anzenbacher Jr., and coworkers combined multivariate analysis methods with array-based sensing by cyclic and acyclic cucurbit[*n*]urils (**C9.4** and **C9.5** in Figure 214) for the detection and classification of addictive over-the-counter (OTC) drugs.[235] These fluorescent cucurbit[*n*]uril analogues, previously introduced in the amino acid section of this review (see section 2.3, **C2.5**), show strong binding affinities for hydrophobic and/or positively charged analytes such as acetaminophen ($K_a$ = 6.9 × $10^3$ $M^{-1}$ for **C9.4**), pseudoephedrine ($K_a$ = 8.6 × $10^3$ $M^{-1}$ for **C9.5**), doxylamine ($K_a$ = 1.1 × $10^5$ $M^{-1}$ for **C9.5**), and histamine ($K_a$ = 5.1 × $10^4$ $M^{-1}$ for **C9.4**), which are found as mixtures in OTC cold remedies. Additionally, antihistamines such as ranitidine ($K_a$ = 1.7 × $10^5$ $M^{-1}$ for **C9.5**) and famotidine ($K_a$ = 1.1 × $10^3$ $M^{-1}$ for **C9.5**) were bound to the chemosensors on account of their positive charge. The analyte binding selectivity was expectedly higher for the cyclic CB6-chemosensor than for the acyclic variant (pre-organization and lock-and-key effect). Importantly, the authors demonstrated that OTC drugs can be quantified at μM concentrations even within binary and ternary mixtures, both in water (pH 3.0 or pH 5.0) and in human urine of properly hydrated volunteers that ingested the manufacturer-recommended amount of cold medication. The authors concluded that their chemosensor-based method provides a higher throughput, sensitivity, and a better LOD than extraction-based methods available at that time (and likely still to date). Nevertheless, care must be taken to avoid false positive results in the presence of other substances excreted in the urine, *e.g.*, drugs or food components, due to the low binding selectivity of CB*n*-based chemosensors.

Our group recently reported a covalently-tethered host−dye conjugate that functions as a unimolecular chemosensor (**C9.6** in Figure 215) for the selective micromolar detection of Parkinson's drug amantadine in urine and saliva.[274] **C9.6** was obtained by covalently linking the macrocyclic host CB7 to the fluorescent indicator dye berberine *via* a flexible tether through a copper-catalyzed click reaction. As a result of the design, **C9.6** is dilution-stable and salt tolerant (*e.g.*, remains in its folded form even in 10X PBS), whereas other noncovalently bound CB*n*•dye ensembles are prone to disaggregate upon dilution or in saline media.[40,880] The unimolecular chemosensor **C9.6** displayed an excellent selectivity for amantadine in human urine and saliva over potential interferents such as polyamines (cadaverine, spermidine, and spermine) or the steroid nortestosterone. Moreover, physiologically relevant

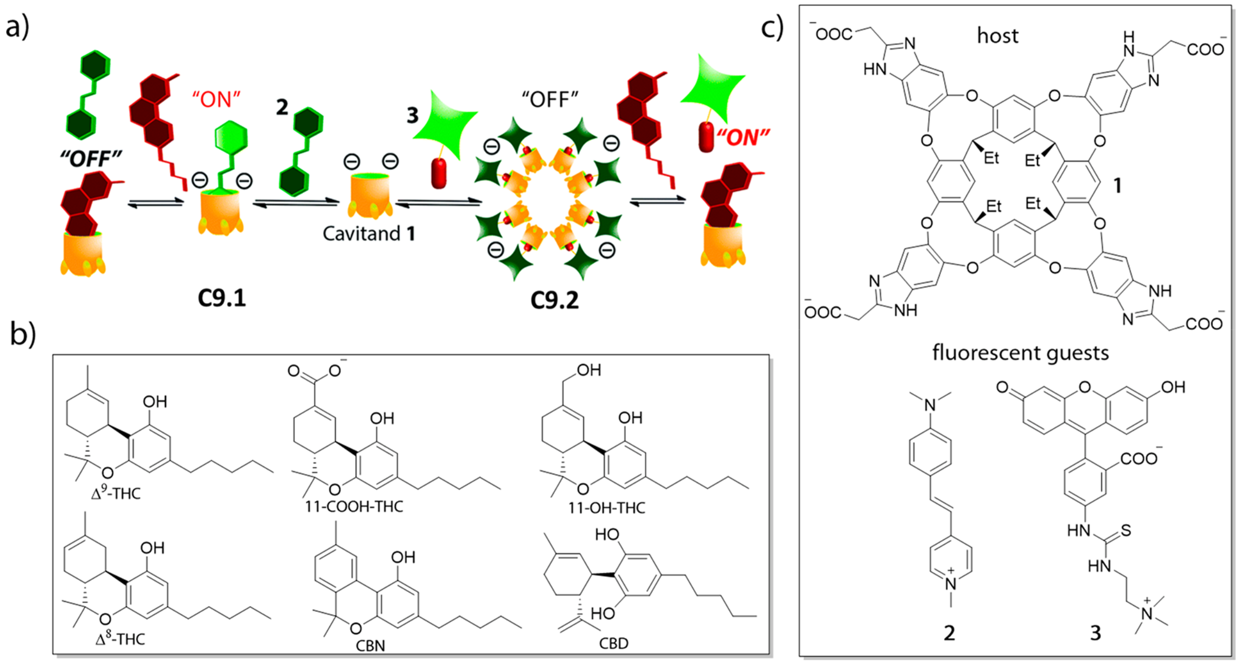

**Figure 212.** (a) Sensing mechanism of chemosensors **C9.1**−**C9.2** for cannabinols. (b) Chemical structures of cannabinols. (c) Chemical structures of components used in the chemosensor array. Adapted with permission from ref 946. Copyright 2020 The Royal Society of Chemistry.

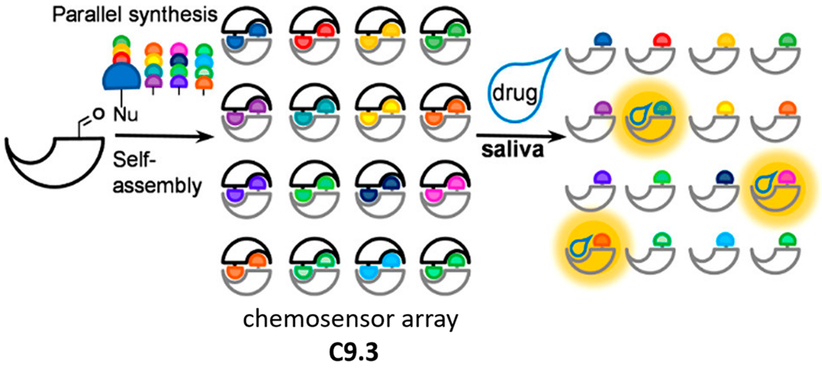

**Figure 213.** Schematic representation of the DimerDyes (DDs)-based chemosensor array (**C9.3**) used for the detection of cationic drugs in biological media. Reproduced with permission from ref 276. Copyright 2019 America Chemistry Society.

concentrations of amantadine were successfully determined in saliva and urine with **C9.6** by a matrix-independent method, which provides a potential clinical application scenario for amantadine monitoring in biofluids.

In 2019, we had communicated the first cucurbit[*n*]uril-based chemosensing system that is applicable in blood serum. Specifically, chemosensor **C9.7** was assembled from CB8 and a novel methyl-pyridinium-paracyclophane indicator dye (MPCP), see Figure 216, that possesses a very high binding affinity ($K_a > 10^{12}$ $M^{-1}$ in water). The required binding strength of the indicator dye was rationally derived by mathematically simulating the performance of different indicator dye−CB8 combinations for the matrix-independent detection of Alzheimer's drug memantine. As input parameters typical concentration ranges of other metabolites and bioactive compounds occurring in blood serum and their binding affinities for CB8 were considered. **C9.6** allowed for memantine quantification through IDA in blood serum at the physiologically-relevant, low micromolar concentration range.[949]

Self-assembling probes (SAPs, Figure 217a) can offer a much higher information content than IDA-type chemosensors, making the concept attractive for future diagnostic application developments. A representative example was introduced by us in which a self-assembled luminescent metal−organic probe (**C9.8** in Figure 217b) responded to a number of aza-heterocyclic compounds, such as histamine, histidine, and the drugs nicotine, clotrimazole, fluconazole, and miconazole in 1× PBS, pH 7.4 (Figure 217d).[184] In contrast to the previously described chemosensor assays, which establish analyte discrimination by different binding affinities in an array-based system, the use of only one probe was demonstrated to be sufficient to distinguish 24 different analytes by emerging analyte-characteristic spectroscopic fingerprints, *e.g.*, emission colors.

### 9.2. Nanosensors for Drug Sensing

Compared to the limited number of dedicated and selective probes and chemosensors for drug sensing, there are considerably more reports on nanoparticle-based sensors for the detection of drugs in aqueous media or biofluids.

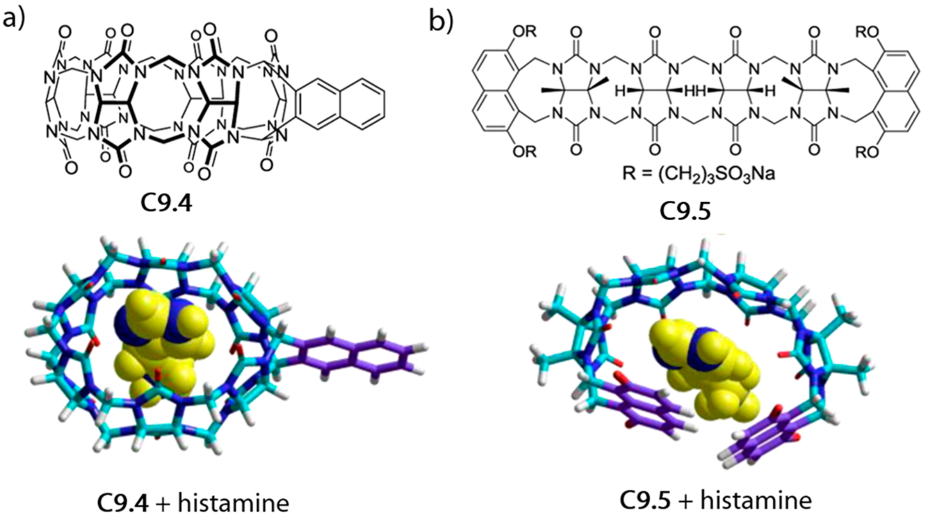

**C9.4**

**C9.5**

**C9.4** + histamine

**C9.5** + histamine

**Figure 214.** Chemical structure and 3D rendering of the (a) cyclic cucurbit[*n*]uril chemosensors (**C9.4**) and (b) acyclic cucurbit[*n*]uril chemosensors (**C9.5**) used for the micromolar detection of addictive over-the-counter (OTC) drugs (*e.g.*, histamine, acetaminophen, and pseudoephedrine) in water. Adapted with permission from ref 235. Copyright 2013 American Chemical Society.

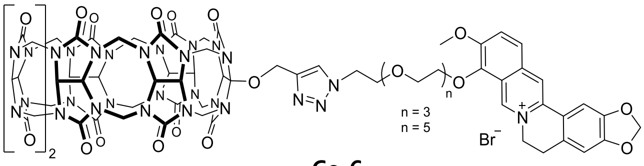

**C9.6**

**Figure 215.** Chemical structure of the unimolecular chemosensor **C9.6** that can be used for the micromolar detection of the drug amantadine in urine and saliva.

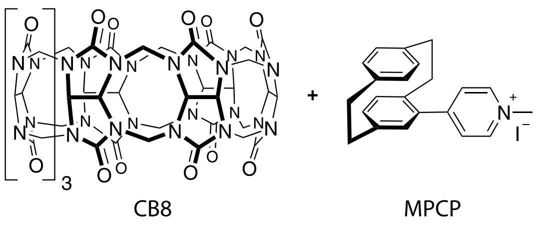

**C9.7**

**Figure 216.** Chemical structure for chemosensor **C9.7** that we employed for memantine sensing in the physiologically relevant micromolar concentration range in blood serum.

Bahram and coworkers reported the use of melamine functionalized AuNPs for the colorimetric detection of morphine and codeine in 10 mM phosphate buffer, pH 7.0, serum and urine samples (**N9.1** in Figure 218).[950] Opioids are bound to the melamine moieties of **N9.1** *via* H-bonding interactions and induce particle aggregation by functioning as "molecular bridges". As a result of aggregation, the surface plasmon resonances of **N9.1** change in the presence of opioids, which was used for their quantification at low $\mu$M concentrations in opioid spiked-blood and urine samples (recovery rates <95 %). The authors showed that potential interfering cations and anions (*e.g.*, $Fe^{3+}$, $Al^{3+}$, $Na^+$, $K^+$, $PO_4^{3-}$, $SO_4^{2-}$, $NO_3^-$, $CH_3COO^-$), biomolecules (*e.g.*, ascorbic acid, glucose, urea, and several amino acids), and other illicit drugs (*e.g.*, tramadol, amphetamine, and methamphetamine) do not produce a similar colorimetric response. However, codeine and morphine cannot be distinguished from each other by **N9.1**.

Sheta and coworkers recently reported the use of metal−organic framework (MOF) nanoparticles (**N9.2** in Figure 219) for the fluorescence-based detection of morphine at nM concentrations in water and biological samples, *i.e.*, urine and serum samples.[951] The $Cr^{III}$-based MOFs prepared in this work are characterized by good stability in aqueous media and have high surface areas, which is a beneficial feature for sensing applications in biological fluids. Quantitative detection of morphine was possible due to its strong H-bonding interactions with the pore interior of **N9.2**, thereby altering photoinduced electron transfer (PET) processes and causing a blue-shift in the photoluminescence spectrum of the nanosensor. The authors showed that other inorganic ions (*e.g.*, $Na^+$, $Ca^{2+}$, and $Cl^-$) and organic molecules (*e.g.*, ascorbic acid, uric acid, caffeine, and methamphetamine) did not produce a similar change in the photophysical properties as observed for morphine. However, the ability to discriminate various structurally analogous opioids was not investigated. Finally, it was demonstrated that the nanosensor was able to detect morphine in spiked (0.5−100 nM) urine and serum samples with good recovery (>96%).

Mesoporous silica particles (MSPs) are interesting candidates for the preparation of nanosensors based on "gated materials". In this respect, reporter molecules (*e.g.*, fluorescent dyes) are loaded in the pores of MSPs and subsequent pore blocking units (or "gatekeepers") are introduced, which prevent reporter dye diffusion from the pores. The gatekeepers can be designed in such a way that the presence of the target analyte triggers its disassembly, allowing for the spontaneous release of the reporter molecules. In this way, an amplified signal generation can be achieved, as few analyte molecules can trigger the release of many reporter dyes. With this in mind, Sancenón, Martínez-Máñez, and coworkers developed fluorescein-loaded and pseudorotaxane-capped MSPs as "gated material" for the detection of MDMA in water, pH 7.0, at $\mu$M concentrations (**N9.3** in Figure 220).[952] In their design, the gatekeeper consisted of pseudorotaxanes formed between cyclobis(paraquat-*p*-phenylene) (CBPQT, the stop-cock) and naphthalene ligands immobilized on the surface of the particles. It was shown that MDMA displaced CBPQT from the naphthalene pending group due to its higher affinity to this

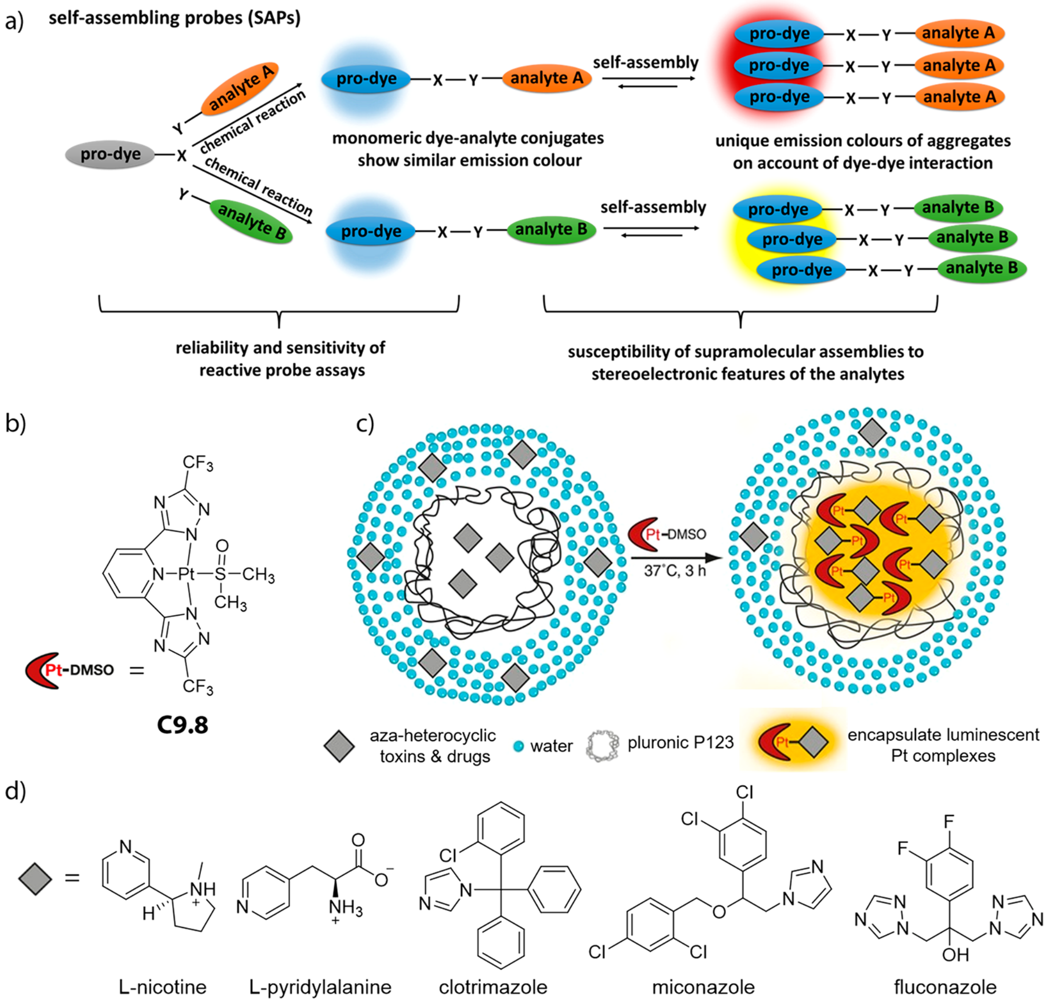

**Figure 217.** (a) Operational principle of self-assembling probes (SAPs) and their capability to provide analyte-indicative spectroscopic fingerprints. (b) Chemical structure of the $Pt^{II}$-complex used as fluorescence turn-on chemosensor (**C9.8**). (c) Representative example of a luminescent platinum complex-based SAP (**C9.8**) for the detection and differentiation of aza-heterocyclic drugs and toxins in 0.5% P123 as surfactant in 1× PBS. Adapted with permission from ref 184. Copyright 2017 Wiley-VCH. (d) Chemical structures of aza-heterocyclic drugs and toxins.

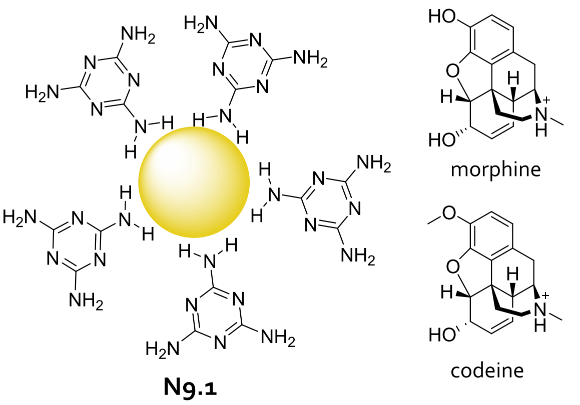

**Figure 218.** Schematic representation of melamine functionalized AuNPs (**N9.1**) used for the colorimetric detection of morphine and codeine in 10 mM phosphate buffer, pH 7.0, serum, and urine samples at $\mu$M concentrations.

macrocycle. The selectivity of the nanosensor was tested towards other opioids (*e.g.*, morphine, methadone, and heroin) and the tropane alkaloid cocaine, demonstrating that fluorescein release only occurs in the presence of MDMA.

An AuNPs-based displacement assay for the detection of phenethylamine (a designer drugs) was reported by Mancin and coworkers (**N9.4** in Figure 220).[953] In this work, AuNPs were decorated with sulfonic acid derivatives, which form a negatively charged monolayer that functions as the "binding unit" for phenethylamine drugs in deuterated solvents (10 mM HEPES buffer/$D_2O$) *via* hydrophobic and electrostatic interactions. Analyte detection at $\mu$M to mM concentrations was achieved though NMR spectroscopy, particularly, by diffusion-based experiments (DOSY or diffusion filters) along with magnetization (NOE-pumping) or saturation transfer protocols. Drugs that strongly interact with the sulfonic acid monolayer experience a greater shortening in the transverse $T_2$ relaxation times, a parameter that strongly varies on the association/dissociation rates between analyte and nanoparticle. Thus, different analytes were quantitatively distinguishable from each other, as their interaction strength with the sulfonic acid monolayer is analytically indicative. However, the analysis of multicomponent mixtures was not attempted.

Recently, Dadfarnia, and coworkers reported the use of $\beta$-cyclodextrin ($\beta$-CD) surface-functionalized AuNPs for the colorimetric detection of the nonsteroidal anti-inflammatory drug (NSAID) nabumetone in urine and wastewater samples

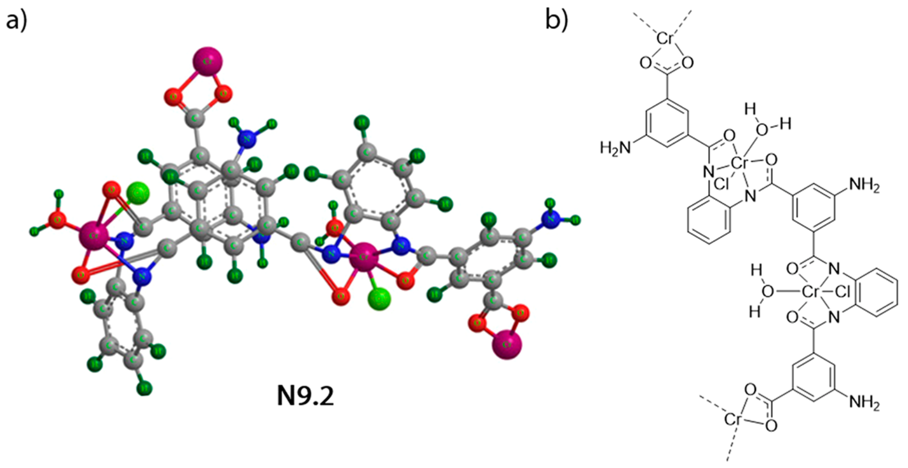

**Figure 219.** (a) 3D structural representation of the monomeric unit in $Cr^{III}$−MOF (**N9.2**). Reproduced with permission from ref 951. Copyright 2020 American Chemical Society. (b) Chemical structure of $Cr^{III}$-based MOF-NPs (**N9.2**) used for fluorescence-based detection of morphine at nM concentrations in water, urine, and serum samples.

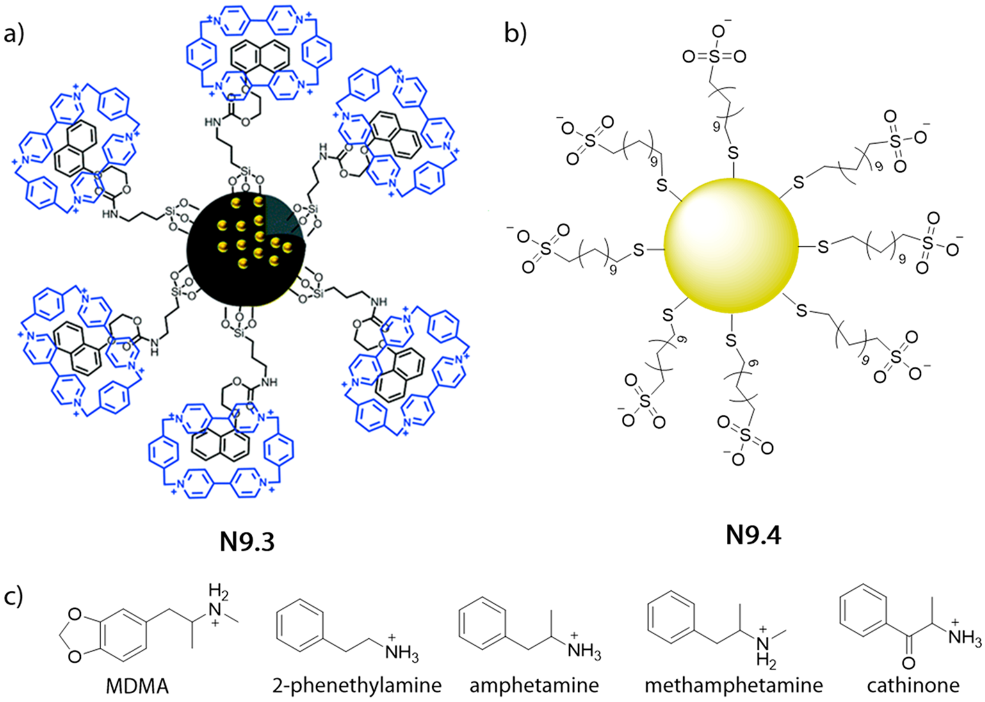

**Figure 220.** (a) Schematic representation of fluorescein-loaded and pseudorotaxane-capped mesoporous silica particles (MSPs, **N9.3**) that can be used for $\mu$M detection of MDMA in water. Adapted with permission from ref 952. Copyright 2017 The Royal Society of Chemistry. (b) Sulfonic acid functionalized AuNPs (**N9.4**) for NMR-based detection of phenethylamine related drugs at $\mu$M concentrations in deuterated water/HEPES buffer. (c) Chemical structures of phenethylamine related drugs.

(**N9.5** in Figure 221).[954] Nabumetone was shown to form strong inclusion complexes with $\beta$-CD in the presence of polyvinylpyrrolidone, which triggered particle aggregation and acted as a supramolecular bridge. The aggregation of **N9.5** is accompanied by a significant color change of the dispersion, allowing for colorimetric-based nabumetone detection at $\mu$M concentrations (LOD, 0.8 nM) in aqueous solutions (10 $\mu$M NaCl). Minor interferences were observed from other drugs (*e.g.*, salicylic acid, mefenamic acid, paracetamol, 6-methoxy-2-naphthylacetic acid, or naproxen) or biomolecules (*e.g.*, sucrose, glucose, or lactose). When the assay was applied to human urine and wastewater samples spiked with nabumetone, good recoveries (> 96%) were found.

The Heller group recently showcased the use of DNA-functionalized single-walled carbon nanotubes (SWCNTs) for *in vivo* detection of doxorubicin in mice (**N9.6** in Figure 222).[955] The authors functionalized SWCNTs with $(GT)_{15}$ oligomers, which were bound to the nanotube *via* $\pi$−$\pi$ interactions and further increased the dispersibility of these hydrophobic nanoparticles in water. In the presence of doxorubicin, the analyte irreversibly intercalated between the DNA nucleobases *via* hydrophobic and stacking interactions, thereby altering the corona composition and the photoluminescent properties of **N9.6** (see section 8.2, Figure 210). The red-shifted and quenched emission from the SWCNTs upon doxorubicin binding was used to quantify the drug at $\mu$M

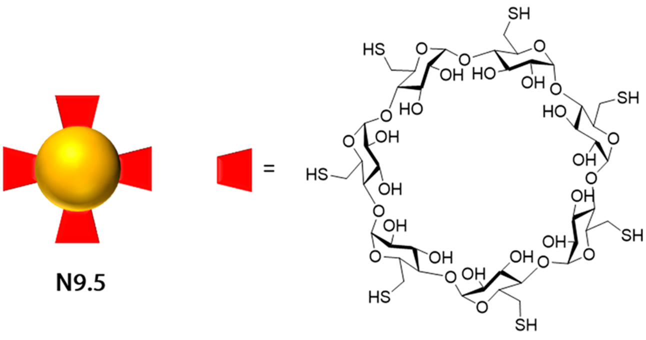

**N9.5**

**Figure 221.** Schematic representation of $\beta$-CD functionalized AuNPs (**N9.5**) used for colorimetric detection of the nonsteroidal anti-inflammatory drugs nabumetone in urine and wastewater samples at $\mu$M concentrations.

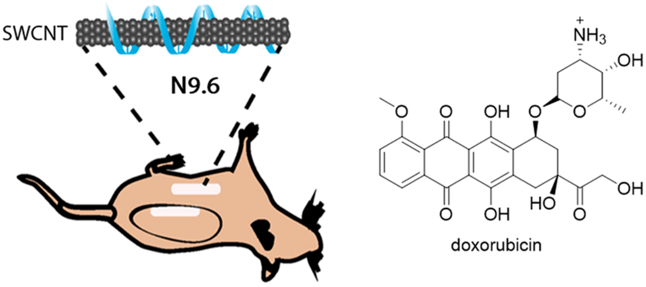

**Figure 222.** Subcutaneous implanted ssDNA functionalized SWCNTs (**N9.6**) allow for $\mu$M detection of doxorubicin. Reproduced with permission from ref 955. Copyright 2019 American Chemical Society.

concentrations in 20 mM HEPES buffer. However, the authors observed some cross-reactivity of **N9.6** with other DNA intercalators, *e.g.*, ethidium bromide or HOECHST 33258. Impressively, by immobilizing **N9.6** in a hydrogel matrix, the authors were able to prepare a nanosensor-based composite that can be implanted subcutaneously in mice. The authors demonstrated that the implanted composite produced a fluorescent response in mice 30 min after an intraperitoneal injection of doxorubicin (dose: 1 mL, 500 $\mu$M).

A molecularly imprinted polymer (MIP)-based sensing approach for the detection of the chemotherapeutic irinotecan at nM concentrations (LOD, 16 nM) in water containing 75% acetonitrile and in deproteinized human plasma was recently reported by Toffoli, Resmini, Berti, and coworkers (**N9.7** in Figure 223).[956] The MIP was prepared by radical polymerization of acrylamides in the presence of irinotecan as the binding pocket template. Specifically, the reaction mixture was composed of acrylamide (monomer), ethylene glycol dimethacrylate (crosslinker), and 7-acryloyloxy-coumarin (fluorescent dye). After completion of polymerization, the drug template was removed from the polymeric network by dialysis so that the final MIPs had "imprinted" free binding sites for subsequent irinotecan binding, which triggers a quenching of the fluorescence by energy transfer processes. The degree of fluorescence quenching was successfully correlated with the concentration of the target drug in spiked human serum samples that were beforehand deproteinized to avoid blocking of the MIP binding pockets.

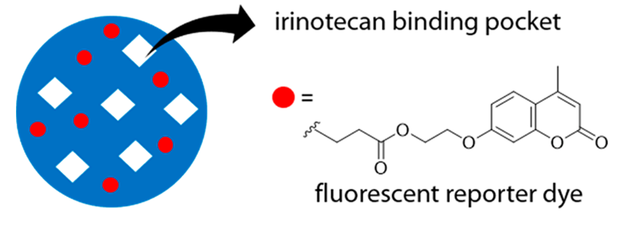

**N9.7**

**Figure 223.** A molecularly imprinted polymer (**N9.7**) offers binding pockets for irinotecan and thereby can be employed for its fluorescence-based nanomolar detection in aqueous-organic mixtures and in deproteinized plasma.

It transpires that many of the currently available macrocyclic hosts and chemosensors display particularly high binding affinities to certain drug classes, *e.g.*, adamantane-based drugs, amphetamine-related structures, and alkaloids. This observation has led many scientists (ourselves included) to direct the focus and efforts to those targets to which the currently available chemosensor classes and probes can efficiently and selectively bind. For the novice reader, this approach may cause an overenthusiastic impression of the current abilities. We are still far away from being able to design functional and selective chemosensors for most available drugs. Nevertheless, those drug classes that can be targeted by reported probes and chemosensors do have practical relevance, such that establishing optical assays in the praxis for these compounds could already have an important impact (see Table 33 for some concentration ranges found in individuals treated with these drugs). We are optimistic that additional classes of drugs can be (selectively) targeted, such that drug monitoring by chemosensors and related systems may find wide practical utility for diagnostics in the future.

**Table 33. Summary of Typical Concentrations of Some Synthetic Drugs and Phenylephrine in Biofluids**[a]

| concentration range | media | ref |
|---|---|---|
| | Codeine Analyte | |
| 2.0−15 nM | blood (infant, 0−1 years old) | 957 |
| | Procaine Analyte | |
| 8.9 $\mu$M | urine | 958 |
| | Phenylephrine Analyte | |
| 0.029−3.0 $\mu$M | blood | 959 |
| 30 nM | urine | 958 |
| | Famotidine Analyte | |
| 0.3−9.0 $\mu$M | blood | 960 |
| | Ranitidine Analyte | |
| 0.63−16.0 $\mu$M | blood | 960 |

[a] Urinary analyte concentrations were converted assuming a representative creatinine level of 10 mmol/L.

## 10. CHEMOSENSORS AND NANOSENSORS FOR XENOBIOTICS, TOXINS, AND HYDROCARBONS

Xenobiotics are defined as anthropogenic compounds that occur in living organisms or ecosystems and that have the potential to cause undesirable adverse effects.[961] As such, the term "xenobiotics" can be applied to a wide range of chemical compounds that can enter the environment *via* pollution. Xenobiotic aromatic compounds (*e.g.*, polyaromatic hydrocarbons) are produced, for example, during various industrial processes such as petroleum extraction, petroleum refining, or are formed during incomplete combustion. Figure 224 shows a

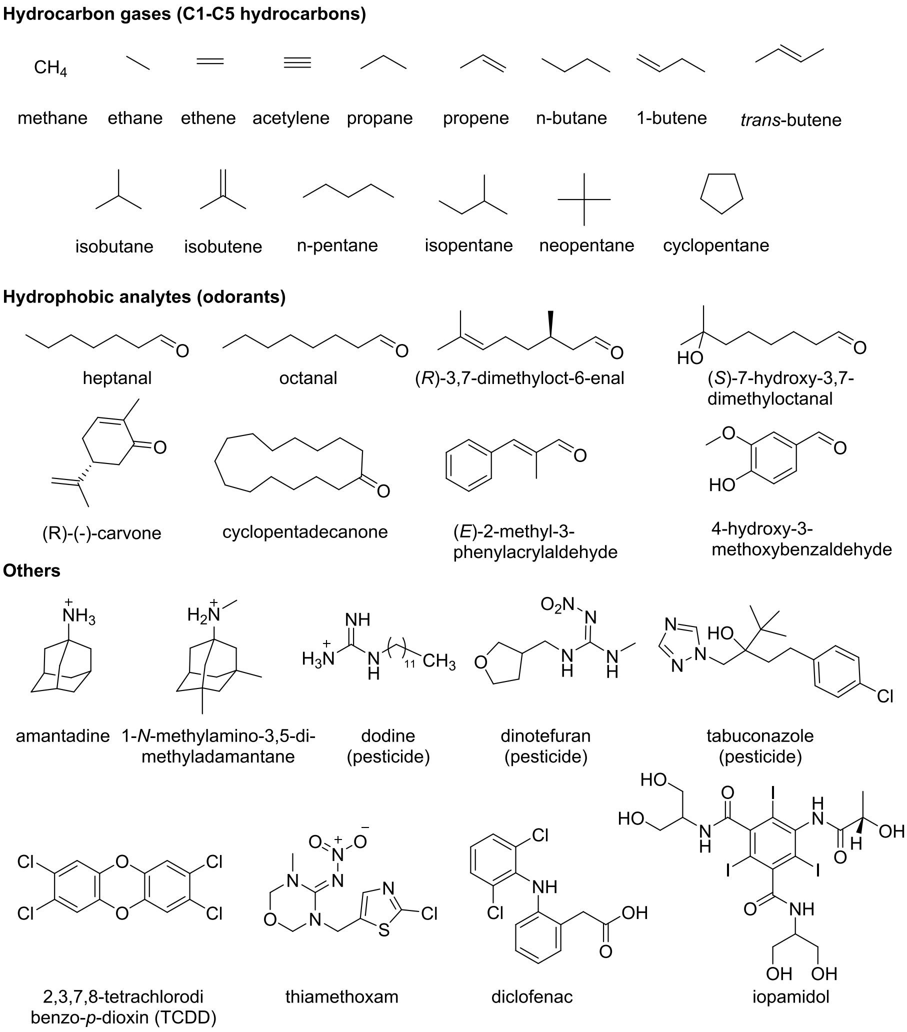

**Figure 224.** Chemical structures of selected xenobiotics.

selection of xenobiotics, toxins, and hydrocarbons. The "Seveso disaster" is a well-known case of man-made pollution in which a polychlorinated dibenzo-*p*-dioxin, namely 2,3,7,8-tetrachlorodibenzo-*p*-dioxin (TCDD), was released into the air and soil as a result of a factory explosion.[962] TCDD is a known human carcinogen and a potent endocrine disruptor that has a long half-life in humans due to its lipophilicity.[963,964] Common examples of man-made water pollution come from the textile, cosmetics, leather, food, pharmaceutical, paint, and paper industries. Many toxic dyes such as methylene blue, rhodamine B, methyl orange, congo red, methyl red, and crystal violet, used by these industries often end up, accidentally or not, in freshwater.[965] Compounds of pharmacological interest that are used deliberately for medical and surgical purposes such as drugs (*e.g.*, diclofenac) or contrast agents (*e.g.*, iopamidol) can be defined as xenobiotics, too, as these compounds enter the environment after use through excretion with urine or feces. Indeed, alarming studies indicate a worrying accumulation of xenobiotic substances in the environment and drinking water.[966−969]

Xenobiotic aromatic compounds are usually more hydrophobic (*e.g.*, polycyclic aromatic hydrocarbons) than other metabolites or naturally occurring substances and thus can often be readily targeted by artificial binders and chemosensors. Nevertheless, a practical scenario is the detection of trace amounts of xenobiotics in soil, waste-, or drinking water, which in turn places stringent sensitivity and accuracy requirements on the selected analytical detection method. For example, guideline maximum concentration levels for benzene (1 $\mu$g/L, 78 nM) and benzo[*a*]pyrene (0.01 $\mu$g/L, 0.04 nM) in drinking water are rather difficult to reach with currently available chemosensors and probes due to affinity limitations.[970] Furthermore, the certified detection of xenobiotics is already widely established and can be routinely carried out by specialized laboratories with powerful instrumental-analytical capabilities. Whether probes and chemosensors will have a real application scenario in this context remains an open question. However, in certain specialized niche applications, probes and chemosensors for xenobiotics may be of fundamental interest and potential practical utility, which is described in the following. The chemosensors and nanosensors discussed within this section are summarized in Table 34.

For instance, the Nau group demonstrated that hydrocarbon gases (*e.g.*, C1 to C5 hydrocarbons) can be detected at micromolar concentrations in water or 50 mM acetate buffer, pH 5.5, using a preassembled fluorescent host−dye complex formed from CB6 and a putrescine-anchored 1-naphtylamine-5-sulfonate indicator dye (**C10.1** in Figure 225a).[971] Purging aqueous solutions of **C10.1** with hydrocarbon gases resulted in

## Table 34. Summary of Chemo- and Nanosensors for Xenobiotics, Toxins, and Hydrocarbons

| chemosensor/ nanosensor | media | concentration range | ref |
|---|---|---|---|
| | Amantadine Analyte | | |
| **C10.2** | water, pH 4.0 | $\mu$M range | 972 |
| | 1-Amino-3,5-dimethyladamantane Analyte | | |
| **C10.2** | water, pH 4.0 | $\mu$M range | 972 |
| | Dodine Analyte | | |
| **C10.3** | $D_2O$ | mM range | 973 |
| | Cyclic Hydrocarbons Analyte | | |
| **C10.4** | water, pH 4.0; food samples | 0−400 $\mu$M | 974 |
| | Volatile Hydrocarbons Analyte | | |
| **C10.1** | aq. HCl solution, pH 3.0; 50 mM acetate buffer, pH 5.5 | $\mu$M range | 971 |
| | Odorants[a] (Small Hydrophobic Aldehydes and Ketones) Analyte | | |
| **N10.1** | 10 mM Tris buffer containing 107 mM NaCl, pH 7.4 | $\mu$M range | 975 |

[a]Analytes were dissolved in DMSO.

the displacement of the dye as evidenced by its reduced emission intensities (factor >2, see Figure 225b). In another example, Isaacs and co-workers have successfully employed the same indicator dye to monitor gas uptake by acyclic CB*n* derivatives, which were already described in section 2.3 (**C2.8** in Figure 50).[245]

The dye *N,N*-dimethylaminophenyltropylium perchlorate (DMAT) investigated by Nau, Pischel, and coworkers, is an interesting chromophoric indicator dye that displays strong color changes when bound inside hydrophobic cavities.[972] The macrocyclic hosts CB7 and CB8 (**C10.2** in Figure 226) were used in this assay in combination with DMAT as a chemosensor ensemble in water, pH 4.0, to distinguish terpenes (*e.g.*, geraniol or linalool) and adamantanes (*e.g.*, 1-amino-3,5-dimethyladamantane) from each. Because of the high and similar binding affinities of DMAT for both CB7 ($K_a$ = 2.1 × $10^7$ $M^{-1}$) and CB8 ($K_{a,\text{effective}}$ = 1.6 × $10^7$ $M^{-1}$; 1:2 complex formed) in water, the chemosensor ensemble **C10.2** can be used in the submicromolar concentration regime for the detection of strongly binding analytes. Because the fluorescence response of the chemosensor ensemble was only tested in deionized water, it remains to be seen if such systems can be applied in situations with potential interferents, *e.g.*, CB*n*-binding salts.[40]

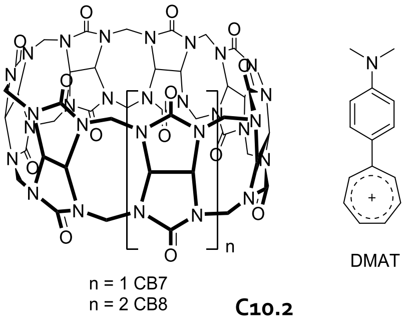

**Figure 226.** Chemical structures of the macrocyclic hosts CB7 and CB8 and the dye *N,N*-dimethylaminophenyltropylium perchlorate (DMAT).

The Mason group prepared a homoternary complex (CB8-based ABA chemosensor) from two $CF_3$-bearing $Ru^{II}$-complexes and CB8 that can be used for NMR-based detection of cyclic hydrocarbons in deuterated water (**C10.3**, in Figure 227).[973] Upon analyte binding, a ternary heterocomplex is formed and the resulting $^{19}F$ NMR "fingerprints" are analytically indicative. The binding affinities for cyclic hydrocarbons were given relative to benzene: $K_{\text{rel,cyclohexane}}$ = 160, $K_{\text{rel,cyclooctane}}$ = 130, $K_{\text{rel,}\mathit{cis}\text{-decalin}}$ = 8700, $K_{\text{rel,}\mathit{trans}\text{-decalin}}$ = 7500). CH−$\pi$ interactions and differences in hydrocarbon solvation were proposed to significantly contribute to the binding process. Because the binding studies were carried out *via* NMR experiments, the applicability of this chemosensor for optical detection remains an open question awaiting future analysis.

Very recently, an indicator displacement assay using a 1:2 cucurbit[10]uril-acridine complex (**C10.4** in Figure 228) was developed by Xiao, Liu, and coworkers for the detection of the pesticide dodine (LOD, 1.8 $\mu$M) in water and food samples.[974] In the absence of dodine, the emission of acridine is strongly quenched, whereas in the presence of the analyte, emission turn-on was observed as acridine is displaced from the macrocycle. Beside acridine, other 19 commonly used pesticides (dinotefuran, oxadixyl, penconazole, thiamethoxam, carbaryl, flutriafol, acetamiprid, ethiofencarb, flusilazole, pyroquilon, pymetrozine, triadimefon, azaconazole, tricyclazole, metalaxyl, triadimenol isomer A, paraquat, pyrimethanil, and tebuconazole) were also detected when added in a 10-fold concentration excess to solutions of **C10.4**. In addition, the

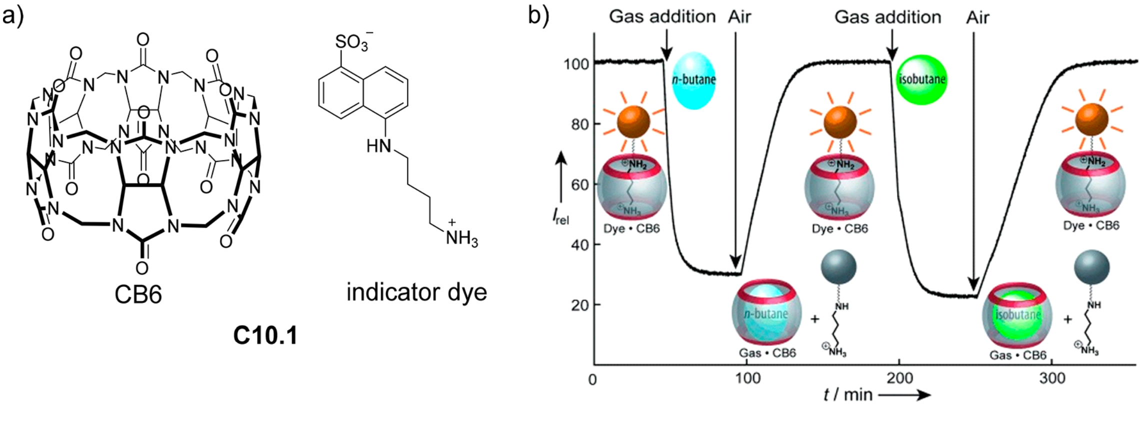

**Figure 225.** (a) Chemical structures of CB6 and the indicator dye, which form the chemosensor ensemble for the detection of hydrocarbon gases (**C10.1**). (b) Schematic representation of the fluorescence-based detection on *n*-butane and isobutane in water. The traces refer to the sequential analyte uptake and release. Reproduced with permission from ref 971. Copyright 2011 Wiley-VCH.

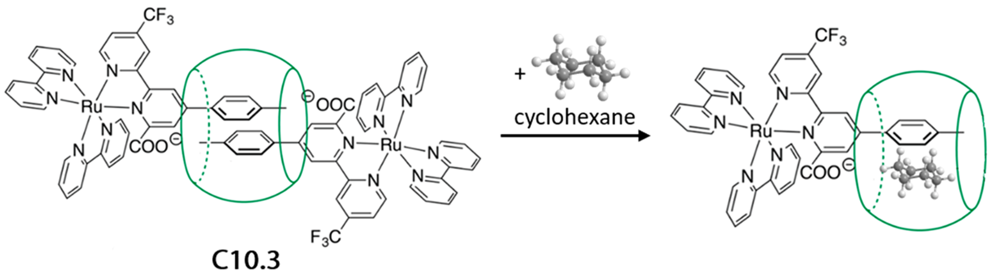

**C10.3**

**Figure 227.** Schematic representation of the homoternary complex **C10.3**, which binds cyclic hydrocarbons in water allowing for NMR-based detection of such analytes in $D_2O$. Reproduced with permission from ref 973. Copyright 2017 American Chemical Society.

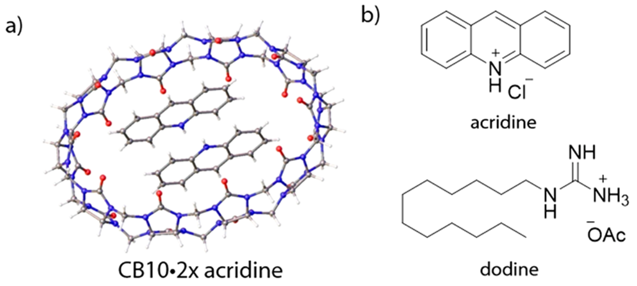

**C10.4**

**Figure 228.** (a) Crystal structure of the CB10−acridine chemosensor ensemble for IDA-based detection of dodine at μM concentration in water, pH 4.0. Reproduced with permission from ref 974. Copyright 2002 American Chemical Society. (b) Chemical structure of dodine acetate.

authors demonstrated the ability of their chemosensor to visualize pesticide residues in samples of plant leaves and beans that had previously been exposed to the pesticide.

Hydrophobic analytes are notoriously difficult to detect with structures composed of bilipid layers because they simply tend to accumulate in the hydrophobic membrane, making them inaccessible for detection by probes or chemosensors. However, the Matile group showed that this problem can be circumvented by using synthetic unilamellar vesicles (**N10.1**) in combination with a polyion-counterion transport system in 10 mM Tris-buffer containing 107 mM NaCl, pH 7.4. Their assay allows for fluorescence-based detection of common hydrophobic odorants (typically aldehydes and ketones) at μM concentrations.[975,976] As shown in Figure 229, the vesicles used in this example were loaded with the anionic reporter dye (8-hydroxy-1,3,6-pyrenetrisulfonate) and the cationic fluorescence quencher (*p*-xylene-bis-pyridinium bromide), resulting in an overall low fluorescence intensity of the system. However, when the polyion-counterion transport system (cationic amphiphiles complexes with calf-thymus DNA) was activated by a chemical reaction of cationic peptidic hydrazides (the amphiphile precursor) with aldehyde- functional odorant (the analyte), the transporter assisted translocation of the fluorescent quencher out of the vesicle, and, in turn, the fluorescence of the reporter dye increases. The authors showed that overlap-free detection of many aldehyde/ketone-functional odorants is possible by determining dose−response curves for individual analytes with a large number of different reactive counterions in combination with hierarchical clustering and principal component analysis (PCA).

We are aware that there are many reports on probes and chemosensors dealing with the detection of organic toxins and xenobiotics, such as pesticides. Nevertheless, we have only presented a few example cases in this review because we feel that their practical utility remains too limited unless it becomes clear how these assays can be used for the detection of these analytes at trace levels, as for instance required for drinking, fresh, and wastewater analysis. Moreover, selectivity must be ensured such that xenobiotics can be detected in the presence

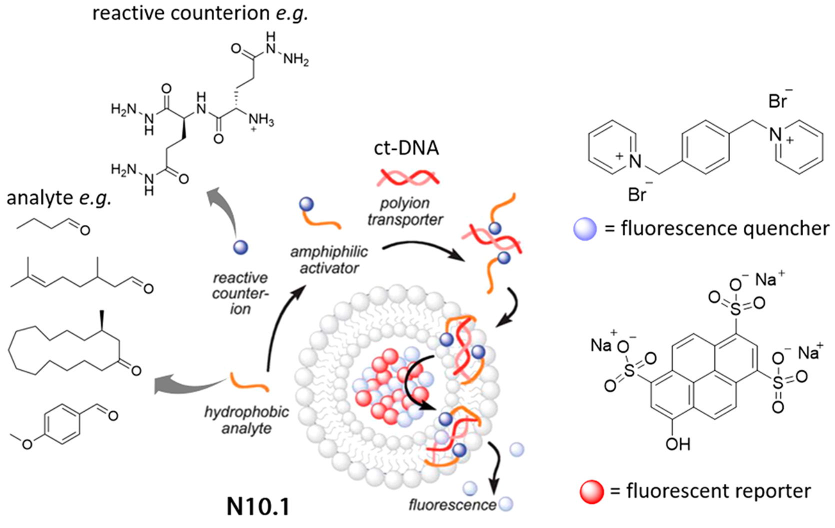

**Figure 229.** Schematic representation of the fluorescence-based detection mechanism for odorants using dye-loaded unilamellar vesicles (**N10.1**) and the polyion-counterion transport system. Adapted with permission from ref 975. Copyright 2011 The Royal Society of Chemistry.

**Table 35. Summary of Molecular Probes and Chemosensors for Metal Cations (LOD, Limit of Detection)**

| probe/chemosensor | media | concentration range | ref |
|---|---|---|---|
| Aluminium ($Al^{3+}$) Analyte | | | |
| **C11.16**[a] | 2% DMSO and 5% MeCN in water; cells | μM range; LOD, 22 nM | 1047 |
| Barium ($Ba^{2+}$) Analyte | | | |
| **C11.11** | 10 mM Tris buffer, pH 10.2 | μM range | 1031 |
| Cadmium ($Cd^{2+}$) Analyte | | | |
| **P11.1** | 100 mM $NaClO_4$ aq | LOD, 1 nM | 1010 |
| **C11.26** | 10 mM $Na_2HPO_4$–$NaH_2PO_4$ buffer, pH 6.5 | μM range | 1053 |
| Calcium ($Ca^{2+}$) Analyte | | | |
| **C11.12** | in cells and biological tissues | μM range | 1035,1038,1039 |
| Cesium ($Cs^{+}$) Analyte | | | |
| **C11.8**[b] | 50 mM MES buffer, pH 7.0 | 0–100 μM (linear range); LOD, 3.7 μM | 1029 |
| Iron ($Fe^{2+}$) Analyte | | | |
| **P11.2** | 1% THF in water | μM range | 1011 |
| Iron ($Fe^{3+}$) Analyte | | | |
| **P11.3** | 50% EtOH in water | 15–210 μM | 1012 |
| **P11.4** | 20 mM HEPES buffer, pH 7.2 | 0–1.2 mM | 1013 |
| **C11.27** | aq solution | 20–500 μM; LOD, 0.2 μM | 1056 |
| Magnesium ($Mg^{2+}$) Analyte | | | |
| **C11.9** | DPBS buffer[c], pH 7.0 | 0–1.0 mM | 1030 |
| **C11.10** | DPBS buffer[c], pH 7.0 | 0–1.0 mM | 1030 |
| Mercury ($Hg^{2+}$) Analyte | | | |
| **P11.5** | 20 mM HEPES buffer, pH 7.0 | μM range in buffer; LOD, 60 nM in buffer | 1014 |
| | fish tissue (meat) | 0.5–40 μM in tissue | |
| **P11.6** | 20 mM HEPES buffer, pH 7.0 | 0–6.7 μM | 1016 |
| | fish tissue (meat) | 0.03–13 ppm | |
| **P11.7** | MeOH/water mixtures | LOD, 110 ± 16 nM | 1017 |
| | drinking water | ∼4.4 nM | |
| | human blood serum; milk | ∼110 nM | |
| **C11.29** | 33% MeCN in water | 0–125 μM (linear range); LOD, 0.37 μM | 1060 |
| Potassium ($K^{+}$) Analyte | | | |
| **C11.1** | Tris-HEPES buffer, pH 7.4; serum | 0–200 mM | 1019 |
| **C11.5** | 5 mM HEPES, pH 7.0 | 0–200 mM | 1024 |
| | brain cortex in mice | 0–40.0 mM | |
| **C11.6** | HEPES buffer, pH 7.0 | 0–200 mM | 1026 |
| **C11.7** | 10 mM HEPES buffer, pH 7.2 | up to 1.6 M | 1028 |
| Silver ($Ag^{+}$) Analyte | | | |
| **C11.28** | 17% THF in water | 0–75 μM (linear range); LOD, 0.34 μM | 1060 |
| Sodium ($Na^{+}$) Analyte | | | |
| **C11.2** | HEPES buffer, pH 7.4 | 100–180 mM | 1020 |
| **C11.3** | 50% MeOH in 10 mM Tris buffer, pH 7.5; blood | 100–300 mM in buffer <145 mM in blood | 1022 |
| **C11.4** | water | 1–1000 mM | 1023 |
| Zinc ($Zn^{2+}$) Analyte | | | |
| **P11.2** | 1% THF in water | μM range | 1011 |
| **C11.13** | 100 mM KCl in 50 mM PIPES buffer, pH 7.0 | LOD, ∼0.1 nM | 1042 |
| **C11.14** | 100 mM KCl in 50 mM PIPES buffer, pH 7.0 | 0–1.0 mM | 1043 |
| **C11.15**[d] | 5% DMSO in 500 mM HEPES buffer, pH 7.4 | μM range | 1046 |
| (**C11.17**–**C11.25**) chemosensor array[e] | water | 0–500 μM | 1048 |
| **C11.26** | 10 mM phosphate buffer, pH 6.5 | nM range | 1053 |

[a] Listed cations did not interfere: $Li^+$, $Na^+$, $K^+$, $Ag^+$, $Mg^{2+}$, $Ca^{2+}$, $Ba^{2+}$, $Pb^{2+}$, $Fe^{2+}$, $Ni^{2+}$, $Cu^{2+}$, $Zn^{2+}$, $Hg^{2+}$, $Fe^{3+}$, and $Cr^{3+}$. [b] Binds also $K^+$ but much weaker than $Cs^+$. [c] 1.4 mM PBS without $Ca^{2+}$ and $Mg^{2+}$ salts but contains 136 mM NaCl and 270 μM KCl. [d] $Cd^{2+}$, $Pb^{2+}$, and $Hg^{2+}$ give distinguishable emission signals. [e] Chemosensor array can distinguish cationic analytes, *e.g.*, $Ca^{2+}$, $Cd^{2+}$, and $Al^{3+}$.

of a large concentration excess of naturally occurring substances, *e.g.*, metabolites, when such assays should be applied for diagnostic purposes.

## 11. METAL CATIONS

Although in this review we focus on the state of the art in the development of molecular probes and chemosensors for the detection of small biorelevant molecules in aqueous media and biofluids, we will nevertheless briefly review some of the successes that have been achieved in the development of such sensors for metal cations. In general, two categories of metal cations can be distinguished for the human body, namely essential and nonessential metal cations. About 10 metal cations have been classified to be essential for humans. Of these, the alkali and alkaline earth metal cations $Na^+$, $K^+$, $Ca^{2+}$, and $Mg^{2+}$ account together for about 99% of the metal ion

Table 36. Summary of Typical Concentrations of Metal Cations in Environment and Biofluids[a]

| concentration range | media | ref |
|---|---|---|
| Aluminium (Al$^{3+}$) Analyte | | |
| 19.0–482 nM | blood (> 18 years old) | 642 |
| 0.0–1.26 $\mu$mol/mmol creatinine = 0–12.6 $\mu$M | urine | 50 |
| 157–299 $\mu$M | saliva | 62 |
| Barium (Ba$^{2+}$) Analyte | | |
| 4.5–12.4 nM | blood (>18 years old) | 1062 |
| 0.1–65.5 nmol/mmol creatinine = 1.0–655 $\mu$M | urine | 50 |
| 80–182 nM | saliva | 62 |
| Calcium (Ca$^{2+}$) Analyte | | |
| 1.40–1.68 mM | blood (>45 years old) | 1063 |
| 2.12–2.70 mM | blood (1–13 years old) | 1064 |
| 17.0–520 $\mu$mol/mmol creatinine = 0.17–5.20 mM | urine | 50 |
| 0.29–1.10 mM | saliva | 62 |
| Cadmium (Cd$^{2+}$) Analyte | | |
| 1.80–11.0 nM | blood (>18 years old) | 642 |
| 0–5.2 nM | blood (>45 years old) | 1063 |
| 0.2–1.0 nmol/mmol creatinine = 2.0–10 nM | urine | 50 |
| 82.0–338 pM | saliva | 1065 |
| Cesium (Cs$^{+}$) Analyte | | |
| 4.1–7.1 nM | blood | 642 |
| 0.5–11.0 nmol/mmol creatinine = 5.0–110 nM | urine | 50 |
| 10–24 nM | saliva | 62 |
| Iron (Fe$^{2+}$) Analyte | | |
| 8.6–11.0 mM | blood | 1062 |
| 30.0–458 nmol/mmol creatinine = 0.03–4.58 $\mu$M | urine | 50 |
| 2.9–8.4 $\mu$M | saliva | 62 |
| Iron (Fe$^{3+}$) Analyte | | |
| 2.7–40.3 $\mu$M | blood | 1066 |
| 20.0–830 nmol/mmol creatinine = 0.2–8.3 $\mu$M | urine (newborn 0–30 days old) | 1067 |
| Magnesium (Mg$^{2+}$) Analyte | | |
| 620–1080 $\mu$M | blood (1–13 years old) | 1064 |
| 693–741 $\mu$M | blood (> 45 years old) | 1063 |
| 42.0–1190 $\mu$mol/mmol creatinine = 0.42–11.9 $\mu$M | urine | 50 |
| 150–732 mM | saliva | 62 |
| Mercury (Hg$^{2+}$) Analyte | | |
| 6.1–16.1 nM | blood (>18 years old) | 642 |
| 3.4–10.6 nM | blood (>45 years old) | 1063 |
| 0–3.8 nmol/mmol creatinine = 0–38 nM | urine | 1068 |
| 0.5 $\mu$g/L; 2.5 nM | drinking water | 1069 |
| Potassium (K$^{+}$) Analyte | | |
| 4.1–5.1 mM | blood (1–35 months) | 642 |
| 3.6–4.8 mM | blood (>18 years old) | 642 |
| 0.5–8.0 mmol/mmol creatinine = 5.3–80.8 mM | urine | 50 |
| 11.2–26.8 mM | saliva | 62 |
| Sodium (Na$^{+}$) Analyte | | |
| 138–150 mM | blood, newborn (0–30 days old) | 642 |
| 137–141 mM | blood, infant (0–1 years old) | 642 |
| 138–146 mM | blood, adult (>18 years old) | 642 |
| 1.80–37.0 mmol/mmol creatinine = 18.0–370 mM | urine | 50 |
| 5.4–19.2 mM | saliva | 62 |
| Zinc (Zn$^{2+}$) Analyte | | |
| 10.3–14.5 $\mu$M | blood (>45 years old) | 1063 |
| 58.0–948 nmol/mmol creatinine = 0.58–9.48 $\mu$M | urine | 50 |
| 684–800 nM | saliva | 62 |

[a] Urinary analyte concentrations were converted assuming a representative creatinine level of 10 mmol/L.

content in the human body. The other five essential metal cations are those of manganese, iron, cobalt, copper, zinc, and molybdenum. Most nonessential metal cations, *e.g.*, mercury, lead, cadmium, or arsenic, are considered toxic.[977] Exposure to nonessential and toxic metal cations can have several origins. First, some of the contrast agents and drugs used for the diagnosis and treatment of disease are complexes of nonessential transition metal cations. For example, $^{89}$Zr and $^{68}$Ga cations are common metals in contrast agents[978,979] for positron emission tomography (PET), Gd$^{\mathrm{III}}$ complexes are used as contrast agents for magnetic resonance imaging (MRI), and Pt$^{\mathrm{II}}$-complexes are well-known cancer drugs.[980] On the other hand, a typical source of exposure to toxic metal cations comes from environmental pollution, which leads to inhalation and ingestion of these cations. While exposure from medically relevant contrast agents and drugs is still somewhat acceptable because the doses administered are generally safe and treatment with such agents contributes to an overall improved treatment of diseases, bioaccumulation of toxic cations from environmental pollution is a serious problem with disastrous health consequences. Mercury poisoning, for example, manifests itself in typical neurological and behavioral disorders. The mode of action by which mercury causes severe toxicity is due to its irreversible inhibition of enzymes by binding to sulfhydryl, phosphoryl, carboxyl, amide, and amine groups. Cadmium is commonly used in industry, *e.g.*, as an anticorrosion agent, as a stabilizer in PVC products, as a color pigment, as a neutron absorber in nuclear power plants, and in the production of nickel–cadmium batteries. There are three possible routes of cadmium uptake: gastrointestinal, pulmonary, and dermal, leading to various diseases in acute exposure, such as renal failure, bone damage (Itai–Itai disease),[981] respiratory distress, pulmonary edema, and destruction of mucous membranes by cadmium-induced pneumonitis.[982] In addition, cadmium can act as a metalloestrogen and as an endocrine disruptor on reproductive tissues and fetal development in mammals, including humans.[983] Aluminum ions are suspected of causing adverse health effects in humans, *e.g.*, as a potential cause of tumors and neurogenerative diseases,[984] and therefore the detection and imaging of Al$^{3+}$ cations in living organism has gained importance.

Despite the important functions of essential metal cations, abnormal concentrations of these ions in the human body are known to cause or be associated with disease and abnormal health conditions. Sodium and potassium are found in all known biological systems and generally function as electrolytes inside and outside of cells. Among alkali metal cations, sodium cations are the most abundant species in the extracellular fluid and account for about 90% of inorganic cations in plasma (Na$^{+}$ concentration in serum of healthy individuals is around 136–

145 mM).[985,986] The kidney is the major organ regulating extracellular $Na^+$ concentrations in the body.[985] Hyponatremia is a condition that results from decreased plasma $Na^+$ concentration, causing symptoms such as nausea, general weakness, and mental confusion at levels below 120 mM and confusion and seizures at levels below 105 mM.[987] On the contrary, the increased $Na^+$ concentration leads to hypernatremia with $Na^+$ concentrations in serum above 150 mM.[988] Potassium ions are the most abundant intracellular alkali metal cations and a major component in the generation of the cell's action potential with their intracellular concentration regulated by ion transporters (potassium ion channels). Known conditions associated with abnormal $K^+$ concentrations caused by altered potassium intake, excretion, or transcellular shifts are hypokalemia (plasma $K^+$ level <3.5 mM) or hyperkalemia (plasma K+ level <5.0 mM).[989,990] Typical symptoms of hypokalemia include muscle weakness, irritability, and paralysis and commonly occur in cancer patients.[991] Hyperkalemia includes symptoms such as mental confusion, weakness, tingling, and flaccid paralysis of the extremities. The alkaline earth metal cation $Ca^{2+}$ has vital functions in the human body, *e.g.*, it is involved in processes of skeletal mineralization, signal transmission, muscle contraction, and blood clotting.[992,993] Calcium deficiency, referred to as hypocalcemia, in which serum $Ca^{2+}$ levels are below 2.2 mM,[992] is manifested by the development of tetany associated with numbness and tingling in the mouth and fingertips as well as painful aches and muscle spasms.[994] $Mg^{2+}$ deficiency is associated with a number of diseases, including stroke, brain injury, Parkinson's disease, and some other brain pathologies such as neurosis, stress, and Alzheimer's disease.[995] Copper cations are essential transition metal cations for the function of enzyme activity. For example, copper is an essential component of the catalytic center of cytochrome-c oxidase, which catalyzes the reduction of molecular oxygen to water, a key step in the mitochondrial respiratory chain.[996] Abnormal copper levels are associated with the development of liver disorders, neurodegenerative changes, and other diseases.[997] For example, copper and other metal cations such as iron and zinc have been shown to play a critical role in the pathogenesis of Alzheimer's disease (AD).[998−1000] Metal cations and their metabolism are also involved in many other diseases, such as Parkinson's disease,[1001,1002] Friedreich's ataxia,[1003,1004] transfusion-related iron overload,[1005] and Wilson's diseases.[1006] The metabolism of metal cations and its relationship to disease is a broad topic that is beyond the scope of our work. In general, the detection and monitoring of metal cations in body fluids such as urine, plasma, and sweat are important measures in clinical diagnosis, and therefore the development of low-cost, easy-to-use probes and sensors is attractive to chemists.

All discussed molecular probes and chemosensors are summarized in Tables 35, and 36 lists the typical concentration levels of metal cations that are considered in this section.

## 11.1. Molecular Probes and Chemosensors for Metal Cations

Many successful probes and chemosensors for metal cations are already available and have even achieved real diagnostic utility, *e.g.*, for real-time monitoring of concentrations of sodium and potassium in the blood of clinic patients.[1007,1008] Likewise, commercially available probes and chemosensors for $Na^+$, $K^+$, and $Ca^{2+}$ are frequently used by biologists to monitor cellular processes, *e.g.*, signaling events.[1009] These target analytes have in common that they occur endogenously in the millimolar concentration range, which have significantly lower sensitivity requirements for the probes and chemosensors than, for example, the detection of neurotransmitters, hormones, or even aromatic xenobiotics. Molecular probes and chemosensors for the detection of trace metals or xenobiotic metals, *e.g.*, $Fe^{2+/3+}$, $Ni^{2+}$, $Cu^{+/2+}$, $Cd^{2+}$, $Hg^{+/2+}$, and $Pb^{2+}$, are also common. These metals have serious adverse effects on plant, animal, and human health, and therefore detection and quantification of their presence in the environment is well justified. While ("soft" or highly charged "hard") transition metal ions are chemically easier to attack, probes and chemosensors for the detection of toxic trace metals must be sensitive enough to operate in the (ultra) low concentration range. For example, the current limit for lead in drinking water is 10 $\mu$g/L (< 50 nM) and for cadmium, and mercury it is only 3 $\mu$g/L (<30 nM) and 1 $\mu$g/L (<0.5 nM), respectively.[970]

In 2008, Thummel, Hancock, and coworkers demonstrated that 2,9-di-(pyrid-2-yl)-1,10-phenanthroline (DPP, **P11.1** in Figure 230) has a high affinity (log $K_{a,1}$ = 12.2) and a good selectivity for $Cd^{2+}$ ions in the presence of other monovalent and divalent cations.[1010] The ligand exhibited a strong chelation-enhanced fluorescence (CHEF) upon $Cd^{2+}$ binding and target analyte concentrations down to $10^{-9}$ M were detectable in 100 mM $NaClO_4$ aq solutions. In comparison, millimolar and molar concentrations of $Ca^{2+}$ and $Na^+$, respectively, were needed to achieve a similar effect. Additionally, the probe **P11.1** also complexes, but weaker, $Zn^{2+}$ (log $K_{a,1}$ = 8.7), $Pb^{2+}$ (log $K_{a,1}$ = 7.8), $Ni^{2+}$ (log $K_{a,1}$ = 6.8), and $Gd^{3+}$ (log $K_{a,1}$ = 5.1).

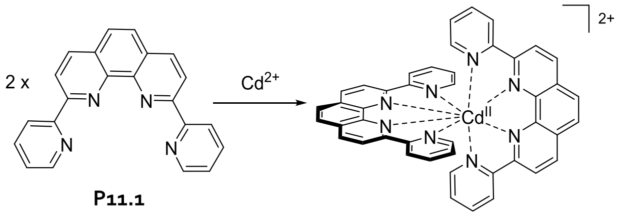

**Figure 230.** Schematic representation of the $Cd^{2+}$ binding probe 2,9-di-(pyrid-2-yl)-1,10-phenanthroline (**P11.1**) for nanomolar $Cd^{2+}$ detection in aqueous solutions of 100 mM $NaClO_4$.

Terpyridine-substituted tetraphenylethylenes were used by Tang and co-workers in combination with a library of divalent and trivalent metal cations (**P11.2** in Figure 231) for fluorescence-based detection of $Zn^{2+}$ at $\mu$M concentrations in 1% THF in water.[1011] The binding of $Zn^{2+}$ resulted in a fluorescence emission enhancement of **P11.2** concomitant with a bathochromic shift of the signal. The metal ions $Na^+$, $K^+$, and $Ag^+$ only weakly quenched molecular probe **P11.2**, whereas $Fe^{2+}$, $Co^{2+}$, $Ni^{2+}$, $Ru^{3+}$, and $Rh^{3+}$ were efficient fluorescence quencher. Interestingly, no colorimetric response was observed in the presence of $Fe^{3+}$, consistent with the proposed signal transduction mechanism, which arises from a combination of the metal ion binding event and subsequent structure/size changes of the nanoaggregates formed by **P11.2**. In contrast, Shah and coworkers found that an amide derivative of 1,10-phenanthroline (**P11.3** in Figure 231) gives a chromophoric response to $Fe^{3+}$ at micromolar concentrations in water containing 50% EtOH at pH 6.2.[1012] Furthermore, Liu and coworkers reported a coumarin-based probe (**P11.4** in Figure 231) for $Fe^{3+}$ detection at mM concentrations in 20

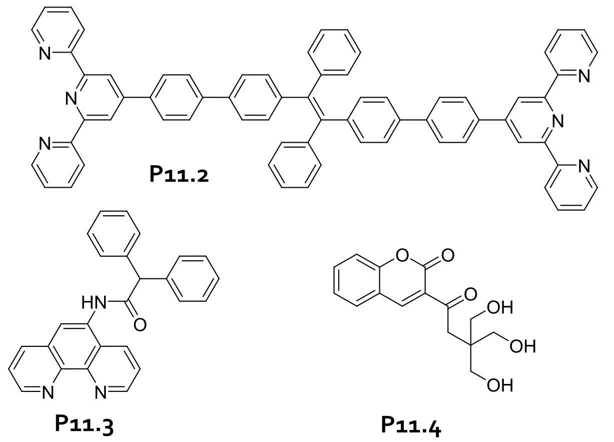
**P11.2** **P11.3** **P11.4**

**Figure 231.** Chemical structures of a terpyridine-substituted and tetraphenylethylene-based probe (**P11.2**) for $Zn^{2+}$ detection. The 1,10-phenanthroline-based probe (**P11.3**) and the coumarin-based probe (**P11.4**) can be used for the detection of $Fe^{3+}$ in aqueous solutions.

mM HEPES buffer, pH 7.2.[1013] The effect of $Fe^{2+}$ on **P11.4** was not tested.

Chang and coworkers reported a fluorescein-based emission turn-on probe (**P11.5** in Figure 232), which allowed for the selective detection of $Hg^{2+}$ over other metal cations (*e.g.*, $Zn^{2+}$, $Pb^{2+}$, $Cd^{2+}$ and $Cu^{2+}$) in 20 mM HEPES buffer, pH 7.0, at $\mu$M concentrations.[1014] Mercury levels in the analytically relevant concentration range (0.1−8.0 ppm, corresponding to 0.5 $\mu$M to 40 $\mu$M) were shown to be detectable in fish tissue samples, demonstrating that **P11.5** was able to distinguish safe and toxic (>0.55 ppm, U.S. Environmental Protection Agency (EPA) standard in 2005) levels of mercury in edibles.[1015] Two years later, the authors prepared a fluorescein-based probe (**P11.6** in Figure 232) in which the rotational modes of the probe are restricted by the presence of an additional methyl group.[1016] As a result, a high emission quantum yield of 0.72 in the presence of $Hg^{2+}$ was observed. Rao and coworkers reported the use of an anthracenylimino glucosyl conjugate, which formed a 2:1 complex (**P11.7** in Figure 232) with $Hg^{2+}$ ions in MeOH/water mixtures. The authors demonstrated that **P11.7** can be used for fluorescence-based detection of $Hg^{2+}$ in blood serum and milk, fulfilling EPA detection standards.[1017]

Frequently, dyes can form nonfluorescent aggregates in aqueous media, which obstructs their use as probes. Supramolecular host−guest chemistry can be employed to overcome such obstacles. Pang and coworkers reported the assembly of squaraine dye with cucurbit[8]uril as 1:1 complex ($K_a = 2.4 \times 10^5\ M^{-1}$ in water) that bound two equivalents of $Hg^{2+}$, forming a ternary complex ($K_a = 4.6 \times 10^{10}\ M^{-2}$) in water.[1018] Upon $Hg^{2+}$ binding, the emission of the CB8−squaraine complex was strongly quenched, allowing for the detection of $Hg^{2+}$ in the micromolar concentration range.

In 2003, He and coworkers described an immobilizable, visible light emission turn-on chemosensor (**C11.1** in Figure 233) for the detection of extracellular potassium levels in Tris-HEPES buffer, pH 7.4, serum, or whole blood, which was adopted and brought into clinical use by Roche.[1019] The chemosensor responded rapidly and reversibly to changes in potassium concentrations (mM range) typical for whole blood samples. Sodium interference was found to be minor, while no interference was caused by physiological pH or the presence of $Ca^{2+}$. In the same year, the He group reported a chemosensor (**C11.2** in Figure 233) for the detection of $Na^+$ in HEPES buffer, pH 7.4, in serum and whole blood samples that was operational in the physiological concentration range (120−160 mM).[1020] Also, this chemosensor was introduced into clinical practice by Roche and mainly differs from chemosensor **C11.1** in its ionophore moiety. The mechanism of signal generation for both chemosensors is based on the interruption of the PET from the cryptand moiety to the dye upon binding of a metal ion.[4301021] It is worth noting that two years earlier, the Gunnlaugsson group reported a chromophoric azobenzene-based chemosensor (**C11.3** in Figure 233) that has the required affinity for $Na^+$ over other cations in both 10 mM Tris buffer, pH 7.5, containing 50% MeOH and importantly also in blood samples.[1022] More recently, a crown-ether binding motif (**C11.4** in Figure 233) for $Na^+$ was used by Wipf and coworkers for selective sodium sensing (1−1000 mM in water) in combination with gold-coated silicon nanowire field effect transistors.[1023]

In 2005, the Verkman group designed and evaluated a water-soluble and cell-membrane-impermeable chemosensor for $K^+$, consisting of triazacryptands coupled to a 3,6-bis-(dimethylamino)xanthylium fluorophore (**C11.5** in Figure 234).[1024] An up to 14-fold increase in fluorescence of **C11.5** was observed in the presence of $K^+$ ions (0−50 mM) in 5 mM HEPES buffer, pH 7.0, which was attributed to a decreased PET quenching due to metal ion binding. The chemosensor showed high $K^+$-to-$Na^+$ selectivity (ratio >30) and rapid responses (<1 ms) to $K^+$ concentration changes and has therefore been successfully used for dynamic $K^+$ imaging in the cerebral cortex of mice. Later, a cell-based fluorescence assay for $K^+$ transport across cell membranes was developed in which the chemosensor was bound to dextran polymers.[1025] The same group also reported a slightly modified ionophore design (**C11.6** in Figure 234) that further increased the selectivity for $K^+$ over other alkali salts (especially $Cs^+$ and $Rb^+$) in HEPES buffer, pH 7.0.[1026] However, the abovementioned ionophores are quickly saturated by intracellular potassium concentrations (∼150 mM)[1027] due to their high binding affinity to $K^+$ and thus cannot respond to dynamic concentration changes in

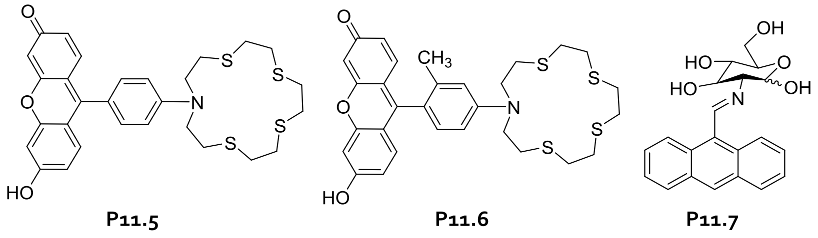
**P11.5** **P11.6** **P11.7**

**Figure 232.** Chemical structures of the probes **P11.5**−**P11.7** used for the detection of $Hg^{2+}$.

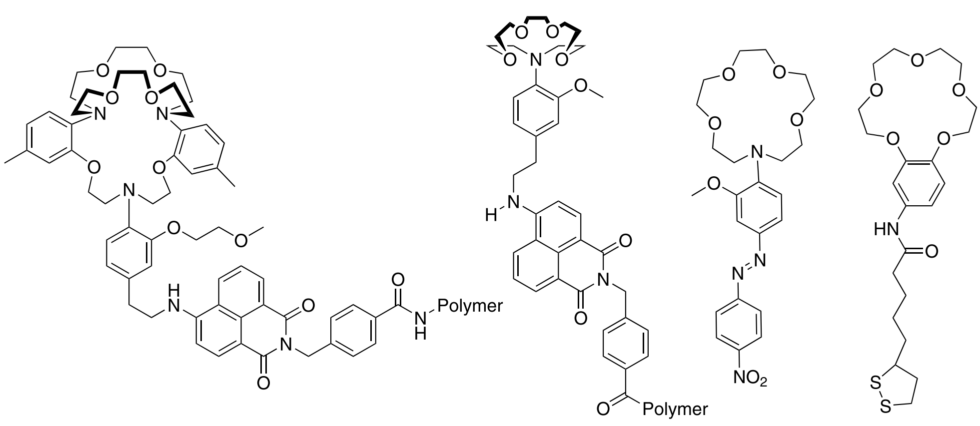

**C11.1** **C11.2** **C11.3** **C11.4**

**Figure 233.** Chemical structures of the chemosensors **C11.1**−**C11.4**.

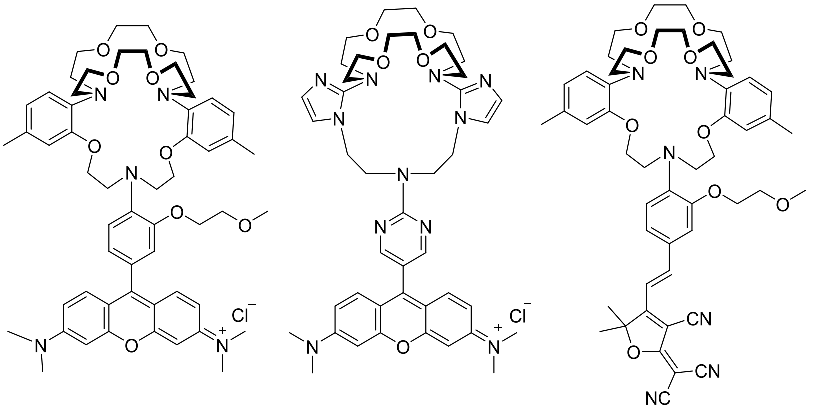

**C11.5** **C11.6** **C11.7**

**Figure 234.** Chemical structures of the chemosensors **C11.5**−**C11.7**.

cells. The "obvious" attempt to use ionophores with lower binding affinities, *e.g.*, crown ethers, would cause detrimental reduction of the cation selectivity by the chemosensor. Tian and coworkers overcame this problem by maintaining a cryptand-like ionophore structure (ensuring high binding selectivity for $K^+$), whose affinity was reduced by the use of a strong electron-withdrawing group in combination with an electron-donating group (**C11.7** in Figure 234).[1028] As a consequence of the strong delocalization of electrons in the fluorophore, the binding strength of the ionophore for cations decreased significantly. This new chemosensor responded to $K^+$ over a wide concentration range up to 1.6 M in 10 mM HEPES buffer, pH 7.2, and was shown to be suitable for the detection and imaging of $K^+$ levels in living cells.

There are comparatively fewer reports for the detection of $Cs^+$, which is understandable given its lesser biological significance. One representative system for micromolar $Cs^+$ detection in 50 mM MES buffer, pH 7.0, was introduced by Leray, Valeur, and coworkers (**C11.8** in Figure 235).[1029] The water-soluble fluorescence turn-on chemosensor is based on sulfonated calix[4]arene-bis(crown-6-ether) ionophore incorporating two coumarin reporter dyes. The chemosensor is highly selective for $Cs^+$ (log $K_a$ = 4.1 for the 1:1 complex and log $K_a$ = 3.82 for the 2:1 complex) over $K^+$ (log $K_a$ = 1.71 for the 1:1 complex) and other cations (*e.g.*, $Li^+$, $Mg^{2+}$, $Ca^{2+}$, and $Sr^{2+}$).

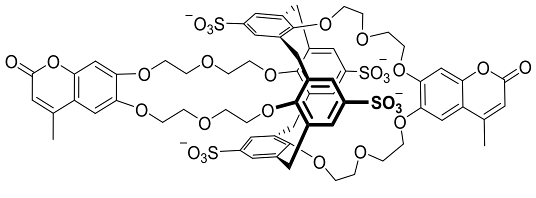

**C11.8**

**Figure 235.** Chemical structure of the chemosensor **C11.8** used for fluorescence-based detection of $Cs^+$ at $\mu$M concentrations in 50 mM MES buffer, pH 7.0.

Chemosensor designs for biorelevant divalent metal cations, *e.g.*, $Mg^{2+}$, $Ca^{2+}$, and $Zn^{2+}$, are also advanced and fulfill applicability criteria for use in biological systems. For instance, two 8-hydroxyquinoline-based chemosensors introduced by Farruggia, Iotti, Prodi, Savage, and Wolf (**C11.9** and **C11.10** in Figure 236) bind $Mg^{2+}$ with micromolar affinity ($K_a = 2.27 \times 10^4$ $M^{-1}$ for **C11.9** and $K_a = 1.37 \times 10^4$ $M^{-1}$ for **C11.10**) in Dulbecco phosphate buffer (DPBS ≙ 1.4 mM PBS without $Ca^{2+}$ and $Mg^{2+}$ salts but containing 136 mM NaCl and 270 $\mu$M KCl) and in cells.[1030] These chemosensors exhibit the usual fluorescence turn-on behavior as the process of photoinduced electron transfer (PET) quenching is interrupted upon metal ion complexation.

A conceptually related design has been established for $Ba^{2+}$ ion sensing at low micromolar concentrations in 10 mM Tris

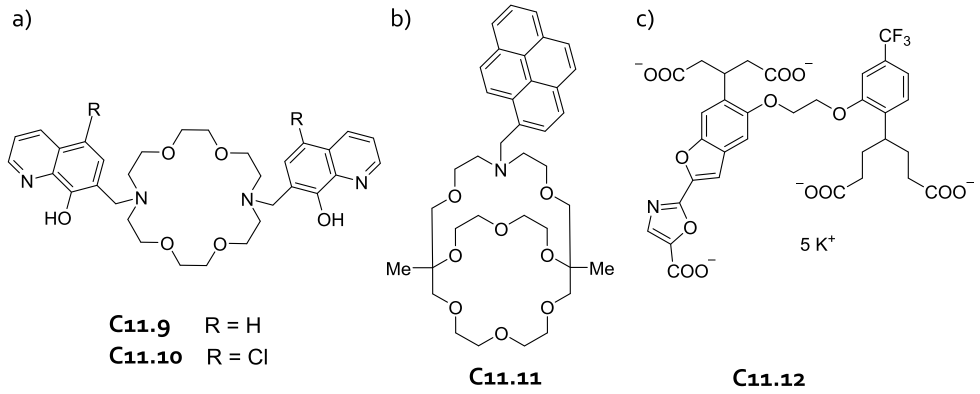

**C11.9** R = H
**C11.10** R = Cl

**C11.11**

**C11.12**

**Figure 236.** (a) Chemical structures of the chemosensors **C11.9**−**C11.10** used for $\mu$M detection of $Mg^{2+}$ in DPBS buffer, pH 7.0. (b) Chemical structure of the chemosensor **C11.11** used for $Ba^{2+}$ detection at $\mu$M concentrations in 10 mM Tris buffer, pH 10.2. (c) Chemical structure of the fura-2 chemosensor **C11.12** used for $Ca^{2+}$ detection at $\mu$M concentrations in biofluids and in cells.

buffer, pH 10.2, by Nakatsuji, Akashi, and coworkers using pyrene as a fluorophore and a monoazacryptand (**C11.11** in Figure 236) as the ionophore.[1031] The authors showed that other cations, such as $Li^+$, $Na^+$, $K^+$, $Rb^+$, $Cs^+$, $Mg^{2+}$, and $Ca^{2+}$ do not produce the same fluorescence response as $Ba^{2+}$ ions, indicating the good selectivity of this chemosensor.

Many different chemosensors for $Ca^{2+}$ have been reported, which work in the low concentration regime (*i.e.*, high-affinity chemosensors; $Ca^{2+}$ concentration is <50 nM), and high concentration regime (i.e., low-affinity chemosensors; Ca2+ concentration is <50 $\mu$M)[1032−1034] and several $Ca^{2+}$ chemosensors for imaging are now commercially available, such as the "Fura" (**C11.12** in Figure 236) and "Indo" dyes.[1035−1040] These chemosensors typically do not contain ionophores, but multiple copies of negatively charged carboxylates that function as "EDTA-like" binding motifs, where signal transduction again occurs by disrupting the PET quenching processes of fluorescence upon cation binding. The development of additional chemosensors for $Ca^{2+}$ detection and imaging may still be necessary for special applications. However, $Ca^{2+}$ detection in biofluids or *in vivo* seems no longer to be a conceptual challenge.

Intra- and extracellular sensing of $Zn^{2+}$ ions can be achieved with a 2,7-dichloro-fluorescein-based chemosensor (**C11.13** in Figure 237a), which was introduced by Lippard and coworkers.[1041,1042] The chemosensor was cell membrane permeable and showed a remarkably low detection limit of 0.1 nM for $Zn^{2+}$ in 50 mM PIPES buffer, pH 7.0, containing 100 mM KCl, with an emission turn-on response in the visible wavelength region and near-unity emission quantum yields. In 2010, the Lippard group presented a highly $Zn^{2+}$-selective rhodamine-based chemosensor (**C11.14** in Figure 237b) that shows a much enhanced emission response (factor 220 compared to factor 5 of the aforementioned fluorescein-based chemosensor) at micromolar concentrations of the target cation ($K_a$ = 1.37 × $10^4$ $M^{-1}$).[1043] Any new probe developed for the detection of $Zn^{2+}$ in biological media, *e.g.*, to study the structural and catalytic role of $Zn^{2+}$ in proteins[1044] and its function in neurobiology,[1045] must be compared to these outstanding systems.

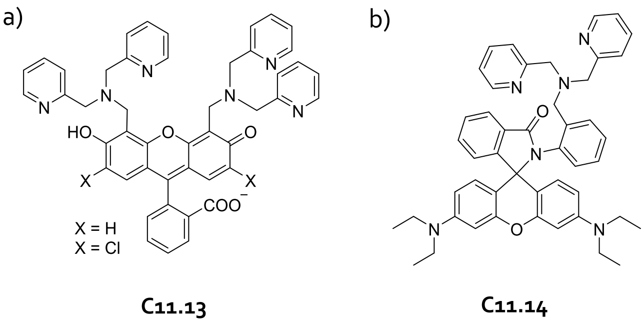

**C11.13**

**C11.14**

**Figure 237.** (a) Chemical structure of the chemosensor **C11.13** used for luminescence-based intra- and extracellular sensing of $Zn^{2+}$. (b) Chemical structure of the chemosensor **C11.14** used for luminescence-based $Zn^{2+}$ detection in PIPES buffer at mM concentrations.

While the usual and arguably "best" approach in biological and diagnostic application contexts is to design selectively binding chemosensors, nonselective chemosensors can also be useful when the binding of different analytes elicits unique responses. For instance, chemosensor **C11.15**, which was introduced by Xu, Spring, and coworkers, can be employed to detect several divalent metal ions, *i.e.*, $Zn^{2+}$, $Cd^{2+}$, $Pb^{2+}$, and $Hg^{2+}$ (Figure 238).[1046] However, a conformational change of the chemosensor occurred only in the presence of bound $Zn^{2+}$, which led to the formation of an imidic acid tautomer that showed a significantly different emission spectrum, which enabled $Zn^{2+}$ detection in the low micromolar concentration range in 500 mM HEPES buffer, pH 7.4, containing 5% DMSO.

A structurally simple but powerful fluorescence turn-on chemosensor for highly selective micromolar detection and imaging of $Al^{3+}$ in water containing 7% organic solvent and in living cells was recently presented by Yan, Zhang, Zhao, and coworkers (**C11.16** in Figure 239).[1047] For this purpose, a negatively charged tetraphenylvinyl-type chromophore was used. $Al^{3+}$ triggered the aggregation of **C11.16** by binding with the carboxyl moiety, causing aggregation-induced emission (AIE). This allowed for the detection of $Al^{3+}$ in the low micromolar concentration range, which was consistent with EPA and U.S. FDA guidelines for $Al^{3+}$ in bottled drinking water ($c_{max}$ = 7.4 $\mu$M). The chemosensor was found to be highly selective for $Al^{3+}$ over other metal cations, *e.g.*, alkaline and earth alkaline metal cations as well as several transition metal cations and was used for $Al^{3+}$ imaging in HeLa cells.

The ability to differentiate metal ions can be further improved by using sensor arrays that contain differentially selective cation receptors, as demonstrated by the Anzenbacher Jr. group in 2007.[1049,1050] The authors reported eight

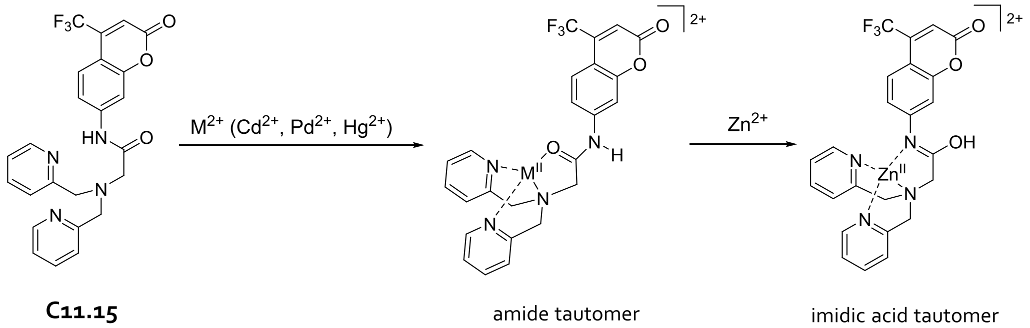

**Figure 238.** Mechanism for Zn$^{2+}$ detection by chemosensor **C11.15** in 5% DMSO in 500 mM HEPES buffer, pH 7.4. Adapted with permission from ref 1046. Copyright 2012 The Royal Society of Chemistry.

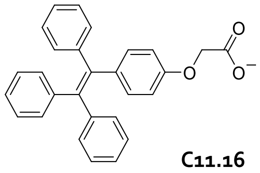

**Figure 239.** Chemical structure of chemosensor **C11.16** for aggregation-induced emission (AIE)-based detection of Al$^{3+}$ at $\mu$M concentrations in water/acetonitrile mixtures and within cells.

hydroxyquinoline-based ligands with extended conjugated fluorophores that provided a ratiometric emission turn-on signal output upon metal binding. The observed changes in the blue and green channels of the RGB signal were used to distinguish various metal cations, *e.g.,* Mg$^{2+}$, Ca$^{2+}$, Zn$^{2+}$, Cd$^{2+}$, and Al$^{3+}$, in the low micromolar to millimolar concentration range. The following year, the same group reported the ability to discriminate 10 metal ions in water at different pH values with over 90% accuracy in the concentration range between 10 $\mu$M and 5 mM, using nine cross-reactive metal binders (**C11.17**−**C11.25** in Figure 240).[1048] In addition, array-based metal discrimination strategies using three structurally similar water-soluble bis-triazolyl benzochalcogendiazole cycloadducts for the detection and differentiation of Cu$^{2+}$, Ni$^{2+}$, and Ag$^{+}$ in the low micromolar concentration range in water were reported by Bunz and coworkers.[1051]

For a pattern recognition-based application scenario, it may be of interest to exploit the relatively strong binding affinity (millimolar to micromolar) of cucurbit[*n*]urils for a wide range of metal cations in water (see Figure 241).[40] The macrocyclic hosts CB5, CB6, CB7, and CB8 each exhibit differential selectivity due to different size matching (and other factors) that can likely be exploited to distinguish metal ions from one to another. A chromophoric or fluorescent optical readout can be readily achieved by IDA-based assays.[40,44,1052]

Self-assembled 1:1 complexes of CB7 and cation-binding dye molecules (*e.g.,* *N*-(2-benz-imidazolylmethyl)-*N*,*N*-bis(2-pyridylmethyl)-amine, BIBPA), reported by Cong, Lindoy, Wei, Fedorova, Isaacs, and Aliaga, showed promising sensing properties for the detection of transition metal cati-

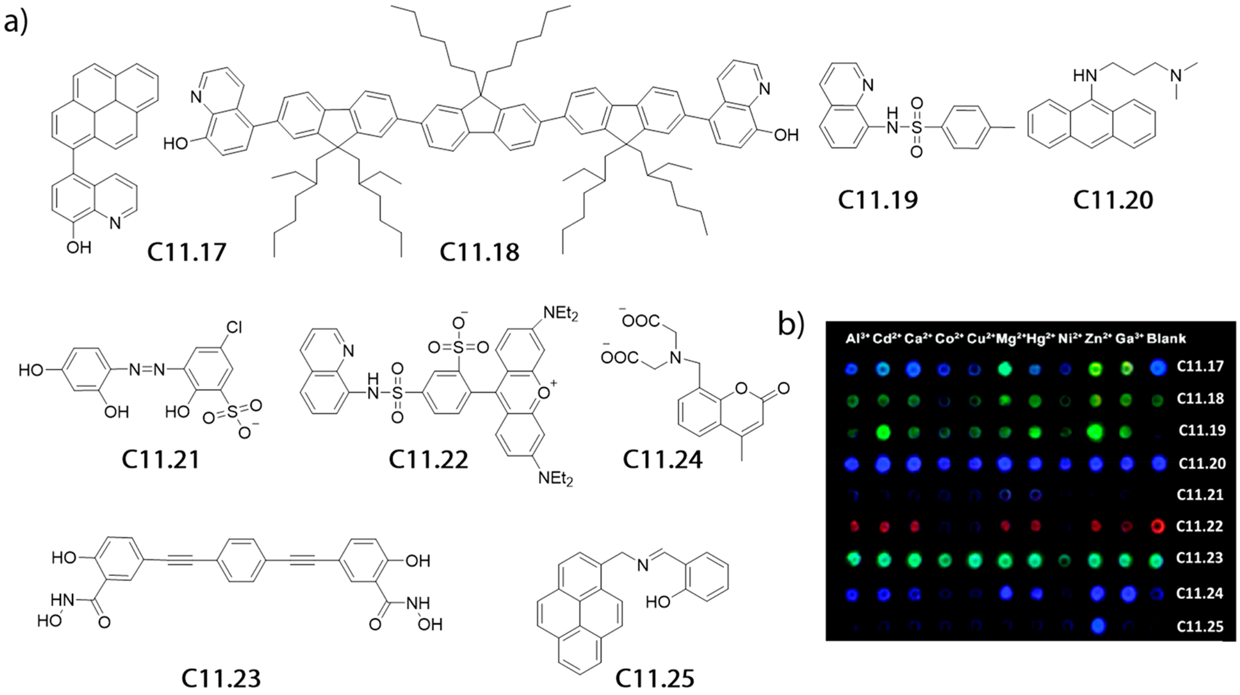

**Figure 240.** (a) Chemical structures of chemosensors **C11.17**−**C11.25**. (b) Fluorescence response of the chemosensor array in the presence of 1 mM of different cations in water, pH 7.0. Adapted with permission from ref 1048. Copyright 2008 American Chemical Society.

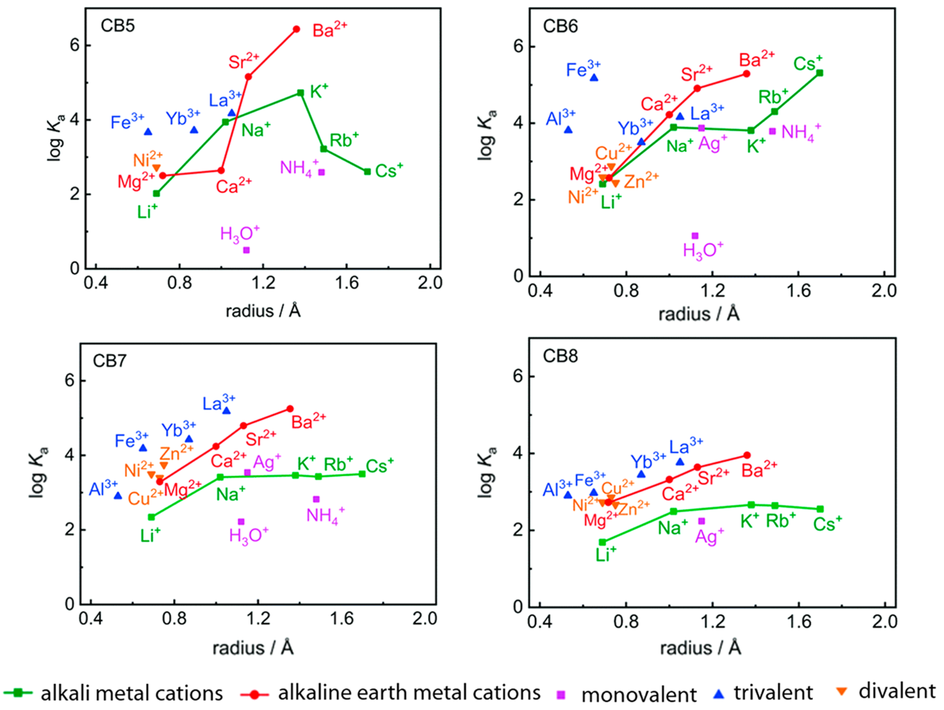

**Figure 241.** Plots of log $K_a$ *vs* cation radius for different cucurbit[*n*]urils that function as metal cation binders in aqueous solutions. Reproduced with permission from ref 40. Copyright 2019 The Royal Society of Chemistry.

ons.[1053−1055] In the example reported by Cong and coworkers, cation binding did not displace the indicator (BIBPA) from the macrocycle but led to the formation of a 1:1:1 ternary complex (**C11.26** in Figure 242), in which both the stabilizing interactions with the carbonyl-fringed CB*n* portals and the rigid chromic effect played a role.[1053] It was observed that fluorescence enhancement occurs upon $Zn^{2+}$ or $Cd^{2+}$ binding in 10 mM phosphate buffer, pH 6.5, while other cations (*e.g.*, $Cr^{3+}$, $Mn^{2+}$, $Co^{2+}$, $Ni^{2+}$, $Ho^{3+}$) did not affect the photoluminescence properties of **C11.26**.

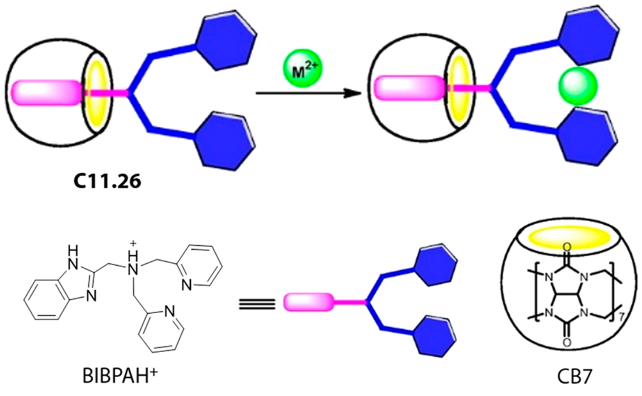

**Figure 242.** Schematic representation of the chemosensor ensemble **C11.26**, composed of CB7 and the cation-binding dye molecule *N*-(2-benzimidazolylmethyl)-*N*,*N*-bis(2-pyridylmethyl)-amine (BIBPA), allows for $\mu$M detection of $Zn^{2+}$ and $Cd^{2+}$ in 10 mM phosphate buffer, pH 6.5. Adapted with permission from ref 1053. Copyright 2020 Taylor & Francis.

A supramolecular chemosensor (**C11.27** in Figure 243) composed of carboxylate-functionalized pillar[5]arenes and water-soluble perylenebisdiimide (PDI) derivatives was used for the detection of $Fe^{3+}$ at $\mu$M concentrations in aqueous solution by Yin and coworkers.[1056] The binding of $Fe^{3+}$ induced a significant fluorescence enhancement of the chemosensor, most likely due to an interruption of the PET quenching mechanism. Other metal cations tested, *e.g.*, $Fe^{2+}$, $Zn^{2+}$, $Cd^{2+}$, and $Hg^{2+}$, did not cause a change in emission or a modulated chromophoric signal.

While we have given preference to optical signal transduction principles, particularly to absorbance- and emission-based probes and chemosensors, it is worth noting that a strong signal amplification can also be achieved by chemical exchange saturation transfer (CEST), *e.g.*, in combination with $^{19}F$ magnetic resonance imaging (MRI). For instance, Bulte, McMahon, and coworkers demonstrated that low $Ca^{2+}$ levels, *e.g.*, 500 nM, can be detected by using 5,5′-difluorinated 1,2-bis(*o*-aminophenoxy)ethane-*N*,*N*,*N*′,*N*′-tetraacetic acid (0.5 mM) as the ligand that undergoes fast exchange reactions with the bound metal cations.[1057] Note that this approach required large concentration excess of the fluorinated species. In recent years, the Bar-Shir group applied this concept to supramolecular host–guest complexes, through which significant improvements of analyte detection in biofluids by NMR/MRI can be expected and realized.[1058,1059]

Taking advantage of the AIE from tetraphenylethylenes, Zhang and coworkers reported the fluorescence turn-on based chemosensors **C11.28** and **C11.29** (see Figure 244) for the micromolar detection of $Ag^+$ and $Hg^{2+}$ in water containing either 20% THF (**C11.28**) or 50% acetonitrile (**C11.29**).[1060] The addition of $Ag^+$ or $Hg^{2+}$ salts led to the formation of aggregates that had increased emission intensities. Importantly, it was observed that other cations such as $K^+$, $Cs^+$, $Ag^+$, $Mg^{2+}$, $Ca^{2+}$, $Ba^{2+}$, $Mn^{2+}$, $Fe^{2+}$, $Fe^{3+}$, $Co^{2+}$, $Ni^{2+}$, $Pb^{2+}$, $Cu^{2+}$, $Zn^{2+}$, and $Cd^{2+}$ did not cause any change in fluorescence. Although it is not the focus of this review, we would like to highlight that Minami and coworkers have recently developed an organic field-effect transistor (OFET) with an extended gate modified

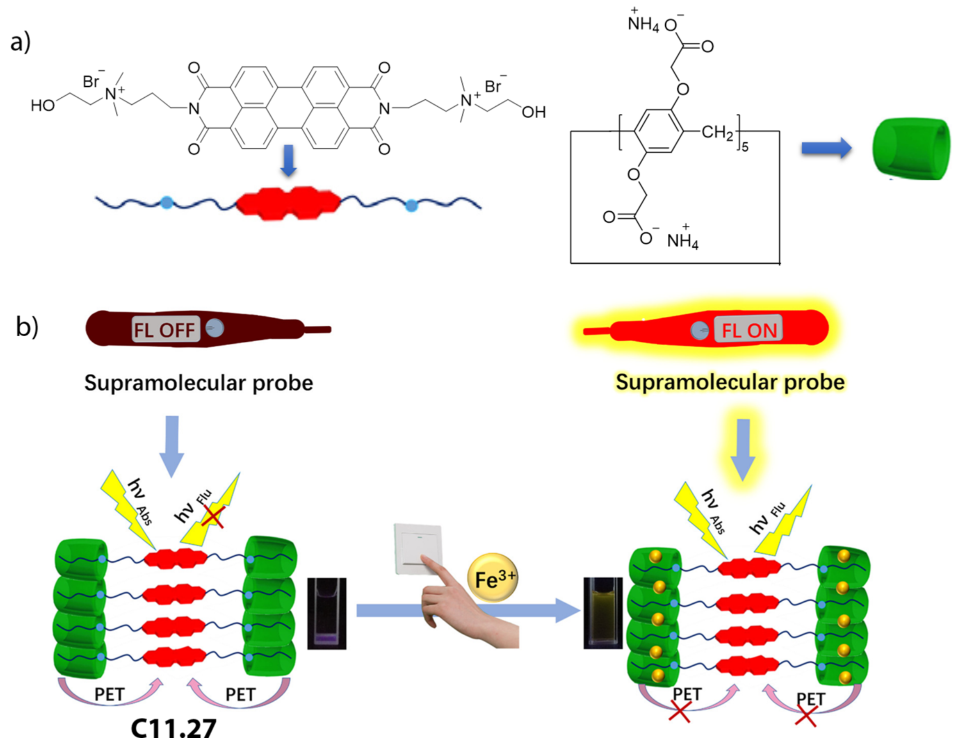

**Figure 243.** (a) Chemical structure of the chemosensor **C11.27** formed from carboxylate-functionalized pillar[5]arenes and PDI. (b) Schematic representation of the detection mechanism for $Fe^{3+}$ with **C11.27.** Reproduced with permission from ref 1056. Copyright 2017 American Chemical Society.

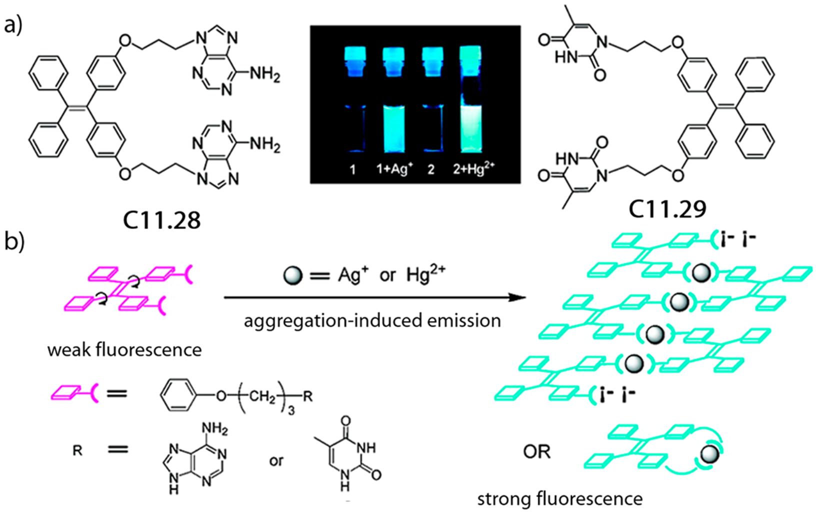

**Figure 244.** (a,b) Schematic representation of the fluorescence-based sensing mechanism of $Ag^+$ and $Hg^{2+}$ by the chemosensors **C11.28** and **C11.29**. Both chemosensors allow for $\mu$M detection of $Ag^+$ and $Hg^{2+}$ in acetonitrile/water mixtures. Reproduced with permission from ref 1060. Copyright 2008 American Chemical Society.

by an artificial receptor for the detection of $Hg^{2+}$ in water.[1061] The authors reported that the OFET sensors, which had a remarkably low detection limit of 9.9 ppb (<50 nM) for $Hg^{2+}$, can be used for low-cost on-site $Hg^{2+}$ detection because they are easy to prepare, reusable, disposable, and portable.

On the one hand, the chemosensor-based detection of $Na^+$, $K^+$, and $Ca^{2+}$ ions has proven to be practically feasible and has already reached commercial viability and wide applicability in medical settings. Systems for sensing $Mg^{2+}$, $Zn^{2+}$, and even for $Al^{3+}$ are also rather advanced, making them competitive options for practical use. On the other hand, the instruments available in analytical technology are still far superior in terms of sensitivity and accuracy for the trace-detection of metal cations in the environment. Usually, state-funded analytical laboratories can afford such technologies to provide legally water-tight concentration values for toxic heavy metals, *e.g.*, in drinking water, food, or soil. This limits a realistic application scenario for optical-based molecular probes and chemosensors for the detection of trace metals at present, even though their sensitivity and selectivity values have already surpassed the legal thresholds for certain trace metals (*e.g.*, $Hg^{2+}$). Molecular probes, chemosensors, and nanosensors may become competitive options for routine sensing applications if their scope is widened, *e.g.*, if all legally relevant metal pollutants can be assessed by the same optical technology, enabling the complete replacement of chromatographic equipment in analytical laboratories.

Besides the "classical" approach of developing highly selective binders, alternative concepts such as the development of sensor arrays containing differently selective cation receptors and pattern recognition-based analysis have been attracting attention in recent years. It remains to be seen if such methods have a real application potential for molecular diagnostics or environmental pollution monitoring in the future.

## 12. INORGANIC ANIONS

Chloride ($Cl^-$) is the major inorganic anion found in extracellular fluids, and normal chloride plasma concentrations range from approximately 99 to 109 mM (see Table 40). Chloride anions are essential for a variety of vital functions, such as the regulation of fluid secretion, *e.g.*, of pancreatic juice into the small intestine, and they are responsible for maintaining normal blood volume, blood pressure, and blood pH.[1070,1071] The kidney is the main organ involved in maintaining the total amount of chloride in the body. Therefore, abnormal chloride concentration in the urine and blood is an important indicator of kidney problems.[1072] For example, chloride loss in the body is caused by suboptimal reabsorption by the kidney, which manifests as hypochloremia ($Cl^-$ in plasma <96−101 mM).[1073] Furthermore, when blood chloride levels are low, bicarbonate reabsorption often increases proportionally, leading to metabolic alkalosis (blood pH above 7.45).[1074] In contrast, a high plasma chloride content, *i.e.*, hyperchloremia ($Cl^-$ in plasma >106−111 mM), is also an important indicator of renal dysfunction, *e.g.*, renal damage due to sepsis.[1075] Cystic fibrosis (CF) is an inherited disease in which the function of the CF transmembrane conductance regulator, a $Cl^-$ ion channel, is impaired.[1076,1077] As a result, $Cl^-$ is inefficiently transported outside the cell, leading to liver damage and sticky mucus accumulation in the lungs, which in turn results in increased susceptibility to respiratory infections.[1078] Therefore, information on chloride concentration in biofluids such as urine or blood is important. Hydrogen sulfide ($H_2S$) is an inorganic compound that due to its $pK_a$ value of about 6.8 occurs at physiological pH values predominantly in its deprotonated state, *i.e.*, as hydrogen sulfide anion ($HS^-$).[1079,1080] Although the understanding of $H_2S/HS^-$ metabolism and its biological functions in humans is still not fully understood, many studies have already shown that it plays a role in a number of biological processes, such as blood vessel dilation, acting as a neuromodulator or neurotransmitter, and regulating endocrine functions.[1081−1083] $H_2S$ is formed in the body from cysteine by enzymatic activity, such as cystathionine-$\beta$-synthase and cystathionine-$\gamma$-lyase.[1084] Abnormal $H_2S/HS^-$ concentrations in biofluids, are associated with neurodegenerative diseases, heart muscle damage, and eye diseases.[1085,1086]

Inorganic nitrate ($NO_3^-$) and nitrite ($NO_2^-$) from endogenous or dietary sources are metabolized in vivo to nitric oxide (NO) and other bioactive nitric oxides. The nitrate−nitrite−NO pathway is shown to be an important mediator in the regulation of blood flow, cell signaling, energy supply, and tissue response to hypoxia.[1087] In addition, $NO_2^-$ and $NO_3^-$ levels in biofluids are important biomarkers for the presence of oxidative and nitrosative stress and cardiovascular disease.[1088−1090] For example, elevated $NO_2^-$ levels cause hypotension and restricts oxygen transport and delivery in the body through the formation of methemoglobin. As a result of increased $NO_2^-$ exposure, hypoxia, impaired consciousness, cardiac arrhythmias, and death may occur.[1091] Adverse health effects, particularly to infants and babies, are also known to be caused by elevated $NO_3^-$ levels in drinking water.[1092] Currently, 50 mg $L^{-1}$ (800 $\mu$M) of nitrate in drinking water is the legally accepted concentration limit (see also Table 40).[970] In addition to nitrate, anions such as sulfate ($SO_4^{2-}$), and phosphate ($PO_4^{3-}$), which are introduced into the environment on a large scale through the use of inorganic and organic (slurry) fertilizers, are recognized as environmental pollutants if their occurrence exceeds the "natural" threshold. Cyanides ($CN^-$) are highly toxic anions and strong inhibitors of the enzyme cytochrome C oxidase, an enzyme important for aerobic respiration.[1093] As a result of cyanide inhibition of cytochrome C oxidase, the electron transport chain is interrupted so that the cell cannot produce ATP for energy production. Thiocyanate ($SCN^-$), as a final product of detoxification of $CN^-$, is correlated with daily cigarette consumption and is considered as a biomarker for distinguishing smokers and nonsmokers.[1094] The toxicity of thiocyanate is due to its potent inhibition of the thyroid sodium-iodide symporter, a transmembrane glycol protein that transports sodium and iodide anions into cells.[1095] It is generally accepted that exposure to fluoride ions ($F^-$) promotes oral health, which is why many countries add fluoride to drinking water at a concentration of 0.7−1.5 ppm. The beneficial properties of $F^-$ for dental health are based on its reaction with tooth enamel ($Ca_{10}(PO_4)_6$), replacing the hydroxide anion and forming a more stable fluorapatite ($Ca_5(PO_4)_3F$) that is more resistant to acidic pH levels caused by bacteria. However, exposure to high fluoride concentrations (above 100 ppm) leads to a wide range of adverse effects including oxidative stress, organelle damage, and apoptosis in individual cells.[1096] Because it is again not the goal to discuss the biological role of inorganic anions in detail, we instead refer the interested reader to other comprehensive literature examples.[977,1070,1097,1098]

### 12.1. Molecular Probes for Inorganic Anions

The cyanide anion is a nucleophilic anionic species and an excellent ligand for many metals. Thus, many cyanide probes have been developed capitalizing on these properties. In this review, we highlight only a few representative examples, which are summarized in Table 37.

For instance, in 2016, Shiraishi and coworkers introduced a hydrogenated coumarin−spiropyran dyad probe (**P12.1** in Figure 245a) that enables fluorescence-based detection of cyanide at $\mu$M concentrations in 30% MeOH in 100 mM CHES buffer, pH 9.6. As depicted in Figure 245a, the nucleophilic attack of $CN^-$ on **P12.1** promotes the opening of the spirocycle, resulting in a strong emission increase (the emission quantum yields prior and after reaction with $CN^-$ are <0.01 and 0.52, respectively).[1099] No fluorescence response was observed for other anions such as $F^-$, $Cl^-$, $Br^-$, $I^-$, $AcO^-$, $H_2PO_4^-$, $ClO_4^-$, $NO_3^-$, $SCN^-$, $S^{2-}$, and organic molecules (*e.g*, Cys, thiophenol, or *n*-propanethiol). This design proved to be a major advance over previously reported spiropyrans, which required UV irradiation to open the spiropyran form into a cyanide-reactive merocyanine.[11001101] A conceptually related approach was reported by Guo, Yang, and coworkers, in which nucleophilic attack of cyanide on coumarin−hemicyanine dyes

### Table 37. Summary of the Herein Discussed Molecular Probes for Inorganic Anions (LOD, Limit of Detection)

| probe | media | concentration range | ref |
|---|---|---|---|
| | Cyanide ($CN^-$) Analyte | | |
| **P12.1** | 30% MeCN in 100 mM CHES buffer, pH 9.6 | 1−50 $\mu$M (linear range); LOD, 1.0 $\mu$M | 1099 |
| **P12.2** | 50% MeOH in 10 mM carbonate buffer, pH 9.4 | 10−2000 $\mu$M; LOD, 9.8 $\mu$M | 1102 |
| **P12.3** | 20% DMSO in water | 0−28 $\mu$M; LOD, 97 nM | 1103 |
| **P12.4** | water | 0−5.2 $\mu$M; LOD, ≤11 nM | 1104 |
| **P12.5**−**P12.6** | 1% DMSO in water containing 2 mM CTAB | 0−120 $\mu$M (**P12.6**); LOD, 0.2 $\mu$M (**P12.6**) | 1105 |
| **P12.7** | 30% THF in water; environmental water; food samples | 0−20 $\mu$M; LOD, 39.9 nM | 1106 |
| **P12.8** | 30% DMSO in HEPES buffer, pH 7.4 | 0−35 $\mu$M; LOD, 200 nM | 1107 |
| **P12.9** | 0.4% MeCN in 10 mM HEPES buffer, pH 7.6 | 0−0.8 mM; LOD, 32 nM | 1108 |
| **P12.10** | 0.5% MeCN in 20 mM HEPES buffer, pH 7.4 | 50−500 $\mu$M; LOD, 5 $\mu$M | 1109 |
| **P12.12** | 1% DMSO in 10 mM HEPES buffer, pH 7.4; fresh mouse serum | 0−350 $\mu$M; LOD, 5.7 $\mu$M | 1111 |
| **P12.11** | 20 mM HEPES buffer, pH 7.2 | 0−40 $\mu$M; LOD, 1.3 $\mu$M | 1110 |
| | Fluoride ($F^-$) Analyte | | |
| **P12.20** | 1% THF in $H_2O$ containing 2 mM CTAB | 0−91 $\mu$M; LOD, 5 $\mu$M | 1125 |
| **P12.21** | 0.5% MeCN in water; HEPES buffer, pH 7.4 | 0.13−3.82 mM | 1126 |
| **P12.22** | 30% EtOH in 20 mM PBS, pH 7.4 | 0−60 mM; LOD, 0.08 mM | 1127 |
| **P12.23** | 20% MeCN in 10 mM HEPES buffer, pH 7.4 | 0−84 mM; LOD, 0.2 mM | 1128 |
| **P12.24** | HEPES buffer containing 100 $\mu$M CTAB, pH 7.4 | 0−1.0 mM; LOD, 1.0 $\mu$M | 1129 |
| **P12.25** | 50% THF in water | 0−90.0 $\mu$M | 1130 |
| **P12.26** | 5% DCM in water | 5.2−79 $\mu$M; LOD, 5.2 $\mu$M | 1131 |
| | Hydrogen Sulfide ($HS^-$) Analyte | | |
| **P12.17** | 30% MeCN in 10 mM PBS, pH 7.4 | 0−200 $\mu$M; LOD, 140 nM | 1121 |
| **P12.18** | 2% DMSO in 20 mM PBS, pH 7.4 | 0−200 $\mu$M | 1122 |
| **P12.19** | 30% MeCN in 10 mM PBS, pH 7.4 | 0−300 $\mu$M; LOD, 68 nM | 1123 |
| | Iodide ($I^-$) Analyte | | |
| **P12.14**[a] | 10% EtOH in water | $\mu$M range | 1118 |
| **P12.15** | 20 mM MES buffer, pH 6.0 | 0−25 $\mu$M; LOD, 7.1 $\mu$M | 1119 |
| | Sulfide ($S^{2-}$) Analyte | | |
| **P12.13** | water, pH 6.0−11.0 | 0−200 $\mu$M; LOD, 37.0 $\mu$M | 1112 |
| **P12.16** | 10 mM BisTris buffer, pH 7.0; living zebrafish | 0−40.0 $\mu$M; LOD, 2.39 $\mu$M | 1120 |

[a] Reacts also with $Ag^{2+}$ and $Hg^{2+}$.

(**P12.2** in Figure 245b), yields a rapid (3 min) colorimetric response, which can be used for the detection of $CN^-$ in the low micromolar concentration range in 50% MeOH in 10 mM carbonate buffer as solvent.[1102]

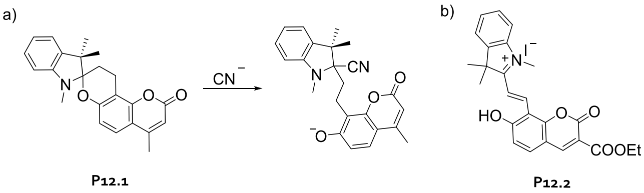

**Figure 245.** (a) Schematic representation of the detection mechanism for $CN^-$ with probe **P12.1**. The probe allows for the $\mu$M detection of $CN^-$ in 30% MeOH in 100 mM CHES buffer, pH 9.6. (b) Chemical structure of **P12.2** used for $\mu$M to mM detection of $CN^-$ in 50% MeOH in 10 mM $Na_2CO_3$−$NaHCO_3$ buffer, pH 9.4.

Lin, Zhang, and coworkers reported that the acylhydrazone-based probe (**P12.3** in Figure 246a) can selectively react with cyanide in aqueous-organic mixtures (water:DMSO 4:1 v/v), resulting in fluorescence enhancement. **P12.3** can be used to detect cyanide at $\mu$M concentrations (LOD, 97 nM). The authors further showed that possible anion interferents (*e.g.*, $OAc^-$, $F^-$, $Cl^-$, $Br^-$, $I^-$, $NO_3^-$, $HSO_4^-$, $H_2PO_4^-$, $ClO_4^-$, $S^{2-}$, and $SCN^-$) did not cause a signal change.[1103] In 2013, Wu, Hua, and coworkers described a triphenylamine fluorescence turn-off probe that was used for the detection of $CN^-$ in pure water and in living cells at $\mu$M concentrations (LOD, <11 nM, **P12.4** in Figure 246b).[1104] Again, no emission response was observed in the presence of other anions (*e.g.*, $F^-$, $Cl^-$, $Br^-$, $I^-$, $NO_2^-$, $N_3^-$, $AcO^-$, $H_2PO_4^-$, $ClO_4^-$, $NO_3^-$, $SCN^-$, $S^{2-}$ $CO_3^{2-}$, $SO_3^{2-}$, $HPO_4^{2-}$, and $PO_4^{3-}$). A year later, a structurally similar probe (**P12.5** and **P12.6** in Figure 246) bearing a luminogenic moiety with the ability of AIE was communicated by the Yu group. This luminescence turn-off probe can detect $CN^-$ (LOD, 0.2 $\mu$M with a response time of 100 s) in water/CTAB mixtures containing 1% DMSO.[1105]

It can be advantageous in certain applications, such as imaging, to employ fluorescence turn-on probes for the detection of cyanide. Niu and coworkers achieved this by designing an oligothiophene-based probe that was linked to a barbituric acid derivative (**P12.7** in Figure 247a), which can act as both an electron-acceptor fluorescence quencher and as a cyanide reactive moiety.[1106] Upon addition of $CN^-$ to the probe, its fluorescence is activated as intramolecular charge transfer (ICT) is interrupted. Other anions, such as $F^-$, $Cl^-$, $Br^-$, $NO_3^-$, $N_3^-$, $AcO^-$, $NO_3^-$, $SCN^-$, $HSO_4^-$, $HCO_3^-$, $S^{2-}$, $CO_3^{2-}$, and $SO_4^{2-}$, did not produce a fluorescence response. By using **P12.7**, low detection limits (40 nM) and fast reaction times (20 s) were achieved for the detection of $CN^-$ in 30% THF in water in various fresh water sources and food extracts. Several years earlier, Hua and coworkers reported a conceptually related design idea in which the nucleophilic addition of cyanides to emission-quenched probes restored their fluorescence properties, making them applicable for cell imaging and as a chemodosimeter for cyanide with submicromolar detection limits in HEPES buffer, pH 7.4, containing 30% DMSO (**P12.8** in Figure 247b).[1107] Unfortunately, this probe required up to 60 min reaction time for full conversion.

There are also several reports where $Cu^{2+}$ complexes were used as intermediary species for the detection of $CN^-$. For such probes, $Cu^{2+}$ is first bound to a cation-binding indicator dye and is subsequently displaced by $CN^-$ anions due to the stronger affinity of copper for cyanides (Figure 248). For instance, Ghosh, Das, and coworkers designed a cyanide-specific turn-on phosphorescent probe (**P12.9** in Figure 248a) that can be applied for cell imaging and for enzymatic reaction monitoring.[1108] The probe **P12.9** showed a 0.2 ppm (32 nM) detection limit in 10 mM HEPES buffer, pH 7.6, containing

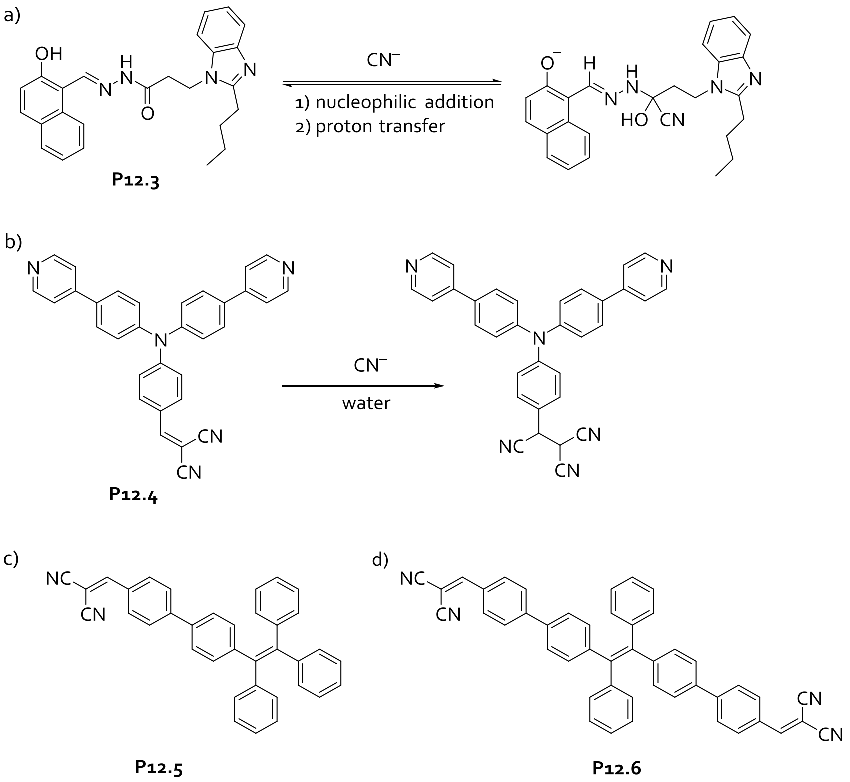

**Figure 246.** (a) Schematic representation of the detection of CN$^-$ by probes **P12.3**. The probe allows for the $\mu$M detection of CN$^-$ in 20% DMSO in water. (b) Schematic representation of the nucleophilic attack of CN$^-$ on **P12.4** resulting in a quenched fluorescence of the probe. (c,d) Chemical structures of probes **P12.5** and **P12.6** for fluorescence-based detection of CN$^-$ at $\mu$M concentration in water containing 1% DMSO and 2 mM CTAB.

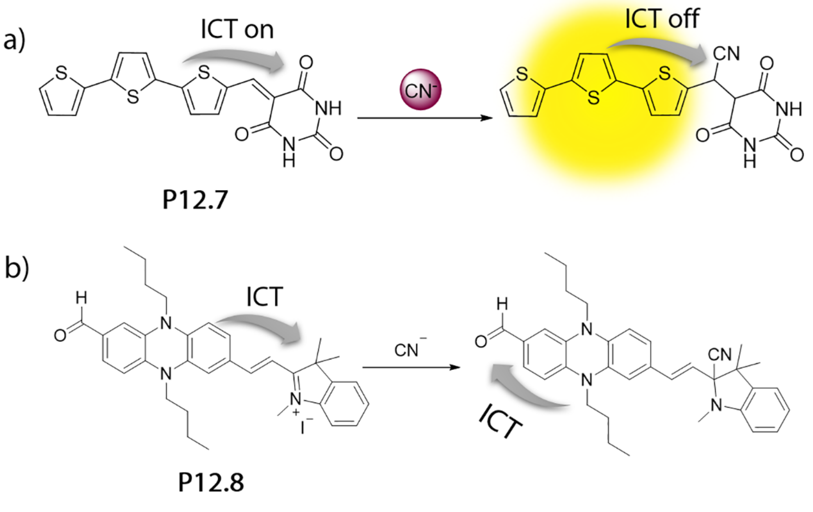

**Figure 247.** (a) Schematic representation of the fluorescence turn-on detection of CN$^-$ at low $\mu$M concentration by **P12.7** in 30% THF in water. (b) Schematic representation of the fluorescence turn-on detection of CN$^-$ at low $\mu$M concentration by **P12.8** in 30% DMSO in HEPES buffer, pH 7.4.

0.4% acetonitrile with no cross-reactivity towards other anions, such as OAc$^-$, F$^-$, Cl$^-$, Br$^-$, I$^-$, NO$_2^-$, NO$_3^-$, HSO$_4^-$, H$_2$PO$_4^-$, P$_2$O$_7^{4-}$, ClO$_4^-$, IO$_4^-$, N$_3^-$, and benzoate. Park, Yoon, and coworkers (**P12.10** in Figure 248b),[1109] Yang and coworkers (**P12.11** in Figure 248c),[1110] as well as Jose and coworkers (**P12.12** in Figure 248d),[1111] established similar concepts for micromolar detection of cyanide in water.

It is worth mentioning that a Cu$^{2+}$ mediated indicator-displacement assay that is functional in aqueous media has been established for sulfide detection at micromolar concentrations, capitalizing on the strong interaction of Cu$^{2+}$ with S$^{2-}$ ions (**P12.13** in Figure 249).[1112] Thus, the detection of cyanide or sulfide with Cu$^{2+}$-based systems is always subject to possible interferences from other Cu$^{2+}$-binding anions.[1113−1117]

Following a similar design strategy, the Wei group[1118] and Jiang group[1119] reported probes **P12.14** (in water containing 10% EtOH) and **P12.15** (in 20 mM MES buffer, pH 6.0) for

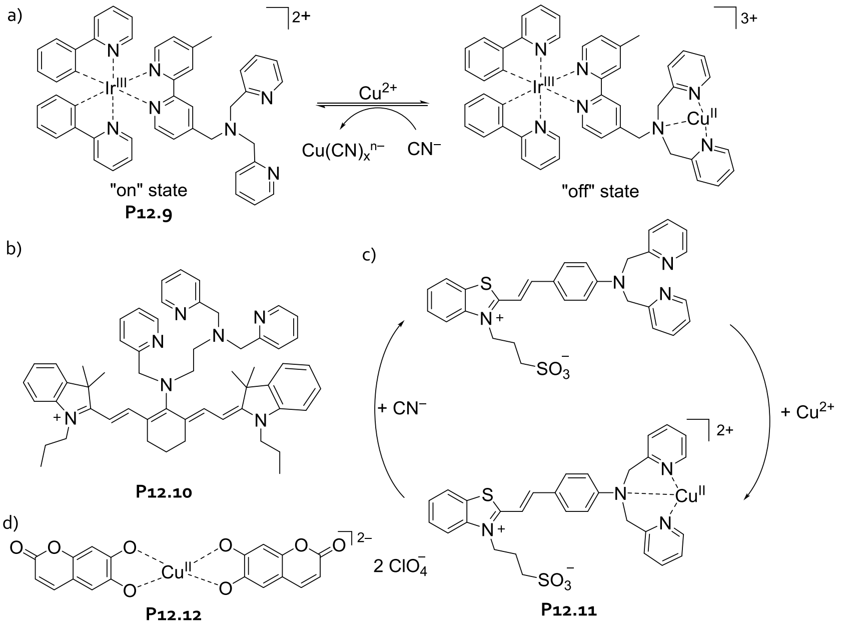

**Figure 248.** (a) Schematic representation of the detection of CN$^-$ at $\mu$M concentrations by **P12.9** in HEPES buffer containing 0.4% MeCN, pH 7.0. (b) Chemical structure of probe **P12.10**, which allows for fluorescence-based detection of CN$^-$ at $\mu$M concentrations in 20 mM HEPES buffer containing 0.5% MeCN. (c) Schematic representation of the detection for CN$^-$ at $\mu$M concentrations in 20 mM HEPES buffer, pH 7.2, by **P12.11**. (d) Chemical structure of probe **P12.12** used for $\mu$M detection of CN$^-$ in 1% DMSO in HEPES buffer.

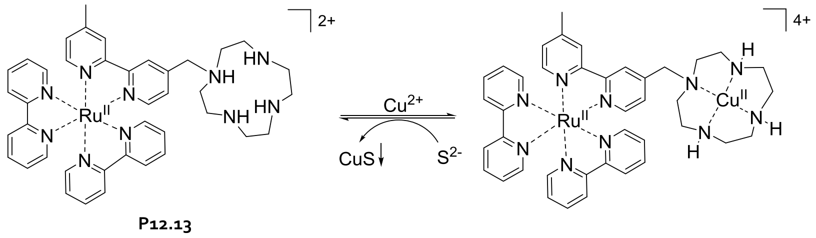

**Figure 249.** Schematic representation of the detection of S$^{2-}$ by **P12.13**.

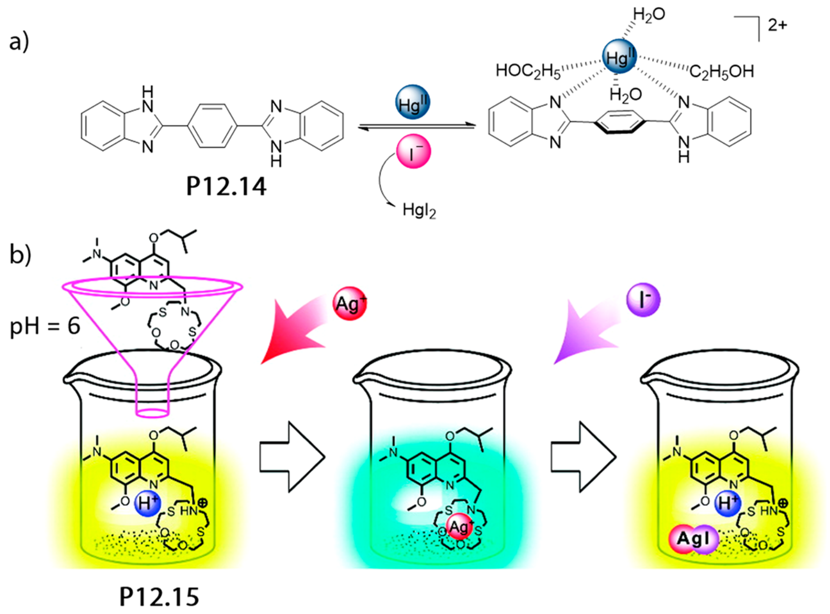

**Figure 250.** (a) Schematic representation of the sensing of I$^-$ by probe **P12.14**. I$^-$ disrupts the complexation of **P12.14** with Hg$^{2+}$ cations resulting in quenched fluorescence which allows for $\mu$M iodide detection in 10% EtOH in water. Reproduced with permission from ref 1118. Copyright 2014 Elsevier BV. (b) Schematic representation of the detection of I$^-$ at $\mu$M concentrations in water containing 1% DMSO and 2 mM CTAB by **P12.15**. Reproduced with permission from ref 1119. Copyright 2011 American Chemical Society.

iodide Figure 250) that exploit the high affinity of $I^-$ for $Hg^{2+}$ and $Ag^+$, respectively, which competitively displaced the metal cations from the indicator dyes (probes). Besides anion selectivity concerns (*e.g.*, potential cross-reactivities with $CN^-$ and $S^{2-}$) the use of heavy metal ion additives may raise additional concerns for handling of these probes.

The Kim group recently reported a $Zn^{2+}$-based IDA (**P12.16** in Figure 251) for $S^{2-}$ detection which was tolerant to other anions, including $CN^-$ and $I^-$, in 10 mM Bis-Tris buffer, pH 7.0, and even allowed for the $Zn^{2+}$ detection in zebrafish.[1120] The detection limit of **P12.16** for $Zn^{2+}$ and for $S^{2-}$ were 0.3 and 2.4 $\mu$M, respectively, and therefore lower than the requirements specified by the WHO guidelines (76.0 and 14.7 $\mu$M) for drinking water.

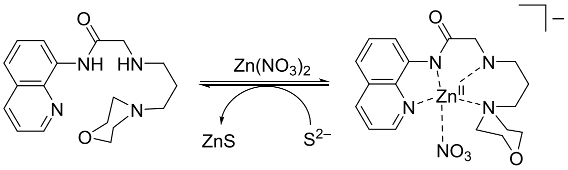

**P12.16**

**Figure 251.** Schematic representation of the micromolar detection of $S^{2-}$ by probe **P12.16** in 10 mM Bis-Tris buffer, pH 7.0.

Exploiting the reactivity characteristics of $S^{2-}$ (and its conjugate acids $HS^-$ and $H_2S$) is a promising alternative for sulfide detection, similar to the probes discussed for cyanide detection. In 2013, Guo and coworkers designed the (hydrogen)sulfide reactive probe **P12.17** (Figure 252a) that undergoes a change from NIR to visible emission by breaking the $\pi$-conjugation upon $H_2S$ addition.[1121] A detection limit of 0.14 $\mu$M was reached in 10 mM PBS containing 30% acetonitrile, pH 7.4. Additionally, **P12.17** can be used for intracellular $H_2S$ detection and for $HS^-$ sensing in blood serum, as it is not cross-reactive towards other anions, including $CN^-$ and $I^-$, and biological thiols such as glutathione. In the same year, Guo, He, and coworkers reported a ratiometric fluorescent probe (**P12.18** in Figure 252b) that can be used for rapid detection of hydrogen sulfide in 20 mM PBS buffer, pH 7.4, and in mitochondria.[1122] **P12.18** was shown to be highly $H_2S$-selective over other anions (*e.g.*, $F^-$, $Cl^-$, $Br^-$, $I^-$, $CN^-$, $NO_3^-$, and $SO_4^{2-}$) and biothiols (*e.g.*, Cys, Hcys, and GSH).

Two years later, a highly sensitive ratiometric probe for $H_2S$ with a 70 nM detection limit and a fast response time (15 s) was introduced by Peng and coworkers (**P12.19** in Figure 253).[1123] A large emission shift (220 nm) and a strong signal response factor (168-fold in ratiometric value) were observed when **P12.19** reacted with $H_2S$ in 10 mM PBS, pH 7.4, containing 30% acetonitrile. The probe can be applied for imaging applications as the authors demonstrated with MCF-7 cells and in living mice. The selectivity of **P12.19** for $HS^-$ was tested in the presence of other ions (*e.g*, $K^+$, $Na^+$, $Mg^{2+}$, $Zn^{2+}$, $NO_2^-$, $NO_3^-$, and $SCN^-$) and thiols (Cys and GSH), which did not affect the signal response.

Fluoride ions have also received widespread interest for the development of chromophoric and fluorescent probes. They have unique properties, such as a small ionic radius and a relatively high charge state ("hard" anion), which makes it easy to exploit their characteristic chemical reaction modes in a probe design. One of the unique properties of $F^-$ is their ability to cleave silyl ether protecting groups driven by the formation of strong Si−F bonds. Silyl-protected phenols are an attractive moiety for designing fluoride-responsive probes as the fluoride-induced deprotection realizes strong chromophoric and fluorescence changes through phenolate formation. Indeed, this approach has first been pioneered by the Swager group for the detection of fluoride in organic solvents[1124] and was later adopted for sensing in aqueous media. Several of such systems have been described were the reaction rates, the selectivity, the optoelectronic properties, and the solubility have been optimized. We showcase here only a few representative examples.

Overcoming shortcomings of previous fluoride probes, *e.g.*, reaction times >10 min for deprotection of the silyl group, Yang and coworkers developed a rapid reacting probe (**P12.20** in Figure 254a) for the detection of fluoride ions at $\mu$M concentrations in water (1% THF, 2 mM CTAB).[1125] The probe **P12.20** displayed high sensitivity (LOD, 5 $\mu$M) and provided two independent modes of signal transduction, one based on the emission color and the other based on the intensity of the fluorescence signal. A similar detection limit was achieved by Lee and coworkers with a silyl protected and fully water-soluble coumarin-based system (**P12.21** in Figure 254b), which required 10 min reaction time prior to the signal read-out.[1126]

At the same time, Ma, Du, Zhang, and coworkers reported a simple but selective colorimetric and ratiometric fluorescent chemodosimeter (**P12.22**) for the detection of $F^-$ in 20 mM PBS containing 30% EtOH, pH 7.4, at $\mu$M to mM concentrations and in live cells (**P12.22** in Figure 255).[1127]

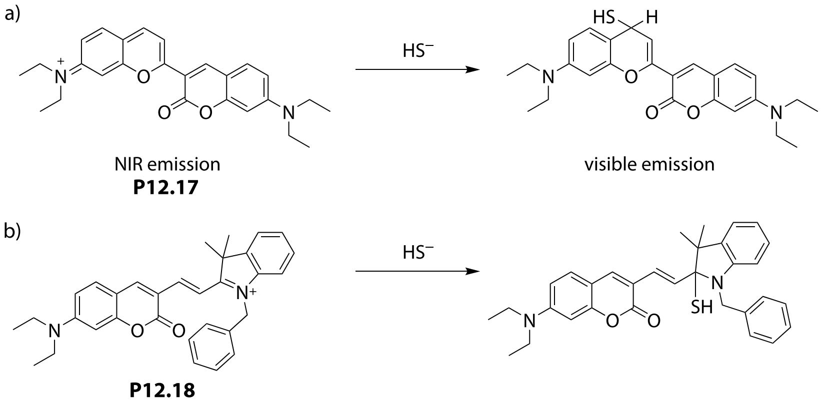

**Figure 252.** Schematic representation of the detection of $HS^-$ by (a) probe **P12.17** and (b) probe **P12.18**.

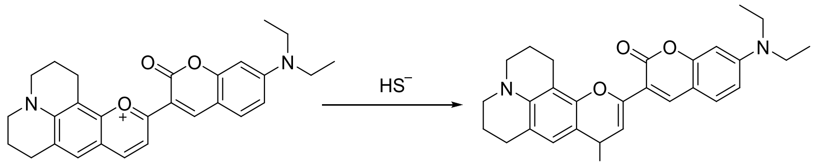

**P12.19**

**Figure 253.** Schematic representation of the reaction between $HS^-$ and the probe **P12.19** used for hydrogen sulfide detection at μM concentration in 10 mM PBS containing 30% MeCN.

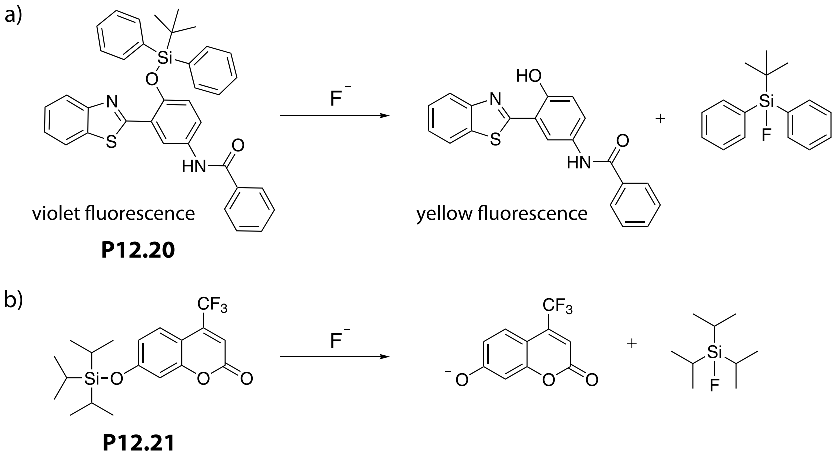

**Figure 254.** (a) Schematic representation of the phenol deprotection reaction promoted by $F^-$ leading to a colorimetric response of **P12.20**. (b) Schematic representation of the alcohol deprotection reaction promoted by $F^-$, allowing for mM detection of $F^-$ by **P12.21** in HEPES buffer.

As previously described for other probes, **P12.22** operated through the fluoride-based silyl deprotection mechanism.

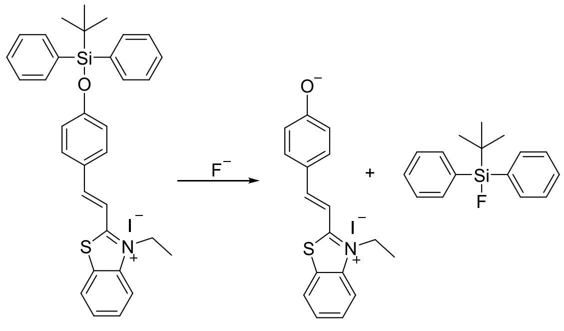

**P12.22**

**Figure 255.** Schematic representation of the phenol deprotection reaction promoted by $F^-$ resulting in the colorimetric reaction of **P12.22** in the presence of $F^-$ at mM concentrations in 20 mM PBS, pH 7.4, containing 30% EtOH.

*In vivo* two-photon imaging of fluoride ions, for instance in zebrafish, is feasible using silyl-protected probes that undergo a subsequent ring closure reaction after fluoride-based deprotection, which was demonstrated by Lee, Kim, and Ahn (**P12.23** in Figure 256).[1128] Also, fluorescein-based dyes can be readily transformed into fluoride-probes through protection of their OH groups with silyl entities (**P12.24** in Figure 257).[1129] Deprotection of aliphatic silyl ethers by fluoride ions can also be exploited for $F^-$ sensing if this structural change induce stacking/orientation differences in the aggregates formed by the probe, as was demonstrated by Li, Lu, Shen, and coworkers, using a pyrene-based probe design (**P12.25** in Figure 257).[1130] This probe was used in water (containing 50% THF) to detect fluoride ions at micromolar concentrations.

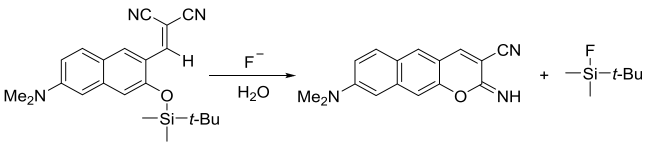

**P12.23**

**Figure 256.** Schematic representation of fluoride-induced deprotection of **P12.23** used to detect $F^-$ in 10 mM HEPES buffer containing 20% MeCN, pH 7.4, at mM concentrations.

In some cases, the direct influence of fluoride ions on aggregating probes, *e.g.*, based on a pyrene scaffold with an attached boronic acid functioning as a fluoride recognition motif, is sufficient to cause optical changes that can be used for micromolar fluoride detection in water containing 5% dichloromethane (**P12.26** in Figure 257).[1131] Likewise, there have been attempts to utilize fluoride-promoted formation of strong H-bonds to design new $F^-$-selective systems.[1132]

## 12.2. Chemosensors for Inorganic Anions

Several groups have mastered the design of inorganic anion binders, and their contributions were summarized in a recent book section.[1133] Some representative examples of high-affinity anion binders are the bambus[*n*]urils[1058,1134−1140] (Sindelar group), biotin[*n*]urils[1141−1143] (Pittelkow group), cyclopeptides,[1144−1151] (Kubik group) and anion binding rotaxanes[1152−1156] (Beer group). In the spirit of this review, we briefly discuss those anion binding systems that provide an optical response to anion binding and thus can be used as chemosensors (see also Table 38).

It has been a considerable challenge introducing a signal transduction mechanism into the anion binding receptors, as

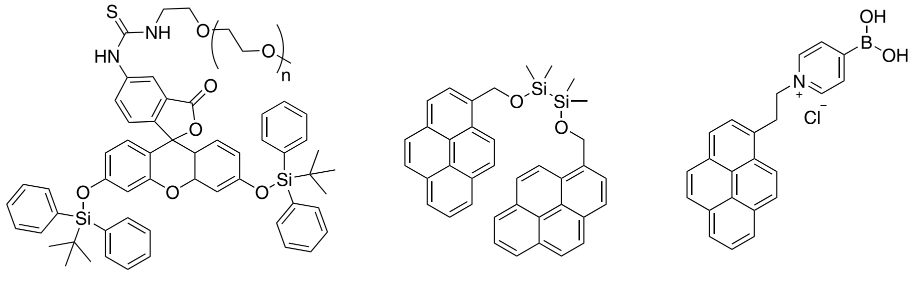

**P12.24** **P12.25** **P12.26**

**Figure 257.** Chemical structures of the fluoride-reactive probes **P12.24**−**P12.26**.

**Table 38. Summary of Some Representative Chemosensors for Inorganic Anions (LOD, Limit of Detection)**

| chemosensor | media | concentration range | ref |
|---|---|---|---|
| Cyanide ($CN^-$) Analyte | | | |
| **C12.2** | water | 0−220 μM;<br>LOD, 320 nM | 1157 |
| **C12.3** | 20 mM HEPES buffer, pH 7.0 | 0−10 mM;<br>LOD, 5 μM | 1158 |
| Chloride ($Cl^-$) Analyte | | | |
| **C12.4** | 4 mM CTAB in 50 mM MOPS buffer, pH 7.0 | 0−2.0 mM;<br>LOD, ∼5 μM | 1163 |
| Iodide ($I^-$) Analyte | | | |
| **C12.1** | water | 0−1.0 mM | 1154 |

for instance the use of PET quenching-based emission turn-on/off is less useful for anion than for cation sensing. Thus, more advanced signal transduction strategies were utilized. For instance, Beer and coworkers recently introduced luminescent tris(bipyridine)ruthenium$^{II}$ moiety into their anion-binding rotaxane (**C12.1** in Figure 258), with the expectation that the luminescence of the chemosensor would decrease upon iodide binding, as was found for the acyclic complex.[1154] However, a notable emission increase (6%) was observed upon $I^-$ binding ($K_a = 1.6 \times 10^3$ $M^{-1}$ in $D_2O$), which the authors attributed to the increased rigidity of the anion bound system. Thus, the chemosensor **C12.1** allowed for fluorescence-based detection of $I^-$ at mM concentrations in water. Other anions such as $SO_4^{2-}$ also bind to **C12.1** ($K_a = 4.5 \times 10^2$ $M^{-1}$ in $D_2O$), generating an even higher fluorescence response (10% emission increase). In comparison, the structurally related acyclic system showed at least one order of magnitude lower affinities.

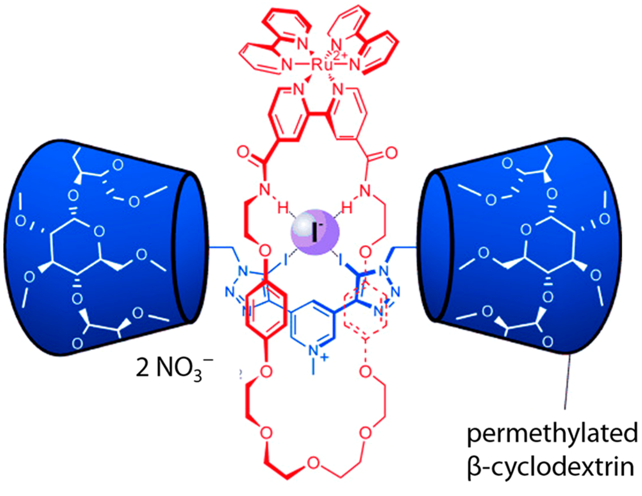

C12.1

**Figure 258.** Chemical structure of the halogen binding [Ru$^{II}$(bpy)$_3$]-based rotaxane chemosensor **C12.1**. The chemosensor **C12.1** allows for luminescence-based detection of $I^-$ at mM concentrations in water ($D_2O$). Reproduced with permission from ref 1154. Copyright 2016 Wiley-VCH.

In some cases, the time of the assays for anion detection, *e.g.*, of cyanides, can be inconveniently long for probes that undergo covalent bond formation with the target analyte. Zhang and coworker overcame this problem by exploiting the self-assembly of 4-amino-3-hydroxynaphthalene-1-sulfonic acid into fluorescent aggregates (**C12.2** in Figure 259) that are selectively and rapidly emission-quenched by cyanide ($K_a = 2.2 \times 10^9$ $M^{-2}$) in water.[1157] The chemosensor detection limit for $CN^-$ in water was given as 0.4 μM, while other anions (*e.g.*, $F^-$, $Cl^-$, $Br^-$, $I^-$, $AcO^-$, $H_2PO_4^-$, $HSO_4^-$, and $ClO_4^-$) had nearly no effect on the emission properties of **C12.2**. The authors also showcased that their chemosensor can be used to prepare paper strips for testing cyanides.

Ye and coworkers had shown that cyanides can be effectively bound by the chemosensor **C12.3** (Figure 260) through a relay of hydrogen bonding contacts in 20 mM HEPES buffer, pH 7.0, reaching binding affinities up to 900 $M^{-1}$ and a detection limit as low as 5 μM.[1158] Furthermore, this chemosensor design that utilized Ru(bpy)$_n$ complexes as luminescent signaling units was shown to be tolerant towards other hard and soft inorganic anions, *i.e.*, $OAc^-$, $F^-$, $Cl^-$, $Br^-$, $I^-$, $NO_3^-$, $HSO_4^-$, $H_2PO_4^-$, $ClO_4^-$, $N_3^-$, $HCO_3^-$, and $SCN^-$.

Intracellular and extracellular concentrations of chlorides differ significantly, *e.g.*, ∼10 mM intracellular and ∼100 mM extracellular in mammalian cells.[1159] Chloride imaging is therefore of particular interest for neuroscientists that typically use either genetically encoded, protein-based bioreceptors or fluorescent dyes, which are dynamically quenched by chloride ions.[1160−1162] Both methods have their advantages and disadvantages but are not in the scope of this review.

Probes and chemosensors that are applicable in aqueous media for the (selective) detection of chloride are rather rare. This biologically relevant target anion has an intermediate softness−hardness characteristic that makes it less likely to trigger chemical transformation or to engage in binding interactions as previously shown with cyanide, fluoride, iodide, or multiply charged anions such as phosphates (see section 13). An elegant approach to increase the apparent affinity of a chemosensor (**C12.4** in Figure 261) for chloride by nearly two order of magnitude was demonstrated by the Severin group.[1163] The authors exploited the enhanced partition of an anion-binding Rh-based metal−organic complex into

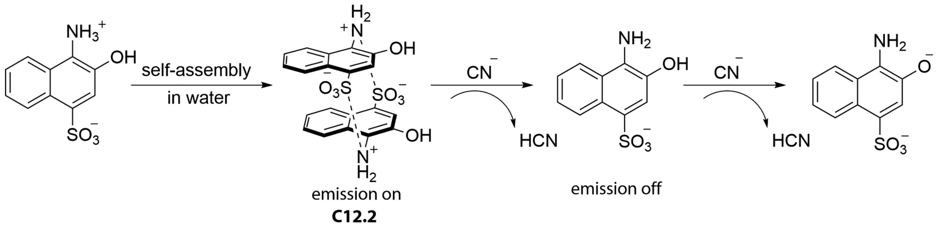

**Figure 259.** Schematic representation of the proposed sensing mechanism for $CN^-$ with chemosensor **C12.2**. Fluorescence-based $CN^-$ detection was achieved at $\mu$M concentrations in water.

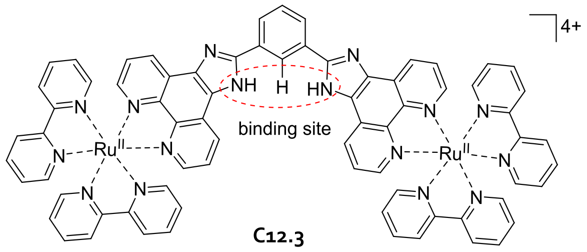

**Figure 260.** Chemical structure of the chemosensor **C12.3** used for fluorescence-based detection of $CN^-$ at mM concentrations in 20 mM HEPES buffer, pH 7.0.

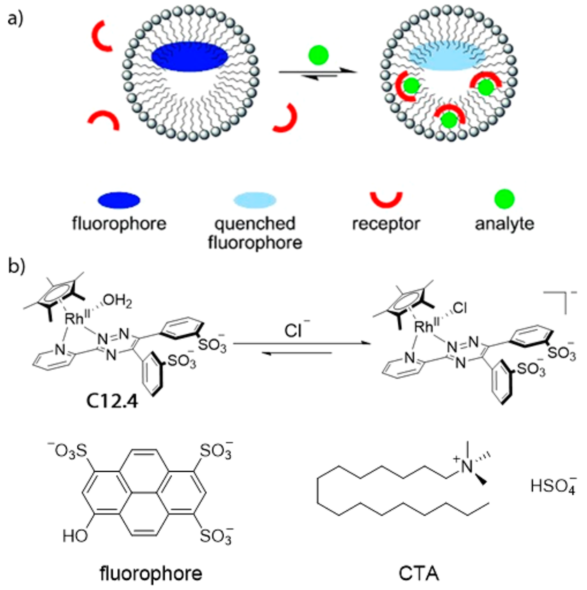

**Figure 261.** (a) Chloride sensing (mM range) in 50 mM MOPS buffer, pH 7.0, with a Rh-based anion-binding metal complex that partitions into a CTA micelle, where it then quenches the emission of the fluorescent dye 8-hydroxypyrene-1,3,6-trisulfonate (HPTS). (b) Chemical structure of the Rh-complex (**C12.4**), the fluorophore (HPTS) and the surfactant CTA. Adapted with permission from ref 1163. Copyright 2010 Wiley-VCH.

cetyltrimethylammonium (CTA) hydrogen sulfate micelles after chloride binding ($K_a$ = 660 $M^{-1}$ and $K_{app}$ > $10^4$ $M^{-1}$ for $Cl^-$ in the absence and presence of >20 mM CTA, respectively; both in 50 mM MOPS buffer, pH 7.0). Moreover, the CTA micelles were co-loaded with 8-hydroxypyrene-1,3,6-trisulfonate (HPTS) as a fluorophore, whose emission is quenched in the presence of the metal complex, thereby providing a fluorescent signal transduction readout for the detection of chloride in water samples at $\mu$M to mM concentrations. Most hard anions such as $SO_4^{2-}$, $NO_3^-$, $F^-$, and $HCO_3^-$, some of which occur in millimolar concentrations in mineral waters, do not interfere the quantitative sensing of chloride ions. Conversely, metal-binding anions such as cyanide, bromide, and iodide were discussed as potential interferents, but their concentration in biofluids and natural water sources is low, if present at all.

Considering the accepted concentration limit for nitrates in drinking water, its concentration level appears attractive for the development of probes and chemosensors for nitrate (or sulfates and phosphates), nevertheless, the difficulties in targeting these hydrophilic "hard" anions in a selective manner are considerable. Thus, many reports have rather focused on the design of probes and chemosensors for inorganic anions whose detection is easier, *e.g.*, the "soft" cyanide. Yet, cyanides typically only occur in the environment due to accidental or deliberate spills, and thus their sensing is of lower practical relevance.

### 12.3. Nanosensors for Inorganic Anions

Several nanoparticle-based sensors have been reported for the detection of toxic cyanide anions in aqueous solutions and in biological samples (see Table 39 for a summary of the within this section discussed nanosensors). For example, Kim, Jung, and coworkers reported the use of bisindole-functionalized mesoporous silica particles (**N12.1** in Figure 262) for the colorimetric-based detection of cyanides in water/acetonitrile (7:1 v/v) mixtures at $\mu$M concentrations.[1164] When cyanide salts were added to aqueous dispersions of **N12.1**, a distinct color change from orange to deep-yellow was observed and quantified *via* UV-Vis absorption spectroscopy. The color change was explained by the Michael addition reaction occurring between the cyanide and bisindole, which alters the absorption properties of the reporter dye. The photophysical properties of **N12.1** were not influenced by other anionic species, such as $F^-$, $Cl^-$, $Br^-$, $I^-$, $AcO^-$, $H_2PO_4^-$, and $HSO_4^-$.

A new type of metal complex-doped silica nanoparticles (**N12.2** in Figure 263) was reported by Wei and coworkers for the detection of cyanides at $\mu$M concentrations (LOD, 80 nM) in carbonate buffer, pH 11.0.[1165] The particles were prepared by a micelle assisted synthesis method[1166,1167] by using the surfactant Pluronic F127 and yielded silica-core polyethylene glycol shell particles that were emissive due to aggregation-induced emission (AIE) of the encapsulated metal complexes. Fluorescence quenching was observed in the presence of $CN^-$. However, the exact mechanism remains unclear. In fact, the authors demonstrated that the $CN^-$ anions did not react with the metal complex. The nanosensor **N12.2** showed a good selectivity towards $CN^-$ anions, as other possible interferants such as $F^-$, $Cl^-$, $Br^-$, $CH_3COO^-$, $SCN^-$, $NO_2^-$, $NO_3^-$, $IO_3^-$, $S^{2-}$, $SO_3^{2-}$, $CO_3^{2-}$, $HPO_4^{2-}$, $PO_4^{3-}$, and $EDTA^{4-}$ did not cause fluorescence quenching of **N12.2**.

### Table 39. Summary of Herein Discussed Representative Nanosensors for Inorganic Anions (LOD, Limit of Detection)

| nanosensor | media | concentration range | ref |
|---|---|---|---|
| | Cyanide ($CN^-$) Analyte | | |
| **N12.1** | 12.5% MeCN in water | $\mu$M range | 1164 |
| **N12.2** | $NaHCO_3$−NaOH buffer, pH 11.0 | 0.1−10 $\mu$M (linear range);<br>LOD, 80 nM | 1165 |
| **N12.3** | PBS, pH 7.4 | 0.5−2 mM | 1168 |
| **N12.4** | water | $\mu$M range | 1169 |
| **N12.5** | 400 mM NaCl in 40 mM phosphate buffer, pH 7.4; | 0−300 $\mu$M;<br>LOD, 100 nM | 1170 |
| | waste water samples | $\mu$M range | |
| **N12.6** | water | 16−133 $\mu$M;<br>LOD, 1.8 $\mu$M | 1172 |
| | Chloride ($Cl^-$) Analyte | | |
| **N12.16** | PBS, pH 7.4; in cells | 0−200 mM | 1184 |
| | Fluoride ($F^-$) Analyte | | |
| **N12.15** | 70% MeCN in water containing 100 mM KHP and HCl, pH 2.5 | mM range | 1183 |
| | Hydrogen sulfide ($HS^-$) Analyte | | |
| **N12.9** | 10 mM phosphate buffer solution containing 20 mM NaCl, pH 9.0 | 0−30 $\mu$M;<br>LOD, 0.2 $\mu$M | 1175 |
| | waste water samples, pH 9.0 | LOD, 0.5 $\mu$M in waste water | |
| **N12.10** | water containing 400 $\mu$M CTAB | 0−100 $\mu$M;<br>LOD, 103 nM | 1176 |
| | 1 % serum samples; 10 % urine samples | 0−200 $\mu$M in biofluids | |
| **N12.11** | 500 $\mu$M phosphate buffer, pH 7.4 | 0−200 $\mu$M;<br>LOD, 15 $\mu$M | 1178 |
| | real water samples | $\mu$M range in real water samples | |
| | Iodide ($I^-$) Analyte | | |
| **N12.13** | 10 mM HEPES buffer, pH 7.2 | 10−120 $\mu$M;<br>LOD, 80 nM | 1180 |
| | real water samples | $\mu$M range in real water samples | |
| **N12.14** | 200 mM phosphate buffer, pH 7.2 | 0−3.8 $\mu$M; | 1182 |
| | real water samples | LOD, 108 nM | |
| | urine, blood, serum, and food samples | | |
| | Permanganate ($MnO_4^-$)[a] Analyte | | |
| **N12.12** | water | 0−50 $\mu$M | 1179 |
| | sebrafish | LOD, 0.5 $\mu$M | |
| | Sulfide ($SO_4^{2-}$) Analyte | | |
| **N12.7** | 10 mM acetate buffer, pH 4.0 | 0−50 $\mu$M;<br>LOD, 0.34 $\mu$M | 1173 |
| **N12.8** | water containing 23.3 mM NaCl and 23.3 mM $Na_2HPO_4$ | 0−12.5 mM | 1174 |

[a] Can also be used to detect $Cu^{2+}$ (LOD, 200 nM) and $Hg^{2+}$ (LOD, 500 nM).

Lin and coworkers prepared fluorescein-loaded mesoporous silica particles in combination with cyanide-responsive pseudorotaxanes as gatekeepers (**N12.3** in Figure 264) for fluorescent-based detection of cyanide anions at millimolar concentrations in PBS, pH 7.4.[1168] The cyanide-responsive gatekeeper consisted of a $Pd^{II}$-templated pseudo-rotaxane that disassembled in the presence of cyanide anions due to a demetallation process that yields the water-soluble $[Pd(CN)_4]^{2-}$ complex. After disassembly of the gatekeeper, the reporter dye spontaneously diffused out of the particle pores, resulting in restored emissivity of the dye that was recorded in the supernatant. Nanosensor **N12.3** allows for mM detection of $CN^-$. None of the other potential interferants tested (*e.g.*, $F^-$, $Cl^-$, $N_3^-$, and $AcO^-$) triggered a gatekeeper disassembly.

Recently, Klajn, and coworkers reported the use of water-soluble polycationic $[Pd_6L_4]^{12+}$ nanocages with an encapsulated H-aggregate of 4,4-difluoro-4-bora-3a,4a-diaza-*s*-indacene (BODIPY) as a potential colorimetric nanosensors for cyanide anions in water (**N12.4** in Figure 265).[1169] The formation of the nanocage BODIPY ensemble was induced by adding empty nanocages to aqueous suspensions of the dye. The cage undergoes structural deformation to trap a single H-dimer of BODIPY in its hydrophobic cavity. In the presence of micromolar concentrations of $CN^-$, the dye-loaded nanocage disassembled and released BODIPY, which reassembled in water to form *J*-aggregates that were detected by their distinct spectroscopic features and correlated with the amount of $CN^-$ present in water.

A sensitive (LOD, 100 nM) nanosensor for the detection of cyanide anions at $\mu$M concentrations in 40 mM phosphate buffer (pH 7.4) was reported by Ko and coworkers using polysorbate-stabilized and fluorescein-doped gold nanoparticles (**N12.5** in Figure 266).[1170] Fluorescence-based detection was possible because the surface of **N12.5** is etched in the presence of $CN^-$,[1171] which leads to depletion of the polysorbate and fluorescein from the surface of the particles, causing an increase in the fluorescence of the dye as it is no longer subject to quenching by an energy transfer process with the gold surface. Alternatively, the authors showed that **N12.5** was able to detect $CN^-$ *via* a colorimetric mode, as depletion of polysorbate also triggered aggregation of the particles, resulting in a distinct color change that was correlated with the concentration of the analyte. As expected, the fluorescence signal response was more sensitive (0−10 $\mu$M) than colorimetric detection (150−300 $\mu$M). The robustness of **N12.5** was investigated, and no cross-reactivity was observed with $F^-$, $Cl^-$, $Br^-$, $CH_3COO^-$, $NO_3^-$, $CO_3^{2-}$, $SO_3^{2-}$, $SO_4^{2-}$, $HPO_4^{2-}$, $PO_4^{3-}$, $EDTA^{4-}$, and citrate.

The same year, Farhadi and coworkers prepared sodium dodecyl sulfate (SDS) stabilized silver nanoparticles, which were used for colorimetric detection of cyanides at $\mu$M concentrations in water samples (**N12.6** in Figure 267).[1172] In the presence of $CN^-$, the particles dissolve, which can be observed by a change in color of the particle dispersion as localized surface plasmon resonances disappear. No colorimetric response was observed with other anions such as $F^-$, $Cl^-$, $Br^-$, $NO_2^-$, $NO_3^-$, $SCN^-$, $H_2PO_4^-$, $HPO_4^{2-}$, $C_2O_4^{2-}$, $CO_3^{2-}$, $SO_3^{2-}$, and $SO_4^{2-}$, but the applicability to biofluids containing biothiols or proteins remains to be investigated.

A colorimetric nanosensor for the detection of sulfate anions at $\mu$M concentrations in 10 mM acetate buffer, pH 4.0, was reported by Ye and coworkers.[1173] To this end, cysteamine decorated gold nanoparticles (**N12.7** in Figure 268) were prepared, which possessed good colloidal stability in acidic media. However, sulfate anions adsorb on the surface of **N12.7** and neutralize positive charges, which promotes particle aggregation, and thus a color change due to a change of surface plasmon resonances. The aggregation degree was quantified spectroscopically and correlated to the amount of sulfate present in buffer solutions. No cross-reactivity with $F^-$, $Cl^-$, $NO_3^-$, $HCO_3^-$, $IO_3^-$, $B_4O_7^{2-}$, $S_2O_3^{2-}$, $CO_3^{2-}$, $PO_4^{3-}$, and $BO_3^{3-}$ was observed. In the presence of $SO_3^{2-}$, some aggregation was observed.

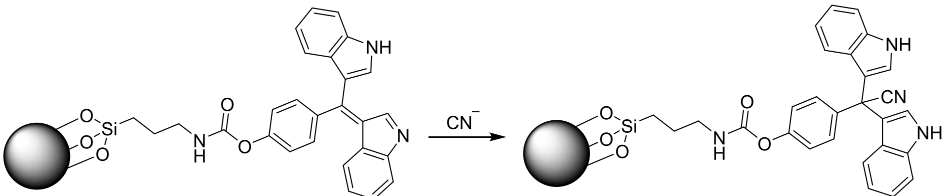

**N12.1**

**Figure 262.** Schematic representation for the detection of CN− with bisindole functionalized mesoporous silica particles (**N12.1**). Colorimetric detection allows for CN− quantification at μM concentrations in water/MeCN mixtures (7:1 v/v).

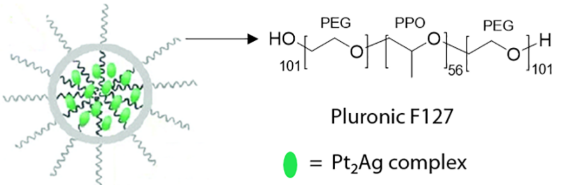

**N12.2**

**Figure 263.** $Pt_2Ag$-complex-loaded hybrid silica particles (**N12.2**) designed for fluorescence-based detection of cyanides at μM concentrations in carbonate buffer, pH 11.0. Adapted with permission from ref 1165. Copyright 2014 The Royal Society of Chemistry.

More recently, Kubik and coworkers reported the use of water-soluble cyclopeptide-decorated and triethylene glycol-protected gold nanoparticles (**N12.8**) for colorimetric-based detection of sulfates in water containing 23 mM NaCl and 23 mM $Na_2HPO_4$ at mM concentrations (Figure 269).[1174] Colorimetric detection was possible because the cyclopeptides bind to sulfate on the surface of the nanoparticles in such a way that a supramolecular bridge is formed between the nanoparticles, triggering the aggregation of **N12.8**. The degree of aggregation can be determined spectroscopically as modified plasmon resonances emanate from these aggregates. The response of the nanosensor to possible interfering species was evaluated and no aggregation of particles was observed in the presence of $Cl^-$, $Br^-$, $NO_3^-$, $CO_3^{2-}$, $HPO_4^{2-}$, $HAsO_4^{2-}$, and $P_2O_7^{4-}$.

Chang, Ye, and coworkers communicated glutathione-capped gold nanoparticles, which have been surface-functionalized with a sulfide responsive aromatic azide moiety and an amine reactive crosslinker (NHS-ester; **N12.9** in Figure 270). This nanosensor allowed for the detection of $H_2S/HS^-$ at μM concentrations in 10 mM phosphate buffer, pH 9.0.[1175] In the absence of sulfides, these particles display good colloidal stability, whereas in the presence of sulfides, the aromatic azide was reduced to an aniline functionality, which subsequently reacted with the NHS ester moieties, leading to the formation of particle-crosslinking amide bonds. Consequently, aggregation occurred which was detected spectroscopically and correlated to the amount of the analyte. Presumably, this system will show a cross-reactivity towards amine-functional analytes and thus cannot be applied in biofluids.

Ding and coworkers reported the use of pyronine-functionalized mesoporous silica particles (**N12.10** in Figure 271) for the detection of $H_2S/HS^-$ at μM concentrations in water containing 400 μM CTAB and in sulfide-spiked blood and urine samples (recovery <99%).[1176] Pyronines are known $H_2S$-selective probes as the $HS^-$ are nucleophilic species which react with such dyes through Michael addition, leading to the formation of nonfluorescent derivatives.[1177] Thus, the characteristic fluorescence quenching of the dye allowed for the spectroscopic detection of $H_2S/HS^-$ with dispersions of **N12.10**. Interestingly, the authors found that the addition of cetyltrimethylammonium bromide (CTAB) to an aqueous dispersion of **N12.10** increased the sensitivity of the nanosensors because the surfactant neutralized negative charges on the surface of the particles, facilitating the diffusion of $HS^-$ anions to the pyronine moieties. The authors found no cross-reactivity with $F^-$, $Br^-$, $NO_3^-$, $H_2PO_4^-$, $HCO_3^-$, Cys, Hcys, GSH, $H_2O_2$, or $Na_2S$.

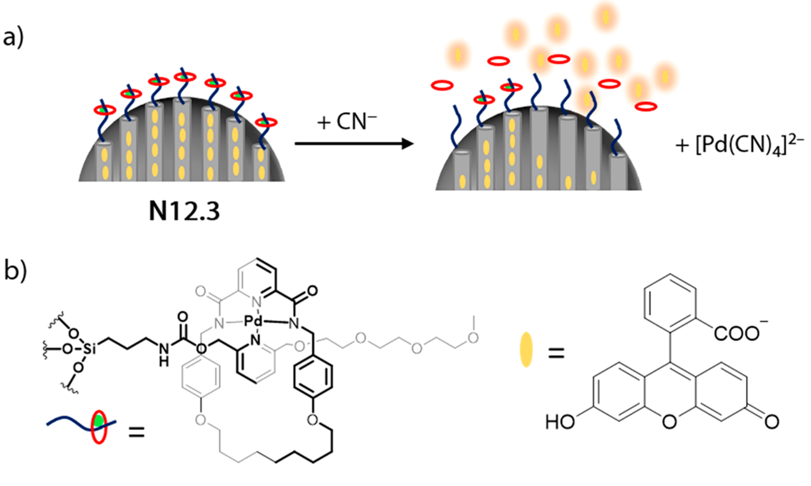

**Figure 264.** (a) Schematic representation for the detection mechanism of CN− using fluorescent reporter-loaded and nanovalve-capped mesoporous silica particles (**N12.3**). CN− anions were detected at millimolar concentrations in PBS, pH 7.4. (b) Chemical structure of the pseudorotaxane-based nanovalve and the fluorescent reporter dye fluorescein.

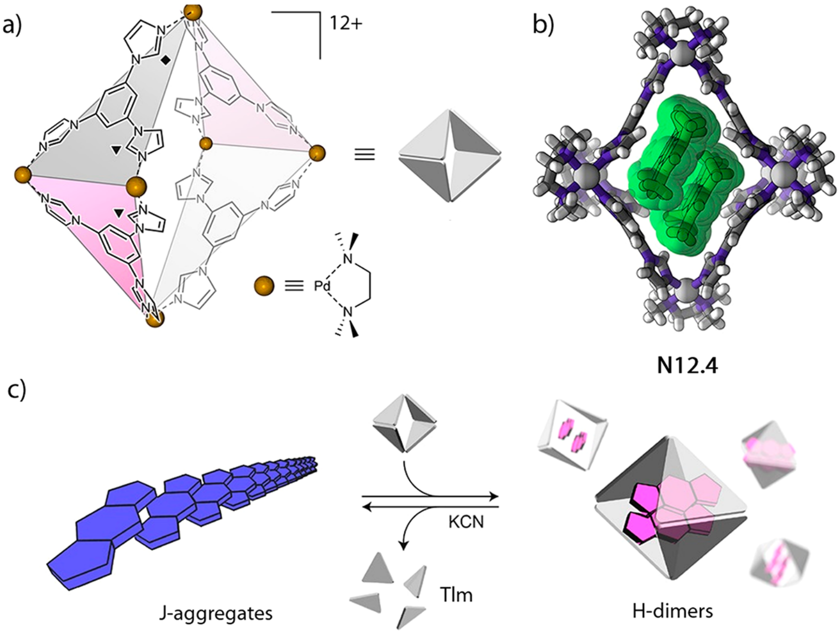

**Figure 265.** (a) Chemical structure of the $[Pd_6L_4]^{12+}$ (L = 1,3,5-triimidazoylbenzene) nanocage BODIPY ensemble (**N12.4**) used for fluorescence-based $CN^-$ detection at $\mu$M concentrations in water. (b) 3D-structure of **N12.4**. (c) Schematic representation of the sensing mechanism using **N12.4**. In the presence of $CN^-$ the nanocage disassembles to release BODIPY, which is detected spectroscopically. Adapted with permission from ref 1169. Copyright 2020 American Chemical Society.

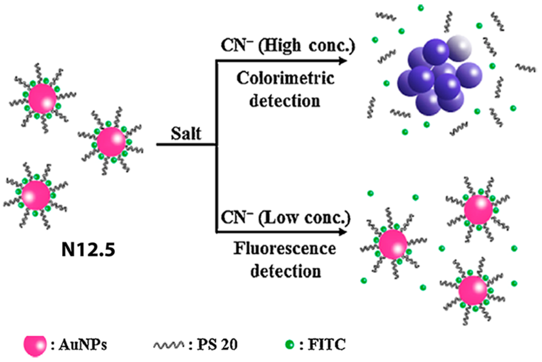

**Figure 266.** Polysorbate-stabilized and fluorescein decorated gold nanoparticles (**N12.5**) used for dual, colorimetric, and fluorescence-based detection of cyanides at $\mu$M concentrations in 40 mM phosphate buffer, pH 7.4. Reproduced with permission from ref 1170. Copyright 2016 Elsevier BV.

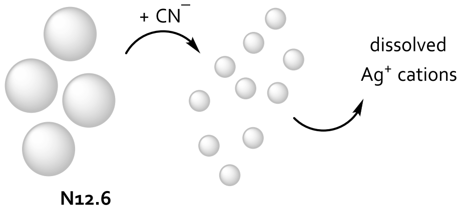

**Figure 267.** Sodium dodecyl sulfate (SDS) stabilized silver nanoparticles (**N12.6**) used for colorimetric $\mu$M detection of cyanide anions in water and wastewater samples.

Recently, Hatai, Niemeyer, and coworkers described the use of Pd(II)-based metallosupramolecular coordination polymers (**N12.11** in Figure 272) as fluorescent probes for the detection of $HS^-$ at $\mu$M concentrations in 500 $\mu$M phosphate buffer, pH 7.4 (LOD, 15 $\mu$M), and real water samples.[1178] **N12.11** was formed by the complexation of the coumarin-bearing hydrazone ligand with $Pd^{II}$ cations. The emission of coumarin was quenched due to intramolecular charge-transfer (ICT) processes arising from the presence of $Pd^{II}$. An increased emission intensity was observed in the presence of $HS^-$ anions, which is explained by the ability of $HS^-$ to scavenge and deplete $Pd^{II}$ from **N12.11**, such that coumarin is no longer subject to an ICT quenching process. Other anions, such as $F^-$, $Cl^-$, $Br^-$, $I^-$, $SCN^-$, $CO_3^{2-}$, $SO_4^{2-}$, $SO_3^{2-}$, $S_2O_3^{2-}$, and acetate (120 $\mu$M) did not affect the emission signal of **N12.11**.

Cuboid mesoporous silica particles functionalized with *o*-safranin were designed as permanganate selective fluorometric nanosensors (**N12.12** in Figure 273) by Yang, Liang, and coworkers.[1179] In this example, the particles were covalently linked with the fluorescent reporter dye *o*-safranin. In the presence of permanganate anions, fluorescence quenching was observed and used to for quantification (LOD, 0.5 $\mu$M). The observed decrease in fluorescence was explained by the formation of strong $R_2NH^+$ and $MnO_4^-$ interactions ($R_2NH^+\cdots O{=}Mn$) between the analyte and the urea moiety, giving rise to charge transfer processes. Fluorescence quenching was not observed in the presence of other anions, such as $F^-$, $Cl^-$, $Br^-$, $I^-$, $NO_3^-$, $HCO_3^-$, $CO_3^{2-}$, $SO_4^{2-}$, $HSO_3^-$, $SO_3^{2-}$, $Cr_2O_7^{2-}$, $CrO_4^{2-}$, $HPO_4^{2-}$, and $PO_4^{3-}$. The authors demonstrated in a proof-of-concept experiment that **N12.12** can be used for *in vivo* imaging of artificially administered permanganate ions in zebrafish models.

Paul and coworkers reported the use of sulfonated-calix[4]arene (Cx4) decorated gold nanoparticles (**N12.13** in Figure 274) for colorimetric detection of iodide at $\mu$M levels in 10 mM HEPES buffer, pH 7.4. **N12.13** showed a good selectivity over other common anions, *e.g.*, $F^-$, $Br^-$, $H_2PO_4^-$, $ClO_4^-$, $NO_3^-$, $IO_4^-$, $BF_4^-$, $CN^-$, $SCN^-$, $CH_3COO^-$, $HSO_4^-$, $HSO_3^-$, $SO_3^{2-}$, and $S_2O_4^{2-}$.[1180] In the presence of $I^-$ anions, particle aggregation was observed and monitored by UV−vis absorption spectroscopy. It was reasoned that iodide adsorbed on the surface of the nanoparticle, driven by energetic

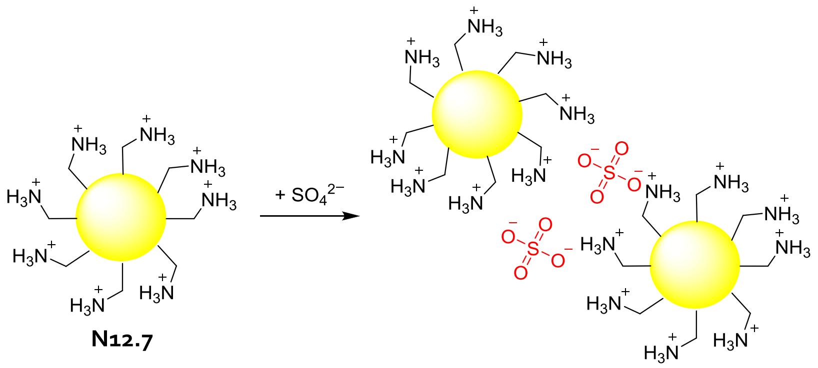

**Figure 268.** Cysteamine decorated gold nanoparticles (**N12.7**) used for colorimetric-based detection of sulfate anions at $\mu$M concentrations in acetate buffer.

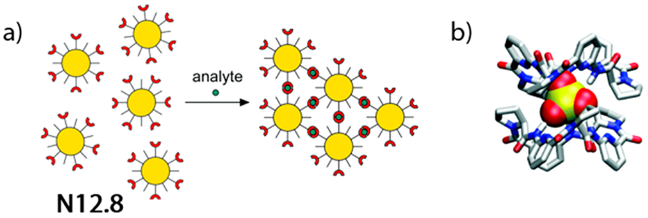

**Figure 269.** (a) Cyclopeptide functionalized gold nanoparticles (**N12.8**) for colorimetric detection of sulfate anions at mM concentrations in water. (b) The cyclopeptide binds with the sulfate anion in a 2:1 ratio. Adapted with permission from ref 1174. Copyright 2020 The Royal Society of Chemistry.

induction ($I^- - e^- \rightarrow I_{adsorbed} + e^-$).[1181] The adsorption of iodide leads to a decrease of negative charges on the surface of **N12.13**, causing the detachment of Cx4, which in turn promotes particle aggregation.

A colorimetric-based detection for iodide at micromolar concentrations in 200 mM phosphate buffer, pH 7.2, urine, blood, and food samples with the use of chitosan oligosaccharide lactate-capped plasmonic silver nanoparticles (**N12.14** in Figure 275) was reported by Vasimalai and coworkers.[1182] The authors showed that the presence of $I^-$ modulated the characteristic surface plasmon resonance of the particles (decrease in absorbance), which was explained by the formation of a new layer of insoluble AgI layer surrounding **N12.14**. Other anions, such as $F^-$, $Br^-$, $NO_3^-$, $NO_2^-$, $H_2PO_4^-$, $CN^-$, $SCN^-$, $SO_4^{2-}$, and $CO_3^{2-}$, did not affect the surface plasmon resonance of **N12.14**. The authors showed that **N12.14** can be used for $\mu$M detection of $I^-$ in spiked urine and blood with good recovery (>98%). Finally, it was demonstrated that the nanosensor can be immobilized on paper-strips and used for easy and practical $I^-$ detection.

A mesoporous silica-based nanosensor for the detection of fluoride anions was introduced by Sarkar and coworkers (**N12.15** in Figure 276).[1183] Covalent immobilization of nitrobenzoxadiazole dyes in the pores of mesoporous silica particles results in strong emission quenching due to nonradiative energy transfer processes occurring in this confined space (aggregation-induced quenching). In the presence of $F^-$, the covalent Si−O−C bond which links the fluorescent molecule with the silica surface is hydrolyzed. As a result, the dye molecules diffuse out of the pores into the aqueous bulk, where their fluorescence intensity is restored. Fluorometric analysis allowed for selective $F^-$ detection at micromolar concentrations in acidic MeCN/water (7:3 v/v) mixtures, pH 2.5.

Recently, a ratiometric sensing strategy which is selective for chloride anions has been evaluated by Wang and coworkers and used for intracellular $Cl^-$ quantification.[1184] For this purpose, dual fluorescent silica particles (**N12.16** in Figure 277) were prepared physically entrapping the [$Ru^{II}$(1,10-phenanthroline)$_3$] complex (reference dye) and bearing on their surface the $Cl^-$ responsive fluorescent dye *N*,*N*′-bis(carboxypropyl)-9,9′-biacridine[1185] (reporter dye), which was grafted onto the surface of the particles by alkoxysilane chemistry. In the presence of $Cl^-$, the fluorescence lifetime of the reporter dye decreases significantly as chloride quenches its fluorescence, while the fluorescence lifetime of the reference dye remains unchanged. This allowed the quantification of chloride anions in the concentration range of 0−200 mM. Cell uptake experiments showed that **N12.16** accumulates in lysosomes, where it remains functional. Because the $Cl^-$

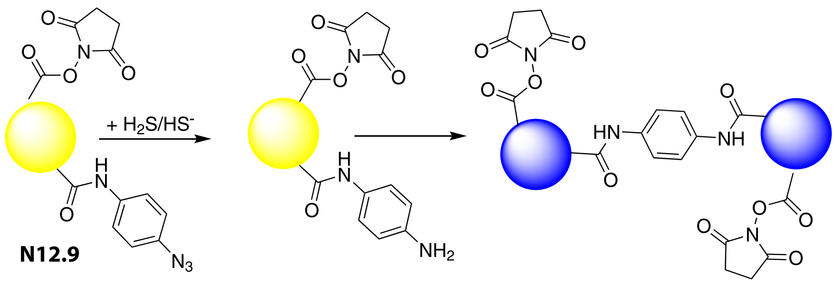

**Figure 270.** Schematic representation of the sensing mechanism for the detection of $H_2S/HS^-$ in phosphate buffer using gold nanoparticles that have been surface-functionalized with hydrogen sulfide and amine reactive crosslinkers (**N12.9**). Note that, for better visualization, only the reactive and truncated chemical structures are shown.

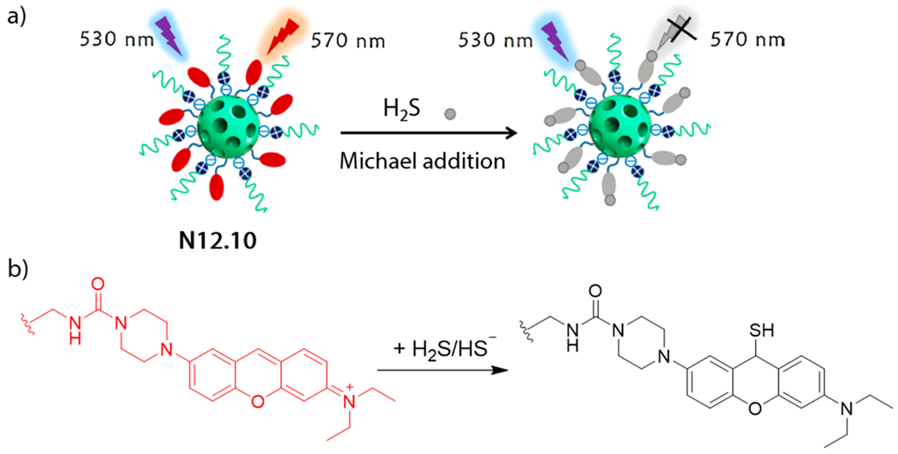

**Figure 271.** (a) Pyronine functionalized mesoporous silica particles (**N12.10**) used for fluorescence-based detection of $H_2S/HS^-$ at $\mu$M concentration in water, blood, and urine samples. (b) Schematic representation of the Michael-type addition reaction occurring between pyronine and of $H_2S/HS^-$. Adapted with permission from ref 1176. Copyright 2019 Elsevier BV.

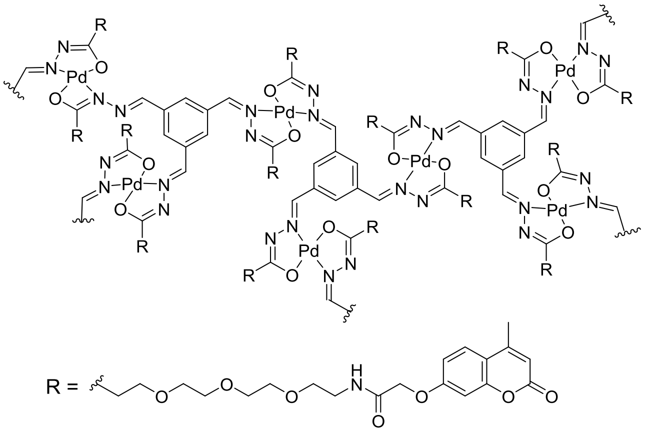

**N12.11**

**Figure 272.** Chemical structure of the metallosupramolecular coordination polymer (**N12.11**) for fluorescence turn-on detection of hydrogen sulfide $HS^-$ at $\mu$M concentrations in PBS, pH 7.4.

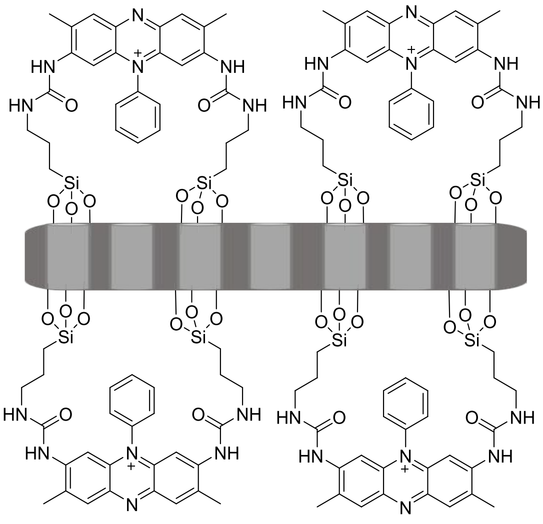

**N12.12**

**Figure 273.** *o*-Safranin functionalized cuboid mesoporous silica particles (**N12.12**) used for fluorescence-based detection of permanganate anions at $\mu$M concentrations in water and *in vivo*.

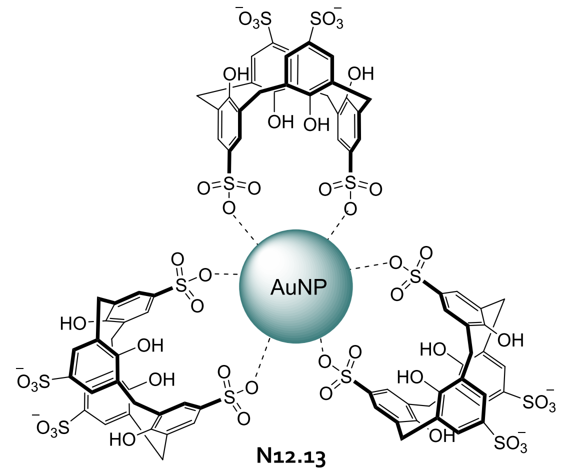

**N12.13**

**Figure 274.** Calix[4]arene functionalized AuNPs (**N12.13**) can be used for the colorimetric detection of iodides at $\mu$M concentrations in 10 mM HEPES buffer, pH 7.4.

concentration is different in various cell compartments, *e.g.*, 5–20 mM in cytosol and more than 80 mM in lysosomes,[1186,1187] **N12.16** holds the potential to serve as a nanosensor for chloride imaging in living cells, especially for studying lysosomal function.

In summary, for the sensing of some inorganic anions, namely cyanide, fluoride, and (hydrogen)sulfides, powerful probes, chemosensors, and nanosensors have become available that are usable in water, in biofluids, and for imaging applications. Reactive probes and some nanosensors appear to outperform chemosensors for these target anions in terms of detection limits and anion selectivity. However, reversible anion-binding chemosensors will be advantageous for monitoring of dynamic anion concentration changes, *e.g.*, in biological systems. Again, the number of molecular probes, chemosensors, and nanosensors available for a particular anion does not correspond to its biological or environmental importance; cyanides and fluorides are rather rarely encountered in biofluids and fresh water sources, and if, such as in the event of a spillage, instrumental analytical methods may be applicable and preferable (Table 40). On the contrary, the choice of molecular probes, chemosensors, and nanosensors with an

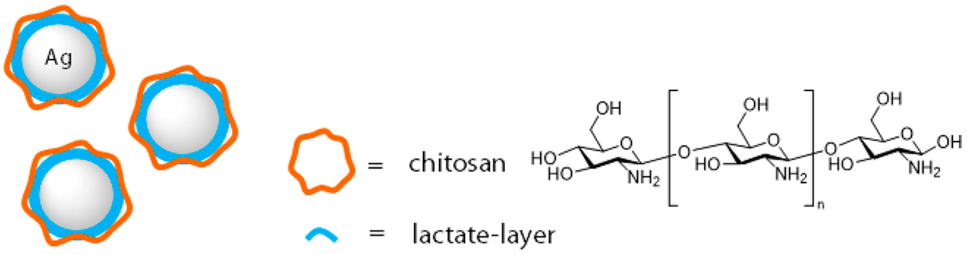

**N12.14**

**Figure 275.** Schematic representation of the detection mechanism of I$^-$ with **N12.14**. The nanosensor **N12.4** allows for the detection of I$^-$ at $\mu$M concentrations in 200 mM phosphate buffer.

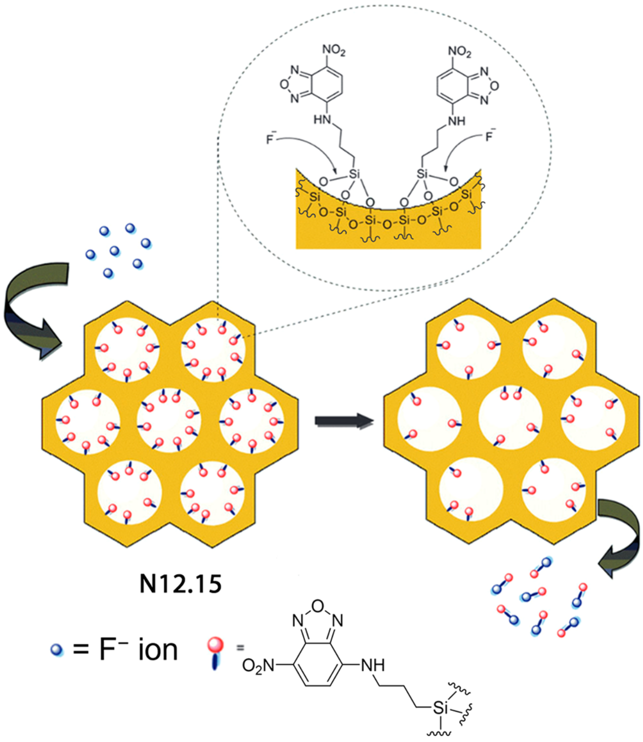

**Figure 276.** Nitrobenzoxadiazole functionalized mesoporous silica particles (**N12.15**) used for fluorometric detection of F$^-$ at $\mu$M concentrations in 70% MeCN in water containing 100 mM potassium hydrogen phthalate and HCl, pH 2.5. Adapted with permission from ref 1183. Copyright 2015 The Royal Society of Chemistry.

optical readout is much more limited for the frequently encountered anions such as sulfate, chloride, and nitrate.

## 13. PHOSPHATES

### 13.1. Biological Role and Structure of Common Inorganic Phosphates

Inorganic phosphates are essential anions for all organisms as they are constituents hard tissues such as bone, teeth, and cartilage.[1194] In addition, inorganic phosphates are used by the body to synthesize vital biomolecules already discussed in section 6 and section 8, such as DNA, phospholipids, adenosine triphosphate, and are important functional groups involved in posttranslational protein modifications.[1195,1196] Therefore, phosphates are crucial for maintaining homeostasis of energy metabolism, cell signaling, regulation of protein synthesis, skeletal development, and bone integrity.[1194,1197] Although calcium phosphates are the major inorganic constituents of biological hard tissue, their insoluble precipitates can crystallize in the body in undesirable ways, causing a variety of diseases, such as urinary stones,[1198,1199] atherosclerosis,[1200−1202] dental calculus,[1203,1204] and chondrocalcinosis.[1205] In addition, elevated urinary phosphate levels are also considered a biomarker for chronic kidney disease.[1206] The intake of inorganic phosphates in Europe has been found to have doubled since 1990, mainly due to the increasing consumption of processed foods, while their use is based on their ability to increase shelf life.[1207] Therefore, monitoring inorganic phosphates in biofluids is an interesting topic for further risk assessment. For example, high serum phosphate concentrations have been shown to be an important risk factor for increased cardiovascular and overall mortality in patients with renal disease.[1208,1209] Because the focus of this review is not on a detailed explanation of the metabolism of inorganic phosphates, we refer the interested reader instead to other excellent reviews on this topic.[1210,1211] Table 43 lists the typical phosphate concentrations found in biofluids.

The smallest inorganic phosphate is the orthophosphate anion ($PO_4^{3-}$), in which the central phosphorus atom is surrounded by four tetrahedrally arranged oxygen atoms. Orthophosphate is derived directly from phosphoric acid (Figure 278a). As depicted in Figure 278b, phosphoric acids/phosphates are involved in a pH-dependent dissociation equilibrium, with only undissociated $H_3PO_4$ existing at pH < 1.0, while dihydrogen phosphate ($H_2PO_4^-$) species predominate at pH 4.2 and hydrogen phosphate ($HPO_4^{2-}$) species at pH 8.2. Only in strongly basic solutions (pH < 10), the fully deprotonated orthophosphate prevails. Therefore, when designing molecular probes, chemosensors, or nanosensors, it must be considered that $H_2PO_4^-$ and $HPO_4^{2-}$ predominate in biological media. In addition to the net negative charge of the phosphate anions, the H-bond capability of phosphates is of interest for the design of selective sensors.

Another important class of phosphates are pyrophosphates, which consist of two phosphorus atoms connected by a P−O−P bond (Figure 278a). The pyrophosphate anion is a polyvalent anion that has a strong binding affinity to divalent cations, *e.g.*, $Zn^{2+}$ or $Ca^{2+}$, which is the property most exploited property for phosphate detection by probes and chemosensors.

### 13.2. Molecular Probes and Chemosensors for Phosphate and Pyrophosphate Anions

To date, the most efficient strategy to bind phosphates is based on the use of "hard" transition metal cations such as $Zn^{2+}$, $Cu^{2+}$, and $Fe^{3+}$ that form strong Lewis acid−base interactions with phosphate anions. When compared to other anions, the detection limits for inorganic phosphates are not that stringent. Phosphates are commonly found in urine at 4−12 mM and in

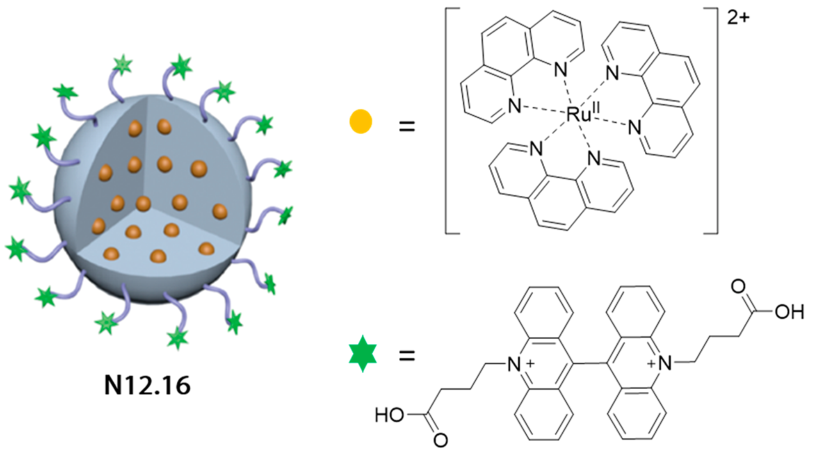

**Figure 277.** Fluorescent silica nanoparticles (**N12.16**) used for ratiometric fluorescence-based detection of chloride anions in cells. Reproduced with permission from ref 1184. Copyright 2020 American Chemical Society.

### Table 40. Summary of the Typical Concentration Ranges of Inorganic Anions in Drinking Water and Biofluids

| concentration range | media | ref |
|---|---|---|
| Cyanide ($CN^-$) Analyte | | |
| 1.3–19.4 $\mu$M | blood | 642 |
| 0.05–151 $\mu$mol/mmol creatinine = 0.052–151 $\mu$M | urine | 642 |
| <3.5 $\mu$g/L | drinking water | 1188 |
| <0.13 $\mu$M | | |
| Chloride ($Cl^-$) Analyte | | |
| 99–109 mM | blood | 1189 |
| 5.26–17.8 $\mu$mol/mmol creatinine = 526–178 mM | urine | 642 |
| 0–533 mM | saliva | 1190 |
| Fluoride ($F^-$) Analyte | | |
| 3.00–6.49 $\mu$M | blood | 642 |
| 1.05–2.95 $\mu$mol/mmol creatinine = 10.5–29.5 $\mu$M | urine | 642 |
| 0–2.2 mM | saliva | 1190 |
| Hydrogen Sulfide ($HS^-$) Analyte | | |
| 60.2–71.2 $\mu$M | blood (1–13 years old) | 1191 |
| 0–68.7 $\mu$M | blood (>18 years old) | 1192 |
| Iodide ($I^-$) Analyte | | |
| 0.20–1.65 $\mu$mol/mmol creatinine = 2.00–16.5 $\mu$M | urine (1–13 years old) | 642 |
| 161–559 nmol/mmol creatinine = 1.61–5.59 $\mu$M | urine (13–18 years old) | 642 |
| Sulfide ($S^{2-}$) Analyte | | |
| <0.003 $\mu$M | blood | 1193 |

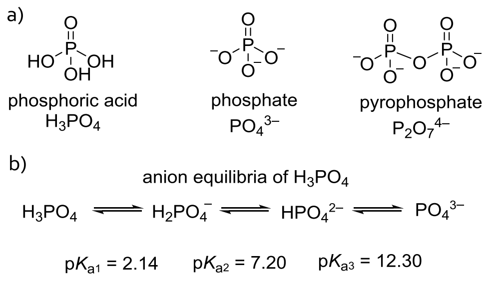

**Figure 278.** (a) Chemical structures and formula of different phosphate species. (b) Dissociation equilibria of phosphoric acid in water.

blood at 1.4–2.2 mM concentrations.[501212] In this subsection, we mainly focus on recent examples of chemosensors and recommend that the reader consult the review by Yoon and coworkers for examples published before 2009.[1213] The chemosensors discussed within this section are summarized in Table 41.

### Table 41. Summary of Some Representative Chemosensors for Phosphates (LOD, Limit of Detection)

| chemosensor | media | concentration range | ref |
|---|---|---|---|
| | Dihydrogen Phosphate Analyte | | |
| **C13.4** | hexamethylenetetramine-HCl buffer, pH 7.0 | 4–80 $\mu$M (linear range); LOD, 0.4 $\mu$M | 1220 |
| | human saliva samples | mM range | |
| | Orthophosphate Analyte | | |
| **C13.1** | 10% urine sample in DMSO | mM range; LOD, 1.68 mM | 1217 |
| | Pyrophosphate Analyte | | |
| **C13.2** | 10 mM HEPES buffer, pH 7.4 | 0–110 $\mu$M; LOD, 0.1 $\mu$M | 1218 |
| **C13.3** | 17% DMSO in 8 mM HEPES buffer, pH 7.3 | 0–40 $\mu$M | 1219 |
| **C13.4** | hexamethylenetetramine-HCl buffer, pH 7.0; | 0.1–7 $\mu$M (linear range); LOD, 34 nM | 1220 |
| | saliva samples | $\mu$M concentrations | |
| **C13.5** | 100 mM KCl in 10 mM Tris-HCl buffer, pH 7.2 | 10 nM–1 mM | 1221 |

The Molybdenum Blue reaction is the most common approach for the detection of orthophosphate anions in aqueous solutions and biological fluids (**P13.1** in Figure 279). In strongly acidic solutions (pH < 1.0), $Mo^{IV}$ salts react with phosphates to form a Keggin-type anionic complex, which after reduction, *e.g.*, by ascorbic acid, forms a deep-blue solution.[1214] The total amount of phosphate (inorganic and organic) can thus be quantified by monitoring this distinct color change using UV–vis spectroscopy. However, while the harsh acidic environment is suitable for urine and deproteinized serum measurements,[1215] the Molybdenum Blue reaction cannot be applied for live cell analysis and *in vivo* monitoring of phosphates. More recently, the molybdenum reagent-based assay has been simplified by the use of paper strips impregnated with molybdenum blue,[1216] allowing for the

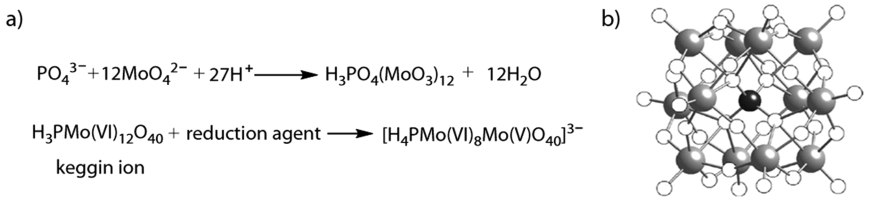

**P13.1**

**Figure 279.** (a) Schematic representation of the molybdate blue reaction for phosphate detection at $\mu$M concentrations in aqueous media and biological fluids. (b) 3D rendering of the Keggin ion $[PW_{12}O_{40}]^{3-}$. Reproduced with permission from ref 1214. Copyright 2015 Elsevier BV.

detection of phosphates at $\mu$M concentrations in aqueous media. Here, the molybdenum blue agent was applied as an ethylene-glycol stabilized complex, allowing not only an improved stability, sensitivity, and selectivity but also a decreased risk of the exposure towards the toxic molybdenum. The detection and quantification of phosphate was achieved by a colorimetric readout resulting in a detection limit between 1.3 and 2.8 $\mu$M in various aqueous media including seawater.

A surprisingly simple chemosensor based on the small molecule 1,3,5-trinitro-2,4-dimethyl-benzene (**C13.1** in Figure 280a) used for the detection of phosphate in urine at mM concentrations (LOD, 168 $\mu$M) was reported by Lowdon and coworkers.[1217] In this example, the detection of phosphates in urine samples was possible as the analyte triggers a color change of **C13.1** in 90% DMSO in water, which can be explained by the coordination of the phosphate to the electron-deficient trinitro compound, giving rise to charge transfer (CT) interactions. The authors reported that the spectroscopic properties of **C13.1** are also affected by $K^+$, $Ca^{2+}$, $Cl^-$, and $SO_4^{2-}$ ions that suppress the CT absorbance of the **C13.1**–phosphate complex, whereas $Na^+$ and $HCO_3^-$ slightly enhance the signal. The phosphate content of untreated urine samples was determined to be 560 ± 20 $\mu$g mL$^{-1}$ when applying chemosensor **C13.2**, whereas the molybdenite assay typically used for phosphate quantification indicated a value of 740 ± 10 $\mu$g mL$^{-1}$. The lower values obtained with **C13.1** can be attributed to possible negative interference from biomolecules that do not affect the molybdenite assay. Although this example may not be the most convenient alternative to existing phosphate probes, the work presented demonstrates how a small and relatively simple molecule can be utilized for the rapid and semi-quantitative detection of biorelevant chemical species.

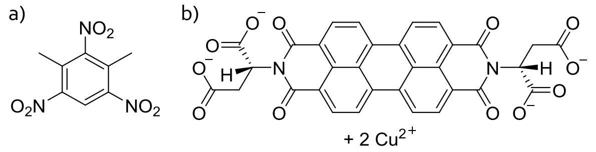

**C13.1** **C13.2**

**Figure 280.** (a) Chemical structure of 1,3,5-trinitro-2,4-dimethylbenzene (**C13.1**) for fluorescence-based detection of $PO_4^{3-}$ at mM concentrations in urine. (b) Chemical structure of perylene diimide and Cu$^{II}$ ensemble (**C13.2**) used for the detection of pyrophosphate at mM concentrations in 10 mM HEPES buffer, pH 7.4.

Pyrophosphate anions are typically found at much lower concentrations (low $\mu$M range)[642] than orthophosphates, and therefore the sensitivity requirements for probes and chemosensors for pyrophosphate detection are more critical. Sukul and coworkers were able to show that a chemosensor ensemble formed by aspartic acid-functionalized perylene diimide and $Cu^{2+}$ cations (**C13.2** in Figure 280b) can be used for the detection of pyrophosphate at $\mu$M concentrations in 10 mM HEPES buffer, pH 7.4.[1218] In aqueous solutions, **C13.2** forms nonemissive aggregates due to aggregation-induced quenching. However, pyrophosphate anions have been shown to strongly coordinate to $Cu^{2+}$ and thereby disrupting aggregation, thus leading to the formation of a highly emissive monomeric species of **C13.2** in aqueous solution. Other anions, *e.g.*, $F^-$, $Cl^-$, $Br^-$, $NO_2^-$, $NO_3^-$, $HPO_4^{2-}$, $SO_4^{2-}$, and $CO_3^{2-}$, did not cause interferences, indicating a good selectivity of **C13.2** for pyrophosphate detection.

A chemosensor for the reversible fluorescence turn-off detection of pyrophosphate at $\mu$M concentrations in HEPES buffer containing 20% DMSO and in rat adrenal cells was recently reported by Xu, Qing, and coworkers (**C13.3** in Figure 281).[1219] The chemosensor **C13.3** was prepared by adding $Cu^{2+}$ salts to hemicyanine-labeled 2-(2′-hydroxyphenyl)-4-methyloxazole (dye) yielding a nonemissive complex. The quenched fluorescence was attributed to the paramagnetic nature of Cu$^{II}$, which promotes energy dissipation from the excited state of the dye *via* nonradiative processes. Comparable to **C13.2**, the fluorescence properties of **C13.3** are also restored in the presence of pyrophosphate anions as the analyte depletes Cu$^{II}$ ions from the chemosensor. Interestingly,

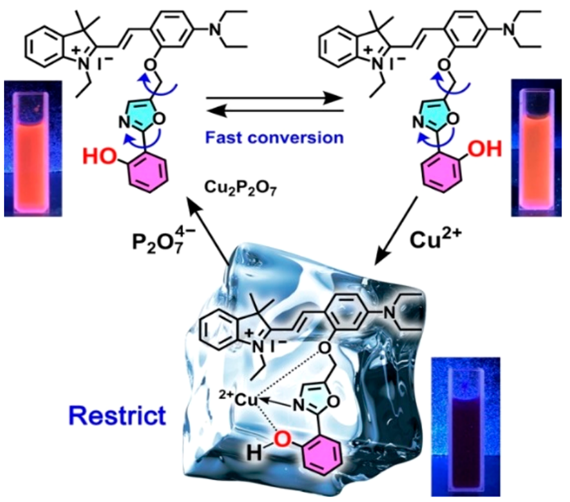

**C13.3**

**Figure 281.** Schematic representation of the fluorescence-based detection of pyrophosphate ($\mu$M concentrations) in HEPES buffer containing 20% DMSO using a Cu(II) complex (**C13.3**). Reproduced with permission from ref 1219. Copyright 2020 American Chemical Society.

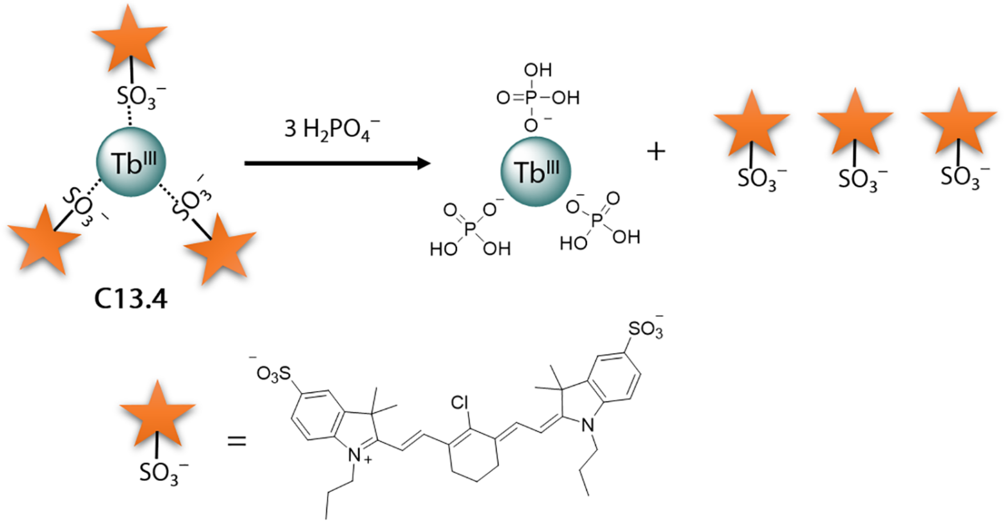

**Figure 282.** Schematic representation of the sensing mechanism for $H_2PO_4^-$ with **C13.4**. The chemosensor **C13.4** enables colorimetric-based detection of phosphate species at $\mu$M concentrations in Tris-HCl buffer solutions and spiked saliva samples.

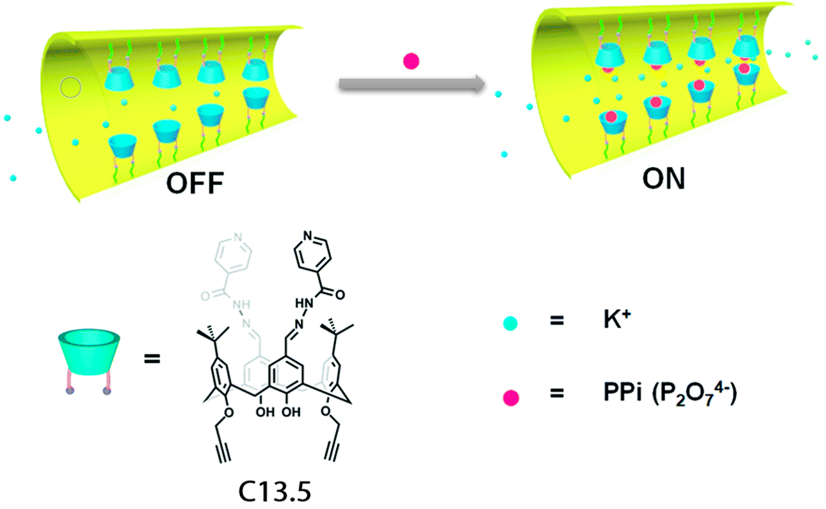

**Figure 283.** Schematic representation of the detection mechanism of pyrophosphate anions at $\mu$M concentrations by isoniazid functionalized calix[4]arene (**C13.5**) in 10 mM Tris-HCl buffer, pH 7.2. Adapted with permission from ref 1221. Copyright 2019 The Royal Society of Chemistry.

the authors showed that the fluorescence properties of **C13.3** switches reversibly upon additions of pyrophosphate and Cu$^{II}$ ions. Additionally, **C13.3** also has a good selectivity for pyrophosphate anions over other phosphate species, such as $PO_4^{3-}$, $H_2PO_4^-$, ADP, and other common anions such as $F^-$, $Cl^-$, $Br^-$, $I^-$, $HCO_3^-$, $NO_3^-$, $HSO_4^-$, $SO_4^{2-}$, and $CO_3^{2-}$.

Recently, Zheng, Wu, and coworkers described sulfonated cyanine dye derivatives in combination with Tb$^{III}$ cations as a chemosensor ensemble for the micromolar detection of $H_2PO_4^-$ and pyrophosphate in hexamethylenetetramine-HCl buffer, pH 7.0 (**C13.4** in Figure 282).[1220] In the absence of phosphates, **C13.4** forms aggregates that can be distinguished from the nonaggregated dye by their characteristic absorption spectrum. However, because of the stronger binding of phosphates to the "hard" Tb$^{III}$ ions, the cyanine dye was depleted from the chemosensor in the presence of phosphates. The authors showed that other ions (*e.g.*, $Cl^-$, $Br^-$, $I^-$, $SO_4^{2-}$, $HCO_3^-$, $NO_3^-$, $Cu^{2+}$, $Zn^{2+}$, $Mg^{2+}$, $Hg^{2+}$, $Cd^{2+}$, $Co^{2+}$, $Ba^{2+}$, $Al^{3+}$, and $Fe^{3+}$) or amino acids do not interfere with the detection of $H_2PO_4^-$ or pyrophosphate. However, the distinction between phosphate and pyrophosphate anions remains difficult, as both elicit a similar concentration dependent optical response. Furthermore, **C13.4** was observed to give cross-reactivities with organic phosphates (*e.g.*, ATP and ADP) as they also coordinate Tb$^{III}$ cations. Finally, the authors investigated the use of **C13.4** for the detection of phosphates in spiked saliva samples and found that their chemosensor provided robust detection with good recoveries (>97%). Additionally, the concentration results obtained were consistent with measurements obtained from ion chromatography analysis.

In the quest of chemosensors with selectivity for pyrophosphate anions, Li and coworkers recently reported a isoniazid functionalized calix[4]arene chemosensor (**C13.5** in Figure 283) that binds pyrophosphate anions ($K_a = 6.68 \times 10^5$ $M^{-1}$ for 1:1 complex) in 10 mM Tris-HCl solutions, pH 7.2, containing 100 mM KCl.[1221] Inspired by naturally occurring ion channels of cells, the authors prepared polyimide-based tubular nanostructures whose channels were functionalized with **C13.5**. Conductivity measurements showed low $K^+$ ion mobility in the absence of pyrophosphate. In the presence of

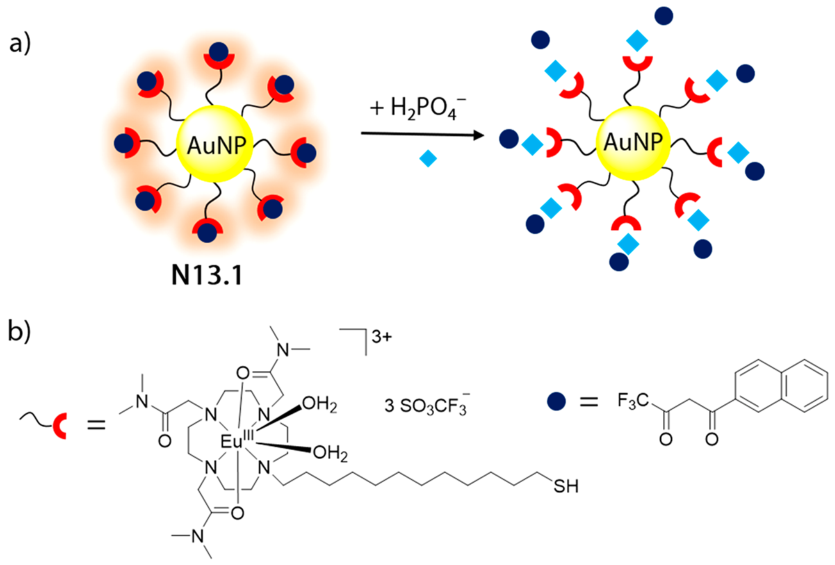

**Figure 284.** (a) $Eu^{III}$−cyclen functionalized gold nanoparticles (**N13.1**) used for fluorescence turn-off sensing of phosphate anions in HEPES buffer solutions at $\mu$M concentrations. (b) Chemical structure of $Eu^{III}$−cyclen and the $\beta$-diketone.

pyrophosphate anions and due to their binding affinity to **C13.5**, an increased $K^+$ mobility was observed, which was correlated to the amount of pyrophosphate (10−1 mM range). The increased potassium ion mobility can be explained by the overlap of the electrical double layer at the tip side of the negatively charged channel, resulting in a concentration gradient that produces higher ionic conductivity and ionic current. The authors showed that **C13.5** offers good selectivity towards pyrophosphate over $H_2PO_4^{2-}$, ATP, and ADP. The use of this chemosensor has yet to be evaluated for real biological applications as the presence of other cations typically found in such biofluids can potentially negatively affect the performance of the sensor.

### 13.3. Nanosensors for Phosphate and Pyrophosphate Anions

An early example for the detection of phosphates by nanosensors was reported by Gunnlaugsson and coworkers (**N13.1** in Figure 284).[1222] Although the authors focused on the detection of the organic phosphate flavin, the possibility to detect $H_2PO_4^-$ anions at $\mu$M concentrations in 100 mM HEPES buffer, pH 7.4, was also considered. In this example, gold nanoparticles were decorated with a $Eu^{III}$−cyclen complex, which forms a highly emissive complex upon addition of an aryl-substituted $\beta$-diketone (Table 42). However, in the presence of phosphate anions, the emission of the lanthanides is quenched because the phosphate displaces the $\beta$-diketone from the lanthanide complex, allowing for the solvent molecules ($H_2O$) to bind to the metal center, which in turn results in O−H-mediated vibrational quenching of its emission.

**Table 42. Summary of Some Representative Nanosensors for Phosphates (LOD, Limit of Detection)**

| probe | media | concentration range | ref |
|---|---|---|---|
| | Dihydrogen Phosphate Analyte | | |
| **N13.1** | 100 mM HEPES buffer, pH 7.4 | $\mu$M range | 1222 |
| | Pyrophosphate Analyte | | |
| **N13.2** | 25 mM Tris-HCl buffer, pH 7.4 | 0−30 $\mu$M | 1223 |
| **N13.3** | 8 mM HEPES buffer, pH 7.4 | 0−160 $\mu$M;<br>LOD, 140 nM | 1224 |
| **N13.4** | water | 0−20 $\mu$M | 1225 |
| | canned meat samples | LOD, 1 $\mu$M | |
| **N13.5** | Britton−Robinson buffer, pH 7.0 | 0−800 $\mu$M; 100−700 $\mu$M (linear range) | 1226 |
| | urine sample | LOD, 6.7 $\mu$M in buffer | |
| **N13.6** | water, pH 7.0 | 2−600 $\mu$M (linear range);<br>LOD, 0.86 $\mu$M | 1227 |
| | urine | 0−100 $\mu$M (urine) | |
| | Orthophosphate Analyte | | |
| **N13.7** | 10 mM Tris-HCl buffer, pH 8.6 | 1−50 $\mu$M (linear range);<br>LOD, 0.23 $\mu$M | 1229 |
| **N13.8** | 15 mM HEPES buffer, pH 7.4; urine samples; saliva samples | 10−60 $\mu$M in buffer;<br>LOD, 4.65 $\mu$M in buffer | 1230 |

Li and coworkers designed a colorimetric assay using carboxylic acid-functionalized AuNPs that aggregate in the presence of $Eu^{III}$ cations (**N13.2** in Figure 285).[1223] This phenomena can be explained by the ability of $Eu^{III}$ to bind to carboxylates, which thus neutralizes the negative charges on the surface of the particles responsible for the repulsive forces (see Figure 285). However, pyrophosphate anions prevent aggregation of **N13.2** due to their high binding affinity to $Eu^{III}$. Therefore, by measuring the degree of **N13.2** aggregation *via* UV−vis absorption spectroscopy (surface plasmon resonances change upon particle aggregation), a colorimetric-based detection of pyrophosphate at $\mu$M concentrations was achieved in 25 mM Tris-HCl buffer, pH 7.4. The authors showed that the nanosensor is not affected by other possible interferents such as $Cl^-$, $Br^-$, $NO_2^-$, $NO_3^-$, $ClO^-$, $SO_4^{2-}$, $SO_3^{2-}$, $ClO_3^-$, $S^{2-}$, $S_2O_3^{2-}$, SDS, Cys, acetic acid, $Ca^{2+}$, $Mg^{2+}$, and $Mn^{2+}$. Potential cross-reactivities with nucleosides, $H_2PO_4^-$, or $PO_4^{3-}$ were not investigated.

A sensitive colorimetric-based nanosensor for the detection of pyrophosphate at $\mu$M concentrations (LOD, 140 nM) in 10 mM HEPES buffer, pH 7.4, was reported by Balasubramanian and co-workers (**N13.3** in Figure 286).[1224] In this example, gold nanoparticles were decorated with positively charged resorcinarenes that served as recognition units for negatively charged pyrophosphate anions. Thus, in the

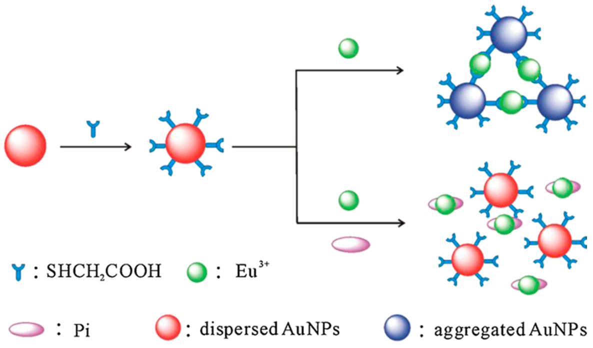

**N13.2**

**Figure 285.** Carboxylic acid-functionalized AuNPs used in combination with $Eu^{III}$ ions (**N13.2**) used for colorimetric detection of pyrophosphate at $\mu$M concentrations in 25 mM Tris-HCl buffer, pH 7.4. Reproduced with permission from ref 1223. Copyright 2013 Elsevier BV.

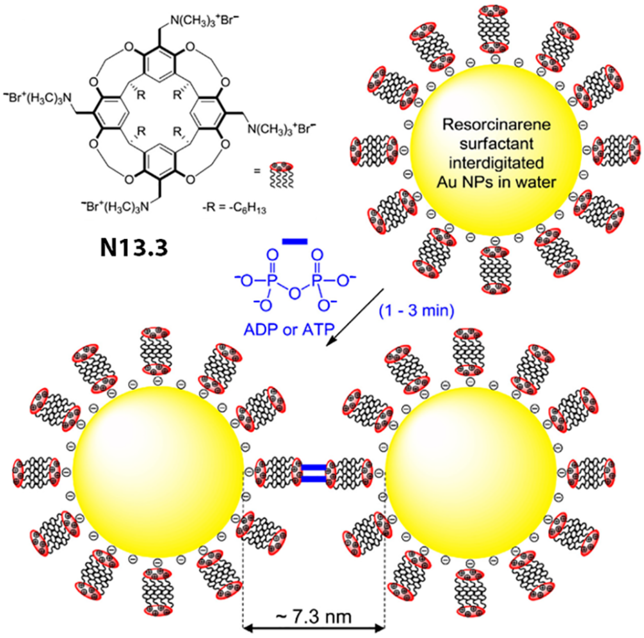

**Figure 286.** Resorcinarene-functionalized AuNPs (**N13.3**) used for colorimetric detection of phosphates at $\mu$M concentrations in 10 mM HEPES buffer, pH 7.4. Adapted with permission from ref 1224. Copyright 2017 Elsevier BV.

presence of pyrophosphates, aggregation of **N13.3** occurs, akin to the sensing mechanism for **N13.2**. The aggregation of **N13.3** was determined by UV−vis absorption spectroscopy and correlated with the concentration of pyrophosphate. The authors showed that other anions such as $F^-$, $Cl^-$, $CO_3^{2-}$, $AcO^-$, $SO_4^{2-}$, and $NO_3^-$ do not trigger any colorimetric response. The authors also confirmed that $H_2PO_4^-$ and $PO_4^{3-}$ did not cause any colorimetric response. However, organic phosphates such as ADP and ATP were found to interfere. The authors argued that the selectivity of **N13.3** for pyrophosphate over $H_2PO_4^-$ and $PO_4^{3-}$ may be attributed the strength of pyrophosphate binding by the resorcinarene cavitand.

Recently, Wu, Zhang, and coworkers reported a smartphone-based detection system for pyrophosphate (LOD, 1 $\mu$M) in water and in meat samples.[1225] To this end, polyvinylpyrrolidone (PVP)-capped silver nanoparticles (**N13.4** in Figure 287) were prepared that aggregate in the presence of divalent ions such as $Pb^{2+}$, which can be monitored colorimetrically. However, pyrophosphate, which binds strongly to $Pb^{2+}$, prevents aggregation of the nanoparticles. Data analysis was performed by a smartphone camera with a specially programmed application. Good selectivity of **N13.4** was demonstrated, as the nanosensor is not affected by $F^-$, $Cl^-$, $Br^-$, $I^-$, $S^{2-}$, $CO_3^{2-}$, $AcO^-$, $NO_3^-$, $SO_3^{2-}$, $SO_4^{2-}$, $HCO_3^-$, $H_2PO_4^-$, $HPO_4^{2-}$, and $PO_4^{3-}$. Although the authors found that anions such as $S^{2-}$ and $SO_4^{2-}$ do not cause a colorimetric response in their specific setup, they could be potential cross-reactants in different scenarios. This is because they are known to form $Pb^{2+}$ salts with low solubility, leading to PbS and $PbSO_4$ precipitates, which are not detected by **N13.4**.

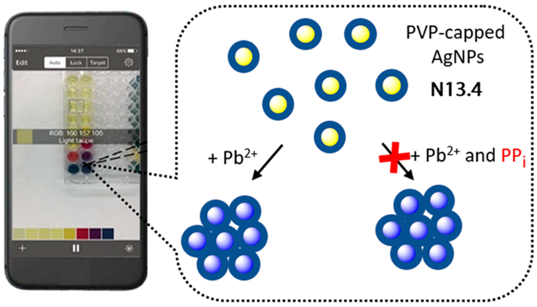

**Figure 287.** AgNPs-based and smartphone-assisted sensor (**N13.4**) used for sensitive detection (1 $\mu$M) of pyrophosphate in water and food samples. Adapted with permission from ref 1225. Copyright 2020 Elsevier BV.

A simple fluorescent turn-on nanosensor based on silk-fibroin capped plasmonic silver nanoparticles for $\mu$M detection of pyrophosphate in Britton−Robinson buffer and spiked urine samples was reported by Shuang, Zhang, and coworkers (**N13.5** in Figure 288).[1226] The authors observed that the characteristic fluorescence of **N13.5** is quenched when the particles are doped with $Cu^{2+}$ ions ($Cu^{2+}$ cations are complexed by fibroid). However, the presence of pyrophosphate restores the fluorescence of the nanoparticles as it binds to $Cu^{2+}$ and thus sequesters the fluorescence quencher (indicator displacement assay). Cross-reactivity with other ions (*e.g.,* $I^-$, $NO_3^-$, $CN^-$, $PO_4^{3-}$, $K^+$, $Ca^{2+}$, $Mg^{2+}$, $Hg^{2+}$, $Zn^{2+}$, $Ni^{2+}$, $Pb^{2+}$, and $Fe^{3+}$) was not observed, and the nanosensor **N13.5** can be used to detect pyrophosphate in diluted and spiked urine samples with good recovery (>99%).

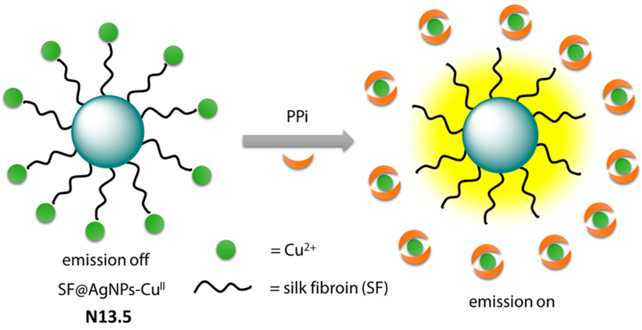

**Figure 288.** Plasmonic silver nanoparticles coated with silk fibroin for fluorescence turn-on detection of pyrophosphate ($\mu$M) in Britton−Robinson buffer and urine.

Good detection limits for pyrophosphate anions (LOD, 860 $\mu$M) in urine samples were reported by Hu, Han, and coworkers using $Fe^{3+}$-doped carbon dots (**N13.6** in Figure 289).[1227] The fluorescence of the carbon dots is initially quenched by $Fe^{3+}$ through energy transfer processes. However, in the presence of pyrophosphates, $Fe^{3+}$ ions were efficiently complexed and depleted from the surface of the nanoparticles, resulting in increased fluorescence of the carbon dots. No interference of other anions or biomolecules (*e.g.*, $F^-$, $Cl^-$, $Br^-$, $I^-$, $NO_3^-$, $S^{2-}$, $BrO_3^{2-}$, $SO_4^{2-}$, $SO_3^{2-}$, $S_2O_3^{2-}$, $S_2O_8^{2-}$, $CO_3^{2-}$, $HCO_3^-$, $H_2PO_4^-$, $HPO_4^{2-}$, Cys, deoxyribose, ribose, lactic acid, folic acid, uric acid, and cholesterol) was observed, and the authors demonstrated that **N13.6** can be applied for the detection of pyrophosphate at $\mu$M concentrations in spiked urine samples with recoveries of up to 99%.

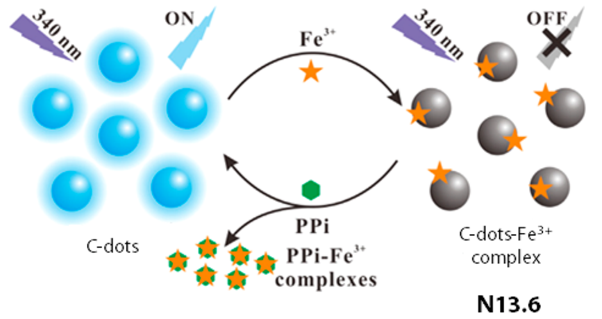

**Figure 289.** $Fe^{3+}$-doped carbon-dots (**N13.6**) used for fluorescence turn-on detection of pyrophosphate at $\mu$M concentration in urine samples. Reproduced with permission from ref 1227. Copyright 2019 Elsevier BV.

The detection of orthophosphate anions ($PO_4^{3-}$) with hybrid carbon dot/zeolitic imidazole framework-90 (ZIF-90) particles was recently reported by Hu and coworkers (**N13.7** in Figure 290).[1229] In this work, carbon dots were incorporated into the $Zn^{II}$-based metal-organic framework (ZIF-90), where their fluorescence was efficiently quenched by energy transfer processes. However, the luminescence was restored upon the addition of *ortho*-phosphate anions, as the ZIF-90 framework disassembled through the complexation of phosphates with the $Zn^{II}$ centers. Fluorescence-based detection of orthophosphate at $\mu$M concentrations in 10 mM Tris-HCl buffer, pH 8.6, tap and lake water samples was demonstrated with good selectivity over $Na^+$, $K^+$, $Mg^{2+}$, $Ca^{2+}$, $Ba^{2+}$, $Hg^{2+}$, $Cd^{2+}$, $Mn^{2+}$, $Pb^{2+}$, $Cu^{2+}$, $Co^{2+}$, $Ni^{2+}$, $Fe^{3+}$, $Cr^{3+}$, $ClO^-$, $CO_3^{2-}$, and $S_2O_3^{2-}$.

Shu, Wang, and coworkers reported that the addition of orthophosphate or pyrophosphate to a mixture of $Eu^{III}$, adenine, and 2,6-pyridinecarboxylic acid triggers the formation of fluorescent nanoparticles (**N13.8** in Figure 291) that can be used to determine the $\mu$M concentrations of phosphates in 15 mM HEPES buffer, pH 7.4, and in diluted urine samples.[1230] It was suggested that through phosphate cobinding, the $Eu^{III}$−carboxylate bonds shorten and that therefore energy transfer from the carboxylate-ligands to $Eu^{III}$ becomes more efficient. No interferences were caused by metal cations, anions, or other phosphor-containing substances. Finally, **N13.9** was shown to be useful for sensing inorganic phosphates (orthophosphate and pyrophosphate) in diluted urine samples without further sample treatment; the results obtained were in good agreement with a phosphomolybdate blue assay.

The chemical properties of phosphates, such as their pH-dependent anion equilibria or ability to bind strongly to hard metal cations, can be exploited to develop sensors for the rapid, simple, and reliable detection of phosphates in biological fluids (Table 43). Indeed, commercial assays for the detection of total phosphate (organic and inorganic) in biofluids already exist (*e.g.*, molybdenum-based assays), but such assays require harsh reaction conditions (use of $Mo^{IV}$ salts and pH values <2) and typically only indicate the amount of total phosphate (organic and inorganic) in biological samples. Most assays currently in use for phosphate detection are based on electrochemical and enzymatic reactions, which we do not cover in this review.[1231−1236] Despite the promising recently reported molecular probes, chemosensors, and nanosensors, the development of selective probes and sensors that can distinguish, for example, orthophosphate and pyrophosphates or pyrophosphates from ADP and ATP, is still a task of great interest.

## 14. CONCLUDING REMARKS

In this review, we have attempted to provide an overview of the current status of probes and chemosensors for analytical applications. We have focused our attention on systems that are already capable of detecting small molecule targets in aqueous media or even biofluids because we believe that functional supramolecular analytical assays for clinics, for point-of-care applications, and for home use may become a game changer in the area of medical diagnostics. In reviewing the many systems and studies available, we noticed that there is already a wealth of data and detailed understanding available.

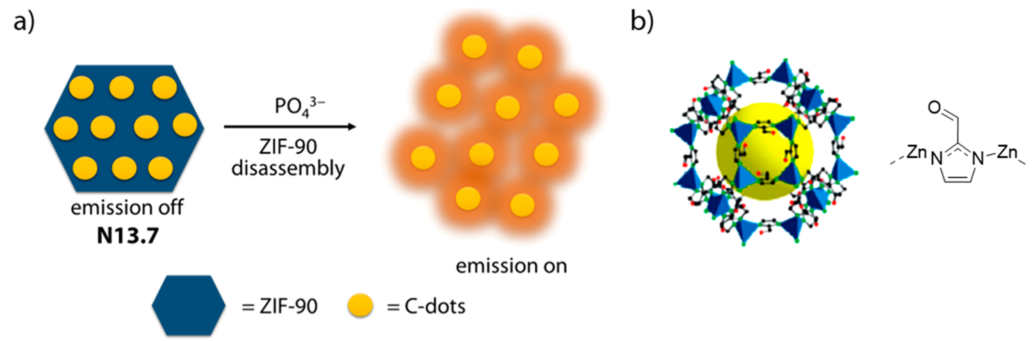

**Figure 290.** (a) Schematic representation of the detection of orthophosphates at $\mu$M concentrations with carbon dot/ZIF-90 nanoparticles in 10 mM Tris-HCl buffer, pH 8.6. (b) Crystal structure and chemical composition of ZIF-90 MOF. Adapted with permission from ref 1228. Copyright 2010 American Chemistry Society.

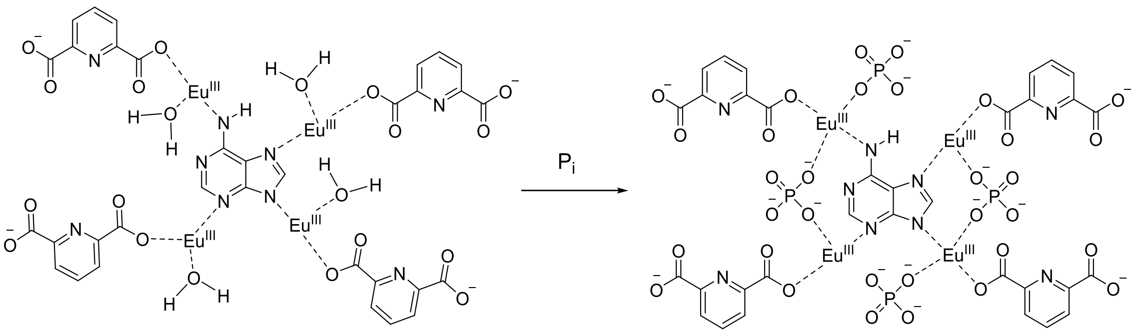

**N13.8**

Figure 291. Chemical structure of the nanoaggregates (**N13.8**) formed when inorganic phosphates are added to a solution of $Eu^{III}$ salts, adenine, and 2,6-pyridinecarboxylic. These fluorescent nanoparticles allow for luminescence-based detection of phosphate at $\mu$M concentrations in 15 mM HEPES buffer, pH 7.4.

### Table 43. Summary of the Normal Concentration of the Phosphate in Biofluids

| concentration range | media | ref |
|---|---|---|
| Phosphate Analyte | | |
| 1.4−2.2 mM | blood (>18 years old) | 1212 |
| 400−684 $\mu$M | blood (1−13 years old) | 1237 |
| 425−1170 $\mu$M/mM creatinine = 4.25−11.7 mM | urine | 50 |
| 3.4−42.0 $\mu$M | saliva | 1190 |
| Pyrophosphate Analyte | | |
| 0.62−2.96 $\mu$M | blood | 642 |
| 1.34−3.78 $\mu$M/mM creatinine = 13.4−37.8 $\mu$M | urine (1−13 years old) | 642 |

Yet almost all studies using probes and chemosensors are executed and communicated from the chemists' perspective and rarely involving clinical or "pure" analytical experts. Furthermore, the studies are usually restricted to a very small number of biofluid samples. In those few reports that had a strong focus on the medical diagnostic use of molecular probes, chemo- and nanosensors, only simple probes, *e.g.*, a general thiol-reactive probe, were investigated.

When comparing the status quo to other molecular recognition-based research areas in which fundamental research and application are already more closely linked, the question arises which hurdles need to be overcome for bringing molecular probes, chemo- and nanosensors into real-life use. Surely, the performance parameters of some molecular probes and chemosensors still do not meet the practical requirements, for instance, in terms of binding affinity and especially analyte selectivity, but recent developments seem to close the gap. We believe that one major obstacle is the imbalance between the modest number and types of analytes tested in research laboratories and the richness of the molecular composition of biofluids. Obviously, it is difficult for chemists to evaluate their new chemosensor designs against hundreds of possible small molecule target compounds. However, the common routine of selecting a (very) small number of "cherry picked" analytes and evaluation of their interaction with the molecular probes, chemo- and nanosensors may lead to false conclusions. Moreover, many reports differ in the assay medium, *e.g.*, buffer type, ionic strength, pH, cosolvents, or additives, whose selection is surely guided by the best of intentions, but this strategy obscures the comparison between different studies and may lead away from the typical composition of biofluids. Also, the commonly performed spiking experiments have to be critically evaluated unless different biofluid matrixes, *e.g.*, different urine or blood serum samples from different sources/donors, are used in a blinded fashion. Oftentimes, the molecular probes, chemo- and nanosensors were evaluated by comparing the optical signal readouts of spiked samples versus blank samples, but in a realistic scenario it is of utmost importance that matrix-to-matrix variations do not affect the target analyte quantification.

Moreover, compared to biochemists (*e.g.*, from the area of proteomics, genomics, and metabolomics), there is still a lack in electronically accessible databases and repositories when it comes to pure chemistry. This complicates the evaluation of newly designed molecular probes or chemosensors in comparison to findings with other structurally related compounds and against previously used experimental conditions. To improve this situation, our group has recently launched the community-based, open-access, non-profit repository SupraBank.org, where the thermodynamic, kinetic, and spectroscopic data of chemosensor−analyte (generally host−guest) pairs can be stored and made electronically accessible to the community. We hereby warmly invite any interest party to join this undertaking.

Probes and chemosensors are likely to remain rather unselective binders compared to biosensors and are certainly not reaching the detection limit and accuracy of instrumental-based analytical methods such as HPLC-MS/MS in the near future. Therefore, we believe it is unlikely that they will replace established analytical methods in any application where legally reliable, and watertight data is needed, for instance, in monitoring of drinking water quality or for identifying subjects committing drug abuse in sports. In contrast, all kinds of high-throughput applications, *e.g.*, screening of a large fraction of the society for tumor markers, development of a metabolomic warning system for cardiovascular malfunctions, or personalized drug dose adjustments for patients based on their individual drug bioavailability levels, are currently not feasible with established methods for socioeconomic reasons. Therefore, we believe that molecular probes, chemo- and nanosensors will find a particularly great future in these application areas where cost-effectiveness, robustness, parallelizability, and handiness are of upmost importance and where demands on the sensitivity and precisions levels are more modest.

## ASSOCIATED CONTENT

### Supporting Information

The Supporting Information is available free of charge at https://pubs.acs.org/doi/10.1021/acs.chemrev.1c00746.

Abbreviations used in this review (PDF)

### Special Issue Paper

This paper is an additional review for *Chem. Rev.* **2021**, volume *121*, issue 22, "Molecular Self-Assembly".

## AUTHOR INFORMATION

### Corresponding Authors

**Frank Biedermann** − *Institute of Nanotechnology, Karlsruhe Institute of Technology (KIT), 76344 Eggenstein-Leopoldshafen, Germany;* orcid.org/0000-0002-1077-6529; Email: frank.biedermann@kit.edu

**Pierre Picchetti** − *Institute of Nanotechnology, Karlsruhe Institute of Technology (KIT), 76344 Eggenstein-Leopoldshafen, Germany;* orcid.org/0000-0002-0689-5998; Email: pierre.picchetti@kit.edu

### Authors

**Joana Krämer** − *Institute of Nanotechnology, Karlsruhe Institute of Technology (KIT), 76344 Eggenstein-Leopoldshafen, Germany;* orcid.org/0000-0003-0498-7298

**Rui Kang** − *Institute of Nanotechnology, Karlsruhe Institute of Technology (KIT), 76344 Eggenstein-Leopoldshafen, Germany*

**Laura M. Grimm** − *Institute of Nanotechnology, Karlsruhe Institute of Technology (KIT), 76344 Eggenstein-Leopoldshafen, Germany;* orcid.org/0000-0002-1808-2206

**Luisa De Cola** − *Institute of Nanotechnology, Karlsruhe Institute of Technology (KIT), 76344 Eggenstein-Leopoldshafen, Germany; Dipartimento DISFARM, University of Milano, 20133 Milano, Italy; Department of Molecular Biochemistry and Pharmacology, Instituto di Ricerche Farmacologiche Mario Negri, IRCCS, 20156 Milano, Italy;* orcid.org/0000-0002-2152-6517

Complete contact information is available at: https://pubs.acs.org/10.1021/acs.chemrev.1c00746

### Author Contributions

‖J.K., R.K., and L.M.G. contributed equally to this work.

### Notes

The authors declare no competing financial interest.

### Biographies

Joana Krämer studied chemistry at the Karlsruhe Institute of Technology (KIT) in Germany and completed her M.Sc. degree in 2019. Afterwards, she joined the group of Dr. Frank Biedermann for her Ph.D. at the Institute of Nanotechnology (INT) at KIT with an Evonik scholarship, where she is working on the design of supramolecular chemosensors for the detection of small bioanalytes such as amino acids.

Rui Kang received her Master's degree in Chemistry from Shaanxi Normal University (SNNU), China, in 2018. She is currently pursuing her Ph.D. studies at the Institute of Nanotechnology (INT) of Karlsruhe Institute of Technology (KIT) under the supervision of Prof. Luisa De Cola and Dr. Frank Biedermann. Her research is mainly focused on the development of optical spectroscopy-based assays (e.g., fluorescence, absorbance, and chiral dichroism) for the detection of biorelevant small molecules in aqueous media and biofluids.

Laura M. Grimm received her M.Sc. from the Ruprecht-Karls-University Heidelberg in 2017 before moving to the Karlsruhe Institute of Technology (KIT), where she completed her Ph.D. in 2021. She is presently a Postdoctoral Fellow with a Vector Stipendium in the group of Dr. Frank Biedermann at the Institute of Nanotechnology (INT), KIT. Her research focuses on in biofluids functional chemo- and nanosensors by utilization of inorganic porous materials and fluorescent dyes.

Luisa De Cola is a full professor at the University of Milan and holds a position as a researcher at the Mario Negri Institute. She also holds a part-time position at KIT. She works in the field of nanomaterials for biomedical applications and luminescent systems. She is a member of the German Academy of Sciences, Leopoldina, and Chevalier de la Légion d'Honneur. She has received an ERC advanced grant, was recently awarded the 2019 Izatt-Christensen Prize in Supramolecular Chemistry, and is the 2020 winner of the "Giulio Natta" Gold Medal of the Italian Chemical Society.

Pierre Picchetti was born in Brunico, Italy. He studied Chemistry at the University of Vienna (Austria) and the University of Bologna—Alma Mater Studiorum, Italy, and completed his Ph.D. in Chemistry with special focus on functional and photonic materials at the University of Strasbourg, France, under the supervision of Prof. Luisa De Cola. In 2019, he had the opportunity to join the group of Prof. Hanadi Sleiman at McGill University, Canada, where he worked on the design of oligonucleotide-based nanoparticles as part of the MSCA-RISE-778133-Nano-OligoMed project. He is currently a postdoctoral fellow in the group of Dr. Frank Biedermann at the Institute of Nanotechnology (INT) at the Karlsruhe Institute of Technology (KIT) in Germany, where his research focuses on the design and preparation of chemosensors for bioanalyte detection.

Frank Biedermann is a trained supramolecular chemist. In 2003, he received his Ph.D. with Oren A. Scherman at the University of Cambridge, UK. In the following years, he joined the groups of Werner M. Nau (Jacobs University Bremen, Germany) and Luisa De Cola (Institute de Science et d'Ingénierie Supramoléculaires, Strasbourg, France) as a postdoctoral fellow to gather expertise in supramolecular-analytical chemistry, materials chemistry, and photophysics. In 2016, Frank started his independent career as an Emmy—Noether junior group leader at the Institute of Nanotechnology (INT) at the Karlsruhe Institute of Technology (KIT), Germany. His group is dedicated toward the development of self-assembling probes, macrocyclic chemosensors, and microporous nanosensors for the detection, imaging, and label-free reaction monitoring of small bioactive molecules such as metabolites and neurotransmitters. In 2021, Frank Biedermann received an Aventis Life Science Bridge Award for his contributions to the development of synthetic chemosensors and assays. Besides, he coordinates the SupraBank.org[41] development, an open-access repository where thermodynamic and kinetic binding parameters of host−guest complexes and supramolecular systems can be deposited and found.

## ACKNOWLEDGMENTS

J.K., R.K., L.M.G., P.P., and F.B. acknowledge the Deutsche Forschungsgemeinschaft (Emmy-Noether grant BI-1805/2-1). J.K. thanks the Evonik foundation for financial support. R.K. acknowledges the China Scholarship Council (CSC) for financial support. L.M.G. and F.B. thank the Vector Stiftung for financial support (P2020-0135). L.D.C. acknowledges financial support from the European Research Council for ERC Advanced Grant (grant agreement no. 2009-247365) and AXA Fundings.

## REFERENCES

(1) Cram, D. J. The Design of Molecular Hosts, Guests, and Their Complexes (Nobel Lecture). *Angew. Chem., Int. Ed. Engl.* **1988**, *27*, 1009−1020.

(2) Pedersen, C. J. The Discovery of Crown Ethers (Noble Lecture). *Angew. Chem., Int. Ed. Engl.* **1988**, *27*, 1021−1027.

(3) Lehn, J.-M. Supramolecular Chemistry: Where From? Where To? *Chem. Soc. Rev.* **2017**, *46*, 2378−2379.

(4) Sauvage, J.-P. From Chemical Topology to Molecular Machines (Nobel Lecture). *Angew. Chem., Int. Ed.* **2017**, *56*, 11080−11093.

(5) Stoddart, J. F. Mechanically Interlocked Molecules (Mims)−Molecular Shuttles, Switches, and Machines (Nobel Lecture). *Angew. Chem., Int. Ed.* **2017**, *56*, 11094−11125.

(6) Feringa, B. L. The Art of Building Small: From Molecular Switches to Motors (Nobel Lecture). *Angew. Chem., Int. Ed.* **2017**, *56*, 11060−11078.

(7) Lehn, J.-M. Supramolecular Chemistry: Receptors, Catalysts, and Carriers. *Science* **1985**, *227*, 849−856.

(8) Tighe, P. J.; Ryder, R. R.; Todd, I.; Fairclough, L. C. Elisa in the Multiplex Era: Potentials and Pitfalls. *Proteomics: Clin. Appl.* **2015**, *9*, 406−422.

(9) Konstantinou, G. N. Enzyme-Linked Immunosorbent Assay (Elisa). *Methods Mol. Biol.* **2017**, *1592*, 79−94.

(10) Greenwald, E. C.; Mehta, S.; Zhang, J. Genetically Encoded Fluorescent Biosensors Illuminate the Spatiotemporal Regulation of Signaling Networks. *Chem. Rev.* **2018**, *118*, 11707−11794.

(11) Nolan, T.; Hands, R. E.; Bustin, S. A. Quantification of Mrna Using Real-Time Rt-Pcr. *Nat. Protoc.* **2006**, *1*, 1559−1582.

(12) Ranallo, S.; Porchetta, A.; Ricci, F. DNA-Based Scaffolds for Sensing Applications. *Anal. Chem.* **2019**, *91*, 44−59.

(13) Rossetti, M.; Del Grosso, E.; Ranallo, S.; Mariottini, D.; Idili, A.; Bertucci, A.; Porchetta, A. Programmable Rna-Based Systems for Sensing and Diagnostic Applications. *Anal. Bioanal. Chem.* **2019**, *411*, 4293−4302.

(14) Bisswanger, H. Enzyme Assays. *Perspect. Sci.* **2014**, *1*, 41−55.

(15) Goddard, J. P.; Reymond, J. L. Enzyme Assays for High-Throughput Screening. *Curr. Opin. Biotechnol.* **2004**, *15*, 314−322.

(16) Wolfbeis, O. S. Editorial: Probes, Sensors, and Labels: Why Is Real Progress Slow? *Angew. Chem., Int. Ed.* **2013**, *52*, 9864−9865.

(17) Mortellaro, M.; DeHennis, A. Performance Characterization of an Abiotic and Fluorescent-Based Continuous Glucose Monitoring System in Patients with Type 1 Diabetes. *Biosens. Bioelectron.* **2014**, *61*, 227−231.

(18) Crane, B. C.; Barwell, N. P.; Gopal, P.; Gopichand, M.; Higgs, T.; James, T. D.; Jones, C. M.; Mackenzie, A.; Mulavisala, K. P.; Paterson, W. The Development of a Continuous Intravascular Glucose Monitoring Sensor. *J. Diabetes Sci. Technol.* **2015**, *9*, 751−761.

(19) de Silva, A. P.; Vance, T. P.; West, M. E. S.; Wright, G. D. Bright Molecules with Sense, Logic, Numeracy and Utility. *Org. Biomol. Chem.* **2008**, *6*, 2468−2480.

(20) de Silva, A. P. Bright Molecules for Sensing, Computing and Imaging: A Tale of Two Once-Troubled Cities. *Beilstein J. Org. Chem.* **2015**, *11*, 2774−2784.

(21) You, L.; Zha, D.; Anslyn, E. V. Recent Advances in Supramolecular Analytical Chemistry Using Optical Sensing. *Chem. Rev.* **2015**, *115*, 7840−7892.

(22) Mako, T. L.; Racicot, J. M.; Levine, M. Supramolecular Luminescent Sensors. *Chem. Rev.* **2019**, *119*, 322−477.

(23) Wang, B.; Anslyn, E. V. *Chemosensors: Principles, Strategies, and Applications*; John Wiley & Sons, 2011; pp 1−496.

(24) Mirsky, V. M.; Yatsimirsky, A. *Artificial Receptors for Chemical Sensors*; Wiley-VCH: Weinheim, 2011; pp 1−460.

(25) Vert, M.; Doi, Y.; Hellwich, K.-H.; Hess, M.; Hodge, P.; Kubisa, P.; Rinaudo, M.; Schué, F. Terminology for Biorelated Polymers and Applications (Iupac Recommendations 2012). *Pure Appl. Chem.* **2012**, *84*, 377−410.

(26) Potocnik, J. *Commission Recommendation of 18 October 2011 on the Definition of Nanomaterials (Text with EEA Relevance)*; European Union, 2011; http://data.europa.eu/eli/reco/2011/696/oj (accessed 2021-03-21).

(27) Rosi, N. L.; Mirkin, C. A. Nanostructures in Biodiagnostics. *Chem. Rev.* **2005**, *105*, 1547−1562.

(28) Astruc, D. Introduction: Nanoparticles in Catalysis. *Chem. Rev.* **2020**, *120*, 461−463.

(29) Anselmo, A. C.; Mitragotri, S. Nanoparticles in the Clinic: An Update. *Bioeng. Transl. Med.* **2019**, *4*, No. e10143.

(30) Auffan, M.; Rose, J.; Bottero, J.-Y.; Lowry, G. V.; Jolivet, J.-P.; Wiesner, M. R. Towards a Definition of Inorganic Nanoparticles from an Environmental, Health and Safety Perspective. *Nat. Nanotechnol.* **2009**, *4*, 634−641.

(31) Kim, D.; Shin, K.; Kwon, S. G.; Hyeon, T. Synthesis and Biomedical Applications of Multifunctional Nanoparticles. *Adv. Mater.* **2018**, *30*, 1802309.

(32) Lim, E.-K.; Kim, T.; Paik, S.; Haam, S.; Huh, Y.-M.; Lee, K. Nanomaterials for Theranostics: Recent Advances and Future Challenges. *Chem. Rev.* **2015**, *115*, 327−394.

(33) Saha, K.; Agasti, S. S.; Kim, C.; Li, X.; Rotello, V. M. Gold Nanoparticles in Chemical and Biological Sensing. *Chem. Rev.* **2012**, *112*, 2739−2779.

(34) Daniel, M. C.; Astruc, D. Gold Nanoparticles: Assembly, Supramolecular Chemistry, Quantum-Size-Related Properties, and Applications toward Biology, Catalysis, and Nanotechnology. *Chem. Rev.* **2004**, *104*, 293−346.

(35) Drechsler, U.; Erdogan, B.; Rotello, V. M. Nanoparticles: Scaffolds for Molecular Recognition. *Chem.−Eur. J.* **2004**, *10*, 5570−5579.

(36) Zeng, S.; Baillargeat, D.; Ho, H. P.; Yong, K. T. Nanomaterials Enhanced Surface Plasmon Resonance for Biological and Chemical Sensing Applications. *Chem. Soc. Rev.* **2014**, *43*, 3426−3452.

(37) Rekharsky, M. V.; Mori, T.; Yang, C.; Ko, Y. H.; Selvapalam, N.; Kim, H.; Sobransingh, D.; Kaifer, A. E.; Liu, S.; Isaacs, L.; Chen, W.; Moghaddam, S.; Gilson, M. K.; Kim, K.; Inoue, Y. A Synthetic Host-Guest System Achieves Avidin-Biotin Affinity by Overcoming Enthalpy-Entropy Compensation. *Proc. Natl. Acad. Sci. U. S. A.* **2007**, *104*, 20737−20742.

(38) Cao, L.; Šekutor, M.; Zavalij, P. Y.; Mlinarić-Majerski, K.; Glaser, R.; Isaacs, L. Cucurbit[7]Uril·Guest Pair with an Attomolar Dissociation Constant. *Angew. Chem., Int. Ed.* **2014**, *53*, 988−993.

(39) Nau, W. M.; Florea, M.; Assaf, K. I. Deep inside Cucurbiturils: Physical Properties and Volumes of Their Inner Cavity Determine the Hydrophobic Driving Force for Host-Guest Complexation. *Isr. J. Chem.* **2011**, *51*, 559−577.

(40) Zhang, S.; Grimm, L.; Miskolczy, Z.; Biczók, L.; Biedermann, F.; Nau, W. M. Binding Affinities of Cucurbit[N]Urils with Cations. *Chem. Commun.* **2019**, *55*, 14131−14134.

(41) *Suprabank*; Biedermann Labs, 2021; www.suprabank.org (accessed 2021-10-29).

(42) Sedgwick, A. C.; Brewster, J. T.; Wu, T.; Feng, X.; Bull, S. D.; Qian, X.; Sessler, J. L.; James, T. D.; Anslyn, E. V.; Sun, X. Indicator Displacement Assays (Idas): The Past, Present and Future. *Chem. Soc. Rev.* **2021**, *50*, 9−38.

(43) Wright, A. T.; Anslyn, E. V. Differential Receptor Arrays and Assays for Solution-Based Molecular Recognition. *Chem. Soc. Rev.* **2006**, *35*, 14−28.

(44) Sinn, S.; Biedermann, F. Chemical Sensors Based on Cucurbit[N]Uril Macrocycles. *Isr. J. Chem.* **2018**, *58*, 357−412.

(45) Wiskur, S. L.; Ait-Haddou, H.; Lavigne, J. J.; Anslyn, E. V. Teaching Old Indicators New Tricks. *Acc. Chem. Res.* **2001**, *34*, 963−972.

(46) Nguyen, B. T.; Anslyn, E. V. Indicator-Displacement Assays. *Coord. Chem. Rev.* **2006**, *250*, 3118−3127.

(47) Prabodh, A.; Sinn, S.; Grimm, L.; Miskolczy, Z.; Megyesi, M.; Biczok, L.; Bräse, S.; Biedermann, F. Teaching Indicators to Unravel the Kinetic Features of Host-Guest Inclusion Complexes. *Chem. Commun.* **2020**, *56*, 12327−12330.

(48) Sinn, S.; Krämer, J.; Biedermann, F. Teaching Old Indicators Even More Tricks: Binding Affinity Measurements with the Guest-Displacement Assay (Gda). *Chem. Commun.* **2020**, *56*, 6620−6623.

(49) Biedermann, F.; Hathazi, D.; Nau, W. M. Associative Chemosensing by Fluorescent Macrocycle-Dye Complexes−a Versatile Enzyme Assay Platform Beyond Indicator Displacement. *Chem. Commun.* **2015**, *51*, 4977−4980.

(50) Bouatra, S.; Aziat, F.; Mandal, R.; Guo, A. C.; Wilson, M. R.; Knox, C.; Bjorndahl, T. C.; Krishnamurthy, R.; Saleem, F.; Liu, P.; Dame, Z. T.; Poelzer, J.; Huynh, J.; Yallou, F. S.; Psychogios, N.; Dong, E.; Bogumil, R.; Roehring, C.; Wishart, D. S. The Human Urine Metabolome. *PLoS One* **2013**, *8*, No. e73076.

(51) Wojtowicz, W.; Zabek, A.; Deja, S.; Dawiskiba, T.; Pawelka, D.; Glod, M.; Balcerzak, W.; Mlynarz, P. Serum and Urine 1h Nmr-Based Metabolomics in the Diagnosis of Selected Thyroid Diseases. *Sci. Rep.* **2017**, *7*, 9108.

(52) Ahn, J. K.; Kim, J.; Hwang, J.; Song, J.; Kim, K. H.; Cha, H.-S. Urinary Metabolomic Profiling to Identify Potential Biomarkers for the Diagnosis of Behcet's Disease by Gas Chromatography/Time-of-Flight-Mass Spectrometry. *Int. J. Mol. Sci.* **2017**, *18*, 2309.

(53) Dinges, S. S.; Hohm, A.; Vandergrift, L. A.; Nowak, J.; Habbel, P.; Kaltashov, I. A.; Cheng, L. L. Cancer Metabolomic Markers in Urine: Evidence, Techniques and Recommendations. *Nat. Rev. Urol.* **2019**, *16*, 339−362.

(54) Alonso, A.; Julià, A.; Vinaixa, M.; Domènech, E.; Fernández-Nebro, A.; Cañete, J. D.; Ferrándiz, C.; Tornero, J.; Gisbert, J. P.; Nos, P.; Casbas, A. G.; Puig, L.; González-Álvaro, I.; Pinto-Tasende, J. A.; Blanco, R.; Rodríguez, M. A.; Beltran, A.; Correig, X.; Marsal, S.; Fernández, E.; Sanmartí, R.; Gratacós, J.; Martínez-Taboada, V. M.; Gomollón, F.; Daudén, E.; Maymó, J.; Queiró, R.; López-Longo, F. J.; Garcia-Planella, E.; Sánchez-Carazo, J. L.; Alperi-López, M.; Montilla, C.; Pérez-Venegas, J. J.; Fernández-Gutiérrez, B.; Mendoza, J. L.; López-Estebaranz, J. L.; Olivé, À.; Torre-Alonso, J. C.; Barreiro-de Acosta, M.; Moreno-Ramírez, D.; Corominas, H.; Muñoz-Fernández, S.; Andreu, J. L.; Muñoz, F.; de la Cueva, P.; Erra, A.; González, C. M.; Aguirre-Zamorano, M. Á.; Vera, M.; Vanaclocha, F.; Roig, D.; Vela, P.; Saro, C.; Herrera, E.; Zarco, P.; Nolla, J. M.; Esteve, M.; Marenco de la Fuente, J. L.; Pego-Reigosa, J. M.; García-Sánchez, V.; Panés, J.; Fonseca, E.; Blanco, F.; Rodríguez-Moreno, J.; Carreira, P.; Ramírez, J.; Ávila, G.; Codó, L.; Gelpí, J. L.; García-Montero, A. C.; Palau, N.; López-Lasanta, M.; Tortosa, R. Urine Metabolome Profiling of Immune-Mediated Inflammatory Diseases. *BMC Med.* **2016**, *14*, 133.

(55) Emwas, A.-H.; Roy, R.; McKay, R. T.; Ryan, D.; Brennan, L.; Tenori, L.; Luchinat, C.; Gao, X.; Zeri, A. C.; Gowda, G. A. N.; Raftery, D.; Steinbeck, C.; Salek, R. M.; Wishart, D. S. Recommendations and Standardization of Biomarker Quantification Using Nmr-Based Metabolomics with Particular Focus on Urinary Analysis. *J. Proteome Res.* **2016**, *15*, 360−373.

(56) Rocca-Serra, P.; Salek, R. M.; Arita, M.; Correa, E.; Dayalan, S.; Gonzalez-Beltran, A.; Ebbels, T.; Goodacre, R.; Hastings, J.; Haug, K.; Koulman, A.; Nikolski, M.; Oresic, M.; Sansone, S.-A.; Schober, D.; Smith, J.; Steinbeck, C.; Viant, M. R.; Neumann, S. Data Standards Can Boost Metabolomics Research, and If There Is a Will, There Is a Way. *Metabolomics* **2016**, *12*, 14.

(57) Müller, O. J.; Heckmann, M. B.; Ding, L.; Rapti, K.; Rangrez, A. Y.; Gerken, T.; Christiansen, N.; Rennefahrt, U. E. E.; Witt, H.; González Maldonado, S.; Ternes, P.; Schwab, D. M.; Ruf, T.; Hille, S.; Remes, A.; Jungmann, A.; Weis, T. M.; Kreußer, J. S.; Gröne, H.-J.; Backs, J.; Schatz, P.; Katus, H. A.; Frey, N. Comprehensive Plasma and Tissue Profiling Reveals Systemic Metabolic Alterations in Cardiac Hypertrophy and Failure. *Cardiovasc. Res.* **2019**, *115*, 1296−1305.

(58) Clarkson, M. R.; Magee, C. N.; Brenner, B. M. *Pocket Companion to Brenner and Rector's the Kidney*; 8th ed.; W.B. Saunders Co Ltd: London, 2010, Chapter 2, pp 21−42.

(59) Kale, N. S.; Haug, K.; Conesa, P.; Jayseelan, K.; Moreno, P.; Rocca-Serra, P.; Nainala, V. C.; Spicer, R. A.; Williams, M.; Li, X.; Salek, R. M.; Griffin, J. L.; Steinbeck, C. Metabolights: An Open-Access Database Repository for Metabolomics Data. *Curr. Protoc. Bioinform.* **2016**, *53*, 14.13.11.

(60) Kuhn, S.; Egert, B.; Neumann, S.; Steinbeck, C. Building Blocks for Automated Elucidation of Metabolites: Machine Learning Methods for Nmr Prediction. *BMC Bioinf.* **2008**, *9*, 400.

(61) Rifai, N. *Tietz Textbook of Clinical Chemistry and Molecular Diagnostics*; Elsevier Health Sciences: London, 2011; pp 684.

(62) Dame, Z. T.; Aziat, F.; Mandal, R.; Krishnamurthy, R.; Bouatra, S.; Borzouie, S.; Guo, A. C.; Sajed, T.; Deng, L.; Lin, H.; Liu, P.; Dong, E.; Wishart, D. S. The Human Saliva Metabolome. *Metabolomics* **2015**, *11*, 1864−1883.

(63) Berg, J. M.; Tymoczko, J. L.; Gattro, G. J., Jr; Stryer, L. *Biochemistry*, 8th ed.; Springer, 2018; pp 79−126.

(64) Aliu, E.; Kanungo, S.; Arnold, G. L. Amino Acid Disorders. *Ann. Transl. Med.* **2018**, *6*, 471.

(65) Sugimoto, M.; Wong, D. T.; Hirayama, A.; Soga, T.; Tomita, M. Capillary Electrophoresis Mass Spectrometry-Based Saliva Metabolomics Identified Oral, Breast and Pancreatic Cancer-Specific Profiles. *Metabolomics* **2010**, *6*, 78−95.

(66) Richter, M. E.; Neugebauer, S.; Engelmann, F.; Hagel, S.; Ludewig, K.; La Rosée, P.; Sayer, H. G.; Hochhaus, A.; von Lilienfeld-Toal, M.; Bretschneider, T.; Pausch, C.; Engel, C.; Brunkhorst, F. M.; Kiehntopf, M. Biomarker Candidates for the Detection of an Infectious Etiology of Febrile Neutropenia. *Infection* **2016**, *44*, 175−186.

(67) Aliu, E.; Kanungo, S.; Arnold, G. L. Amino Acid Disorders. *Ann. Transl Med.* **2018**, *6*, 471−471.

(68) Knerr, I. Amino Acid-Related Diseases. In *The Molecular Nutrition of Amino Acids and Proteins*; Academic Press, 2016; pp 305−314.

(69) Kumar, A.; Palfrey, H. A.; Pathak, R.; Kadowitz, P. J.; Gettys, T. W.; Murthy, S. N. The Metabolism and Significance of Homocysteine in Nutrition and Health. *Nutr. Metab.* **2017**, *14*, 78.

(70) Townsend, D. M.; Tew, K. D.; Tapiero, H. Sulfur Containing Amino Acids and Human Disease. *Biomed. Pharmacother.* **2004**, *58*, 47−55.

(71) Zinellu, A.; Zinellu, E.; Sotgiu, E.; Fois, A. G.; Paliogiannis, P.; Scano, V.; Piras, B.; Sotgia, S.; Mangoni, A. A.; Carru, C.; Pirina, P. Systemic Transsulfuration Pathway Thiol Concentrations in Chronic Obstructive Pulmonary Disease Patients. *Eur. J. Clin. Invest.* **2020**, *50*, No. e13267.

(72) Comai, S.; Bertazzo, A.; Brughera, M.; Crotti, S. Tryptophan in Health and Disease. In *Advances in Clinical Chemistry*; Elsevier, 2020; Vol. *95*; Chapter 5, pp 165−218.

(73) Holeček, M. Histidine in Health and Disease: Metabolism, Physiological Importance, and Use as a Supplement. *Nutrients* **2020**, *12*, 848.

(74) Bouchereau, J.; Schiff, M. Inherited Disorders of Lysine Metabolism: A Review. *J. Nutr.* **2020**, *150*, 2556s.

(75) Grosse, G. M.; Schwedhelm, E.; Worthmann, H.; Choe, C.-U. Arginine Derivatives in Cerebrovascular Diseases: Mechanisms and Clinical Implications. *Int. J. Mol. Sci.* **2020**, *21*, 1798.

(76) Hillert, A.; Anikster, Y.; Belanger-Quintana, A.; Burlina, A.; Burton, B. K.; Carducci, C.; Chiesa, A. E.; Christodoulou, J.; Đorđević, M.; Desviat, L. R. The Genetic Landscape and Epidemiology of Phenylketonuria. *Am. J. Hum. Genet.* **2020**, *107*, 234−250.

(77) Yildiz Celik, S.; Bebek, N.; Gurses, C.; Baykan, B.; Gokyigit, A. Clinical and Electrophysiological Findings in Patients with Phenylketonuria and Epilepsy: Reflex Features. *Epilepsy Behav.* **2018**, *82*, 46−51.

(78) Murphy, G. H.; Johnson, S. M.; Amos, A.; Weetch, E.; Hoskin, R.; Fitzgerald, B.; Lilburn, M.; Robertson, L.; Lee, P. Adults with

Untreated Phenylketonuria: Out of Sight, out of Mind. *Br. J. Psychiatry* **2008**, *193*, 501−502.

(79) Chinsky, J. M.; Singh, R.; Ficicioglu, C.; van Karnebeek, C. D. M.; Grompe, M.; Mitchell, G.; Waisbren, S. E.; Gucsavas-Calikoglu, M.; Wasserstein, M. P.; Coakley, K.; Scott, C. R.; et al. Diagnosis and Treatment of Tyrosinemia Type I: A Us and Canadian Consensus Group Review and Recommendations. *Genet. Med.* **2017**, *19*, 1380.

(80) Gostner, J. M.; Geisler, S.; Stonig, M.; Mair, L.; Sperner-Unterweger, B.; Fuchs, D. Tryptophan Metabolism and Related Pathways in Psychoneuroimmunology: The Impact of Nutrition and Lifestyle. *Neuropsychobiology* **2020**, *79*, 89−99.

(81) Sun, M.; Ma, N.; He, T.; Johnston, L. J.; Ma, X. Tryptophan (Trp) Modulates Gut Homeostasis Via Aryl Hydrocarbon Receptor (Ahr). *Crit. Rev. Food Sci. Nutr.* **2020**, *60*, 1760−1768.

(82) Gao, J.; Xu, K.; Liu, H.; Liu, G.; Bai, M.; Peng, C.; Li, T.; Yin, Y. Impact of the Gut Microbiota on Intestinal Immunity Mediated by Tryptophan Metabolism. *Front. Cell. Infect. Microbiol.* **2018**, *8*, 13.

(83) Friedman, M. Analysis, Nutrition, and Health Benefits of Tryptophan. *Int. J. Tryptophan Res.* **2018**, *11*, 117864691880228.

(84) Sandyk, R. L-Tryptophan in Neuropsychiatry Disorders: A Review. *Int. J. Neurosci.* **1992**, *67*, 127−144.

(85) Zhai, G.; Wang-Sattler, R.; Hart, D. J.; Arden, N. K.; Hakim, A. J.; Illig, T.; Spector, T. D. Serum Branched-Chain Amino Acid to Histidine Ratio: A Novel Metabolomic Biomarker of Knee Osteoarthritis. *Ann. Rheum. Dis.* **2010**, *69*, 1227.

(86) Ueland, P. M.; Refsum, H. Plasma Homocysteine, a Risk Factor for Vascular Disease: Plasma Levels in Health, Disease, and Drug Therapy. *J. Lab. Clin. Med.* **1989**, *114*, 473−501.

(87) Streifler, J. Y.; Rosenberg, N.; Chetrit, A.; Eskaraev, R.; Sela, B. A.; Dardik, R.; Zivelin, A.; Ravid, B.; Davidson, J.; Seligsohn, U.; Inbal, A. Cerebrovascular Events in Patients with Significant Stenosis of the Carotid Artery Are Associated with Hyperhomocysteinemia and Platelet Antigen-1 (Leu33pro) Polymorphism. *Stroke* **2001**, *32*, 2753−2758.

(88) Zhou, Y.; Yoon, J. Recent Progress in Fluorescent and Colorimetric Chemosensors for Detection of Amino Acids. *Chem. Soc. Rev.* **2012**, *41*, 52−67.

(89) Moore, S.; Stein, W. H. A Modified Ninhydrin Reagent for the Photometric Determination of Amino Acids and Related Compounds. *J. Biol. Chem.* **1954**, *211*, 907−913.

(90) Yemm, E.; Cocking, E.; Ricketts, R. The Determination of Amino-Acids with Ninhydrin. *Analyst* **1955**, *80*, 209−214.

(91) Rosen, H. A Modified Ninhydrin Colorimetric Analysis for Amino Acids. *Arch. Biochem. Biophys.* **1957**, *67*, 10−15.

(92) Friedman, M. Applications of the Ninhydrin Reaction for Analysis of Amino Acids, Peptides, and Proteins to Agricultural and Biomedical Sciences. *J. Agric. Food Chem.* **2004**, *52*, 385−406.

(93) Harding, V. J.; MacLean, R. M. The Ninhydrin Reaction with Amines and Amides. *J. Biol. Chem.* **1916**, *25*, 337−350.

(94) West, R. Siegfried Ruhemann and the Discovery of Ninhydrin. *J. Chem. Educ.* **1965**, *42*, 386.

(95) McCaldin, D. J. The Chemistry of Ninhydrin. *Chem. Rev.* **1960**, *60*, 39−51.

(96) Kalant, H. Colorimetric Ninhydrin Reaction for Measurement of α-Amino Nitrogen. *Anal. Chem.* **1956**, *28*, 265−266.

(97) Odén, S.; Von Hofsten, B. Detection of Fingerprints by the Ninhydrin Reaction. *Nature* **1954**, *173*, 449−450.

(98) Wiesner, S.; Springer, E.; Sasson, Y.; Almog, J. Chemical Development of Latent Fingerprints: 1, 2-Indanedione Has Come of Age. *J. Forensic Sci.* **2001**, *46*, 1082−1084.

(99) Azman, A. M. Fast, Easy, Reproducible Method for Planting Fingerprints for Ninhydrin, Iodine Development. *J. Chem. Educ.* **2020**, *97*, 571−573.

(100) Brunelle, E.; Huynh, C.; Le, A. M.; Halámková, L.; Agudelo, J.; Halámek, J. New Horizons for Ninhydrin: Colorimetric Determination of Gender from Fingerprints. *Anal. Chem.* **2016**, *88*, 2413−2420.

(101) Udenfriend, S.; Stein, S.; Böhlen, P.; Dairman, W.; Leimgruber, W.; Weigele, M. Fluorescamine: A Reagent for Assay of Amino Acids, Peptides, Proteins, and Primary Amines in the Picomole Range. *Science* **1972**, *178*, 871−872.

(102) Weigele, M.; DeBernardo, S.; Leimgruber, W. Fluorometric Assay of Secondary Amino Acids. *Biochem. Biophys. Res. Commun.* **1973**, *50*, 352−356.

(103) Bridges, M. A.; McErlane, K. M.; Kwong, E.; Katz, S.; Applegarth, D. A. Fluorometric Determination of Nanogram Quantities of Protein in Small Samples: Application to Calcium-Transport Adenosine Triphosphatase. *Clin. Chim. Acta* **1986**, *157*, 73−79.

(104) Funk, G. M.; Hunt, C. E.; Epps, D. E.; Brown, P. K. Use of a Rapid and Highly Sensitive Fluorescamine-Based Procedure for the Assay of Plasma Lipoproteins. *J. Lipid Res.* **1986**, *27*, 792−795.

(105) Stein, S.; Böhlen, P.; Udenfriend, S. Studies on the Kinetics of Reaction and Hydrolysis of Fluorescamine. *Arch. Biochem. Biophys.* **1974**, *163*, 400−403.

(106) Benson, J. R.; Hare, P. E. O-Phthalaldehyde: Fluorogenic Detection of Primary Amines in the Picomole Range. Comparison with Fluorescamine and Ninhydrin. *Proc. Natl. Acad. Sci. U. S. A.* **1975**, *72*, 619−622.

(107) De Montigny, P.; Stobaugh, J. F.; Givens, R. S.; Carlson, R. G.; Srinivasachar, K.; Sternson, L. A.; Higuchi, T. Naphthalene-2,3-Dicarboxyaldehyde/Cyanide Ion: A Rationally Designed Fluorogenic Reagent for Primary Amines. *Anal. Chem.* **1987**, *59*, 1096−1101.

(108) Leroy, P.; Nicolas, A.; Gavriloff, C.; Matt, M.; Netter, P.; Bannwarth, B.; Hercelin, B.; Mazza, M. Determination of 2-Mercaptopropionylglycine and Its Metabolite, 2-Mercaptopropionic Acid, in Plasma by Ion-Pair Reversed-Phase High-Performance Liquid Chromatography with Post-Column Derivatization. *J. Chromatogr., Biomed. Appl.* **1991**, *564*, 258−265.

(109) Nakamura, H.; Tamura, Z. Fluorometric Determination of Thiols by Liquid Chromatography with Postcolumn Derivatization. *Anal. Chem.* **1981**, *53*, 2190−2193.

(110) Kobayashi, M.; Ichishima, E. Use of Water-Soluble 1-Ethyl-3(3-Dimethylaminopropyl)Carbodiimide for the Fluorescent Determination of Uronic Acids and Carboxylic Acids. *Anal. Biochem.* **1990**, *189*, 122−125.

(111) Sano, A.; Takezawa, M.; Takitani, S. Spectrofluorimetric Determination of Cyanide in Blodd and Urine with Naphthalene-2,3-Dialdehyde and Taurine. *Anal. Chim. Acta* **1989**, *225*, 351−358.

(112) Jeon, S.; Kim, T. I.; Jin, H.; Lee, U.; Bae, J.; Bouffard, J.; Kim, Y. Amine-Reactive Activated Esters of Meso-Carboxybodipy: Fluorogenic Assays and Labeling of Amines, Amino Acids, and Proteins. *J. Am. Chem. Soc.* **2020**, *142*, 9231−9239.

(113) Buryak, A.; Severin, K. A Chemosensor Array for the Colorimetric Identification of 20 Natural Amino Acids. *J. Am. Chem. Soc.* **2005**, *127*, 3700−3701.

(114) Leung, D.; Folmer-Andersen, J. F.; Lynch, V. M.; Anslyn, E. V. Using Enantioselective Indicator Displacement Assays to Determine the Enantiomeric Excess of Alpha-Amino Acids. *J. Am. Chem. Soc.* **2008**, *130*, 12318−12327.

(115) Feuster, E. K.; Glass, T. E. Detection of Amines and Unprotected Amino Acids in Aqueous Conditions by Formation of Highly Fluorescent Iminium Ions. *J. Am. Chem. Soc.* **2003**, *125*, 16174−16175.

(116) Peng, H.; Chen, W.; Cheng, Y.; Hakuna, L.; Strongin, R.; Wang, B. Thiol Reactive Probes and Chemosensors. *Sensors* **2012**, *12*, 15907−15946.

(117) Jung, H. S.; Chen, X.; Kim, J. S.; Yoon, J. Recent Progress in Luminescent and Colorimetric Chemosensors for Detection of Thiols. *Chem. Soc. Rev.* **2013**, *42*, 6019−6031.

(118) Yin, C.; Huo, F.; Zhang, J.; Martinez-Manez, R.; Yang, Y.; Lv, H.; Li, S. Thiol-Addition Reactions and Their Applications in Thiol Recognition. *Chem. Soc. Rev.* **2013**, *42*, 6032−6059.

(119) Niu, L. Y.; Chen, Y. Z.; Zheng, H. R.; Wu, L. Z.; Tung, C. H.; Yang, Q. Z. Design Strategies of Fluorescent Probes for Selective Detection among Biothiols. *Chem. Soc. Rev.* **2015**, *44*, 6143−6160.

(120) Pak, Y. L.; Swamy, K. M.; Yoon, J. Recent Progress in Fluorescent Imaging Probes. *Sensors* **2015**, *15*, 24374−24396.

(121) Matsumoto, T.; Urano, Y.; Shoda, T.; Kojima, H.; Nagano, T. A Thiol-Reactive Fluorescence Probe Based on Donor-Excited Photoinduced Electron Transfer: Key Role of Ortho Substitution. *Org. Lett.* **2007**, *9*, 3375−3377.

(122) Kand, D.; Kalle, A. M.; Varma, S. J.; Talukdar, P. A Chromenoquinoline-Based Fluorescent Off-on Thiol Probe for Bioimaging. *Chem. Commun.* **2012**, *48*, 2722−2724.

(123) McMahon, B. K.; Gunnlaugsson, T. Selective Detection of the Reduced Form of Glutathione (Gsh) over the Oxidized (Gssg) Form Using a Combination of Glutathione Reductase and a Tb(Iii)-Cyclen Maleimide Based Lanthanide Luminescent 'Switch on' Assay. *J. Am. Chem. Soc.* **2012**, *134*, 10725−10728.

(124) Lin, W.; Yuan, L.; Cao, Z.; Feng, Y.; Long, L. A Sensitive and Selective Fluorescent Thiol Probe in Water Based on the Conjugate 1,4-Addition of Thiols to A, B-Unsaturated Ketones. *Chem.−Eur. J.* **2009**, *15*, 5096−5103.

(125) Kwon, H.; Lee, K.; Kim, H. J. Coumarin-Malonitrile Conjugate as a Fluorescence Turn-on Probe for Biothiols and Its Cellular Expression. *Chem. Commun.* **2011**, *47*, 1773−1775.

(126) Jung, H. S.; Han, J. H.; Pradhan, T.; Kim, S.; Lee, S. W.; Sessler, J. L.; Kim, T. W.; Kang, C.; Kim, J. S. A Cysteine-Selective Fluorescent Probe for the Cellular Detection of Cysteine. *Biomaterials* **2012**, *33*, 945−953.

(127) Isik, M.; Ozdemir, T.; Turan, I. S.; Kolemen, S.; Akkaya, E. U. Chromogenic and Fluorogenic Sensing of Biological Thiols in Aqueous Solutions Using Bodipy-Based Reagents. *Org. Lett.* **2013**, *15*, 216−219.

(128) Sreejith, S.; Divya, K. P.; Ajayaghosh, A. A near-Infrared Squaraine Dye as a Latent Ratiometric Fluorophore for the Detection of Aminothiol Content in Blood Plasma. *Angew. Chem., Int. Ed.* **2008**, *47*, 7883−7887.

(129) Ellman, G. L. Tissue Sulfhydryl Groups. *Arch. Biochem. Biophys.* **1959**, *82*, 70−77.

(130) Winther, J. R.; Thorpe, C. Quantification of Thiols and Disulfides. *Biochim. Biophys. Acta, Gen. Subj.* **2014**, *1840*, 838−846.

(131) Moser, M.; Schneider, R.; Behnke, T.; Schneider, T.; Falkenhagen, J.; Resch-Genger, U. Ellman's and Aldrithiol Assay as Versatile and Complementary Tools for the Quantification of Thiol Groups and Ligands on Nanomaterials. *Anal. Chem.* **2016**, *88*, 8624−8631.

(132) Yang, X.; Guo, Y.; Strongin, R. M. Conjugate Addition/Cyclization Sequence Enables Selective and Simultaneous Fluorescence Detection of Cysteine and Homocysteine. *Angew. Chem.* **2011**, *123*, 10878−10881.

(133) Chen, X.; Zhou, Y.; Peng, X.; Yoon, J. Fluorescent and Colorimetric Probes for Detection of Thiols. *Chem. Soc. Rev.* **2010**, *39*, 2120−2135.

(134) Townsend, D. M.; Tew, K. D.; Tapiero, H. The Importance of Glutathione in Human Disease. *Biomed. Pharmacother.* **2003**, *57*, 145−155.

(135) Refsum, H.; Ueland, P. M.; Nygård, O.; Vollset, S. E. Homocysteine and Cardiovascular Disease. *Annu. Rev. Med.* **1998**, *49*, 31−62.

(136) Shi, J. M.; Wang, Y. J.; Tang, X. L.; Liu, W.; Jiang, H. E.; Dou, W.; Liu, W. S. A Colorimetric and Fluorescent Probe for Thiols Based on 1, 8-Naphthalimide and Its Application for Bioimaging. *Dyes Pigm.* **2014**, *100*, 255−260.

(137) Niu, W.; Guo, L.; Li, Y.; Shuang, S.; Dong, C.; Wong, M. S. Highly Selective Two-Photon Fluorescent Probe for Ratiometric Sensing and Imaging Cysteine in Mitochondria. *Anal. Chem.* **2016**, *88*, 1908−1914.

(138) Zhang, P.; Guo, Z.-Q.; Yan, C.-X.; Zhu, W.-H. Near-Infrared Mitochondria-Targeted Fluorescent Probe for Cysteine Based on Difluoroboron Curcuminoid Derivatives. *Chin. Chem. Lett.* **2017**, *28*, 1952−1956.

(139) Wang, H.; Zhou, G.; Gai, H.; Chen, X. A Fluorescein-Based Probe with High Selectivity to Cysteine over Homocysteine and Glutathione. *Chem. Commun.* **2012**, *48*, 8341−8343.

(140) Chen, H.; Zhou, B.; Ye, R.; Zhu, J.; Bao, X. Synthesis and Evaluation of a New Fluorescein and Rhodamine B-Based Chemosensor for Highly Sensitive and Selective Detection of Cysteine over Other Amino Acids and Its Application in Living Cell Imaging. *Sens. Actuators, B* **2017**, *251*, 481−489.

(141) Lee, H. Y.; Choi, Y. P.; Kim, S.; Yoon, T.; Guo, Z.; Lee, S.; Swamy, K. M.; Kim, G.; Lee, J. Y.; Shin, I.; Yoon, J. Selective Homocysteine Turn-on Fluorescent Probes and Their Bioimaging Applications. *Chem. Commun.* **2014**, *50*, 6967−6969.

(142) Lin, W.; Long, L.; Yuan, L.; Cao, Z.; Chen, B.; Tan, W. A Ratiometric Fluorescent Probe for Cysteine and Homocysteine Displaying a Large Emission Shift. *Org. Lett.* **2008**, *10*, 5577−5580.

(143) Mei, J.; Tong, J. Q.; Wang, J.; Qin, A. J.; Sun, J. Z.; Tang, B. Z. Discriminative Fluorescence Detection of Cysteine, Homocysteine and Glutathione Via Reaction-Dependent Aggregation of Fluorophore-Analyte Adducts. *J. Mater. Chem.* **2012**, *22*, 17063−17070.

(144) Freudenberg, J.; Kumpf, J.; Schafer, V.; Sauter, E.; Worner, S. J.; Brodner, K.; Dreuw, A.; Bunz, U. H. Water-Soluble Cruciforms and Distyrylbenzenes: Synthesis, Characterization, and Ph-Dependent Amine-Sensing Properties. *J. Org. Chem.* **2013**, *78*, 4949−4959.

(145) Wang, W.; Rusin, O.; Xu, X.; Kim, K. K.; Escobedo, J. O.; Fakayode, S. O.; Fletcher, K. A.; Lowry, M.; Schowalter, C. M.; Lawrence, C. M.; Fronczek, F. R.; Warner, I. M.; Strongin, R. M. Detection of Homocysteine and Cysteine. *J. Am. Chem. Soc.* **2005**, *127*, 15949−15958.

(146) Wang, P.; Liu, J.; Lv, X.; Liu, Y.; Zhao, Y.; Guo, W. A Naphthalimide-Based Glyoxal Hydrazone for Selective Fluorescence Turn-on Sensing of Cys and Hcy. *Org. Lett.* **2012**, *14*, 520−523.

(147) Hou, X.; Guo, X.; Chen, B.; Liu, C.; Gao, F.; Zhao, J.; Wang, J. Rhodamine-Based Fluorescent Probe for Highly Selective Detection of Glutathione over Cysteine and Homocysteine. *Sens. Actuators, B* **2015**, *209*, 838−845.

(148) Zhang, D.; Yang, Z.; Li, H.; Pei, Z.; Sun, S.; Xu, Y. A Simple Excited-State Intramolecular Proton Transfer Probe Based on a New Strategy of Thiol-Azide Reaction for the Selective Sensing of Cysteine and Glutathione. *Chem. Commun.* **2016**, *52*, 749−752.

(149) Wang, L.; Chen, H. Y.; Wang, H. L.; Wang, F.; Kambam, S.; Wang, Y.; Zhao, W. B.; Chen, X. Q. A Fluorescent Probe with High Selectivity to Glutathione over Cysteine and Homocysteine Based on Positive Effect of Carboxyl on Nucleophilic Substitution in Ctab. *Sens. Actuators, B* **2014**, *192*, 708−713.

(150) Yang, X. F.; Huang, Q.; Zhong, Y.; Li, Z.; Li, H.; Lowry, M.; Escobedo, J. O.; Strongin, R. M. A Dual Emission Fluorescent Probe Enables Simultaneous Detection of Glutathione and Cysteine/Homocysteine. *Chem. Sci.* **2014**, *5*, 2177−2183.

(151) Zhang, H.; Zhang, C.; Liu, R.; Yi, L.; Sun, H. A Highly Selective and Sensitive Fluorescent Thiol Probe through Dual-Reactive and Dual-Quenching Groups. *Chem. Commun.* **2015**, *51*, 2029−2032.

(152) Wei, M.; Yin, P.; Shen, Y.; Zhang, L.; Deng, J.; Xue, S.; Li, H.; Guo, B.; Zhang, Y.; Yao, S. A New Turn-on Fluorescent Probe for Selective Detection of Glutathione and Cysteine in Living Cells. *Chem. Commun.* **2013**, *49*, 4640−4642.

(153) Fan, J.; Han, Z.; Kang, Y.; Peng, X. A Two-Photon Fluorescent Probe for Lysosomal Thiols in Live Cells and Tissues. *Sci. Rep.* **2016**, *6*, 19562.

(154) Wang, F.; Zhou, L.; Zhao, C.; Wang, R.; Fei, Q.; Luo, S.; Guo, Z.; Tian, H.; Zhu, W. H. A Dual-Response Bodipy-Based Fluorescent Probe for the Discrimination of Glutathione from Cystein and Homocystein. *Chem. Sci.* **2015**, *6*, 2584−2589.

(155) Lu, J.; Song, Y.; Shi, W.; Li, X.; Ma, H. A Long-Wavelength Fluorescent Probe for Imaging Reduced Glutathione in Live Cells. *Sens. Actuators, B* **2012**, *161*, 615−620.

(156) Lu, J.; Sun, C.; Chen, W.; Ma, H.; Shi, W.; Li, X. Determination of Non-Protein Cysteine in Human Serum by a Designed Bodipy-Based Fluorescent Probe. *Talanta* **2011**, *83*, 1050−1056.

(157) Wang, Z.; Han, D. M.; Jia, W. P.; Zhou, Q. Z.; Deng, W. P. Reaction-Based Fluorescent Probe for Selective Discrimination of

Thiophenols over Aliphaticthiols and Its Application in Water Samples. *Anal. Chem.* **2012**, *84*, 4915−4920.

(158) Jiang, W.; Cao, Y.; Liu, Y.; Wang, W. Rational Design of a Highly Selective and Sensitive Fluorescent Pet Probe for Discrimination of Thiophenols and Aliphatic Thiols. *Chem. Commun.* **2010**, *46*, 1944−1946.

(159) Lv, H.; Yang, X. F.; Zhong, Y.; Guo, Y.; Li, Z.; Li, H. Native Chemical Ligation Combined with Spirocyclization of Benzopyrylium Dyes for the Ratiometric and Selective Fluorescence Detection of Cysteine and Homocysteine. *Anal. Chem.* **2014**, *86*, 1800−1807.

(160) Niu, L.-Y.; Zheng, H.-R.; Chen, Y.-Z.; Wu, L.-Z.; Tung, C.-H.; Yang, Q.-Z. Fluorescent Sensors for Selective Detection of Thiols: Expanding the Intramolecular Displacement Based Mechanism to New Chromophores. *Analyst* **2014**, *139*, 1389−1395.

(161) Chen, W.; Luo, H.; Liu, X.; Foley, J. W.; Song, X. Broadly Applicable Strategy for the Fluorescence Based Detection and Differentiation of Glutathione and Cysteine/Homocysteine: Demonstration in Vitro and in Vivo. *Anal. Chem.* **2016**, *88*, 3638−3646.

(162) Lee, D.; Kim, G.; Yin, J.; Yoon, J. An Aryl-Thioether Substituted Nitrobenzothiadiazole Probe for the Selective Detection of Cysteine and Homocysteine. *Chem. Commun.* **2015**, *51*, 6518−6520.

(163) Lou, Z.; Li, P.; Sun, X.; Yang, S.; Wang, B.; Han, K. A Fluorescent Probe for Rapid Detection of Thiols and Imaging of Thiols Reducing Repair and H2o2 Oxidative Stress Cycles in Living Cells. *Chem. Commun.* **2013**, *49*, 391−393.

(164) Wang, R.; Chen, L.; Liu, P.; Zhang, Q.; Wang, Y. Sensitive near-Infrared Fluorescent Probes for Thiols Based on Se-N Bond Cleavage: Imaging in Living Cells and Tissues. *Chem.−Eur. J.* **2012**, *18*, 11343−11349.

(165) Tang, B.; Yin, L.; Wang, X.; Chen, Z.; Tong, L.; Xu, K. A Fast-Response, Highly Sensitive and Specific Organoselenium Fluorescent Probe for Thiols and Its Application in Bioimaging. *Chem. Commun.* **2009**, 5293−5295.

(166) Lee, M. H.; Han, J. H.; Lee, J.-H.; Choi, H. G.; Kang, C.; Kim, J. S. Mitochondrial Thioredoxin-Responding Off-on Fluorescent Probe. *J. Am. Chem. Soc.* **2012**, *134*, 17314−17319.

(167) Niu, L.-Y.; Guan, Y.-S.; Chen, Y.-Z.; Wu, L.-Z.; Tung, C.-H.; Yang, Q.-Z. Bodipy-Based Ratiometric Fluorescent Sensor for Highly Selective Detection of Glutathione over Cysteine and Homocysteine. *J. Am. Chem. Soc.* **2012**, *134*, 18928−18931.

(168) Liu, J.; Sun, Y. Q.; Huo, Y.; Zhang, H.; Wang, L.; Zhang, P.; Song, D.; Shi, Y.; Guo, W. Simultaneous Fluorescence Sensing of Cys and Gsh from Different Emission Channels. *J. Am. Chem. Soc.* **2014**, *136*, 574−577.

(169) Kang, R.; Talamini, L.; D'Este, E.; Estevão, B. M.; De Cola, L.; Klopper, W.; Biedermann, F. Discovery of a Size-Record Breaking Green-Emissive Fluorophore: Small, Smaller, Hina. *Chem. Sci.* **2021**, *12*, 1392−1397.

(170) Tong, W.-L.; Chan, M. C. W.; Yiu, S.-M. Congested Cyclometalated Platinum(Ii) Ditopic Frameworks and Their Phosphorescent Responses to S-Containing Amino Acids. *Organometallics* **2010**, *29*, 6377−6383.

(171) Yang, Y. K.; Shim, S.; Tae, J. Rhodamine-Sugar Based Turn-on Fluorescent Probe for the Detection of Cysteine and Homocysteine in Water. *Chem. Commun.* **2010**, *46*, 7766−7768.

(172) Yang, X.-F.; Liu, P.; Wang, L.; Zhao, M. A Chemosensing Ensemble for the Detection of Cysteine Based on the Inner Filter Effect Using a Rhodamine B Spirolactam. *J. Fluoresc.* **2008**, *18*, 453−459.

(173) Mahapatra, A. K.; Roy, J.; Sahoo, P.; Mukhopadhyay, S. K.; Banik, A.; Mandal, D. Carbazole Phenylthiosemicarbazone-Based Ensemble of Hg2+ as Selective Fluorescence Turn-on Sensor toward Cysteine in Water. *Tetrahedron Lett.* **2013**, *54*, 2946−2951.

(174) Huang, H.; Shi, F.; Li, Y.; Niu, L.; Gao, Y.; Shah, S. M.; Su, X. Water-Soluble Conjugated Polymer-Cu(Ii) System as a Turn-on Fluorescence Probe for Label-Free Detection of Glutathione and Cysteine in Biological Fluids. *Sens. Actuators, B* **2013**, *178*, 532−540.

(175) Ros-Lis, J. V.; García, B.; Jiménez, D.; Martínez-Máñez, R.; Sancenón, F.; Soto, J.; Gonzalvo, F.; Valldecabres, M. C. Squaraines as Fluoro-Chromogenic Probes for Thiol-Containing Compounds and Their Application to the Detection of Biorelevant Thiols. *J. Am. Chem. Soc.* **2004**, *126*, 4064−4065.

(176) Zhang, M.; Yu, M.; Li, F.; Zhu, M.; Li, M.; Gao, Y.; Li, L.; Liu, Z.; Zhang, J.; Zhang, D.; Yi, T.; Huang, C. A Highly Selective Fluorescence Turn-on Sensor for Cysteine/Homocysteine and Its Application in Bioimaging. *J. Am. Chem. Soc.* **2007**, *129*, 10322−10323.

(177) Kuśmierek, K.; Chwatko, G.; Głowacki, R.; Bald, E. Determination of Endogenous Thiols and Thiol Drugs in Urine by Hplc with Ultraviolet Detection. *J. Chromatogr. B: Anal. Technol. Biomed. Life Sci.* **2009**, *877*, 3300−3308.

(178) Pastore, A.; Massoud, R.; Motti, C.; Lo Russo, A.; Fucci, G.; Cortese, C.; Federici, G. Fully Automated Assay for Total Homocysteine, Cysteine, Cysteinylglycine, Glutathione, Cysteamine, and 2-Mercaptopropionylglycine in Plasma and Urine. *Clin. Chem.* **1998**, *44*, 825−832.

(179) Zappacosta, B.; Manni, A.; Persichilli, S.; Scribano, D.; Minucci, A.; Lazzaro, D.; De Sole, P.; Giardina, B. Hplc Analysis of Some Sulphur Compounds in Saliva: Comparison between Healthy Subjects and Periodontopathic Patients. *Clin. Chim. Acta* **2003**, *338*, 57−60.

(180) Bald, E.; Głowacki, R. Analysis of Saliva for Glutathione and Metabolically Related Thiols by Liquid Chromatography with Ultraviolet Detection. *Amino Acids* **2005**, *28*, 431−433.

(181) Kuśmierek, K.; Bald, E. Determination of N-Acetylcysteine and Thioglycolic Acid in Human Urine. *Chromatographia* **2008**, *67*, 23−29.

(182) Ma, D. L.; Wong, W. L.; Chung, W. H.; Chan, F. Y.; So, P. K.; Lai, T. S.; Zhou, Z. Y.; Leung, Y. C.; Wong, K. Y. A Highly Selective Luminescent Switch-on Probe for Histidine/Histidine-Rich Proteins and Its Application in Protein Staining. *Angew. Chem., Int. Ed.* **2008**, *47*, 3735−3739.

(183) Wang, H.; Xu, B.; Chen, H.; Li, D.; Shen, X.; Cai, F.; Xu, Y.; Zhou, L.; Hu, L. A Fluorescent Probe Based on Ir(Iii) Solvent Complex for Specific Recognition of Histidine in Aqueous Solution and the Application in Cell Imaging. *Inorg. Chim. Acta* **2020**, *511*, 119799.

(184) Sinn, S.; Biedermann, F.; De Cola, L. Platinum Complex Assemblies as Luminescent Probes and Tags for Drugs and Toxins in Water. *Chem.−Eur. J.* **2017**, *23*, 1965−1971.

(185) Mutihac, L.; Lee, J. H.; Kim, J. S.; Vicens, J. Recognition of Amino Acids by Functionalized Calixarenes. *Chem. Soc. Rev.* **2011**, *40*, 2777−2796.

(186) Schneider, H.-J.; Yatsimirsky, A. K. Selectivity in Supramolecular Host-Guest Complexes. *Chem. Soc. Rev.* **2008**, *37*, 263−277.

(187) Biedermann, F.; Schneider, H.-J. Experimental Binding Energies in Supramolecular Complexes. *Chem. Rev.* **2016**, *116*, 5216−5300.

(188) Yang, K.; Pei, Y.; Wen, J.; Pei, Z. Recent Advances in Pillar[N]Arenes: Synthesis and Applications Based on Host-Guest Interactions. *Chem. Commun.* **2016**, *52*, 9316−9326.

(189) Sousa, F.; Cruz, C.; Queiroz, J. A. Amino Acids-Nucleotides Biomolecular Recognition: From Biological Occurrence to Affinity Chromatography. *J. Mol. Recognit.* **2010**, *23*, 505−518.

(190) Urbach, A. R.; Ramalingam, V. Molecular Recognition of Amino Acids, Peptides, and Proteins by Cucurbit[N]Uril Receptors. *Isr. J. Chem.* **2011**, *51*, 664−678.

(191) James, L. I.; Beaver, J. E.; Rice, N. W.; Waters, M. L. A Synthetic Receptor for Asymmetric Dimethyl Arginine. *J. Am. Chem. Soc.* **2013**, *135*, 6450−6455.

(192) Buschmann, H. J.; Mutihac, L.; Schollmeyer, E. Complexation of Some Amino Acids and Peptides by P-Sulfonatocalix[4]Arene and Hexasodium P-Sulfonatocalix[6]Arene in Aqueous Solution. *J. Inclusion Phenom. Mol. Recognit. Chem.* **2003**, *46*, 133−137.

(193) Da Silva, E.; Coleman, A. W. Synthesis and Complexation Properties Towards Amino Acids of Mono-Substituted P-Sulphonato-Calix-[N]-Arenes. *Tetrahedron* **2003**, *59*, 7357−7364.

(194) Dziemidowicz, J.; Witt, D.; Rachoń, J. Complexation of Amino Acids Derivatives in Water by Calix[4]Arene Phosphonic Acids. *J. Inclusion Phenom. Mol. Recognit. Chem.* **2008**, *61*, 381−391.

(195) Bonaccorso, C.; Gentile, S.; Gulino, F.; Sciotto, D. Molecular Recognition of Alkylammonium, N-Methylpyridinium Cations and Native L-A-Amino Acids by Water Soluble Penta- and Tetra-Sulfonatocalixarenes. *Lett. Org. Chem.* **2009**, *6*, 598−603.

(196) Rajgariah, P.; Urbach, A. R. Scope of Amino Acid Recognition by Cucurbit[8]Uril. *J. Inclusion Phenom. Mol. Recognit. Chem.* **2008**, *62*, 251−254.

(197) Lee, J. W.; Lee, H. H. L.; Ko, Y. H.; Kim, K.; Kim, H. I. Deciphering the Specific High-Affinity Binding of Cucurbit[7]Uril to Amino Acids in Water. *J. Phys. Chem. B* **2015**, *119*, 4628−4636.

(198) Gao, Q.; Zhang, W.; Song, B.; Zhang, R.; Guo, W.; Yuan, J. Development of a Novel Lysosome-Targeted Ruthenium(Ii) Complex for Phosphorescence/Time-Gated Luminescence Assay of Biothiols. *Anal. Chem.* **2017**, *89*, 4517−4524.

(199) Caso, J. V.; Russo, L.; Palmieri, M.; Malgieri, G.; Galdiero, S.; Falanga, A.; Isernia, C.; Iacovino, R. Investigating the Inclusion Properties of Aromatic Amino Acids Complexing Beta-Cyclodextrins in Model Peptides. *Amino Acids* **2015**, *47*, 2215−2227.

(200) Roy, A.; Saha, S.; Roy, M. N. Study to Explore Host-Guest Inclusion Complexes of Cyclodextrins with Biologically Active Molecules in Aqueous Environment. *Fluid Phase Equilib.* **2016**, *425*, 252−258.

(201) Kahle, C.; Holzgrabe, U. Determination of Binding Constants of Cyclodextrin Inclusion Complexes with Amino Acids and Dipeptides by Potentiometric Titration. *Chirality* **2004**, *16*, 509−515.

(202) Barrow, S. J.; Kasera, S.; Rowland, M. J.; del Barrio, J.; Scherman, O. A. Cucurbituril-Based Molecular Recognition. *Chem. Rev.* **2015**, *115*, 12320−12406.

(203) Ayhan, M. M.; Karoui, H.; Hardy, M.; Rockenbauer, A.; Charles, L.; Rosas, R.; Udachin, K.; Tordo, P.; Bardelang, D.; Ouari, O. Comprehensive Synthesis of Monohydroxy-Cucurbit[N]Urils (N = 5, 6, 7, 8): High Purity and High Conversions. *J. Am. Chem. Soc.* **2015**, *137*, 10238−10245.

(204) Biedermann, F.; Nau, W. M.; Schneider, H.-J. The Hydrophobic Effect Revisited−Studies with Supramolecular Complexes Imply High-Energy Water as a Noncovalent Driving Force. *Angew. Chem., Int. Ed.* **2014**, *53*, 11158−11171.

(205) Biedermann, F.; Uzunova, V. D.; Scherman, O. A.; Nau, W. M.; De Simone, A. Release of High-Energy Water as an Essential Driving Force for the High-Affinity Binding of Cucurbit[N]Urils. *J. Am. Chem. Soc.* **2012**, *134*, 15318−15323.

(206) Biedermann, F.; Vendruscolo, M.; Scherman, O. A.; De Simone, A.; Nau, W. M. Cucurbit[8]Uril and Blue-Box: High-Energy Water Release Overwhelms Electrostatic Interactions. *J. Am. Chem. Soc.* **2013**, *135*, 14879−14888.

(207) He, S.; Biedermann, F.; Vankova, N.; Zhechkov, L.; Heine, T.; Hoffman, R. E.; De Simone, A.; Duignan, T. T.; Nau, W. M. Cavitation Energies Can Outperform Dispersion Interactions. *Nat. Chem.* **2018**, *10*, 1252−1257.

(208) Reczek, J. J.; Kennedy, A. A.; Halbert, B. T.; Urbach, A. R. Multivalent Recognition of Peptides by Modular Self-Assembled Receptors. *J. Am. Chem. Soc.* **2009**, *131*, 2408−2415.

(209) Smith, L. C.; Leach, D. G.; Blaylock, B. E.; Ali, O. A.; Urbach, A. R. Sequence-Specific, Nanomolar Peptide Binding Via Cucurbit[8]Uril-Induced Folding and Inclusion of Neighboring Side Chains. *J. Am. Chem. Soc.* **2015**, *137*, 3663−3669.

(210) Heitmann, L. M.; Taylor, A. B.; Hart, P. J.; Urbach, A. R. Sequence-Specific Recognition and Cooperative Dimerization of N-Terminal Aromatic Peptides in Aqueous Solution by a Synthetic Host. *J. Am. Chem. Soc.* **2006**, *128*, 12574−12581.

(211) Chinai, J. M.; Taylor, A. B.; Ryno, L. M.; Hargreaves, N. D.; Morris, C. A.; Hart, P. J.; Urbach, A. R. Molecular Recognition of Insulin by a Synthetic Receptor. *J. Am. Chem. Soc.* **2011**, *133*, 8810−8813.

(212) Guo, D.-S.; Liu, Y. Supramolecular Chemistry of P-Sulfonatocalix[N]Arenes and Its Biological Applications. *Acc. Chem. Res.* **2014**, *47*, 1925−1934.

(213) Nau, W. M.; Ghale, G.; Hennig, A.; Bakirci, H. S.; Bailey, D. M. Substrate-Selective Supramolecular Tandem Assays: Monitoring Enzyme Inhibition of Arginase and Diamine Oxidase by Fluorescent Dye Displacement from Calixarene and Cucurbituril Macrocycles. *J. Am. Chem. Soc.* **2009**, *131*, 11558−11570.

(214) Ghale, G.; Nau, W. M. Dynamically Analyte-Responsive Macrocyclic Host-Fluorophore Systems. *Acc. Chem. Res.* **2014**, *47*, 2150−2159.

(215) Dsouza, R. N.; Hennig, A.; Nau, W. M. Supramolecular Tandem Enzyme Assays. *Chem.−Eur. J.* **2012**, *18*, 3444−3459.

(216) Ghale, G.; Lanctôt, A. G.; Kreissl, H. T.; Jacob, M. H.; Weingart, H.; Winterhalter, M.; Nau, W. M. Chemosensing Ensembles for Monitoring Biomembrane Transport in Real Time. *Angew. Chem., Int. Ed.* **2014**, *53*, 2762−2765.

(217) Guo, D.-S.; Uzunova, V. D.; Su, X.; Liu, Y.; Nau, W. M. Operational Calixarene-Based Fluorescent Sensing Systems for Choline and Acetylcholine and Their Application to Enzymatic Reactions. *Chem. Sci.* **2011**, *2*, 1722−1734.

(218) Hennig, A.; Bakirci, H.; Nau, W. M. Label-Free Continuous Enzyme Assays with Macrocycle-Fluorescent Dye Complexes. *Nat. Methods* **2007**, *4*, 629−632.

(219) Norouzy, A.; Azizi, Z.; Nau, W. M. Indicator Displacement Assays inside Live Cells. *Angew. Chem., Int. Ed.* **2015**, *54*, 792−795.

(220) Barba-Bon, A.; Pan, Y.-C.; Biedermann, F.; Guo, D.-S.; Nau, W. M.; Hennig, A. Fluorescence Monitoring of Peptide Transport Pathways into Large and Giant Vesicles by Supramolecular Host-Dye Reporter Pairs. *J. Am. Chem. Soc.* **2019**, *141*, 20137−20145.

(221) Ghale, G.; Ramalingam, V.; Urbach, A. R.; Nau, W. M. Determining Protease Substrate Selectivity and Inhibition by Label-Free Supramolecular Tandem Enzyme Assays. *J. Am. Chem. Soc.* **2011**, *133*, 7528−7535.

(222) Biedermann, F.; Nau, W. M. Noncovalent Chirality Sensing Ensembles for the Detection and Reaction Monitoring of Amino Acids, Peptides, Proteins, and Aromatic Drugs. *Angew. Chem., Int. Ed.* **2014**, *53*, 5694−5699.

(223) Biedermann, F.; Ghale, G.; Hennig, A.; Nau, W. M. Fluorescent Artificial Receptor-Based Membrane Assay (Farma) for Spatiotemporally Resolved Monitoring of Biomembrane Permeability. *Commun. Biol.* **2020**, *3*, 383.

(224) He, S.; Zhiti, A.; Barba-Bon, A.; Hennig, A.; Nau, W. M. Real-Time Parallel Artificial Membrane Permeability Assay Based on Supramolecular Fluorescent Artificial Receptors. *Front. Chem.* **2020**, *8*, 597927.

(225) Shaikh, M.; Mohanty, J.; Singh, P. K.; Nau, W. M.; Pal, H. Complexation of Acridine Orange by Cucurbit[7]Uril and B-Cyclodextrin: Photophysical Effects and Pka Shifts. *Photochem. Photobiol. Sci.* **2008**, *7*, 408−414.

(226) Bailey, D. M.; Hennig, A.; Uzunova, V. D.; Nau, W. M. Supramolecular Tandem Enzyme Assays for Multiparameter Sensor Arrays and Enantiomeric Excess Determination of Amino Acids. *Chem.−Eur. J.* **2008**, *14*, 6069−6077.

(227) Wang, Y.; Dmochowski, I. J. Cucurbit[6]Uril Is an Ultrasensitive 129xe Nmr Contrast Agent. *Chem. Commun.* **2015**, *51*, 8982−8985.

(228) Schnurr, M.; Sloniec-Myszk, J.; Döpfert, J.; Schröder, L.; Hennig, A. Supramolecular Assays for Mapping Enzyme Activity by Displacement-Triggered Change in Hyperpolarized 129xe Magnetization Transfer Nmr Spectroscopy. *Angew. Chem., Int. Ed.* **2015**, *54*, 13444−13447.

(229) Hane, F. T.; Li, T.; Smylie, P.; Pellizzari, R. M.; Plata, J. A.; DeBoef, B.; Albert, M. S. In Vivo Detection of Cucurbit[6]Uril, a Hyperpolarized Xenon Contrast Agent for a Xenon Magnetic Resonance Imaging Biosensor. *Sci. Rep.* **2017**, *7*, 41027.

(230) Jayapaul, J.; Schroder, L. Probing Reversible Guest Binding with Hyperpolarized 129xe-Nmr: Characteristics and Applications for Cucurbit[N]Urils. *Molecules* **2020**, *25*, 957.

(231) Li, W.; Bockus, A. T.; Vinciguerra, B.; Isaacs, L.; Urbach, A. R. Predictive Recognition of Native Proteins by Cucurbit[7]Uril in a Complex Mixture. *Chem. Commun.* **2016**, *52*, 8537−8540.

(232) Bhasikuttan, A. C.; Mohanty, J.; Nau, W. M.; Pal, H. Efficient Fluorescence Enhancement and Cooperative Binding of an Organic Dye in a Supra-Biomolecular Host-Protein Assembly. *Angew. Chem., Int. Ed.* **2007**, *46*, 4120.

(233) Lagona, J.; Wagner, B. D.; Isaacs, L. Molecular-Recognition Properties of a Water-Soluble Cucurbit[6]Uril Analogue. *J. Org. Chem.* **2006**, *71*, 1181−1190.

(234) Minami, T.; Esipenko, N. A.; Zhang, B.; Isaacs, L.; Anzenbacher, P. Turn-on" Fluorescent Sensor Array for Basic Amino Acids in Water. *Chem. Commun.* **2014**, *50*, 61−63.

(235) Minami, T.; Esipenko, N. A.; Akdeniz, A.; Zhang, B.; Isaacs, L.; Anzenbacher, P. Multianalyte Sensing of Addictive over-the-Counter (Otc) Drugs. *J. Am. Chem. Soc.* **2013**, *135*, 15238−15243.

(236) Bai, Q.; Zhang, S.; Chen, H.; Sun, T.; Redshaw, C.; Zhang, J.-X.; Ni, X.-L.; Wei, G.; Tao, Z. Alkyl Substituted Cucurbit[6]Uril Assisted Competitive Fluorescence Recognition of Lysine and Methionine in Aqueous Solution. *ChemistrySelect* **2017**, *2*, 2569−2573.

(237) Yang, B.; Zheng, L.-M.; Gao, Z.-Z.; Xiao, X.; Zhu, Q.-J.; Xue, S.-F.; Tao, Z.; Liu, J.-X.; Wei, G. Extended and Contorted Conformations of Alkanediammonium Ions in Symmetrical Tetramethylcucurbit[6]Uril Cavity. *J. Org. Chem.* **2014**, *79*, 11194−11198.

(238) Ma, D.; Zavalij, P. Y.; Isaacs, L. Acyclic Cucurbit[N]Uril Congeners Are High Affinity Hosts. *J. Org. Chem.* **2010**, *75*, 4786−4795.

(239) Sigwalt, D.; Moncelet, D.; Falcinelli, S.; Mandadapu, V.; Zavalij, P. Y.; Day, A.; Briken, V.; Isaacs, L. Acyclic Cucurbit[N]Uril-Type Molecular Containers: Influence of Linker Length on Their Function as Solubilizing Agents. *ChemMedChem* **2016**, *11*, 980−989.

(240) Deng, C.-L.; Murkli, S. L.; Isaacs, L. D. Supramolecular Hosts as in Vivo Sequestration Agents for Pharmaceuticals and Toxins. *Chem. Soc. Rev.* **2020**, *49*, 7516−7532.

(241) Shen, C.; Ma, D.; Meany, B.; Isaacs, L.; Wang, Y. H. Acyclic Cucurbit[N]Uril Molecular Containers Selectively Solubilize Single-Walled Carbon Nanotubes in Water. *J. Am. Chem. Soc.* **2012**, *134*, 7254−7257.

(242) Ma, D.; Hettiarachchi, G.; Nguyen, D.; Zhang, B.; Wittenberg, J. B.; Zavalij, P. Y.; Briken, V.; Isaacs, L. Acyclic Cucurbit[N]Uril Molecular Containers Enhance the Solubility and Bioactivity of Poorly Soluble Pharmaceuticals. *Nat. Chem.* **2012**, *4*, 503−510.

(243) Ma, D.; Zhang, B.; Hoffmann, U.; Sundrup, M. G.; Eikermann, M.; Isaacs, L. Acyclic Cucurbit[N]Uril-Type Molecular Containers Bind Neuromuscular Blocking Agents in Vitro and Reverse Neuromuscular Block in Vivo. *Angew. Chem., Int. Ed.* **2012**, *51*, 11358−11362.

(244) Ma, D.; Glassenberg, R.; Ghosh, S.; Zavalij, P. Y.; Isaacs, L. Acyclic Cucurbituril Congener Binds to Local Anaesthetics. *Supramol. Chem.* **2012**, *24*, 325−332.

(245) Lu, X.; Isaacs, L. Uptake of Hydrocarbons in Aqueous Solution by Encapsulation in Acyclic Cucurbit[N]Uril-Type Molecular Containers. *Angew. Chem.* **2016**, *128*, 8208−8212.

(246) Prabodh, A.; Bauer, D.; Kubik, S.; Rebmann, P.; Klarner, F. G.; Schrader, T.; Delarue Bizzini, L.; Mayor, M.; Biedermann, F. Chirality Sensing of Terpenes, Steroids, Amino Acids, Peptides and Drugs with Acyclic Cucurbit[N]Urils and Molecular Tweezers. *Chem. Commun.* **2020**, *56*, 4652−4655.

(247) Dutt, S.; Wilch, C.; Gersthagen, T.; Talbiersky, P.; Bravo-Rodriguez, K.; Hanni, M.; Sanchez-Garcia, E.; Ochsenfeld, C.; Klarner, F. G.; Schrader, T. Molecular Tweezers with Varying Anions: A Comparative Study. *J. Org. Chem.* **2013**, *78*, 6721−6734.

(248) Schrader, T.; Bitan, G.; Klarner, F. G. Molecular Tweezers for Lysine and Arginine−Powerful Inhibitors of Pathologic Protein Aggregation. *Chem. Commun.* **2016**, *52*, 11318−11334.

(249) Fokkens, M.; Schrader, T.; Klarner, F. G. A Molecular Tweezer for Lysine and Arginine. *J. Am. Chem. Soc.* **2005**, *127*, 14415−14421.

(250) Talbiersky, P.; Bastkowski, F.; Klarner, F. G.; Schrader, T. Molecular Clip and Tweezer Introduce New Mechanisms of Enzyme Inhibition. *J. Am. Chem. Soc.* **2008**, *130*, 9824−9828.

(251) Klarner, F. G.; Schrader, T. Aromatic Interactions by Molecular Tweezers and Clips in Chemical and Biological Systems. *Acc. Chem. Res.* **2013**, *46*, 967−978.

(252) Ferreira, N.; Pereira-Henriques, A.; Attar, A.; Klärner, F.-G.; Schrader, T.; Bitan, G.; Gales, L.; Saraiva, M. J.; Almeida, M. R. Molecular Tweezers Targeting Transthyretin Amyloidosis. *Neurotherapeutics* **2014**, *11*, 450−461.

(253) Lump, E.; Castellano, L. M.; Meier, C.; Seeliger, J.; Erwin, N.; Sperlich, B.; Stürzel, C. M.; Usmani, S.; Hammond, R. M.; von Einem, J.; et al. A Molecular Tweezer Antagonizes Seminal Amyloids and Hiv Infection. *eLife* **2015**, *4*, No. e05397.

(254) Lulla, A.; Barnhill, L.; Bitan, G.; Ivanova, M. I.; Nguyen, B.; O'Donnell, K.; Stahl, M. C.; Yamashiro, C.; Klärner, F.-G.; Schrader, T.; Sagasti, A.; Bronstein, J. M. Neurotoxicity of the Parkinson Disease-Associated Pesticide Ziram Is Synuclein-Dependent in Zebrafish Embryos. *Environ. Health Perspect.* **2016**, *124*, 1766−1775.

(255) Kim, H.-J.; Heo, J.; Jeon, W. S.; Lee, E.; Kim, J.; Sakamoto, S.; Yamaguchi, K.; Kim, K. Selective Inclusion of a Hetero-Guest Pair in a Molecular Host: Formation of Stable Charge-Transfer Complexes in Cucurbit[8]Uril. *Angew. Chem., Int. Ed.* **2001**, *40*, 1526−1529.

(256) Jeon, W. S.; Kim, H.-J.; Lee, C.; Kim, K. Control of the Stoichiometry in Host-Guest Complexation by Redox Chemistry of Guests: Inclusion of Methylviologen in Cucurbit[8]Uril. *Chem. Commun.* **2002**, 1828−1829.

(257) Jeon, W. S.; Ziganshina, A. Y.; Lee, J. W.; Ko, Y. H.; Kang, J.-K.; Lee, C.; Kim, K. A [2]Pseudorotaxane-Based Molecular Machine: Reversible Formation of a Molecular Loop Driven by Electrochemical and Photochemical Stimuli. *Angew. Chem., Int. Ed.* **2003**, *42*, 4097−4100.

(258) Ko, Y. H.; Kim, K.; Kang, J. K.; Chun, H.; Lee, J. W.; Sakamoto, S.; Yamaguchi, K.; Fettinger, J. C.; Kim, K. Designed Self-Assembly of Molecular Necklaces Using Host-Stabilized Charge-Transfer Interactions. *J. Am. Chem. Soc.* **2004**, *126*, 1932−1933.

(259) Jeon, W. S.; Kim, E.; Ko, Y. H.; Hwang, I.; Lee, J. W.; Kim, S.-Y.; Kim, H.-J.; Kim, K. Molecular Loop Lock: A Redox-Driven Molecular Machine Based on a Host-Stabilized Charge-Transfer Complex. *Angew. Chem., Int. Ed.* **2005**, *44*, 87−91.

(260) Bush, M. E.; Bouley, N. D.; Urbach, A. R. Charge-Mediated Recognition of N-Terminal Tryptophan in Aqueous Solution by a Synthetic Host. *J. Am. Chem. Soc.* **2005**, *127*, 14511−14517.

(261) Biedermann, F.; Scherman, O. A. Cucurbit[8]Uril Mediated Donor-Acceptor Ternary Complexes: A Model System for Studying Charge-Transfer Interactions. *J. Phys. Chem. B* **2012**, *116*, 2842−2849.

(262) Appel, E. A.; Biedermann, F.; Hoogland, D.; del Barrio, J.; Driscoll, M. D.; Hay, S.; Wales, D. J.; Scherman, O. A. Decoupled Associative and Dissociative Processes in Strong yet Highly Dynamic Host-Guest Complexes. *J. Am. Chem. Soc.* **2017**, *139*, 12985−12993.

(263) Sindelar, V.; Cejas, M. A.; Raymo, F. M.; Chen, W.; Parker, S. E.; Kaifer, A. E. Supramolecular Assembly of 2,7-Dimethyldiazapyrenium and Cucurbit[8]Uril: A New Fluorescent Host for Detection of Catechol and Dopamine. *Chem.−Eur. J.* **2005**, *11*, 7054−7059.

(264) Ling, Y.; Wang, W.; Kaifer, A. E. A New Cucurbit[8]Uril-Based Fluorescent Receptor for Indole Derivatives. *Chem. Commun.* **2007**, 610−612.

(265) Biedermann, F.; Rauwald, U.; Cziferszky, M.; Williams, K. A.; Gann, L. D.; Guo, B. Y.; Urbach, A. R.; Bielawski, C. W.; Scherman, O. A. Benzobis(Imidazolium)-Cucurbit[8]Uril Complexes for Binding and Sensing Aromatic Compounds in Aqueous Solution. *Chem.−Eur. J.* **2010**, *16*, 13716−13722.

(266) Biedermann, F.; Elmalem, E.; Ghosh, I.; Nau, W. M.; Scherman, O. A. Strongly Fluorescent, Switchable Perylene Bis-(Diimide) Host-Guest Complexes with Cucurbit[8]Uril in Water. *Angew. Chem., Int. Ed.* **2012**, *51*, 7739−7743.

(267) Aryal, G. H.; Huang, L.; Hunter, K. W. Highly Fluorescent Cucurbit[8]Uril-Perylenemonoimide Host-Guest Complexes as Efficient Fluorescent Probes for N-Terminal Phenylalanine. *RSC Adv.* **2016**, *6*, 82566−82570.

(268) Xu, Q.; Wang, J.-L.; Luo, Y.-L.; Li, J.-J.; Wang, K.-R.; Li, X.-L. Host-Guest Interactions and Controllable Capture and Release of Proteins Based on Cationic Perylene Bisimides. *Chem. Commun.* **2017**, *53*, 2241−2244.

(269) Jia, J.; Wen, H.; Zhao, S.; Wang, L.; Qiao, H.; Shen, H.; Yu, Z.; Di, B.; Xu, L.; Hu, C. Displacement Induced Off-on Fluorescent Biosensor Targeting Ido1 Activity in Live Cells. *Anal. Chem.* **2019**, *91*, 14943−14950.

(270) Wang, B.; Han, J.; Bojanowski, N. M.; Bender, M.; Ma, C.; Seehafer, K.; Herrmann, A.; Bunz, U. H. F. An Optimized Sensor Array Identifies All Natural Amino Acids. *ACS Sens.* **2018**, *3*, 1562−1568.

(271) Zhang, F.; Lu, C.; Wang, M.; Yu, X.; Wei, W.; Xia, Z. A Chiral Sensor Array for Peptidoglycan Biosynthesis Monitoring Based on Mos2 Nanosheet-Supported Host-Guest Recognitions. *ACS Sens.* **2018**, *3*, 304−312.

(272) Ramalingam, V.; Urbach, A. R. Cucurbit[8]Uril Rotaxanes. *Org. Lett.* **2011**, *13*, 4898−4901.

(273) Bockus, A. T.; Smith, L. C.; Grice, A. G.; Ali, O. A.; Young, C. C.; Mobley, W.; Leek, A.; Roberts, J. L.; Vinciguerra, B.; Isaacs, L.; Urbach, A. R. Cucurbit[7]Uril-Tetramethylrhodamine Conjugate for Direct Sensing and Cellular Imaging. *J. Am. Chem. Soc.* **2016**, *138*, 16549−16552.

(274) Hu, C.; Grimm, L.; Prabodh, A.; Baksi, A.; Siennicka, A.; Levkin, P. A.; Kappes, M. M.; Biedermann, F. Covalent Cucurbit[7]-Uril-Dye Conjugates for Sensing in Aqueous Saline Media and Biofluids. *Chem. Sci.* **2020**, *11*, 11142−11153.

(275) Beatty, M. A.; Borges-González, J.; Sinclair, N. J.; Pye, A. T.; Hof, F. Analyte-Driven Disassembly and Turn-on Fluorescent Sensing in Competitive Biological Media. *J. Am. Chem. Soc.* **2018**, *140*, 3500−3504.

(276) Beatty, M. A.; Selinger, A. J.; Li, Y.; Hof, F. Parallel Synthesis and Screening of Supramolecular Chemosensors That Achieve Fluorescent Turn-on Detection of Drugs in Saliva. *J. Am. Chem. Soc.* **2019**, *141*, 16763−16771.

(277) Liu, Y.; Perez, L.; Mettry, M.; Easley, C. J.; Hooley, R. J.; Zhong, W. Self-Aggregating Deep Cavitand Acts as a Fluorescence Displacement Sensor for Lysine Methylation. *J. Am. Chem. Soc.* **2016**, *138*, 10746−10749.

(278) Bastug, E.; Kursunlu, A. N.; Guler, E. A Fluorescent Clever Macrocycle: Deca-Bodipy Bearing a Pillar [5]Arene and Its Selective Binding of Asparagine in Half-Aqueous Medium. *J. Lumin.* **2020**, *225*, 117343.

(279) Ueno, A.; Kuwabara, T.; Nakamura, A.; Toda, F. A Modified Cyclodextrin as a Guest Responsive Colour-Change Indicator. *Nature* **1992**, *356*, 136−137.

(280) Ikeda, H.; Nakamura, M.; Ise, N.; Oguma, N.; Nakamura, A.; Ikeda, T.; Toda, F.; Ueno, A. Fluorescent Cyclodextrins for Molecule Sensing: Fluorescent Properties, Nmr Characterization, and Inclusion Phenomena of N-Dansylleucine-Modified Cyclodextrins. *J. Am. Chem. Soc.* **1996**, *118*, 10980−10988.

(281) Almenar, E.; Costero, A. M.; Gaviña, P.; Gil, S.; Parra, M. Towards the Fluorogenic Detection of Peroxide Explosives through Host-Guest Chemistry. *R. Soc. Open Sci.* **2018**, *5*, 171787.

(282) Huang, Q.; Jiang, L.; Liang, W.; Gui, J.; Xu, D.; Wu, W.; Nakai, Y.; Nishijima, M.; Fukuhara, G.; Mori, T.; Inoue, Y.; Yang, C. Inherently Chiral Azonia[6]Helicene-Modified B-Cyclodextrin: Synthesis, Characterization, and Chirality Sensing of Underivatized Amino Acids in Water. *J. Org. Chem.* **2016**, *81*, 3430−3434.

(283) Corradini, R.; Paganuzzi, C.; Marchelli, R.; Pagliari, S.; Sforza, S.; Dossena, A.; Galaverna, G.; Duchateau, A. Fast Parallel Enantiomeric Analysis of Unmodified Amino Acids by Sensing with Fluorescent B-Cyclodextrins. *J. Mater. Chem.* **2005**, *15*, 2741−2746.

(284) Chen, Z.-H.; He, Y.-B.; Hu, C.-G.; Huang, X.-H. Preparation of a Metal-Ligand Fluorescent Chemosensor and Enantioselective Recognition of Carboxylate Anions in Aqueous Solution. *Tetrahedron: Asymmetry* **2008**, *19*, 2051−2057.

(285) Klug, A.; Schwabe, J. W. Zinc Fingers. *FASEB J.* **1995**, *9*, 597−604.

(286) Isernia, C.; Malgieri, G.; Russo, L.; D'Abrosca, G.; Baglivo, I.; Pedone, P. V.; Fattorusso, R. Zinc Fingers. In *Transition Metals and Sulfur—A Strong Relationship for Life*; De Gruyter, 2020; pp 415−436.

(287) Michalek, J. L.; Besold, A. N.; Michel, S. L. J. Cysteine and Histidine Shuffling: Mixing and Matching Cysteine and Histidine Residues in Zinc Finger Proteins to Afford Different Folds and Function. *Dalton Trans.* **2011**, *40*, 12619−12632.

(288) Reddy, B. A.; Etkin, L. D. A Unique Bipartite Cysteine-Histidine Motif Defines a Subfamily of Potential Zinc-Finger Proteins. *Nucleic Acids Res.* **1991**, *19*, 6330−6330.

(289) Zhang, Y.; Yang, R.; Liu, F.; Li, K. Fluorescent Sensor for Imidazole Derivatives Based on Monomer-Dimer Equilibrium of a Zinc Porphyrin Complex in a Polymeric Film. *Anal. Chem.* **2004**, *76*, 7336−7345.

(290) Du, J.; Huang, Z.; Yu, X. Q.; Pu, L. Highly Selective Fluorescent Recognition of Histidine by a Crown Ether-Terpyridine-Zn(Ii) Sensor. *Chem. Commun.* **2013**, *49*, 5399−5401.

(291) Hou, J. T.; Li, K.; Yu, K. K.; Wu, M. Y.; Yu, X. Q. Coumarin-Dpa-Cu(Ii) as a Chemosensing Ensemble Towards Histidine Determination in Urine and Serum. *Org. Biomol. Chem.* **2013**, *11*, 717−720.

(292) You, Q.-H.; Lee, A. W.-M.; Chan, W.-H.; Zhu, X.-M.; Leung, K. C.-F. A Coumarin-Based Fluorescent Probe for Recognition of Cu2+and Fast Detection of Histidine in Hard-to-Transfect Cells by a Sensing Ensemble Approach. *Chem. Commun.* **2014**, *50*, 6207−6210.

(293) Reddy, G. U.; Agarwalla, H.; Taye, N.; Ghorai, S.; Chattopadhyay, S.; Das, A. A Novel Fluorescence Probe for Estimation of Cysteine/Histidine in Human Blood Plasma and Recognition of Endogenous Cysteine in Live Hct116 Cells. *Chem. Commun.* **2014**, *50*, 9899−9902.

(294) Yang, Y.; Li, Y.; Zhi, X.; Xu, Y.; Li, M. A Red-Emitting Luminescent Probe for Sequentially Detecting Cu2+ and Cysteine/Histidine in Aqueous Solution and Its Imaging Application in Living Zebrafish. *Dyes Pigm.* **2020**, *183*, 108690.

(295) Huang, Z.; Du, J.; Zhang, J.; Yu, X. Q.; Pu, L. A Simple and Efficient Fluorescent Sensor for Histidine. *Chem. Commun.* **2012**, *48*, 3412−3414.

(296) Qiu, S.; Miao, M.; Wang, T.; Lin, Z.; Guo, L.; Qiu, B.; Chen, G. A Fluorescent Probe for Detection of Histidine in Cellular Homogenate and Ovalbumin Based on the Strategy of Click Chemistry. *Biosens. Bioelectron.* **2013**, *42*, 332−336.

(297) Hortala, M. A.; Fabbrizzi, L.; Marcotte, N.; Stomeo, F.; Taglietti, A. Designing the Selectivity of the Fluorescent Detection of Amino Acids: A Chemosensing Ensemble for Histidine. *J. Am. Chem. Soc.* **2003**, *125*, 20−21.

(298) Gao, Q.; Song, B.; Ye, Z.; Yang, L.; Liu, R.; Yuan, J. A Highly Selective Phosphorescence Probe for Histidine in Living Bodies. *Dalton Trans.* **2015**, *44*, 18671−18676.

(299) Fu, Y.; Li, H.; Hu, W. Design and Syntheses of New Fluorescent Probes for Histidine and Fluoride Ion: A Reinvestigation of Chemosensing Ensemble Method. *Sens. Actuators, B* **2008**, *131*, 167−173.

(300) Hengen, P. N. Purification of His-Tag Fusion Proteins from Escherichia Coli. *Trends Biochem. Sci.* **1995**, *20*, 285−286.

(301) Patel, J. D.; O'Carra, R.; Jones, J.; Woodward, J. G.; Mumper, R. J. Preparation and Characterization of Nickel Nanoparticles for Binding to His-Tag Proteins and Antigens. *Pharm. Res.* **2007**, *24*, 343−352.

(302) Li, S.; Yang, K.; Liu, J.; Jiang, B.; Zhang, L.; Zhang, Y. Surface-Imprinted Nanoparticles Prepared with a His-Tag-Anchored Epitope as the Template. *Anal. Chem.* **2015**, *87*, 4617−4620.

(303) Uchinomiya, S.; Nonaka, H.; Wakayama, S.; Ojida, A.; Hamachi, I. In-Cell Covalent Labeling of Reactive His-Tag Fused Proteins. *Chem. Commun.* **2013**, *49*, 5022−5024.

(304) Oliveira, E.; Santos, C.; Poeta, P.; Capelo, J. L.; Lodeiro, C. Turn-on Selective Vitamin B6 Derivative Fluorescent Probe for Histidine Detection in Biological Samples. *Analyst* **2013**, *138*, 3642−3645.

(305) Aït-Haddou, H.; Wiskur, S. L.; Lynch, V. M.; Anslyn, E. V. Achieving Large Color Changes in Response to the Presence of Amino Acids: A Molecular Sensing Ensemble with Selectivity for Aspartate. *J. Am. Chem. Soc.* **2001**, *123*, 11296−11297.

(306) Zhou, X.; Jin, X.; Li, D.; Wu, X. Selective Detection of Zwitterionic Arginine with a New Zn(Ii)-Terpyridine Complex: Potential Application in Protein Labeling and Determination. *Chem. Commun.* **2011**, *47*, 3921−3923.

(307) Zwicker, V. E.; Oliveira, B. L.; Yeo, J. H.; Fraser, S. T.; Bernardes, G. J. L.; New, E. J.; Jolliffe, K. A. A Fluorogenic Probe for Cell Surface Phosphatidylserine Using an Intramolecular Indicator Displacement Sensing Mechanism. *Angew. Chem., Int. Ed.* **2019**, *58*, 3087−3091.

(308) Patel, G.; Menon, S. Recognition of Lysine, Arginine and Histidine by Novel P-Sulfonatocalix[4]Arene Thiol Functionalized Gold Nanoparticles in Aqueous Solution. *Chem. Commun.* **2009**, 3563−3565.

(309) Freeman, R.; Finder, T.; Bahshi, L.; Willner, I. B-Cyclodextrin-Modified Cdse/Zns Quantum Dots for Sensing and Chiroselective Analysis. *Nano Lett.* **2009**, *9*, 2073−2076.

(310) Gill, R.; Zayats, M.; Willner, I. Semiconductor Quantum Dots for Bioanalysis. *Angew. Chem., Int. Ed.* **2008**, *47*, 7602−7625.

(311) Han, C.; Li, H. Chiral Recognition of Amino Acids Based on Cyclodextrin-Capped Quantum Dots. *Small* **2008**, *4*, 1344−1350.

(312) Zhou, J.; Liu, Y.; Zhang, Z.; Yang, S.; Tang, J.; Liu, W.; Tang, W. Cyclodextrin-Clicked Silica/Cdte Fluorescent Nanoparticles for Enantioselective Recognition of Amino Acids. *Nanoscale* **2016**, *8*, 5621−5626.

(313) Hardman, R. A Toxicologic Review of Quantum Dots: Toxicity Depends on Physicochemical and Environmental Factors. *Environ. Health Perspect.* **2006**, *114*, 165−172.

(314) Zhang, G.; Jiang, L.; Zhou, J.; Hu, L.; Feng, S. Epitope-Imprinted Mesoporous Silica Nanoparticles for Specific Recognition of Tyrosine Phosphorylation. *Chem. Commun.* **2019**, *55*, 9927−9930.

(315) Zhao, Q.; Yang, J.; Zhang, J.; Wu, D.; Tao, Y.; Kong, Y. Single-Template Molecularly Imprinted Chiral Sensor for Simultaneous Recognition of Alanine and Tyrosine Enantiomers. *Anal. Chem.* **2019**, *91*, 12546−12552.

(316) Budhathoki-Uprety, J.; Shah, J.; Korsen, J. A.; Wayne, A. E.; Galassi, T. V.; Cohen, J. R.; Harvey, J. D.; Jena, P. V.; Ramanathan, L. V.; Jaimes, E. A.; Heller, D. A. Synthetic Molecular Recognition Nanosensor Paint for Microalbuminuria. *Nat. Commun.* **2019**, *10*, 3605.

(317) Heller, D. A.; Jeng, E. S.; Yeung, T. K.; Martinez, B. M.; Moll, A. E.; Gastala, J. B.; Strano, M. S. Optical Detection of DNA Conformational Polymorphism on Single-Walled Carbon Nanotubes. *Science* **2006**, *311*, 508−511.

(318) Muller, A.; Konig, B. Vesicular Aptasensor for the Detection of Thrombin. *Chem. Commun.* **2014**, *50*, 12665−12668.

(319) Banerjee, S.; Konig, B. Molecular Imprinting of Luminescent Vesicles. *J. Am. Chem. Soc.* **2013**, *135*, 2967−2970.

(320) Müller, A.; König, B. Preparation of Luminescent Chemosensors by Post-Functionalization of Vesicle Surfaces. *Org. Biomol. Chem.* **2015**, *13*, 1690−1699.

(321) Leong, J.; Teo, J. Y.; Aakalu, V. K.; Yang, Y. Y.; Kong, H. Engineering Polymersomes for Diagnostics and Therapy. *Adv. Healthcare Mater.* **2018**, *7*, No. 1701276.

(322) Ferrer-Tasies, L.; Moreno-Calvo, E.; Cano-Sarabia, M.; Aguilella-Arzo, M.; Angelova, A.; Lesieur, S.; Ricart, S.; Faraudo, J.; Ventosa, N.; Veciana, J. Quatsomes: Vesicles Formed by Self-Assembly of Sterols and Quaternary Ammonium Surfactants. *Langmuir* **2013**, *29*, 6519−6528.

(323) Sun, T.; Fan, R.; Xiao, R.; Xing, T.; Qin, M.; Liu, Y.; Hao, S.; Chen, W.; Yang, Y. Anionic Ln-Mof with Tunable Emission for Heavy Metal Ion Capture and L-Cysteine Sensing in Serum. *J. Mater. Chem. A* **2020**, *8*, 5587−5594.

(324) Xu, H.; Cao, C.-S.; Kang, X.-M.; Zhao, B. Lanthanide-Based Metal-Organic Frameworks as Luminescent Probes. *Dalton Trans.* **2016**, *45*, 18003−18017.

(325) Peveler, W. J.; Landis, R. F.; Yazdani, M.; Day, J. W.; Modi, R.; Carmalt, C. J.; Rosenberg, W. M.; Rotello, V. M. A Rapid and Robust Diagnostic for Liver Fibrosis Using a Multichannel Polymer Sensor Array. *Adv. Mater.* **2018**, *30*, 1800634.

(326) De, M.; Rana, S.; Akpinar, H.; Miranda, O. R.; Arvizo, R. R.; Bunz, U. H. F.; Rotello, V. M. Sensing of Proteins in Human Serum Using Conjugates of Nanoparticles and Green Fluorescent Protein. *Nat. Chem.* **2009**, *1*, 461−465.

(327) Li, X.; Wen, F.; Creran, B.; Jeong, Y.; Zhang, X.; Rotello, V. M. Colorimetric Protein Sensing Using Catalytically Amplified Sensor Arrays. *Small* **2012**, *8*, 3589−3592.

(328) Miranda, O. R.; Chen, H.-T.; You, C.-C.; Mortenson, D. E.; Yang, X.-C.; Bunz, U. H. F.; Rotello, V. M. Enzyme-Amplified Array Sensing of Proteins in Solution and in Biofluids. *J. Am. Chem. Soc.* **2010**, *132*, 5285−5289.

(329) Geng, Y.; Peveler, W. J.; Rotello, V. M. Array-Based "Chemical Nose" Sensing in Diagnostics and Drug Discovery. *Angew. Chem., Int. Ed.* **2019**, *58*, 5190−5200.

(330) Miranda, O. R.; Creran, B.; Rotello, V. M. Array-Based Sensing with Nanoparticles: 'Chemical Noses' for Sensing Biomolecules and Cell Surfaces. *Curr. Opin. Chem. Biol.* **2010**, *14*, 728−736.

(331) Cynober, L. A. Plasma Amino Acid Levels with a Note on Membrane Transport: Characteristics, Regulation, and Metabolic Significance. *Nutrition* **2002**, *18*, 761−766.

(332) Nakamura, Y.; Kodama, H.; Satoh, T.; Adachi, K.; Watanabe, S.; Yokote, Y.; Sakagami, H. Diurnal Changes in Salivary Amino Acid Concentrations. *In Vivo* **2010**, *24*, 837−842.

(333) Psychogios, N.; Hau, D. D.; Peng, J.; Guo, A. C.; Mandal, R.; Bouatra, S.; Sinelnikov, I.; Krishnamurthy, R.; Eisner, R.; Gautam, B.; Young, N.; Xia, J.; Knox, C.; Dong, E.; Huang, P.; Hollander, Z.; Pedersen, T. L.; Smith, S. R.; Bamforth, F.; Greiner, R.; McManus, B.; Newman, J. W.; Goodfriend, T.; Wishart, D. S. The Human Serum Metabolome. *PLoS One* **2011**, *6*, No. e16957.

(334) Gatti, R.; Gioia, M. G. Liquid Chromatographic Fluorescence Determination of Amino Acids in Plasma and Urine after Derivatization with Phanquinone. *Biomed. Chromatogr.* **2008**, *22*, 207−213.

(335) Sugimoto, M.; Saruta, J.; Matsuki, C.; To, M.; Onuma, H.; Kaneko, M.; Soga, T.; Tomita, M.; Tsukinoki, K. Physiological and Environmental Parameters Associated with Mass Spectrometry-Based Salivary Metabolomic Profiles. *Metabolomics* **2013**, *9*, 454−463.

(336) Hušek, P.; Švagera, Z.; Hanzlíková, D.; Řimnáčová, L.; Zahradníčková, H.; Opekarová, I.; Šimek, P. Profiling of Urinary Amino-Carboxylic Metabolites by in-Situ Heptafluorobutyl Chloroformate Mediated Sample Preparation and Gas Chromatography-Mass Spectrometry. *J. Chromatogr. A* **2016**, *1443*, 211−232.

(337) Tsuruoka, M.; Hara, J.; Hirayama, A.; Sugimoto, M.; Soga, T.; Shankle, W. R.; Tomita, M. Capillary Electrophoresis-Mass Spectrometry-Based Metabolome Analysis of Serum and Saliva from Neurodegenerative Dementia Patients. *Electrophoresis* **2013**, *34*, 2865.

(338) Takeda, I.; Stretch, C.; Barnaby, P.; Bhatnager, K.; Rankin, K.; Fu, H.; Weljie, A.; Jha, N.; Slupsky, C. Understanding the Human Salivary Metabolome. *NMR Biomed.* **2009**, *22*, 577−584.

(339) Novarino, G.; El-Fishawy, P.; Kayserili, H.; Meguid, N. A.; Scott, E. M.; Schroth, J.; Silhavy, J. L.; Kara, M.; Khalil, R. O.; Ben-Omran, T.; Ercan-Sencicek, A. G.; Hashish, A. F.; Sanders, S. J.; Gupta, A. R.; Hashem, H. S.; Matern, D.; Gabriel, S.; Sweetman, L.; Rahimi, Y.; Harris, R. A.; State, M. W.; Gleeson, J. G. Mutations in Bckd-Kinase Lead to a Potentially Treatable Form of Autism with Epilepsy. *Science* **2012**, *338*, 394.

(340) Kurko, J.; Tringham, M.; Tanner, L.; Näntö-Salonen, K.; Vähä-Mäkilä, M.; Nygren, H.; Pöhö, P.; Lietzen, N.; Mattila, I.; Olkku, A.; Hyötyläinen, T.; Orešič, M.; Simell, O.; Niinikoski, H.; Mykkänen, J. Imbalance of Plasma Amino Acids, Metabolites and Lipids in Patients with Lysinuric Protein Intolerance (Lpi). *Metab., Clin. Exp.* **2016**, *65*, 1361−1375.

(341) Jones, M. G.; Cooper, E.; Amjad, S.; Goodwin, C. S.; Barron, J. L.; Chalmers, R. A. Urinary and Plasma Organic Acids and Amino Acids in Chronic Fatigue Syndrome. *Clin. Chim. Acta* **2005**, *361*, 150−158.

(342) Buczko, W.; Cylwik, D.; Stokowska, W. Metabolism of Tryptophan Via the Kynurenine Pathway in Saliva. *Postepy Hig. Med. Dosw.* **2005**, *59*, 283−289.

(343) Tabor, C. W.; Tabor, H. Polyamines. *Annu. Rev. Biochem.* **1984**, *53*, 749−790.

(344) Minois, N.; Carmona-Gutierrez, D.; Madeo, F. Polyamines in Aging and Disease. *Aging* **2011**, *3*, 716−732.

(345) Casero, R. A.; Marton, L. J. Targeting Polyamine Metabolism and Function in Cancer and Other Hyperproliferative Diseases. *Nat. Rev. Drug Discovery* **2007**, *6*, 373−390.

(346) Madeo, F.; Eisenberg, T.; Pietrocola, F.; Kroemer, G. Spermidine in Health and Disease. *Science* **2018**, *359*, 2788.

(347) Kawakita, M.; Hiramatsu, K. Diacetylated Derivatives of Spermine and Spermidine as Novel Promising Tumor Markers. *J. Biochem.* **2006**, *139*, 315−322.

(348) Casero, R. A.; Pegg, A. E. Polyamine Catabolism and Disease. *Biochem. J.* **2009**, *421*, 323.

(349) Tabor, C. W.; Tabor, H. Polyamines in Microorganisms. *Microbiol. Rev.* **1985**, *49*, 81−99.

(350) Conway, L. P.; Rendo, V.; Correia, M. S. P.; Bergdahl, I. A.; Sjöblom, T.; Globisch, D. Unexpected Acetylation of Endogenous Aliphatic Amines by Arylamine N-Acetyltransferase Nat2. *Angew. Chem., Int. Ed.* **2020**, *59*, 14342−14346.

(351) Grasemann, H.; Shehnaz, D.; Enomoto, M.; Leadley, M.; Belik, J.; Ratjen, F. L-Ornithine Derived Polyamines in Cystic Fibrosis Airways. *PLoS One* **2012**, *7*, No. e46618.

(352) Tomitori, H.; Usui, T.; Saeki, N.; Ueda, S.; Kase, H.; Nishimura, K.; Kashiwagi, K.; Igarashi, K. Polyamine Oxidase and Acrolein as Novel Biochemical Markers for Diagnosis of Cerebral Stroke. *Stroke* **2005**, *36*, 2609−2613.

(353) Igarashi, K.; Kashiwagi, K. Use of Polyamine Metabolites as Markers for Stroke and Renal Failure. *Methods Mol. Biol.* **2011**, *720*, 395−408.

(354) Saiki, R.; Park, H.; Ishii, I.; Yoshida, M.; Nishimura, K.; Toida, T.; Tatsukawa, H.; Kojima, S.; Ikeguchi, Y.; Pegg, A. E.; Kashiwagi, K.; Igarashi, K. Brain Infarction Correlates More Closely with Acrolein Than with Reactive Oxygen Species. *Biochem. Biophys. Res. Commun.* **2011**, *404*, 1044−1049.

(355) Igarashi, K.; Ueda, S.; Yoshida, K.; Kashiwagi, K. Polyamines in Renal Failure. *Amino Acids* **2006**, *31*, 477−483.

(356) Gomes-Trolin, C.; Nygren, I.; Aquilonius, S. M.; Askmark, H. Increased Red Blood Cell Polyamines in Als and Parkinson's Disease. *Exp. Neurol.* **2002**, *177*, 515−520.

(357) Cheng, M.-L.; Wang, C.-H.; Shiao, M.-S.; Liu, M.-H.; Huang, Y.-Y.; Huang, C.-Y.; Mao, C.-T.; Lin, J.-F.; Ho, H.-Y.; Yang, N.-I. Metabolic Disturbances Identified in Plasma Are Associated with Outcomes In patients with Heart Failure: Diagnostic and Prognostic Value of Metabolomics. *J. Am. Coll. Cardiol.* **2015**, *65*, 1509−1520.

(358) Sansbury, B. E.; DeMartino, A. M.; Xie, Z.; Brooks, A. C.; Brainard, R. E.; Watson, L. J.; DeFilippis, A. P.; Cummins, T. D.; Harbeson, M. A.; Brittian, K. R.; Prabhu, S. D.; Bhatnagar, A.; Jones, S. P.; Hill, B. G. Metabolomic Analysis of Pressure-Overloaded and Infarcted Mouse Hearts. *Circ.: Heart Failure* **2014**, *7*, 634−642.

(359) Pan, X.; Nasaruddin, M. B.; Elliott, C. T.; McGuinness, B.; Passmore, A. P.; Kehoe, P. G.; Hölscher, C.; McClean, P. L.; Graham, S. F.; Green, B. D. Alzheimer's Disease-Like Pathology Has Transient Effects on the Brain and Blood Metabolome. *Neurobiol. Aging* **2016**, *38*, 151−163.

(360) Graham, S. F.; Chevallier, O. P.; Elliott, C. T.; Hölscher, C.; Johnston, J.; McGuinness, B.; Kehoe, P. G.; Passmore, A. P.; Green, B. D. Untargeted Metabolomic Analysis of Human Plasma Indicates Differentially Affected Polyamine and L-Arginine Metabolism in Mild Cognitive Impairment Subjects Converting to Alzheimer's Disease. *PLoS One* **2015**, *10*, No. e0119452.

(361) Joaquim, H. P. G.; Costa, A. C.; Forlenza, O. V.; Gattaz, W. F.; Talib, L. L. Decreased Plasmatic Spermidine and Increased Spermine in Mild Cognitive Impairment and Alzheimer's Disease Patients. *Arch. Clin. Psychiatry* **2019**, *46*, 120−124.

(362) Park, M. H.; Igarashi, K. Polyamines and Their Metabolites as Diagnostic Markers of Human Diseases. *Biomol. Ther.* **2013**, *21*, 1−9.

(363) Casero, R. A.; Murray Stewart, T.; Pegg, A. E. Polyamine Metabolism and Cancer: Treatments, Challenges And opportunities. *Nat. Rev. Cancer* **2018**, *18*, 681−695.

(364) Xu, H.; Liu, R.; He, B.; Bi, C. W.; Bi, K.; Li, Q. Polyamine Metabolites Profiling for Characterization of Lung and Liver Cancer Using an Lc-Tandem Ms Method with Multiple Statistical Data Mining Strategies: Discovering Potential Cancer Biomarkers in Human Plasma and Urine. *Molecules* **2016**, *21*, 1040.

(365) Liu, R.; Li, P.; Bi, C. W.; Ma, R.; Yin, Y.; Bi, K.; Li, Q. Plasma N-Acetylputrescine, Cadaverine and 1,3-Diaminopropane: Potential Biomarkers of Lung Cancer Used to Evaluate the Efficacy of Anticancer Drugs. *Oncotarget* **2017**, *8*, 88575−88585.

(366) Lo, C.; Hsu, Y.-L.; Cheng, C.-N.; Lin, C.-H.; Kuo, H.-C.; Huang, C.-S.; Kuo, C.-H. Investigating the Association of the Biogenic Amine Profile in Urine with Therapeutic Response to Neoadjuvant Chemotherapy in Breast Cancer Patients. *J. Proteome Res.* **2020**, *19*, 4061−4070.

(367) Stepien, M.; Duarte-Salles, T.; Fedirko, V.; Floegel, A.; Barupal, D. K.; Rinaldi, S.; Achaintre, D.; Assi, N.; Tjønneland, A.; Overvad, K.; Bastide, N.; Boutron-Ruault, M.-C.; Severi, G.; Kühn, T.; Kaaks, R.; Aleksandrova, K.; Boeing, H.; Trichopoulou, A.; Bamia, C.; Lagiou, P.; Saieva, C.; Agnoli, C.; Panico, S.; Tumino, R.; Naccarati, A.; Bueno-de-Mesquita, H. B.; Peeters, P. H.; Weiderpass, E.; Quirós, J. R.; Agudo, A.; Sánchez, M.-J.; Dorronsoro, M.; Gavrila, D.; Barricarte, A.; Ohlsson, B.; Sjöberg, K.; Werner, M.; Sund, M.; Wareham, N.; Khaw, K.-T.; Travis, R. C.; Schmidt, J. A.; Gunter, M.; Cross, A.; Vineis, P.; Romieu, I.; Scalbert, A.; Jenab, M. Alteration of Amino Acid and Biogenic Amine Metabolism in Hepatobiliary Cancers: Findings from a Prospective Cohort Study. *Int. J. Cancer* **2016**, *138*, 348−360.

(368) Agostinelli, E.; Tempera, G.; Molinari, A.; Salvi, M.; Battaglia, V.; Toninello, A.; Arancia, G. The Physiological Role of Biogenic Amines Redox Reactions in Mitochondria. New Perspectives in Cancer Therapy. *Amino Acids* **2007**, *33*, 175−187.

(369) Liu, R.; Li, Q.; Ma, R.; Lin, X.; Xu, H.; Bi, K. Determination of Polyamine Metabolome in Plasma and Urine by Ultrahigh Performance Liquid Chromatography-Tandem Mass Spectrometry Method: Application to Identify Potential Markers for Human Hepatic Cancer. *Anal. Chim. Acta* **2013**, *791*, 36−45.

(370) Kato, M.; Onishi, H.; Matsumoto, K.; Motoshita, J.; Tsuruta, N.; Higuchi, K.; Katano, M. Prognostic Significance of Urine N1, N12-Diacetylspermine in Patients with Non-Small Cell Lung Cancer. *Anticancer Res.* **2014**, *34*, 3053−3059.

(371) Niemi, R. J.; Roine, A. N.; Häkkinen, M. R.; Kumpulainen, P. S.; Keinänen, T. A.; Vepsäläinen, J. J.; Lehtimäki, T.; Oksala, N. K.; Mäenpää, J. U. Urinary Polyamines as Biomarkers for Ovarian Cancer. *Int. J. Gynecol. Cancer* **2017**, *27*, 1360−1366.

(372) Takahashi, Y.; Sakaguchi, K.; Horio, H.; Hiramatsu, K.; Moriya, S.; Takahashi, K.; Kawakita, M. Urinary N1, N12-Diacetylspermine Is a Non-Invasive Marker for the Diagnosis and Prognosis of Non-Small-Cell Lung Cancer. *Br. J. Cancer* **2015**, *113*, 1493−1501.

(373) Bulushi, I. A.; Poole, S.; Deeth, H. C.; Dykes, G. A. Biogenic Amines in Fish: Roles in Intoxication, Spoilage, and Nitrosamine Formation—a Review. *Crit. Rev. Food Sci. Nutr.* **2009**, *49*, 369−377.

(374) Prester, L. Biogenic Amines in Fish, Fish Products and Shellfish: A Review. *Food Addit. Contam., Part A* **2011**, *28*, 1547−1560.

(375) Tittarelli, R.; Mannocchi, G.; Pantano, F.; Romolo, F. Recreational Use, Analysis and Toxicity of Tryptamines. *Curr. Neuropharmacol.* **2015**, *13*, 26.

(376) Malaca, S.; Lo Faro, A. F.; Tamborra, A.; Pichini, S.; Busardò, F. P.; Huestis, M. A. Toxicology and Analysis of Psychoactive Tryptamines. *Int. J. Mol. Sci.* **2020**, *21*, 9279.

(377) Nishimura, K.; Shiina, R.; Kashiwagi, K.; Igarashi, K. Decrease in Polyamines with Aging and Their Ingestion from Food and Drink. *J. Biochem.* **2006**, *139*, 81−90.

(378) Lee, B.; Scopelliti, R.; Severin, K. A Molecular Probe for the Optical Detection of Biogenic Amines. *Chem. Commun.* **2011**, *47*, 9639−9641.

(379) Li, L.; Li, W.; Ran, X.; Wang, L.; Tang, H.; Cao, D. A Highly Efficient, Colorimetric and Fluorescent Probe for Recognition of Aliphatic Primary Amines Based on a Unique Cascade Chromophore Reaction. *Chem. Commun.* **2019**, *55*, 9789−9792.

(380) Waikar, S. S.; Sabbisetti, V. S.; Bonventre, J. V. Normalization of Urinary Biomarkers to Creatinine During Changes in Glomerular Filtration Rate. *Kidney Int.* **2010**, *78*, 486−494.

(381) den Elzen, W. P. J.; Cobbaert, C. M.; Klein Gunnewiek, J. M. T.; Bakkeren, D. L.; van Berkel, M.; Frasa, M. A. M.; Herpers, R. L. J. M.; Kuypers, A. W. H. M.; Ramakers, C.; Roelofsen-de Beer, R. J. A. C.; van der Vuurst, H.; Weykamp, C. Glucose and Total Protein: Unacceptable Interference on Jaffe Creatinine Assays in Patients. *Clin. Chem. Lab. Med.* **2018**, *56*, e185.

(382) Cruickshank, A. M.; Shenkin, A. A Comparison of the Effect of Acetoacetate Concentration on the Measurement of Serum Creatinine Using Technicon Smac Ii, Beckman Astra and Enzymatic Techniques. *Ann. Clin. Biochem.* **1987**, *24*, 317.

(383) Nigam, P. K. Bilirubin Interference in Serum Creatinine Estimation by Jaffe's kinetic Method and Its Rectification in Three Different Kits. *Indian J. Clin. Biochem.* **2016**, *31*, 237−239.

(384) Guder, W. G.; Hoffmann, G. E.; Hubbuch, A.; Poppe, W. A.; Siedel, J.; Price, C. P. Multicentre Evaluation of an Enzymatic Method for Creatinine Determination Using a Sensitive Colour Reagent. *J. Clin. Chem. Clin. Biochem.* **1986**, *24*, 889−902.

(385) Fossati, P.; Prencipe, L.; Berti, G. Enzymic Creatinine Assay: A New Colorimetric Method Based on Hydrogen Peroxide Measurement. *Clin. Chem.* **1983**, *29*, 1494−1496.

(386) Fossati, P.; Ponti, M.; Passoni, G.; Tarenghi, G.; Melzi d'Eril, G. V.; Prencipe, L. A Step Forward in Enzymatic Measurement of Creatinine. *Clin. Chem.* **1994**, *40*, 130−137.

(387) Boyne, P.; Robinson, B. A.; Murphy, P.; McKay, M. Enzymatic Correction of Interference in the Kinetic Jaffé Reaction for Determining Creatinine in Plasma. *Clin. Chem.* **1985**, *31*, 1564−1565.

(388) Stokes, P.; O'Connor, G. Development of a Liquid Chromatography-Mass Spectrometry Method for the High-Accuracy Determination of Creatinine in Serum. *J. Chromatogr. B: Anal. Technol. Biomed. Life Sci.* **2003**, *794*, 125−136.

(389) Soldin, S. J.; Hill, J. G. Micromethod for Determination of Creatinine in Biological Fluids by High-Performance Liquid Chromatography. *Clin. Chem.* **1978**, *24*, 747−750.

(390) Cánovas, R.; Cuartero, M.; Crespo, G. A. Modern Creatinine (Bio)Sensing: Challenges of Point-of-Care Platforms. *Biosens. Bioelectron.* **2019**, *130*, 110−124.

(391) Lewińska, I.; Michalec, M.; Tymecki, L. From the Bottom of an Old Jar: A Fluorometric Method for the Determination of Creatinine in Human Serum. *Anal. Chim. Acta* **2020**, *1135*, 116.

(392) Pal, S.; Lohar, S.; Mukherjee, M.; Chattopadhyay, P.; Dhara, K. A Fluorescent Probe for the Selective Detection of Creatinine in Aqueous Buffer Applicable to Human Blood Serum. *Chem. Commun.* **2016**, *52*, 13706−13709.

(393) Kumpf, J.; Schwaebel, S. T.; Bunz, U. H. Amine Detection with Distyrylbenzenedialdehyde-Based Knoevenagel Adducts. *J. Org. Chem.* **2015**, *80*, 5159−5166.

(394) Kostereli, Z.; Severin, K. Fluorescence Sensing of Spermine with a Frustrated Amphiphile. *Chem. Commun.* **2012**, *48*, 5841−5843.

(395) Tu, J.; Sun, S.; Xu, Y. A Novel Self-Assembled Platform for the Ratiometric Fluorescence Detection of Spermine. *Chem. Commun.* **2016**, *52*, 1040−1043.

(396) Kim, T. I.; Kim, Y. Analyte-Directed Formation of Emissive Excimers for the Selective Detection of Polyamines. *Chem. Commun.* **2016**, *52*, 10648−10651.

(397) Durie, B. G. M.; Salmon, S. E.; Russell, D. H. Polyamines as Markers of Response and Disease Activity in Cancer Chemotherapy. *Cancer Res.* **1977**, *37*, 214.

(398) Bentrad, V. V.; Gogol, S. V.; Zaletok, S. P.; Vitruk, Y. V.; Stakhovskyi, E. O.; Grechko, B. O. P1-114−Urinary Spermine Level as Novel Additional Diagnostic Marker of Prostate Cancer. *Ann. Oncol.* **2019**, *30*, No. vi123.

(399) Park, M. H.; Igarashi, K. Polyamines and Their Metabolites as Diagnostic Markers of Human Diseases. *Biomol. Ther.* **2013**, *21*, 1−9.

(400) D'Urso, A.; Brancatelli, G.; Hickey, N.; Farnetti, E.; De Zorzi, R.; Bonaccorso, C.; Purrello, R.; Geremia, S. Interactions of a Water-Soluble Calix[4]Arene with Spermine: Solution and Solid-State Characterisation. *Supramol. Chem.* **2016**, *28*, 499−505.

(401) Carvalho, C. P.; Ferreira, R.; Da Silva, J. P.; Pischel, U. An Aminonaphthalimide-Putrescine Conjugate as Fluorescent Probe for Cucurbituril Host-Guest Complexes. *Supramol. Chem.* **2013**, *25*, 92−100.

(402) Zhong, C.; Hu, C.; Kumar, R.; Trouillet, V.; Biedermann, F.; Hirtz, M. Cucurbit[N]Uril-Immobilized Sensor Arrays for Indicator-Displacement Assays of Small Bioactive Metabolites. *ACS Appl. Nano Mater.* **2021**, *4*, 4676−4687.

(403) Huang, W. H.; Zavalij, P. Y.; Isaacs, L. Chiral Recognition inside a Chiral Cucurbituril. *Angew. Chem., Int. Ed.* **2007**, *46*, 7425−7427.

(404) Bell, T. W.; Hou, Z.; Luo, Y.; Drew, M. G.; Chapoteau, E.; Czech, B. P.; Kumar, A. Detection of Creatinine by a Designed Receptor. *Science* **1995**, *269*, 671.

(405) Snyder, P.; Lockett, M.; Moustakas, D.; Whitesides, G. Is It the Shape of the Cavity, or the Shape of the Water in the Cavity? *Eur. Phys. J.: Spec. Top.* **2014**, *223*, 853−891.

(406) Sierra, A. F.; Hernández-Alonso, D.; Romero, M. A.; González-Delgado, J. A.; Pischel, U.; Ballester, P. Optical Supramolecular Sensing of Creatinine. *J. Am. Chem. Soc.* **2020**, *142*, 4276−4284.

(407) Han, C.; Zeng, L.; Li, H.; Xie, G. Colorimetric Detection of Pollutant Aromatic Amines Isomers with P-Sulfonatocalix[6]Arene-Modified Gold Nanoparticles. *Sens. Actuators, B* **2009**, *137*, 704−709.

(408) Chen, X.; Parker, S. G.; Zou, G.; Su, W.; Zhang, Q. Β-Cyclodextrin-Functionalized Silver Nanoparticles for the Naked Eye Detection of Aromatic Isomers. *ACS Nano* **2010**, *4*, 6387−6394.

(409) Corma, A.; Garcia, H.; Montes-Navajas, P.; Primo, A.; Calvino, J. J.; Trasobares, S. Gold Nanoparticles in Organic Capsules: A Supramolecular Assembly of Gold Nanoparticles and Cucurbituril. *Chem.−Eur. J.* **2007**, *13*, 6359−6364.

(410) Kim, T. I.; Park, J.; Kim, Y. A Gold Nanoparticle-Based Fluorescence Turn-on Probe for Highly Sensitive Detection of Polyamines. *Chem.−Eur. J.* **2011**, *17*, 11978−11982.

(411) Rawat, K. A.; Bhamore, J. R.; Singhal, R. K.; Kailasa, S. K. Microwave Assisted Synthesis of Tyrosine Protected Gold Nanoparticles for Dual (Colorimetric and Fluorimetric) Detection of Spermine and Spermidine in Biological Samples. *Biosens. Bioelectron.* **2017**, *88*, 71−77.

(412) Bhaskar, S.; Kowshik, N.; Chandran, S. P.; Ramamurthy, S. S. Femtomolar Detection of Spermidine Using Au Decorated Sio2 Nanohybrid on Plasmon-Coupled Extended Cavity Nanointerface: A Smartphone-Based Fluorescence Dequenching Approach. *Langmuir* **2020**, *36*, 2865−2876.

(413) Cai, W. P.; Zhai, Y. Y.; Cao, S. H.; Liu, Q.; Weng, Y. H.; Xie, K. X.; Lin, G. C.; Li, Y. Q. High Performance Dual-Mode Surface Plasmon Coupled Emission Imaging Apparatus Integrating Kretsch-

mann and Reverse Kretschmann Configurations for Flexible Measurements. *Rev. Sci. Instrum.* **2016**, *87*, 013705.

(414) Chopra, S.; Singh, A.; Venugopalan, P.; Singh, N.; Kaur, N. Organic Nanoparticles for Visual Detection of Spermidine and Spermine in Vapors and Aqueous Phase. *ACS Sustainable Chem. Eng.* **2017**, *5*, 1287−1296.

(415) Nair, R. R.; Debnath, S.; Das, S.; Wakchaure, P.; Ganguly, B.; Chatterjee, P. B. A Highly Selective Turn-on Biosensor for Measuring Spermine/Spermidine in Human Urine and Blood. *ACS Appl. Bio Mater.* **2019**, *2*, 2374−2387.

(416) Fu, Y.; Wu, S.; Zhou, H.; Zhao, S.; Lan, M.; Huang, J.; Song, X. Carbon Dots and a Cdte Quantum Dot Hybrid-Based Fluorometric Probe for Spermine Detection. *Ind. Eng. Chem. Res.* **2020**, *59*, 1723−1729.

(417) del Pozo, M.; Casero, E.; Quintana, C. Visual and Spectrophotometric Determination of Cadaverine Based on the Use of Gold Nanoparticles Capped with Cucurbiturils or Cyclodextrins. *Microchim. Acta* **2017**, *184*, 2107−2114.

(418) Comes, M.; Marcos, M. D.; Martínez-Máñez, R.; Sancenón, F.; Soto, J.; Villaescusa, L. A.; Amorós, P.; Beltrán, D. Chromogenic Discrimination of Primary Aliphatic Amines in Water with Functionalized Mesoporous Silica. *Adv. Mater.* **2004**, *16*, 1783−1786.

(419) Du, J.; Zhu, B.; Leow, W. R.; Chen, S.; Sum, T. C.; Peng, X.; Chen, X. Colorimetric Detection of Creatinine Based on Plasmonic Nanoparticles Via Synergistic Coordination Chemistry. *Small* **2015**, *11*, 4104−4110.

(420) Du, J.; Zhu, B.; Chen, X. Urine for Plasmonic Nanoparticle-Based Colorimetric Detection of Mercury Ion. *Small* **2013**, *9*, 4104−4111.

(421) Parmar, A. K.; Valand, N. N.; Solanki, K. B.; Menon, S. K. Picric Acid Capped Silver Nanoparticles as a Probe for Colorimetric Sensing of Creatinine in Human Blood and Cerebrospinal Fluid Samples. *Analyst* **2016**, *141*, 1488−1498.

(422) Goswami, N.; Zheng, K.; Xie, J. Bio-Ncs−the Marriage of Ultrasmall Metal Nanoclusters with Biomolecules. *Nanoscale* **2014**, *6*, 13328−13347.

(423) Mathew, M. S.; Joseph, K. Green Synthesis of Gluten-Stabilized Fluorescent Gold Quantum Clusters: Application as Turn-on Sensing of Human Blood Creatinine. *ACS Sustainable Chem. Eng.* **2017**, *5*, 4837−4845.

(424) Alula, M. T.; Karamchand, L.; Hendricks, N. R.; Blackburn, J. M. Citrate-Capped Silver Nanoparticles as a Probe for Sensitive and Selective Colorimetric and Spectrophotometric Sensing of Creatinine in Human Urine. *Anal. Chim. Acta* **2018**, *1007*, 40−49.

(425) Ortiz-Gomez, I.; Ramirez-Rodriguez, G. B.; Capitan-Vallvey, L. F.; Salinas-Castillo, A.; Delgado-Lopez, J. M. Highly Stable Luminescent Europium-Doped Calcium Phosphate Nanoparticles for Creatinine Quantification. *Colloids Surf., B* **2020**, *196*, 111337.

(426) Wang, F.; Tan, W. B.; Zhang, Y.; Fan, X.; Wang, M. Luminescent Nanomaterials for Biological Labelling. *Nanotechnology* **2006**, *17*, R1−R13.

(427) Yuan, P.; Walt, D. R. Calculation for Fluorescence Modulation by Absorbing Species and Its Application to Measurements Using Optical Fibers. *Anal. Chem.* **1987**, *59*, 2391−2394.

(428) Chio, W.-I K.; Moorthy, S.; Perumal, J.; U. S., D.; Parkin, I. P.; Olivo, M.; Lee, T.-C. Dual-Triggered Nanoaggregates of Cucurbit[7]-Uril and Gold Nanoparticles for Multi-Spectroscopic Quantification of Creatinine in Urinalysis. *J. Mater. Chem. C* **2020**, *8*, 7051.

(429) Qu, S.; Cao, Q.; Ma, J.; Jia, Q. A Turn-on Fluorescence Sensor for Creatinine Based on the Quinoline-Modified Metal Organic Frameworks. *Talanta* **2020**, *219*, 121280.

(430) Daly, B.; Ling, J.; de Silva, A. P. Current Developments in Fluorescent Pet (Photoinduced Electron Transfer) Sensors and Switches. *Chem. Soc. Rev.* **2015**, *44*, 4203−4211.

(431) Rochat, S.; Swager, T. M. Fluorescence Sensing of Amine Vapors Using a Cationic Conjugated Polymer Combined with Various Anions. *Angew. Chem., Int. Ed.* **2014**, *53*, 9792−9796.

(432) Fu, Y.; Yao, J.; Xu, W.; Fan, T.; He, Q.; Zhu, D.; Cao, H.; Cheng, J. Reversible and "Fingerprint" Fluorescence Differentiation of Organic Amine Vapours Using a Single Conjugated Polymer Probe. *Polym. Chem.* **2015**, *6*, 2179−2182.

(433) Yu, J.; Zhang, C. Fluorescent Sensing for Amines with a Low Detection Limit Based on Conjugated Porous Polymers. *J. Mater. Chem. C* **2020**, *8*, 16463−16469.

(434) Rochat, S.; Swager, T. M. Conjugated Amplifying Polymers for Optical Sensing Applications. *ACS Appl. Mater. Interfaces* **2013**, *5*, 4488−4502.

(435) Bentley, K. W.; Nam, Y. G.; Murphy, J. M.; Wolf, C. Chirality Sensing of Amines, Diamines, Amino Acids, Amino Alcohols, and A-Hydroxy Acids with a Single Probe. *J. Am. Chem. Soc.* **2013**, *135*, 18052−18055.

(436) Pilicer, S. L.; Wolf, C. Ninhydrin Revisited: Quantitative Chirality Recognition of Amines and Amino Alcohols Based on Nondestructive Dynamic Covalent Chemistry. *J. Org. Chem.* **2020**, *85*, 11560−11565.

(437) Hassan, D. S.; Thanzeel, F. Y.; Wolf, C. Stereochemical Analysis of Chiral Amines, Diamines, and Amino Alcohols: Practical Chiroptical Sensing Based on Dynamic Covalent Chemistry. *Chirality* **2020**, *32*, 457−463.

(438) De los Santos, Z. A.; Ding, R.; Wolf, C. Quantitative Chirality Sensing of Amines and Amino Alcohols Via Schiff Base Formation with a Stereodynamic Uv/Cd Probe. *Org. Biomol. Chem.* **2016**, *14*, 1934−1939.

(439) Thanzeel, F. Y.; Sripada, A.; Wolf, C. Quantitative Chiroptical Sensing of Free Amino Acids, Biothiols, Amines, and Amino Alcohols with an Aryl Fluoride Probe. *J. Am. Chem. Soc.* **2019**, *141*, 16382−16387.

(440) Pilicer, S. L.; Bakhshi, P. R.; Bentley, K. W.; Wolf, C. Biomimetic Chirality Sensing with Pyridoxal-5′-Phosphate. *J. Am. Chem. Soc.* **2017**, *139*, 1758−1761.

(441) Jo, H. H.; Lin, C.-Y.; Anslyn, E. V. Rapid Optical Methods for Enantiomeric Excess Analysis: From Enantioselective Indicator Displacement Assays to Exciton-Coupled Circular Dichroism. *Acc. Chem. Res.* **2014**, *47*, 2212−2221.

(442) van den Berg, G. A.; Muskiet, F. A.; Kingma, A. W.; van der Slik, W.; Halie, M. R. Simultaneous Gas-Chromatographic Determination of Free and Acetyl-Conjugated Polyamines in Urine. *Clin. Chem.* **1986**, *32*, 1930−1937.

(443) Löser, C.; Fölsch, U. R.; Paprotny, C.; Creutzfeldt, W. Polyamines in Colorectal Cancer. Evaluation of Polyamine Concentrations in the Colon Tissue, Serum, and Urine of 50 Patients with Colorectal Cancer. *Cancer* **1990**, *65*, 958−966.

(444) Gill, D. S.; Fonseca, V. A.; Barradas, M. A.; Balliod, R.; Moorhead, J. F.; Dandona, P. Plasma Histamine in Patients with Chronic Renal Failure and Nephrotic Syndrome. *J. Clin. Pathol.* **1991**, *44*, 243.

(445) Bruce, C.; Weatherstone, R.; Seaton, A.; Taylor, W. H. Histamine Levels in Plasma, Blood, and Urine in Severe Asthma, and the Effect of Corticosteroid Treatment. *Thorax* **1976**, *31*, 724.

(446) Vanholder, R.; De Smet, R.; Glorieux, G.; Argilés, A.; Baurmeister, U.; Brunet, P.; Clark, W.; Cohen, G.; De Deyn, P. P.; Deppisch, R.; Descamps-Latscha, B.; Henle, T.; Jörres, A.; Lemke, H. D.; Massy, Z. A.; Passlick-Deetjen, J.; Rodriguez, M.; Stegmayr, B.; Stenvinkel, P.; Tetta, C.; Wanner, C.; Zidek, W. For the European Uremic Toxin Work, G. Review on Uremic Toxins: Classification, Concentration, and Interindividual Variability. *Kidney Int.* **2003**, *63*, 1934−1943.

(447) Hyman, S. E. Neurotransmitters. *Curr. Biol.* **2005**, *15*, R154−R158.

(448) Stanford, S. C. Depression. In *Neurotransmitters, Drugs and Brain Function*; John Wiley & Sons, Ltd., 2001; pp 425−452.

(449) Webster, R.; Stanford, S. C. Sleep and Waking. In *Neurotransmitters, Drugs and Brain Function*; John Wiley & Sons, Ltd., 2001; pp 475−498.

(450) Webster, R. Alzheimer's Disease. In *Neurotransmitters, Drugs and Brain Function*; John Wiley & Sons, Ltd., 2001; pp 375−393.

(451) Godfrey, K. E.; Gardner, A. C.; Kwon, S.; Chea, W.; Muthukumaraswamy, S. D. Differences in Excitatory and Inhibitory

Neurotransmitter Levels between Depressed Patients and Healthy Controls: A Systematic Review and Meta-Analysis. *J. Psychiatr. Res.* **2018**, *105*, 33−44.

(452) Durant, C.; Christmas, D.; Nutt, D. The Pharmacology of Anxiety. In *Behavioral Neurobiology of Anxiety and Its Treatment*; Springer-Verlag, 2009; pp 303−330.

(453) Dulawa, S. C.; Janowsky, D. S. Cholinergic Regulation of Mood: From Basic and Clinical Studies to Emerging Therapeutics. *Mol. Psychiatry* **2019**, *24*, 694−709.

(454) Cousins, D. A.; Butts, K.; Young, A. H. The Role of Dopamine in Bipolar Disorder. *Bipolar Disord.* **2009**, *11*, 787−806.

(455) Masato, A.; Plotegher, N.; Boassa, D.; Bubacco, L. Impaired Dopamine Metabolism in Parkinson's Disease Pathogenesis. *Mol. Neurodegener.* **2019**, *14*, 35.

(456) Chagraoui, A.; Boulain, M.; Juvin, L.; Anouar, Y.; Barrière, G.; Deurwaerdère, P. D. L-Dopa in Parkinson's Disease: Looking at the "False" Neurotransmitters and Their Meaning. *Int. J. Mol. Sci.* **2020**, *21*, 294.

(457) Muthuraman, M.; Koirala, N.; Ciolac, D.; Pintea, B.; Glaser, M.; Groppa, S.; Tamás, G.; Groppa, S. Deep Brain Stimulation and L-Dopa Therapy: Concepts of Action and Clinical Applications in Parkinson's Disease. *Front. Neurol.* **2018**, *9*, 711.

(458) Nagatsu, T. The Catecholamine System in Health and Disease -Relation to Tyrosine 3-Monooxygenase and Other Catecholamine-Synthesizing Enzymes. *Proc. Jpn. Acad., Ser. B* **2006**, *82*, 388−415.

(459) Pan, X.; Kaminga, A. C.; Jia, P.; Wen, S. W.; Acheampong, K.; Liu, A. Catecholamines in Alzheimer's Disease: A Systematic Review and Meta-Analysis. *Front. Aging Neurosci.* **2020**, *12*, 184.

(460) Kruk, J.; Kotarska, K.; Aboul-Enein, B. H. Physical Exercise and Catecholamines Response: Benefits and Health Risk: Possible Mechanisms. *Free Radical Res.* **2020**, *54*, 105−125.

(461) Reisch, N.; Peczkowska, M.; Januszewicz, A.; Neumann, H. P. Pheochromocytoma: Presentation, Diagnosis and Treatment. *J. Hypertens.* **2006**, *24*, 2331−2339.

(462) Tsirlin, A.; Oo, Y.; Sharma, R.; Kansara, A.; Gliwa, A.; Banerji, M. Pheochromocytoma: A Review. *Maturitas* **2014**, *77*, 229−238.

(463) Laug, W. E.; Siegel, S. E.; Shaw, K. N.; Landing, B.; Baptista, J.; Gutenstein, M. Initial Urinary Catecholamine Metabolite Concentrations and Prognosis in Neuroblastoma. *Pediatrics* **1978**, *62*, 77−83.

(464) Strenger, V.; Kerbl, R.; Dornbusch, H. J.; Ladenstein, R.; Ambros, P. F.; Ambros, I. M.; Urban, C. Diagnostic and Prognostic Impact of Urinary Catecholamines in Neuroblastoma Patients. *Pediatr. Blood Cancer* **2007**, *48*, 504−509.

(465) Oaklander, M. New Hope for Depression. *Time Magazine* **2017**, *190*, 38−45.

(466) Haynes, R. L.; Frelinger, A. L.; Giles, E. K.; Goldstein, R. D.; Tran, H.; Kozakewich, H. P.; Haas, E. A.; Gerrits, A. J.; Mena, O. J.; Trachtenberg, F. L.; et al. High Serum Serotonin in Sudden Infant Death Syndrome. *Proc. Natl. Acad. Sci. U. S. A.* **2017**, *114*, 7695.

(467) Mulkey, M. A.; Hardin, S. R.; Olson, D. M.; Munro, C. L. Pathophysiology Review: Seven Neurotransmitters Associated with Delirium. *Clin. Nurse Spec.* **2018**, *32*, 195−211.

(468) Jiang, S.-H.; Hu, L.-P.; Wang, X.; Li, J.; Zhang, Z.-G. Neurotransmitters: Emerging Targets in Cancer. *Oncogene* **2020**, *39*, 503−515.

(469) Marc, D. T.; Ailts, J. W.; Campeau, D. C. A.; Bull, M. J.; Olson, K. L. Neurotransmitters Excreted in the Urine as Biomarkers of Nervous System Activity: Validity and Clinical Applicability. *Neurosci. Biobehav. Rev.* **2011**, *35*, 635−644.

(470) Gershon, M. D. Review Article: Serotonin Receptors and Transporters−Roles in Normal and Abnormal Gastrointestinal Motility. *Aliment. Pharmacol. Ther.* **2004**, *20*, 3−14.

(471) Luan, H.; Liu, L.-F.; Meng, N.; Tang, Z.; Chua, K.-K.; Chen, L.-L.; Song, J.-X.; Mok, V. C. T.; Xie, L.-X.; Li, M.; Cai, Z. Lc-Ms-Based Urinary Metabolite Signatures in Idiopathic Parkinson's Disease. *J. Proteome Res.* **2015**, *14*, 467−478.

(472) Mittal, R.; Debs, L. H.; Patel, A. P.; Nguyen, D.; Patel, K.; O'Connor, G.; Grati, M. H.; Mittal, J.; Yan, D.; Eshraghi, A. A.; Deo, S. K.; Daunert, S.; Liu, X. Z. Neurotransmitters: The Critical Modulators Regulating Gut-Brain Axis. *J. Cell. Physiol.* **2017**, *232*, 2359−2372.

(473) Sarkodie, E. K.; Zhou, S.; Baidoo, S. A.; Chu, W. Influences of Stress Hormones on Microbial Infections. *Microb. Pathog.* **2019**, *131*, 270−276.

(474) Rakers, F.; Bischoff, S.; Schiffner, R.; Haase, M.; Rupprecht, S.; Kiehntopf, M.; Kühn-Velten, W. N.; Schubert, H.; Witte, O. W.; Nijland, M. J.; et al. Role of Catecholamines in Maternal-Fetal Stress Transfer in Sheep. *Am. J. Obstet. Gynecol.* **2015**, *213*, 684.

(475) Fischer, A. G.; Ullsperger, M. An Update on the Role of Serotonin and Its Interplay with Dopamine for Reward. *Front. Hum. Neurosci.* **2017**, *11*, 484.

(476) Wu, H.; Denna, T. H.; Storkersen, J. N.; Gerriets, V. A. Beyond a Neurotransmitter: The Role of Serotonin in Inflammation and Immunity. *Pharmacol. Res.* **2019**, *140*, 100−114.

(477) Kema, I. P.; Schellings, A. M. J.; Hoppenbrouwers, C. J. M.; Rutgers, H. M.; de Vries, E. G. E.; Muskiet, F. A. J. High Performance Liquid Chromatographic Profiling of Tryptophan and Related Indoles in Body Fluids and Tissues of Carcinoid Patients. *Clin. Chim. Acta* **1993**, *221*, 143−158.

(478) Sarrouilhe, D.; Clarhaut, J.; Defamie, N.; Mesnil, M. Serotonin and Cancer: What Is the Link? *Curr. Mol. Med.* **2015**, *15*, 62−77.

(479) Zisapel, N. New Perspectives on the Role of Melatonin in Human Sleep, Circadian Rhythms and Their Regulation. *Br. J. Pharmacol.* **2018**, *175*, 3190−3199.

(480) Rawashdeh, O.; Maronde, E. The Hormonal Zeitgeber Melatonin: Role as a Circadian Modulator in Memory Processing. *Front. Mol. Neurosci.* **2012**, *5*, 27.

(481) Berger, M.; Gray, J. A.; Roth, B. L. The Expanded Biology of Serotonin. *Annu. Rev. Med.* **2009**, *60*, 355−366.

(482) Nichkova, M.; Wynveen, P. M.; Marc, D. T.; Huisman, H.; Kellermann, G. H. Validation of an Elisa for Urinary Dopamine: Applications in Monitoring Treatment of Dopamine-Related Disorders. *J. Neurochem.* **2013**, *125*, 724−735.

(483) Marvin, J. S.; Shimoda, Y.; Magloire, V.; Leite, M.; Kawashima, T.; Jensen, T. P.; Kolb, I.; Knott, E. L.; Novak, O.; Podgorski, K.; Leidenheimer, N. J.; Rusakov, D. A.; Ahrens, M. B.; Kullmann, D. M.; Looger, L. L. A Genetically Encoded Fluorescent Sensor for in Vivo Imaging of Gaba. *Nat. Methods* **2019**, *16*, 763−770.

(484) Patriarchi, T.; Cho, J. R.; Merten, K.; Howe, M. W.; Marley, A.; Xiong, W.-H.; Folk, R. W.; Broussard, G. J.; Liang, R.; Jang, M. J.; et al. Ultrafast Neuronal Imaging of Dopamine Dynamics with Designed Genetically Encoded Sensors. *Science* **2018**, *360*, No. eaat4422.

(485) Banerjee, S.; McCracken, S.; Hossain, M. F.; Slaughter, G. Electrochemical Detection of Neurotransmitters. *Biosensors* **2020**, *10*, 101.

(486) Hall, D. G. *Boronic Acids: Preparation and Applications in Organic Synthesis, Medicine and Materials*, 2nd ed.; Wiley, 2011; pp 1−133.

(487) Hettie, K. S.; Liu, X.; Gillis, K. D.; Glass, T. E. Selective Catecholamine Recognition with Neurosensor 521: A Fluorescent Sensor for the Visualization of Norepinephrine in Fixed and Live Cells. *ACS Chem. Neurosci.* **2013**, *4*, 918−923.

(488) Zhang, L.; Liu, X. A.; Gillis, K. D.; Glass, T. E. A High-Affinity Fluorescent Sensor for Catecholamine: Application to Monitoring Norepinephrine Exocytosis. *Angew. Chem., Int. Ed.* **2019**, *58*, 7611−7614.

(489) Coskun, A.; Akkaya, E. U. Three-Point Recognition and Selective Fluorescence Sensing of L-Dopa. *Org. Lett.* **2004**, *6*, 3107−3109.

(490) Jang, Y. J.; Jun, J.-H.; Koh, H. S. Fluorescence Sensing of Dopamine. *Bull. Korean Chem. Soc.* **2005**, *26*, 2041.

(491) Maue, M.; Schrader, T. A Color Sensor for Catecholamines. *Angew. Chem., Int. Ed.* **2005**, *44*, 2265−2270.

(492) Chandra, F.; Dutta, T.; Koner, A. L. Supramolecular Encapsulation of a Neurotransmitter Serotonin by Cucurbit[7]Uril. *Front. Chem.* **2020**, *8*, 582757.

(493) Kasera, S.; Walsh, Z.; del Barrio, J.; Scherman, O. A. A Selective Supramolecular Photochemical Sensor for Dopamine. *Supramol. Chem.* **2014**, *26*, 280−285.

(494) Baumes, L. A.; Buaki Sogo, M.; Montes-Navajas, P.; Corma, A.; Garcia, H. A Colorimetric Sensor Array for the Detection of the Date-Rape Drug Γ-Hydroxybutyric Acid (Ghb): A Supramolecular Approach. *Chem.−Eur. J.* **2010**, *16*, 4489−4495.

(495) Kitamura, M.; Shabbir, S. H.; Anslyn, E. V. Guidelines for Pattern Recognition Using Differential Receptors and Indicator Displacement Assays. *J. Org. Chem.* **2009**, *74*, 4479−4489.

(496) Guo, D.-S.; Yang, J.; Liu, Y. Specifically Monitoring Butyrylcholinesterase by Supramolecular Tandem Assay. *Chem.−Eur. J.* **2013**, *19*, 8755−8759.

(497) Abd El-Rahman, M. K.; Mazzone, G.; Mahmoud, A. M.; Sicilia, E.; Shoeib, T. Spectrophotometric Determination of Choline in Pharmaceutical Formulations Via Host-Guest Complexation with a Biomimetic Calixarene Receptor. *Microchem. J.* **2019**, *146*, 735−741.

(498) Jin, T. Near-Infrared Fluorescence Detection of Acetylcholine in Aqueous Solution Using a Complex of Rhodamine 800 and P-Sulfonato-Calix[8]Arene. *Sensors* **2010**, *10*, 2438−2449.

(499) Maintz, L.; Novak, N. Histamine and Histamine Intolerance. *Am. J. Clin. Nutr.* **2007**, *85*, 1185−1196.

(500) Pereira, A. R.; Araújo, A. N.; Montenegro, M. C. B. S. M.; Amorim, C. M. P. G. A Simpler Potentiometric Method for Histamine Assessment in Blood Sera. *Anal. Bioanal. Chem.* **2020**, *412*, 3629−3637.

(501) Sahudin, M. A.; Su'ait, M. S.; Tan, L. L.; Lee, Y. H.; Abd Karim, N. H. Zinc(Ii) Salphen Complex-Based Fluorescence Optical Sensor for Biogenic Amine Detection. *Anal. Bioanal. Chem.* **2019**, *411*, 6449−6461.

(502) Khurana, R.; Barooah, N.; Bhasikuttan, A. C.; Mohanty, J. Supramolecular Assembly Induced Emission of Thiazole Orange with Sulfobutylether Β-Cyclodextrin: A Stimuli-Responsive Fluorescence Sensor for Tyramine. *ChemPhysChem* **2019**, *20*, 2498−2505.

(503) Oshikawa, Y.; Furuta, K.; Tanaka, S.; Ojida, A. Cell Surface-Anchored Fluorescent Probe Capable of Real-Time Imaging of Single Mast Cell Degranulation Based on Histamine-Induced Coordination Displacement. *Anal. Chem.* **2016**, *88*, 1526−1529.

(504) Seto, D.; Soh, N.; Nakano, K.; Imato, T. An Amphiphilic Fluorescent Probe for the Visualization of Histamine in Living Cells. *Bioorg. Med. Chem. Lett.* **2010**, *20*, 6708−6711.

(505) Jang, Y.; Jang, M.; Kim, H.; Lee, S. J.; Jin, E.; Koo, J. Y.; Hwang, I.-C.; Kim, Y.; Ko, Y. H.; Hwang, I.; Oh, J. H.; Kim, K. Point-of-Use Detection of Amphetamine-Type Stimulants with Host-Molecule-Functionalized Organic Transistors. *Chem.* **2017**, *3*, 641−651.

(506) Pradhan, T.; Jung, H. S.; Jang, J. H.; Kim, T. W.; Kang, C.; Kim, J. S. Chemical Sensing of Neurotransmitters. *Chem. Soc. Rev.* **2014**, *43*, 4684−4713.

(507) Feng, J. J.; Guo, H.; Li, Y. F.; Wang, Y. H.; Chen, W. Y.; Wang, A. J. Single Molecular Functionalized Gold Nanoparticles for Hydrogen-Bonding Recognition and Colorimetric Detection of Dopamine with High Sensitivity and Selectivity. *ACS Appl. Mater. Interfaces* **2013**, *5*, 1226−1231.

(508) Godoy-Reyes, T. M.; Costero, A. M.; Gaviña, P.; Martínez-Máñez, R.; Sancenón, F. A Colorimetric Probe for the Selective Detection of Norepinephrine Based on a Double Molecular Recognition with Functionalized Gold Nanoparticles. *ACS Appl. Nano Mater.* **2019**, *2*, 1367−1373.

(509) Godoy-Reyes, T. M.; Llopis-Lorente, A.; Costero, A. M.; Sancenón, F.; Gaviña, P.; Martínez-Máñez, R. Selective and Sensitive Colorimetric Detection of the Neurotransmitter Serotonin Based on the Aggregation of Bifunctionalised Gold Nanoparticles. *Sens. Actuators, B* **2018**, *258*, 829−835.

(510) Kong, B.; Zhu, A.; Luo, Y.; Tian, Y.; Yu, Y.; Shi, G. Sensitive and Selective Colorimetric Visualization of Cerebral Dopamine Based on Double Molecular Recognition. *Angew. Chem., Int. Ed.* **2011**, *50*, 1837−1840.

(511) Leng, Y.; Xie, K.; Ye, L.; Li, G.; Lu, Z.; He, J. Gold-Nanoparticle-Based Colorimetric Array for Detection of Dopamine in Urine and Serum. *Talanta* **2015**, *139*, 89−95.

(512) Huang, X.; El-Sayed, M. A. Gold Nanoparticles: Optical Properties and Implementations in Cancer Diagnosis and Photothermal Therapy. *J. Adv. Res.* **2010**, *1*, 13−28.

(513) Chen, Z.; Zhang, C.; Zhou, T.; Ma, H. Gold Nanoparticle Based Colorimetric Probe for Dopamine Detection Based on the Interaction between Dopamine and Melamine. *Microchim. Acta* **2015**, *182*, 1003−1008.

(514) Zheng, Y.; Wang, Y.; Yang, X. Aptamer-Based Colorimetric Biosensing of Dopamine Using Unmodified Gold Nanoparticles. *Sens. Actuators, B* **2011**, *156*, 95−99.

(515) Zhang, Y.; Qi, S.; Liu, Z.; Shi, Y.; Yue, W.; Yi, C. Rapid Determination of Dopamine in Human Plasma Using a Gold Nanoparticle-Based Dual-Mode Sensing System. *Mater. Sci. Eng., C* **2016**, *61*, 207−213.

(516) Liu, X.; He, F.; Zhang, F.; Zhang, Z.; Huang, Z.; Liu, J. Dopamine and Melamine Binding to Gold Nanoparticles Dominates Their Aptamer-Based Label-Free Colorimetric Sensing. *Anal. Chem.* **2020**, *92*, 9370−9378.

(517) Chávez, J. L.; Hagen, J. A.; Kelley-Loughnane, N. Fast and Selective Plasmonic Serotonin Detection with Aptamer-Gold Nanoparticle Conjugates. *Sensors* **2017**, *17*, 681.

(518) Gabrielli, L.; Carril, M.; Padro, D.; Mancin, F. Multimodal (19) F Nmr Dopamine Detection and Imaging with a Nanoparticle-Based Displacement Assay. *Chem.−Eur. J.* **2018**, *24*, 13036−13042.

(519) Ji, C.; Zhou, Y.; Leblanc, R. M.; Peng, Z. Recent Developments of Carbon Dots in Biosensing: A Review. *ACS Sens.* **2020**, *5*, 2724−2741.

(520) LeCroy, G. E.; Messina, F.; Sciortino, A.; Bunker, C. E.; Wang, P.; Fernando, K. A. S.; Sun, Y.-P. Characteristic Excitation Wavelength Dependence of Fluorescence Emissions in Carbon "Quantum" Dots. *J. Phys. Chem. C* **2017**, *121*, 28180−28186.

(521) Liu, X.; Hu, X.; Xie, Z.; Chen, P.; Sun, X.; Yan, J.; Zhou, S. In Situ Bifunctionalized Carbon Dots with Boronic Acid and Amino Groups for Ultrasensitive Dopamine Detection. *Anal. Methods* **2016**, *8*, 3236−3241.

(522) Qu, K.; Wang, J.; Ren, J.; Qu, X. Carbon Dots Prepared by Hydrothermal Treatment of Dopamine as an Effective Fluorescent Sensing Platform for the Label-Free Detection of Iron(Iii) Ions and Dopamine. *Chem.−Eur. J.* **2013**, *19*, 7243−7249.

(523) Luo, K.; Jiang, X. Fluorescent Carbon Quantum Dots with Fe(Iii/Ii) Irons as Bridge for the Detection of Ascorbic Acid and H2o2. *J. Fluoresc.* **2019**, *29*, 769−777.

(524) Hsieh, V.; Okada, S.; Wei, H.; Garcia-Alvarez, I.; Barandov, A.; Alvarado, S. R.; Ohlendorf, R.; Fan, J.; Ortega, A.; Jasanoff, A. Neurotransmitter-Responsive Nanosensors for T2-Weighted Magnetic Resonance Imaging. *J. Am. Chem. Soc.* **2019**, *141*, 15751−15754.

(525) Kruss, S.; Landry, M. P.; Vander Ende, E.; Lima, B. M.; Reuel, N. F.; Zhang, J.; Nelson, J.; Mu, B.; Hilmer, A.; Strano, M. Neurotransmitter Detection Using Corona Phase Molecular Recognition on Fluorescent Single-Walled Carbon Nanotube Sensors. *J. Am. Chem. Soc.* **2014**, *136*, 713−724.

(526) Qian, C. G.; Zhu, S.; Feng, P. J.; Chen, Y. L.; Yu, J. C.; Tang, X.; Liu, Y.; Shen, Q. D. Conjugated Polymer Nanoparticles for Fluorescence Imaging and Sensing of Neurotransmitter Dopamine in Living Cells and the Brains of Zebrafish Larvae. *ACS Appl. Mater. Interfaces* **2015**, *7*, 18581−18589.

(527) Justice, J. B., Jr Quantitative Microdialysis of Neurotransmitters. *J. Neurosci. Methods* **1993**, *48*, 263−276.

(528) Wang, J.; Dai, J.; Xu, Y.; Dai, X.; Zhang, Y.; Shi, W.; Sellergren, B.; Pan, G. Molecularly Imprinted Fluorescent Test Strip for Direct, Rapid, and Visual Dopamine Detection in Tiny Amount of Biofluid. *Small* **2019**, *15*, No. e1803913.

(529) Ling, X.; Shi, R.; Zhang, J.; Liu, D.; Weng, M.; Zhang, C.; Lu, M.; Xie, X.; Huang, L.; Huang, W. Dual-Signal Luminescent Detection of Dopamine by a Single Type of Lanthanide-Doped Nanoparticles. *ACS Sens.* **2018**, *3*, 1683−1689.

(530) Kumar, B.; Murali, A.; Giri, S. Upconversion Nanoplatform for Fret-Based Sensing of Dopamine and Ph. *ChemistrySelect* **2019**, *4*, 5407−5414.

(531) Rabie, H.; Zhang, Y.; Pasquale, N.; Lagos, M. J.; Batson, P. E.; Lee, K. B. Nir Biosensing of Neurotransmitters in Stem Cell-Derived Neural Interface Using Advanced Core-Shell Upconversion Nanoparticles. *Adv. Mater.* **2019**, *31*, 1806991.

(532) Murillo Pulgarín, J. A.; Alañón Molina, A.; Jiménez García, E.; García Gómez, L. A Sensitive Resonance Rayleigh Scattering Sensor for Dopamine in Urine Using Upconversion Nanoparticles. *J. Raman Spectrosc.* **2020**, *51*, 406−413.

(533) Li, H.; Liu, J.; Yang, M.; Kong, W.; Huang, H.; Liu, Y. Highly Sensitive, Stable, and Precise Detection of Dopamine with Carbon Dots/Tyrosinase Hybrid as Fluorescent Probe. *RSC Adv.* **2014**, *4*, 46437−46443.

(534) Zhu, L.; Xu, G.; Song, Q.; Tang, T.; Wang, X.; Wei, F.; Hu, Q. Highly Sensitive Determination of Dopamine by a Turn-on Fluorescent Biosensor Based on Aptamer Labeled Carbon Dots and Nano-Graphite. *Sens. Actuators, B* **2016**, *231*, 506−512.

(535) Anjali Devi, J. S.; Anulekshmi, A. H.; Salini, S.; Aparna, R. S.; George, S. Boronic Acid Functionalized Nitrogen Doped Carbon Dots for Fluorescent Turn-on Detection of Dopamine. *Microchim. Acta* **2017**, *184*, 4081−4090.

(536) Jana, J.; Chung, J. S.; Hur, S. H. Zno-Associated Carbon Dot-Based Fluorescent Assay for Sensitive and Selective Dopamine Detection. *ACS Omega* **2019**, *4*, 17031−17038.

(537) Jin, T.; Fujii, F.; Sakata, H.; Tamura, M.; Kinjo, M. Amphiphilic P-Sulfonatocalix[4]Arene-Coated Cdse/Zns Quantum Dots for the Optical Detection of the Neurotransmitter Acetylcholine. *Chem. Commun.* **2005**, 4300−4302.

(538) Freeman, R.; Bahshi, L.; Finder, T.; Gill, R.; Willner, I. Competitive Analysis of Saccharides or Dopamine by Boronic Acid-Functionalized Cdse-Zns Quantum Dots. *Chem. Commun.* **2009**, 764−766.

(539) Diaz-Diestra, D.; Thapa, B.; Beltran-Huarac, J.; Weiner, B. R.; Morell, G. L-Cysteine Capped Zns:Mn Quantum Dots for Room-Temperature Detection of Dopamine with High Sensitivity and Selectivity. *Biosens. Bioelectron.* **2017**, *87*, 693−700.

(540) Xu, Y.; Wang, J.; Lu, Y.; Dai, X.; Yan, Y. Preparation of Functionalized Double Ratio Fluorescent Imprinted Sensors for Visual Determination and Recognition of Dopamine in Human Serum. *Spectrochim. Acta, Part A* **2019**, *219*, 225−231.

(541) Zhao, X.; Cui, Y.; He, Y.; Wang, S.; Wang, J. Synthesis of Multi-Mode Quantum Dots Encoded Molecularly Imprinted Polymers Microspheres and Application in Quantitative Detection for Dopamine. *Sens. Actuators, B* **2020**, *304*, 127265.

(542) Zhang, X.; Chen, X.; Kai, S.; Wang, H. Y.; Yang, J.; Wu, F. G.; Chen, Z. Highly Sensitive and Selective Detection of Dopamine Using One-Pot Synthesized Highly Photoluminescent Silicon Nanoparticles. *Anal. Chem.* **2015**, *87*, 3360−3365.

(543) Wu, S.; Lin, Y.; Liu, J.; Shi, W.; Yang, G.; Cheng, P. Rapid Detection of the Biomarkers for Carcinoid Tumors by a Water Stable Luminescent Lanthanide Metal-Organic Framework Sensor. *Adv. Funct. Mater.* **2018**, *28*, 1707169.

(544) Lin, V. S.-Y.; Lai, C.-Y.; Huang, J.-L.; Song, S.-A.; Xu, S. Molecular Recognition inside of Multifunctionalized Mesoporous Silicas: Toward Selective Fluorescence Detection of Dopamine and Glucosamine. *J. Am. Chem. Soc.* **2001**, *123*, 11510−11511.

(545) Radu, D. R.; Lai, C.-Y.; Wiench, J. W.; Pruski, M.; Lin, V. S. Y. Gatekeeping Layer Effect: A Poly(Lactic Acid)-Coated Mesoporous Silica Nanosphere-Based Fluorescence Probe for Detection of Amino-Containing Neurotransmitters. *J. Am. Chem. Soc.* **2004**, *126*, 1640−1641.

(546) Sun, Y.; Lin, Y.; Ding, C.; Sun, W.; Dai, Y.; Zhu, X.; Liu, H.; Luo, C. An Ultrasensitive and Ultraselective Chemiluminescence Aptasensor for Dopamine Detection Based on Aptamers Modified Magnetic Mesoporous Silica @ Graphite Oxide Polymers. *Sens. Actuators, B* **2018**, *257*, 312−323.

(547) Grimm, L. M.; Sinn, S.; Krstić, M.; D'Este, E.; Sonntag, I.; Prasetyanto, E. A.; Kuner, T.; Wenzel, W.; De Cola, L.; Biedermann, F. Fluorescent Nanozeolite Receptors for the Highly Selective and Sensitive Detection of Neurotransmitters in Water and Biofluids. *Adv. Mater.* **2021**, 2104614.

(548) Watanabe, M.; Kimura, A.; Akasaka, K.; Hayashi, S. Determination of Acetylcholine in Human Blood. *Biochem. Med. Metab. Biol.* **1986**, *36*, 355−362.

(549) Kirsch, S. H.; Herrmann, W.; Rabagny, Y.; Obeid, R. Quantification of Acetylcholine, Choline, Betaine, and Dimethylglycine in Human Plasma and Urine Using Stable-Isotope Dilution Ultra Performance Liquid Chromatography-Tandem Mass Spectrometry. *J. Chromatogr. B: Anal. Technol. Biomed. Life Sci.* **2010**, *878*, 3338−3344.

(550) Kvitvang, H. F. N.; Andreassen, T.; Adam, T.; Villas-Bôas, S. G.; Bruheim, P. Highly Sensitive Gc/Ms/Ms Method for Quantitation of Amino and Nonamino Organic Acids. *Anal. Chem.* **2011**, *83*, 2705−2711.

(551) Trabado, S.; Al-Salameh, A.; Croixmarie, V.; Masson, P.; Corruble, E.; Fève, B.; Colle, R.; Ripoll, L.; Walther, B.; Boursier-Neyret, C.; Werner, E.; Becquemont, L.; Chanson, P. The Human Plasma-Metabolome: Reference Values in 800 French Healthy Volunteers; Impact of Cholesterol, Gender and Age. *PLoS One* **2017**, *12*, No. e0173615.

(552) Cucchi, M. L.; Frattini, P.; Santagostino, G.; Preda, S.; Orecchia, G. Catecholamines Increase in the Urine of Non-Segmental Vitiligo Especially During Its Active Phase. *Pigm. Cell Res.* **2003**, *16*, 111−116.

(553) Lambert, G.; Naredi, S.; Edén, E.; Rydenhag, B.; Friberg, P. Monoamine Metabolism and Sympathetic Nervous Activation Following Subarachnoid Haemorrhage: Influence of Gender and Hydrocephalus. *Brain Res. Bull.* **2002**, *58*, 77−82.

(554) Peyrin, L.; Pequignot, J. M.; Lacour, J. R.; Fourcade, J. Relationships between Catecholamine or 3-Methoxy 4-Hydroxy Phenylglycol Changes and the Mental Performance under Submaximal Exercise in Man. *Psychopharmacology* **1987**, *93*, 188.

(555) Campollo, O.; MacGillivray, B. B.; McIntyre, N. Association of Plasma Ammonia and Gaba Levels and the Degree of Hepatic Encephalopathy. *Rev. Invest. Clin.* **1992**, *44*, 483−490.

(556) Grant, S. L.; Shulman, Y.; Tibbo, P.; Hampson, D. R.; Baker, G. B. Determination of D-Serine and Related Neuroactive Amino Acids in Human Plasma by High-Performance Liquid Chromatography with Fluorimetric Detection. *J. Chromatogr. B: Anal. Technol. Biomed. Life Sci.* **2006**, *844*, 278−282.

(557) Panholzer, T. J.; Beyer, J.; Lichtwald, K. Coupled-Column Liquid Chromatographic Analysis of Catecholamines, Serotonin, and Metabolites in Human Urine. *Clin. Chem.* **1999**, *45*, 262−268.

(558) Andrew, R.; Watson, D. G.; Best, S. A.; Midgley, J. M.; Wenlong, H.; Petty, R. K. H. The Determination of Hydroxydopamines and Other Trace Amines in the Urine of Parkinsonian Patients and Normal Controls. *Neurochem. Res.* **1993**, *18*, 1175−1177.

(559) Kitajima, K.; Sato, C. *Carbohydrate Recognition*; Wiley & Sons, 2011; pp 33−63.

(560) Wang, W.; Song, X.; Wang, L.; Song, L. Pathogen-Derived Carbohydrate Recognition in Molluscs Immune Defense. *Int. J. Mol. Sci.* **2018**, *19*, 721.

(561) Johnson, R. J.; Segal, M. S.; Sautin, Y.; Nakagawa, T.; Feig, D. I.; Kang, D.-H.; Gersch, M. S.; Benner, S.; Sánchez-Lozada, L. G. Potential Role of Sugar (Fructose) in the Epidemic of Hypertension, Obesity and the Metabolic Syndrome, Diabetes, Kidney Disease, and Cardiovascular Disease. *Am. J. Clin. Nutr.* **2007**, *86*, 899.

(562) Vos, M. B.; Lavine, J. E. Dietary Fructose in Nonalcoholic Fatty Liver Disease. *Hepatology* **2013**, *57*, 2525−2531.

(563) Ouyang, X.; Cirillo, P.; Sautin, Y.; McCall, S.; Bruchette, J. L.; Diehl, A. M.; Johnson, R. J.; Abdelmalek, M. F. Fructose Consumption as a Risk Factor for Non-Alcoholic Fatty Liver Disease. *J. Hepatol.* **2008**, *48*, 993−999.

(564) Hannou, S. A.; Haslam, D. E.; McKeown, N. M.; Herman, M. A. Fructose Metabolism and Metabolic Disease. *J. Clin. Invest.* **2018**, *128*, 545−555.

(565) Brewer, R. A.; Gibbs, V. K.; Smith, D. L., Jr Targeting Glucose Metabolism for Healthy Aging. *Nutr. Healthy Aging* **2016**, *4*, 31−46.

(566) Bechmann, L. P.; Hannivoort, R. A.; Gerken, G.; Hotamisligil, G. S.; Trauner, M.; Canbay, A. The Interaction of Hepatic Lipid and Glucose Metabolism in Liver Diseases. *J. Hepatol.* **2012**, *56*, 952−964.

(567) Wittig, R.; Coy, J. F. The Role of Glucose Metabolism and Glucose-Associated Signalling in Cancer. *Perspect. Med. Chem.* **2007**, *1*, 64−82.

(568) Feskens, E. J. M.; Kromhout, D. Glucose Tolerance and the Risk of Cardiovascular Diseases: The Zutphen Study. *J. Clin. Epidemiol.* **1992**, *45*, 1327−1334.

(569) Crook, M. A.; Earle, K.; Morocutti, A.; Yip, J.; Viberti, G.; Pickup, J. C. Serum Sialic Acid, a Risk Factor for Cardiovascular Disease, Is Increased in Iddm Patients with Microalbuminuria and Clinical Proteinuria. *Diabetes Care* **1994**, *17*, 305−310.

(570) Afzali, B.; Bakri, R. S.; Bharma-Ariza, P.; Lumb, P. J.; Dalton, N.; Turner, N. C.; Wierzbicki, A. S.; Crook, M. A.; Goldsmith, D. J. Raised Plasma Total Sialic Acid Levels Are Markers of Cardiovascular Disease in Renal Dialysis Patients. *J. Nephrol.* **2003**, *16*, 540−545.

(571) Varki, A. Sialic Acids in Human Health and Disease. *Trends Mol. Med.* **2008**, *14*, 351−360.

(572) Pickup, J. C.; Mattock, M. B.; Crook, M. A.; Chusney, G. D.; Burt, D.; Fitzgerald, A. P. Serum Sialic Acid Concentration and Coronary Heart Disease in Niddm. *Diabetes Care* **1995**, *18*, 1100.

(573) Hao, C.; Xu, H.; Yu, L.; Zhang, L. Heparin: An Essential Drug for Modern Medicine. In *Progress in Molecular Biology and Translational Science*; Academic Press, 2019; Vol. *163*, Chapter 1, pp 1−19.

(574) Qiu, M.; Huang, S.; Luo, C.; Wu, Z.; Liang, B.; Huang, H.; Ci, Z.; Zhang, D.; Han, L.; Lin, J. Pharmacological and Clinical Application of Heparin Progress: An Essential Drug for Modern Medicine. *Biomed. Pharmacother.* **2021**, *139*, 111561.

(575) Dai, C.; Sagwal, A.; Cheng, Y.; Peng, H.; Chen, W.; Wang, B. Carbohydrate Biomarker Recognition Using Synthetic Lectin Mimics. *Pure Appl. Chem.* **2012**, *84*, 2479−2498.

(576) Cheng, Y.; Ni, N.; Peng, H.; Jin, S.; Wang, B. Carbohydrate Biomarkers. In *Carbohydrate Recognition*; Wiley & Sons, 2011; pp 133−156.

(577) Cheng, X.; Zheng, J.; Lin, A.; Xia, H.; Zhang, Z.; Gao, Q.; Lv, W.; Liu, H. A Review: Roles of Carbohydrates in Human Diseases through Regulation of Imbalanced Intestinal Microbiota. *J. Funct. Foods* **2020**, *74*, 104197.

(578) Hujoel, P. Dietary Carbohydrates and Dental-Systemic Diseases. *J. Dent. Res.* **2009**, *88*, 490−502.

(579) Mann, J. Dietary Carbohydrate: Relationship to Cardiovascular Disease and Disorders of Carbohydrate Metabolism. *Eur. J. Clin. Nutr.* **2007**, *61*, S100−S111.

(580) Englyst, K. N.; Englyst, H. N. Carbohydrate Bioavailability. *Br. J. Nutr.* **2005**, *94*, 1−11.

(581) Ambrosi, M.; Cameron, N. R.; Davis, B. G. Lectins: Tools for the Molecular Understanding of the Glycocode. *Org. Biomol. Chem.* **2005**, *3*, 1593−1608.

(582) Ke, C.; Destecroix, H.; Crump, M. P.; Davis, A. P. A Simple and Accessible Synthetic Lectin for Glucose Recognition and Sensing. *Nat. Chem.* **2012**, *4*, 718−723.

(583) Toone, E. J. Structure and Energetics of Protein-Carbohydrate Complexes. *Curr. Opin. Struct. Biol.* **1994**, *4*, 719−728.

(584) Fehling, H. Quantitative Bestimmung Des Zuckers Im Harn. *Arch. Physiol. Heilkunde* **1848**, *7*, 64−73.

(585) Tollens, B. Ueber Ammon-Alkalische Silberlösung Als Reagens Auf Aldehyd. *Ber. Dtsch. Chem. Ges.* **1882**, *15*, 1635−1639.

(586) Lorand, J. P.; Edwards, J. O. Polyol Complexes and Structure of the Benzeneboronate Ion. *J. Org. Chem.* **1959**, *24*, 769−774.

(587) Wu, X.; Li, Z.; Chen, X.-X.; Fossey, J. S.; James, T. D.; Jiang, Y.-B. Selective Sensing of Saccharides Using Simple Boronic Acids and Their Aggregates. *Chem. Soc. Rev.* **2013**, *42*, 8032−8048.

(588) Davis, A. P.; Wareham, R. S. Carbohydrate Recognition through Noncovalent Interactions: A Challenge for Biomimetic and Supramolecular Chemistry. *Angew. Chem., Int. Ed.* **1999**, *38*, 2978−2996.

(589) Fang, G.; Wang, H.; Bian, Z.; Sun, J.; Liu, A.; Fang, H.; Liu, B.; Yao, Q.; Wu, Z. Recent Development of Boronic Acid-Based Fluorescent Sensors. *RSC Adv.* **2018**, *8*, 29400−29427.

(590) Zhai, W.; Sun, X.; James, T. D.; Fossey, J. S. Boronic Acid-Based Carbohydrate Sensing. *Chem.−Asian J.* **2015**, *10*, 1836−1848.

(591) Springsteen, G.; Wang, B. A Detailed Examination of Boronic Acid-Diol Complexation. *Tetrahedron* **2002**, *58*, 5291−5300.

(592) Springsteen, G.; Wang, B. Alizarin Red S. As a General Optical Reporter for Studying the Binding of Boronic Acids with Carbohydrates. *Chem. Commun.* **2001**, *2001*, 1608.

(593) James, T. D.; Sandanayake, K. R. A. S.; Iguchi, R.; Shinkai, S. Novel Saccharide-Photoinduced Electron Transfer Sensors Based on the Interaction of Boronic Acid and Amine. *J. Am. Chem. Soc.* **1995**, *117*, 8982−8987.

(594) Yoon, J.; Czarnik, A. W. Fluorescent Chemosensors of Carbohydrates. A Means of Chemically Communicating the Binding of Polyols in Water Based on Chelation-Enhanced Quenching. *J. Am. Chem. Soc.* **1992**, *114*, 5874−5875.

(595) James, T. D.; Sandanayake, K. R. A. S.; Shinkai, S. A Glucose-Selective Molecular Fluorescence Sensor. *Angew. Chem., Int. Ed. Engl.* **1994**, *33*, 2207−2209.

(596) Larkin, J. D.; Frimat, K. A.; Fyles, T. M.; Flower, S. E.; James, T. D. Boronic Acid Based Photoinduced Electron Transfer (Pet) Fluorescence Sensors for Saccharides. *New J. Chem.* **2010**, *34*, 2922−2931.

(597) Arimori, S.; Bell, M. L.; Oh, C. S.; Frimat, K. A.; James, T. D. Modular Fluorescence Sensors for Saccharides. *J. Chem. Soc., Perkin Trans. 1* **2002**, 803−808.

(598) Chapin, B. M.; Metola, P.; Vankayala, S. L.; Woodcock, H. L.; Mooibroek, T. J.; Lynch, V. M.; Larkin, J. D.; Anslyn, E. V. Disaggregation Is a Mechanism for Emission Turn-on of Ortho-Aminomethylphenylboronic Acid-Based Saccharide Sensors. *J. Am. Chem. Soc.* **2017**, *139*, 5568−5578.

(599) Sun, X.; James, T. D.; Anslyn, E. V. Arresting "Loose Bolt" Internal Conversion from -B(Oh)2 Groups Is the Mechanism for Emission Turn-on in Ortho-Aminomethylphenylboronic Acid-Based Saccharide Sensors. *J. Am. Chem. Soc.* **2018**, *140*, 2348−2354.

(600) Karnati, V. V.; Gao, X.; Gao, S.; Yang, W.; Ni, W.; Sankar, S.; Wang, B. A Glucose-Selective Fluorescence Sensor Based on Boronicacid-Diol Recognition. *Bioorg. Med. Chem. Lett.* **2002**, *12*, 3373−3377.

(601) Kaur, G.; Fang, H.; Gao, X.; Li, H.; Wang, B. Substituent Effect on Anthracene-Based Bisboronic Acid Glucose Sensors. *Tetrahedron* **2006**, *62*, 2583−2589.

(602) Phillips, M. D.; Fyles, T. M.; Barwell, N. P.; James, T. D. Carbohydrate Sensing Using a Fluorescent Molecular Tweezer. *Chem. Commun.* **2009**, 6557−6559.

(603) Tran, T. M.; Alan, Y.; Glass, T. E. A Highly Selective Fluorescent Sensor for Glucosamine. *Chem. Commun.* **2015**, *51*, 7915−7918.

(604) Aghazadeh-Habashi, A.; Jamali, F. The Glucosamine Controversy; a Pharmacokinetic Issue. *J. Pharm. Pharm. Sci.* **2011**, *14*, 264−273.

(605) Kanzaki, N.; Saito, K.; Maeda, A.; Kitagawa, Y.; Kiso, Y.; Watanabe, K.; Tomonaga, A.; Nagaoka, I.; Yamaguchi, H. Effect of a Dietary Supplement Containing Glucosamine Hydrochloride, Chondroitin Sulfate and Quercetin Glycosides on Symptomatic Knee Osteoarthritis: A Randomized, Double-Blind, Placebo-Controlled Study. *J. Sci. Food Agric.* **2012**, *92*, 862−869.

(606) Zhong, Z.; Anslyn, E. V. A Colorimetric Sensing Ensemble for Heparin. *J. Am. Chem. Soc.* **2002**, *124*, 9014−9015.

(607) Wright, A. T.; Zhong, Z.; Anslyn, E. V. A Functional Assay for Heparin in Serum Using a Designed Synthetic Receptor. *Angew. Chem., Int. Ed.* **2005**, *44*, 5679−5682.

(608) Sun, W.; Bandmann, H.; Schrader, T. A Fluorescent Polymeric Heparin Sensor. *Chem.−Eur. J.* **2007**, *13*, 7701−7707.

(609) Wu, X.; Lin, L.-R.; Huang, Y.-J.; Li, Z.; Jiang, Y.-B. A 2:2 Stilbeneboronic Acid-Γ-Cyclodextrin Fluorescent Ensemble Highly Selective for Glucose in Aqueous Solutions. *Chem. Commun.* **2012**, *48*, 4362−4364.

(610) Shimpuku, C.; Ozawa, R.; Sasaki, A.; Sato, F.; Hashimoto, T.; Yamauchi, A.; Suzuki, I.; Hayashita, T. Selective Glucose Recognition by Boronic Acid Azoprobe/Γ-Cyclodextrin Complexes in Water. *Chem. Commun.* **2009**, 1709−1711.

(611) Hashimoto, T.; Kumai, M.; Maeda, M.; Miyoshi, K.; Tsuchido, Y.; Fujiwara, S.; Hayashita, T. Structural Effect of Fluorophore on Phenylboronic Acid Fluorophore/Cyclodextrin Complex for Selective Glucose Recognition. *Front. Chem. Sci. Eng.* **2020**, *14*, 53−60.

(612) Kumai, M.; Kozuka, S.; Samizo, M.; Hashimoto, T.; Suzuki, I.; Hayashita, T. Glucose Recognition by a Supramolecular Complex of Boronic Acid Fluorophore with Boronic Acid-Modified Cyclodextrin in Water. *Anal. Sci.* **2012**, *28*, 121−121.

(613) Tong, A.-J.; Yamauchi, A.; Hayashita, T.; Zhang, Z.-Y.; Smith, B. D.; Teramae, N. Boronic Acid Fluorophore/Β-Cyclodextrin Complex Sensors for Selective Sugar Recognition in Water. *Anal. Chem.* **2001**, *73*, 1530−1536.

(614) Liu, Y.; Deng, C.; Tang, L.; Qin, A.; Hu, R.; Sun, J. Z.; Tang, B. Z. Specific Detection of D-Glucose by a Tetraphenylethene-Based Fluorescent Sensor. *J. Am. Chem. Soc.* **2011**, *133*, 660−663.

(615) Hansen, J. S.; Ficker, M.; Petersen, J. F.; Christensen, J. B.; Hoeg-Jensen, T. Ortho-Substituted Fluorescent Aryl Monoboronic Acid Displays Physiological Binding of D-Glucose. *Tetrahedron Lett.* **2013**, *54*, 1849−1852.

(616) Hansen, J. S.; Petersen, J. F.; Hoeg-Jensen, T.; Christensen, J. B. Buffer and Sugar Concentration Dependent Fluorescence Response of a Bodipy-Based Aryl Monoboronic Acid Sensor. *Tetrahedron Lett.* **2012**, *53*, 5852−5855.

(617) Zhai, J.; Pan, T.; Zhu, J.; Xu, Y.; Chen, J.; Xie, Y.; Qin, Y. Boronic Acid Functionalized Boron Dipyrromethene Fluorescent Probes: Preparation, Characterization, and Saccharides Sensing Applications. *Anal. Chem.* **2012**, *84*, 10214−10220.

(618) Liu, Y.; Zhu, J.; Xu, Y.; Qin, Y.; Jiang, D. Boronic Acid Functionalized Aza-Bodipy (Azabdpba) Based Fluorescence Optodes for the Analysis of Glucose in Whole Blood. *ACS Appl. Mater. Interfaces* **2015**, *7*, 11141−11145.

(619) Huang, Y. J.; Ouyang, W. J.; Wu, X.; Li, Z.; Fossey, J. S.; James, T. D.; Jiang, Y. B. Glucose Sensing Via Aggregation and the Use of "Knock-out" Binding to Improve Selectivity. *J. Am. Chem. Soc.* **2013**, *135*, 1700−1703.

(620) Liang, X.; Trentle, M.; Kozlovskaya, V.; Kharlampieva, E.; Bonizzoni, M. Carbohydrate Sensing Using Water-Soluble Poly(Methacrylic Acid)-Co-3-(Acrylamido)Phenylboronic Acid Copolymer. *ACS Appl. Polym. Mater.* **2019**, *1*, 1341−1349.

(621) Elsherif, M.; Hassan, M. U.; Yetisen, A. K.; Butt, H. Glucose Sensing with Phenylboronic Acid Functionalized Hydrogel-Based Optical Diffusers. *ACS Nano* **2018**, *12*, 2283−2291.

(622) Arimori, S.; Frimat, K. A.; James, T. D.; Bell, M. L.; Oh, C. S. Modular Fluorescence Sensors for Saccharides. *Chem. Commun.* **2001**, 1836−1837.

(623) Kobayashi, K.; Asakawa, Y.; Kato, Y.; Aoyama, Y. Complexation of Hydrophobic Sugars and Nucleosides in Water with Tetrasulfonate Derivatives of Resorcinol Cyclic Tetramer Having a Polyhydroxy Aromatic Cavity: Importance of Guest-Host Ch-Π Interaction. *J. Am. Chem. Soc.* **1992**, *114*, 10307−10313.

(624) Rios, P.; Carter, T. S.; Mooibroek, T. J.; Crump, M. P.; Lisbjerg, M.; Pittelkow, M.; Supekar, N. T.; Boons, G.-J.; Davis, A. P. Synthetic Receptors for the High-Affinity Recognition of O-Glcnac Derivatives. *Angew. Chem., Int. Ed.* **2016**, *55*, 3387−3392.

(625) Davis, A. P. Synthetic Lectins. *Org. Biomol. Chem.* **2009**, *7*, 3629−3638.

(626) Kubik, S. Synthetic Lectins. *Angew. Chem., Int. Ed.* **2009**, *48*, 1722−1725.

(627) Klein, E.; Crump, M. P.; Davis, A. P. Carbohydrate Recognition in Water by a Tricyclic Polyamide Receptor. *Angew. Chem., Int. Ed.* **2005**, *44*, 298−302.

(628) Ferrand, Y.; Klein, E.; Barwell, N. P.; Crump, M. P.; Jiménez-Barbero, J.; Vicent, C.; Boons, G.-J.; Ingale, S.; Davis, A. P. A Synthetic Lectin for O-Linked Β-N-Acetylglucosamine. *Angew. Chem., Int. Ed.* **2009**, *48*, 1775−1779.

(629) Tromans, R. A.; Carter, T. S.; Chabanne, L.; Crump, M. P.; Li, H.; Matlock, J. V.; Orchard, M. G.; Davis, A. P. A Biomimetic Receptor for Glucose. *Nat. Chem.* **2019**, *11*, 52−56.

(630) Tromans, R. A.; Samanta, S. K.; Chapman, A. M.; Davis, A. P. Selective Glucose Sensing in Complex Media Using a Biomimetic Receptor. *Chem. Sci.* **2020**, *11*, 3223−3227.

(631) Bromfield, S. M.; Barnard, A.; Posocco, P.; Fermeglia, M.; Pricl, S.; Smith, D. K. Mallard Blue: A High-Affinity Selective Heparin Sensor That Operates in Highly Competitive Media. *J. Am. Chem. Soc.* **2013**, *135*, 2911−2914.

(632) Jana, P.; Radhakrishna, M.; Khatua, S.; Kanvah, S. A "Turn-Off" Red-Emitting Fluorophore for Nanomolar Detection of Heparin. *Phys. Chem. Chem. Phys.* **2018**, *20*, 13263−13270.

(633) Jayeoye, T. J.; Cheewasedtham, W.; Putson, C.; Rujiralai, T. A Selective Probe Based on 3-Aminophenyl Boronic Acid Assembly on Dithiobis(Succinimidylpropionate) Functionalized Gold Nanoparticles for Sialic Acid Detection in Human Serum. *J. Mol. Liq.* **2019**, *281*, 407−414.

(634) Zhang, L.; Zhang, Z. Y.; Liang, R. P.; Li, Y. H.; Qiu, J. D. Boron-Doped Graphene Quantum Dots for Selective Glucose Sensing Based on the "Abnormal" Aggregation-Induced Photoluminescence Enhancement. *Anal. Chem.* **2014**, *86*, 4423−4430.

(635) Chung, S.; Revia, R. A.; Zhang, M. Graphene Quantum Dots and Their Applications in Bioimaging, Biosensing, and Therapy. *Adv. Mater.* **2021**, 33, No. 1904362.

(636) Zou, W.-S.; Ye, C.-H.; Wang, Y.-Q.; Li, W.-H.; Huang, X.-H. A Hybrid Ratiometric Probe for Glucose Detection Based on Synchronous Responses to Fluorescence Quenching and Resonance Light Scattering Enhancement of Boronic Acid Functionalized Carbon Dots. *Sens. Actuators, B* **2018**, *271*, 54−63.

(637) Das, P.; Maity, P. P.; Ganguly, S.; Ghosh, S.; Baral, J.; Bose, M.; Choudhary, S.; Gangopadhyay, S.; Dhara, S.; Das, A. K.; Banerjee, S.; Das, N. C. Biocompatible Carbon Dots Derived from Kappa-Carrageenan and Phenyl Boronic Acid for Dual Modality Sensing Platform of Sugar and Its Anti-Diabetic Drug Release Behavior. *Int. J. Biol. Macromol.* **2019**, *132*, 316−329.

(638) Alizadeh, N.; Salimi, A.; Hallaj, R. A Strategy for Visual Optical Determination of Glucose Based on a Smartphone Device Using Fluorescent Boron-Doped Carbon Nanoparticles as a Light-up Probe. *Microchim. Acta* **2020**, *187*, 14.

(639) Wang, C.; Li, Y.; Wei, Y. A Sandwich Boronate Affinity Sorbent Assay for Glucose Detection Facilitated by Boronic Acid-Terminated Fluorescent Polymers. *Sens. Actuators, B* **2017**, *247*, 595−601.

(640) Gaballa, H.; Theato, P. Glucose-Responsive Polymeric Micelles Via Boronic Acid-Diol Complexation for Insulin Delivery at Neutral Ph. *Biomacromolecules* **2019**, *20*, 871−881.

(641) Jia, L. Y.; Liu, G. J.; Ji, Y. M.; Zhang, Y.; Xing, G. W. Assembly of Water-Soluble Sugar-Coated Aie-Active Fluorescent Organic Nanoparticles for the Detection of Ginsenosides Based on Carbohydrate-Carbohydrate Interactions. *ChemNanoMat* **2020**, *6*, 368−372.

(642) Lentner, C. *Geigy Scientific Tables, Physical Chemistry, Composition of Blood, Hematology, Somatometric Data* 8th ed.; Ciba Geigy, 1985; pp 1−241.

(643) Kawasaki, T.; Akanuma, H.; Yamanouchi, T. Increased Fructose Concentrations in Blood and Urine in Patients with Diabetes. *Diabetes Care* **2002**, *25*, 353.

(644) Bruen, D.; Delaney, C.; Florea, L.; Diamond, D. Glucose Sensing for Diabetes Monitoring: Recent Developments. *Sensors* **2017**, *17*, 1866.

(645) *Glucose Urine Test*; University of California San Francisco, 2018; https://www.ucsfhealth.org/medical-tests/glucose-urine-test (accessed 2021-01).

(646) Persiani, S.; Rotini, R.; Trisolino, G.; Rovati, L. C.; Locatelli, M.; Paganini, D.; Antonioli, D.; Roda, A. Synovial and Plasma Glucosamine Concentrations in Osteoarthritic Patients Following Oral Crystalline Glucosamine Sulphate at Therapeutic Dose. *Osteoarthr. Cartil.* **2007**, *15*, 764−772.

(647) Guo, K.; Li, L. Differential 12c-/13c-Isotope Dansylation Labeling and Fast Liquid Chromatography/Mass Spectrometry for Absolute and Relative Quantification of the Metabolome. *Anal. Chem.* **2009**, *81*, 3919−3932.

(648) Volpi, N.; Cusmano, M.; Venturelli, T. Qualitative and Quantitative Studies of Heparin and Chondroitin Sulfates in Normal Human Plasma. *Biochim. Biophys. Acta, Gen. Subj.* **1995**, *1243*, 49−58.

(649) Renlund, M. Clinical and Laboratory Diagnosis of Salla Disease in Infancy and Childhood. *J. Pediatr.* **1984**, *104*, 232−236.

(650) Illes, P.; Klotz, K. N.; Lohse, M. J. Signaling by Extracellular Nucleotides and Nucleosides. *Naunyn-Schmiedeberg's Arch. Pharmacol.* **2000**, *362*, 295−298.

(651) Bodin, P.; Burnstock, G. Purinergic Signalling: Atp Release. *Neurochem. Res.* **2001**, *26*, 959−969.

(652) Pietrocola, F.; Galluzzi, L.; Bravo-San Pedro, J. M.; Madeo, F.; Kroemer, G. Acetyl Coenzyme A: A Central Metabolite and Second Messenger. *Cell Metab.* **2015**, *21*, 805−821.

(653) Xiao, W.; Wang, R. S.; Handy, D. E.; Loscalzo, J. Nad(H) and Nadp(H) Redox Couples and Cellular Energy Metabolism. *Antioxid. Redox Signaling* **2018**, *28*, 251−272.

(654) Spada, F.; Schiffers, S.; Kirchner, A.; Zhang, Y.; Arista, G.; Kosmatchev, O.; Korytiakova, E.; Rahimoff, R.; Ebert, C.; Carell, T. Active Turnover of Genomic Methylcytosine in Pluripotent Cells. *Nat. Chem. Biol.* **2020**, *16*, 1411−1419.

(655) Xie, N.; Zhang, L.; Gao, W.; Huang, C.; Huber, P. E.; Zhou, X.; Li, C.; Shen, G.; Zou, B. Nad+ Metabolism: Pathophysiologic Mechanisms and Therapeutic Potential. *Signal Transduct. Target. Ther.* **2020**, *5*, 227.

(656) Nirody, J. A.; Budin, I.; Rangamani, P. Atp Synthase: Evolution, Energetics, and Membrane Interactions. *J. Gen. Physiol.* **2020**, *152*, No. e201912475.

(657) Seidel, A.; Brunner, S.; Seidel, P.; Fritz, G. I.; Herbarth, O. Modified Nucleosides: An Accurate Tumour Marker for Clinical Diagnosis of Cancer, Early Detection and Therapy Control. *Br. J. Cancer* **2006**, *94*, 1726−1733.

(658) He, L.; Wei, X.; Ma, X.; Yin, X.; Song, M.; Donninger, H.; Yaddanapudi, K.; McClain, C. J.; Zhang, X. Simultaneous Quantification of Nucleosides and Nucleotides from Biological Samples. *J. Am. Soc. Mass Spectrom.* **2019**, *30*, 987−1000.

(659) Nakano, K.; Nakao, T.; Schram, K. H.; Hammargren, W. M.; McClure, T. D.; Katz, M.; Petersen, E. Urinary Excretion of Modified Nucleosides as Biological Marker of Rna Turnover in Patients with Cancer and Aids. *Clin. Chim. Acta* **1993**, *218*, 169−183.

(660) Rasmuson, T.; Björk, G. R. Urinary Excretion of Pseudouridine and Prognosis of Patients with Malignant Lymphoma. *Acta Oncol.* **1995**, *34*, 61−67.

(661) Zheng, Y.-F.; Kong, H.-W.; Xiong, J.-H.; Lv, S.; Xu, G.-W. Clinical Significance and Prognostic Value of Urinary Nucleosides in Breast Cancer Patients. *Clin. Biochem.* **2005**, *38*, 24−30.

(662) Xu, G.; Schmid, H. R.; Lu, X.; Liebich, H. M.; Lu, P. Excretion Pattern Investigation of Urinary Normal and Modified Nucleosides of Breast Cancer Patients by Rp-Hplc and Factor Analysis Method. *Biomed. Chromatogr.* **2000**, *14*, 459−463.

(663) McEntire, J. E.; Kuo, K. C.; Smith, M. E.; Stalling, D. L.; Richens, J. W.; Zumwalt, R. W.; Gehrke, C. W.; Papermaster, B. W. Classification of Lung Cancer Patients and Controls by Chromatography of Modified Nucleosides in Serum. *Cancer Res.* **1989**, *49*, 1057.

(664) Koshida, K.; Harmenberg, J.; Borgström, E.; Wahren, B.; Andersson, L. Pseudouridine and Uridine in Normal Kidney and Kidney Cancer Tissues. *Urol. Res.* **1985**, *13*, 219−221.

(665) Yang, J.; Xu, G.; Zheng, Y.; Kong, H.; Pang, T.; Lv, S.; Yang, Q. Diagnosis of Liver Cancer Using Hplc-Based Metabonomics Avoiding False-Positive Result from Hepatitis and Hepatocirrhosis Diseases. *J. Chromatogr. B: Anal. Technol. Biomed. Life Sci.* **2004**, *813*, 59−65.

(666) Martinow, A. J.; Yuen, K.; Cooper, I. A.; Matthews, J. P.; Juneja, S.; Wolf, M.; Januszewicz, H.; Prince, H. M. Prognostic Markers of Disease Activity in Hodgkin's Disease. *Leuk. Lymphoma* **1998**, *29*, 383−389.

(667) Schwarzenbach, H.; Hoon, D. S. B.; Pantel, K. Cell-Free Nucleic Acids as Biomarkers in Cancer Patients. *Nat. Rev. Cancer* **2011**, *11*, 426−437.

(668) Daniel, C.; Leppkes, M.; Muñoz, L. E.; Schley, G.; Schett, G.; Herrmann, M. Extracellular DNA Traps in Inflammation, Injury and Healing. *Nat. Rev. Nephrol.* **2019**, *15*, 559−575.

(669) Elkon, K. B. Review: Cell Death, Nucleic Acids, and Immunity. *Arthritis Rheumatol.* **2018**, *70*, 805−816.

(670) Vlassov, V. V.; Laktionov, P. P.; Rykova, E. Y. Extracellular Nucleic Acids. *BioEssays* **2007**, *29*, 654−667.

(671) Ralla, B.; Stephan, C.; Meller, S.; Dietrich, D.; Kristiansen, G.; Jung, K. Nucleic Acid-Based Biomarkers in Body Fluids of Patients with Urologic Malignancies. *Crit. Rev. Clin. Lab. Sci.* **2014**, *51*, 200−231.

(672) Zorofchian, S.; Iqbal, F.; Rao, M.; Aung, P. P.; Esquenazi, Y.; Ballester, L. Y. Circulating Tumour DNA, Microrna and Metabolites in Cerebrospinal Fluid as Biomarkers for Central Nervous System Malignancies. *J. Clin. Pathol.* **2019**, *72*, 271−280.

(673) Chin, R.-I.; Chen, K.; Usmani, A.; Chua, C.; Harris, P. K.; Binkley, M. S.; Azad, T. D.; Dudley, J. C.; Chaudhuri, A. A. Detection of Solid Tumor Molecular Residual Disease (Mrd) Using Circulating Tumor DNA (Ctdna). *Mol. Diagn. Ther.* **2019**, *23*, 311−331.

(674) Zen, K.; Zhang, C.-Y. Circulating Micrornas: A Novel Class of Biomarkers to Diagnose and Monitor Human Cancers. *Med. Res. Rev.* **2012**, *32*, 326−348.

(675) Mitchell, P. S.; Parkin, R. K.; Kroh, E. M.; Fritz, B. R.; Wyman, S. K.; Pogosova-Agadjanyan, E. L.; Peterson, A.; Noteboom, J.; O'Briant, K. C.; Allen, A.; et al. Circulating Micrornas as Stable Blood-Based Markers for Cancer Detection. *Proc. Natl. Acad. Sci. U. S. A.* **2008**, *105*, 10513.

(676) Jordheim, L. P.; Durantel, D.; Zoulim, F.; Dumontet, C. Advances in the Development of Nucleoside and Nucleotide Analogues for Cancer and Viral Diseases. *Nat. Rev. Drug Discovery* **2013**, *12*, 447−464.

(677) Agrawal, S.; Jiang, Z.; Zhao, Q.; Shaw, D.; Cai, Q.; Roskey, A.; Channavajjala, L.; Saxinger, C.; Zhang, R. Mixed-Backbone Oligonucleotides as Second Generation Antisense Oligonucleotides: In Vitro and in Vivo Studies. *Proc. Natl. Acad. Sci. U. S. A.* **1997**, *94*, 2620−2625.

(678) Kilanowska, A.; Studzińska, S. In Vivo and in Vitro Studies of Antisense Oligonucleotides−a Review. *RSC Adv.* **2020**, *10*, 34501−34516.

(679) Nordhoff, E.; Cramer, R.; Karas, M.; Hillenkamp, F.; Kirpekar, F.; Kristiansen, K.; Roepstorff, P. Ion Stability of Nucleic Acids in Infrared Matrix-Assisted Laser Desorption/Ionization Mass Spectrometry. *Nucleic Acids Res.* **1993**, *21*, 3347−3357.

(680) Zhou, W.; Saran, R.; Liu, J. Metal Sensing by DNA. *Chem. Rev.* **2017**, *117*, 8272−8325.

(681) Morciano, G.; Sarti, A. C.; Marchi, S.; Missiroli, S.; Falzoni, S.; Raffaghello, L.; Pistoia, V.; Giorgi, C.; Di Virgilio, F.; Pinton, P. Use of Luciferase Probes to Measure Atp in Living Cells and Animals. *Nat. Protoc.* **2017**, *12*, 1542−1562.

(682) Chamchoy, K.; Pakotiprapha, D.; Pumirat, P.; Leartsakulpanich, U.; Boonyuen, U. Application of Wst-8 Based Colorimetric Nad(P)H Detection for Quantitative Dehydrogenase Assays. *BMC Biochem.* **2019**, *20*, 4.

(683) Jun, Y. W.; Sarkar, S.; Kim, K. H.; Ahn, K. H. Molecular Probes for Fluorescence Imaging of Atp in Cells and Tissues. *ChemPhotoChem.* **2019**, *3*, 214−219.

(684) Chi, W.; Qi, Q.; Lee, R.; Xu, Z.; Liu, X. A Unified Push-Pull Model for Understanding the Ring-Opening Mechanism of Rhodamine Dyes. *J. Phys. Chem. C* **2020**, *124*, 3793−3801.

(685) Tang, J. L.; Li, C. Y.; Li, Y. F.; Zou, C. X. A Ratiometric Fluorescent Probe with Unexpected High Selectivity for Atp and Its Application in Cell Imaging. *Chem. Commun.* **2014**, *50*, 15411−15414.

(686) Tan, K. Y.; Li, C. Y.; Li, Y. F.; Fei, J.; Yang, B.; Fu, Y. J.; Li, F. Real-Time Monitoring Atp in Mitochondrion of Living Cells: A Specific Fluorescent Probe for Atp by Dual Recognition Sites. *Anal. Chem.* **2017**, *89*, 1749−1756.

(687) Fang, Y.; Shi, W.; Hu, Y.; Li, X.; Ma, H. A Dual-Function Fluorescent Probe for Monitoring the Degrees of Hypoxia in Living Cells: Via the Imaging of Nitroreductase and Adenosine Triphosphate. *Chem. Commun.* **2018**, *54*, 5454−5457.

(688) Tikum, A. F.; Kim, G.; Nasirian, A.; Ko, J. W.; Yoon, J.; Kim, J. Rhodamine-Based near-Infrared Probe for Emission Detection of Atp in Lysosomes in Living Cells. *Sens. Actuators, B* **2019**, *292*, 40−47.

(689) Wu, Z.; Liu, M.; Liu, Z.; Tian, Y. Real-Time Imaging and Simultaneous Quantification of Mitochondrial H2o2and Atp in Neurons with a Single Two-Photon Fluorescence-Lifetime-Based Probe. *J. Am. Chem. Soc.* **2020**, *142*, 7532−7541.

(690) Ren, T. B.; Wen, S. Y.; Wang, L.; Lu, P.; Xiong, B.; Yuan, L.; Zhang, X. B. Engineering a Reversible Fluorescent Probe for Real-Time Live-Cell Imaging and Quantification of Mitochondrial Atp. *Anal. Chem.* **2020**, *92*, 4681−4688.

(691) Wang, L.; Yuan, L.; Zeng, X.; Peng, J.; Ni, Y.; Er, J. C.; Xu, W.; Agrawalla, B. K.; Su, D.; Kim, B.; Chang, Y.-T. A Multisite-Binding Switchable Fluorescent Probe for Monitoring Mitochondrial Atp Level Fluctuation in Live Cells. *Angew. Chem., Int. Ed.* **2016**, *55*, 1773−1776.

(692) Fenniri, H.; Hosseini, M. W.; Lehn, J. M. Molecular Recognition of Nadp(H) and Atp by Macrocyclic Polyamines Bearing Acridine Groups. *Helv. Chim. Acta* **1997**, *80*, 786−803.

(693) Padilla-Tosta, M. E.; Lloris, J. M.; Martínez-Máñez, R.; Pardo, T.; Sancenón, F.; Soto, J.; Marcos, M. D. Atp Recognition through a Fluorescence Change in a Multicomponent Dinuclear System Containing a Ru(Tpy)22+ Fluorescent Core and a Cyclam-Cu2+ Complex. *Eur. J. Inorg. Chem.* **2001**, *2001*, 1221−1226.

(694) Irvin, J. L.; Irvin, E. M. The Interaction of Quinacrine with Adenine Nucleotides. *J. Biol. Chem.* **1954**, *210*, 45−56.

(695) Forveille, S.; Humeau, J.; Sauvat, A.; Bezu, L.; Kroemer, G.; Kepp, O. *Quinacrine-Mediated Detection of Intracellular ATP*; Elsevier, 2019; pp 103−113.

(696) Farshbaf, S.; Anzenbacher, P. Fluorimetric Sensing of Atp in Water by an Imidazolium Hydrazone Based Sensor. *Chem. Commun.* **2019**, *55*, 1770−1773.

(697) Cheng, H.-B.; Sun, Z.; Kwon, N.; Wang, R.; Cui, Y.; Park, C. O.; Yoon, J. A Self-Assembled Atp Probe for Melanoma Cell Imaging. *Chem.−Eur. J.* **2019**, *25*, 3501−3504.

(698) Shuvaev, S.; Fox, M. A.; Parker, D. Monitoring of the Adp/Atp Ratio by Induced Circularly Polarised Europium Luminescence. *Angew. Chem., Int. Ed.* **2018**, *57*, 7488−7492.

(699) He, Y.; Lopez, A.; Zhang, Z.; Chen, D.; Yang, R.; Liu, J. Nucleotide and DNA Coordinated Lanthanides: From Fundamentals to Applications. *Coord. Chem. Rev.* **2019**, *387*, 235−248.

(700) Zhang, Z.; Morishita, K.; Lin, W. T. D.; Huang, P.-J. J.; Liu, J. Nucleotide Coordination with 14 Lanthanides Studied by Isothermal Titration Calorimetry. *Chin. Chem. Lett.* **2018**, *29*, 151−156.

(701) Kitagawa, Y.; Tsurui, M.; Hasegawa, Y. Steric and Electronic Control of Chiral Eu(Iii) Complexes for Effective Circularly Polarized Luminescence. *ACS Omega* **2020**, *5*, 3786−3791.

(702) Marcotte, N.; Taglietti, A. Transition-Metal-Based Chemosensing Ensembles: Atp Sensing in Physiological Conditions. *Supramol. Chem.* **2003**, *15*, 617−625.

(703) Singh, V. R.; Singh, P. K. A Supramolecule Based Fluorescence Turn-on and Ratiometric Sensor for Atp in Aqueous Solution. *J. Mater. Chem. B* **2020**, *8*, 1182−1190.

(704) Kanagaraj, K.; Xiao, C.; Rao, M.; Fan, C.; Borovkov, V.; Cheng, G.; Zhou, D.; Zhong, Z.; Su, D.; Yu, X.; Yao, J.; Hao, T.; Wu, W.; Chruma, J. J.; Yang, C. A Quinoline-Appended Cyclodextrin Derivative as a Highly Selective Receptor and Colorimetric Probe for Nucleotides. *iScience* **2020**, *23*, 100927−100927.

(705) Formoso, C. The Interaction of B-Cyclodextrin with Nucleic Acid Monomer Units. *Biochem. Biophys. Res. Commun.* **1973**, *50*, 999−1005.

(706) Formoso, C. The Interaction of B-Cyclodextrin with Dinucleoside Phosphates. *Biopolymers* **1974**, *13*, 909−917.

(707) Hargrove, A. E.; Nieto, S.; Zhang, T.; Sessler, J. L.; Anslyn, E. V. Artificial Receptors for the Recognition of Phosphorylated Molecules. *Chem. Rev.* **2011**, *111*, 6603−6782.

(708) Sigwalt, D.; Zavalij, P. Y.; Isaacs, L. Cationic Acyclic Cucurbit[N]Uril-Type Containers: Synthesis and Molecular Recognition toward Nucleotides. *Supramol. Chem.* **2016**, *28*, 825−834.

(709) Bazzicalupi, C.; Bencini, A.; Biagini, S.; Faggi, E.; Meini, S.; Giorgi, C.; Spepi, A.; Valtancoli, B. Exploring the Binding Ability of Phenanthroline-Based Polyammonium Receptors for Anions: Hints for Design of Selective Chemosensors for Nucleotides. *J. Org. Chem.* **2009**, *74*, 7349−7363.

(710) Moreno-Corral, R.; Lara, K. O. Complexation Studies of Nucleotides by Tetrandrine Derivatives Bearing Anthraquinone and Acridine Groups. *Supramol. Chem.* **2008**, *20*, 427−435.

(711) Abe, H.; Mawatari, Y.; Teraoka, H.; Fujimoto, K.; Inouye, M. Synthesis and Molecular Recognition of Pyrenophanes with Polycationic or Amphiphilic Functionalities: Artificial Plate-Shaped Cavitant Incorporating Arenes and Nucleotides in Water. *J. Org. Chem.* **2004**, *69*, 495−504.

(712) Bazany-Rodríguez, I. J.; Salomón-Flores, M. K.; Bautista-Renedo, J. M.; González-Rivas, N.; Dorazco-González, A. Chemosensing of Guanosine Triphosphate Based on a Fluorescent Dinuclear Zn(Ii)-Dipicolylamine Complex in Water. *Inorg. Chem.* **2020**, *59*, 7739−7751.

(713) Ojida, A.; Takashima, I.; Kohira, T.; Nonaka, H.; Hamachi, I. Turn-on Fluorescence Sensing of Nucleoside Polyphosphates Using a Xanthene-Based Zn(Ii) Complex Chemosensor. *J. Am. Chem. Soc.* **2008**, *130*, 12095−12101.

(714) Sakamoto, T.; Ojida, A.; Hamachi, I. Molecular Recognition, Fluorescence Sensing, and Biological Assay of Phosphate Anion Derivatives Using Artificial Zn(Ii)-Dpa Complexes. *Chem. Commun.* **2009**, 141−152.

(715) Neelakandan, P. P.; Hariharan, M.; Ramaiah, D. A Supramolecular on-Off-on Fluorescence Assay for Selective Recognition of Gtp. *J. Am. Chem. Soc.* **2006**, *128*, 11334−11335.

(716) Hewitt, S. H.; Macey, G.; Mailhot, R.; Elsegood, M. R. J.; Duarte, F.; Kenwright, A. M.; Butler, S. J. Tuning the Anion Binding Properties of Lanthanide Receptors to Discriminate Nucleoside Phosphates in a Sensing Array. *Chem. Sci.* **2020**, *11*, 3619−3628.

(717) Nairin, R. S.; Dodson, M. L.; Humphrey, R. M. Comparison of Ethidium Bromide and 4′,6-Diamidino-2-Phenylindole as Quantitative Fluorescent Stains for DNA in Agarose Gels. *J. Biochem. Biophys. Methods* **1982**, *6*, 95−103.

(718) Kapuscinski, J. Dapi: A DNA-Specific Fluorescent Probe. *Biotech. Histochem.* **1995**, *70*, 220−233.

(719) Ihmels, H.; Otto, D. *Supermolecular Dye Chemistry*; Springer: Berlin, Heidelberg, 2005; pp 161−204.

(720) Dougherty, G.; Pilbrow, J. R. Physico-Chemical Probes of Intercalation. *Int. J. Biochem.* **1984**, *16*, 1179−1192.

(721) Bucevicius, J.; Lukinavicius, G.; Gerasimaite, R. The Use of Hoechst Dyes for DNA Staining and Beyond. *Chemosensors* **2018**, *6*, 18.

(722) Verma, A.; Halder, K.; Halder, R.; Yadav, V. K.; Rawal, P.; Thakur, R. K.; Mohd, F.; Sharma, A.; Chowdhury, S. Genome-Wide Computational and Expression Analyses Reveal G-Quadruplex DNA Motifs as Conserved Cis-Regulatory Elements in Human and Related Species. *J. Med. Chem.* **2008**, *51*, 5641−5649.

(723) Hänsel-Hertsch, R.; Di Antonio, M.; Balasubramanian, S. DNA G-Quadruplexes in the Human Genome: Detection, Functions

and Therapeutic Potential. *Nat. Rev. Mol. Cell Biol.* **2017**, *18*, 279−284.

(724) Biffi, G.; Tannahill, D.; McCafferty, J.; Balasubramanian, S. Quantitative Visualization of DNA G-Quadruplex Structures in Human Cells. *Nat. Chem.* **2013**, *5*, 182−186.

(725) Kim, N. The Interplay between G-Quadruplex and Transcription. *Curr. Med. Chem.* **2019**, *26*, 2898−2917.

(726) Spiegel, J.; Adhikari, S.; Balasubramanian, S. The Structure and Function of DNA G-Quadruplexes. *Trends Chem.* **2020**, *2*, 123−136.

(727) Xie, X.; Reznichenko, O.; Chaput, L.; Martin, P.; Teulade-Fichou, M. P.; Granzhan, A. Topology-Selective, Fluorescent "Light-up" Probes for G-Quadruplex DNA Based on Photoinduced Electron Transfer. *Chem.−Eur. J.* **2018**, *24*, 12638−12651.

(728) Kikuchi, N.; Reed, A.; Gerasimova, Y. V.; Kolpashchikov, D. M. Split Dapoxyl Aptamer for Sequence-Selective Analysis of Nucleic Acid Sequence Based Amplification Amplicons. *Anal. Chem.* **2019**, *91*, 2667−2671.

(729) Mohanty, J.; Barooah, N.; Dhamodharan, V.; Harikrishna, S.; Pradeepkumar, P. I.; Bhasikuttan, A. C. Thioflavin T as an Efficient Inducer and Selective Fluorescent Sensor for the Human Telomeric G-Quadruplex DNA. *J. Am. Chem. Soc.* **2013**, *135*, 367−376.

(730) Gao, Y.; He, Z.; He, X.; Zhang, H.; Weng, J.; Yang, X.; Meng, F.; Luo, L.; Tang, B. Z. Dual-Color Emissive Aiegen for Specific and Label-Free Double-Stranded DNA Recognition and Single-Nucleotide Polymorphisms Detection. *J. Am. Chem. Soc.* **2019**, *141*, 20097−20106.

(731) Zhang, S.; Assaf, K. I.; Huang, C.; Hennig, A.; Nau, W. M. Ratiometric DNA Sensing with a Host-Guest Fret Pair. *Chem. Commun.* **2019**, *55*, 671−674.

(732) Berdnikova, D. V.; Chernikova, E. Curcubiturils in Nucleic Acids Research. *Chem. Commun.* **2020**, *56*, 15360−15376.

(733) Moro, A. J.; Schmidt, J.; Doussineau, T.; Lapresta-Fernandéz, A.; Wegener, J.; Mohr, G. J. Surface-Functionalized Fluorescent Silica Nanoparticles for the Detection of Atp. *Chem. Commun.* **2011**, *47*, 6066−6068.

(734) Moro, A. J.; Cywinski, P. J.; Körsten, S.; Mohr, G. J. An Atp Fluorescent Chemosensor Based on a Zn(Ii)-Complexed Dipicolylamine Receptor Coupled with a Naphthalimide Chromophore. *Chem. Commun.* **2010**, *46*, 1085−1087.

(735) Banerjee, S.; Bhuyan, M.; Konig, B. Tb(Iii) Functionalized Vesicles for Phosphate Sensing: Membrane Fluidity Controls the Sensitivity. *Chem. Commun.* **2013**, *49*, 5681−5683.

(736) Plajer, A. J.; Percástegui, E. G.; Santella, M.; Rizzuto, F. J.; Gan, Q.; Laursen, B. W.; Nitschke, J. R. Fluorometric Recognition of Nucleotides within a Water-Soluble Tetrahedral Capsule. *Angew. Chem., Int. Ed.* **2019**, *58*, 4200−4204.

(737) Zhou, Y.; Tang, L.; Zeng, G.; Zhang, C.; Zhang, Y.; Xie, X. Current Progress in Biosensors for Heavy Metal Ions Based on Dnazymes/DNA Molecules Functionalized Nanostructures: A Review. *Sens. Actuators, B* **2016**, *223*, 280−294.

(738) Torabi, S.-F.; Lu, Y. Functional DNA Nanomaterials for Sensing and Imaging in Living Cells. *Curr. Opin. Biotechnol.* **2014**, *28*, 88−95.

(739) Pehlivan, Z. S.; Torabfam, M.; Kurt, H.; Ow-Yang, C.; Hildebrandt, N.; Yüce, M. Aptamer and Nanomaterial Based Fret Biosensors: A Review on Recent Advances (2014-2019). *Microchim. Acta* **2019**, *186*, 563.

(740) Lu, C.-H.; Willner, B.; Willner, I. DNA Nanotechnology: From Sensing and DNA Machines to Drug-Delivery Systems. *ACS Nano* **2013**, *7*, 8320−8332.

(741) Traut, T. W. Physiological Concentrations of Purines and Pyrimidines. *Mol. Cell. Biochem.* **1994**, *140*, 1−22.

(742) Kochańska, B.; Smoleński, R. T.; Knap, N. Determination of Adenine Nucleotides and Their Metabolites in Human Saliva. *Acta Biochim. Polym.* **2000**, *47*, 877−879.

(743) Mirtavoos-Mahyari, H.; Ghafouri-Fard, S.; Khosravi, A.; Motevaseli, E.; Esfahani-Monfared, Z.; Seifi, S.; Salimi, B.; Oskooei, V. K.; Ghadami, M.; Modarressi, M. H. Circulating Free DNA Concentration as a Marker of Disease Recurrence and Metastatic Potential in Lung Cancer. *Clin. Transl. Med.* **2019**, *8*, e14.

(744) Czarnecka, J.; Cieślak, M.; Michał, K. Application of Solid Phase Extraction and High-Performance Liquid Chromatography to Qualitative and Quantitative Analysis of Nucleotides and Nucleosides in Human Cerebrospinal Fluid. *J. Chromatogr. B: Anal. Technol. Biomed. Life Sci.* **2005**, *822*, 85−90.

(745) Martínez-Reyes, I.; Chandel, N. S. Mitochondrial Tca Cycle Metabolites Control Physiology and Disease. *Nat. Commun.* **2020**, *11*, 102.

(746) Mastrangelo, D.; Pelosi, E.; Castelli, G.; Lo-Coco, F.; Testa, U. Mechanisms of Anti-Cancer Effects of Ascorbate: Cytotoxic Activity and Epigenetic Modulation. *Blood Cells, Mol., Dis.* **2018**, *69*, 57−64.

(747) Macknight, R. C.; Laing, W. A.; Bulley, S. M.; Broad, R. C.; Johnson, A. A. T.; Hellens, R. P. Increasing Ascorbate Levels in Crops to Enhance Human Nutrition and Plant Abiotic Stress Tolerance. *Curr. Opin. Biotechnol.* **2017**, *44*, 153−160.

(748) Mandl, J.; Szarka, A.; Bánhegyi, G. Vitamin C: Update on Physiology and Pharmacology. *Br. J. Pharmacol.* **2009**, *157*, 1097−1110.

(749) McGregor, G. P.; Biesalski, H. K. Rationale and Impact of Vitamin C in Clinical Nutrition. *Curr. Opin. Clin. Nutr. Metab. Care* **2006**, *9*, 697.

(750) Jacob, R. A.; Sotoudeh, G. Vitamin C Function and Status in Chronic Disease. *Nutrition in Clinical Care* **2002**, *5*, 66−74.

(751) Costello, L. C.; Franklin, R. B. The Intermediary Metabolism of the Prostate: A Key to Understanding the Pathogenesis and Progression of Prostate Malignancy. *Oncology* **2000**, *59*, 269−282.

(752) Costello, L. C.; Franklin, R. B. Citrate Metabolism of Normal and Malignant Prostate Epithelial Cells. *Urology* **1997**, *50*, 3−12.

(753) Costello, L. C.; Franklin, R. B. Effect of Prolactin on the Prostate. *Prostate* **1994**, *24*, 162−166.

(754) Costello, L. C.; Franklin, R. B. Concepts of Citrate Production and Secretion by Prostate: 2. Hormonal Relationships in Normal and Neoplastic Prostate. *Prostate* **1991**, *19*, 181−205.

(755) Costello, L. C.; Franklin, R. B. Concepts of Citrate Production and Secretion by Prostate. 1. Metabolic Relationships. *Prostate* **1991**, *18*, 25−46.

(756) Cooper, J. F.; Farid, I. The Role of Citric Acid in the Physiology of the Prostate: Lactate/Citrate Ratios in Benign and Malignant Prostatic Homogenates as an Index of Prostatic Malignancy. *J. Urol.* **1964**, *92*, 533−536.

(757) Cooper, J. F.; Farid, I. The Role of Citric Acid in the Physiology of the Prostate. A Chromatographic Study of Citric Acid Cycle Intermediates in Benign and Malignant Prostatic Tissue. *J. Surg. Res.* **1963**, *3*, 112−121.

(758) Costello, L. C.; Franklin, R. B. Novel Role of Zinc in the Regulation of Prostate Citrate Metabolism and Its Implications in Prostate Cancer. *Prostate* **1998**, *35*, 285−296.

(759) Goodwin, M. L.; Harris, J. E.; Hernández, A.; Gladden, L. B. Blood Lactate Measurements and Analysis During Exercise: A Guide for Clinicians. *J. Diabetes Sci. Technol.* **2007**, *1*, 558−569.

(760) Dezman, Z. D. W.; Comer, A. C.; Smith, G. S.; Narayan, M.; Scalea, T. M.; Hirshon, J. M. Failure to Clear Elevated Lactate Predicts 24-Hour Mortality in Trauma Patients. *J. Trauma Acute Care Surg.* **2015**, *79*, 580−585.

(761) Doshi, P. B.; Park, A. Y.; Banuelos, R. C.; Akkanti, B. H.; Darger, B. F.; Macaluso, A.; Thangam, M.; Chambers, K. A. The Incidence and Outcome Differences in Severe Sepsis with and without Lactic Acidosis. *J. Emerg. Trauma Shock* **2018**, *11*, 165.

(762) Ceglarek, U.; Schellong, P.; Rosolowski, M.; Scholz, M.; Willenberg, A.; Kratzsch, J.; Zeymer, U.; Fuernau, G.; de Waha-Thiele, S.; Büttner, P.; Jobs, A.; Freund, A.; Desch, S.; Feistritzer, H.-J.; Isermann, B.; Thiery, J.; Pöss, J.; Thiele, H. The Novel Cystatin C, Lactate, Interleukin-6, and N-Terminal Pro-B-Type Natriuretic Peptide (Clip)-Based Mortality Risk Score in Cardiogenic Shock after Acute Myocardial Infarction. *Eur. Heart J.* **2021**, *42*, 2344−2352.

(763) Sakai, T.; Takadate, A.; Otagiri, M. Characterization of Binding Site of Uremic Toxins on Human Serum Albumin. *Biol. Pharm. Bull.* **1995**, *18*, 1755−1761.

(764) Spustová, V.; Dzúrik, R.; Geryková, M. Hippurate Participation in the Inhibition of Glucose Utilization in Renal Failure. *Czech Med.* **1987**, *10*, 79−89.

(765) Mutsaers, H. A. M.; Wilmer, M. J. G.; Reijnders, D.; Jansen, J.; van den Broek, P. H. H.; Forkink, M.; Schepers, E.; Glorieux, G.; Vanholder, R.; van den Heuvel, L. P.; Hoenderop, J. G.; Masereeuw, R. Uremic Toxins Inhibit Renal Metabolic Capacity through Interference with Glucuronidation and Mitochondrial Respiration. *Biochim. Biophys. Acta, Mol. Basis Dis.* **2013**, *1832*, 142−150.

(766) Barshop, B. A.; Breuer, J.; Holm, J.; Leslie, J.; Nyhan, W. L. Excretion of Hippuric Acid During Sodium Benzoate Therapy in Patients with Hyperglycinaemia or Hyperammonaemia. *J. Inherited Metab. Dis.* **1989**, *12*, 72−79.

(767) Yu, T.-H.; Tang, W.-H.; Lu, Y.-C.; Wang, C.-P.; Hung, W.-C.; Wu, C.-C.; Tsai, I. T.; Chung, F.-M.; Houng, J.-Y.; Lan, W.-C.; Lee, Y.-J. Association between Hippuric Acid and Left Ventricular Hypertrophy in Maintenance Hemodialysis Patients. *Clin. Chim. Acta* **2018**, *484*, 47−51.

(768) Kolodziejczyk, J.; Saluk-Juszczak, J.; Wachowicz, B. In Vitro Study of the Antioxidative Properties of the Glucose Derivatives against Oxidation of Plasma Components. *J. Physiol. Biochem.* **2011**, *67*, 175−183.

(769) Hu, Z. P.; Browne, E. R.; Liu, T.; Angel, T. E.; Ho, P. C.; Chan, E. C. Metabonomic Profiling of Tastpm Transgenic Alzheimer's Disease Mouse Model. *J. Proteome Res.* **2012**, *11*, 5903−5913.

(770) Orešič, M.; Hyötyläinen, T.; Herukka, S. K.; Sysi-Aho, M.; Mattila, I.; Seppänan-Laakso, T.; Julkunen, V.; Gopalacharyulu, P. V.; Hallikainen, M.; Koikkalainen, J.; Kivipelto, M.; Helisalmi, S.; Lötjönen, J.; Soininen, H. Metabolome in Progression to Alzheimer's Disease. *Transl. Psychiatry* **2011**, *1*, No. e57.

(771) Kane, R. C. Intravenous Iron Replacement with Sodium Ferric Gluconate Complex in Sucrose for Iron Deficiency Anemia in Adults. *Curr. Ther. Res.* **2003**, *64*, 263−268.

(772) Warady, B. A.; Zobrist, R. H.; Wu, J.; Finan, E. Sodium Ferric Gluconate Complex Therapy in Anemic Children on Hemodialysis. *Pediatr. Nephrol.* **2005**, *20*, 1320−1327.

(773) Mycielska, M. E.; Mohr, M. T. J.; Schmidt, K.; Drexler, K.; Rümmele, P.; Haferkamp, S.; Schlitt, H. J.; Gaumann, A.; Adamski, J.; Geissler, E. K. Potential Use of Gluconate in Cancer Therapy. *Front. Oncol.* **2019**, *9*, 522.

(774) Schrör, K. Aspirin and Reye Syndrome. *Pediatric Drugs* **2007**, *9*, 195−204.

(775) Partin, J.; Schubert, W.; Partin, J.; Hammond, J. Serum Salicylate Concentrations in ReyèS Disease: A Study of 130 Biopsy-Proven Cases. *Lancet* **1982**, *319*, 191−194.

(776) Needs, C. J.; Brooks, P. M. Clinical Pharmacokinetics of the Salicylates. *Clin. Pharmacokinet.* **1985**, *10*, 164−177.

(777) Brotzel, F.; Mayr, H. Nucleophilicities of Amino Acids and Peptides. *Org. Biomol. Chem.* **2007**, *5*, 3814−3820.

(778) Schaller, H. F.; Tishkov, A. A.; Feng, X.; Mayr, H. Direct Observation of the Ionization Step in Solvolysis Reactions: Electrophilicity Versus Electrofugality of Carbocations. *J. Am. Chem. Soc.* **2008**, *130*, 3012−3022.

(779) Minegishi, S.; Mayr, H. How Constant Are Ritchie's "Constant Selectivity Relationships"? A General Reactivity Scale for N-, Π-, and Σ-Nucleophiles. *J. Am. Chem. Soc.* **2003**, *125*, 286−295.

(780) Mayer, R. J.; Ofial, A. R. Nucleophilicity of Glutathione: A Link to Michael Acceptor Reactivities. *Angew. Chem., Int. Ed.* **2019**, *58*, 17704−17708.

(781) Brotzel, F.; Chu, Y. C.; Mayr, H. Nucleophilicities of Primary and Secondary Amines in Water. *J. Org. Chem.* **2007**, *72*, 3679−3688.

(782) Zhu, L.; Anslyn, E. V. Facile Quantification of Enantiomeric Excess and Concentration with Indicator-Displacement Assays: An Example in the Analyses of A-Hydroxyacids. *J. Am. Chem. Soc.* **2004**, *126*, 3676−3677.

(783) Zhao, J.; Fyles, T. M.; James, T. D. Chiral Binol-Bisboronic Acid as Fluorescence Sensor for Sugar Acids. *Angew. Chem., Int. Ed.* **2004**, *43*, 3461−3464.

(784) Hansen, J. S.; Hoeg-Jensen, T.; Christensen, J. B. Redemitting Bodipy Boronic Acid Fluorescent Sensors for Detection of Lactate. *Tetrahedron* **2017**, *73*, 3010−3013.

(785) Couet, W. R.; Brasch, R. C.; Sosnovsky, G.; Tozer, T. N. Factors Affecting Nitroxide Reduction in Ascorbate Solution and Tissue Homogenates. *Magn. Reson. Imaging* **1985**, *3*, 83−88.

(786) Paleos, C. M.; Dais, P. Ready Reduction of Some Nitroxide Free Radicals with Ascorbic Acid. *J. Chem. Soc., Chem. Commun.* **1977**, 345−346.

(787) Matsuoka, Y.; Ohkubo, K.; Yamasaki, T.; Yamato, M.; Ohtabu, H.; Shirouzu, T.; Fukuzumi, S.; Yamada, K.-I. A Profluorescent Nitroxide Probe for Ascorbic Acid Detection and Its Application to Quantitative Analysis of Diabetic Rat Plasma. *RSC Adv.* **2016**, *6*, 60907−60915.

(788) Nam, H.; Kwon, J. E.; Choi, M.-W.; Seo, J.; Shin, S.; Kim, S.; Park, S. Y. Highly Sensitive and Selective Fluorescent Probe for Ascorbic Acid with a Broad Detection Range through Dual-Quenching and Bimodal Action of Nitronyl-Nitroxide. *ACS Sens.* **2016**, *1*, 392−398.

(789) Yang, T.; Zheng, B.; Liang, H.; Wan, Y.; Du, J.; Xiao, D. A Sensitive and Selective Chemosensor for Ascorbic Acid Based on a Fluorescent Nitroxide Switch. *Talanta* **2015**, *132*, 191−196.

(790) Bao, B.; Tao, N.; Ma, M.; Zhang, L.; Yuwen, L.; Fan, Q.; Wang, L.; Huang, W. Fluorescence Turn-on Sensing of Ascorbic Acid Based on a Hyperbranched Conjugated Polyelectrolyte. *Soft Mater.* **2014**, *12*, 73−78.

(791) Peerannawar, S. R.; Gejji, S. P. Electronic Structure, Molecular Electrostatic Potential and Spectral Characteristics of Pillar[6]Arene Hosts and Their Complexes with N-Octyltriethylammonium Ions. *Phys. Chem. Chem. Phys.* **2012**, *14*, 8711−8722.

(792) Sullivan, M. R.; Yao, W.; Tang, D.; Ashbaugh, H. S.; Gibb, B. C. The Thermodynamics of Anion Complexation to Nonpolar Pockets. *J. Phys. Chem. B* **2018**, *122*, 1702−1713.

(793) Gibb, C. L. D.; Gibb, B. C. Anion Binding to Hydrophobic Concavity Is Central to the Salting-in Effects of Hofmeister Chaotropes. *J. Am. Chem. Soc.* **2011**, *133*, 7344−7347.

(794) Gibb, C. L. D.; Oertling, E. E.; Velaga, S.; Gibb, B. C. Thermodynamic Profiles of Salt Effects on a Host-Guest System: New Insight into the Hofmeister Effect. *J. Phys. Chem. B* **2015**, *119*, 5624−5638.

(795) Raker, J.; Glass, T. E. Selectivity Via Cooperative Interactions: Detection of Dicarboxylates in Water by a Pinwheel Chemosensor. *J. Org. Chem.* **2002**, *67*, 6113−6116.

(796) Bencini, A.; Coluccini, C.; Garau, A.; Giorgi, C.; Lippolis, V.; Messori, L.; Pasini, D.; Puccioni, S. A Binol-Based Chiral Polyammonium Receptor for Highly Enantioselective Recognition and Fluorescence Sensing of (S, S)-Tartaric Acid in Aqueous Solution. *Chem. Commun.* **2012**, *48*, 10428−10430.

(797) Sedgwick, A. C.; Wu, L.; Han, H.-H.; Bull, S. D.; He, X.-P.; James, T. D.; Sessler, J. L.; Tang, B. Z.; Tian, H.; Yoon, J. Excited-State Intramolecular Proton-Transfer (Esipt) Based Fluorescence Sensors and Imaging Agents. *Chem. Soc. Rev.* **2018**, *47*, 8842−8880.

(798) Arnaut, L. G.; Formosinho, S. J. Excited-State Proton Transfer Reactions I. Fundamentals and Intermolecular Reactions. *J. Photochem. Photobiol., A* **1993**, *75*, 1−20.

(799) Huang, X.; Wang, X.; Quan, M.; Yao, H.; Ke, H.; Jiang, W. Biomimetic Recognition and Optical Sensing of Carboxylic Acids in Water by Using a Buried Salt Bridge and the Hydrophobic Effect. *Angew. Chem., Int. Ed.* **2021**, *60*, 1929−1935.

(800) Liu, Y.; Minami, T.; Nishiyabu, R.; Wang, Z.; Anzenbacher, P. Sensing of Carboxylate Drugs in Urine by a Supramolecular Sensor Array. *J. Am. Chem. Soc.* **2013**, *135*, 7705−7712.

(801) Han, J.; Wang, B.; Bender, M.; Seehafer, K.; Bunz, U. H. F. Water-Soluble Poly(P-Aryleneethynylene)S: A Sensor Array Discriminates Aromatic Carboxylic Acids. *ACS Appl. Mater. Interfaces* **2016**, *8*, 20415−20421.

(802) Gunnlaugsson, T.; Harte, A. J.; Leonard, J. P.; Nieuwenhuyzen, M. Delayed Lanthanide Luminescence Sensing of Aromatic Carboxylates Using Heptadentate Triamide Tb(Iii) Cyclen Complexes: The Recognition of Salicylic Acid in Water. *Chem. Commun.* **2002**, 2134−2135.

(803) Gunnlaugsson, T.; Harte, A. J.; Leonard, J. P.; Nieuwenhuyzen, M. The Formation of Luminescent Supramolecular Ternary Complexes in Water: Delayed Luminescence Sensing of Aromatic Carboxylates Using Coordinated Unsaturated Cationic Heptadentate Lanthanide Ion Complexes. *Supramol. Chem.* **2003**, *15*, 505−519.

(804) He, C.; Qian, X.; Xu, Y.; Yang, C.; Yin, L.; Zhu, W. A Ratiometric Fluorescent Probe for Oxalate Based on Alkyne-Conjugated Carboxamidoquinolines in Aqueous Solution and Imaging in Living Cells. *Dalton Trans.* **2011**, *40*, 1034−1037.

(805) Sheini, A.; Khajehsharifi, H.; Shahbazy, M.; Kompany-Zareh, M. A Chemosensor Array for the Colorimetric Identification of Some Carboxylic Acids in Human Urine Samples. *Sens. Actuators, B* **2017**, *242*, 288−298.

(806) Youk, K.-S.; Kim, K. M.; Chatterjee, A.; Ahn, K. H. Selective Recognition of Fumarate from Maleate with a Gold Nanoparticle-Based Colorimetric Sensing System. *Tetrahedron Lett.* **2008**, *49*, 3652−3655.

(807) Kim, D. S.; Miyaji, H.; Chang, B. Y.; Park, S. M.; Ahn, K. H. Selective Recognition and Electrochemical Sensing of Dicarboxylates with a Ferrocene-Based Bis(O-Trifluoroacetylcarboxanilide) Receptor. *Chem. Commun.* **2006**, 3314−3316.

(808) Song, G.; Xu, C.; Li, B. Visual Chiral Recognition of Mandelic Acid Enantiomers with L-Tartaric Acid-Capped Gold Nanoparticles as Colorimetric Probes. *Sens. Actuators, B* **2015**, *215*, 504−509.

(809) Xie, F.; Bai, Q.; Jiang, X.; Yu, X.; Xia, Z.; Wei, W. Visual and Colorimetric High-Throughput Analysis of Chiral Carboxylic Acids Based on Enantioselective Charge Shielding of Gold Nanoparticles. *ACS Appl. Mater. Interfaces* **2018**, *10*, 11872−11879.

(810) Calero, P.; Aznar, E.; Lloris, J. M.; Marcos, M. D.; Martinez-Manez, R.; Ros-Lis, J. V.; Soto, J.; Sancenon, F. Chromogenic Silica Nanoparticles for the Colorimetric Sensing of Long-Chain Carboxylates. *Chem. Commun.* **2008**, 1668−1670.

(811) Nishizawa, S.; Kato, R.; Hayashita, T.; Teramae, N. Anion Sensing by a Thiourea Based Chromoionophore Via Hydrogen Bonding. *Anal. Sci.* **1998**, *14*, 595−597.

(812) López, K. A.; Piña, M. N.; Morey, J. Squaramide-Coated Fe3o4 Nanoparticles and Their Selective Complexation with Carboxylate Anions in Water. *Sens. Actuators, B* **2013**, *181*, 267−273.

(813) Malerich, J. P.; Hagihara, K.; Rawal, V. H. Chiral Squaramide Derivatives Are Excellent Hydrogen Bond Donor Catalysts. *J. Am. Chem. Soc.* **2008**, *130*, 14416−14417.

(814) Marchetti, L. A.; Kumawat, L. K.; Mao, N.; Stephens, J. C.; Elmes, R. B. P. The Versatility of Squaramides: From Supramolecular Chemistry to Chemical Biology. *Chem.* **2019**, *5*, 1398−1485.

(815) Li, N.; Li, Y.; Han, Y.; Pan, W.; Zhang, T.; Tang, B. A Highly Selective and Instantaneous Nanoprobe for Detection and Imaging of Ascorbic Acid in Living Cells and in Vivo. *Anal. Chem.* **2014**, *86*, 3924−3930.

(816) Bi, J.; Wang, H.; Kamal, T.; Zhu, B.-W.; Tan, M. A Fluorescence Turn-Off-on Chemosensor Based on Carbon Nanocages for Detection of Ascorbic Acid. *RSC Adv.* **2017**, *7*, 30481−30487.

(817) Shamsipur, M.; Molaei, K.; Molaabasi, F.; Alipour, M.; Alizadeh, N.; Hosseinkhani, S.; Hosseini, M. Facile Preparation and Characterization of New Green Emitting Carbon Dots for Sensitive and Selective Off/on Detection of Fe(3+) Ion and Ascorbic Acid in Water and Urine Samples and Intracellular Imaging in Living Cells. *Talanta* **2018**, *183*, 122−130.

(818) Müller, O. J.; Heckmann, M. B.; Ding, L.; Rapti, K.; Rangrez, A. Y.; Gerken, T.; Christiansen, N.; Rennefahrt, U. E. E.; Witt, H.; González Maldonado, S.; Ternes, P.; Schwab, D. M.; Ruf, T.; Hille, S.; Remes, A.; Jungmann, A.; Weis, T. M.; Kreußer, J. S.; Gröne, H. J.; Backs, J.; Schatz, P.; Katus, H. A.; Frey, N. Comprehensive Plasma and Tissue Profiling Reveals Systemic Metabolic Alterations in Cardiac Hypertrophy and Failure. *Cardiovasc. Res.* **2019**, *115*, 1296−1305.

(819) Craig, S. A. Betaine in Human Nutrition. *Am. J. Clin. Nutr.* **2004**, *80*, 539−549.

(820) Wang, Z. Y.; Liu, Y. Y.; Liu, G. H.; Lu, H. B.; Mao, C. Y. L-Carnitine and Heart Disease. *Life Sci.* **2018**, *194*, 88−97.

(821) Kanemitsu, Y.; Mishima, E.; Maekawa, M.; Matsumoto, Y.; Saigusa, D.; Yamaguchi, H.; Ogura, J.; Tsukamoto, H.; Tomioka, Y.; Abe, T.; Mano, N. Comprehensive and Semi-Quantitative Analysis of Carboxyl-Containing Metabolites Related to Gut Microbiota on Chronic Kidney Disease Using 2-Picolylamine Isotopic Labeling Lc-Ms/Ms. *Sci. Rep.* **2019**, *9*, 19075.

(822) Tavazzi, B.; Lazzarino, G.; Leone, P.; Amorini, A. M.; Bellia, F.; Janson, C. G.; Di Pietro, V.; Ceccarelli, L.; Donzelli, S.; Francis, J. S.; Giardina, B. Simultaneous High Performance Liquid Chromatographic Separation of Purines, Pyrimidines, N-Acetylated Amino Acids, and Dicarboxylic Acids for the Chemical Diagnosis of Inborn Errors of Metabolism. *Clin. Biochem.* **2005**, *38*, 997−1008.

(823) Rai, B.; Kharb, S.; Jain, R.; Anand, S. C. Salivary Vitamins E and C in Oral Cancer. *Redox Rep.* **2007**, *12*, 163−164.

(824) Hoffmann, G. F.; Meier-Augenstein, W.; Stöckler, S.; Surtees, R.; Rating, D.; Nyhan, W. L. Physiology and Pathophysiology of Organic Acids in Cerebrospinal Fluid. *J. Inherited Metab. Dis.* **1993**, *16*, 648−669.

(825) Koike, S.; Bundo, M.; Iwamoto, K.; Suga, M.; Kuwabara, H.; Ohashi, Y.; Shinoda, K.; Takano, Y.; Iwashiro, N.; Satomura, Y.; Nagai, T.; Natsubori, T.; Tada, M.; Yamasue, H.; Kasai, K. A Snapshot of Plasma Metabolites in First-Episode Schizophrenia: A Capillary Electrophoresis Time-of-Flight Mass Spectrometry Study. *Transl. Psychiatry* **2014**, *4*, No. e379.

(826) Hoffmann, G.; Aramaki, S.; Blum-Hoffmann, E.; Nyhan, W. L.; Sweetman, L. Quantitative Analysis for Organic Acids in Biological Samples: Batch Isolation Followed by Gas Chromatographic-Mass Spectrometric Analysis. *Clin. Chem.* **1989**, *35*, 587−595.

(827) Duranton, F.; Cohen, G.; De Smet, R.; Rodriguez, M.; Jankowski, J.; Vanholder, R.; Argiles, A. Normal and Pathologic Concentrations of Uremic Toxins. *J. Am. Soc. Nephrol.* **2012**, *23*, 1258−1270.

(828) Jonas, A. J.; Lin, S. N.; Conley, S. B.; Schneider, J. A.; Williams, J. C.; Caprioli, R. C. Urine Glyceraldehyde Excretion Is Elevated in the Renal Fanconi Syndrome. *Kidney Int.* **1989**, *35*, 99−104.

(829) Honda, A.; Yamashita, K.; Ikegami, T.; Hara, T.; Miyazaki, T.; Hirayama, T.; Numazawa, M.; Matsuzaki, Y. Highly Sensitive Quantification of Serum Malonate, a Possible Marker for De Novo Lipogenesis, by Lc-Esi-Ms/Ms. *J. Lipid Res.* **2009**, *50*, 2124−2130.

(830) Loke, W. M.; Jenner, A. M.; Proudfoot, J. M.; McKinley, A. J.; Hodgson, J. M.; Halliwell, B.; Croft, K. D. A Metabolite Profiling Approach to Identify Biomarkers of Flavonoid Intake in Humans. *J. Nutr.* **2009**, *139*, 2309−2314.

(831) Rios, L. Y.; Gonthier, M. P.; Rémésy, C.; Mila, I.; Lapierre, C.; Lazarus, S. A.; Williamson, G.; Scalbert, A. Chocolate Intake Increases Urinary Excretion of Polyphenol-Derived Phenolic Acids in Healthy Human Subjects. *Am. J. Clin. Nutr.* **2003**, *77*, 912−918.

(832) Turchany, J. M.; Leung, P. S.; Iwayama, T.; Jefferson, D. M.; Ishida, J.; Yamaguchi, M.; Munoz, S.; Danner, D. J.; Dickson, E. R.; Gershwin, M. E. Comparative Metabolism and Structure of Bckd-E2 in Primary Biliary Cirrhosis. *J. Autoimmun.* **1993**, *6*, 459−466.

(833) Lee, S. H.; Kim, S. O.; Chung, B. C. Gas Chromatographic-Mass Spectrometric Determination of Urinary Oxoacids Using O-(2,3,4,5,6-Pentafluorobenzyl)Oxime-Trimethylsilyl Ester Derivatization and Cation-Exchange Chromatography. *J. Chromatogr., Biomed. Appl.* **1998**, *719*, 1−7.

(834) Magera, M. J.; Helgeson, J. K.; Matern, D.; Rinaldo, P. Methylmalonic Acid Measured in Plasma and Urine by Stable-Isotope Dilution and Electrospray Tandem Mass Spectrometry. *Clin. Chem.* **2000**, *46*, 1804−1810.

(835) Fahy, E.; Subramaniam, S.; Murphy, R. C.; Nishijima, M.; Raetz, C. R. H.; Shimizu, T.; Spener, F.; van Meer, G.; Wakelam, M. J.

O.; Dennis, E. A. Update of the Lipid Maps Comprehensive Classification System for Lipids. *J. Lipid Res.* **2009**, *50*, S9−S14.

(836) Gaudl, A.; Kratzsch, J.; Bae, Y. J.; Kiess, W.; Thiery, J.; Ceglarek, U. Liquid Chromatography Quadrupole Linear Ion Trap Mass Spectrometry for Quantitative Steroid Hormone Analysis in Plasma, Urine, Saliva and Hair. *J. Chromatogr. A* **2016**, *1464*, 64−71.

(837) Orozco-Beltran, D.; Gil-Guillen, V. F.; Redon, J.; Martin-Moreno, J. M.; Pallares-Carratala, V.; Navarro-Perez, J.; Valls-Roca, F.; Sanchis-Domenech, C.; Fernandez-Gimenez, A.; Perez-Navarro, A.; et al. Lipid Profile, Cardiovascular Disease and Mortality in a Mediterranean High-Risk Population: The Escarval-Risk Study. *PLoS One* **2017**, *12*, No. e0186196.

(838) Eberlin, L. S.; Norton, I.; Dill, A. L.; Golby, A. J.; Ligon, K. L.; Santagata, S.; Cooks, R. G.; Agar, N. Y. R. Classifying Human Brain Tumors by Lipid Imaging with Mass Spectrometry. *Cancer Res.* **2012**, *72*, 645−654.

(839) Levy, B. D.; Clish, C. B.; Schmidt, B.; Gronert, K.; Serhan, C. N. Lipid Mediator Class Switching During Acute Inflammation: Signals in Resolution. *Nat. Immunol.* **2001**, *2*, 612−619.

(840) Delikatny, E. J.; Chawla, S.; Leung, D.-J.; Poptani, H. Mr-Visible Lipids and the Tumor Microenvironment. *NMR Biomed.* **2011**, *24*, 592.

(841) Krahmer, N.; Farese, R. V., Jr; Walther, T. C. Balancing the Fat: Lipid Droplets and Human Disease. *EMBO Mol. Med.* **2013**, *5*, 973−983.

(842) Baenke, F.; Peck, B.; Miess, H.; Schulze, A. Hooked on Fat: The Role of Lipid Synthesis in Cancer Metabolism and Tumour Development. *Dis. Models &amp; Mech.* **2013**, *6*, 1353−1363.

(843) Mueller-Hennessen, M.; Düngen, H.-D.; Lutz, M.; Trippel, T. D.; Kreuter, M.; Sigl, J.; Müller, O. J.; Tahirovic, E.; Witt, H.; Ternes, P.; Carvalho, S.; Peter, E.; Rein, D.; Schatz, P.; Herth, F.; Giannitsis, E.; Weis, T.; Frey, N.; Katus, H. A. A Novel Lipid Biomarker Panel for the Detection of Heart Failure with Reduced Ejection Fraction. *Clin. Chem.* **2017**, *63*, 267−277.

(844) Khaliq, W.; Großmann, P.; Neugebauer, S.; Kleyman, A.; Domizi, R.; Calcinaro, S.; Brealey, D.; Gräler, M.; Kiehntopf, M.; Schäuble, S.; Singer, M.; Panagiotou, G.; Bauer, M. Lipid Metabolic Signatures Deviate in Sepsis Survivors Compared to Non-Survivors. *Comput. Struct. Biotechnol. J.* **2020**, *18*, 3678−3691.

(845) Neugebauer, S.; Giamarellos-Bourboulis, E. J.; Pelekanou, A.; Marioli, A.; Baziaka, F.; Tsangaris, I.; Bauer, M.; Kiehntopf, M. Metabolite Profiles in Sepsis: Developing Prognostic Tools Based on the Type of Infection. *Crit. Care Med.* **2016**, *44*, 1649.

(846) Calder, P. C. Functional Roles of Fatty Acids and Their Effects on Human Health. *JPEN, J. Parenter. Enteral Nutr.* **2015**, *39*, 18S−32S.

(847) Spiller, S.; Blüher, M.; Hoffmann, R. Plasma Levels of Free Fatty Acids Correlate with Type 2 Diabetes Mellitus. *Diabetes, Obes. Metab.* **2018**, *20*, 2661−2669.

(848) Sobczak, A. I. S.; Blindauer, C. A.; Stewart, A. J. Changes in Plasma Free Fatty Acids Associated with Type-2 Diabetes. *Nutrients* **2019**, *11*, 2022.

(849) Castro-Gómez, P.; Garcia-Serrano, A.; Visioli, F.; Fontecha, J. Relevance of Dietary Glycerophospholipids and Sphingolipids to Human Health. *Prostaglandins, Leukotrienes Essent. Fatty Acids* **2015**, *101*, 41−51.

(850) Munro, S. Lipid Rafts: Elusive or Illusive? *Cell* **2003**, *115*, 377−388.

(851) Hishikawa, D.; Hashidate, T.; Shimizu, T.; Shindou, H. Diversity and Function of Membrane Glycerophospholipids Generated by the Remodeling Pathway in Mammalian Cells. *J. Lipid Res.* **2014**, *55*, 799−807.

(852) Kraft, M. L. Sphingolipid Organization in the Plasma Membrane and the Mechanisms That Influence It. *Front. Cell Dev. Biol.* **2017**, *4*, 154.

(853) Farooqui, A. A.; Horrocks, L. A.; Farooqui, T. Glycerophospholipids in Brain: Their Metabolism, Incorporation into Membranes, Functions, and Involvement in Neurological Disorders. *Chem. Phys. Lipids* **2000**, *106*, 1−29.

(854) Farooqui, A. A.; Horrocks, L. A.; Farooqui, T. Interactions between Neural Membrane Glycerophospholipid and Sphingolipid Mediators: A Recipe for Neural Cell Survival or Suicide. *J. Neurosci. Res.* **2007**, *85*, 1834−1850.

(855) Stace, C. L.; Ktistakis, N. T. Phosphatidic Acid- and Phosphatidylserine-Binding Proteins. *Biochim. Biophys. Acta, Mol. Cell Biol. Lipids* **2006**, *1761*, 913−926.

(856) Hussain, G.; Anwar, H.; Rasul, A.; Imran, A.; Qasim, M.; Zafar, S.; Imran, M.; Kamran, S. K. S.; Aziz, N.; Razzaq, A.; Ahmad, W.; Shabbir, A.; Iqbal, J.; Baig, S. M.; Ali, M.; Gonzalez de Aguilar, J.-L.; Sun, T.; Muhammad, A.; Muhammad Umair, A. Lipids as Biomarkers of Brain Disorders. *Crit. Rev. Food Sci. Nutr.* **2020**, *60*, 351−374.

(857) de Diego, I.; Peleg, S.; Fuchs, B. The Role of Lipids in Aging-Related Metabolic Changes. *Chem. Phys. Lipids* **2019**, *222*, 59−69.

(858) Vijayan, R.; Biggin, P. C. A Steroid in a Lipid Bilayer: Localization, Orientation, and Energetics. *Biophys. J.* **2008**, *95*, L45−L47.

(859) Barnes, P. J.; Adcock, I.; Spedding, M.; Vanhoutte, P. M. Anti-Infalmmatory Actions of Steroids: Molecular Mechanism. *Trends Pharmacol. Sci.* **1993**, *14*, 436.

(860) Adriaenssens, E.; Lottin, S.; Dugimont, T.; Fauquette, W.; Coll, J.; Dupouy, J. P.; Boilly, B.; Curgy, J. J. Steroid Hormones Modulate H19 Gene Expression in Both Mammary Gland and Uterus. *Oncogene* **1999**, *18*, 4460.

(861) Faulds, M. H.; Zhao, C.; Dahlman-Wright, K.; Gustafsson, J. A. The Diversity of Sex Steroid Action: Regulation of Metabolism by Estrogen Signaling. *J. Endocrinol.* **2012**, *212*, 3−12.

(862) Anand, P. K. Lipids, Inflammasomes, Metabolism, and Disease. *Immunol. Rev.* **2020**, *297*, 108−122.

(863) Ceglarek, U.; Dittrich, J.; Leopold, J.; Helmschrodt, C.; Becker, S.; Staab, H.; Richter, O.; Rohm, S.; Aust, G. Free Cholesterol, Cholesterol Precursor and Plant Sterol Levels in Atherosclerotic Plaques Are Independently Associated with Symptomatic Advanced Carotid Artery Stenosis. *Atherosclerosis* **2020**, *295*, 18−24.

(864) Bratusch-Marrain, P. R. Insulin-Counteracting Hormones: Their Impact on Glucose Metabolism. *Diabetologia* **1983**, *24*, 74−79.

(865) Vedhara, K.; Hyde, J.; Gilchrist, I. D.; Tytherleigh, M.; Plummer, S. Acute Stress, Memory, Attention and Cortisol. *Psychoneuroendocrinology* **2000**, *25*, 535−549.

(866) Ericson-Neilsen, W.; Kaye, A. D. Steroids: Pharmacology, Complications, and Practice Delivery Issues. *Ochsner J.* **2014**, *14*, 203−207.

(867) Curtis, J. R.; Westfall, A. O.; Allison, J.; Bijlsma, J. W.; Freeman, A.; George, V.; Kovac, S. H.; Spettell, C. M.; Saag, K. G. Population-Based Assessment of Adverse Events Associated with Long-Term Glucocorticoid Use. *Arthritis Rheum.* **2006**, *55*, 420−426.

(868) Gupta, S. K.; Dubé, M. P. Exogenous Cushing Syndrome Mimicking Human Immunodeficiency Virus Lipodystrophy. *Clin. Infect. Dis.* **2002**, *35*, e69.

(869) Kapoor, D.; Malkin, C. J.; Channer, K. S.; Jones, T. H. Androgens, Insulin Resistance and Vascular Disease in Men. *Clin. Endocrinol.* **2005**, *63*, 239−250.

(870) LeMoult, J.; Joormann, J. Depressive Rumination Alters Cortisol Decline in Major Depressive Disorder. *Biol. Psychol.* **2014**, *100*, 50−55.

(871) Yahyavi, S. T.; Zarghami, M.; Naghshvar, F.; Danesh, A. Relationship of Cortisol, Norepinephrine, and Epinephrine Levels with War-Induced Posttraumatic Stress Disorder in Fathers and Their Offspring. *Braz. J. Psychiatry* **2015**, *37*, 93−98.

(872) Holsboer, F.; Ising, M. Stress Hormone Regulation: Biological Role and Translation into Therapy. *Annu. Rev. Psychol.* **2010**, *61*, 81.

(873) Albar, W. F.; Russell, E. W.; Koren, G.; Rieder, M. J.; Van Umm, S. H. Human Hair Cortisol Analysis: Comparison of the Internationallyreported Elisa Methods. *Clin. Invest. Med.* **2013**, *36*, 312−316.

(874) Wymann, M. P.; Schneiter, R. Lipid Signalling in Disease. *Nat. Rev. Mol. Cell Biol.* **2008**, *9*, 162−176.

(875) Lee, C.-H.; Olson, P.; Evans, R. M. Minireview: Lipid Metabolism, Metabolic Diseases, and Peroxisome Proliferator-Activated Receptors. *Endocrinology* **2003**, *144*, 2201−2207.

(876) Long, J.; Zhang, C.-J.; Zhu, N.; Du, K.; Yin, Y.-F.; Tan, X.; Liao, D.-F.; Qin, L. Lipid Metabolism and Carcinogenesis, Cancer Development. *Am. J. Cancer Res.* **2018**, *8*, 778−791.

(877) Walther, T. C.; Farese, R. V. Lipid Droplets and Cellular Lipid Metabolism. *Annu. Rev. Biochem.* **2012**, *81*, 687−714.

(878) Lazar, A. I.; Biedermann, F.; Mustafina, K. R.; Assaf, K. I.; Hennig, A.; Nau, W. M. Nanomolar Binding of Steroids to Cucurbit[N]Urils: Selectivity and Applications. *J. Am. Chem. Soc.* **2016**, *138*, 13022−13029.

(879) Das, D.; Assaf, K. I.; Nau, W. M. Applications of Cucurbiturils in Medicinal Chemistry and Chemical Biology. *Front. Chem.* **2019**, *7*, 619.

(880) Miskolczy, Z.; Megyesi, M.; Biczók, L.; Prabodh, A.; Biedermann, F. Kinetics and Mechanism of Cation-Induced Guest Release from Cucurbit[7]Uril. *Chem.−Eur. J.* **2020**, *26*, 7433−7441.

(881) Stahl, A.; Lazar, A. I.; Muchemu, V. N.; Nau, W. M.; Ullrich, M. S.; Hennig, A. A Fluorescent, Supramolecular Chemosensor to Follow Steroid Depletion in Bacterial Cultures. *Anal. Bioanal. Chem.* **2017**, *409*, 6485−6494.

(882) Zheng, Z.; Geng, W.-C.; Gao, J.; Wang, Y.-Y.; Sun, H.; Guo, D.-S. Ultrasensitive and Specific Fluorescence Detection of a Cancer Biomarker Via Nanomolar Binding to a Guanidinium-Modified Calixarene. *Chem. Sci.* **2018**, *9*, 2087−2091.

(883) Shorthill, B. J.; Avetta, C. T.; Glass, T. E. Shape-Selective Sensing of Lipids in Aqueous Solution by a Designed Fluorescent Molecular Tube. *J. Am. Chem. Soc.* **2004**, *126*, 12732−12733.

(884) Murray, J.; Kim, K.; Ogoshi, T.; Yao, W.; Gibb, B. C. The Aqueous Supramolecular Chemistry of Cucurbit[N]Urils, Pillar[N]-Arenes and Deep-Cavity Cavitands. *Chem. Soc. Rev.* **2017**, *46*, 2479−2496.

(885) Jordan, J. H.; Gibb, B. C. Molecular Containers Assembled through the Hydrophobic Effect. *Chem. Soc. Rev.* **2015**, *44*, 547−585.

(886) Avetta, C. T.; Shorthill, B. J.; Ren, C.; Glass, T. E. Molecular Tubes for Lipid Sensing: Tube Conformations Control Analyte Selectivity and Fluorescent Response. *J. Org. Chem.* **2012**, *77*, 851−857.

(887) Ren, C.; Lee, J. S.; Glass, T. E. A Novel Fluorescent Sensor for Hydrophobic Amines in Aqueous Solution. *Supramol. Chem.* **2014**, *26*, 607−611.

(888) Bai, L. M.; Zhou, H.; Liu, W. E.; Chai, H.; Yang, L. P.; Yan, W.; Zhang, W.; Yang, H. H.; Jiang, W. Fluorescent Monitoring of the Reaction Kinetics of Nonfluorescent Molecules Enabled by a Fluorescent Receptor. *Chem. Commun.* **2019**, *55*, 3128−3131.

(889) Huang, G. B.; Wang, S. H.; Ke, H.; Yang, L. P.; Jiang, W. Selective Recognition of Highly Hydrophilic Molecules in Water by Endo-Functionalized Molecular Tubes. *J. Am. Chem. Soc.* **2016**, *138*, 14550−14553.

(890) Wang, L. L.; Chen, Z.; Liu, W. E.; Ke, H.; Wang, S. H.; Jiang, W. Molecular Recognition and Chirality Sensing of Epoxides in Water Using Endo-Functionalized Molecular Tubes. *J. Am. Chem. Soc.* **2017**, *139*, 8436−8439.

(891) Yang, L. P.; Wang, X.; Yao, H.; Jiang, W. Naphthotubes: Macrocyclic Hosts with a Biomimetic Cavity Feature. *Acc. Chem. Res.* **2020**, *53*, 198−208.

(892) Yao, H.; Ke, H.; Zhang, X.; Pan, S. J.; Li, M. S.; Yang, L. P.; Schreckenbach, G.; Jiang, W. Molecular Recognition of Hydrophilic Molecules in Water by Combining the Hydrophobic Effect with Hydrogen Bonding. *J. Am. Chem. Soc.* **2018**, *140*, 13466−13477.

(893) Manna, A.; Goswami, S. Ratiometric Detection of Hypochlorite Applying the Restriction to 2-Way Esipt: Simple Design for "Naked-Eye" Tap Water Analysis. *New J. Chem.* **2015**, *39*, 4424−4429.

(894) Yin, J.; Peng, M.; Ma, Y.; Guo, R.; Lin, W. Rational Design of a Lipid-Droplet-Polarity Based Fluorescent Probe for Potential Cancer Diagnosis. *Chem. Commun.* **2018**, *54*, 12093−12096.

(895) Lakowicz, J. R. *Principles of Fluorescence Spectroscopy*; Springer, 2006; pp 205.

(896) Mandal, M.; Chatterjee, T.; Das, A.; Mandal, S.; Sen, A.; Ta, M.; Mandal, P. K. Meta-Fluors—a Unique Way to Create a 200 Da Ultrasmall Fluorophore Emitting in Red with Intense Stokes/Solvatochromic Shift: Imaging Subcellular Nanopolarity in Live Stem Cells. *J. Phys. Chem. C* **2019**, *123*, 24786−24792.

(897) Xiao, H.; Li, P.; Tang, B. Recent Progresses in Fluorescent Probes for Detection of Polarity. *Coord. Chem. Rev.* **2021**, *427*, 213582.

(898) Fan, L.; Wang, X.; Ge, J.; Li, F.; Wang, X.; Wang, J.; Shuang, S.; Dong, C. A Lysosome-Targeting and Polarity-Specific Fluorescent Probe for Cancer Diagnosis. *Chem. Commun.* **2019**, *55*, 4703−4706.

(899) Shi, X.; Sung, S. H. P.; Lee, M. M. S.; Kwok, R. T. K.; Sung, H. H. Y.; Liu, H.; Lam, J. W. Y.; Williams, I. D.; Liu, B.; Tang, B. Z. A Lipophilic Aiegen for Lipid Droplet Imaging and Evaluation of the Efficacy of Hif-1 Targeting Drugs. *J. Mater. Chem. B* **2020**, *8*, 1516−1523.

(900) Zhang, F.; Liu, Y.; Yang, B.; Wen, G.; Liu, B. Near-Infrared Aiegens for Lipid Droplets Imaging in Corpus Adiposum or Trachea of Locusta Migratoria and Its Application in Photodynamic Therapy. *Sens. Actuators, B* **2020**, *322*, 128589.

(901) Zhang, F.; Li, Z.; Liu, Y.; Yang, B.; Qiao, H.; Chai, J.; Wen, G.; Liu, B. Rational Construction of Aiegens with Wide Color Tunability and Their Specific Lipid Droplet Imaging Applications. *J. Mater. Chem. B* **2020**, *8*, 9533−9543.

(902) Wei, X.; Zhang, H.; Sun, Y.; Liu, J.; Li, Z. Engineering a Lipid Droplet Targeting Fluorescent Probe with a Large Stokes Shift through Ester Substituent Rotation for in Vivo Tumor Imaging. *Analyst* **2021**, *146*, 495−501.

(903) Wang, K.-N.; Peng, X.-J.; Li, Y.; Tang, H.-T.; Pan, Y.-M.; He, L. Photostable Fluorescent Probes for 3d Imaging and Monitoring the Metabolism of Lipid Droplets. *Dyes Pigm.* **2020**, *180*, 108502.

(904) Zhang, X.; Yuan, L.; Jiang, J.; Hu, J.; du Rietz, A.; Cao, H.; Zhang, R.; Tian, X.; Zhang, F.; Ma, Y.; Zhang, Z.; Uvdal, K.; Hu, Z. Light-up Lipid Droplets Dynamic Behaviors Using a Red-Emitting Fluorogenic Probe. *Anal. Chem.* **2020**, *92*, 3613−3619.

(905) Valanciunaite, J.; Kempf, E.; Seki, H.; Danylchuk, D. I.; Peyriéras, N.; Niko, Y.; Klymchenko, A. S. Polarity Mapping of Cells and Embryos by Improved Fluorescent Solvatochromic Pyrene Probe. *Anal. Chem.* **2020**, *92*, 6512−6520.

(906) Yin, J.; Peng, M.; Lin, W. Two-Photon Fluorescence Imaging of Lipid Drops Polarity toward Cancer Diagnosis in Living Cells and Tissue. *Sens. Actuators, B* **2019**, *288*, 251−258.

(907) Lai, Z.-L.; Chang, J.-S.; Chan, Y.-C.; Chang, C.-C.; Li, C.-Y.; Huang, S.-W. Tumor Tissues Diagnosis with Piee Lipid Droplet Vesicles. *Sens. Actuators, B* **2021**, *330*, 129269.

(908) Samanta, S.; Huang, M.; Lin, F.; Das, P.; Chen, B.; Yan, W.; Chen, J.-J.; Ji, K.; Liu, L.; Qu, J.; Yang, Z. Solo Smart Fluorogenic Probe for Potential Cancer Diagnosis and Tracking in Vivo Tumorous Lymphatic Systems Via Distinct Emission Signals. *Anal. Chem.* **2020**, *92*, 1541−1548.

(909) Li, L.; Xu, Y.; Chen, Y.; Zheng, J.; Zhang, J.; Li, R.; Wan, H.; Yin, J.; Yuan, Z.; Chen, H. A Family of Push-Pull Bio-Probes for Tracking Lipid Droplets in Living Cells with the Detection of Heterogeneity and Polarity. *Anal. Chim. Acta* **2020**, *1096*, 166−173.

(910) Pal, K.; Kumar, P.; Koner, A. L. Deciphering Interior Polarity of Lysosome in Live Cancer and Normal Cells Using Spectral Scanning Microscopy. *J. Photochem. Photobiol., B* **2020**, *206*, 111848.

(911) Tian, H.; Sedgwick, A. C.; Han, H.-H.; Sen, S.; Chen, G.-R.; Zang, Y.; Sessler, J. L.; James, T. D.; Li, J.; He, X.-P. Fluorescent Probes for the Imaging of Lipid Droplets in Live Cells. *Coord. Chem. Rev.* **2021**, *427*, 213577.

(912) Park, S. J.; Juvekar, V.; Jo, J. H.; Kim, H. M. Combining Hydrophilic and Hydrophobic Environment Sensitive Dyes to Detect a Wide Range of Cellular Polarity. *Chem. Sci.* **2020**, *11*, 596−601.

(913) Eustis, S.; el-Sayed, M. A. Why Gold Nanoparticles Are More Precious Than Pretty Gold: Noble Metal Surface Plasmon Resonance

and Its Enhancement of the Radiative and Nonradiative Properties of Nanocrystals of Different Shapes. *Chem. Soc. Rev.* **2006**, *35*, 209−217.

(914) Amendola, V.; Pilot, R.; Frasconi, M.; Marago, O. M.; Iati, M. A. Surface Plasmon Resonance in Gold Nanoparticles: A Review. *J. Phys.: Condens. Matter* **2017**, *29*, 203002.

(915) Leung, F. C.; Au, V. K.; Song, H. O.; Yam, V. W. Dual Esterase- and Steroid-Responsive Energy Transfer Modulation of Ruthenium(Ii) and Rhenium(I) Complex Functionalized Gold Nanoparticles. *Chem.−Eur. J.* **2015**, *21*, 16448−16454.

(916) Butterfield, S. M.; Miyatake, T.; Matile, S. Amplifier-Mediated Activation of Cell-Penetrating Peptides with Steroids: Multifunctional Anion Transporters for Fluorogenic Cholesterol Sensing in Eggs and Blood. *Angew. Chem.* **2009**, *121*, 331−334.

(917) Tanaka, H.; Matile, S. Chirality Sensing with Synthetic Pores. *Chirality* **2008**, *20*, 307−312.

(918) Shi, W.; Friedman, A. K.; Baker, L. A. Nanopore Sensing. *Anal. Chem.* **2017**, *89*, 157−188.

(919) Hagihara, S.; Tanaka, H.; Matile, S. Signal Amplification by Conjugate Addition for Differential Sensing with Synthetic Pores. *Org. Biomol. Chem.* **2008**, *6*, 2259−2262.

(920) Litvinchuk, S.; Tanaka, H.; Miyatake, T.; Pasini, D.; Tanaka, T.; Bollot, G.; Mareda, J.; Matile, S. Synthetic Pores with Reactive Signal Amplifiers as Artificial Tongues. *Nat. Mater.* **2007**, *6*, 576−580.

(921) Lee, M. A.; Wang, S.; Jin, X.; Bakh, N. A.; Nguyen, F. T.; Dong, J.; Silmore, K. S.; Gong, X.; Pham, C.; Jones, K. K.; Muthupalani, S.; Bisker, G.; Son, M.; Strano, M. S. Implantable Nanosensors for Human Steroid Hormone Sensing in Vivo Using a Self-Templating Corona Phase Molecular Recognition. *Adv. Healthcare Mater.* **2020**, *9*, No. 2000429.

(922) Krupke, R.; Hennrich, F.; Löhneysen, H. V.; Kappes, M. M. Separation of Metallic from Semiconducting Single-Walled Carbon Nanotubes. *Science* **2003**, *301*, 344−347.

(923) Gerstel, P.; Klumpp, S.; Hennrich, F.; Altintas, O.; Eaton, T. R.; Mayor, M.; Barner-Kowollik, C.; Kappes, M. M. Selective Dispersion of Single-Walled Carbon Nanotubes Via Easily Accessible Conjugated Click Polymers. *Polym. Chem.* **2012**, *3*, 1966−1970.

(924) Janas, D. Towards Monochiral Carbon Nanotubes: A Review of Progress in the Sorting of Single-Walled Carbon Nanotubes. *Mater. Chem. Front.* **2018**, *2*, 36−63.

(925) Lemasson, F.; Berton, N.; Tittmann, J.; Hennrich, F.; Kappes, M. M.; Mayor, M. Polymer Library Comprising Fluorene and Carbazole Homo- and Copolymers for Selective Single-Walled Carbon Nanotubes Extraction. *Macromolecules* **2012**, *45*, 713−722.

(926) Hennrich, F.; Li, W.; Fischer, R.; Lebedkin, S.; Krupke, R.; Kappes, M. M. Length-Sorted, Large-Diameter, Polyfluorene-Wrapped Semiconducting Single-Walled Carbon Nanotubes for High-Density, Short-Channel Transistors. *ACS Nano* **2016**, *10*, 1888−1895.

(927) Li, H.; Gordeev, G.; Wasserroth, S.; Chakravadhanula, V. S. K.; Neelakandhan, S. K. C.; Hennrich, F.; Jorio, A.; Reich, S.; Krupke, R.; Flavel, B. S. Inner- and Outer-Wall Sorting of Double-Walled Carbon Nanotubes. *Nat. Nanotechnol.* **2017**, *12*, 1176−1182.

(928) Harvey, J. D.; Baker, H. A.; Mercer, E.; Budhathoki-Uprety, J.; Heller, D. A. Control of Carbon Nanotube Solvatochromic Response to Chemotherapeutic Agents. *ACS Appl. Mater. Interfaces* **2017**, *9*, 37947−37953.

(929) Kannel, W. B. Range of Serum Cholesterol Values in the Population Developing Coronary Artery Disease. *Am. J. Cardiol.* **1995**, *76*, 69C−77C.

(930) Miller, M.; Seidler, A.; Moalemi, A.; Pearson, T. A. Normal Triglyceride Levels and Coronary Artery Disease Events: The Baltimore Coronary Observational Long-Term Study 11this Study Was Supported by Grants Hl02263 and Hl52663 from the National Heart, Lung, and Blood Institute, National Institutes of Health, Bethesda, Maryland. *J. Am. Coll. Cardiol.* **1998**, *31*, 1252−1257.

(931) Liu, Q.; Boyd, B. J. Liposomes in Biosensors. *Analyst* **2013**, *138*, 391−409.

(932) Vargas, K. M.; Shon, Y.-S. Hybrid Lipid-Nanoparticle Complexes for Biomedical Applications. *J. Mater. Chem. B* **2019**, *7*, 695−708.

(933) Report of the National Cholesterol Education Program Expert Panel on Detection, Evaluation, and Treatment of High Blood Cholesterol in Adults. The Expert Panel. *Arch. Intern. Med.* **1988**, *148*, 36−69.

(934) Higashijima, H.; Ichimiya, H.; Nakano, T.; Yamashita, H.; Kuroki, S.; Satoh, H.; Chijiiwa, K.; Tanaka, M. Deconjugation of Bilirubin Accelerates Coprecipitation of Cholesterol, Fatty Acids, and Mucin in Human Bile–in Vitro Study. *J. Gastroenterol.* **1996**, *31*, 828−835.

(935) Donner, K. M.; Hiltunen, T. P.; Jänne, O. A.; Sane, T.; Kontula, K. Generalized Glucocorticoid Resistance Caused by a Novel Two-Nucleotide Deletion in the Hormone-Binding Domain of the Glucocorticoid Receptor Gene Nr3c1. *Eur. J. Endocrinol.* **2013**, *168*, K9−K18.

(936) Epstein, M. T.; Espiner, E. A.; Donald, R. A.; Hughes, H.; Cowles, R. J.; Lun, S. Licorice Raises Urinary Cortisol in Man. *J. Clin. Endocrinol. Metab.* **1978**, *47*, 397−400.

(937) Toone, R. J.; Peacock, O. J.; Smith, A. A.; Thompson, D.; Drawer, S.; Cook, C.; Stokes, K. A. Measurement of Steroid Hormones in Saliva: Effects of Sample Storage Condition. *Scand. J. Clin. Lab. Invest.* **2013**, *73*, 615−621.

(938) Reichman, M. E.; Judd, J. T.; Longcope, C.; Schatzkin, A.; Clevidence, B. A.; Nair, P. P.; Campbell, W. S.; Taylor, P. R. Effects of Alcohol Consumption on Plasma and Urinary Hormone Concentrations in Premenopausal Women. *J. Natl. Cancer Inst.* **1993**, *85*, 722−727.

(939) Thompson, T. N. Optimization of Metabolic Stability as a Goal of Modern Drug Design. *Med. Res. Rev.* **2001**, *21*, 412−449.

(940) Schilsky, R. L. Personalized Medicine in Oncology: The Future Is Now. *Nat. Rev. Drug Discovery* **2010**, *9*, 363−366.

(941) Abrahams, E.; Silver, M. The Case for Personalized Medicine. *J. Diabetes Sci. Technol.* **2009**, *3*, 680−684.

(942) Balashova, E. E.; Maslov, D. L.; Lokhov, P. G. A Metabolomics Approach to Pharmacotherapy Personalization. *J. Pers. Med.* **2018**, *8*, 28.

(943) Bhide, A.; Ganguly, A.; Parupudi, T.; Ramasamy, M.; Muthukumar, S.; Prasad, S. Next-Generation Continuous Metabolite Sensing toward Emerging Sensor Needs. *ACS Omega* **2021**, *6*, 6031−6040.

(944) *European Drug Report 2018: Trends and Developments*; European Union; European Monitoring Centre for Drugs and Drug Addiction: Luxembourg, 2018.

(945) *Overdose Death Rates*; National Center for Health Statistics (NCHS), CDC Wonder; National Institute on Drug Abuse (NIH)—Advancing Addiction Sicence, 2017.

(946) Gill, A. D.; Hickey, B. L.; Zhong, W.; Hooley, R. J. Selective Sensing of Thc and Related Metabolites in Biofluids by Host:Guest Arrays. *Chem. Commun.* **2020**, *56*, 4352−4355.

(947) Gill, A. D.; Perez, L.; Salinas, I. N. Q.; Byers, S. R.; Liu, Y.; Hickey, B. L.; Zhong, W.; Hooley, R. J. Selective Array-Based Sensing of Anabolic Steroids in Aqueous Solution by Host-Guest Reporter Complexes. *Chem.−Eur. J.* **2019**, *25*, 1740−1745.

(948) Wang, G.-S.; Zhang, H.-Y.; Ding, F.; Liu, Y. Preparation and Characterization of Inclusion Complexes of Topotecan with Sulfonatocalixarene. *J. Inclusion Phenom. Mol. Recognit. Chem.* **2011**, *69*, 85−89.

(949) Sinn, S.; Spuling, E.; Bräse, S.; Biedermann, F. Rational Design and Implementation of a Cucurbit[8]Uril-Based Indicator-Displacement Assay for Application in Blood Serum. *Chem. Sci.* **2019**, *10*, 6584−6593.

(950) Mohseni, N.; Bahram, M. Mean Centering of Ratio Spectra for Colorimetric Determination of Morphine and Codeine in Pharmaceuticals and Biological Samples Using Melamine Modified Gold Nanoparticles. *Anal. Methods* **2016**, *8*, 6739−6747.

(951) Alhaddad, M.; Sheta, S. M. Dual Naked-Eye and Optical Chemosensor for Morphine Detection in Biological Real Samples

Based on Cr(Iii) Metal-Organic Framework Nanoparticles. *ACS Omega* **2020**, *5*, 28296−28304.

(952) Lozano-Torres, B.; Pascual, L.; Bernardos, A.; Marcos, M. D.; Jeppesen, J. O.; Salinas, Y.; Martinez-Manez, R.; Sancenon, F. Pseudorotaxane Capped Mesoporous Silica Nanoparticles for 3,4-Methylenedioxymethamphetamine (Mdma) Detection in Water. *Chem. Commun.* **2017**, *53*, 3559−3562.

(953) Gabrielli, L.; Rosa-Gastaldo, D.; Salvia, M.-V.; Springhetti, S.; Rastrelli, F.; Mancin, F. Detection and Identification of Designer Drugs by Nanoparticle-Based Nmr Chemosensing. *Chem. Sci.* **2018**, *9*, 4777−4784.

(954) Khodaveisi, J.; Dadfarnia, S.; Shabani, A. H.; Saberi, D. Colorimetric Determination of Nabumetone Based on Localized Surfaceplasmon Resonance of Functionalized Gold Nanoparticles as a Chemicalsensor. *Sens. Actuators, B* **2017**, *239*, 1300−1306.

(955) Harvey, J. D.; Williams, R. M.; Tully, K. M.; Baker, H. A.; Shamay, Y.; Heller, D. A. An in Vivo Nanosensor Measures Compartmental Doxorubicin Exposure. *Nano Lett.* **2019**, *19*, 4343−4354.

(956) Tommasini, M.; Pellizzoni, E.; Iacuzzi, V.; Marangon, E.; Posocco, P.; Forzato, C.; Bertoncin, P.; Toffoli, G.; Resmini, M.; Berti, F. Fluorescent Imprinted Nanoparticles for the Effective Monitoring of Irinotecan in Human Plasma. *Nanomaterials* **2020**, *10*, 1707.

(957) Meny, R. G.; Naumburg, E. G.; Alger, L. S.; Brill-Miller, J. L.; Brown, S. Codeine and the Breastfed Neonate. *J. Hum. Lact.* **1993**, *9*, 237−240.

(958) Guo, K.; Li, L. Differential 12c-/13c-Isotope Dansylation Labeling and Fast Liquid Chromatography/Mass Spectrometry for Absolute and Relative Quantification of the Metabolome. *Anal. Chem.* **2009**, *81*, 3919−3932.

(959) Yamaguchi, M.; Monji, H.; Aoki, I.; Yashiki, T. High-Performance Liquid Chromatographic Determination of Phenylephrine in Human Serum Using Column Switching with Fluorescence Detection. *J. Chromatogr., Biomed. Appl.* **1994**, *661*, 93−99.

(960) Wu, S. M.; Ho, Y. H.; Wu, H. L.; Chen, S. H.; Ko, H. S. Head-Column Field-Amplified Sample Stacking in Capillary Electrophoresis for the Determination of Cimetidine, Famotidine, Nizatidine, and Ranitidine-Hcl in Plasma. *Electrophoresis* **2001**, *22*, 2717−2722.

(961) Hicks, R. J.; Stotzky, G.; Van Voris, P. Review and Evaluation of the Effects of Xenobiotic Chemicals on Microorganisms in Soil. *Adv. Appl. Microbiol.* **1990**, *35*, 195−253.

(962) Eskenazi, B.; Warner, M.; Brambilla, P.; Signorini, S.; Ames, J.; Mocarelli, P. The Seveso Accident: A Look at 40 Years of Health Research and Beyond. *Environ. Int.* **2018**, *121*, 71−84.

(963) Ayres, S. M.; Webb, K. B.; Evans, R. G.; Mikes, J. Is 2,3,7,8-Tcdd (Dioxin) a Carcinogen for Humans? *Environ. Health Perspect.* **1985**, *62*, 329−335.

(964) Bruner-Tran, K. L.; Gnecco, J.; Ding, T.; Glore, D. R.; Pensabene, V.; Osteen, K. G. Exposure to the Environmental Endocrine Disruptor Tcdd and Human Reproductive Dysfunction: Translating Lessons from Murine Models. *Reprod. Toxicol.* **2017**, *68*, 59−71.

(965) Dutta, S.; Gupta, B.; Srivastava, S. K.; Gupta, A. K. Recent Advances on the Removal of Dyes from Wastewater Using Various Adsorbents: A Critical Review. *Mater. Adv.* **2021**, *2*, 4497−4531.

(966) Zuccato, E.; Calamari, D.; Natangelo, M.; Fanelli, R. Presence of Therapeutic Drugs in the Environment. *Lancet* **2000**, *355*, 1789−1790.

(967) Rowney, N. C.; Johnson, A. C.; Williams, R. J. Cytotoxic Drugs in Drinking Water: A Prediction and Risk Assessment Exercise for the Thames Catchment in the United Kingdom. *Environ. Toxicol. Chem.* **2009**, *28*, 2733−2743.

(968) Debroux, J.-F.; Soller, J. A.; Plumlee, M. H.; Kennedy, L. J. Human Health Risk Assessment of Non-Regulated Xenobiotics in Recycled Water: A Review. *Hum. Ecol. Risk Assess.* **2012**, *18*, 517−546.

(969) Davoli, E.; Zuccato, E.; Castiglioni, S. Illicit Drugs in Drinking Water. *Curr. Opin. Environ. Sci. Health* **2019**, *7*, 92−97.

(970) *Drinking Water Parameter Cooperation Project*; European Union, 2017; https://ec.europa.eu/environment/water/water-drink/pdf/20171215_EC_project_report_final_corrected.pdf (accessed 2021-03-16).

(971) Florea, M.; Nau, W. M. Strong Binding of Hydrocarbons to Cucurbituril Probed by Fluorescent Dye Displacement: A Supramolecular Gas-Sensing Ensemble. *Angew. Chem., Int. Ed.* **2011**, *50*, 9338−9342.

(972) Vázquez, J.; Remón, P.; Dsouza, R. N.; Lazar, A. I.; Arteaga, J. F.; Nau, W. M.; Pischel, U. A Simple Assay for Quality Binders to Cucurbiturils. *Chem.−Eur. J.* **2014**, *20*, 9897−9901.

(973) Rabbani, R.; Masson, E. Probing Interactions between Hydrocarbons and Auxiliary Guests inside Cucurbit[8]Uril. *Org. Lett.* **2017**, *19*, 4303−4306.

(974) Xu, W.-T.; Luo, Y.; Zhao, W.-W.; Liu, M.; Luo, G.-Y.; Fan, Y.; Lin, R.-L.; Tao, Z.; Xiao, X.; Liu, J.-X. Detecting Pesticide Dodine by Displacement of Fluorescent Acridine from Cucurbit[10]Uril Macrocycle. *J. Agric. Food Chem.* **2021**, *69*, 584−591.

(975) Takeuchi, T.; Montenegro, J.; Hennig, A.; Matile, S. Pattern Generation with Synthetic Sensing Systems in Lipid Bilayer Membranes. *Chem. Sci.* **2011**, *2*, 303−307.

(976) Takeuchi, T.; Bagnacani, V.; Sansone, F.; Matile, S. Amphiphilic Counterion Activators for DNA: Stimuli-Responsive Cation Transporters and Biosensors in Bulk and Lipid Bilayer Membranes. *ChemBioChem* **2009**, *10*, 2793−2799.

(977) Scott, L. E.; Orvig, C. Medicinal Inorganic Chemistry Approaches to Passivation and Removal of Aberrant Metal Ions in Disease. *Chem. Rev.* **2009**, *109*, 4885−4910.

(978) Sedgwick, A. C.; Brewster, J. T.; Harvey, P.; Iovan, D. A.; Smith, G.; He, X.-P.; Tian, H.; Sessler, J. L.; James, T. D. Metal-Based Imaging Agents: Progress Towards Interrogating Neurodegenerative Disease. *Chem. Soc. Rev.* **2020**, *49*, 2886−2915.

(979) Caravan, P.; Begley, T. P. Metals in Medicine: Imaging Agents. In *Wiley Encyclopedia of Chemical Biology*; John Wiley & Sons, 2007.

(980) Johnstone, T. C.; Park, G. Y.; Lippard, S. J. Understanding and Improving Platinum Anticancer Drugs—Phenanthriplatin. *Anticancer Res.* **2014**, *34*, 471−476.

(981) Baba, H.; Tsuneyama, K.; Yazaki, M.; Nagata, K.; Minamisaka, T.; Tsuda, T.; Nomoto, K.; Hayashi, S.; Miwa, S.; Nakajima, T.; Nakanishi, Y.; Aoshima, K.; Imura, J. The Liver in Itai-Itai Disease (Chronic Cadmium Poisoning): Pathological Features and Metallothionein Expression. *Mod. Pathol.* **2013**, *26*, 1228−1234.

(982) Godt, J.; Scheidig, F.; Grosse-Siestrup, C.; Esche, V.; Brandenburg, P.; Reich, A.; Groneberg, D. A. The Toxicity of Cadmium and Resulting Hazards for Human Health. *J. Occup. Med. Toxicol.* **2006**, *1*, 22.

(983) Stasenko, S.; Bradford, E. M.; Piasek, M.; Henson, M. C.; Varnai, V. M.; Jurasović, J.; Kušec, V. Metals in Human Placenta: Focus on the Effects of Cadmium on Steroid Hormones and Leptin. *J. Appl. Toxicol.* **2010**, *30*, 242−253.

(984) Igbokwe, I. O.; Igwenagu, E.; Igbokwe, N. A. Aluminium Toxicosis: A Review of Toxic Actions and Effects. *Interdiscip. Toxicol.* **2019**, *12*, 45−70.

(985) Rifai, N. *Tietz Textbook of Clinical Chemistry and Molecular DiagnosticsE-Book*; Elsevier Health Sciences, 2017.

(986) Reynolds, R. M.; Padfield, P. L.; Seckl, J. R. Disorders of Sodium Balance. *BMJ.* **2006**, *332*, 702−705.

(987) Verbalis, J. G.; Goldsmith, S. R.; Greenberg, A.; Schrier, R. W.; Sterns, R. H. Hyponatremia Treatment Guidelines 2007: Expert Panel Recommendations. *Am. J. Med.* **2007**, *120*, S1−21.

(988) Muhsin, S. A.; Mount, D. B. Diagnosis and Treatment of Hypernatremia. *Best Pract. Res. Clin. Endocrinol. Metab.* **2016**, *30*, 189−203.

(989) Emmett, M. Disorders of Potassium Balance: Hypokalemia & Hyperkalemia. In *Current Diagnosis & Treatment: Nephrology & Hypertension*; McGraw-Hill, 2009.

(990) McDonald, R. A. Disorders of Potassium Balance. *Pediatric Ann.* **1995**, *24*, 31−37.

(991) Berardi, R.; Torniai, M.; Lenci, E.; Pecci, F.; Morgese, F.; Rinaldi, S. Electrolyte Disorders in Cancer Patients: A Systematic Review. *J. Cancer Metastasis Treat.* **2019**, *2019*, 79.

(992) Tinawi, M. Disorders of Calcium Metabolism: Hypocalcemia and Hypercalcemia. *Cureus* **2021**, *13*, No. e12420.

(993) Sun, M.; Wu, X.; Yu, Y.; Wang, L.; Xie, D.; Zhang, Z.; Chen, L.; Lu, A.; Zhang, G.; Li, F. Disorders of Calcium and Phosphorus Metabolism and the Proteomics/Metabolomics-Based Research. *Front. Cell Dev. Biol.* **2020**, 8−576110.

(994) Edmondson, J. W.; Brashear, R. E.; Li, T. K. Tetany: Quantitative Interrelationships between Calcium and Alkalosis. *Am. J. Physiol.* **1975**, *228*, 1082−1086.

(995) de Baaij, J. H. F.; Hoenderop, J. G. J.; Bindels, R. J. M. Magnesium in Man: Implications for Health and Disease. *Physiol. Rev.* **2015**, *95*, 1−46.

(996) Horn, D.; Barrientos, A. Mitochondrial Copper Metabolism and Delivery to Cytochrome C Oxidase. *IUBMB Life* **2008**, *60*, 421−429.

(997) Gaetke, L. M.; Chow-Johnson, H. S.; Chow, C. K. Copper: Toxicological Relevance and Mechanisms. *Arch. Toxicol.* **2014**, *88*, 1929−1938.

(998) Budimir, A. Metal Ions, Alzheimer's Disease and Chelation Therapy. *Acta Pharm.* **2011**, *61*, 1−14.

(999) Liu, Y.; Nguyen, M.; Robert, A.; Meunier, B. Metal Ions in Alzheimer's Disease: A Key Role or Not? *Acc. Chem. Res.* **2019**, *52*, 2026−2035.

(1000) Hajji, N.; Calvert, C.; Ritchie, C. W.; Sastre, M. The Role of Metals in Alzheimer's Disease. In *Mechanisms and Metal Involvement in Neurodegenerative Diseases*; Royal Society of Chemistry, 2013; pp 80−97.

(1001) Enochs, W. S.; Sarna, T.; Zecca, L.; Riley, P. A.; Swartz, H. M. The Roles of Neuromelanin, Binding of Metal Ions, and Oxidative Cytotoxicity in the Pathogenesis of Parkinson's Disease: A Hypothesis. *J. Neural Transm.: Parkinson's Dis. Dementia Sect.* **1994**, *7*, 83−100.

(1002) Deas, E.; Cremades, N.; Angelova, P. R.; Ludtmann, M. H. R.; Yao, Z.; Chen, S.; Horrocks, M. H.; Banushi, B.; Little, D.; Devine, M. J.; Gissen, P.; Klenerman, D.; Dobson, C. M.; Wood, N. W.; Gandhi, S.; Abramov, A. Y. Alpha-Synuclein Oligomers Interact with Metal Ions to Induce Oxidative Stress and Neuronal Death in Parkinson's Disease. *Antioxid. Redox Signaling* **2016**, *24*, 376−391.

(1003) Waldvogel, D.; Van Gelderen, P.; Hallett, M. Increased Iron in the Dentate Nucleus of Patients with Friedreich's Ataxia. *Ann. Neurol.* **1999**, *46*, 123−125.

(1004) Boddaert, N.; Le Quan Sang, K. H.; Rötig, A.; Leroy-Willig, A.; Gallet, S.; Brunelle, F.; Sidi, D.; Thalabard, J. C.; Munnich, A.; Cabantchik, Z. I. Selective Iron Chelation in Friedreich Ataxia: Biologic and Clinical Implications. *Blood* **2007**, *110*, 401−408.

(1005) Kontoghiorghes, G. J.; Weinberg, E. D. Iron: Mammalian Defense Systems, Mechanisms of Disease, and Chelation Therapy Approaches. *Blood Rev.* **1995**, *9*, 33−45.

(1006) Kitzberger, R.; Madl, C.; Ferenci, P. Wilson Disease. *Metab. Brain Dis.* **2005**, *20*, 295−302.

(1007) Tusa, J. K.; He, H. Critical Care Analyzer with Fluorescent Optical Chemosensors for Blood Analytes. *J. Mater. Chem.* **2005**, *15*, 2640−2647.

(1008) Frost, M. C.; Meyerhoff, M. E. Real-Time Monitoring of Critical Care Analytes in the Bloodstream with Chemical Sensors: Progress and Challenges. *Annu. Rev. Anal. Chem.* **2015**, *8*, 171−192.

(1009) Carter, K. P.; Young, A. M.; Palmer, A. E. Fluorescent Sensors for Measuring Metal Ions in Living Systems. *Chem. Rev.* **2014**, *114*, 4564−4601.

(1010) Cockrell, G. M.; Zhang, G.; VanDerveer, D. G.; Thummel, R. P.; Hancock, R. D. Enhanced Metal Ion Selectivity of 2,9-Di-(Pyrid-2-Yl)-1,10-Phenanthroline and Its Use as a Fluorescent Sensor for Cadmium(Ii). *J. Am. Chem. Soc.* **2008**, *130*, 1420−1430.

(1011) Hong, Y.; Chen, S.; Leung, C. W. T.; Lam, J. W. Y.; Liu, J.; Tseng, N.-W.; Kwok, R. T. K.; Yu, Y.; Wang, Z.; Tang, B. Z. Fluorogenic Zn(Ii) and Chromogenic Fe(Ii) Sensors Based on Terpyridine-Substituted Tetraphenylethenes with Aggregation-Induced Emission Characteristics. *ACS Appl. Mater. Interfaces* **2011**, *3*, 3411−3418.

(1012) Nadeem, S.; Shah, M. R.; Khan, B.; Hoda, N.; Topel, Ö. Supramolecular Chemosensor for Selective Detection of Iron in Aqueous Medium. *Supramol. Chem.* **2013**, *25*, 798−805.

(1013) Yao, J.; Dou, W.; Qin, W.; Liu, W. A New Coumarin-Based Chemosensor for Fe3+ in Water. *Inorg. Chem. Commun.* **2009**, *12*, 116−118.

(1014) Yoon, S.; Albers, A. E.; Wong, A. P.; Chang, C. J. Screening Mercury Levels in Fish with a Selective Fluorescent Chemosensor. *J. Am. Chem. Soc.* **2005**, *127*, 16030−16031.

(1015) *Regulatory Impact Analysis of the Clean Air Mercury Rule*; EPA-452, R-05-003; U.S. EPA, 2005.

(1016) Yoon, S.; Miller, E. W.; He, Q.; Do, P. H.; Chang, C. J. A Bright and Specific Fluorescent Sensor for Mercury in Water, Cells, and Tissue. *Angew. Chem., Int. Ed.* **2007**, *46*, 6658−6661.

(1017) Mitra, A.; Mittal, A. K.; Rao, C. P. Carbohydrate Assisted Fluorescence Turn-on Gluco-Imino-Anthracenyl Conjugate as a Hg(Ii) Sensor in Milk and Blood Serum Milieu. *Chem. Commun.* **2011**, *47*, 2565−2567.

(1018) Xu, Y.; Panzner, M. J.; Li, X.; Youngs, W. J.; Pang, Y. Host-Guest Assembly of Squaraine Dye in Cucurbit[8]Uril: Its Implication in Fluorescent Probe for Mercury Ions. *Chem. Commun.* **2010**, *46*, 4073−4075.

(1019) He, H.; Mortellaro, M. A.; Leiner, M. J. P.; Fraatz, R. J.; Tusa, J. K. A Fluorescent Sensor with High Selectivity and Sensitivity for Potassium in Water. *J. Am. Chem. Soc.* **2003**, *125*, 1468−1469.

(1020) He, H.; Mortellaro, M. A.; Leiner, M. J. P.; Young, S. T.; Fraatz, R. J.; Tusa, J. K. A Fluorescent Chemosensor for Sodium Based on Photoinduced Electron Transfer. *Anal. Chem.* **2003**, *75*, 549−555.

(1021) de Silva, A. P.; Moody, T. S.; Wright, G. D. Fluorescent Pet (Photoinduced Electron Transfer) Sensors as Potent Analytical Tools. *Analyst* **2009**, *134*, 2385−2393.

(1022) Gunnlaugsson, T.; Nieuwenhuyzen, M.; Richard, L.; Thoss, V. A Novel Optically Based Chemosensor for the Detection of Blood Na+. *Tetrahedron Lett.* **2001**, *42*, 4725−4728.

(1023) Wipf, M.; Stoop, R. L.; Tarasov, A.; Bedner, K.; Fu, W.; Wright, I. A.; Martin, C. J.; Constable, E. C.; Calame, M.; Schönenberger, C. Selective Sodium Sensing with Gold-Coated Silicon Nanowire Field-Effect Transistors in a Differential Setup. *ACS Nano* **2013**, *7*, 5978−5983.

(1024) Padmawar, P.; Yao, X.; Bloch, O.; Manley, G. T.; Verkman, A. S. K+ Waves in Brain Cortex Visualized Using a Long-Wavelength K+-Sensing Fluorescent Indicator. *Nat. Methods* **2005**, *2*, 825−827.

(1025) Namkung, W.; Padmawar, P.; Mills, A. D.; Verkman, A. S. Cell-Based Fluorescence Screen for K+ Channels and Transporters Using an Extracellular Triazacryptand-Based K+ Sensor. *J. Am. Chem. Soc.* **2008**, *130*, 7794−7795.

(1026) Carpenter, R. D.; Verkman, A. S. Synthesis of a Sensitive and Selective Potassium-Sensing Fluoroionophore. *Org. Lett.* **2010**, *12*, 1160−1163.

(1027) Thier, S. O. Potassium Physiology. *Am. J. Med.* **1986**, *80*, 3−7.

(1028) Zhou, X.; Su, F.; Tian, Y.; Youngbull, C.; Johnson, R. H.; Meldrum, D. R. A New Highly Selective Fluorescent K+ Sensor. *J. Am. Chem. Soc.* **2011**, *133*, 18530−18533.

(1029) Souchon, V.; Leray, I.; Valeur, B. Selective Detection of Cesium by a Water-Soluble Fluorescent Molecular Sensor Based on a Calix[4]Arene-Bis(Crown-6-Ether). *Chem. Commun.* **2006**, 4224−4226.

(1030) Farruggia, G.; Iotti, S.; Prodi, L.; Montalti, M.; Zaccheroni, N.; Savage, P. B.; Trapani, V.; Sale, P.; Wolf, F. I. 8-Hydroxyquinoline Derivatives as Fluorescent Sensors for Magnesium in Living Cells. *J. Am. Chem. Soc.* **2006**, *128*, 344−350.

(1031) Nakahara, Y.; Kida, T.; Nakatsuji, Y.; Akashi, M. A Novel Fluorescent Indicator for Ba2+ in Aqueous Micellar Solutions. *Chem. Commun.* **2004**, 224−225.

(1032) Paredes, R. M.; Etzler, J. C.; Watts, L. T.; Zheng, W.; Lechleiter, J. D. Chemical Calcium Indicators. *Methods* **2008**, *46*, 143−151.

(1033) Tsien, R. Y. Fluorescence Measurement and Photochemical Manipulation of Cytosolic Free Calcium. *Trends Neurosci.* **1988**, *11*, 419−424.

(1034) Stosiek, C.; Garaschuk, O.; Holthoff, K.; Konnerth, A. In Vivo Two-Photon Calcium Imaging of Neuronal Networks. *Proc. Natl. Acad. Sci. U. S. A.* **2003**, *100*, 7319−7324.

(1035) Roe, M. W.; Lemasters, J. J.; Herman, B. Assessment of Fura-2 for Measurements of Cytosolic Free Calcium. *Cell Calcium* **1990**, *11*, 63−73.

(1036) Malgaroli, A.; Milani, D.; Meldolesi, J.; Pozzan, T. Fura-2 Measurement of Cytosolic Free Ca2+ in Monolayers and Suspensions of Various Types of Animal Cells. *J. Cell Biol.* **1987**, *105*, 2145−2155.

(1037) Neher, E. The Use of Fura-2 for Estimating Ca Buffers and Ca Fluxes. *Neuropharmacology* **1995**, *34*, 1423−1442.

(1038) Williams, D. A.; Fogarty, K. E.; Tsien, R. Y.; Fay, F. S. Calcium Gradients in Single Smooth Muscle Cells Revealed by the Digital Imaging Microscope Using Fura-2. *Nature* **1985**, *318*, 558−561.

(1039) Almers, W.; Neher, E. The Ca Signal from Fura-2 Loaded Mast Cells Depends Strongly on the Method of Dye-Loading. *FEBS Lett.* **1985**, *192*, 13−18.

(1040) Bannwarth, M.; Corrêa, I. R., Jr; Sztretye, M.; Pouvreau, S.; Fellay, C.; Aebischer, A.; Royer, L.; Ríos, E.; Johnsson, K. Indo-1 Derivatives for Local Calcium Sensing. *ACS Chem. Biol.* **2009**, *4*, 179−190.

(1041) Burdette, S. C.; Walkup, G. K.; Spingler, B.; Tsien, R. Y.; Lippard, S. J. Fluorescent Sensors for Zn2+ Based on a Fluorescein Platform: Synthesis, Properties and Intracellular Distribution. *J. Am. Chem. Soc.* **2001**, *123*, 7831−7841.

(1042) Walkup, G. K.; Burdette, S. C.; Lippard, S. J.; Tsien, R. Y. A New Cell-Permeable Fluorescent Probe for Zn2+. *J. Am. Chem. Soc.* **2000**, *122*, 5644−5645.

(1043) Du, P.; Lippard, S. J. A Highly Selective Turn-on Colorimetric, Red Fluorescent Sensor for Detecting Mobile Zinc in Living Cells. *Inorg. Chem.* **2010**, *49*, 10753−10755.

(1044) Ishida, T. Review on the Role of Zn2+ Ions in Viral Pathogenesis and the Effect of Zn2+ Ions for Host Cell-Virus Growth Inhibition. *Am. J. Biomed. Sci.* **2019**, *2*, 28−37.

(1045) Frederickson, C. J.; Koh, J.-Y.; Bush, A. I. The Neurobiology of Zinc in Health and Disease. *Nat. Rev. Neurosci.* **2005**, *6*, 449−462.

(1046) Xu, Z.; Liu, X.; Pan, J.; Spring, D. R. Coumarin-Derived Transformable Fluorescent Sensor for Zn2+. *Chem. Commun.* **2012**, *48*, 4764−4766.

(1047) Gui, S.; Huang, Y.; Hu, F.; Jin, Y.; Zhang, G.; Yan, L.; Zhang, D.; Zhao, R. Fluorescence Turn-on Chemosensor for Highly Selective and Sensitive Detection and Bioimaging of Al3+ in Living Cells Based on Ion-Induced Aggregation. *Anal. Chem.* **2015**, *87*, 1470−1474.

(1048) Wang, Z.; Palacios, M. A.; Anzenbacher, P. Fluorescence Sensor Array for Metal Ion Detection Based on Various Coordination Chemistries: General Performance and Potential Application. *Anal. Chem.* **2008**, *80*, 7451−7459.

(1049) Palacios, M. A.; Wang, Z.; Montes, V. A.; Zyryanov, G. V.; Hausch, B. J.; Jursíková, K.; Anzenbacher, P., Jr Hydroxyquinolines with Extended Fluorophores: Arrays for Turn-on and Ratiometric Sensing of Cations. *Chem. Commun.* **2007**, 3708−3710.

(1050) Palacios, M. A.; Wang, Z.; Montes, V. A.; Zyryanov, G. V.; Anzenbacher, P. Rational Design of a Minimal Size Sensor Array for Metal Ion Detection. *J. Am. Chem. Soc.* **2008**, *130*, 10307−10314.

(1051) Bryant, J. J.; Lindner, B. D.; Bunz, U. H. F. Water-Soluble Bis-Triazolyl Benzochalcogendiazole Cycloadducts as Tunable Metal Ion Sensors. *J. Org. Chem.* **2013**, *78*, 1038−1044.

(1052) Dsouza, R. N.; Pischel, U.; Nau, W. M. Fluorescent Dyes and Their Supramolecular Host/Guest Complexes with Macrocycles in Aqueous Solution. *Chem. Rev.* **2011**, *111*, 7941−7980.

(1053) Geng, Q.-X.; Cong, H.; Tao, Z.; Lindoy, L. F.; Wei, G. Cucurbit[7]Uril-Improved Recognition by a Fluorescent Sensor for Cadmium and Zinc Cations. *Supramol. Chem.* **2016**, *28*, 784−791.

(1054) Chernikova, E.; Berdnikova, D.; Fedorov, Y.; Fedorova, O.; Peregudov, A.; Isaacs, L. Self-Assembly of a Ternary Architecture Driven by Cooperative Hg2+ Ion Binding between Cucurbit[7]Uril and Crown Ether Macrocyclic Hosts. *Chem. Commun.* **2012**, *48*, 7256−7258.

(1055) Aliaga, M. E.; Garcia-Rio, L.; Pessego, M.; Montecinos, R.; Fuentealba, D.; Uribe, I.; Martin-Pastor, M.; Garcia-Beltran, O. Host-Guest Interaction of Coumarin-Derivative Dyes and Cucurbit[7]Uril: Leading to the Formation of Supramolecular Ternary Complexes with Mercuric Ions. *New J. Chem.* **2015**, *39*, 3084−3092.

(1056) Yao, Q.; Lü, B.; Ji, C.; Cai, Y.; Yin, M. Supramolecular Host-Guest System as Ratiometric Fe3+ Ion Sensor Based on Water-Soluble Pillar[5]Arene. *ACS Appl. Mater. Interfaces* **2017**, *9*, 36320−36326.

(1057) Bar-Shir, A.; Gilad, A. A.; Chan, K. W. Y.; Liu, G.; van Zijl, P. C. M.; Bulte, J. W. M.; McMahon, M. T. Metal Ion Sensing Using Ion Chemical Exchange Saturation Transfer 19f Magnetic Resonance Imaging. *J. Am. Chem. Soc.* **2013**, *135*, 12164−12167.

(1058) Avram, L.; Havel, V.; Shusterman-Krush, R.; Iron, M. A.; Zaiss, M.; Šindelář, V.; Bar-Shir, A. Dynamic Interactions in Synthetic Receptors: A Guest Exchange Saturation Transfer Study. *Chem.−Eur. J.* **2019**, *25*, 1604.

(1059) Avram, L.; Wishard, A. D.; Gibb, B. C.; Bar-Shir, A. Quantifying Guest Exchange in Supramolecular Systems. *Angew. Chem., Int. Ed.* **2017**, *56*, 15314−15318.

(1060) Liu, L.; Zhang, G.; Xiang, J.; Zhang, D.; Zhu, D. Fluorescence "Turn on" Chemosensors for Ag+ and Hg2+ Based on Tetraphenylethylene Motif Featuring Adenine and Thymine Moieties. *Org. Lett.* **2008**, *10*, 4581−4584.

(1061) Minami, T.; Sasaki, Y.; Minamiki, T.; Koutnik, P.; Anzenbacher, P.; Tokito, S. A Mercury(Ii) Ion Sensor Device Based on an Organic Field Effect Transistor with an Extended-Gate Modified by Dipicolylamine. *Chem. Commun.* **2015**, *51*, 17666−17668.

(1062) Forte, G.; Visconti, A.; Santucci, S.; Ghazaryan, A.; Figà-Talamanca, L.; Cannoni, S.; Bocca, B.; Pino, A.; Violante, N.; Alimonti, A.; Salvetti, M.; Ristori, G. Quantification of Chemical Elements in Blood of Patients Affected by Multiple Sclerosis. *Ann. Ist. Super. Sanita* **2005**, *41*, 213−216.

(1063) Bocca, B.; Forte, G.; Petrucci, F.; Pino, A.; Marchione, F.; Bomboi, G.; Senofonte, O.; Giubilei, F.; Alimonti, A. Monitoring of Chemical Elements and Oxidative Damage in Patients Affected by Alzheimer's Disease. *Ann. Ist. Super. Sanita* **2005**, *41*, 197−203.

(1064) Shalev, H.; Phillip, M.; Galil, A.; Carmi, R.; Landau, D. Clinical Presentation and Outcome in Primary Familial Hypomagnesaemia. *Arch. Dis. Child.* **1998**, *78*, 127−130.

(1065) Kim, Y. J.; Kim, Y. K.; Kho, H. S. Effects of Smoking on Trace Metal Levels in Saliva. *Oral Dis.* **2010**, *16*, 823−830.

(1066) Bulaj, Z. J.; Griffen, L. M.; Jorde, L. B.; Edwards, C. Q.; Kushner, J. P. Clinical and Biochemical Abnormalities in People Heterozygous for Hemochromatosis. *N. Engl. J. Med.* **1996**, *335*, 1799−1805.

(1067) Bocca, B.; Ciccarelli, S.; Agostino, R.; Alimonti, A. Trace Elements, Oxidative Status and Antioxidant Capacity as Biomarkers in Very Low Birth Weight Infants. *Environ. Res.* **2017**, *156*, 705−713.

(1068) Ruha, A. M.; Curry, S. C.; Gerkin, R. D.; Caldwell, K. L.; Osterloh, J. D.; Wax, P. M. Urine Mercury Excretion Following Meso-Dimercaptosuccinic Acid Challenge in Fish Eaters. *Arch. Pathol. Lab. Med.* **2009**, *133*, 87−92.

(1069) *Mercury in Drinking Water*; World Health Organization, 2005; https://www.who.int/water_sanitation_health/dwq/chemicals/mercuryfinal.pdf (accessed 2021-01).

(1070) Berend, K.; van Hulsteijn, L. H.; Gans, R. O. B. Chloride: The Queen of Electrolytes? *Eur. J. Intern. Med.* **2012**, *23*, 203−211.

(1071) George, A. L., Jr; Bianchi, L.; Link, E. M.; Vanoye, C. G. From Stones to Bones: The Biology of Clc Chloride Channels. *Curr. Biol.* **2001**, *11*, R620−R628.

(1072) Khatri, M.; Zitovsky, J.; Lee, D.; Nayyar, K.; Fazzari, M.; Grant, C. The Association between Serum Chloride Levels and Chronic Kidney Disease Progression: A Cohort Study. *BMC Nephrol.* **2020**, *21*, 165.

(1073) Ter Maaten, J. M.; Damman, K.; Hanberg, J. S.; Givertz, M. M.; Metra, M.; O'Connor, C. M.; Teerlink, J. R.; Ponikowski, P.; Cotter, G.; Davison, B.; et al. Hypochloremia, Diuretic Resistance, and Outcome in Patients with Acute Heart Failure. *Circ.: Heart Failure* **2016**, *9*, e003109.

(1074) Galla, J. H. Metabolic Alkalosis. *J. Am. Soc. Nephrol.* **2000**, *11*, 369−375.

(1075) Suetrong, B.; Pisitsak, C.; Boyd, J. H.; Russell, J. A.; Walley, K. R. Hyperchloremia and Moderate Increase in Serum Chloride Are Associated with Acute Kidney Injury in Severe Sepsis and Septic Shock Patients. *Crit. Care* **2016**, *20*, 315.

(1076) Liou, T. G. The Clinical Biology of Cystic Fibrosis Transmembrane Regulator Protein: Its Role and Function in Extrapulmonary Disease. *Chest* **2019**, *155*, 605−616.

(1077) Dalemans, W.; Barbry, P.; Champigny, G.; Jallat, S.; Jallat, S.; Dott, K.; Dreyer, D.; Crystal, R. G.; Pavirani, A.; Lecocq, J.-P.; Lazdunski, M. Altered Chloride Ion Channel Kinetics Associated with the Delta F508 Cystic Fibrosis Mutation. *Nature* **1991**, *354*, 526.

(1078) Cantin, A. M.; Hartl, D.; Konstan, M. W.; Chmiel, J. F. Inflammation in Cystic Fibrosis Lung Disease: Pathogenesis and Therapy. *J. Cystic Fibrosis* **2015**, *14*, 419−430.

(1079) Li, L.; Moore, P. K. Putative Biological Roles of Hydrogen Sulfide in Health and Disease: A Breath of Not So Fresh Air? *Trends Pharmacol. Sci.* **2008**, *29*, 84−90.

(1080) Ono, K.; Akaike, T.; Sawa, T.; Kumagai, Y.; Wink, D. A.; Tantillo, D. J.; Hobbs, A. J.; Nagy, P.; Xian, M.; Lin, J.; Fukuto, J. M. Redox Chemistry and Chemical Biology of H2s, Hydropersulfides, and Derived Species: Implications of Their Possible Biological Activity and Utility. *Free Radical Biol. Med.* **2014**, *77*, 82−94.

(1081) Wallace, J. L.; Wang, R. Hydrogen Sulfide-Based Therapeutics: Exploiting a Unique but Ubiquitous Gasotransmitter. *Nat. Rev. Drug Discovery* **2015**, *14*, 329−345.

(1082) Guidotti, T. L. Hydrogen Sulfide: Advances in Understanding Human Toxicity. *Int. J. Toxicol.* **2010**, *29*, 569−581.

(1083) Whiteman, M.; Le Trionnaire, S.; Chopra, M.; Fox, B.; Whatmore, J. Emerging Role of Hydrogen Sulfide in Health and Disease: Critical Appraisal of Biomarkers and Pharmacological Tools. *Clin. Sci.* **2011**, *121*, 459−488.

(1084) Panthi, S.; Manandhar, S.; Gautam, K. Hydrogen Sulfide, Nitric Oxide, and Neurodegenerative Disorders. *Transl. Neurodegener.* **2018**, *7*, 3.

(1085) Shefa, U.; Kim, M.-S.; Jeong, N. Y.; Jung, J. Antioxidant and Cell-Signaling Functions of Hydrogen Sulfide in the Central Nervous System. *Oxid. Med. Cell. Longevity* **2018**, *2018*, 1873962.

(1086) Han, Y.; Shang, Q.; Yao, J.; Ji, Y. Hydrogen Sulfide: A Gaseous Signaling Molecule Modulates Tissue Homeostasis: Implications in Ophthalmic Diseases. *Cell Death Dis.* **2019**, *10*, 293.

(1087) Lundberg, J. O.; Gladwin, M. T.; Ahluwalia, A.; Benjamin, N.; Bryan, N. S.; Butler, A.; Cabrales, P.; Fago, A.; Feelisch, M.; Ford, P. C.; Freeman, B. A.; Frenneaux, M.; Friedman, J.; Kelm, M.; Kevil, C. G.; Kim-Shapiro, D. B.; Kozlov, A. V.; Lancaster, J. R.; Lefer, D. J.; McColl, K.; McCurry, K.; Patel, R. P.; Petersson, J.; Rassaf, T.; Reutov, V. P.; Richter-Addo, G. B.; Schechter, A.; Shiva, S.; Tsuchiya, K.; van Faassen, E. E.; Webb, A. J.; Zuckerbraun, B. S.; Zweier, J. L.; Weitzberg, E. Nitrate and Nitrite in Biology, Nutrition and Therapeutics. *Nat. Chem. Biol.* **2009**, *5*, 865−869.

(1088) Lundberg, J. O.; Carlström, M.; Larsen, F. J.; Weitzberg, E. Roles of Dietary Inorganic Nitrate in Cardiovascular Health and Disease. *Cardiovasc. Res.* **2011**, *89*, 525−532.

(1089) Lundberg, J. O.; Weitzberg, E.; Gladwin, M. T. The Nitrate-Nitrite-Nitric Oxide Pathway in Physiology and Therapeutics. *Nat. Rev. Drug Discovery* **2008**, *7*, 156−167.

(1090) Bryan, N. S.; Grisham, M. B. Methods to Detect Nitric Oxide and Its Metabolites in Biological Samples. *Free Radical Biol. Med.* **2007**, *43*, 645−657.

(1091) Neth, M. R.; Love, J. S.; Horowitz, B. Z.; Shertz, M. D.; Sahni, R.; Daya, M. R. Fatal Sodium Nitrite Poisoning: Key Considerations for Prehospital Providers. *Prehospital Emergency Care* **2021**, 844, *25*.

(1092) Castranova, V.; Vallyathan, V. Silicosis and Coal Workers' Pneumoconiosis. *Environ. Health Perspect.* **2000**, *108*, 675−684.

(1093) Manoj, K. M.; Ramasamy, S.; Parashar, A.; Gideon, D. A.; Soman, V.; Jacob, V. D.; Pakshirajan, K. Acute Toxicity of Cyanide in Aerobic Respiration: Theoretical and Experimental Support for Murburn Explanation. *Biomol. Concepts* **2020**, *11*, 32−56.

(1094) Yang, P.; Wei, W.; Tao, C. Determination of Trace Thiocyanate with Nano-Silver Coated Multi-Walled Carbon Nanotubes Modified Glassy Carbon Electrode. *Anal. Chim. Acta* **2007**, *585*, 331−336.

(1095) Braverman, L. E.; He, X.; Pino, S.; Cross, M.; Magnani, B.; Lamm, S. H.; Kruse, M. B.; Engel, A.; Crump, K. S.; Gibbs, J. P. The Effect of Perchlorate, Thiocyanate, and Nitrate on Thyroid Function in Workers Exposed to Perchlorate Long-Term. *J. Clin. Endocrinol. Metab.* **2005**, *90*, 700−706.

(1096) Johnston, N. R.; Strobel, S. A. Principles of Fluoride Toxicity and the Cellular Response: A Review. *Arch. Toxicol.* **2020**, *94*, 1051−1069.

(1097) Guo, L.; Wang, Y.; Zheng, Y.; Huang, Z.; Cheng, Y.; Ye, J.; Chu, Q.; Huang, D. Study on the Potential Application of Salivary Inorganic Anions in Clinical Diagnosis by Capillary Electrophoresis Coupled with Contactless Conductivity Detection. *J. Chromatogr. B: Anal. Technol. Biomed. Life Sci.* **2016**, *1014*, 70−74.

(1098) Lundberg, J. O.; Carlström, M.; Weitzberg, E. Metabolic Effects of Dietary Nitrate in Health and Disease. *Cell Metab.* **2018**, *28*, 9−22.

(1099) Shiraishi, Y.; Nakamura, M.; Hayashi, N.; Hirai, T. Coumarin-Spiropyran Dyad with a Hydrogenated Pyran Moiety for Rapid, Selective, and Sensitive Fluorometric Detection of Cyanide Anion. *Anal. Chem.* **2016**, *88*, 6805−6811.

(1100) Shiraishi, Y.; Sumiya, S.; Hirai, T. Highly Sensitive Cyanide Anion Detection with a Coumarin-Spiropyran Conjugate as a Fluorescent Receptor. *Chem. Commun.* **2011**, *47*, 4953−4955.

(1101) Shiraishi, Y.; Adachi, K.; Itoh, M.; Hirai, T. Spiropyran as a Selective, Sensitive, and Reproducible Cyanide Anion Receptor. *Org. Lett.* **2009**, *11*, 3482−3485.

(1102) Peng, M.-J.; Guo, Y.; Yang, X.-F.; Wang, L.-Y.; An, J. A Highly Selective Ratiometric and Colorimetric Chemosensor for Cyanide Detection. *Dyes Pigm.* **2013**, *98*, 327−332.

(1103) Lin, Q.; Liu, X.; Wei, T. B.; Zhang, Y. M. Reaction-Based Ratiometric Chemosensor for Instant Detection of Cyanide in Water with High Selectivity and Sensitivity. *Chem.−Asian J.* **2013**, *8*, 3015−3021.

(1104) Qu, Y.; Jin, B.; Liu, Y.; Wu, Y.; Yang, L.; Wu, J.; Hua, J. A New Triphenylamine Fluorescent Dye for Sensing of Cyanide Anion in Living Cell. *Tetrahedron Lett.* **2013**, *54*, 4942−4944.

(1105) Zhang, Y.; Li, D.; Li, Y.; Yu, J. Solvatochromic Aie Luminogens as Supersensitive Water Detectors in Organic Solvents and Highly Efficient Cyanide Chemosensors in Water. *Chem. Sci.* **2014**, *5*, 2710−2716.

(1106) Sun, T.; Niu, Q.; Li, Y.; Li, T.; Hu, T.; Wang, E.; Liu, H. A Novel Oligothiophene-Based Colorimetric and Fluorescent "Turn on" Sensor for Highly Selective and Sensitive Detection of Cyanide in Aqueous Media and Its Practical Applications in Water and Food Samples. *Sens. Actuators, B* **2018**, *258*, 64−71.

(1107) Yang, L.; Li, X.; Qu, Y.; Qu, W.; Zhang, X.; Hang, Y.; Ågren, H.; Hua, J. Red Turn-on Fluorescent Phenazine-Cyanine Chemodosimeters for Cyanide Anion in Aqueous Solution and Its Application for Cell Imaging. *Sens. Actuators, B* **2014**, *203*, 833−847.

(1108) Reddy G, U.; Das, P.; Saha, S.; Baidya, M.; Ghosh, S. K.; Das, A. A Cn-Specific Turn-on Phosphorescent Probe with Probable

Application for Enzymatic Assay and as an Imaging Reagent. *Chem. Commun.* **2013**, *49*, 255−257.

(1109) Chen, X.; Nam, S. W.; Kim, G. H.; Song, N.; Jeong, Y.; Shin, I.; Kim, S. K.; Kim, J.; Park, S.; Yoon, J. A near-Infrared Fluorescent Sensor for Detection of Cyanide in Aqueous Solution and Its Application for Bioimaging. *Chem. Commun.* **2010**, *46*, 8953−8955.

(1110) Xu, J.-F.; Chen, H.-H.; Chen, Y.-Z.; Li, Z.-J.; Wu, L.-Z.; Tung, C.-H.; Yang, Q.-Z. A Colorimetric and Fluorometric Dual-Modal Chemosensor for Cyanide in Water. *Sens. Actuators, B* **2012**, *168*, 14−19.

(1111) Kaushik, R.; Ghosh, A.; Singh, A.; Gupta, P.; Mittal, A.; Jose, D. A. Selective Detection of Cyanide in Water and Biological Samples by an Off-the-Shelf Compound. *ACS Sens.* **2016**, *1*, 1265−1271.

(1112) Li, M.; Liang, Q.; Zheng, M.; Fang, C.; Peng, S.; Zhao, M. An Efficient Ruthenium Tris(Bipyridine)-Based Luminescent Chemosensor for Recognition of Cu(Ii) and Sulfide Anion in Water. *Dalton Trans.* **2013**, *42*, 13509−13515.

(1113) Hou, F.; Huang, L.; Xi, P.; Cheng, J.; Zhao, X.; Xie, G.; Shi, Y.; Cheng, F.; Yao, X.; Bai, D.; Zeng, Z. A Retrievable and Highly Selective Fluorescent Probe for Monitoring Sulfide and Imaging in Living Cells. *Inorg. Chem.* **2012**, *51*, 2454−2460.

(1114) Wang, M. Q.; Li, K.; Hou, J. T.; Wu, M. Y.; Huang, Z.; Yu, X. Q. Binol-Based Fluorescent Sensor for Recognition of Cu(Ii) and Sulfide Anion in Water. *J. Org. Chem.* **2012**, *77*, 8350−8354.

(1115) Tang, L.; Cai, M.; Huang, Z.; Zhong, K.; Hou, S.; Bian, Y.; Nandhakumar, R. Rapid and Highly Selective Relay Recognition of Cu(Ii) and Sulfide Ions by a Simple Benzimidazole-Based Fluorescent Sensor in Water. *Sens. Actuators, B* **2013**, *185*, 188−194.

(1116) Hao, Y.; Chen, W.; Wang, L.; Zhu, X.; Zhang, Y.; Qu, P.; Liu, L.; Zhou, B.; Liu, Y. N.; Xu, M. A Retrievable, Water-Soluble and Biocompatible Fluorescent Probe for Recognition of Cu(Ii) and Sulfide Based on a Peptide Receptor. *Talanta* **2015**, *143*, 307−314.

(1117) Cao, X.; Lin, W.; He, L. A near-Infrared Fluorescence Turn-on Sensor for Sulfide Anions. *Org. Lett.* **2011**, *13*, 4716−4719.

(1118) Liu, J.; Lin, Q.; Zhang, Y.-M.; Wei, T.-B. A Reversible and Highly Selective Fluorescent Probe for Monitoring Hg2+ and Iodide in Aqueous Solution. *Sens. Actuators, B* **2014**, *196*, 619−623.

(1119) Wang, H.; Xue, L.; Jiang, H. Ratiometric Fluorescent Sensor for Silver Ion and Its Resultant Complex for Iodide Anion in Aqueous Solution. *Org. Lett.* **2011**, *13*, 3844−3847.

(1120) Yun, D.; Chae, J. B.; So, H.; Lee, H.; Kim, K.-T.; Kim, C. Sensing of Zinc Ions and Sulfide Using a Highly Practical and Water-Soluble Fluorescent Sensor: Applications in Test Kits and Zebrafish. *New J. Chem.* **2020**, *44*, 442−449.

(1121) Liu, J.; Sun, Y. Q.; Zhang, J.; Yang, T.; Cao, J.; Zhang, L.; Guo, W. A Ratiometric Fluorescent Probe for Biological Signaling Molecule H2s: Fast Response and High Selectivity. *Chem.−Eur. J.* **2013**, *19*, 4717−4722.

(1122) Chen, Y.; Zhu, C.; Yang, Z.; Chen, J.; He, Y.; Jiao, Y.; He, W.; Qiu, L.; Cen, J.; Guo, Z. A Ratiometric Fluorescent Probe for Rapid Detection of Hydrogen Sulfide in Mitochondria. *Angew. Chem., Int. Ed.* **2013**, *52*, 1688−1691.

(1123) Li, H. D.; Yao, Q. C.; Fan, J. L.; Jiang, N.; Wang, J. Y.; Xia, J.; Peng, X. J. A Fluorescent Probe for H2s in Vivo with Fast Response and High Sensitivity. *Chem. Commun.* **2015**, *51*, 16225−16228.

(1124) Kim, T.-H.; Swager, T. M. A Fluorescent Self-Amplifying Wavelength-Responsive Sensory Polymer for Fluoride Ions. *Angew. Chem., Int. Ed.* **2003**, *42*, 4803−4806.

(1125) Hu, R.; Feng, J.; Hu, D.; Wang, S.; Li, S.; Li, Y.; Yang, G. A Rapid Aqueous Fluoride Ion Sensor with Dual Output Modes. *Angew. Chem., Int. Ed.* **2010**, *49*, 4915−4918.

(1126) Sokkalingam, P.; Lee, C. H. Highly Sensitive Fluorescence "Turn-on" Indicator for Fluoride Anion with Remarkable Selectivity in Organic and Aqueous Media. *J. Org. Chem.* **2011**, *76*, 3820−3828.

(1127) Zhu, B.; Yuan, F.; Li, R.; Li, Y.; Wei, Q.; Ma, Z.; Du, B.; Zhang, X. A Highly Selective Colorimetric and Ratiometric Fluorescent Chemodosimeter for Imaging Fluoride Ions in Living Cells. *Chem. Commun.* **2011**, *47*, 7098−7100.

(1128) Kim, D.; Singha, S.; Wang, T.; Seo, E.; Lee, J. H.; Lee, S. J.; Kim, K. H.; Ahn, K. H. In Vivo Two-Photon Fluorescent Imaging of Fluoride with a Desilylation-Based Reactive Probe. *Chem. Commun.* **2012**, *48*, 10243−10245.

(1129) Zheng, F.; Zeng, F.; Yu, C.; Hou, X.; Wu, S. A Pegylated Fluorescent Turn-on Sensor for Detecting Fluoride Ions in Totally Aqueous Media and Its Imaging in Live Cells. *Chem.−Eur. J.* **2013**, *19*, 936−942.

(1130) Gai, L.; Chen, H.; Zou, B.; Lu, H.; Lai, G.; Li, Z.; Shen, Z. Ratiometric Fluorescence Chemodosimeters for Fluoride Anion Based on Pyrene Excimer/Monomer Transformation. *Chem. Commun.* **2012**, *48*, 10721−10723.

(1131) Nishimura, T.; Xu, S. Y.; Jiang, Y. B.; Fossey, J. S.; Sakurai, K.; Bull, S. D.; James, T. D. A Simple Visual Sensor with the Potential for Determining the Concentration of Fluoride in Water at Environmentally Significant Levels. *Chem. Commun.* **2013**, *49*, 478−480.

(1132) Kumar, G. G. V.; Kesavan, M. P.; Sivaraman, G.; Rajesh, J. Colorimetric and Nir Fluorescence Receptors for F- Ion Detection in Aqueous Condition and Its Live Cell Imaging. *Sens. Actuators, B* **2018**, *255*, 3194−3206.

(1133) Leoni, L.; Dalla Cort, A.; Biedermann, F.; Kubik, S. *Supramolecular Chemistry in Water*; Wiley-VCH: Weinheim, 2019, Chapter 6, pp 193−247.

(1134) Svec, J.; Necas, M.; Sindelar, V. Bambus[6]Uril. *Angew. Chem., Int. Ed.* **2010**, *49*, 2378−2381.

(1135) Havel, V.; Svec, J.; Wimmerova, M.; Dusek, M.; Pojarova, M.; Sindelar, V. Bambus[N]Urils: A New Family of Macrocyclic Anion Receptors. *Org. Lett.* **2011**, *13*, 4000−4003.

(1136) Svec, J.; Dusek, M.; Fejfarova, K.; Stacko, P.; Klán, P.; Kaifer, A. E.; Li, W.; Hudeckova, E.; Sindelar, V. Anion-Free Bambus[6]Uril and Its Supramolecular Properties. *Chem.−Eur. J.* **2011**, *17*, 5605−5612.

(1137) Havel, V.; Sindelar, V.; Necas, M.; Kaifer, A. E. Water-Mediated Inclusion of Benzoates and Tosylates inside the Bambusuril Macrocycle. *Chem. Commun.* **2014**, *50*, 1372−1374.

(1138) Yawer, M. A.; Havel, V.; Sindelar, V. A Bambusuril Macrocycle That Binds Anions in Water with High Affinity and Selectivity. *Angew. Chem., Int. Ed.* **2015**, *54*, 276−279.

(1139) Havel, V.; Yawer, M. A.; Sindelar, V. Real-Time Analysis of Multiple Anion Mixtures in Aqueous Media Using a Single Receptor. *Chem. Commun.* **2015**, *51*, 4666−4669.

(1140) Lizal, T.; Sindelar, V. Bambusuril Anion Receptors. *Isr. J. Chem.* **2018**, *58*, 326−333.

(1141) Lisbjerg, M.; Jessen, B. M.; Rasmussen, B.; Nielsen, B. E.; Madsen, A. O.; Pittelkow, M. Discovery of a Cyclic 6 + 6 Hexamer of D-Biotin and Formaldehyde. *Chem. Sci.* **2014**, *5*, 2647−2650.

(1142) Lisbjerg, M.; Nielsen, B. E.; Milhoj, B. O.; Sauer, S. P. A.; Pittelkow, M. Anion Binding by Biotin[6]Uril in Water. *Org. Biomol. Chem.* **2015**, *13*, 369−373.

(1143) Lisbjerg, M.; Valkenier, H.; Jessen, B. M.; Al-Kerdi, H.; Davis, A. P.; Pittelkow, M. Biotin[6]Uril Esters: Chloride-Selective Transmembrane Anion Carriers Employing C—H···Anion Interactions. *J. Am. Chem. Soc.* **2015**, *137*, 4948−4951.

(1144) Kubik, S.; Goddard, R.; Kirchner, R.; Nolting, D.; Seidel, J. A Cyclic Hexapeptide Containing L-Proline and 6-Aminopicolinic Acid Subunits Binds Anions in Water. *Angew. Chem., Int. Ed.* **2001**, *40*, 2648−2651.

(1145) Kubik, S.; Kirchner, R.; Nolting, D.; Seidel, J. A Molecular Oyster: A Neutral Anion Receptor Containing Two Cyclopeptide Subunits with a Remarkable Sulfate Affinity in Aqueous Solution. *J. Am. Chem. Soc.* **2002**, *124*, 12752−12760.

(1146) Otto, S.; Kubik, S. Dynamic Combinatorial Optimization of a Neutral Receptor That Binds Inorganic Anions in Aqueous Solution. *J. Am. Chem. Soc.* **2003**, *125*, 7804−7805.

(1147) Krause, M. R.; Goddard, R.; Kubik, S. Anion-Binding Properties of a Cyclic Pseudohexapeptide Containing 1,5-Disubstituted 1,2,3-Triazole Subunits. *J. Org. Chem.* **2011**, *76*, 7084−7095.

(1148) Sommer, F.; Kubik, S. Anion Binding of a Neutral Bis(Cyclopeptide) in Water-Methanol Mixtures Containing up to 95% Water. *Org. Biomol. Chem.* **2014**, *12*, 8851−8860.

(1149) Kubik, S. Anion Recognition in Aqueous Media by Cyclopeptides and Other Synthetic Receptors. *Acc. Chem. Res.* **2017**, *50*, 2870−2878.

(1150) Sommer, F.; Marcus, Y.; Kubik, S. Effects of Solvent Properties on the Anion Binding of Neutral Water-Soluble Bis-(Cyclopeptides) in Water and Aqueous Solvent Mixtures. *ACS Omega* **2017**, *2*, 3669−3680.

(1151) Bartl, J.; Kubik, S. Anion Binding of a Cyclopeptide-Derived Molecular Cage in Aqueous Solvent Mixtures. *ChemPlusChem* **2020**, *85*, 963−969.

(1152) Langton, M. J.; Robinson, S. W.; Marques, I.; Félix, V.; Beer, P. D. Halogen Bonding in Water Results in Enhanced Anion Recognition in Acyclic and Rotaxane Hosts. *Nat. Chem.* **2014**, *6*, 1039−1043.

(1153) Langton, M. J.; Blackburn, O. A.; Lang, T.; Faulkner, S.; Beer, P. D. Nitrite-Templated Synthesis of Lanthanide-Containing [2]Rotaxanes for Anion Sensing. *Angew. Chem., Int. Ed.* **2014**, *53*, 11463−11466.

(1154) Langton, M. J.; Marques, I.; Robinson, S. W.; Félix, V.; Beer, P. D. Iodide Recognition and Sensing in Water by a Halogen-Bonding Ruthenium(Ii)-Based Rotaxane. *Chem.−Eur. J.* **2016**, *22*, 185−192.

(1155) Bunchuay, T.; Docker, A.; Martinez-Martinez, A. J.; Beer, P. D. A Potent Halogen-Bonding Donor Motif for Anion Recognition and Anion Template Mechanical Bond Synthesis. *Angew. Chem., Int. Ed.* **2019**, *58*, 13823−13827.

(1156) Langton, M. J.; Beer, P. D. Rotaxane and Catenane Host Structures for Sensing Charged Guest Species. *Acc. Chem. Res.* **2014**, *47*, 1935−1949.

(1157) Shi, B.; Zhang, P.; Wei, T.; Yao, H.; Lin, Q.; Zhang, Y. Highly Selective Fluorescent Sensing for Cn- in Water: Utilization of the Supramolecular Self-Assembly. *Chem. Commun.* **2013**, *49*, 7812−7814.

(1158) Mo, H. J.; Shen, Y.; Ye, B. H. Selective Recognition of Cyanide Anion Via Formation of Multipoint Nh and Phenyl Ch Hydrogen Bonding with Acyclic Ruthenium Bipyridine Imidazole Receptors in Water. *Inorg. Chem.* **2012**, *51*, 7174−7184.

(1159) Walker, W. F.; Johnston, I. D. A. *The Metabolic Basis of Surgical Care*; Elsevier Butterworth-Heinemann, 1971; Chapter 2, pp 13−47.

(1160) Arosio, D.; Ratto, G. M. Twenty Years of Fluorescence Imaging of Intracellular Chloride. *Front. Cell. Neurosci.* **2014**, *8*, 258.

(1161) Sulis Sato, S.; Artoni, P.; Landi, S.; Cozzolino, O.; Parra, R.; Pracucci, E.; Trovato, F.; Szczurkowska, J.; Luin, S.; Arosio, D.; Beltram, F.; Cancedda, L.; Kaila, K.; Ratto, G. M. Simultaneous Two-Photon Imaging of Intracellular Chloride Concentration and Ph in Mouse Pyramidal Neurons in Vivo. *Proc. Natl. Acad. Sci. U. S. A.* **2017**, *114*, E8770.

(1162) Li, P.; Xie, T.; Fan, N.; Li, K.; Tang, B. Ratiometric Fluorescence Imaging for Distinguishing Chloride Concentration between Normal and Ischemic Ventricular Myocytes. *Chem. Commun.* **2012**, *48*, 2077−2079.

(1163) Riis-Johannessen, T.; Severin, K. A Micelle-Based Chemosensing Ensemble for the Fluorimetric Detection of Chloride in Water. *Chem.−Eur. J.* **2010**, *16*, 8291−8295.

(1164) Kim, H. J.; Lee, H.; Lee, J. H.; Choi, D. H.; Jung, J. H.; Kim, J. S. Bisindole Anchored Mesoporous Silica Nanoparticles for Cyanide Sensing in Aqueous Media. *Chem. Commun.* **2011**, *47*, 10918−10920.

(1165) Lin, X. X.; Li, Z. H.; Huang, X. Y.; Jiang, Y.; Wei, Q. H.; Chen, G. N. Pt2ag Acetylide-Doped Silica Nanoparticles: Enabling Luminescence of Pt2ag Complexes in Water and Sensors for Highly Sensitive Detection of Cyanide Anions. *Dalton Trans.* **2014**, *43*, 8861−8867.

(1166) Huo, Q.; Liu, J.; Wang, L.-Q.; Jiang, Y.; Lambert, T. N.; Fang, E. A New Class of Silica Cross-Linked Micellar Core-Shell Nanoparticles. *J. Am. Chem. Soc.* **2006**, *128*, 6447−6453.

(1167) Zanarini, S.; Rampazzo, E.; Bonacchi, S.; Juris, R.; Marcaccio, M.; Montalti, M.; Paolucci, F.; Prodi, L. Iridium Doped Silica-Peg Nanoparticles: Enabling Electrochemiluminescence of Neutral Complexes in Aqueous Media. *J. Am. Chem. Soc.* **2009**, *131*, 14208−14209.

(1168) Ramakrishnam Raju, M. V.; Lin, H.-C. A Cyanide-Responsive Supramolecular Nanovalve Based on Pd(Ii)-Templated Pseudo-Rotaxane. *J. Mater. Chem. A* **2015**, *3*, 6414−6422.

(1169) Gemen, J.; Ahrens, J.; Shimon, L. J. W.; Klajn, R. Modulating the Optical Properties of Bodipy Dyes by Noncovalent Dimerization within a Flexible Coordination Cage. *J. Am. Chem. Soc.* **2020**, *142*, 17721−17729.

(1170) Cheng, C.; Chen, H.-Y.; Wu, C.-S.; Meena, J. S.; Simon, T.; Ko, F.-H. A Highly Sensitive and Selective Cyanide Detection Using a Gold Nanoparticle-Based Dual Fluorescence-Colorimetric Sensor with a Wide Concentration Range. *Sens. Actuators, B* **2016**, *227*, 283−290.

(1171) Hilson, G.; Monhemius, A. J. Alternatives to Cyanide in the Gold Mining Industry: What Prospects for the Future? *J. Cleaner Prod.* **2006**, *14*, 1158−1167.

(1172) Hajizadeh, S.; Farhadi, K.; Forough, M.; Sabzi, R. E. Silver Nanoparticles as a Cyanide Colorimetric Sensor in Aqueous Media. *Anal. Methods* **2011**, *3*, 2599−2603.

(1173) Zhang, M.; Liu, Y. Q.; Ye, B. C. Colorimetric Assay for Sulfate Using Positively-Charged Gold Nanoparticles and Its Application for Real-Time Monitoring of Redox Process. *Analyst* **2011**, *136*, 4558−4562.

(1174) Bartl, J.; Reinke, L.; Koch, M.; Kubik, S. Selective Sensing of Sulfate Anions in Water with Cyclopeptide-Decorated Gold Nanoparticles. *Chem. Commun.* **2020**, *56*, 10457−10460.

(1175) Yuan, Z.; Lu, F.; Peng, M.; Wang, C. W.; Tseng, Y. T.; Du, Y.; Cai, N.; Lien, C. W.; Chang, H. T.; He, Y.; Yeung, E. S. Selective Colorimetric Detection of Hydrogen Sulfide Based on Primary Amine-Active Ester Cross-Linking of Gold Nanoparticles. *Anal. Chem.* **2015**, *87*, 7267−7273.

(1176) Gao, Z. P.; Qiao, M.; Tan, M. M.; Peng, H. N.; Ding, L. P. Surface Functionalization of Mesoporous Silica Nanoparticles with Pyronine Derivative for Selective Detection of Hydrogen Sulfide in Aqueous Solution. *Colloids Surf., A* **2020**, *586*, 124194.

(1177) He, L.; Yang, X.; Liu, Y.; Weiying Lin, W. L. Colorimetric and Ratiometric Fluorescent Probe for Hydrogen Sulfide Using a Coumarin-Pyronine Fret Dyad with a Large Emission Shift. *Anal. Methods* **2016**, *8*, 8022−8027.

(1178) Hatai, J.; Hirschhauser, C.; Schmuck, C.; Niemeyer, J. A Metallosupramolecular Coordination Polymer for the 'Turn-on' Fluorescence Detection of Hydrogen Sulfide. *ChemistryOpen* **2020**, *9*, 786−792.

(1179) Chatterjee, S.; Qin, J.; Li, X.; Liang, F.; Rai, D. K.; Yang, Y. W. Safranin O-Functionalized Cuboid Mesoporous Silica Material for Fluorescent Sensing and Adsorption of Permanganate. *J. Mater. Chem. B* **2020**, *8*, 2238−2249.

(1180) Maity, D.; Bhatt, M.; Paul, P. Calix[4]Arene Functionalized Gold Nanoparticles for Colorimetric and Bare-Eye Detection of Iodide in Aqueous Media and Periodate Aided Enhancement in Sensitivity. *Microchim. Acta* **2015**, *182*, 377−384.

(1181) Cheng, W.; Dong, S.; Wang, E. Iodine-Induced Gold-Nanoparticle Fusion/Fragmentation/Aggregation and Iodine-Linked Nanostructured Assemblies on a Glass Substrate. *Angew. Chem., Int. Ed.* **2003**, *42*, 449−452.

(1182) Maruthupandi, M.; Chandhru, M.; Rani, S. K.; Vasimalai, N. Highly Selective Detection of Iodide in Biological, Food, and Environmental Samples Using Polymer-Capped Silver Nanoparticles: Preparation of a Paper-Based Testing Kit for on-Site Monitoring. *ACS Omega* **2019**, *4*, 11372−11379.

(1183) Jha, G.; N, A.; Rahaman, A.; Sarkar, M. Fluoride Ion Sensing in Aqueous Medium by Employing Nitrobenzoxadiazole-Postgrafted Mesoporous Silica Nanoparticles (Mcm-41). *Phys. Chem. Chem. Phys.* **2015**, *17*, 3525.

(1184) Ding, L.; Lian, Y.; Lin, Z.; Zhang, Z.; Wang, X. D. Long-Term Quantitatively Imaging Intracellular Chloride Concentration

Using a Core-/Shell-Structured Nanosensor and Time-Domain Dual-Lifetime Referencing Method. *ACS Sens.* **2020**, *5*, 3971−3978.

(1185) Geddes, C. D. Optical Halide Sensing Using Fluorescence Quenching: Theory, Simulations and Applications—a Review. *Meas. Sci. Technol.* **2001**, *12*, R53.

(1186) Stauber, T.; Jentsch, T. J. Chloride in Vesicular Trafficking and Function. *Annu. Rev. Physiol.* **2013**, *75*, 453−477.

(1187) Xu, H.; Ren, D. Lysosomal Physiology. *Annu. Rev. Physiol.* **2015**, *77*, 57−80.

(1188) *Cyanide in Drinking Water*; World Health Organization, 2021; https://www.who.int/water_sanitation_health/ (accessed 2021-01-09).

(1189) Nozu, K.; Inagaki, T.; Fu, X. J.; Nozu, Y.; Kaito, H.; Kanda, K.; Sekine, T.; Igarashi, T.; Nakanishi, K.; Yoshikawa, N.; Iijima, K.; Matsuo, M. Molecular Analysis of Digenic Inheritance in Bartter Syndrome with Sensorineural Deafness. *J. Med. Genet.* **2007**, *45*, 182−186.

(1190) Park, Y.-D.; Jang, J.-H.; Oh, Y.-J.; Kwon, H.-J. Analyses of Organic Acids and Inorganic Anions and Their Relationship in Human Saliva before and after Glucose Intake. *Arch. Oral Biol.* **2014**, *59*, 1−11.

(1191) Chen, L.; Ingrid, S.; Ding, Y. G.; Liu, Y.; Qi, J. G.; Tang, C. S.; Du, J. B. Imbalance of Endogenous Homocysteine and Hydrogen Sulfide Metabolic Pathway in Essential Hypertensive Children. *Chin. Med. J.* **2007**, *120*, 389−393.

(1192) Whiteman, M.; Haigh, R.; Tarr, J. M.; Gooding, K. M.; Shore, A. C.; Winyard, P. G. Detection of Hydrogen Sulfide in Plasma and Knee-Joint Synovial Fluid from Rheumatoid Arthritis Patients: Relation to Clinical and Laboratory Measures of Inflammation. *Ann. N. Y. Acad. Sci.* **2010**, *1203*, 146−150.

(1193) Kage, S.; Takekawa, K.; Kurosaki, K.; Imamura, T.; Kudo, K. The Usefulness of Thiosulfate as an Indicator of Hydrogen Sulfide Poisoning: Three Cases. *Int. J. Legal Med.* **1997**, *110*, 220−222.

(1194) Dorozhkin, S. V.; Epple, M. Biological and Medical Significance of Calcium Phosphates. *Angew. Chem., Int. Ed.* **2002**, *41*, 3130−3146.

(1195) Fernández-García, C.; Coggins, A. J.; Powner, M. W. A Chemist's Perspective on the Role of Phosphorus at the Origins of Life. *Life* **2017**, *7*, 31.

(1196) Ubersax, J. A.; Ferrell, J. E., Jr Mechanisms of Specificity in Protein Phosphorylation. *Nat. Rev. Mol. Cell Biol.* **2007**, *8*, 530−541.

(1197) Penido, M. G. M. G.; Alon, U. S. Phosphate Homeostasis and Its Role in Bone Health. *Pediatr. Nephrol.* **2012**, *27*, 2039.

(1198) Achilles, W.; Dekanić, D.; Burk, M.; Schalk, C.; Tucak, A.; Karner, I. Crystal Growth of Calcium Oxalate in Urine of Stone-Formers and Normal Controls. *Urol. Res.* **1991**, *19*, 159−164.

(1199) Achilles, W.; Jöckel, U.; Schaper, A.; Burk, M.; Riedmiller, H. In Vitro Formation of "Urinary Stones": Generation of Spherulites of Calcium Phosphate in Gel and Overgrowth with Calcium Oxalate Using a New Flow Model of Crystallization. *Scanning Microsc.* **1995**, *9*, 24 discussion 585-576.

(1200) Stary, H. C. Natural History of Calcium Deposits in Atherosclerosis Progression and Regression. *Z. Kardiol.* **2000**, *89*, S028.

(1201) Tomazic, B. B. Physicochemical Principles of Cardiovascular Calcification. *Z. Kardiol.* **2001**, *90*, 68.

(1202) Bäck, M.; Michel, J.-B. From Organic and Inorganic Phosphates to Valvular and Vascular Calcifications. *Cardiovasc. Res.* **2021**, *117*, 2016−2029.

(1203) Zapanta Le Geros, R. Variations in the Crystalline Components of Human Dental Calculus. I. Crystallographic and Spectroscopic Methods of Analysis. *J. Dent. Res.* **1974**, *53*, 45−50.

(1204) Schroeder, H. E.; Shanley, D. Formation and Inhibition of Dental Calculus. *J. Periodontol.* **1969**, *40*, 643−646.

(1205) Fisseler-Eckhoff, A.; Müller, K. M. Arthroscopy and Chondrocalcinosis. *Arthrosc.−J. Arthrosc. Relat. Surg.* **1992**, *8*, 98−104.

(1206) Santamaria, R.; Diaz-Tocados, J. M.; Pendon-Ruiz de Mier, M. V.; Robles, A.; Salmeron-Rodriguez, M. D.; Ruiz, E.; Vergara, N.; Aguilera-Tejero, E.; Raya, A.; Ortega, R.; et al. Increased Phosphaturia Accelerates the Decline in Renal Function: A Search for Mechanisms. *Sci. Rep.* **2018**, *8*, 13701.

(1207) Olanbiwonnu, T.; Holden, R. M. Inorganic Phosphate as a Potential Risk Factor for Chronic Disease. *CMAJ.* **2018**, *190*, E784−E785.

(1208) Block, G. A.; Klassen, P. S.; Lazarus, J. M.; Ofsthun, N.; Lowrie, E. G.; Chertow, G. M. Mineral Metabolism, Mortality, and Morbidity in Maintenance Hemodialysis. *J. Am. Soc. Nephrol.* **2004**, *15*, 2208−2218.

(1209) Kestenbaum, B.; Sampson, J. N.; Rudser, K. D.; Patterson, D. J.; Seliger, S. L.; Young, B.; Sherrard, D. J.; Andress, D. L. Serum Phosphate Levels and Mortality Risk among People with Chronic Kidney Disease. *J. Am. Soc. Nephrol.* **2005**, *16*, 520−528.

(1210) Takeda, E.; Yamamoto, H.; Nashiki, K.; Sato, T.; Arai, H.; Taketani, Y. Inorganic Phosphate Homeostasis and the Role of Dietary Phosphorus. *J. Cell. Mol. Med.* **2004**, *8*, 191−200.

(1211) Peacock, M. Phosphate Metabolism in Health and Disease. *Calcif. Tissue Int.* **2021**, *108*, 3−15.

(1212) Calpena, E.; Casado, M.; Martínez-Rubio, D.; Nascimento, A.; Colomer, J.; Gargallo, E.; García-Cazorla, A.; Palau, F.; Artuch, R.; Espinós, C. 5-Oxoprolinuria in Heterozygous Patients for 5-Oxoprolinase (Oplah) Missense Changes. *JIMD Rep.* **2012**, *7*, 123−128.

(1213) Kim, S. K.; Lee, D. H.; Hong, J.-I.; Yoon, J. Chemosensors for Pyrophosphate. *Acc. Chem. Res.* **2009**, *42*, 23−31.

(1214) Bochet, C. G.; Draper, T.; Bocquet, B.; Pope, M. T.; Williams, A. F. 182tungsten Mössbauer Spectroscopy of Heteropolytungstates. *Dalton Trans.* **2009**, 5127−5131.

(1215) Bagniski, E.; Zak, B. Micro-Determination of Serum Phosphate and Phospholipids. *Clin. Chim. Acta* **1960**, *5*, 834−838.

(1216) Racicot, J. M.; Mako, T. L.; Olivelli, A.; Levine, M. A Paper-Based Device for Ultrasensitive, Colorimetric Phosphate Detection in Seawater. *Sensors* **2020**, *20*, 2766.

(1217) Lowdon, J. W.; Ishikura, H.; Radchenko, A.; Arreguin-Campos, R.; Rogosic, R.; Heidt, B.; Jimenez Monroy, K.; Peeters, M.; Dilien, H.; Eersels, K.; Cleij, T. J.; van Grinsven, B. Rapid Colorimetric Screening of Elevated Phosphate in Urine: A Charge-Transfer Interaction. *ACS Omega* **2020**, *5*, 21054−21066.

(1218) Dey, S.; Sukul, P. K. Selective Detection of Pyrophosphate Anions in Aqueous Medium Using Aggregation of Perylene Diimide as a Fluorescent Probe. *ACS Omega* **2019**, *4*, 16191−16200.

(1219) Chang, Y.; Qin, H.; Wang, X.; Li, X.; Li, M.; Yang, H.; Xu, K.; Qing, G. Visible and Reversible Restrict of Molecular Configuration by Copper Ion and Pyrophosphate. *ACS Sens.* **2020**, *5*, 2438−2447.

(1220) Gao, X.; Xu, J.; Ye, B.; Wu, W.; Zheng, H. Determination of Phosphate Anions with a near-Infrared Heptamethine Cyanine Dye in a Neutral Aqueous Solution. *Anal. Methods* **2019**, *11*, 2677−2682.

(1221) Zhu, F.; Yang, G.; Dhinakaran, M. K.; Wang, R.; Song, M.; Li, H. A Pyrophosphate-Activated Nanochannel Inspired by a Trp Ion Channel. *Chem. Commun.* **2019**, *55*, 12833−12836.

(1222) Massue, J.; Quinn, S. J.; Gunnlaugsson, T. Lanthanide Luminescent Displacement Assays: The Sensing of Phosphate Anions Using Eu(Iii)-Cyclen-Conjugated Gold Nanoparticles in Aqueous Solution. *J. Am. Chem. Soc.* **2008**, *130*, 6900−6901.

(1223) Liu, W.; Du, Z.; Qian, Y.; Li, F. A Specific Colorimetric Probe for Phosphate Detection Based on Anti-Aggregation of Gold Nanoparticles. *Sens. Actuators, B* **2013**, *176*, 927−931.

(1224) Skinner, A. V.; Han, S.; Balasubramanian, R. Rapid Selective Colorimetric Sensing of Polyphosphates by Ionic Resorcinarene Cavitand Interdigitated Gold Nanoparticles. *Sens. Actuators, B* **2017**, *247*, 706−712.

(1225) Dong, C.; Ma, X.; Qiu, N.; Zhang, Y.; Wu, A. An Ultra-Sensitive Colorimetric Sensor Based on Smartphone for Pyrophosphate Determination. *Sens. Actuators, B* **2021**, *329*, 129066.

(1226) Zhou, Y.; Zhang, G.; Xu, T.; Wu, Y.; Dong, C.; Shuang, S. Silk Fibroin-Confined Star-Shaped Decahedral Silver Nanoparticles as Fluorescent Probe for Detection of Cu2+ and Pyrophosphate. *ACS Biomater. Sci. Eng.* **2020**, *6*, 2770−2777.

(1227) Hu, Y.; Gao, Z.; Yang, J.; Chen, H.; Han, L. Environmentally Benign Conversion of Waste Polyethylene Terephthalate to Fluorescent Carbon Dots for "on-Off-on" Sensing of Ferric and Pyrophosphate Ions. *J. Colloid Interface Sci.* **2019**, *538*, 481−488.

(1228) Phan, A.; Doonan, C. J.; Uribe-Romo, F. J.; Knobler, C. B.; O'Keeffe, M.; Yaghi, O. M. Synthesis, Structure, and Carbon Dioxide Capture Properties of Zeolitic Imidazolate Frameworks. *Acc. Chem. Res.* **2010**, *43*, 58−67.

(1229) Wu, Z.; Yang, H.; Pan, S.; Liu, H.; Hu, X. Fluorescence-Scattering Dual-Signal Response of Carbon Dots@Zif-90 for Phosphate Ratiometric Detection. *ACS Sens.* **2020**, *5*, 2211−2220.

(1230) Zhao, C. X.; Zhang, X. P.; Shu, Y.; Wang, J. H. Europium-Pyridinedicarboxylate-Adenine Light-up Fluorescence Nanoprobes for Selective Detection of Phosphate in Biological Fluids. *ACS Appl. Mater. Interfaces* **2020**, *12*, 22593−22600.

(1231) Berchmans, S.; Issa, T. B.; Singh, P. Determination of Inorganic Phosphate by Electroanalytical Methods: A Review. *Anal. Chim. Acta* **2012**, *729*, 7−20.

(1232) Villalba, M. M.; McKeegan, K. J.; Vaughan, D. H.; Cardosi, M. F.; Davis, J. Bioelectroanalytical Determination of Phosphate: A Review. *J. Mol. Catal. B: Enzym.* **2009**, *59*, 1−8.

(1233) Yang, H. Enzyme-Based Ultrasensitive Electrochemical Biosensors. *Curr. Opin. Chem. Biol.* **2012**, *16*, 422−428.

(1234) Wongkongkatep, J.; Ojida, A.; Hamachi, I. Fluorescence Sensing of Inorganic Phosphate and Pyrophosphate Using Small Molecular Sensors and Their Applications. *Top. Curr. Chem.* **2017**, *375*, 30.

(1235) Ramakrishnam Raju, M. V.; Harris, S. M.; Pierre, V. C. Design and Applications of Metal-Based Molecular Receptors and Probes for Inorganic Phosphate. *Chem. Soc. Rev.* **2020**, *49*, 1090−1108.

(1236) Lee, S.; Yuen, K. K.; Jolliffe, K. A.; Yoon, J. Fluorescent and Colorimetric Chemosensors for Pyrophosphate. *Chem. Soc. Rev.* **2015**, *44*, 1749−1762.

(1237) Saki, F.; Karamizadeh, Z.; Nasirabadi, S.; Mumm, S.; McAlister, W. H.; Whyte, M. P. Juvenile Paget's Disease in an Iranian Kindred with Vitamin D Deficiency and Novel Homozygous Tnfrsf11b Mutation. *J. Bone Miner. Res.* **2013**, *28*, 1501−1508.